UCRL-PROC-235344

LAWRENCE
LIVERMORE
NATIONAL
LABORATORY

UITI2007-University Information Technical Interchange Review Meeting

V. Franques, R. Williams, S. Schubert, J. Bloch, A. Ostrogorsky, A. Burger, Z. He, J. Derby, K Lynn, J. De Pruneda, D. McGregor, P. Lucas, K. Richardson, S. Hauck, K. Webb, M. Richardson, S. Sharpe, L. Carin, G. Wolberg, J. Gunther, T. Moon, L. J. Latecki, S. Balkir, I. Paschalidis, A. Garrett, G. Tepper, Z. Pizlo, G. Williams, J. Ryan, A. Maccabe, J. Qi, M. W. Hoffman

January 24, 2008

University Information Technical Interchange (UITI) Review Meeting
Orlando, FL, United States
November 27, 2007 through November 28, 2007

UITI2007—University Information Technical Interchange Review Meeting

University of Central Florida • Central Florida Research Park • Orlando • Florida
November 27 - 28, 2007

Agenda

Tuesday, November 27, 2007 • 3100 Technology Parkway • UCF Building 8119 Partnership II, Room 208

0800	Arrival, Registration and Morning Hospitality	
	Review Meeting Opening	
0845	Review Meeting Organizational Details	Dr. Gus Williams Program Chair, Brigham Young University Dr. Martin Richardson Host, University of Central Florida
0855	Welcome	Dr. Victoria Franques Nonproliferation Research and Development Program Manager
	Plenary Session	
0900	Nonproliferation Research and Development Organizational Mission and Overview	Rhys Williams, Ph.D. Nonproliferation Research and Development Deputy Director
0920	University Research Review Program Overview	Dr. Steven Schubert Pacific Northwest National Laboratory, Nonproliferation Research and Development Program Reviews
0940	National Laboratory Overview	Dr. Jeff Bloch Los Alamos National Laboratory
1005	Break	
	Materials	
1020	Heavy Metal Iodides	Professor Aleksander Ostrogorsky Rensselaer Polytechnical Institute Dr. Arnold Burger Fisk University
1045	High Resolution Three-Dimensional CZT Detector	Professor Zhong He University of Michigan
1110	Computational Models	Professor Jeffrey Derby University of Minnesota
1135	CZT Growth	Professor Kelvin G. Lynn Washington State University
1200	Onsite Lunch	All

Sponsor: Department of Energy, Nonproliferation Research and Development
Technical Host: Victoria Franques (Nonproliferation Research and Development) / 202.586.2560
Meeting Coordinators: Donna Raziano (LLNL) / 925.422.8517, Christine Shannon (LLNL) / 202.974.6315
Meeting Classification: Unclassified
Modification Date: 12/4/07 11:04 AM
UCRL No. UCRL-WEB-235344

UITI2007—University Information Technical Interchange Review Meeting

University of Central Florida • Central Florida Research Park • Orlando • Florida
November 27 - 28, 2007

Agenda

Tuesday, November 27, 2007 (continued)

1300	National Laboratory Overview	Jenni H. De Pruneda Lawrence Livermore National Laboratory
1325	Advanced Room Temperature Gamma Spectroscopy	Professor Douglas S. McGregor Kansas State University
	Remote Sensing	
1350	Optical Processing of Chalcogenide Glasses	Dr. Pierre Lucas University of Arizona
1415	Break	
1430	Optical Microsensor Array for Remote Sensing of Chemicals	Dr. Kathleen Richardson Clemson University Dr. Anu Agarwal Massachusetts Institute of Technology
1455	High-Performance, Low-Power Configurable Fabrics for Embedded Applications	Professor Scott Hauck University of Washington
1520	Ultra-Small Imaging and Spectroscopic	Professor Kevin J. Webb Purdue University
	Optics, Lasers and Photonics Laboratories	
1545	Optical Standoff Detection	Dr. Martin Richardson University of Central Florida
1615	Tour Optics, Lasers and Photonics Laboratories	Dr. Martin Richardson University of Central Florida
1700	Adjourn Day One	
1800	No Host Dinner at Peppino's Ristorante Italiano	100 Carrigan Avenue, Oviedo phone (407) 365-4774

UITI2007—University Information Technical Interchange Review Meeting

University of Central Florida • Central Florida Research Park • Orlando • Florida
November 27 - 28, 2007

Agenda

Wednesday, November 28, 2007 • 3100 Technology Parkway • UCF Building 8119 Partnership II, Room 208

0800	Arrival, Registration and Morning Hospitality	
0830	Welcome	Dr. Gus Williams Brigham Young University
	Remote Sensing (continued)	
0835	National Laboratory Overview	Dr. Steve Sharpe Pacific Northwest National Laboratory
0900	Advanced Wavelet-Based Analysis of Hyperspectral Ima	Professor Lawrence Carin Duke University
0925	Feature-Based Data Fusion for Three Dimensional Photography	Dr. George Wolberg The City University of New York
0950	GEOM-ICA: Incorporating Geometric and Other Information into Hyperspectral Independent Component Analysis	Dr. Todd Moon Utah State University Dr. Jake Gunther Utah State University Dr. Gus Williams Brigham Young University
1015	Break	
1030	National Laboratory Overview	Toby Townsend Sandia National Laboratories
1055	Image Recognition/Classification Based on Objects	Dr. Longin Jan Latecki Temple University Professor Zygmunt Pizlo Purdue University
	Simulations and Algorithms	
1120	All Solid-State Wireless Sensor Network for Nuclear Proliferation Detection	Professor Sina Balkir University of Nebraska Professor Michael W. Hoffman University of Nebraska
1145	Distributed Wireless Sensor Networks for Long-Term Deployments	Professor Ioannis Paschalidis Boston University

Sponsor: Department of Energy, Nonproliferation Research and Development
Technical Host: Victoria Franques (Nonproliferation Research and Development) / 202.586.2560
Meeting Coordinators: Donna Raziano (LLNL) / 925.422.8517, Christine Shannon (LLNL) / 202.974.6315
Meeting Classification: Unclassified
Modification Date: 12/4/07 11:04 AM

Agenda

Wednesday, November 28, 2007 (continued)

1210	Onsite Lunch	All
1300	National Laboratory Overview	Dr. Al Garrett Savannah River National Laboratory
1325	Standoff Fluorescence Detection of Uranium in Soil	Dr. Gary C. Tepper Virginia Commonwealth University
1350	Eagle Eyes: Physics-Based Model Development	Professor Chris Winstead University of Southern Mississippi William C. West Radiance Technologies
1415	Break	
1430	National Laboratory Overview – Nevada Test Site/Nonproliferation Research and Development Tests	Dr. Gus Williams Brigham Young University
1455	Simulation, Modeling and Real-Time Algorithm Development for Fast Neutron Imaging Telescopes	Dr. James Ryan University of New Hampshire
1520	A Framework for Dynamic Retasking and Redeployment in Sensors Network	Dr. Arthur Maccabe University of New Mexico
1545	Bayesian Estimation of Muon Scattering Images for Detecting Heavy Radioactive Materials: Algorithms Development and Performance Evaluation	Professor Jinyi Qi University of California, Davis
1610	Meeting Review and Conclusion	Dr. Victoria Franques Nonproliferation Research and Development Dr. Gus Williams Brigham Young University
	Materials Characterization Facility	
1645	Tour Materials Characterization Facility (**optional**)	Dr. Martin Richardson University of Central Florida
1730	Adjourn Day Two	

UITI Conference
Welcome

UITI Conference Goals

- Share information
  - With NNSA NA-22 HQ
  - With NNSA National Laboratories

People

- NA-22 Program Chair
  - Dr. Robert Mayo – Advanced Materials
    - SNM Detection, Radiation Sensors
  - Victoria Franques – Remote Sensing
  - Victoria Franques – Algorithms
    - Simluation and Algorithms
- Technical Chair
  - Dr. Gustavious Williams
- Hosted by UCF
  - Dr. Martin Richardson

Logistics

- All NA-22 Research Grants Represented
- NA-22 Funded National Laboratory Overviews

- NEED TO OBSERVE TIME LIMITS

Victoria Franques

- Remote Sensing Program Manager
- Simulation and Algorithms Program Manager

Dr. Rhys Williams
Deputy Director

NNSA Office of Nonproliferation Research and Development

University of Central Florida

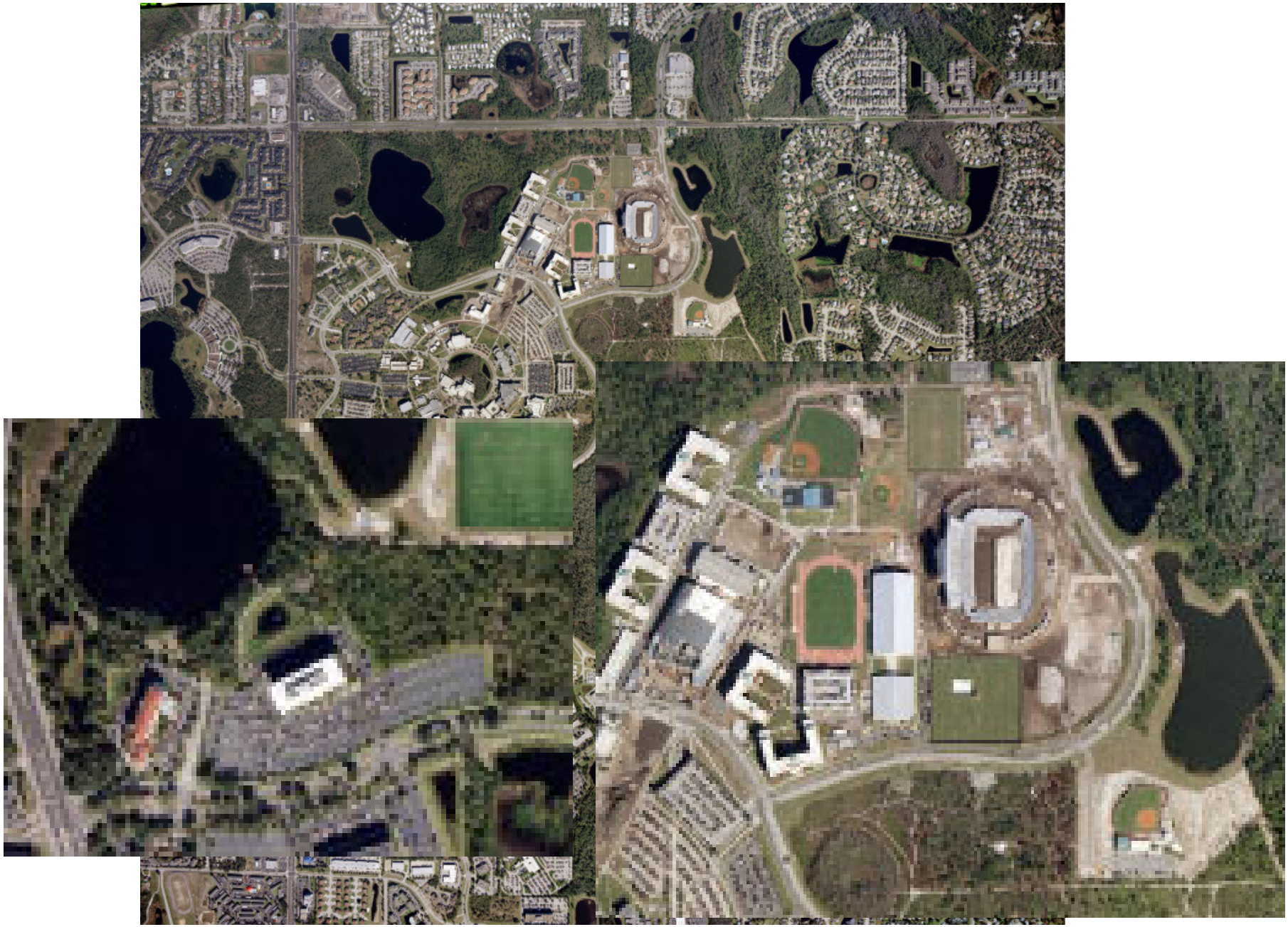

Brighthouse Stadium

A new medical school at Lake Nona

College of Optics and Photonics

The first college of optics
27 faculty (+ 9), ~ 200 graduates
~120,000 sq ft , $20M/yr
Home of CREOL, FPCE and the Townes Laser Institute

Office of Nonproliferation Research and Development

Welcome to the University Information Technical Interchange (UITI) Review Meeting

Victoria Franques
Program Manager

November 27, 2007

National Nuclear Security Administration
Office of Nonproliferation Research and Development

Research for National Missions

Rhys Williams, PhD
Deputy Director

November 27, 2007

Mission & Objectives

Mission:

Reduce the threat to national security posed by nuclear weapons proliferation/detonation or the illicit trafficking of nuclear materials through the development of new and novel technology.

Objectives:

- Develop and demonstrate technologies for detecting the stages of a foreign nuclear weapons program
- Develop, demonstrate, and deliver technologies to detect, report, locate, and identify worldwide nuclear detonations
- Conduct the highest quality, most innovative research and development

Nonproliferation R&D

Office of Nonproliferation Research & Development (NA-22)

T. Jan Cerveny, Ph.D.
Assistant Deputy Administrator

Rhys Williams, Ph.D.
Deputy

Office of Proliferation Detection

Rhys Williams, Ph.D.
Acting Program Manager

COL Vern Davis, Ph.D.
Deputy Program Manager

- Detection of nuclear material production
- Detection of nuclear weapon and material smuggling

Office of Nuclear Detonation Detection

Randy Bell
Program Manager

- Production of nuclear detonation detection systems
- Detonation forensics supporting attribution

Proliferation Detection (PD)

Proliferation Detection

Nonproliferation Mission Areas

- U-235 Production Detection
- Pu Production Detection
- SNM Movement Detection/Radiation Sensing
- Detection of Nuclear Weapons Production and Testing

Nonproliferation Enabling Technologies

- Advanced Material (radiation detection focus)
- Simulation, Algorithms and Modeling
- Nuclear Fuel Cycle Remote Sensing
- Tools, Techniques, Infrastructure and Demonstrations

Signatures &Observables

- Identify & characterize relevant nuclear proliferation signatures and observables

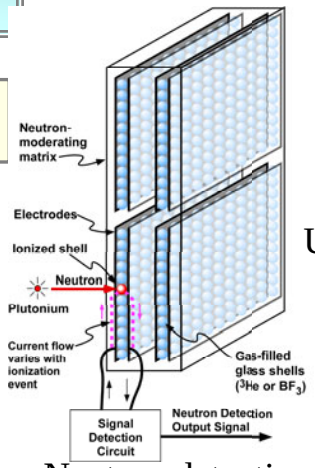

Neutron detection: gas-filled glass beads

Uranium Gas Centrifuge enrichment cascade

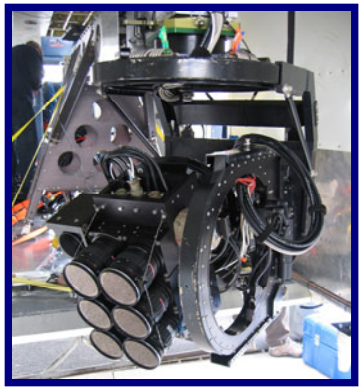

Sonoma Camera Pod

Trivalent Europium luminescence in Lutetium and Scandium phosphate glasses

Nuclear Detonation Detection (NDD)

Nuclear Detonation Detection

Space-Based Systems

- Surface & Atmospheric Burst Detection
- High Altitude & Space Burst Detection

Ground-Based Systems

- Seismic Detection Methods
- Radionuclide Detection Methods

Detonation Forensics

- Prompt Signatures
- Radionuclide Debris Sampling

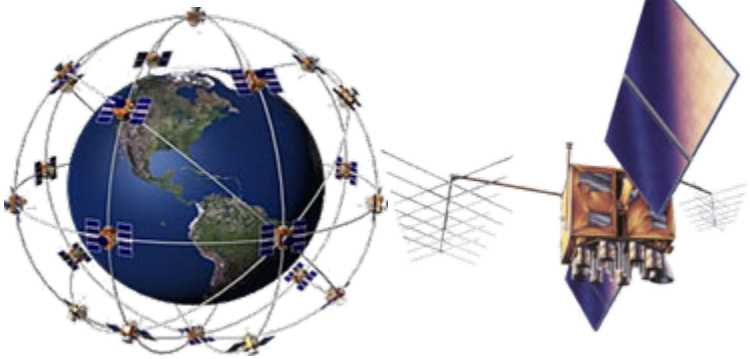

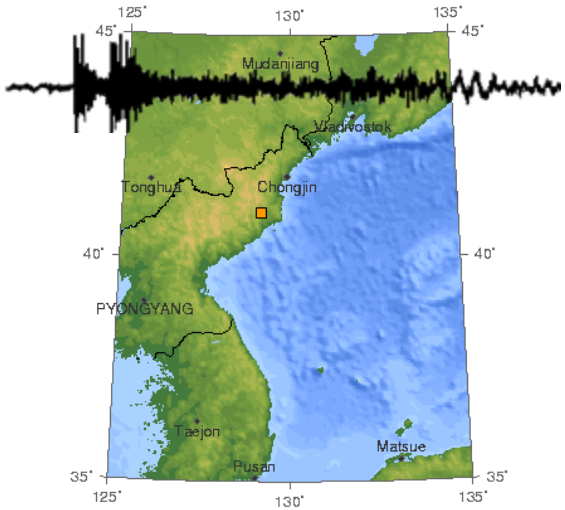

Questions?

National Nuclear Security Administration

Office of Nonproliferation Research and Development

Independent Review Process

Steven A. Schubert, Ph.D.
Chairman, IRP
509.372.6990
509.551.0645 (cell)
steven.schubert@pnl.gov

November 27, 2007

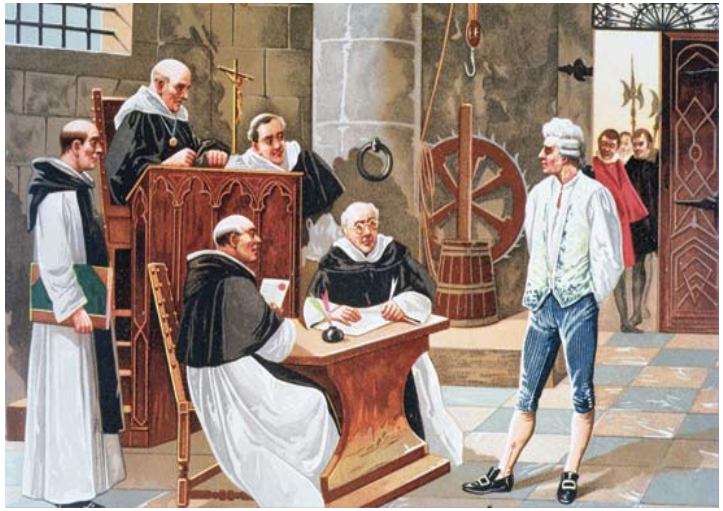

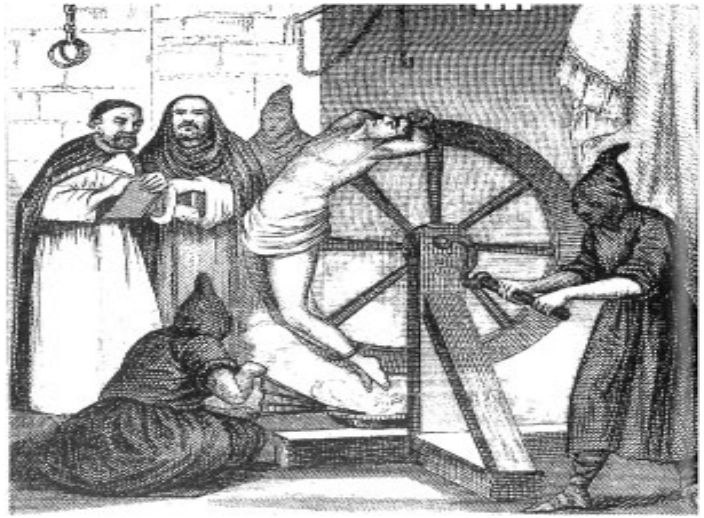

Review?

"We're here to help!"

Non-adversarial

&

Constructive

Process

Introduction

- **Independent Evaluation Strategy**
- **Project Selection**
- **Review Team Structure**
- **Working Guidelines**
- **Review Criteria**
- **Summary**

Independent Evaluation Strategy

The Purpose of Reviews:

- Give the PI an “outside” perspective on the R&D
- Maintain focus on Project objectives
- Evaluate need for mid-course corrections
- Provide NA-22 with input to key project and program decisions

Portfolio Framework & Key Decisions

	Exploratory Research	Research		Development	
Stages	**R1** • Innovative • Advanced concept	**R2** • Concept • Working lab demo • Controlled testing	**R3** • Prototype • Field test & evaluation	**D1** • Pre-production • Performance testing • Partnership	**D2** • Technology transfer
A Typical Project	6 months $50K	24 months $300K-$1M	24 months $750K-$1.2M	24 months $500K- $2M	24 months

Key Decision Points

18 Month Independent Review
- technical achievement
- likely success
- feedback on direction

Mature Project Independent Review
- objectives achieved
- remaining milestones
- rationale for continuing

Project Selection

- 100% of “eligible” R&D projects reviewed by end FY and every 3 years
- Projects normally reviewed 12-24 months after start
- 70 projects/grants selected for Independent Review in FY08
  - 1 at INL, 11 at LANL, 1 at LBNL, 11 at LLNL, 3 at ORNL, 10 at PNNL, 8 at SNL, 3 at SRNL, 1 at Y-12, 1 Earmark, 20 University Grants

Working Guidelines

- “Non-adversarial” process w/constructive goals
- Reviews conducted at performing location
- Each site visit will cover 1 project/day
- Exec session w/Review Team to summarize findings
- PI/POC debrief same day
- Formal Report to NA-22 within 14 days
- Generally unclassified or held at OUO level
- Classified sessions, as needed
- Strict non-disclosure requirements for reviewers

Review Team Structure

Chairperson + outside/academic experts + user reps

- Chairperson appointed by NA-22
- Outside/Academic Experts:
  - selected from academic and/or industrial community
  - strong relevant science background
- User Representatives:
  - technically astute and understand potential applications

Review Criteria

General Evaluation Criteria = same for all projects

Specific Evaluation Criteria = project specific questions in 3 areas

- Scientific & Technical Soundness
- Management/Execution
- Potential User Impact

General Criteria

- the project goals are well defined
- the technical approach is well conceived and adequately addresses the relevant technical issues and decision points in the proper sequence
- the management, management plan, technical staff, consultants, equipment and facilities are adequate to support the proposed effort
- the technical risks associated with the project are understood
- the project will produce or evaluate technology or scientific knowledge potentially useful to the user community
- the funding requirements are not unreasonable (+/-)

Summary

Independent Reviews help insure program excellence:

- Outside reviewers provide a different, non-DOE perspective
- PIs benefit from technical feedback from “subject matter experts” and potential users
- HQ given another reference point for evaluating projects
- Reviewers also gain valuable insight into NA-22 R&D program

Los Alamos National Laboratory Overview

Jeffrey J. Bloch

Senior Project Leader

Threat Reduction Directorate
Nuclear Non-Proliferation Research and Development Program Office

LA-UR-07-1010

Our Mission - 1943: in the span of two years……..
"the physical sciences were turned up-side down."

PAJARITO PLATEAU

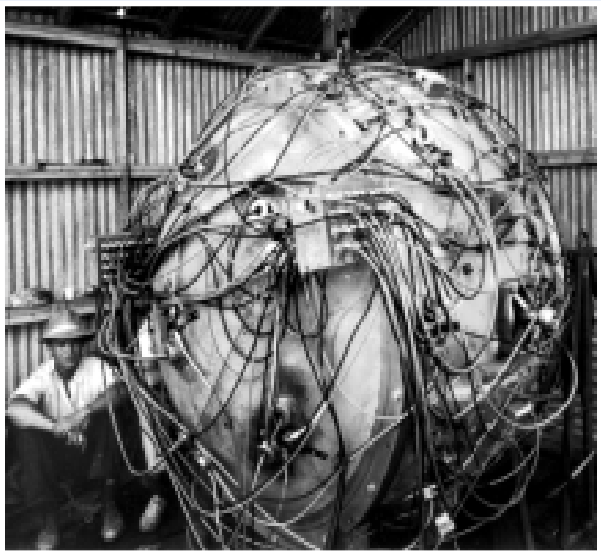

THE GADGET

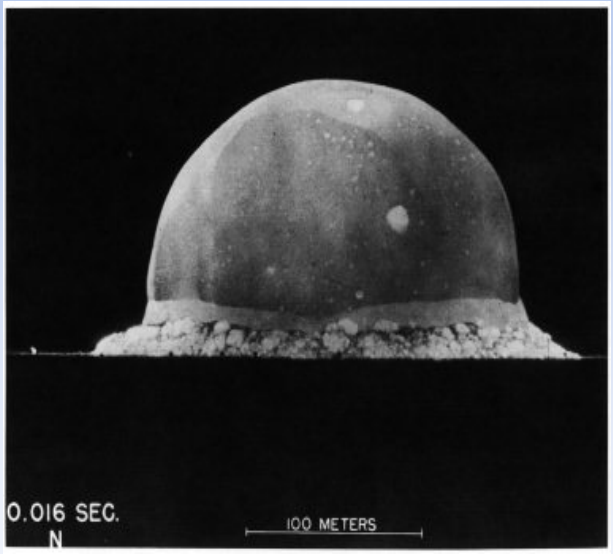

TRINITY SHOT

2007 Mission: Enhance Global Security by

- **Ensuring the safety and reliability of the U.S. nuclear deterrent**
- **Reducing global threats**
- **Solving national problems in defense, energy, environment, infrastructure, and health security**

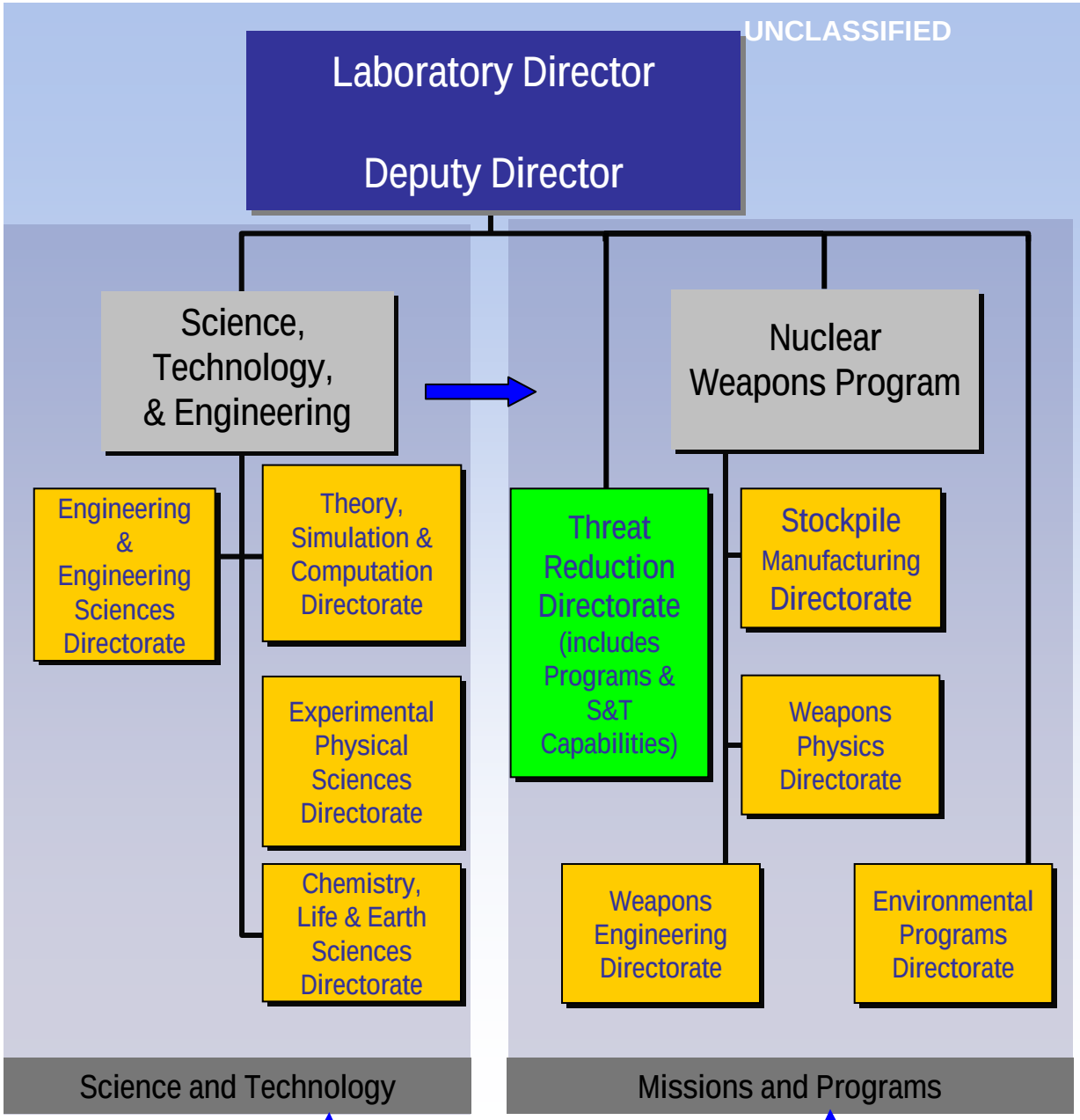

Accelerator Operations & Technology
Applied Engineering & Technology
Applied Physics
Chemistry
Chemistry & Metallurgy Research
Computing, Communications, and Networking
Computer, Computational & Stat. Sci.
Decision Applications
Dynamic & Energetic Materials
Earth and Environmental Sciences
Engineering Sciences and Applications
High Performance Computing
Hydrodynamic Experiments
International & Applied Technology
Information Systems and Technology
International, Space & Response
Los Alamos Neutron Science Center
Manufacturing Systems and Methods
Materials Physics & Applications
Materials Science & Technology
Nuclear Nonproliferation
Physics
Plutonium Manufacturing & Tech.
Theoretical
Weapons Engineering Technology

25 Technical Divisions

Los Alamos National Laboratory executes a large and complex set of programs

Weapons Research

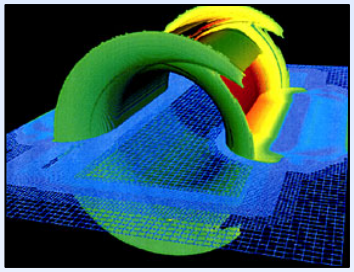

Large-Scale Simulation
Stockpile Stewardship

Pit Manufacturing

B61-11

W80 for Advanced
Cruise Missile

W76, W78, W88
for Trident &
Minuteman III

Basic Research

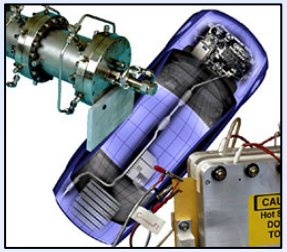

Fuel Cell

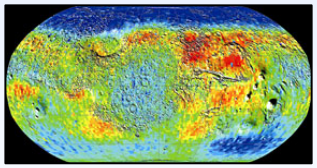

Neutron Spectrometer
Map of Mars

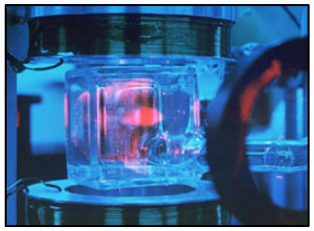

Atom Trapping
and Cooling

Threat Reduction

Nuclear Response

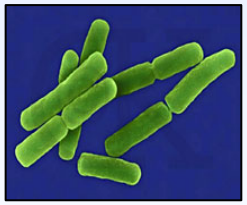

Advanced
Characterization
of Biological Agents

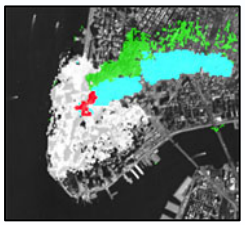

Image Analysis

Los Alamos encompasses a large and complex site

- Core Employees 9000
- Technical Staff 4000
- PhD 2000
- Post-docs 400
- Students 1500
- Operating budget ~$2.2 B
- Land area ~40 square miles

Very broad and deep science and engineering capabilities, driven by critical National needs

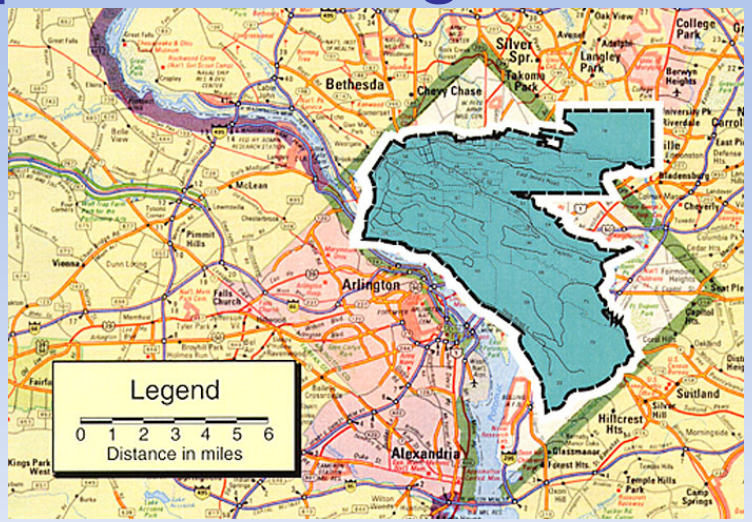

LANL (green) compared with Washington, D.C.

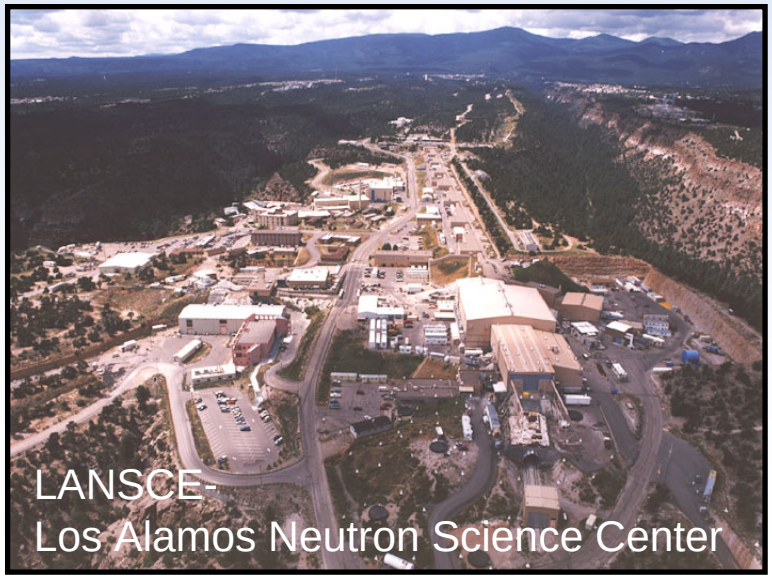

Proliferation Detection and Response:
A complex, multidimensional problem

Think of the problem via the process of acquiring and using a weapon

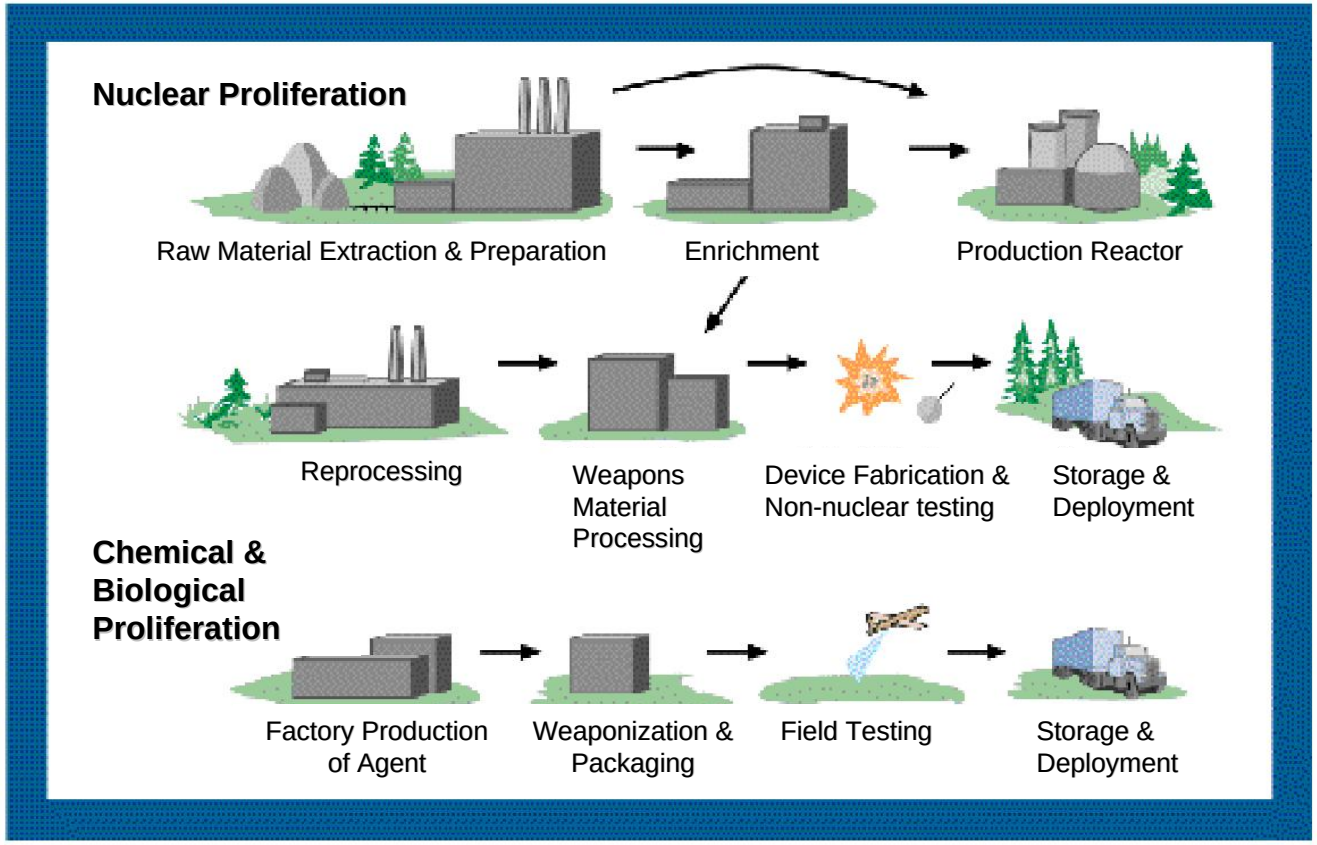

Mission Driven Science is a Los Alamos Hallmark - Satellite-Based Nuclear Explosion Monitoring

New solutions from science resulting from national needs

New Science Contributions

Gamma-ray bursts, water on moon/mars, magnetospheres of earth and planets.

Solutions

Triggering codes, imaging for homeland security, new detectors.

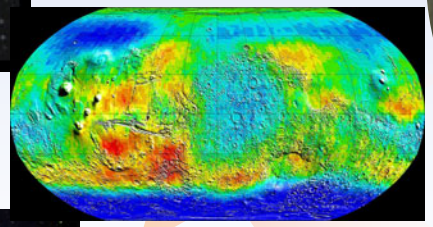

Map of Hydrogen (Water) on Mars

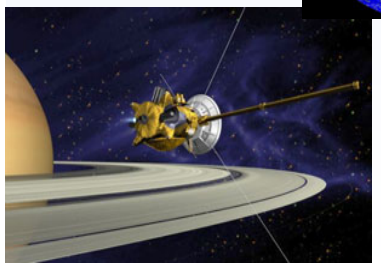

Cassini exploring Saturn's moons and rings 2005

National Need

Detect nuclear explosions in atmosphere and space - everywhere, all the time.

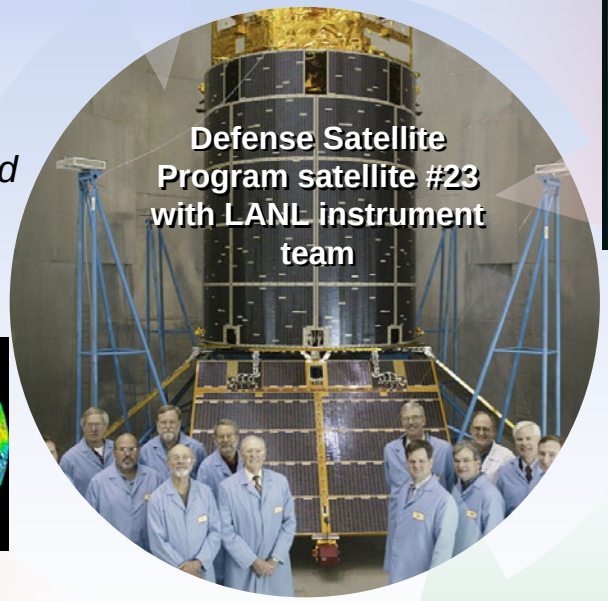

New Capabilities

Coded aperture x-ray imaging, Doppler neutron spectroscopy, neutral-particle imaging.

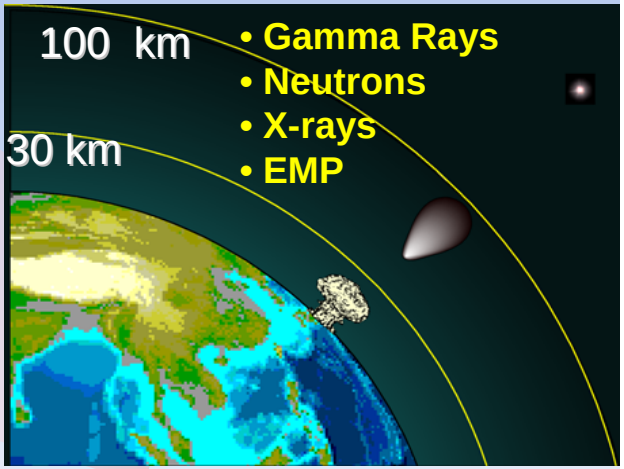

Existing and Emerging S&T

Satellite Instrumentation, x-ray, gamma-ray, neutron, EMP sensors

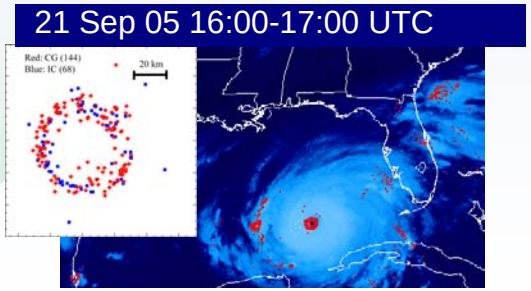

Rita category 5: intense lightning marks boundary of eyewall - EdotX sensors

40 Years of Space Experience - A Headstart on Persistent Surveillance - *1400 sensors, 400 instruments, 60 satellites*

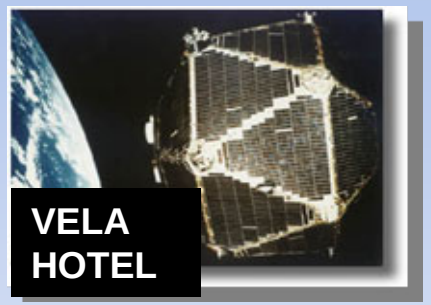

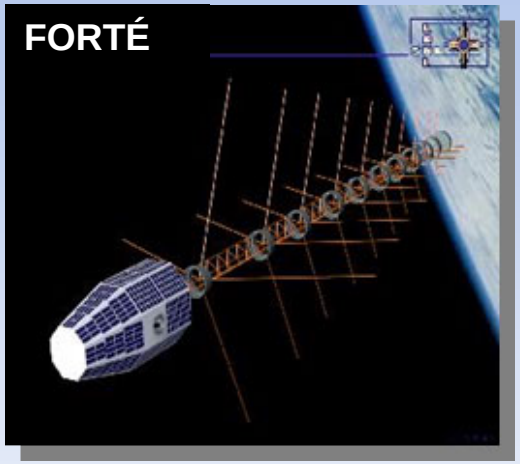

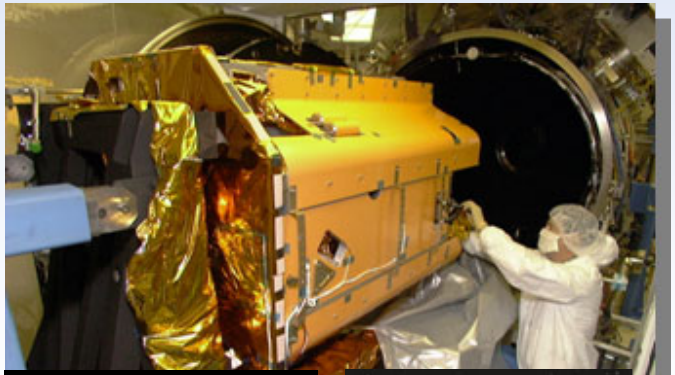

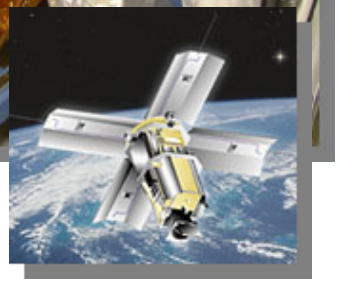

Multi-Spectral Thermal Imager

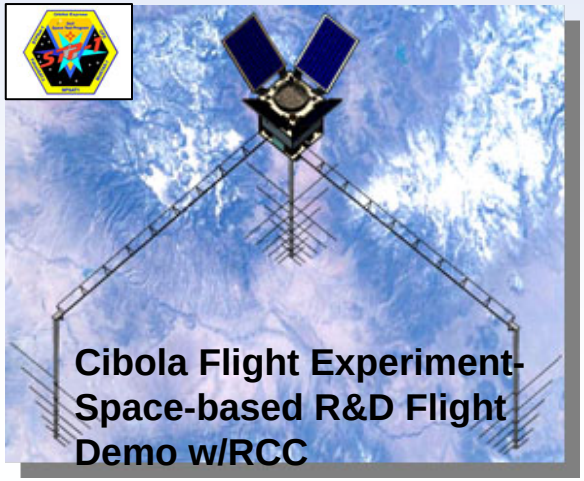

Satellite-Based Nuclear Explosion Monitoring: US Nuclear Detonation Detection System (USNDS)

- GPS Constellation
  - RF, x-ray
- Defense Support Program (DSP)
  - Neutron, γ-ray, space environment, x-ray
  - Space & Atmospheric Burst Reporting System (SABRS): next generation NUDET system
- Space-Based Infrared System (SBIRS)
  - Neutron, γ-ray, space environment
- DOE-sponsored Technology Demonstration Missions
  - Alexis, FORTE, Cibola Flight Experiment

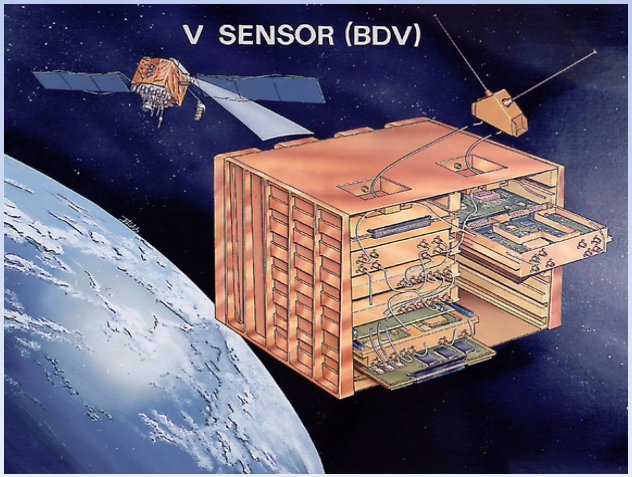

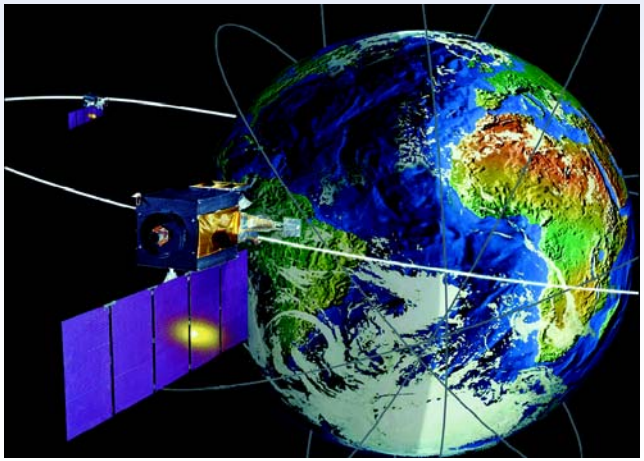

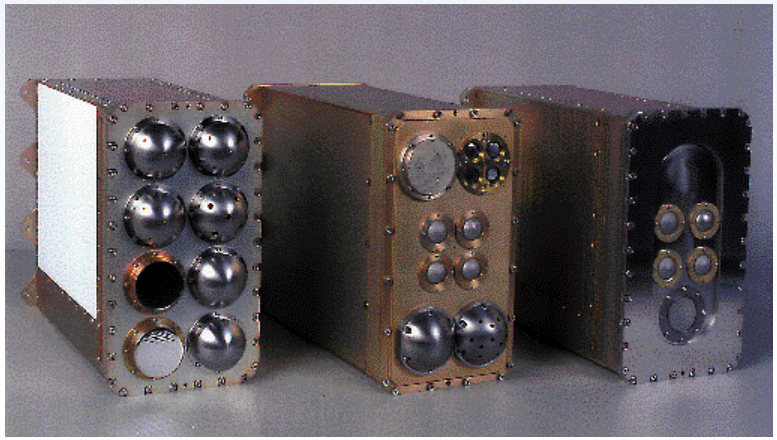

DOE Satellite Programs at Los Alamos Explore the Use of Advanced Technologies for National Security Mission

- Los Alamos in space since early 1960's (VELA)
- Four Dept. of Energy small satellites
- Over 400 instruments flown
  - DOD, NASA platforms
- Complete Capability
  - Design
  - Fabricate
  - Test
  - Operate

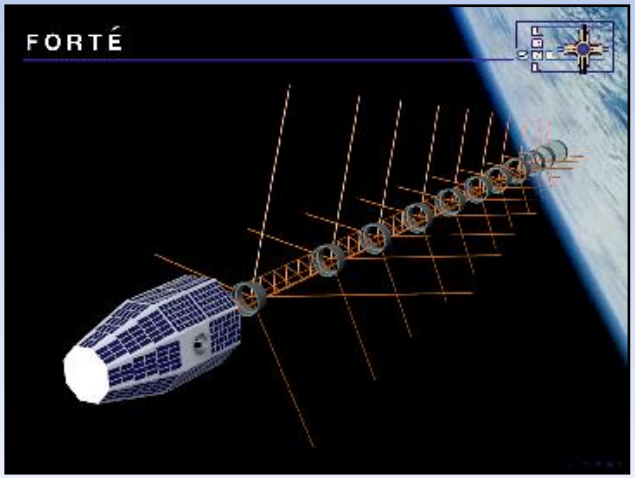

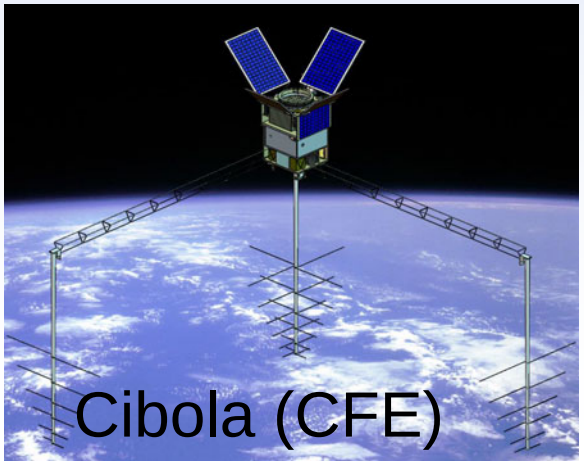

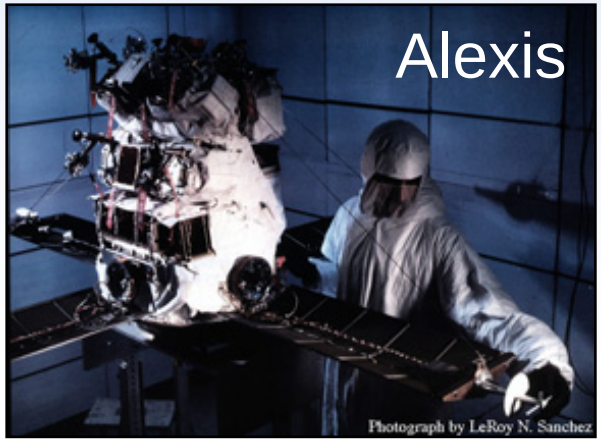

Water on the Moon and Mars: Space-based Nuclear Detection Capability
Advanced neutron, gamma-ray, x-ray, and RF detection

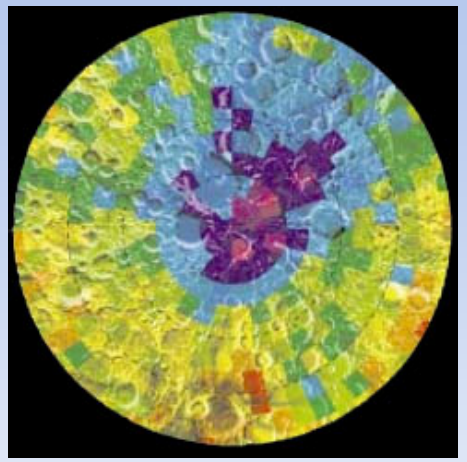

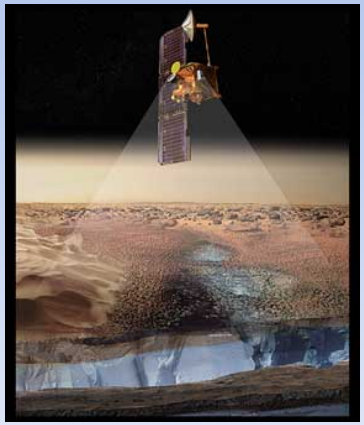

- Los Alamos Neutron Spectrometers on Lunar Prospector and on Mars Odyssey.

- Hydrogen content was detected under the surface.

- Mars' soil richer in hydrogen than the Moon's soil by more than several factors of 10 to several factors of 1,000.

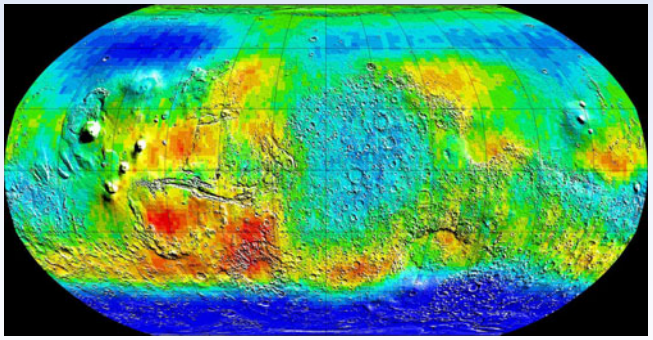

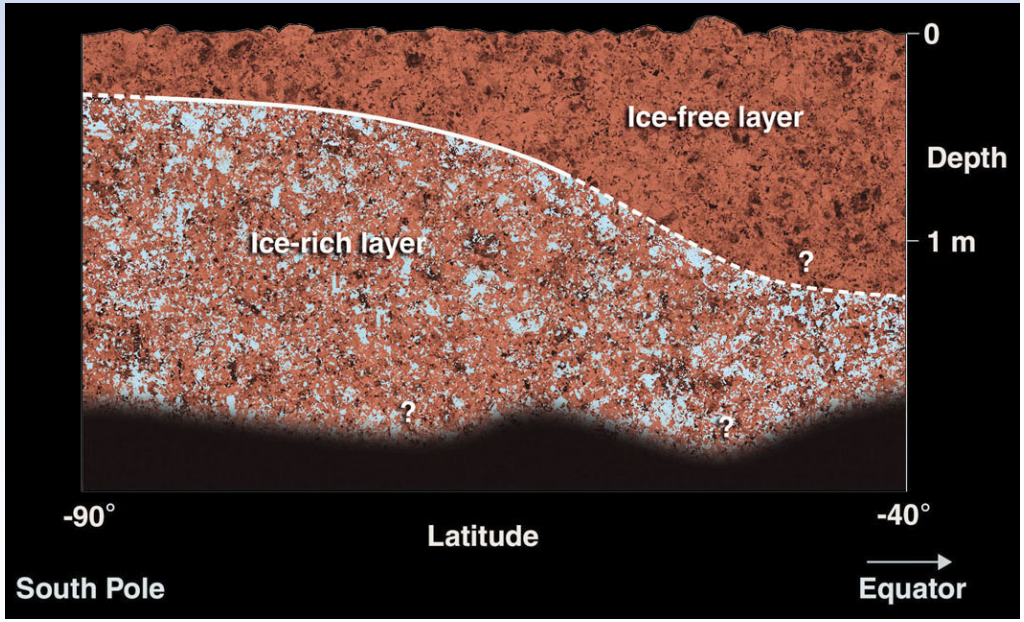

Mapping Hydrogen on Mars:

- Neutrons from cosmic ray spallation are moderated by H
- Presence of H (a signature of water) is noted as a low epithermal neutron flux
- Small signal change on large signal: validation of MCNP-X model

Space Weather: DREAM - A New Real-time Data Assimilation Model of the Radiation Belts

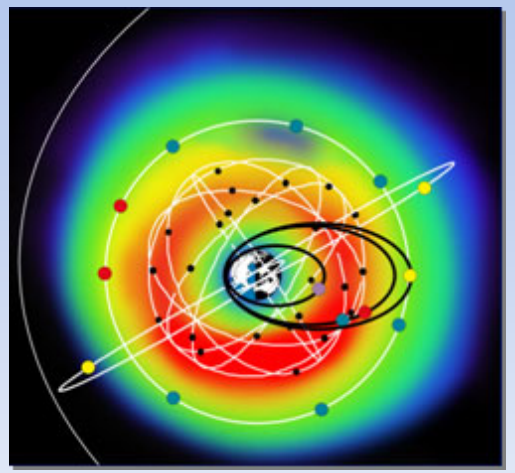

GEO & GPS Data Input

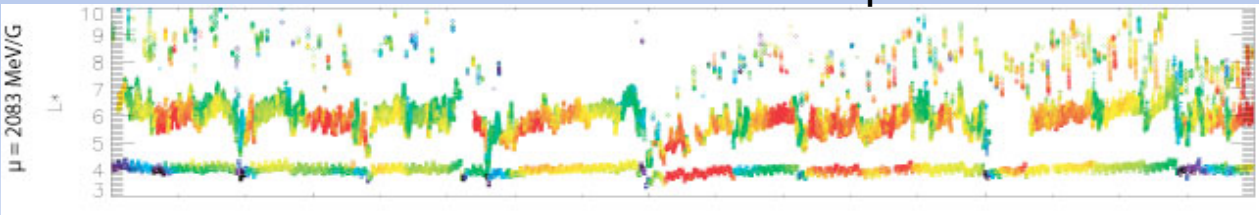

Global Data Assimilation Model (physics units)

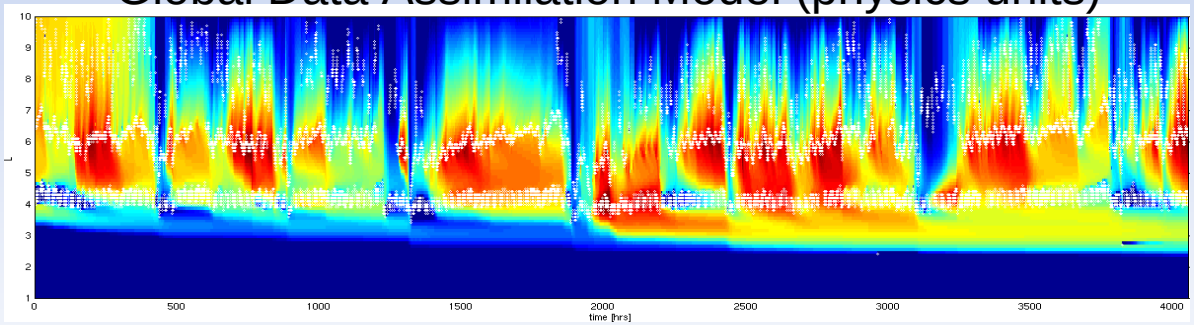

Modeled Fluxes in HEO orbit - spacecraft units

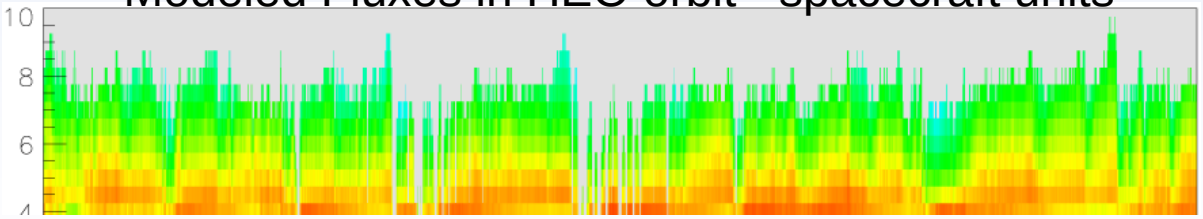

Measured Fluxes by HEO Satellite

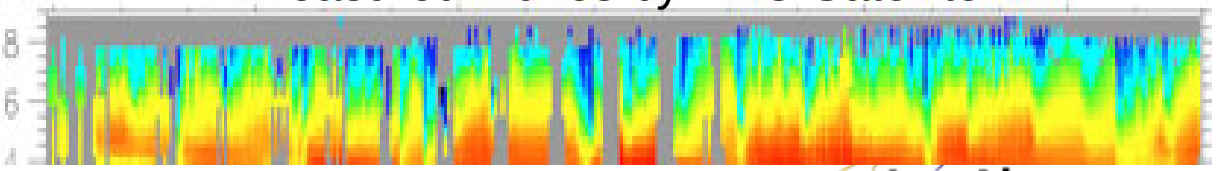

- Input from operational satellite systems in GEO, GPS & HEO orbits
- State-of-the-art physics models
- Data Assimilation produces data-driven, physically accurate specification of the dynamic radiation environment in real time
- Provides global knowledge of radiation fluxes, dose rate, or cumulative dose in any arbitrary satellite orbit

Dynamic Model, Real-Time (60s), Data-Driven, & Accurate

Los Alamos Information S&T Provides the Capability to Derive Actionable Knowledge from Data

Technologies that provide the ability to detect, assess, and disseminate in real time information critical to decision makers

- Surveillance Sensors and Systems
- Modeling & Simulation
- ISIS: Intelligent Searching of Images and Signals (e.g., GENIE: Genetic Imagery Exploitation)
- IKE: integrated Knowledge Engine decision tools

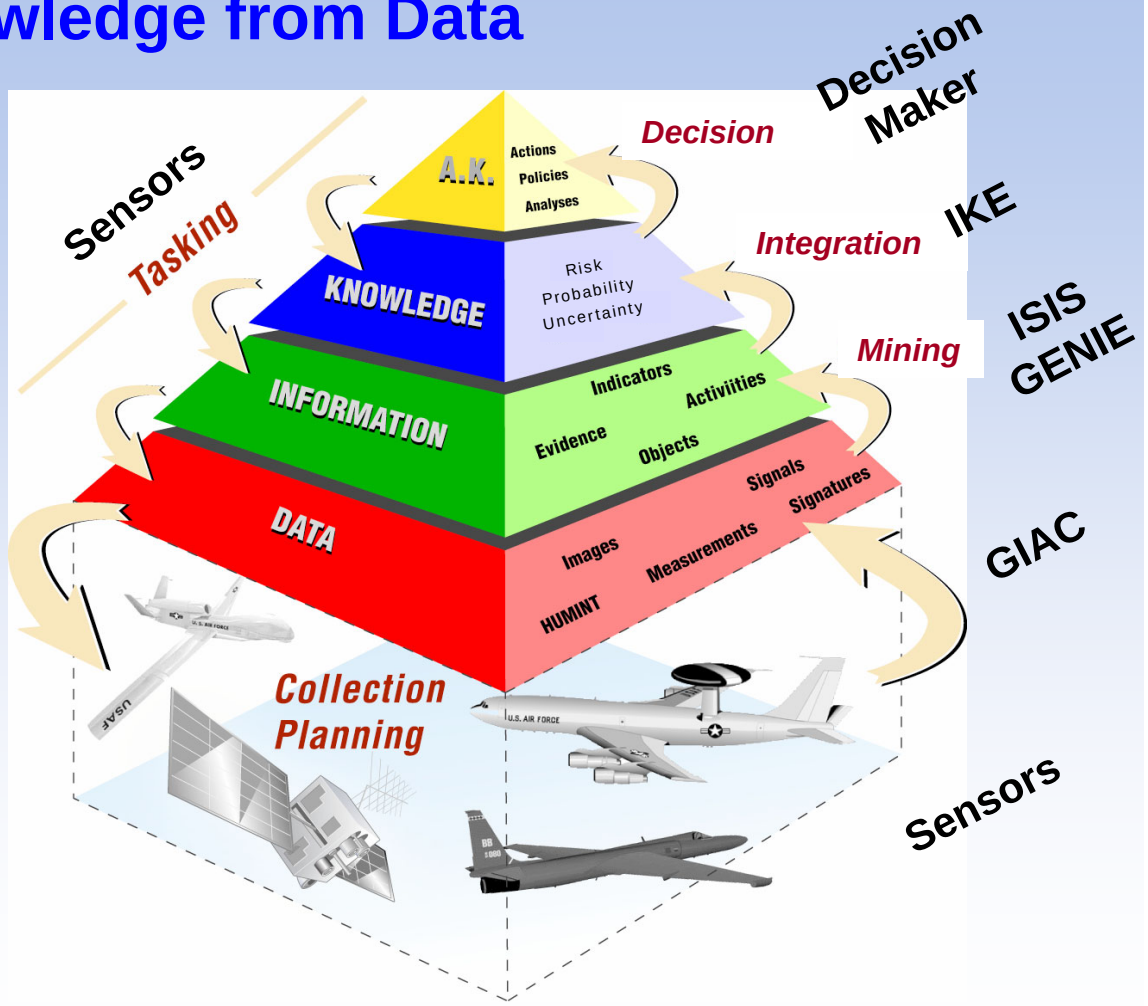

The Challenge: Event to Knowledge to Action *in Real Time*

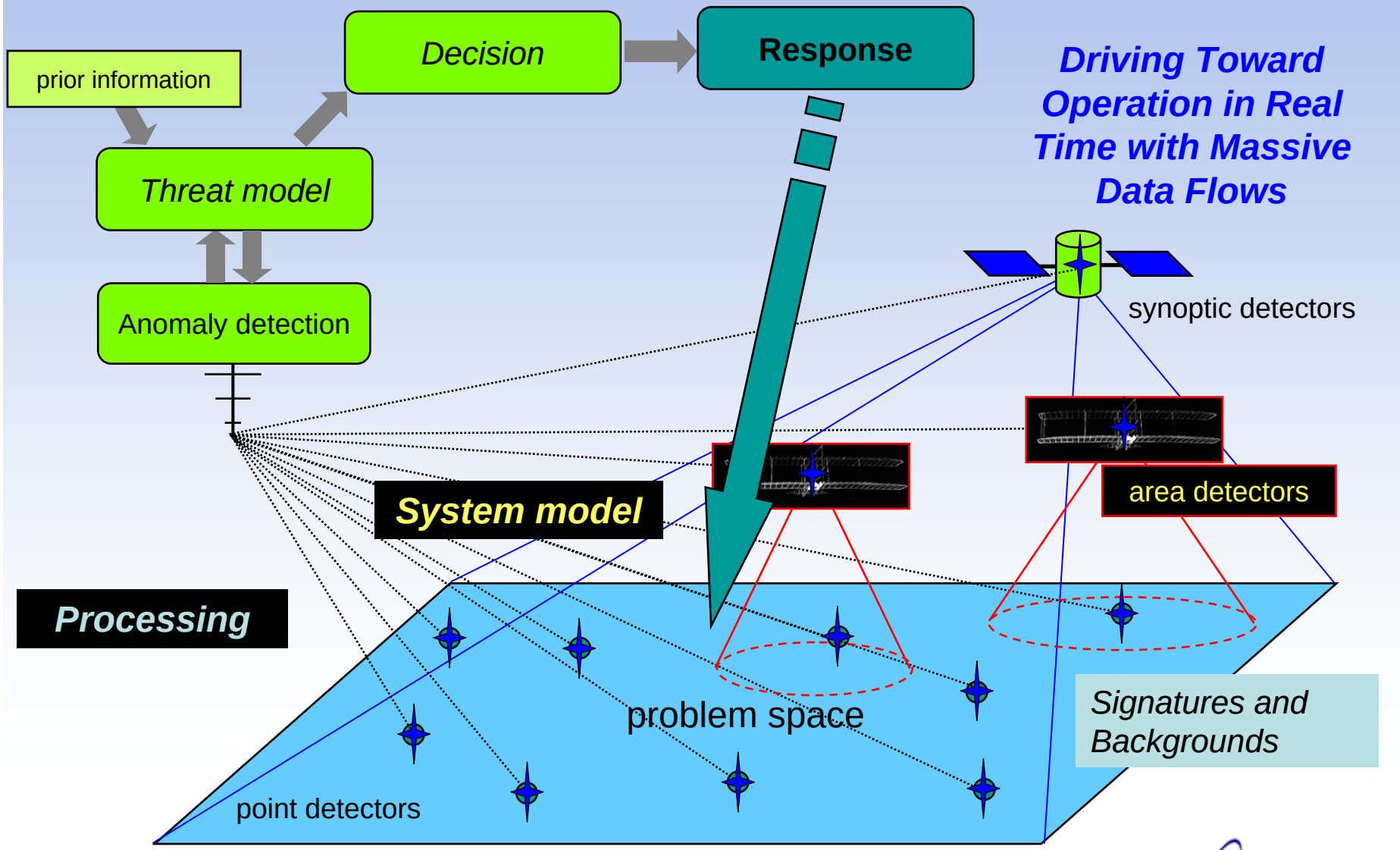

Automated Scene Classification - translation of expert knowledge into automated knowledge extraction

Algorithm evolution using biomorphic strategies

GENIE: Genetic Imagery Exploitation

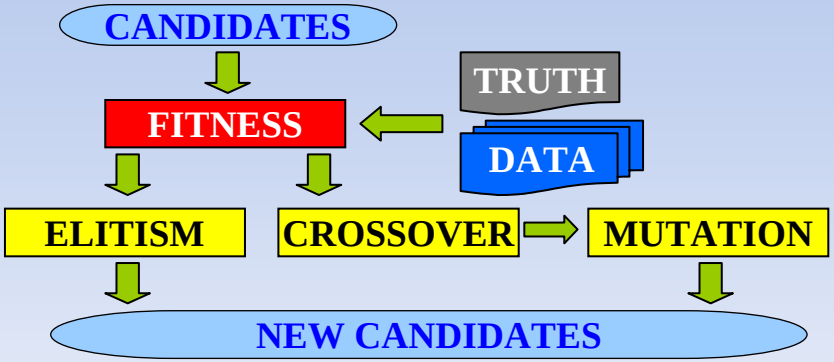

Training

Input Image

Training Image

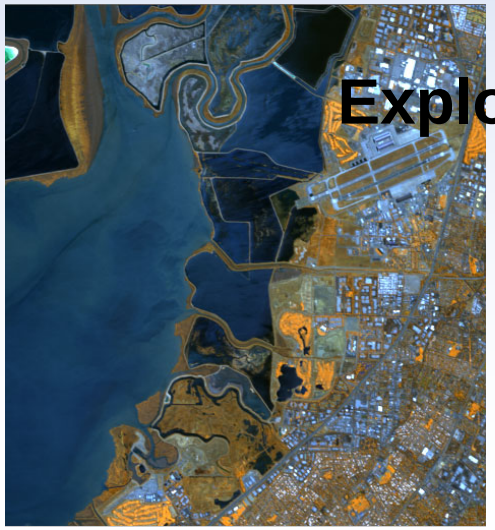

Exploitation

Test Image

Output of GENIE

Contact: Nancy David, 505-667-8896, ndavid@lanl.gov

Los Alamos

GENetic Image Exploitation (GENIE): Analysis of the 9/11 Debris Cloud

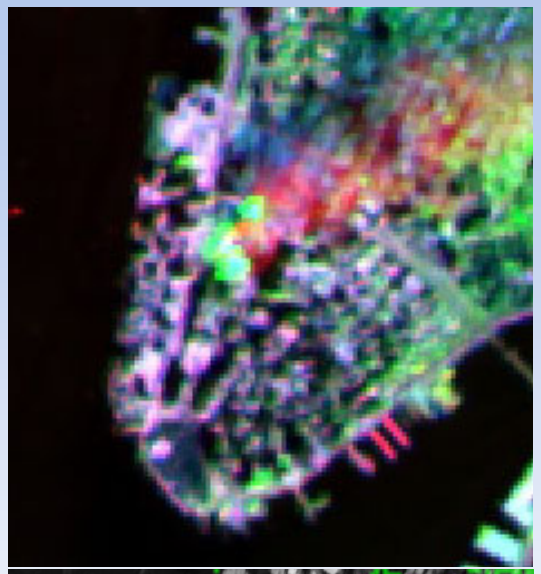

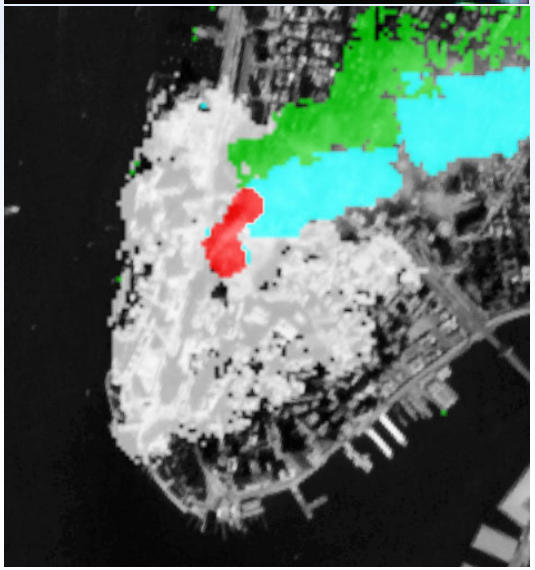

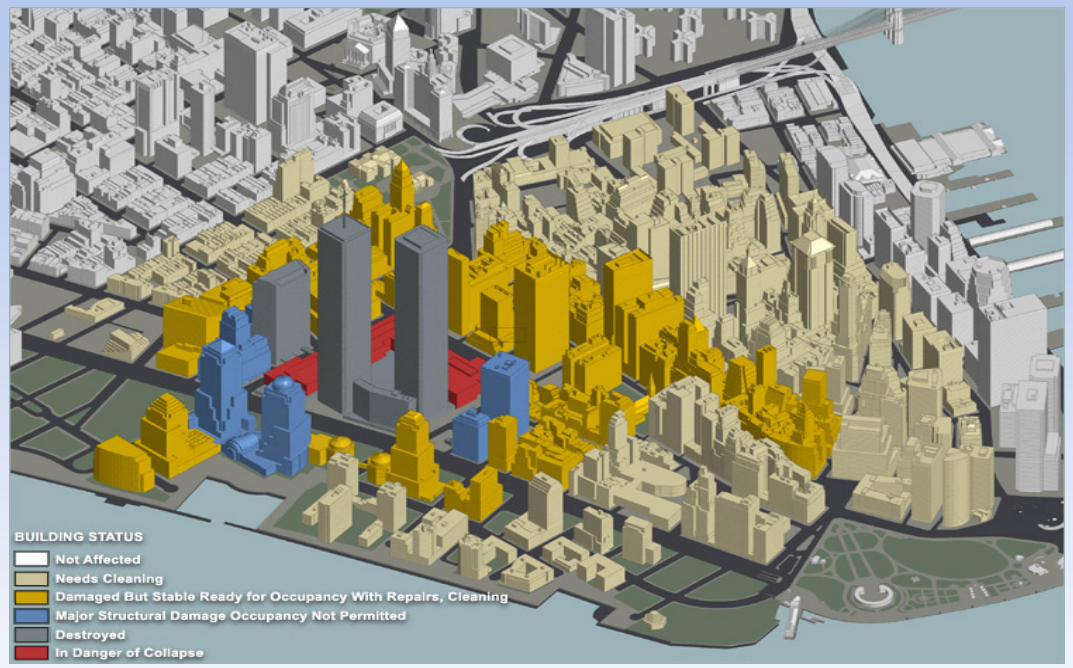

Top Left: Imagery of New York City Sep 13, 2001 from DOE's Multispectral Thermal imager (MTI) Satellite (Launched March 2000).

Lower Left: LANL's GENIE analysis of imagery from Sep 13 2001 and from Sep 2000. Colors: **WTC hotspots, smoke plume,** and **smoke plume's shadow**. The ash/debris field from the WTC collapse is shown as white, and covers an area of approximately 340 acres.

Above: Ground truth later released on CNN confirms result

Automated Change Detection in Remote Sensing Imagery: *Machine Learning Approach to Change Detection*

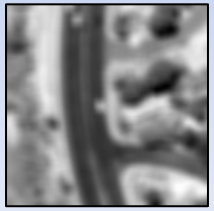

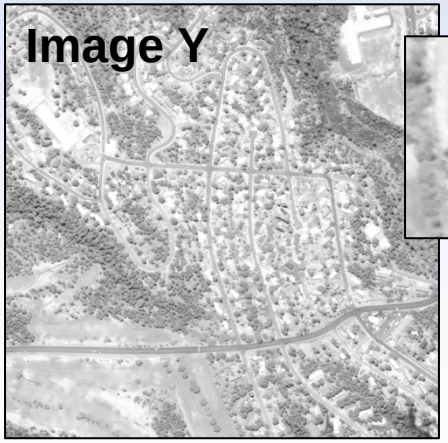

Persistent surveillance requires:

- What has changed in the time between two images?
- What changes are relevant?

In two images of the same scene many things can change

- Pervasive, uninteresting differences
- Illumination (brightness, contrast, focus)
- Camera angle
- Rare, anomalous changes (e.g. disturbed earth, camouflage)

- **Traditional Method**: Difference-based change detection
- **New Method**: Distribution-based anomaly detection

Benefits

- Analyst should be able to work faster by orders of magnitude
- Robust to mis-registration & lower false alarm rate

PI: James Theiler

Rapid Analysis of Polygonized Image Data Allows for High Compression with High Recognition Fidelity

Raster Airfield Image (DigitalGlobe©)

Decomposition into polygonal features

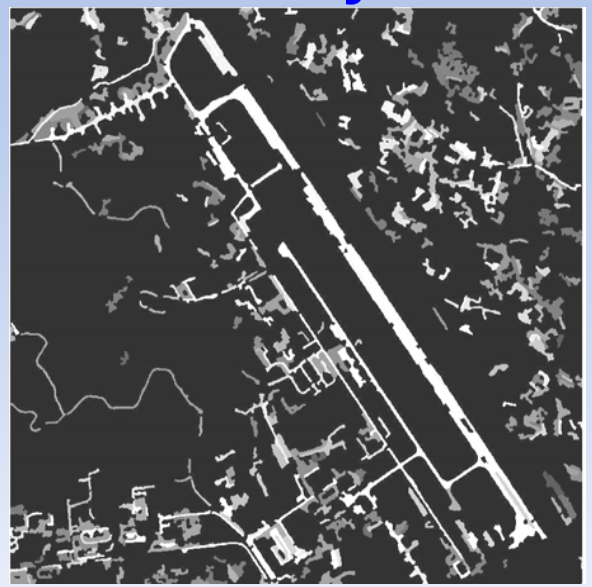

Detection of "thin" features such as roads

NOVELTY

- Conversion of pixel ('raster') images to polygonal ('vector') representation
- Representation of images in terms of features as opposed to pixels
- Emphasis on structural, as opposed to spectral, signature of features for robust identification

ADVANTAGES

- Significant data reduction for rapid analysis of large image datasets
- Structural abstraction of features for tolerating normal feature variability
- Detection and characterization of complex features independent of spectral signatures

APPLICATIONS

- Onboard automated analysis of aerial and satellite imagery
- Feature-based meta data for geospatial information systems (GIS)
- Rapid transmission of tagged UAV imagery to warfighter on ground

Global Intelligence from Merging Astrophysics & Information Science

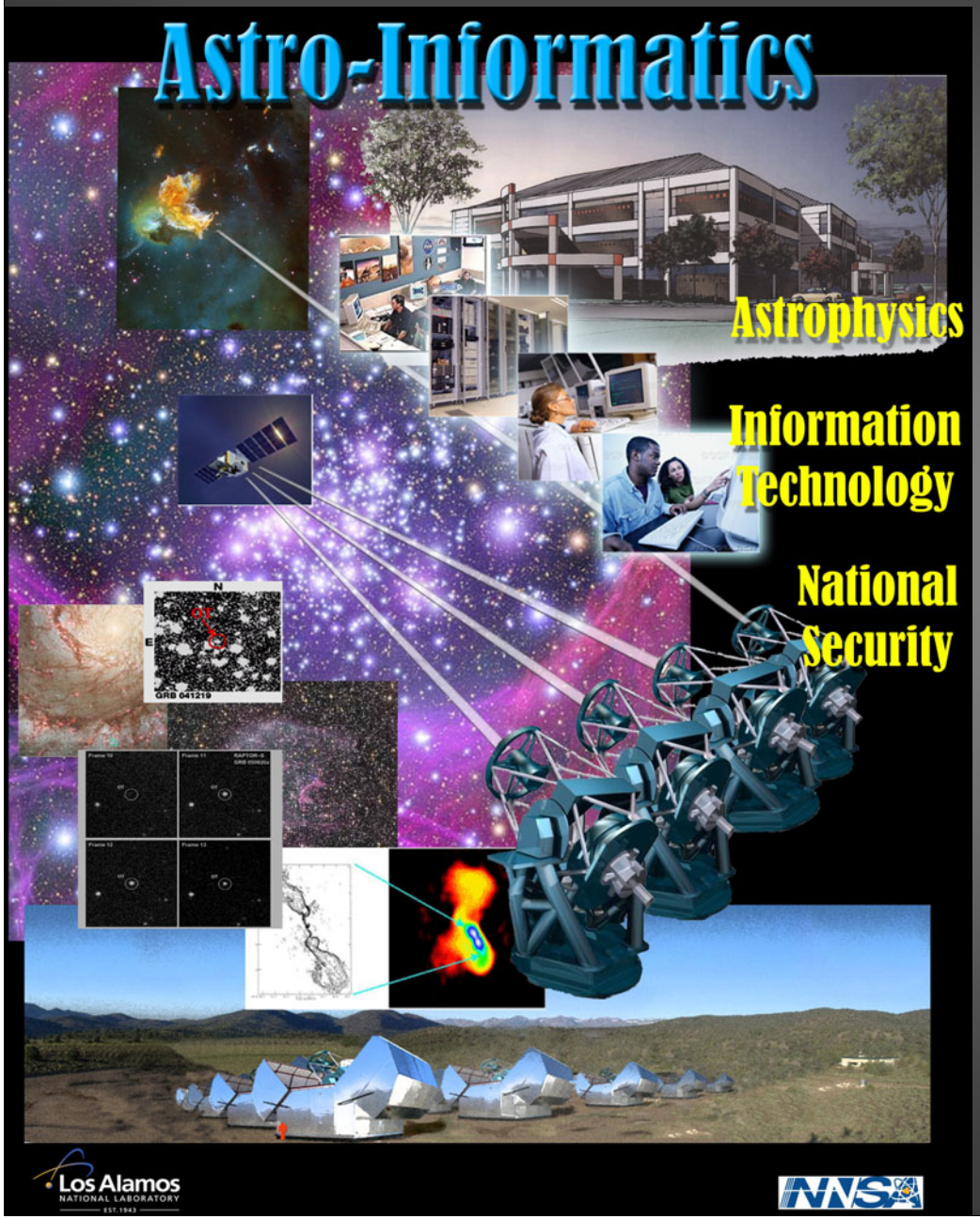

- Great science from global, real-time, coverage of the cosmos
- Space situational awareness
- Building the information science infrastructure for intelligence community applications

Supercomputers in Space Provide Leap in On-board Processing Capability

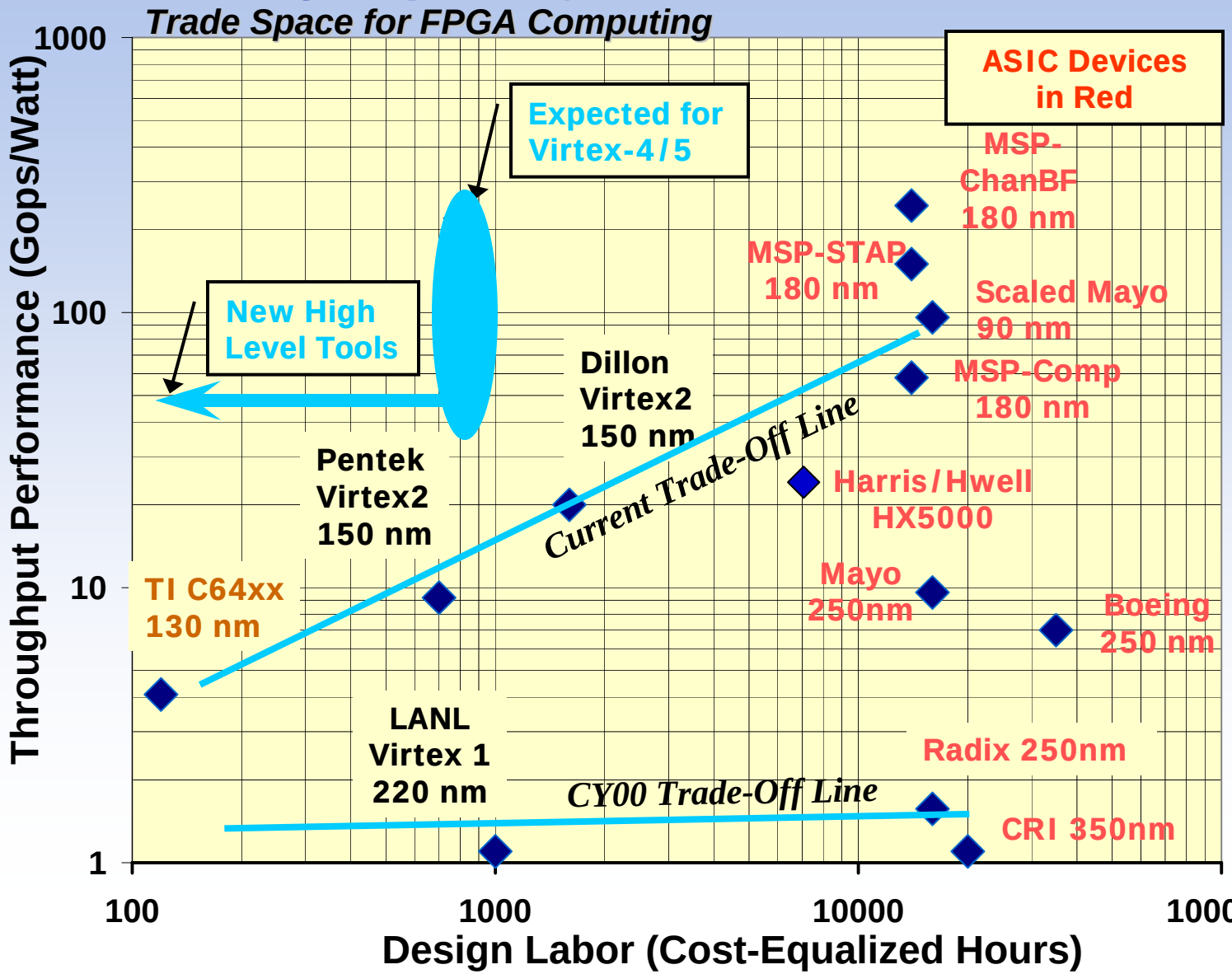

4K Integer FFT Test Case

Notes:

2) Cost Equalized Hrs = Man Hours * (Salary Level + Tools Cost/seat)

3) Hware $/die is ~10% of labor cost in all classes

4) Real compute rate is derived from 4K FFT test case. Gops = 6 * R (Gss)* $\log_2(L)$

4) Trade Lines are not statistically derived from data

Los Alamos

Supercomputers in Space:
Reconfigurable Processor = Responsive Payload

- ***Reconfigurable Payload***
  - Store assets on-orbit and upload new configurations upon need
  - Responsive to changing needs w/o affecting space infrastructure
  - Reconfiguration time ≈1sec
- ***Responsive Mission Capability***
  - Mission capability tailored to specific theater needs
  - Future missions will detect and dynamically adjust payload mission
- ***On-orbit Data Processing***
  - Collect, process, and rapidly disseminate information
  - Data compression allows dissemination of most important information: data products vs raw data

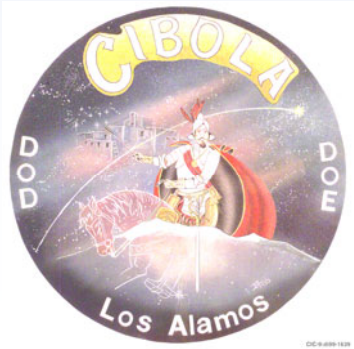

Supercomputers in Space: CFE Concept: Fast on-board processor with COTS parts

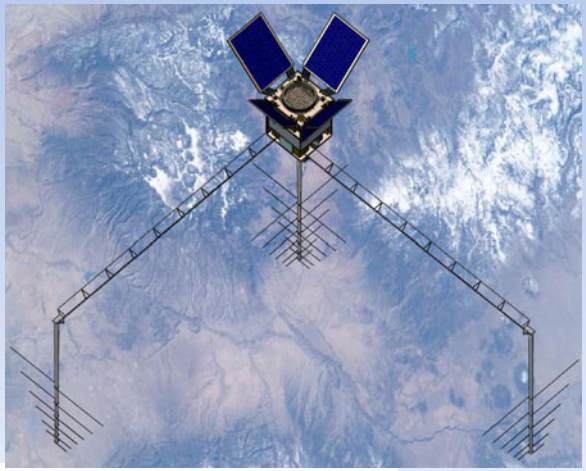

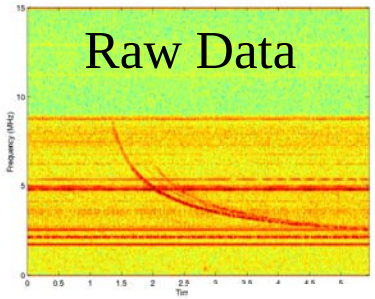

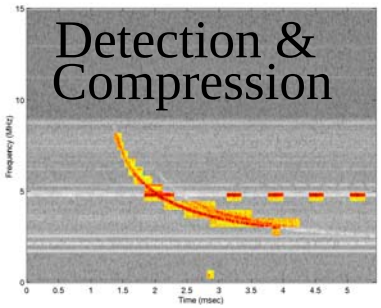

- **Objectives:**
- Demonstrate responsive, flexible, multi-mission RF payload with continuous data processing
  - Detect, geolocate, characterize VHF/UHF EMP & lightning signals
  - Compression & immediate distribution of data products
  - Adaptability: Re-configurable on-orbit
- Validate LANL developed SEU mitigation techniques enabling use of COTS parts
- **Description:**
- Software Radio:
  - Four channels, 20 MHz bandwidth each
  - Tunable from 100 to 500 MHz,
  - 300 Gop/sec Re-Configurable Computer (RCC)
  - 4-element antenna array

Supercomputers in Space: Rad-Hard Space Processing

Lags ground-based processing by 10 years!

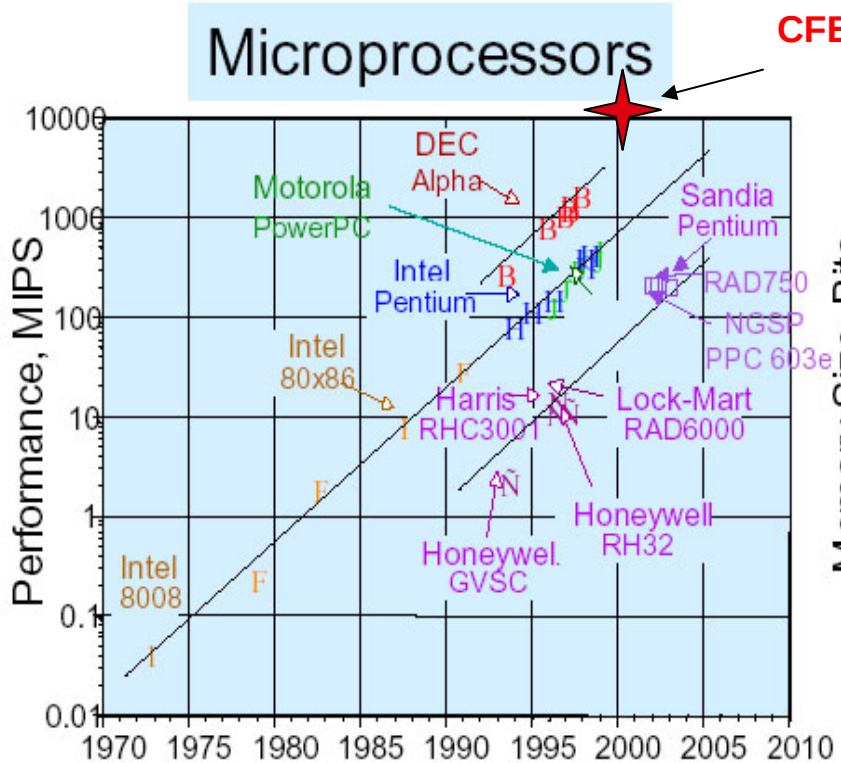

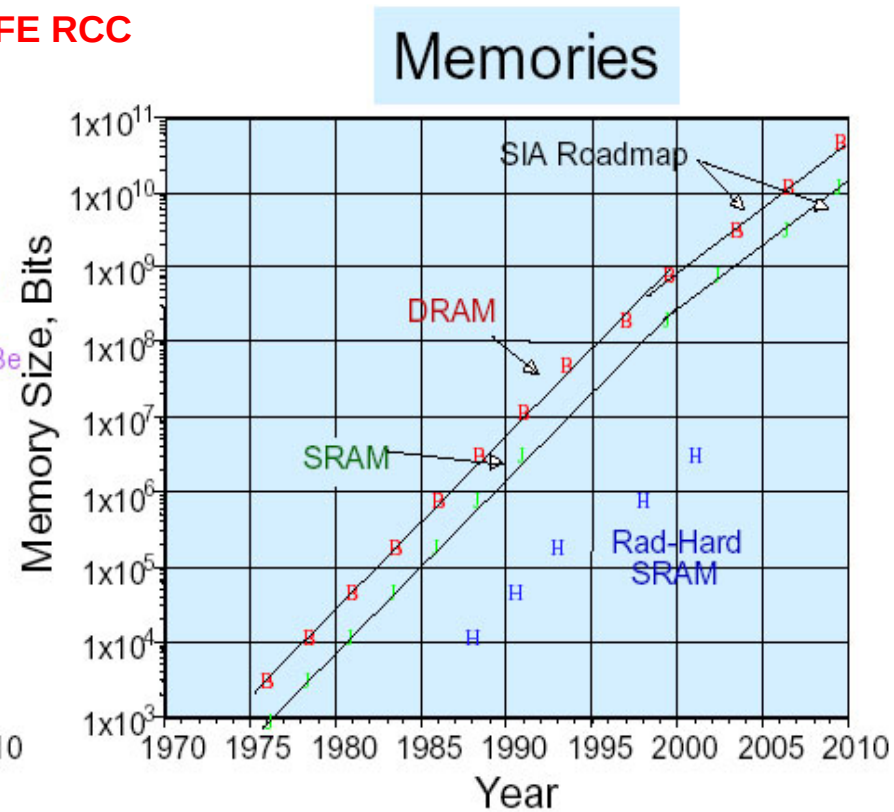

Rad-Hard Lags 2-3 Generations Behind Commercial

Modern Warfighters Need Modern Adaptable Tools

Supercomputers in Space: CFE Has Launched!

STP-1 Mission

STP was provided a Medium Class launch Vehicle by AFSPC.
STP successfully launched the STP-1 mission on 8 March 2007.

Mission Manifest

- Primary Spacecraft is Orbital Express (DARPA)
- EELV Secondary Payload Adapter with 5 Spacecraft
  - MidSTAR-1 (Naval Academy)
  - FalconSat-3 (USAF Academy)
  - STPSat-1 (STP-built w/ NRL & AFRL P/L)
  - CFE (Los Alamos Nat'l Labs)

ESPA

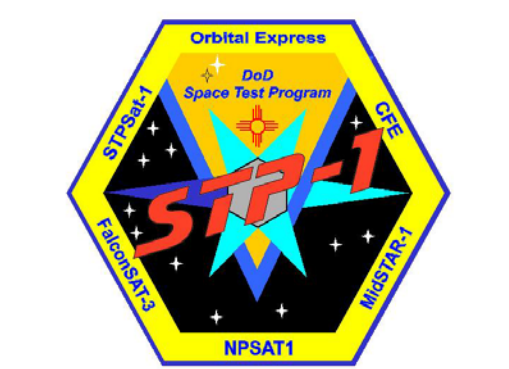

Supercomputers in Space: CFE Satellite Capabilities and Orbit

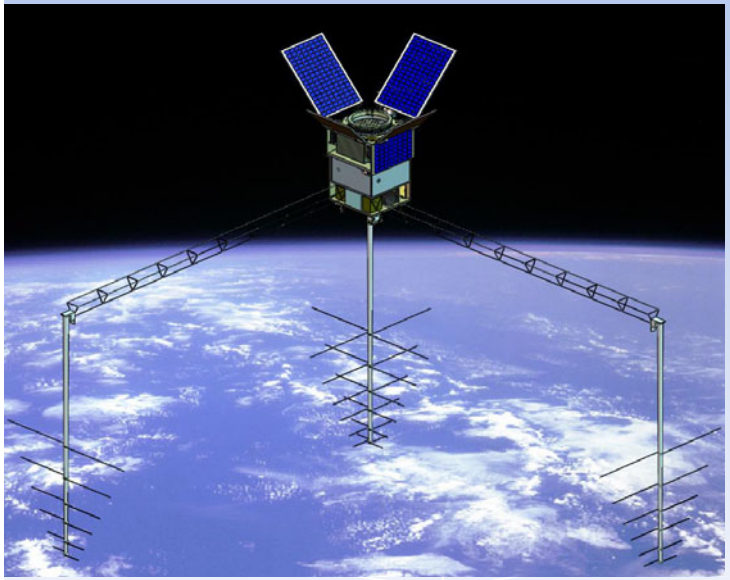

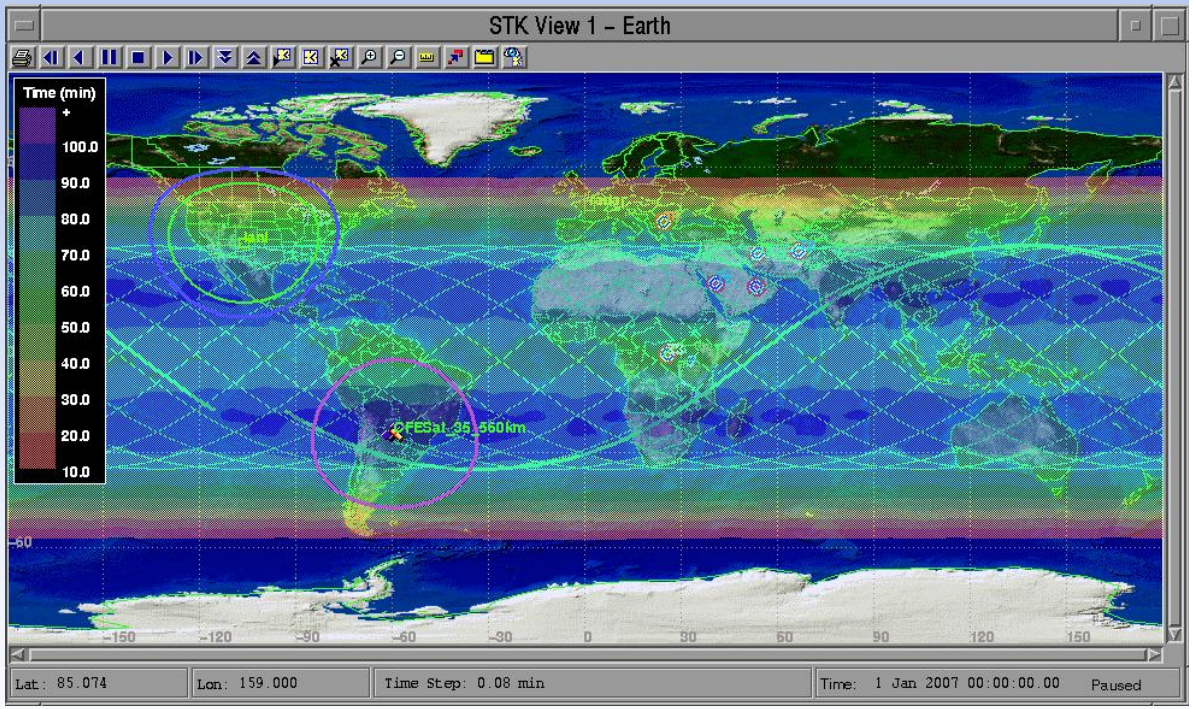

- Orbit 560 km, 35 deg inclination
- On-orbit lifetime: ≈ 3-4 yr
- 4 Mbps downlink, 19.2 Kbps Uplink
- 1 GB storage for data & algorithms
- Fits the ESPA Volume of 24x24x38”

- Weight: ≈ 160 kg
- Satellite generates 120W orbit averaged
- 80W OAP for payload operations

Directed Energy - Response at the Speed of Light

*40 Years of High Average Power Accelerator Experience, Supporting Navy **Free Electron Laser** Development*

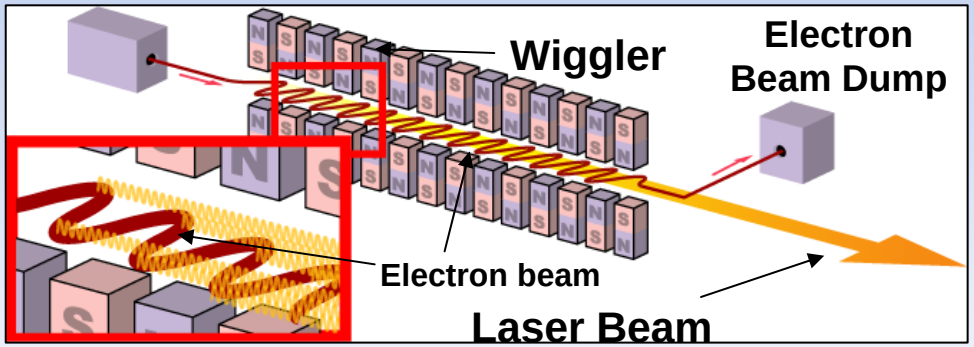

Navy FEL High Current Photoinjector

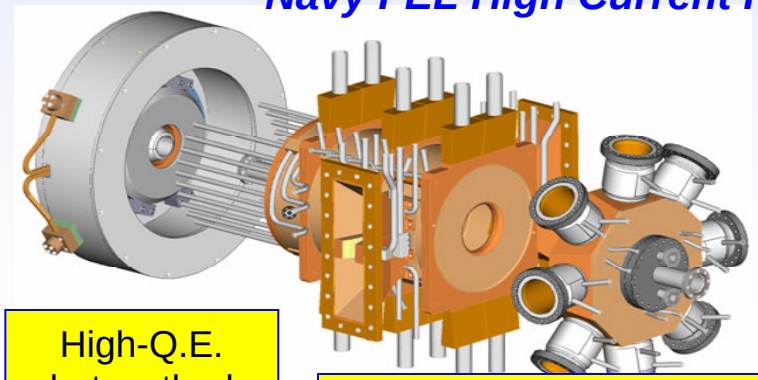

High-Q.E. photocathode

Accelerator with 750 kW of Microchannel cooling

Contact: Bruce Carlsten, bcarlsten@lanl.gov

Revolutionary Ultra-Compact High Power MM Wave Sources

Based on *Sheet* Electron Beams and *Planar* Structures

Unprecedented Power (0.5 MW/10kW) , Bandwidth (50%), and Frequency (100-1000 GHz) with Photonic Bandgap (PBG) Structures

Enabling Technology:

- Sheet beam formation and transport
- Planar RF structures

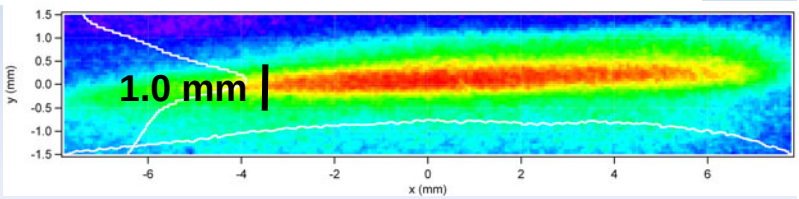

20:1 Aspect ratio sheet beam demonstrated (0.5 mm x 10 mm)

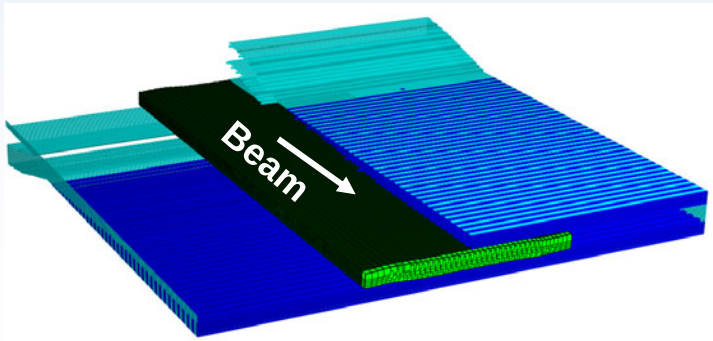

0.5 mm x 10 mm sheet beam in planar RF structure

Pulsed power

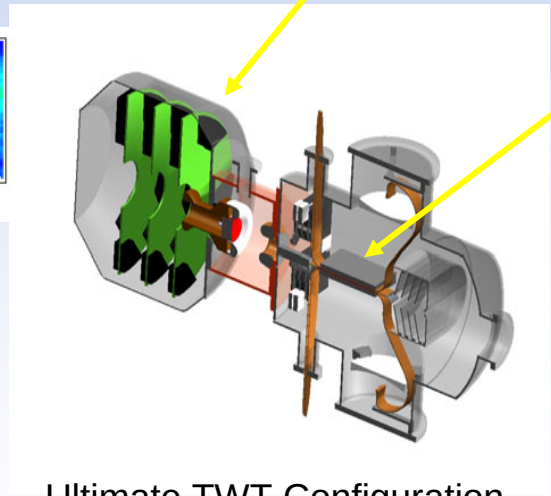

Ultimate TWT Configuration (10 lbs, 3.5 liters, 5 kW avg)

Copper Planar RF structure

Enabling technology for:

- Radar
- Hi-Res Imaging
- Covert Comms
- Remote Sensing
- Active denial

Overmoded Photonic Bandgap Structures

Enable Scaling to THz Frequencies at High Power & Bandwidth

- A PBG can be thought of as a macroscopic crystal structure. Removing an element ("atom") causes localization of the electric field.
- Can replace conventional copper fundamental mode RF structures with overmoded dielectrics such as diamond.

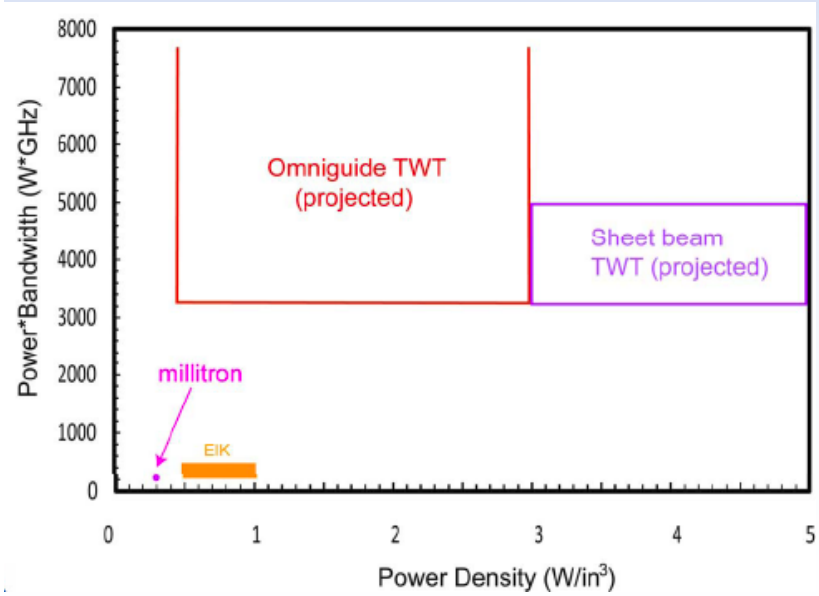

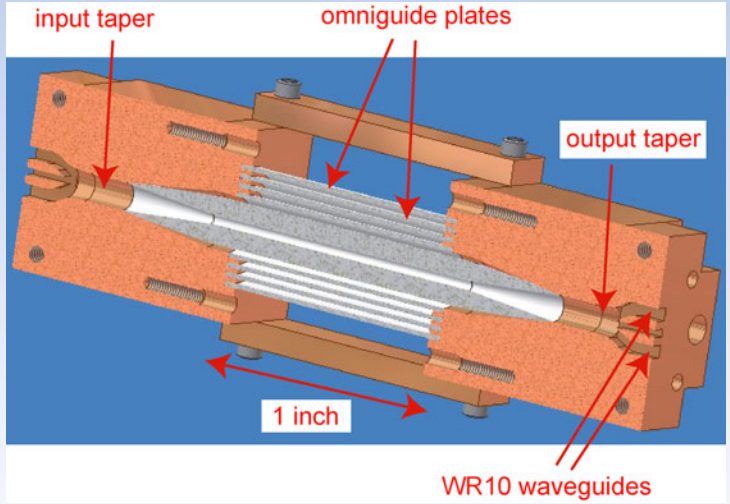

100 GHz Fused Silica Structure

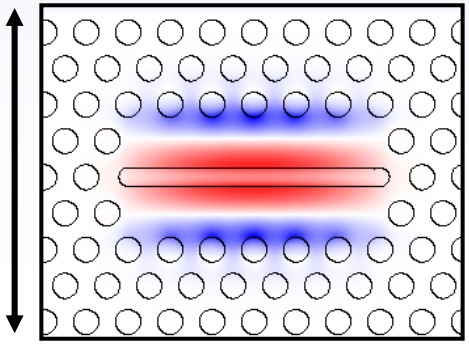

Diamond Photonic Bandgap Structure showing electric field in beam tunnel (view looking down beam axis)

Quantum Cryptography: Information Is Physical

CLASSICAL INFORMATION > WWII

Can be stored and re-measured without error indefinitely

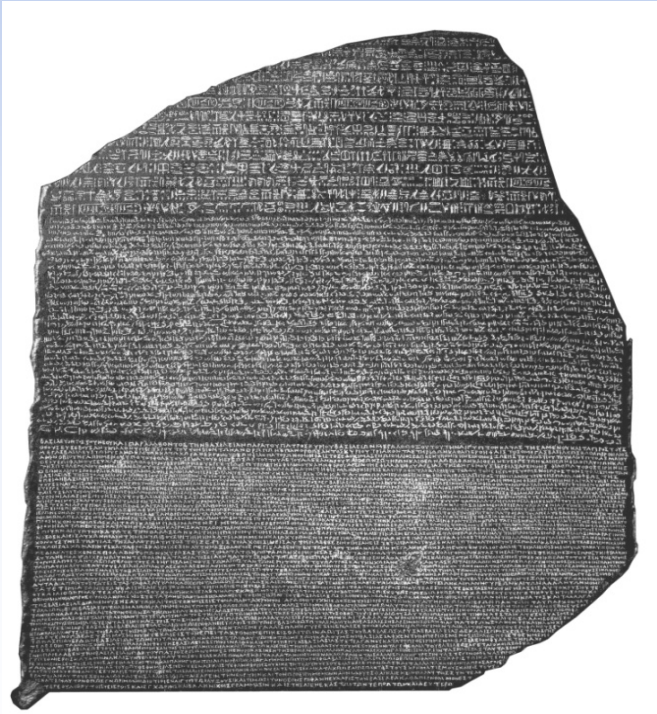

The Rosetta Stone was created in 196 BC, discovered by the French in 1799 at Rosetta, and translated in 1822 by Frenchman Jean-François Champollion.

QUANTUM INFORMATION > 1984

Acquiring information about a system disturbs the system

- **A "qubit" can be represented by a two state system such as a polarized photon**

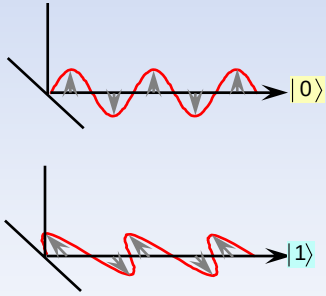

- **Quantum Key Distribution was invented 25 years ago:**

QUANTUM CRYPTOGRAPHY: PUBLIC KEY DISTRIBUTION AND COIN TOSSING

Charles H. Bennett (IBM Research, Yorktown Heights NY 10598 USA)
Gilles Brassard (dept. IRO, Univ. de Montreal, H3C 3J7 Canada)

- **Unconditionally secure cryptographic key transfer by single-photon communications: detectability and defeat of eavesdropping ensured by laws of physics & information theory**

Quantum Cryptography: QKD with LEO Satellites Possible Using Small Terminals

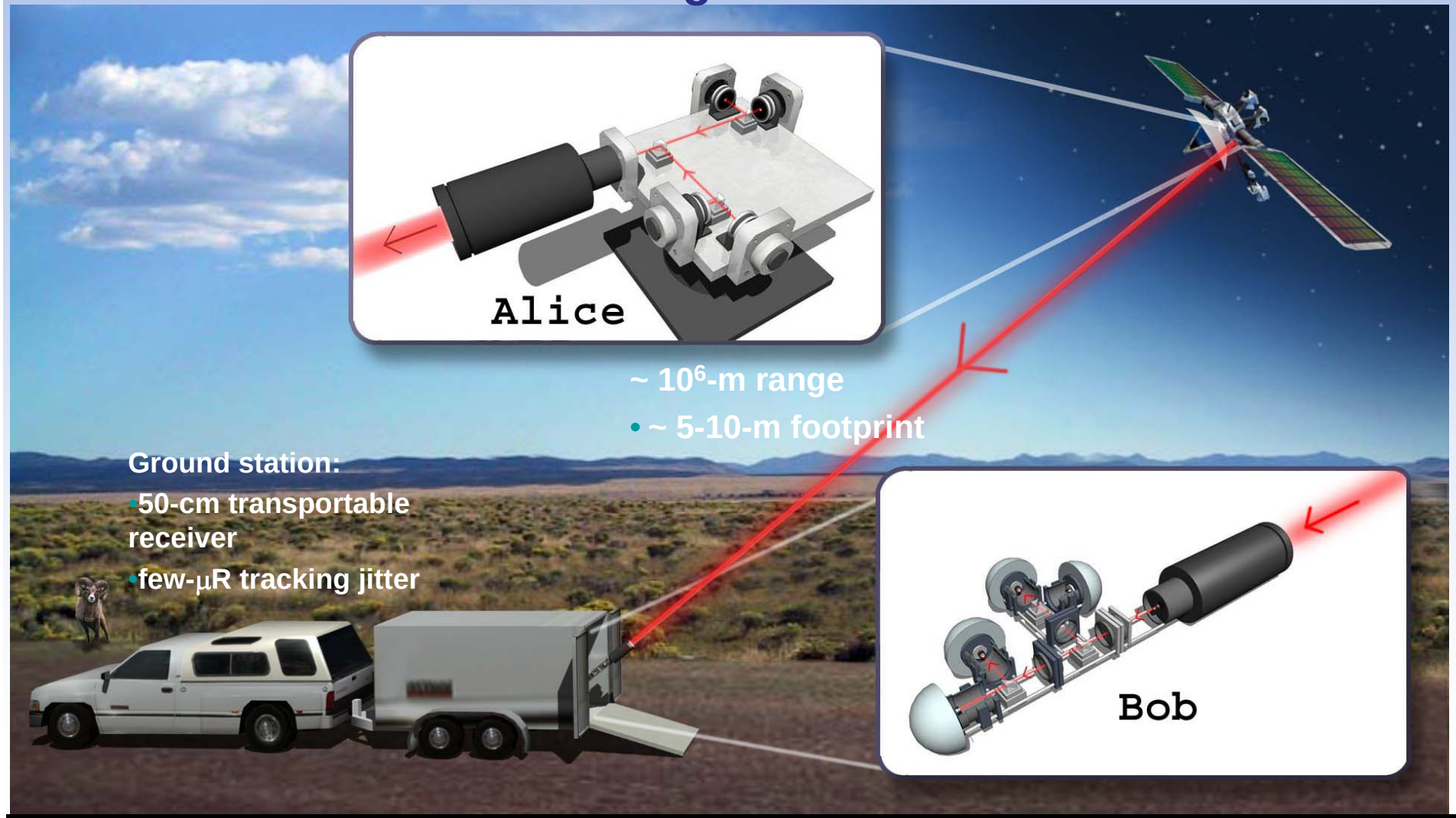

availability: rates ~ "100s secret keys/contact minute/notional day" feasible

Los Alamos Continues a 63 Year History of Paradigm Changing R&D

- Mission-driven science in the National interest
- Underpinned with broad and deep multidisciplinary science and engineering capabilities - *much more than a nuclear weapons laboratory*
- Long history of successfully fielding complex hardware on time scales of days, weeks, & years in harsh environments with autonomous operation
- Portfolio extends across many programs with many sponsors
- Routinely partner and collaborate with other government agencies,industry, and academia

Purification and Growth of Heavy Metal Iodides

$Hg_xCd_{1-x}I_2$, $HgI_{2-x}Br_x$ and InI Single Crystals at High Pressure

Aleksandar G. Ostrogorsky
MANE and Materials Science and Engineering Dept.
Rensselaer Polytechnic Institute, Troy NY 12180
(518) 276-6975; ostroa@rpi.edu

Arnold Burger, PhD
Department of Physics
Fisk University, Nashville, TN 37208
Ph. 615-329-8516, **aburger@fisk.edu**

NNSA NA-22 *Office of Non-Proliferation Research and Development,*
PPD BAA06-39 , DE-FG52-06NA27500
University Information Technical Interchange Program Review Meeting (UITI)
November 27 - 28, at the Central Florida Research Park, Orlando, Florida.

Melt Growth of $Hg_xCd_{1-x}I_2$ at RPI

- *C. Marin, PhD (DOE, SBIR) , 2001*
- *2002-2006, Pacific Northwest National Laboratory, Mary Bliss*
- *Tim Cummings, MS (2005)*

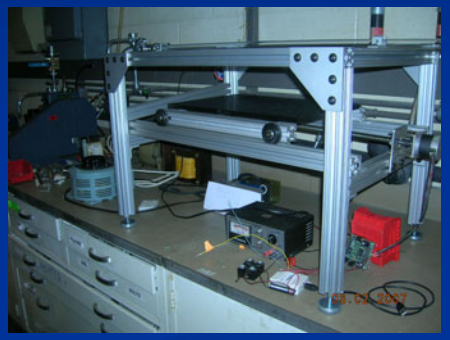

High Pressure Czochralski

T. Cummings et al. , "Tetragonal red and yellow HgI2-CdI2 crystals.."
J. Crystal Growth 297 (2006)334-338.

HgI_2

- For > 30 years, research on crystal growth to fabrication of detectors.
- Large size crystals have been grown. T_m= 259 °C

1. **Soft:** the material quality degrades during the fabrication of the devices. Trapping defects, related with the softness of the structure.
2. At in the vicinity of 130 °C, tetragonal red α-HgI_2 crystals undergo a destructive phase transition to an orthorhombic yellow β-HgI_2 phase

Material	CdTe	ZnTe	$Cd_{0.9}Zn_{0.1}Te$	HgI_2	CdI_2	$HgBr_2$	InI
Av. Atomic Z_{eff}	50.16	46.21	49.1	59.9	51.3	50	51
ρ (g/cm3)	5.85	6.34	5.78	6.4	5.640	6.05	5.31
Eg. (eV)	1.56	2.25	1.549	2.41	3.5	3.6	2.0
ρ [Ω cm]	$\sim 10^9$		3×10^9	10^{13}			$\sim 10^{11}$

- **Rensselaer Polytechnic Institute**
- Dr. Choonho Jung, Postdoctoral Associate
- Moshe Nahmany, August 2007, Nuclear Research Center – Negev (NRCN)
- Undergraduate Students
  - Eric Shaffer
  - Aaron Kendall

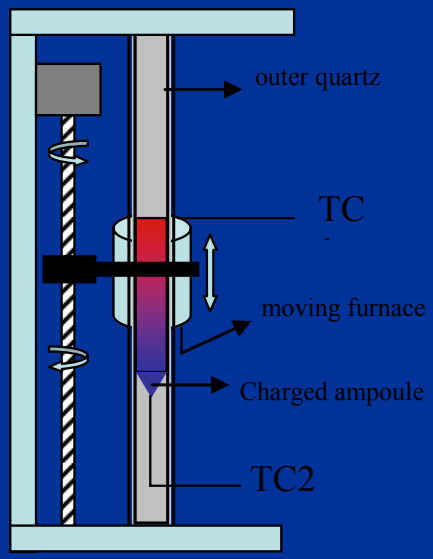

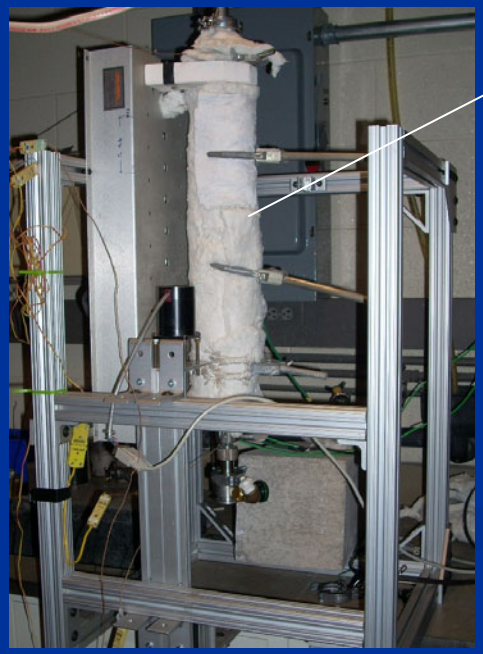

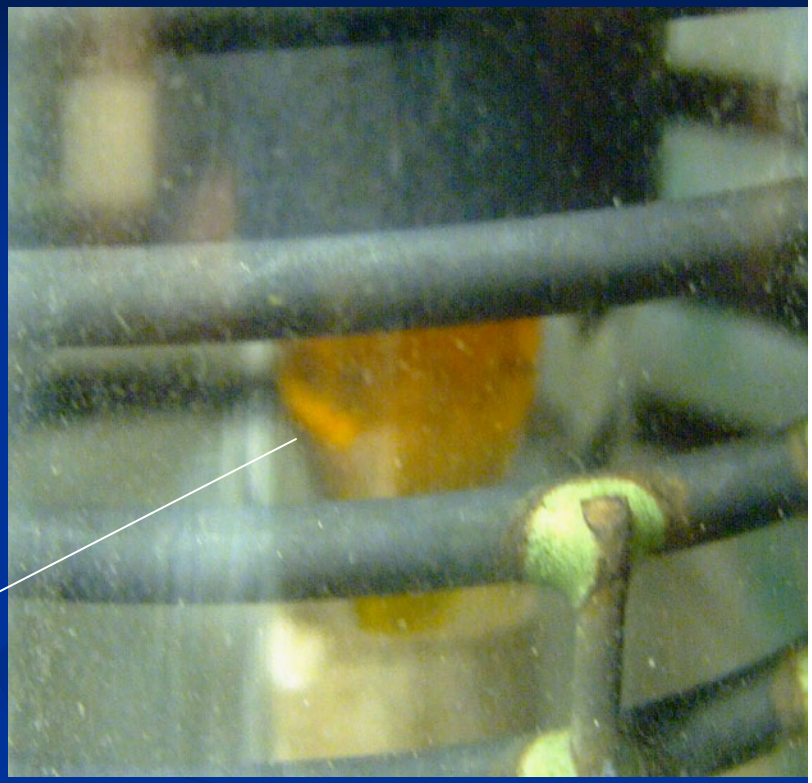

Solid/liquid interface
$HgBr_{1.16}I_{0.84}$

Directional Gradient Freeze (DGF) 18 zone Mellen Furnace

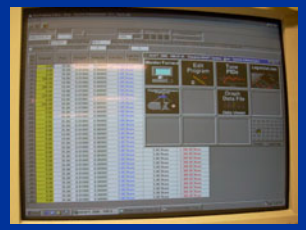

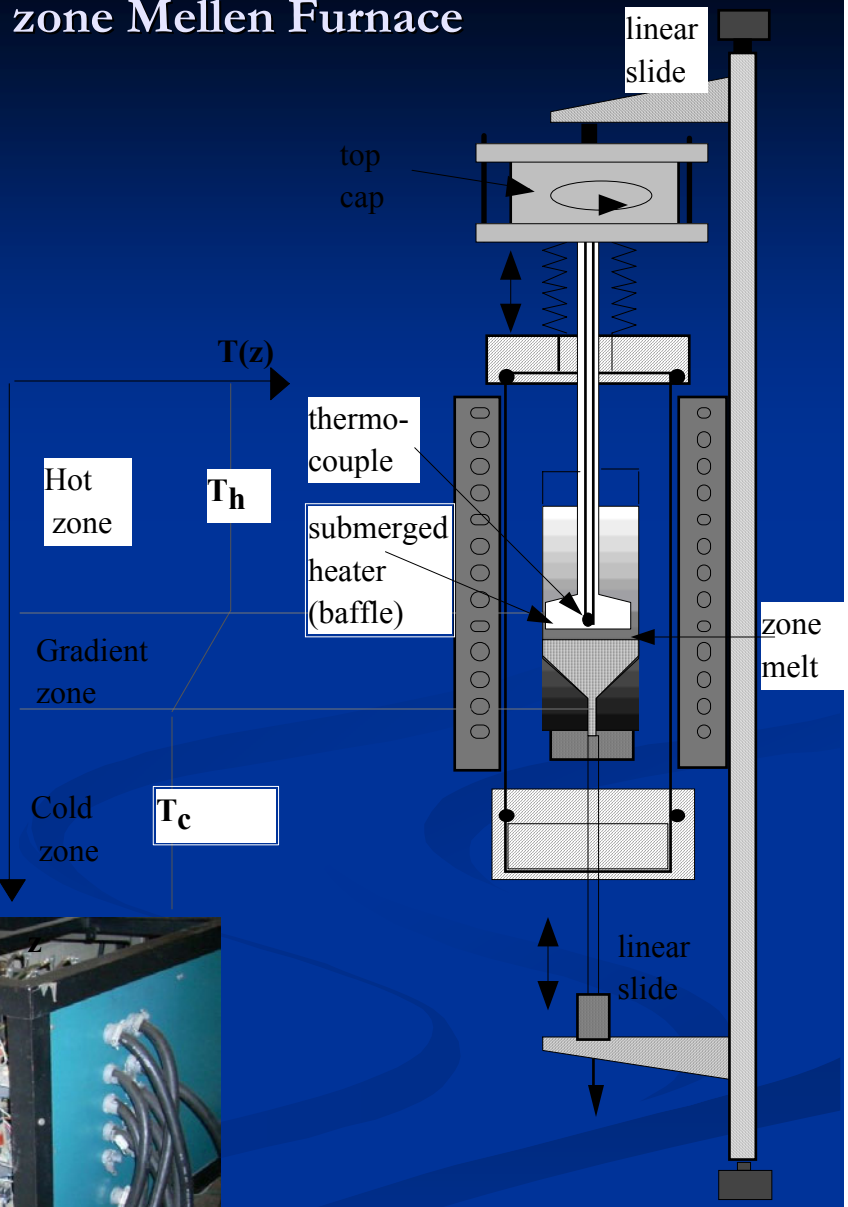

•Arthur D. Little (ADL) MP Czochralski

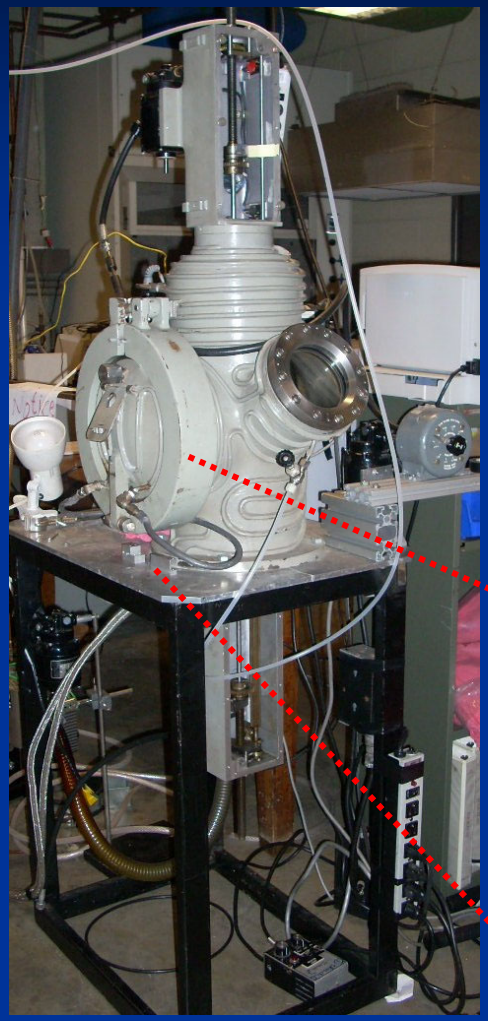

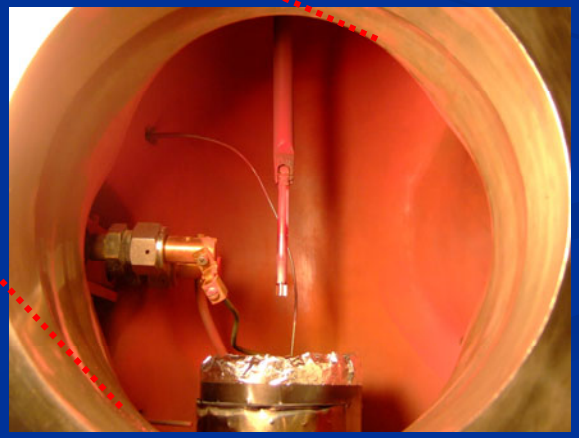

Cutting, polishing and Characterization

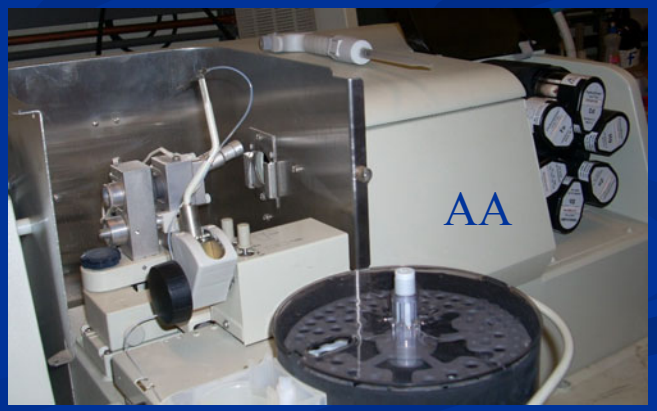

HgI_2-CdI_2

- Gas ambient: 20 atm of 99.999% purity argon
- Alfa Aesar 99.999% α-HgI_2 and CdI_2 pellets
- Quartz ampoules (10 mm ID, 13 mm OD) were used as crucibles.
- BN, floating on the melt free surface was used, to reduce evaporation.
- Melting points of CdI_2 and HgI_2 are 360 C and 253 C respectively; segregation

(0.2778 μm/s).

dT/dz~50 K/cm

Cummings at al., Journal of Crystal Growth 297 2006, Pages 334-338

#30 Initial composition: 22% CdI_2 - 78% HgI_2

•k_{eff}~2 to 3.

•Red crystals, CdI_2 concentration was always $0<x<0.17$.

•In the yellow crystals, the composition was always $x>0.17$.

XRD

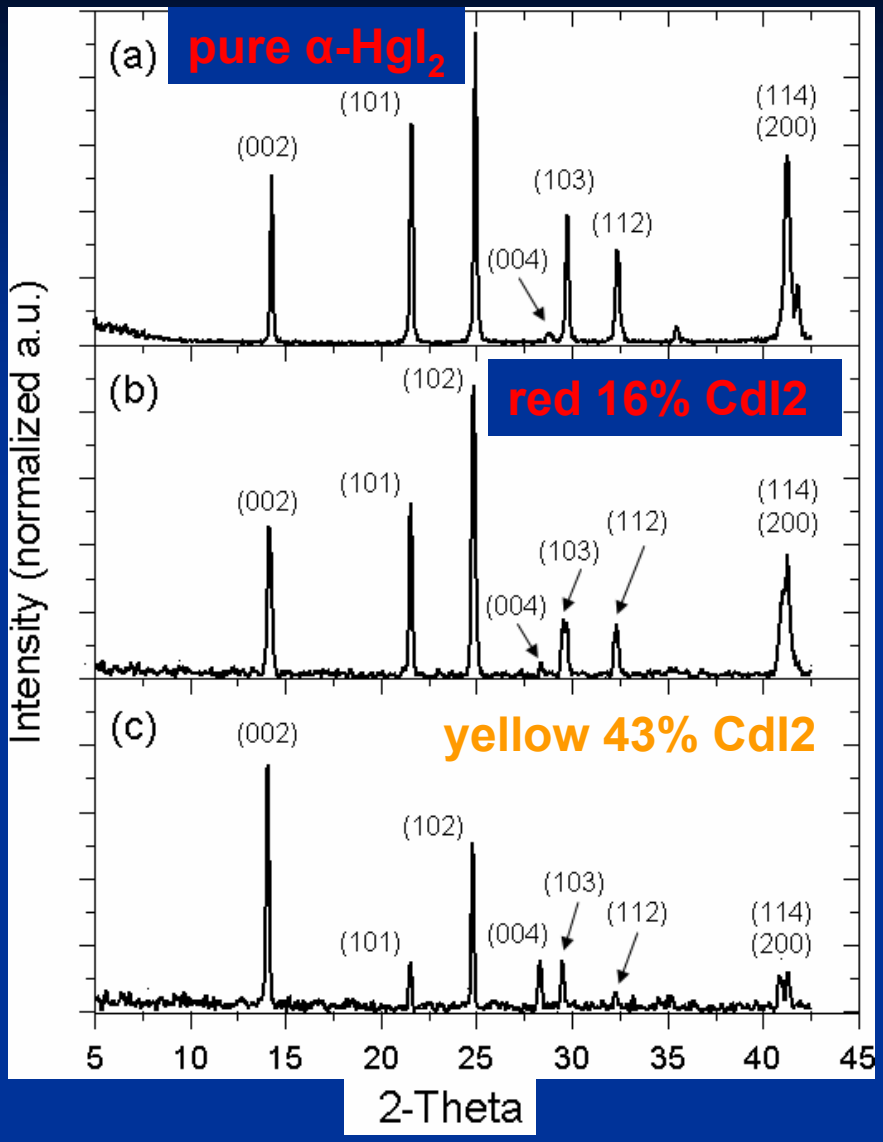

- The melt-grown red grains comprised of $Hg_{84}Cd_{16}I_2$ (x<0.17), have the same structure as the vapor-phase grown α-HgI_2.
- In spite of the difference in color, the melt-grown $Hg_{57}Cd_{43}I_2$ yellow grains (x>0.17)<u>have the same structure as the red grains, i.e., the ***tetragonal α-HgI_2 structure***</u>.

α-HgI_2 structure is preserved by substitution of Hg by Cd.

Indexing of crystallographic planes corresponding to the peaks is assigned using lattice parameters of α-HgI2.

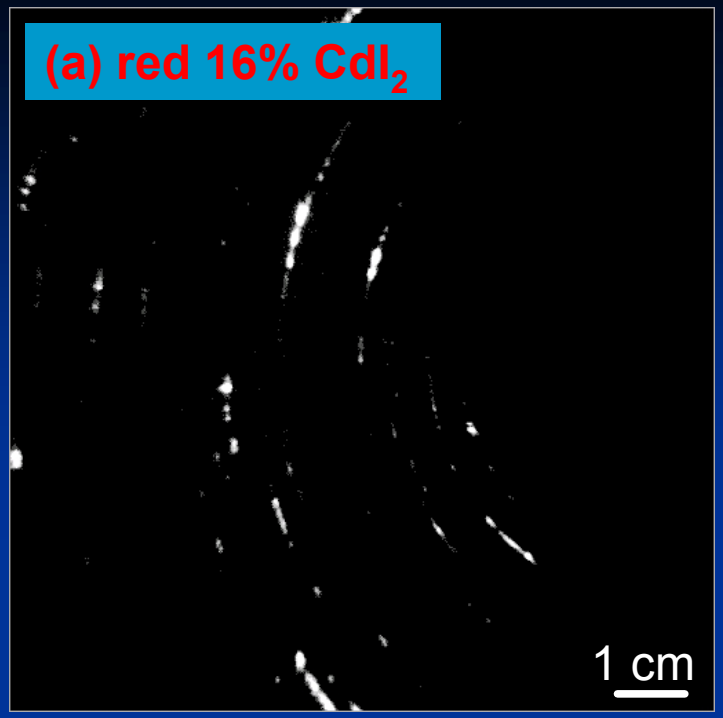

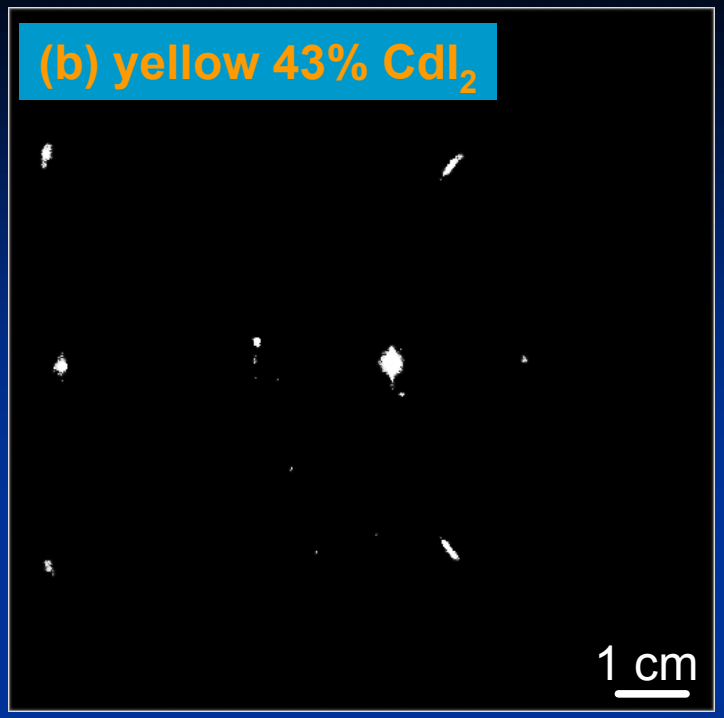

Reflection X-ray Laue technique (Siemens GADDS) with a 1 mm diameter circular cross section collimated beam, white radiation from a Cu source, operating at 15 kV and 60 mA.

- **The same procedure was used to cleave the red and the yellow portion of the crystal**
- Smeared Laue spots are consistent with the highly layered appearance of the samples.
- Red crystal shows much larger smearing –may indicate the presence of plastic deformation that could have occurred during the cleaving process (as it is known to happen in pure α-HgI2 crystals).

- **Yellow crystals have a significantly higher crystalline perfection.**
- **Yellow portion of the crystal is less susceptible to plastic deformation.**

Optical microscope up-close on the color boundary

crystal #30: sample was prepared by cleaving (not a polished).

•Boundary between the yellow and red (darker) regions is not along straight edges.

•Although the image was obtained without filtering, a number of optical fringes caused by stress is visible

Current–voltage measurements

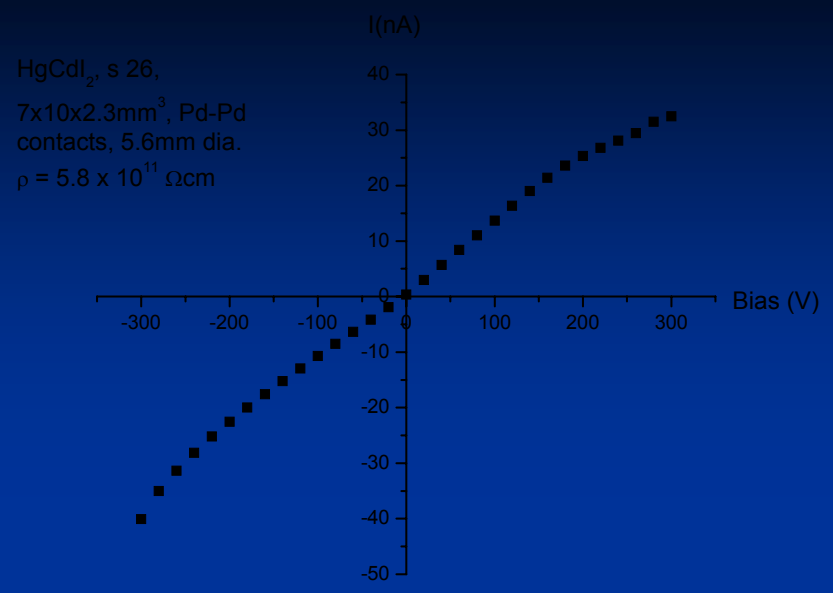

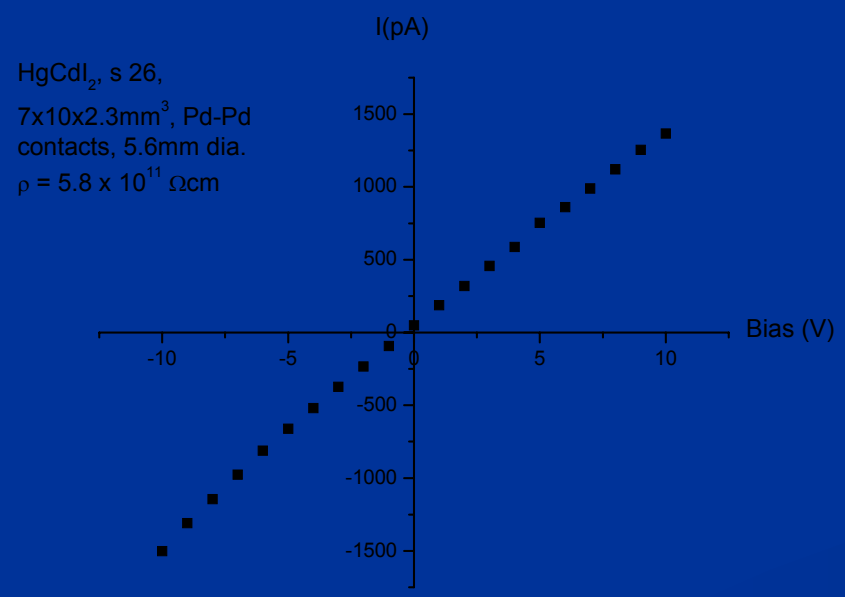

- **Resistivity of pure HgI_2, 4.5×10^{9} Ω cm.**
- **Resistivity of $Hg_xCd_{1-x}I_2$= 5.8×10^{11} Ω cm**
- Higher energy gap and the lower number of point defects.
- HgI_2 and CdI_2 pellets purity = 99.999%

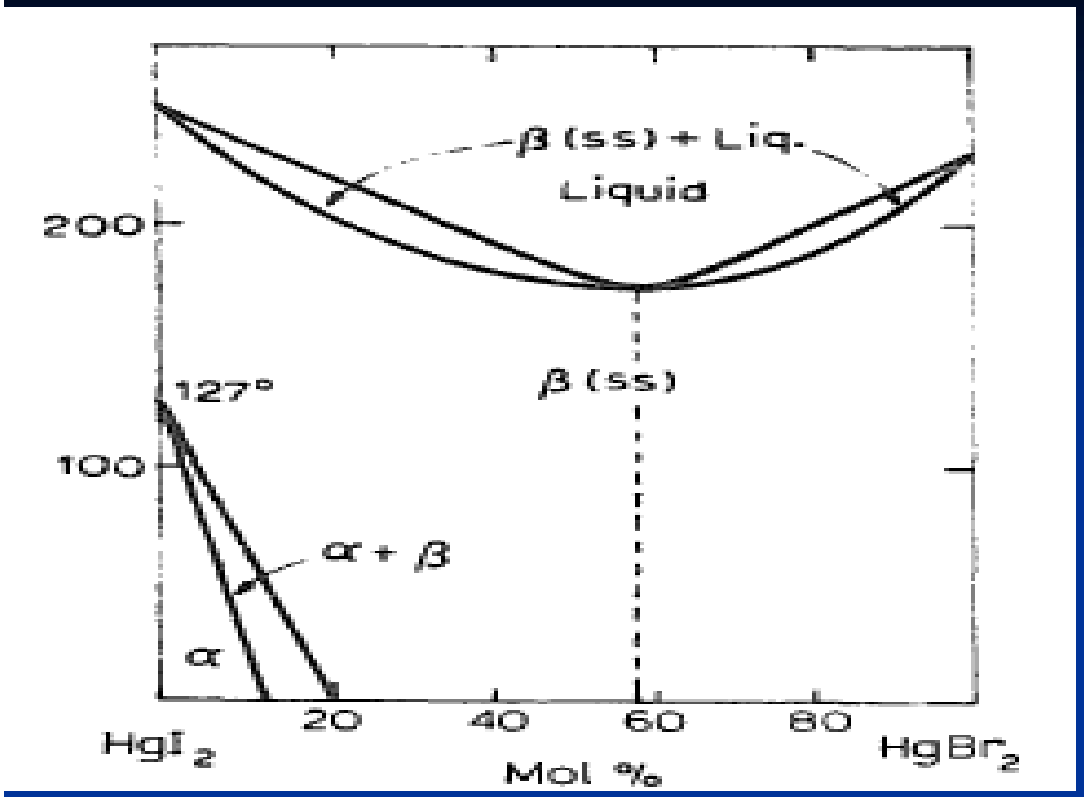

HgI_2 -$HgBr_2$

U.D. Turyanista and V.V. Khiminets, Sov. Phys . Cryst. 18 (1974) 688.

< 20 mol% $HgBr_2$ orthorhombic→ transformation.

K.S. Shah, et. al. Nucl. Intrum. and Meth. in Phys. Res. A 380 (1996) 215-219.

- Inferior charge transport properties ; carrier trapping, by impurities and crystal defects, occurring at the energy levels created within the forbidden gap.
- recommend that the **future research should focus on improving purity and crystalline perfection.**

HgI_2-$HgBr_2$ crystals

Sample #11

$HgI_{2-x}Br_x$

	Nominal Comp. ($HgI_{2-x}Br_x$), X=	mol%$HgBr_2$	crucible	R mm/hr	$\frac{dT}{dx}\left[\frac{K}{cm}\right]$	# zones	Remarks
1	0.6	30	Pyrex	1	7.2	one	
2	0.4	20	Pyrex	1	7.2	one	
3	1.16	58	Pyrex	1	7.2	one	No segregation
4	0.2	10	Pyrex	1	7.2	one	
5	0	0	Pyrex	1	7.2	one	Pure HgI_2
6	1.16	58	Quartz	1	4.24	one	
7	1.16	58	Quartz	1	1.61	one	Gradient still high
8	1.16	58	Quartz	1	0.59	two	failed(crack)
11	**1.16**	**58**	**Quartz**	**1**	**0.52**	**two**	**Best quality so far**
12	1.16	58	Quartz	2	0.52	two	
13	1.16	58	Quartz	1	0.1	Two	thermal fluctuation during the growth
14	1.16	58	Quartz	1	0.1	Two	
15	1.16	58	Quartz	1	0.1	two	

Sample #7

Sample #11

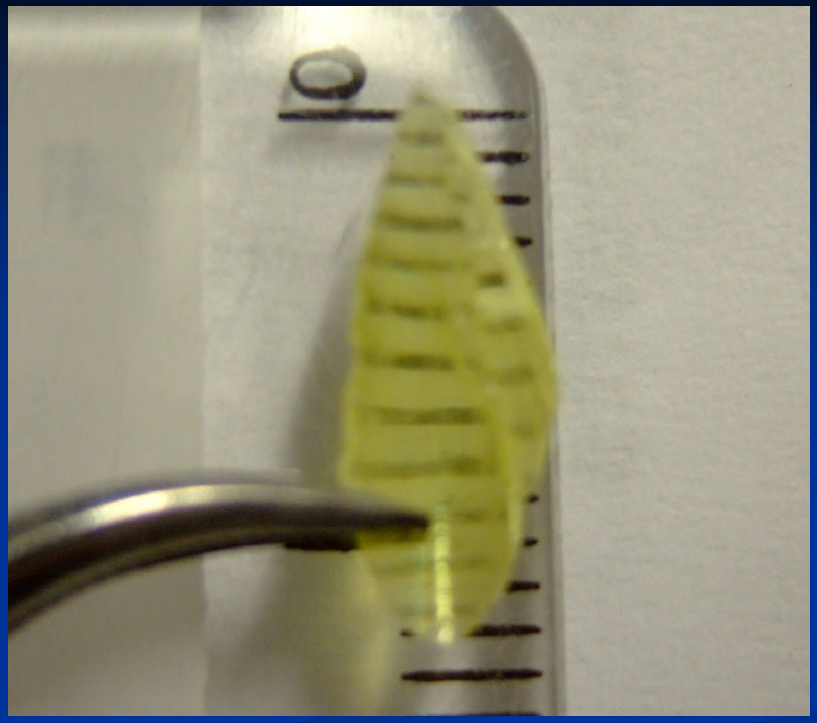

(a) Sample#6 ($HgBr_{1.16}I_{0.84}$) with nominal composition of 58mol% $HgBr_2$ and (b) A cleavage from (a) showing a good transparency

Sample #6

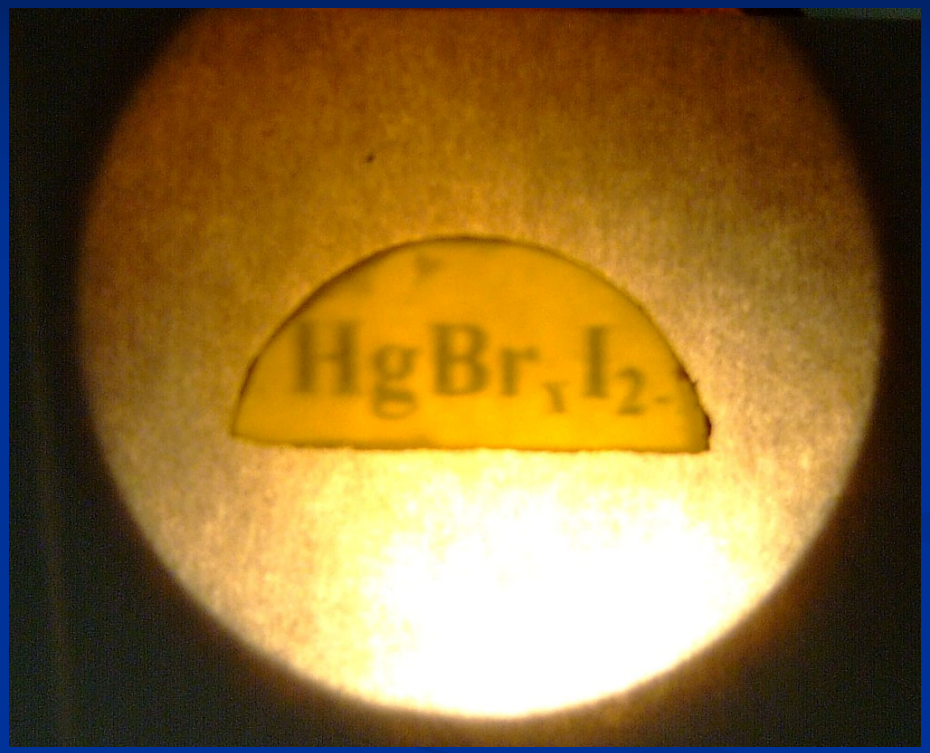

Sample #11

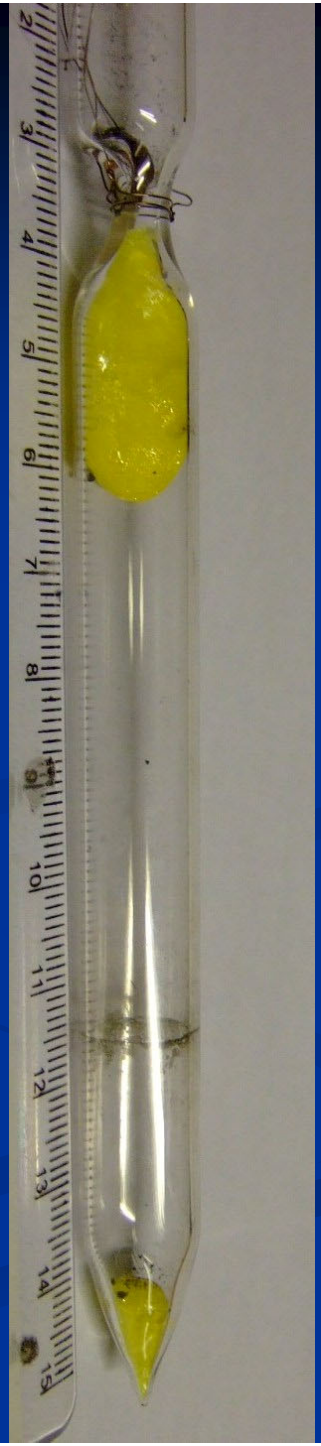

58 mol%HgBr2

16

#17

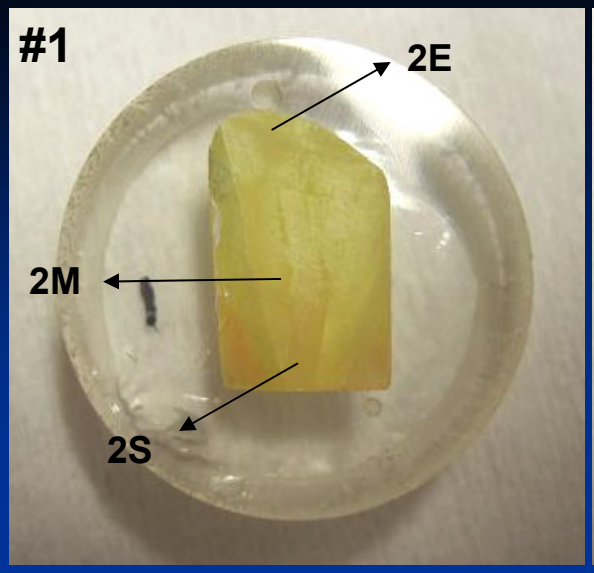

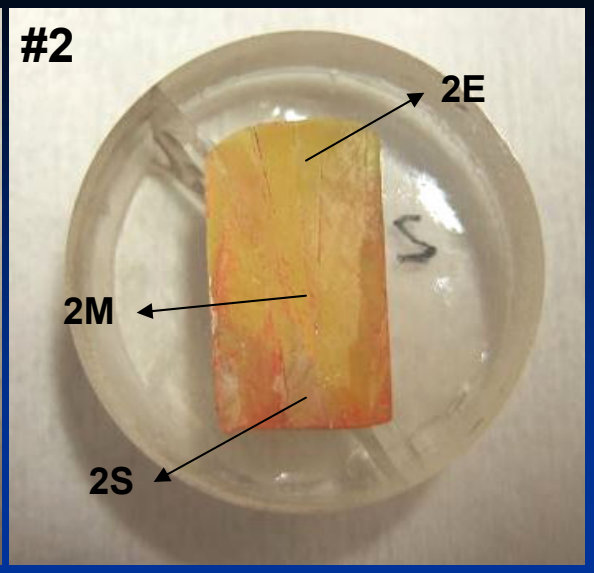

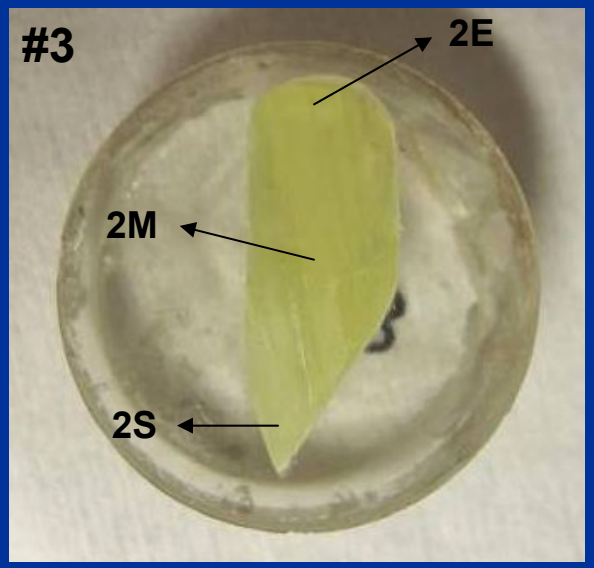

S: Start
M: Middle
E: End

Sections mounted for microprobe analysis.

Micro-probe composition analysis for three samples and initial composition

Initial composition	mol% of $HgBr_2$	Position of the ingot	Atomic %			Normalized composition
			%Hg	%Br	%I	
#1 $HgBr_{0.6}I_{1.4}$	30	Start	30.24	19.73	50.03	$HgBr_{0.65}I_{1.65}$
		Middle	31.01	21.43	47.56	$HgBr_{0.69}I_{1.53}$
		End	30.68	21.16	48.16	$HgBr_{0.69}I_{1.57}$
#2 $HgBr_{0.4}I_{1.6}$	20	Start	30.87	11.54	57.58	$HgBr_{0.37}I_{1.87}$
		Middle	30.73	14.36	54.91	$HgBr_{0.47}I_{1.79}$
		End	31.62	20.9	47.48	$HgBr_{0.66}I_{1.50}$
#3	58	Start	31.43	37.33	31.24	$HgBr_{1.22}I_{0.92}$
		Middle	31.13	39.35	29.52	$HgBr_{1.26}I_{0.95}$
		End	31.9	38.77	29.33	$HgBr_{1.19}I_{0.99}$

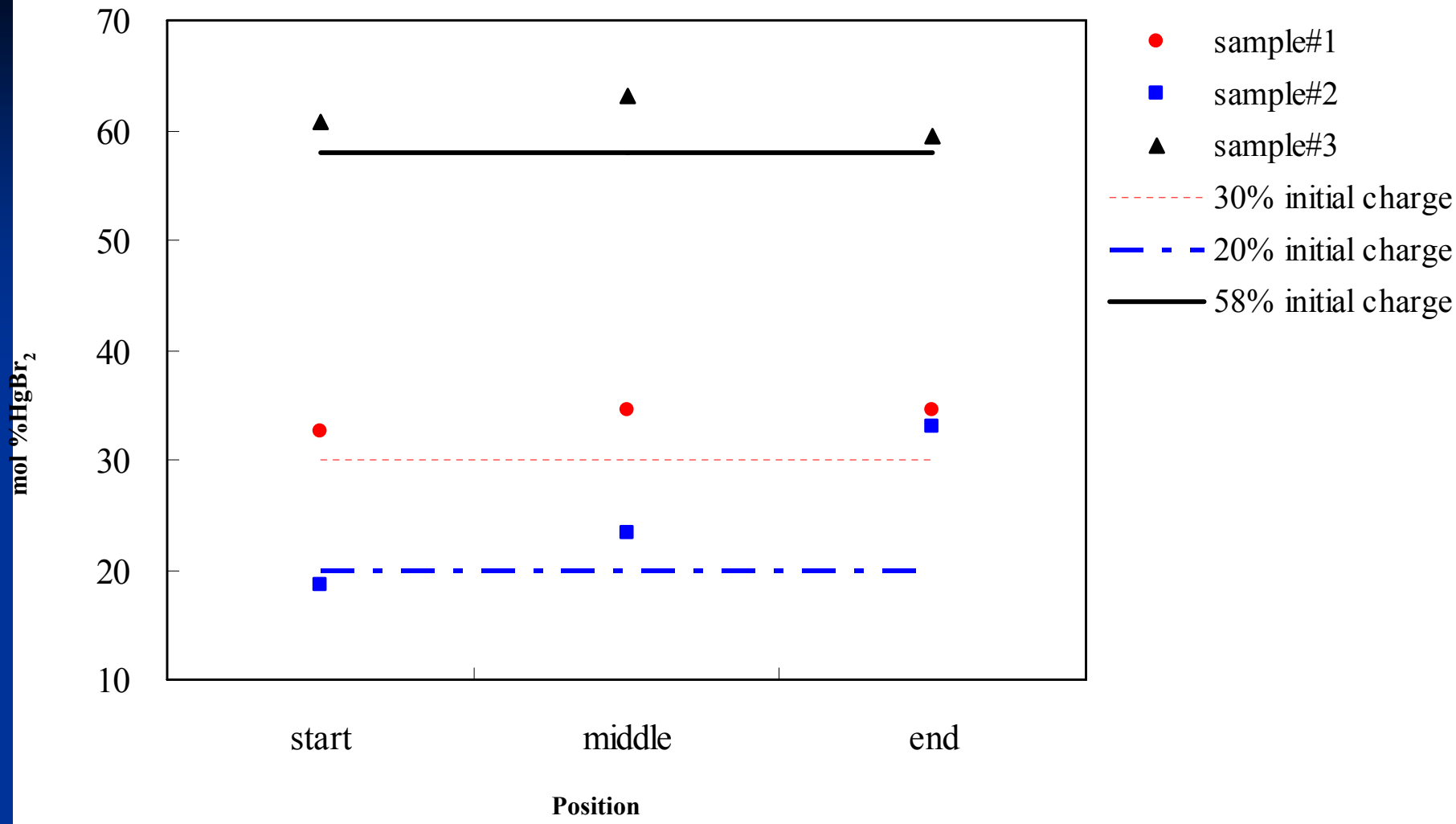

Axial concentration of $HgBr_2$ in samples #1, #2 and #3.

Average micro-hardness (5 measurements)

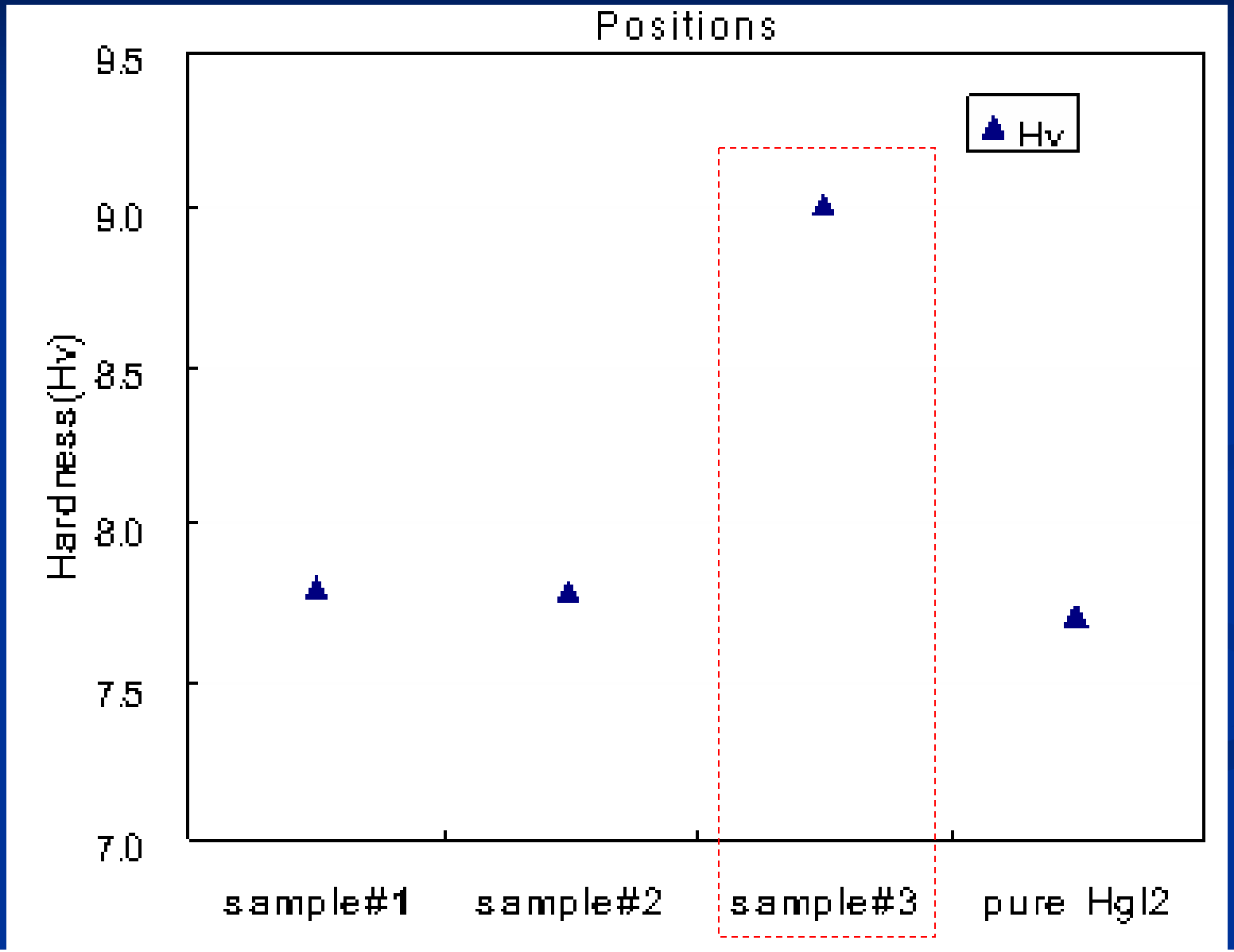

Leakage current vs. bias voltage

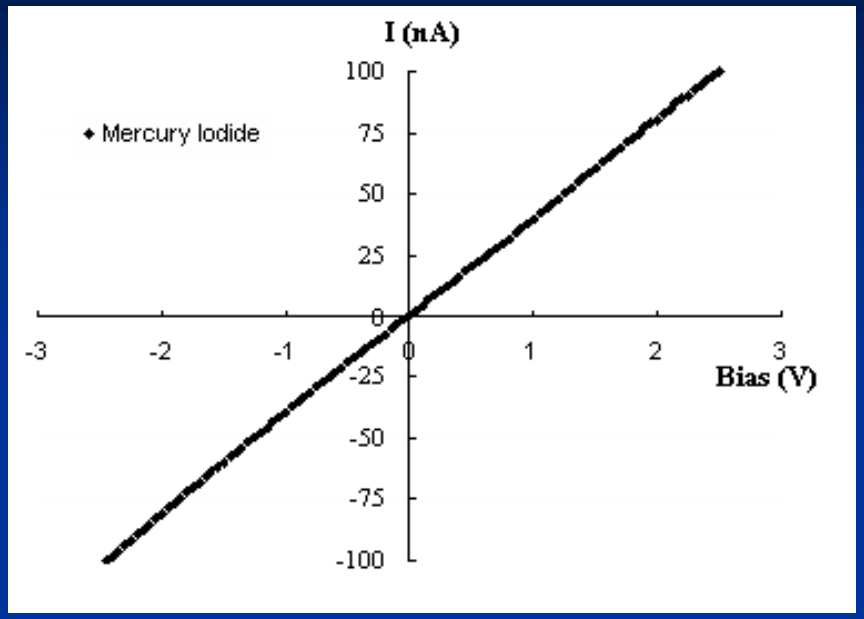

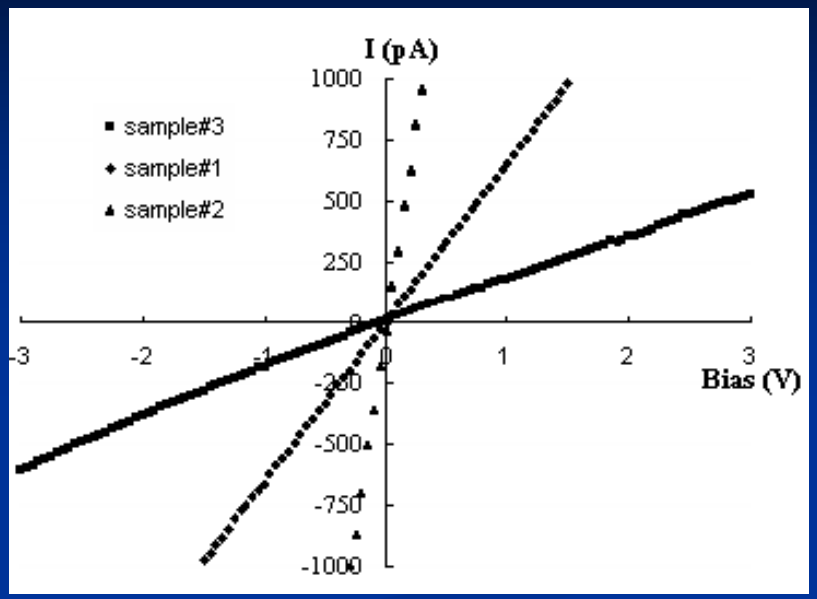

#5: **HgI_2 and ρ = 4.9 x 10^7Ωcm**

#2: 20 mol% $HgBr_2$; ρ = 7.9 x10^8Ωcm

#1: 30 mol% $HgBr_2$; ρ = 1.6 x10^9Ωcm

#3: **58 mol% $HgBr_2$; ρ = 7.6 x10^9Ωcm**

Photocurrent sensitivity of $HgBr_xI_{2-x}$ crystals

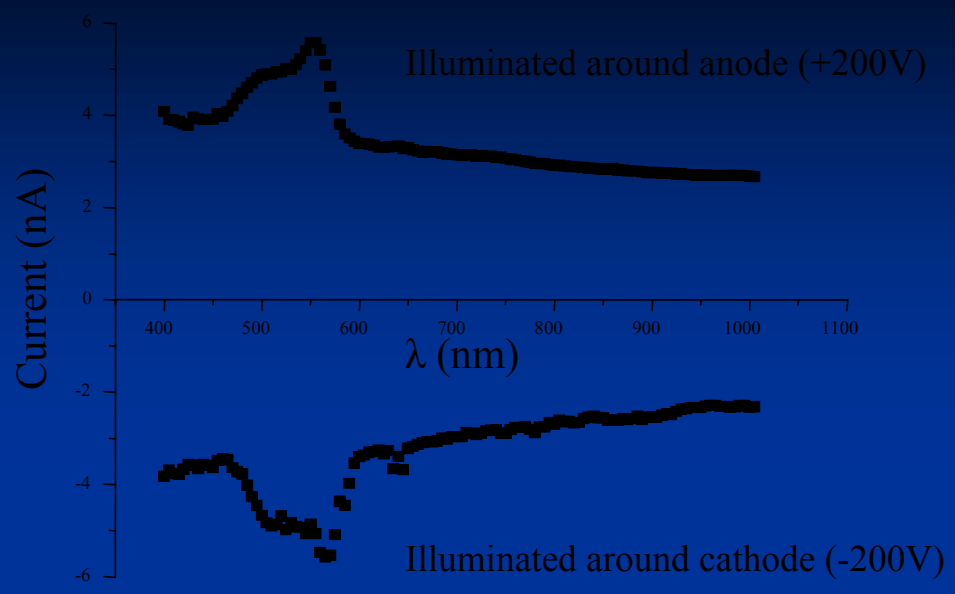

sample#1(30mol% HgBr2

Photocurrent vs waelength

- **Graphite contacts** (non-transparent)
- Surrounding area was illuminated: 2μW; 400 <λ< 1000 nm, (Δ λ = 5 nm, every 5 s). Modest photosensitivity
- **Eg. = 2.24 eV calculated from 555 nm photo-peak (lower than that of HgI_2)at room temperature.**
- Tests with transparent contacts and better crystals should provide more info. on photocurrent sensitivity of $HgBr_xI_{2-x}$ crystals.

InI and CZ –experiments

	Goals	Equipment	Observation
InI-00	Setting up the ADL, heater controller ; Aesar InI	ADL-CZ	Vapor deposition
InI-00-01	Special seed; Partial seeding; InI from Aesar	ADL-CZ	Pressure fluctuations evaporation, deposit
InI-01	Synthesis	ADL 1~2 atm	
InI-02	Synthesis	vertical furnace	+ 5 mm/hr growth several phases
InI-03	Synthesis	vertical furnace	5-6 phases, rotation Rotation, ~2% excess
InI-03-02	Synthesis +growth	vertical furnace, 2 mm/hr	Few grains
InI-03-02	Sample preparation	Polishing	Red semi transparent, few grains
InI – xx	CZ growth/evaporation	ADL	4.6% lost
InI-04	Synthesis	Horizontal furnace (6fl.)	Homogeneous charge 1% excess I
InI-04	Growth	vertical furnace, 1 mm/hr	Homogeneous crystal. Few grains 1% excess I
InI-05	Synthesis	Horizontal furnace (6fl.)	Ampoule exploded 1% excess I, New Pyrex
58%HgI_2-42%$HgBr_2$	CZ growth	ADL	1.8-2 atm; spider-web-like

InI

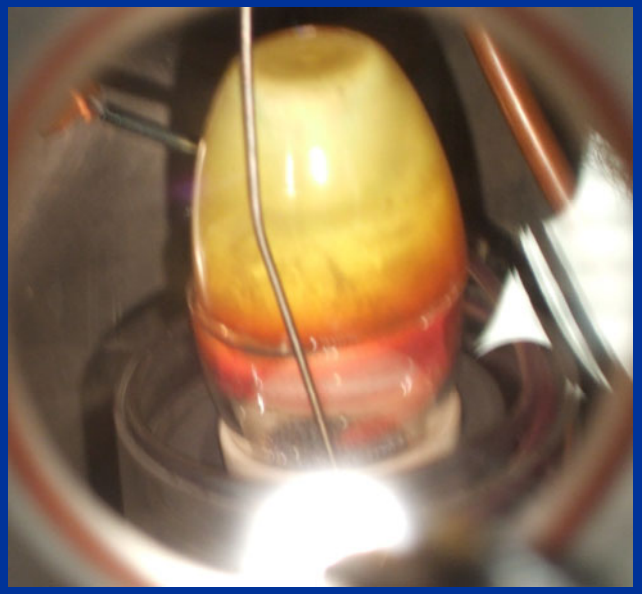

Summary

A. $HgCd_xI_{1-x}$

- Grown form the melt. Tetragonal lattice in the full compositional range. **Red** crystals for $x<0.17$. **Yellow** crystals for $x> 0.17$
- **Yellow** crystals: higher crystalline perfection; degrade less during cleaving. Resistivity = 5.8×10^{11} Ω cm; $k_{eff} \sim 2.5$
- Need to reduce temperature gradients.

B. $HgI_{2-x}Br_x$

- 15 experiments using various equipment. Need to optimize temperature gradients – use VGF Mellen Furnace.
- $k_{eff} \sim 1$ to 1.1
- $\rho = 7.6 \times 10^9 \Omega$cm; Eg. = 2.24 eV
- photoconductive response.

C. InI

~ 10 Charge synthesis/growth. Trying to grow by Czochraski or Kiropulos.

Purification and Growth of Heavy Metal Iodides ($Hg_xCd_{1-x}I_2$, $HgI_{2-x}Br_x$ and InI) Single Crystals at High Pressure

Arnold Burger, PhD
Department of Physics
Fisk University, Nashville, TN 37208
Ph. 615-329-8516, aburger@fisk.edu

NNSA NA-22 *Office of Non-Proliferation Research and Development,*
PPD BAA06-39 , DE-FG52-06NA27500
University Information Technical Interchange Program Review Meeting (UITI)
November 27 - 28, at the Central Florida Research Park, Orlando, Florida.

National Nuclear Security Administration

Radiation Detection Lab – Research Group

- Group leader: Dr. Arnold Burger
- Research Professors:

  Dr. Utpal Roy and Dr. Yunlong Cui
- Postdocs:

  Dr. Mike Guo and Dr. Pijush Bhattacharya
- Research Technicians:

  Ms. Ajanta Bhattacharjee, Mr. Vlad Buliga and Mr. Constantine Coca
- Grads:

  Helen Jackson, George Turner, Kunle Adio, Melissa Harrison, Michael Groza, Vincent Alexander, Tomas Yan, Julia Bodnarik and Thompson LeBlanc
- Undergrads - Summer Interns

  Isaa Smith, Andréa Sease, Jennifer Sanders, Eric Woodward, Everett Samuels

Expertise and activities – RDL

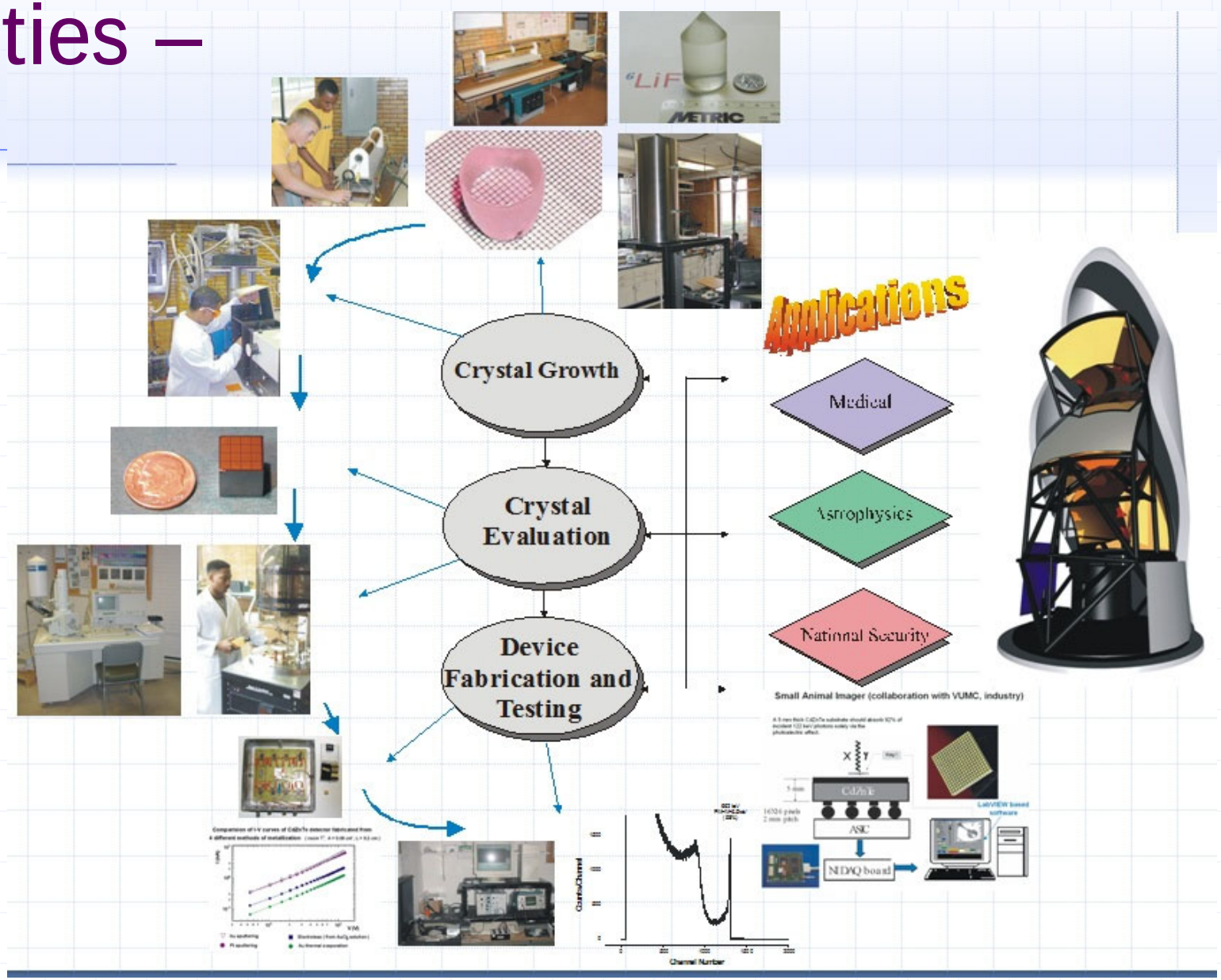

Fabrication **Cutting, polishing, etching**

- Damage of up to 200 μm deep into the crystal is not uncommon during the sectioning of the crystal (blade or wire saw impregnated with abrasive or slurry)
- Polishing with finer and finer abrasive down to 0.05 μm particle size alumina suspension
- Chemical etching (optional): 5% bromine in methanol (BM) solution for two minutes and followed by methanol rinsing.

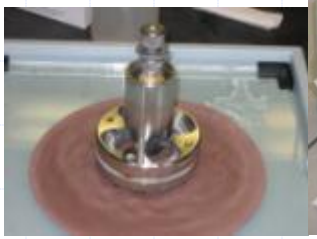

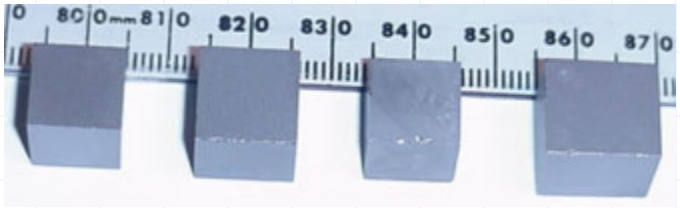

Mask design & fabrication

Photo-plotter

Various masks

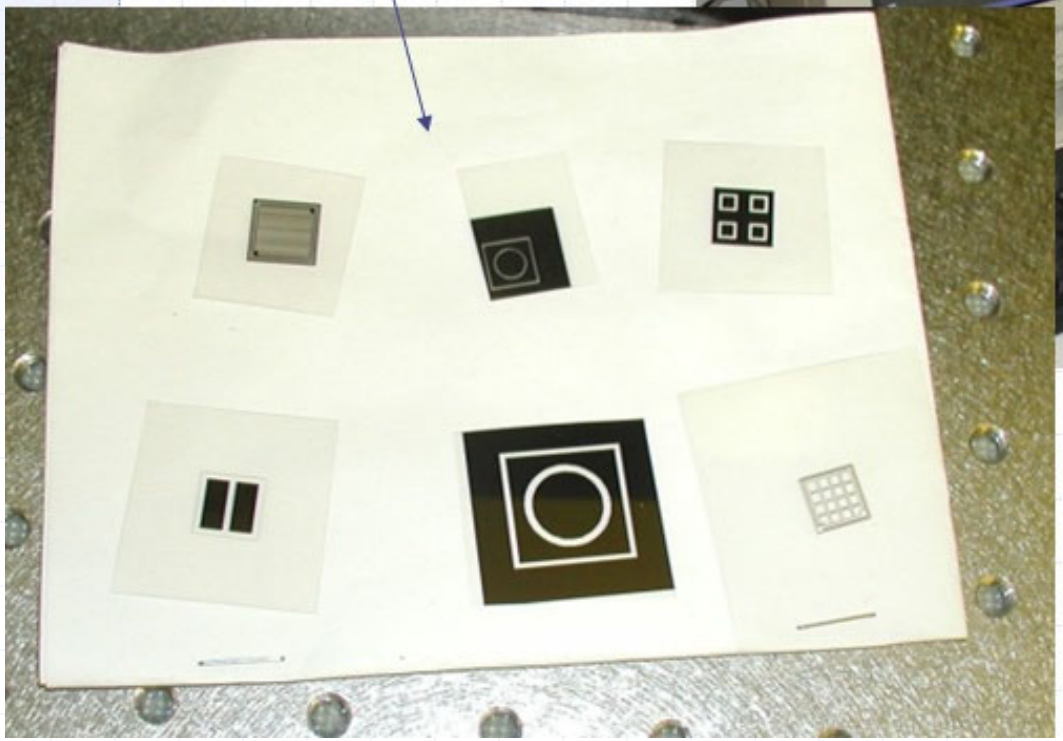

- strip photoresist and inspect

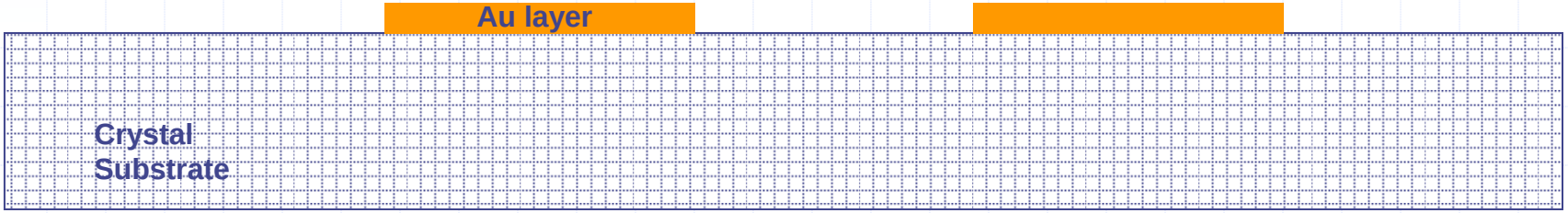

- photoresist is patterned by exposure to UV through the mask

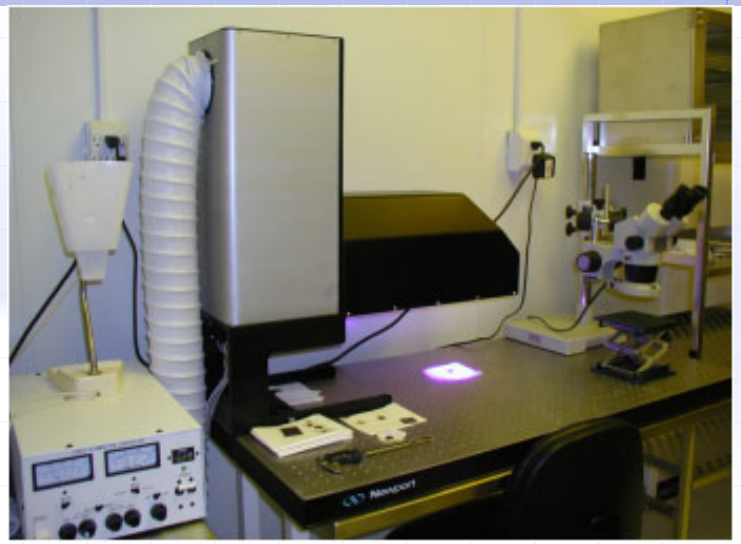

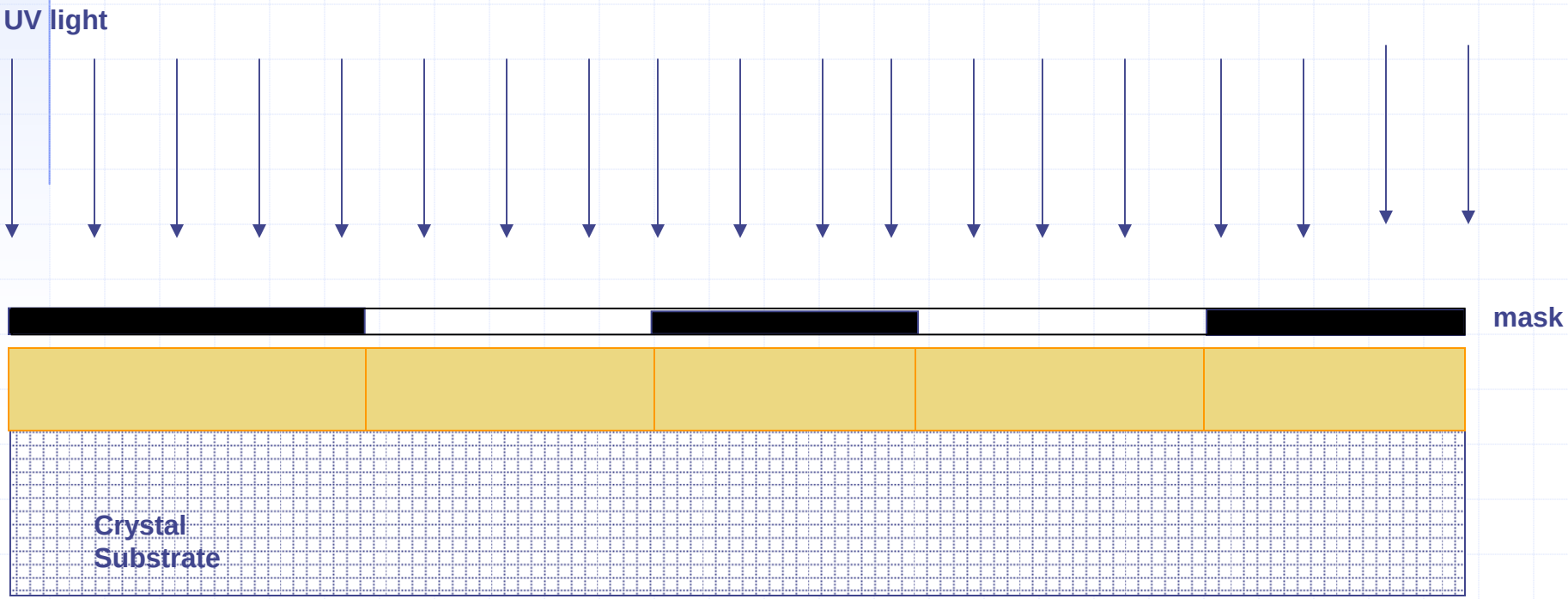

Testing electronics

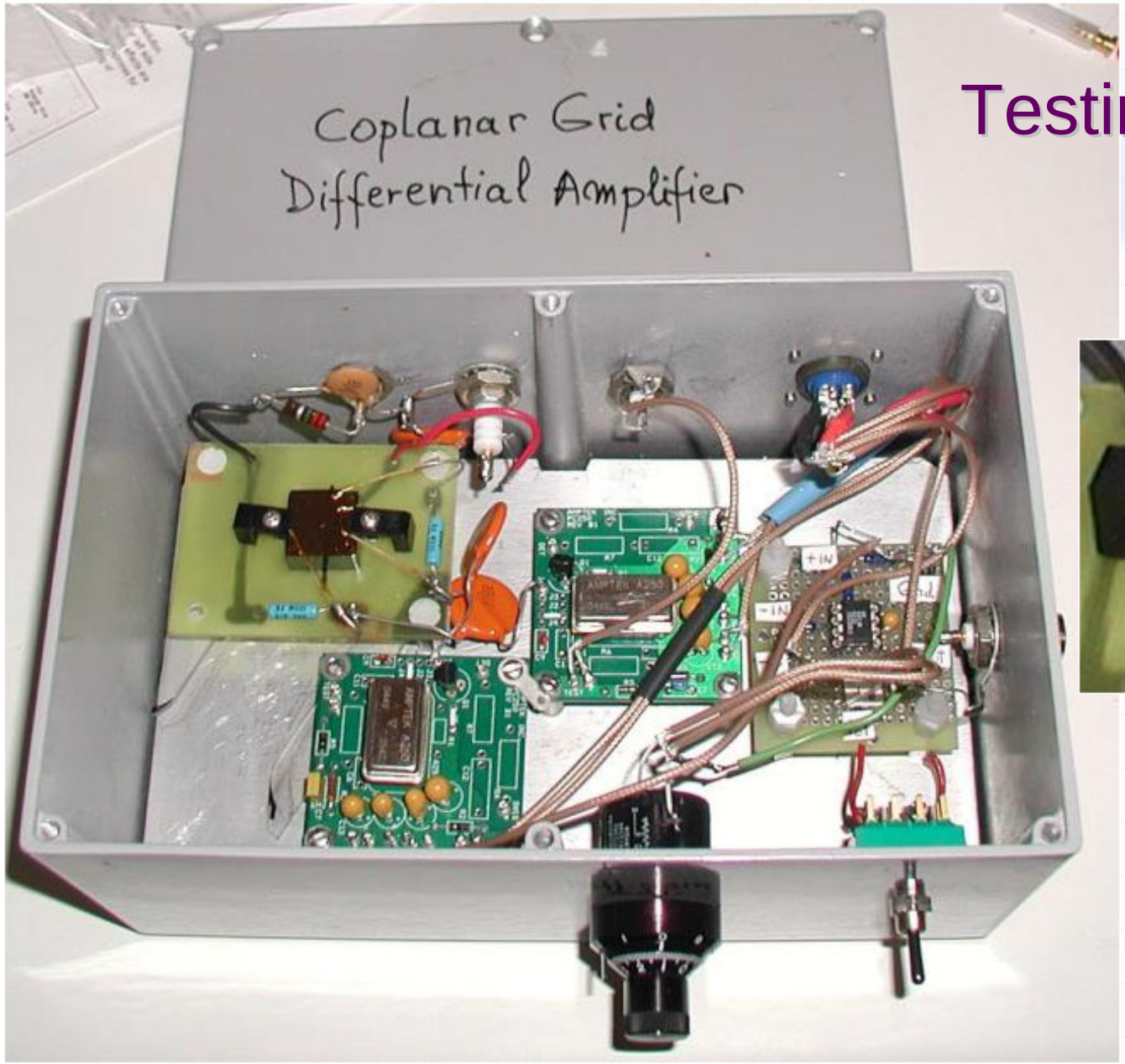

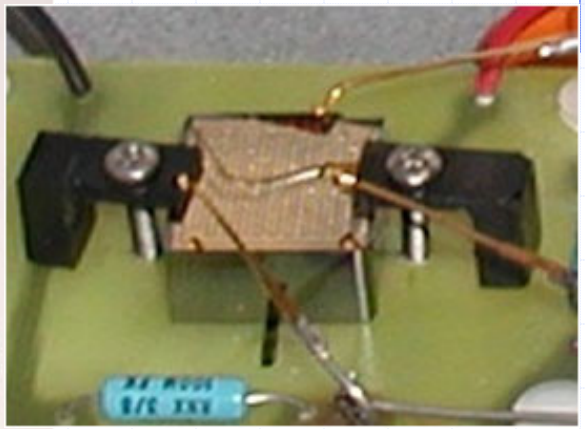

Project Accomplishments

- A potentially exciting iodide for direct or indirect radiation detection is InI.
- Indium iodide has an orthorhombic structure [N. Ohno, M. Yoshida, K. Nakamura. J. Nakahara and K. Kobayashi, J. Phys. Sot. Jpn. 53 (1984)]
- Bandgap of 2.0 eV, 5×10^{11} Ωcm achiavable
- high atomic numbers (Z_{In}: 49 and Z_I: 53)
- high density of 5.31 g/cm^3
- Knoop hardness of 27 (compared with 10 for HgI_2)
- electron-hole pair was reported to be 4 eV [M.R. Squillante, C. Zhou, J. Zhang, L.P. Moy and K.S. Shah, "InI Nuclear Radiation Detectors" IEEE Trans. on Nucl. Sci. 40/ 4 (1993) 364-366]

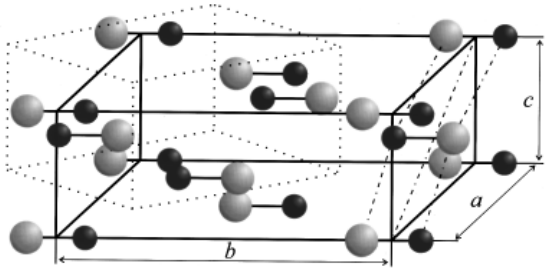

- low melting point (351 °C)
- very low toxicity
- Structure Structure of InI a = 4.75 A, b = 12.76 A, c = 4.91 A (each ±0.2%). [after M. I. Kolinko, Density of states of InI: Theoretical and experimental investigation, Phys. Rev B, 55(7) (1997)4007-4010, also R. E. Jones and D. H. Templeton, Acta Crystallogr. **8**, 847 (1955)]

InI boule and wafer

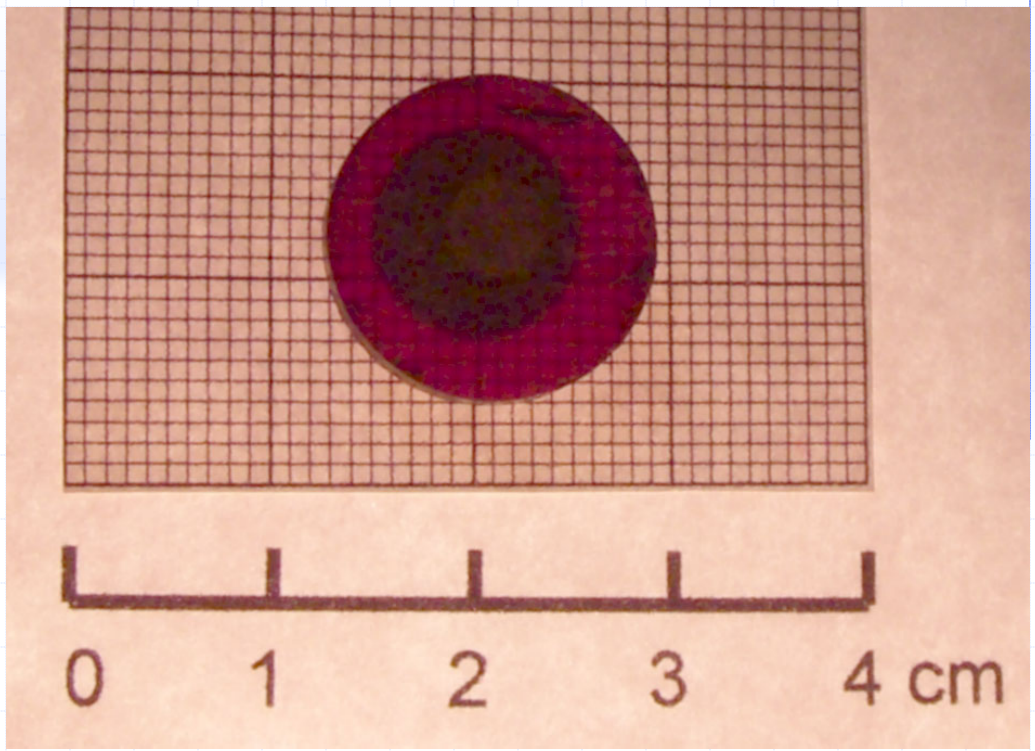

- Boule: grown by vertical Bridgman
- Wafer: 16 mm diameter x 2 mm thick, equipped with Au-Au contacts, 8 mm diameter and 60nm thick

Optical transmission spectrum of an InI wafer

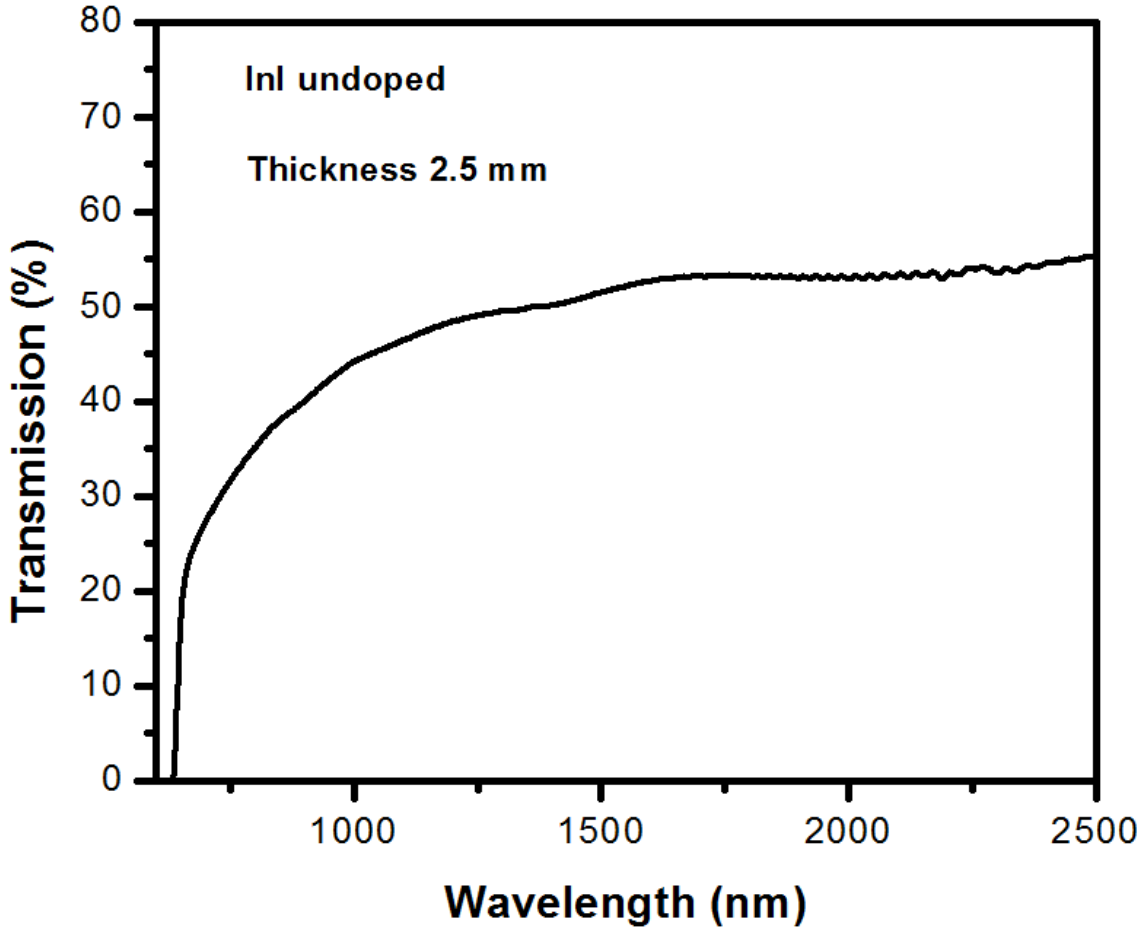

Current-Voltage/Photocurrent measurements setup

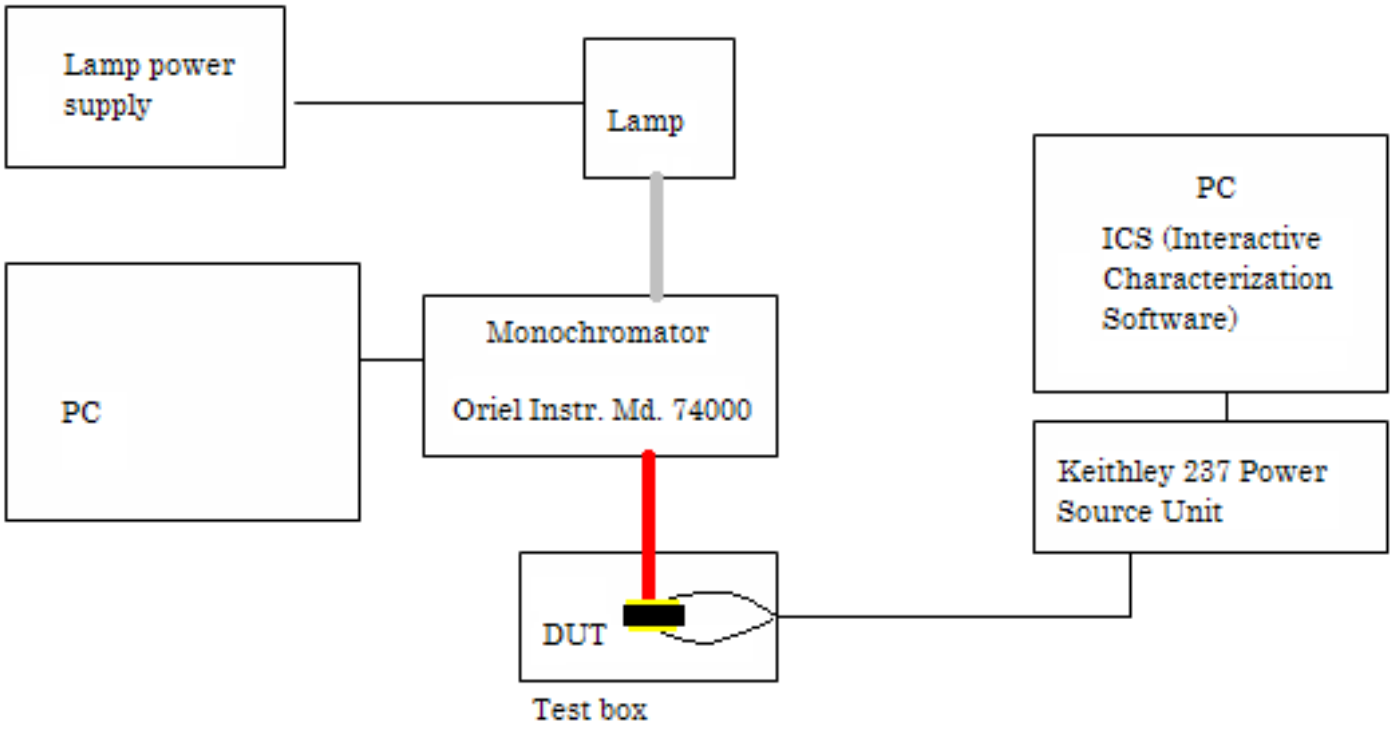

Au/InI/Au, Current-Voltage (I-V) characteristics

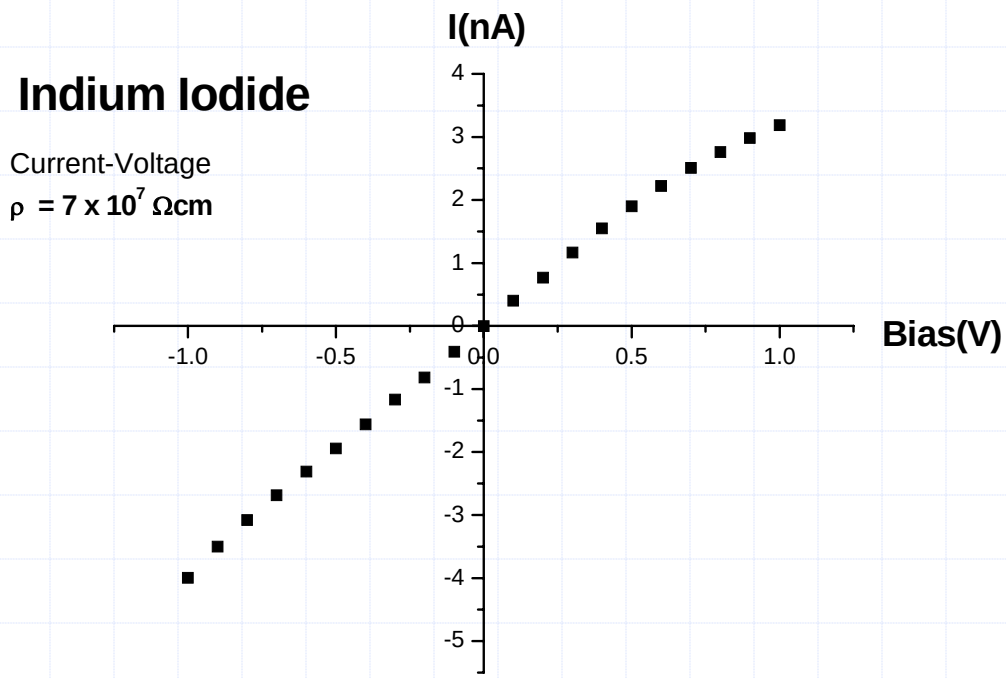

Samples resistivities are calculated from low bias current-voltage characteristics and their physical dimensions

Current-Voltage for thin sample of InI with Pd-Pd contacts

InI (4x5x.34)mm^3
Pd contacts, 1 mm dia.
Current-Voltage
ρ = 4 x 10^8 Ωcm

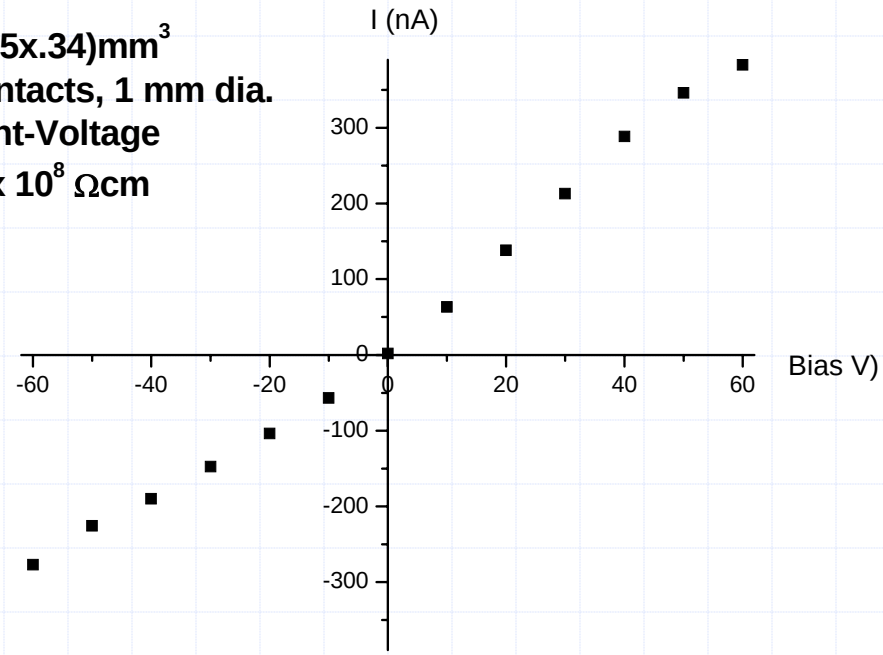

Au/InI/Au , Photocurrent vs. wavelength. Energy badgap 2.02 eV

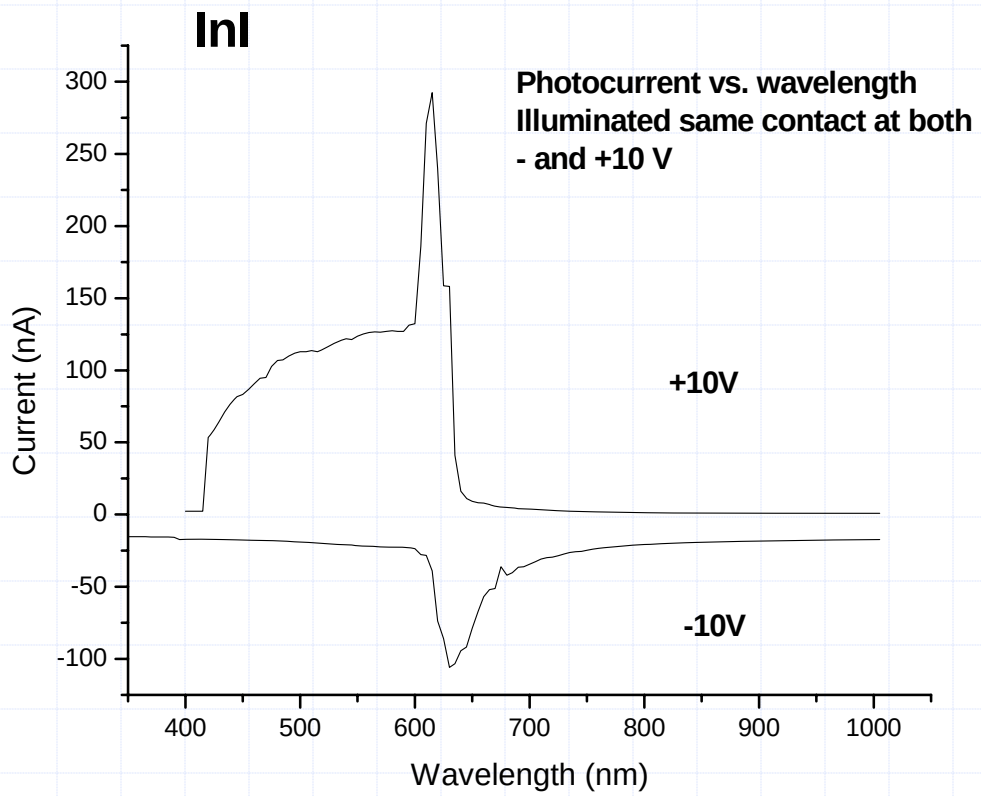

$HgCdI_2$ – Dark current and photocurrent measurements

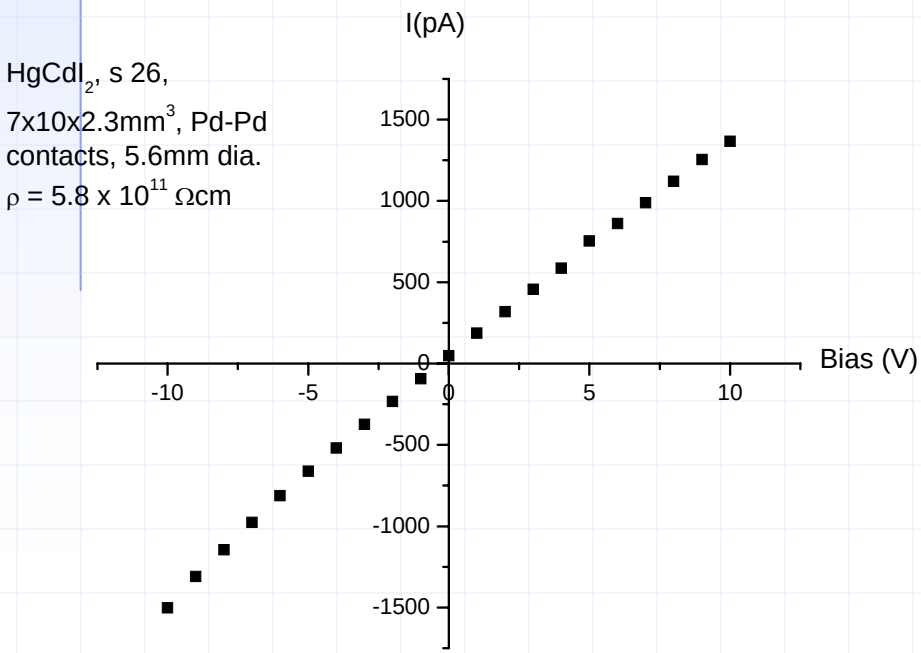

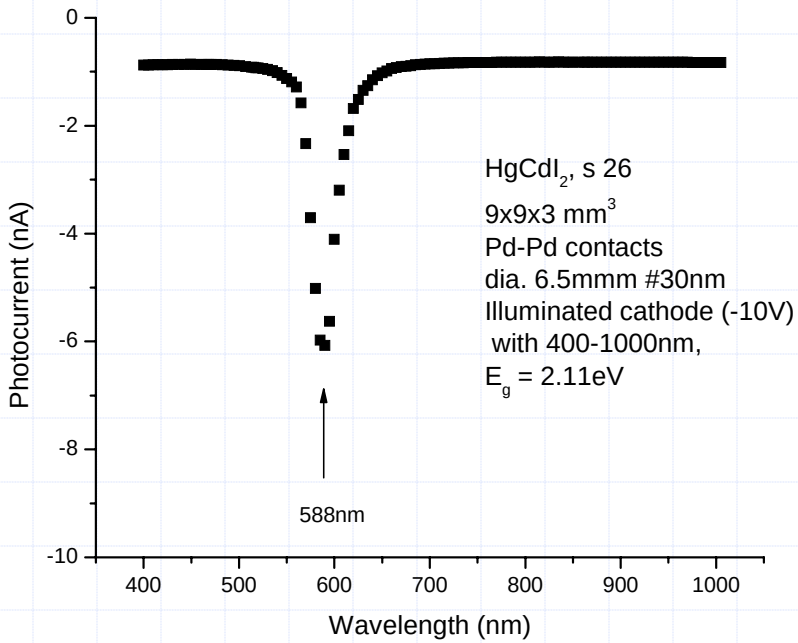

Photocurrent vs. Voltage

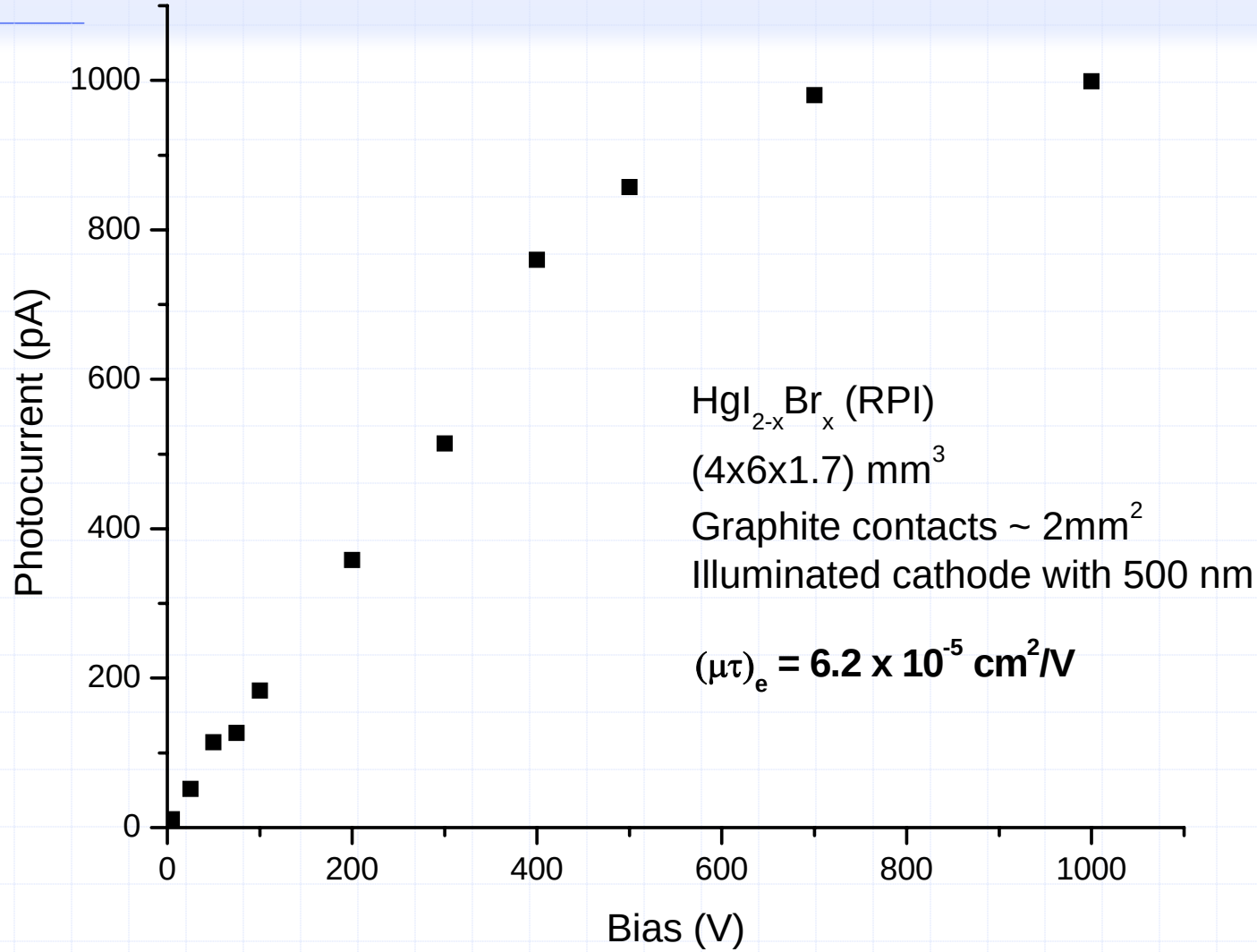

Activity update

- We are continuing to develop the infrastructure by introducing new methods of material preparation, materials characterization and detector fabrication
- New research professor was hired
- New research assistant hired
- Student training is and integral part of the research activities. We are developing collaborations for placing our students as interns at DOE labs.

Computational Models to Improve the Growth of Radiation Detector Crystals: Growth of CZT by the EDG Method

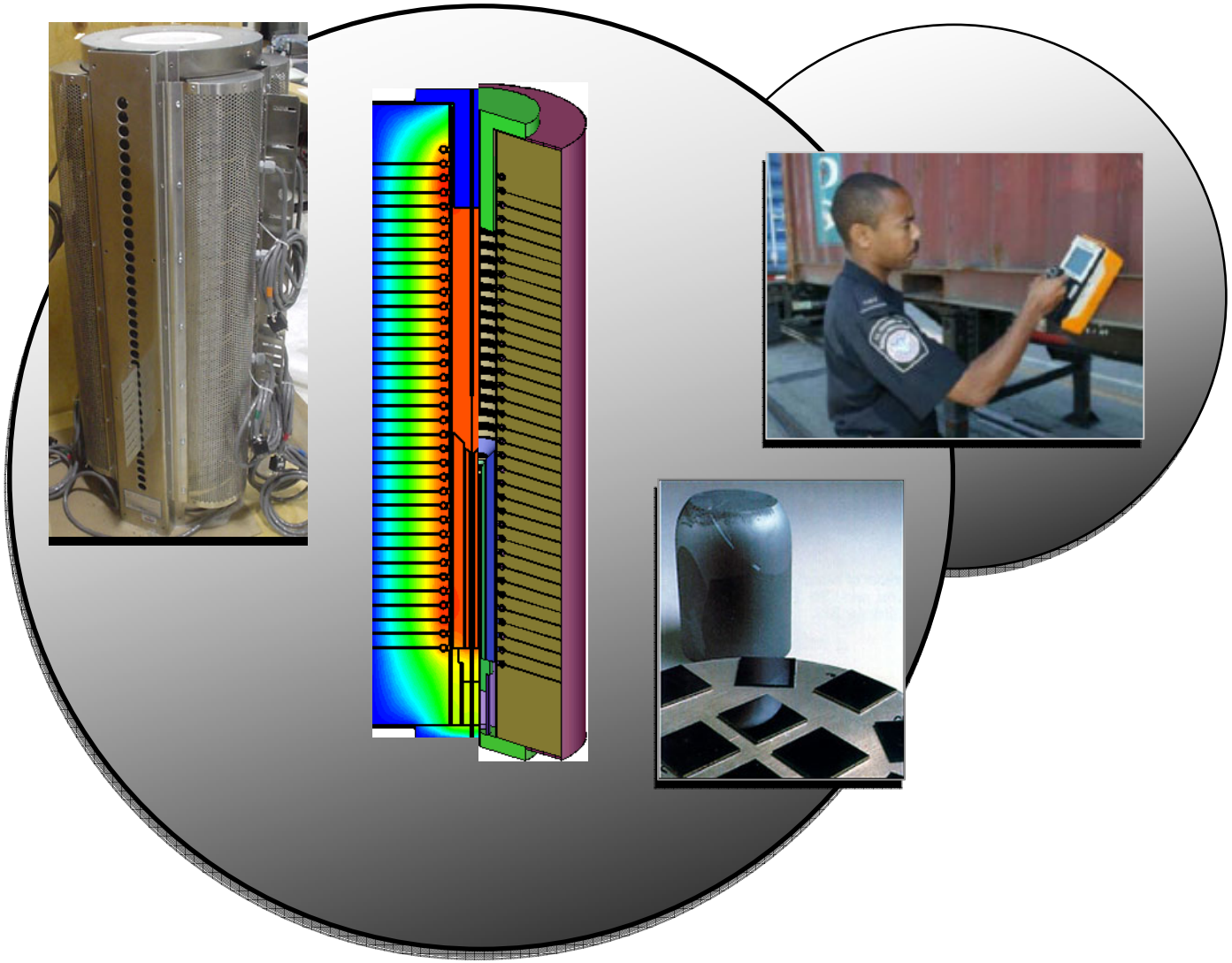

Jeffrey J. Derby
Department of Chemical Engineering & Materials Science
University of Minnesota

QuickTime™ and a GIF decompressor are needed to see this picture.

UITI Meeting
Orlando, FL
November 27-28, 2007

Outline of presentation

QuickTime™ and a
GIF decompressor
are needed to see this picture.

I. Why modeling?

II. CZT crystal growth

III. Modeling and objectives

IV. Results for WSU/PNNL EDG process

V. Future modeling opportunities

VI. Concluding remarks

Why do we model crystal growth?

QuickTime™ and a
GIF decompressor
are needed to see this picture.

"Genius is one percent inspiration and 99 percent perspiration."
--- Thomas Edison

"...a little theory and calculation would have saved him ninety per cent of his labor." --- Nikola Tesla

We model to improve and optimize crystal growth processes.

Why do we model crystal growth?

QuickTime™ and a
GIF decompressor
are needed to see this picture.

"The purpose of models is not to fit the data but to sharpen the questions."
--- Samuel Karlin, 11th R A Fisher Memorial Lecture, Royal Society 20, April 1983.

We model to understand crystal growth.

Outline of presentation

QuickTime™ and a
GIF decompressor
are needed to see this picture.

I. Why modeling?

II. CZT crystal growth

III. Modeling and objectives

IV. Results for WSU/PNNL EDG process

V. Future modeling opportunities

VI. Concluding remarks

The growth of detector-grade, single crystals of CZT has proven to be extremely challenging

- Formation of extended defects; grains, twins, and dislocations
- Cracking caused by thermal stresses
- Nonuniform crystal composition caused by segregation
- Second-phase inclusions; tellurium precipitates and inclusions

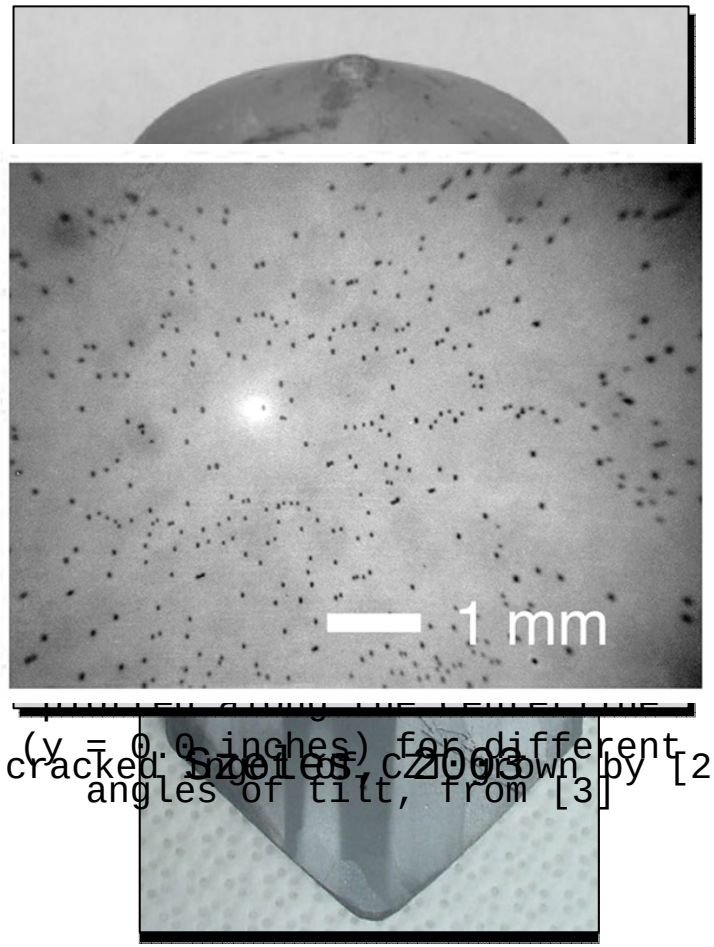

A cracked ingot of CZT grown by [2
angles of tilt, from [3]

[3] Lun *et al*, "Decreasing Lateral Segregation in Cadmium Zinc Telluride via Ampoule Tilting during Vertical Bridgman Growth" Journal of Crystal Growth, **291**, 348, 2006.

Furnace" Journal of Crystal Growth, **289(2)**, 415-748, 2006.

Growing CZT: The Mellen EDG furnace

- A crucible is “charged” with Cd, Te and Zn, and sealed in a quartz

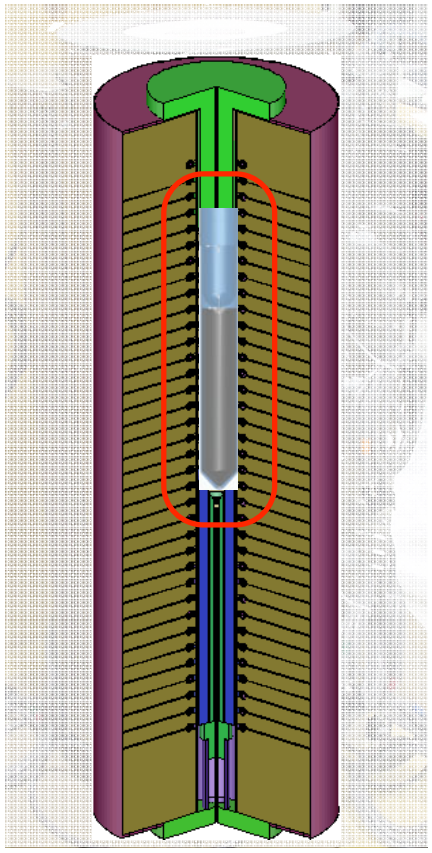

WSU Mellen furnace

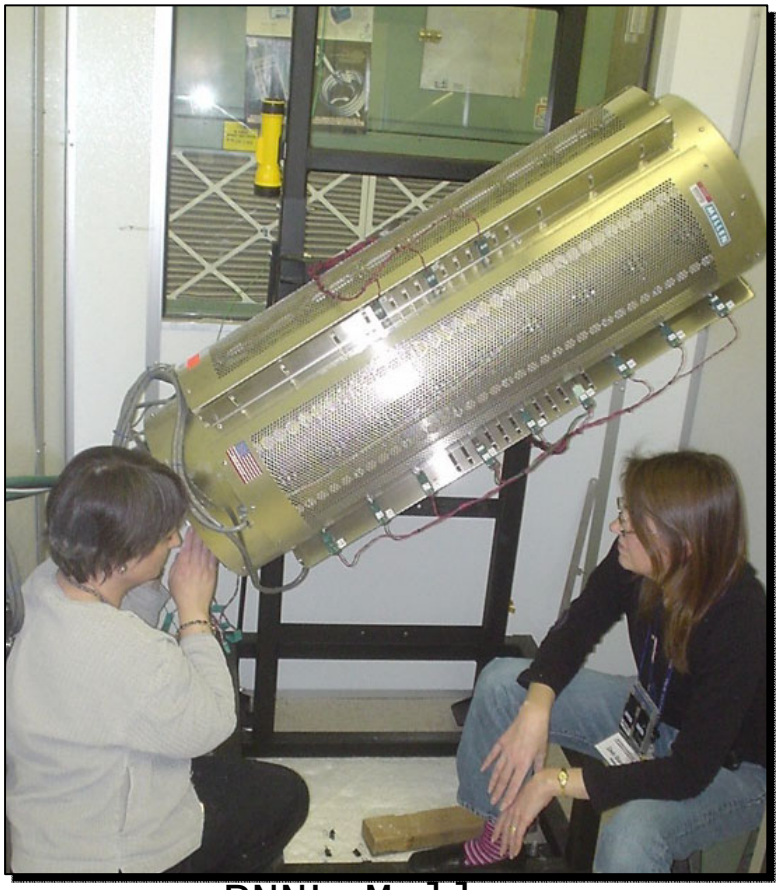

PNNL Mellen furnace

Growth occurs via “moving gradient

Outline of presentation

QuickTime™ and a
GIF decompressor
are needed to see this picture.

I. Why modeling?

II. CZT crystal growth

III. Modeling and objectives

IV. Results for WSU/PNNL EDG process

V. Future modeling opportunities

VI. Concluding remarks

We are developing and applying models to address crystal growth issues for CZT

QuickTime™ and a GIF decompressor are needed to see this picture.

Longer-term goal: Development of flexible, rigorous models

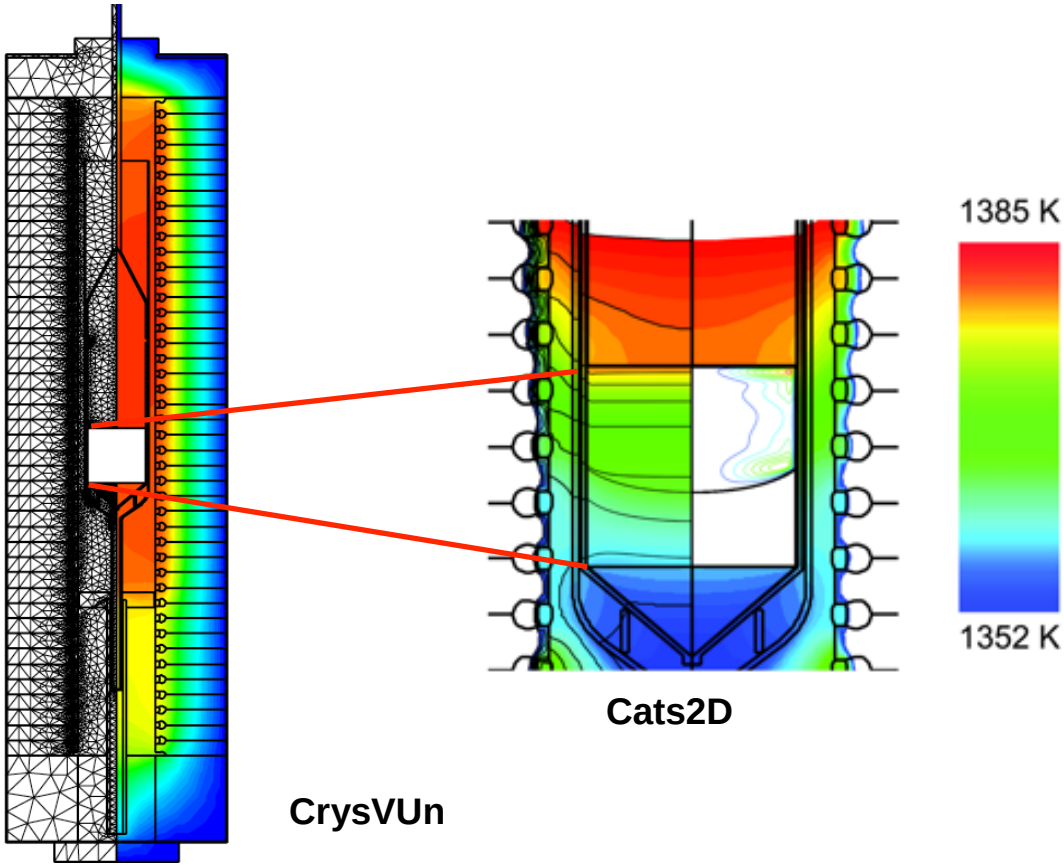

Short-term goal: Develop and apply a detailed process model for EDG growth systems

Research Goal: Characterize conditions in WSU/PNNL furnaces towards furnace modifications for improved CZT growth

Current problem:

Identifying *conditions* for the *reproducible growth* of single crystal CZT ingots

Solution approach:

- Design computational models to accurately predict continuum transport and thermodynamics within experimental growth furnaces
- Verify models within growth zone *(to a known degree of accuracy)*
- Probe alternative furnace materials & heater profiles for enhanced heat transfer control *(crucibles, ampoule supports, liners)*

We are applying CrysMAS to study continuum transport during CZT growth

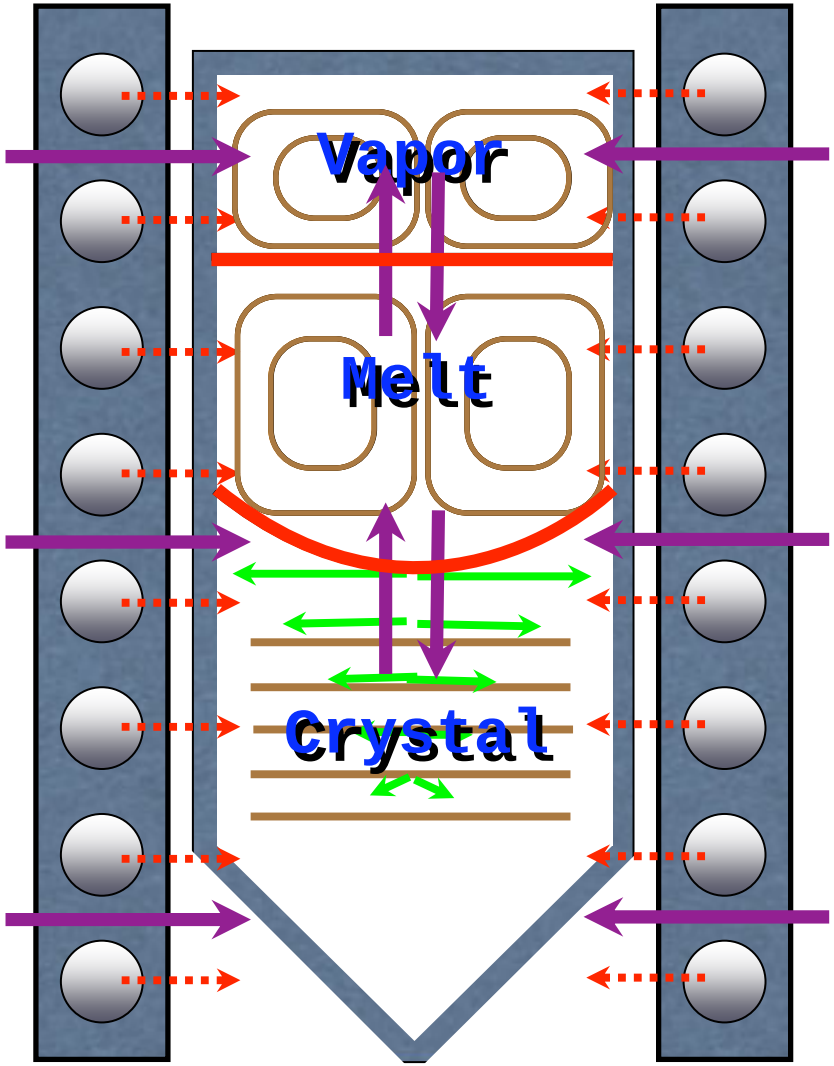

Continuum transport

- Momentum
- Heat
  - Convection
  - Conduction
  - Radiation
- Species
  - Thermodynamic phenomena
  - Phase change
  - Equilibrium partitioning of solutes along solidification front

Generating the computational model

- Physical system assessment for CAD generation: *measurements accurate to 0.1 mm*
- Discretizing the computational domain (meshing)
- Identification of relevant material properties *(20+ materials)*
- Identification of appropriate boundary conditions

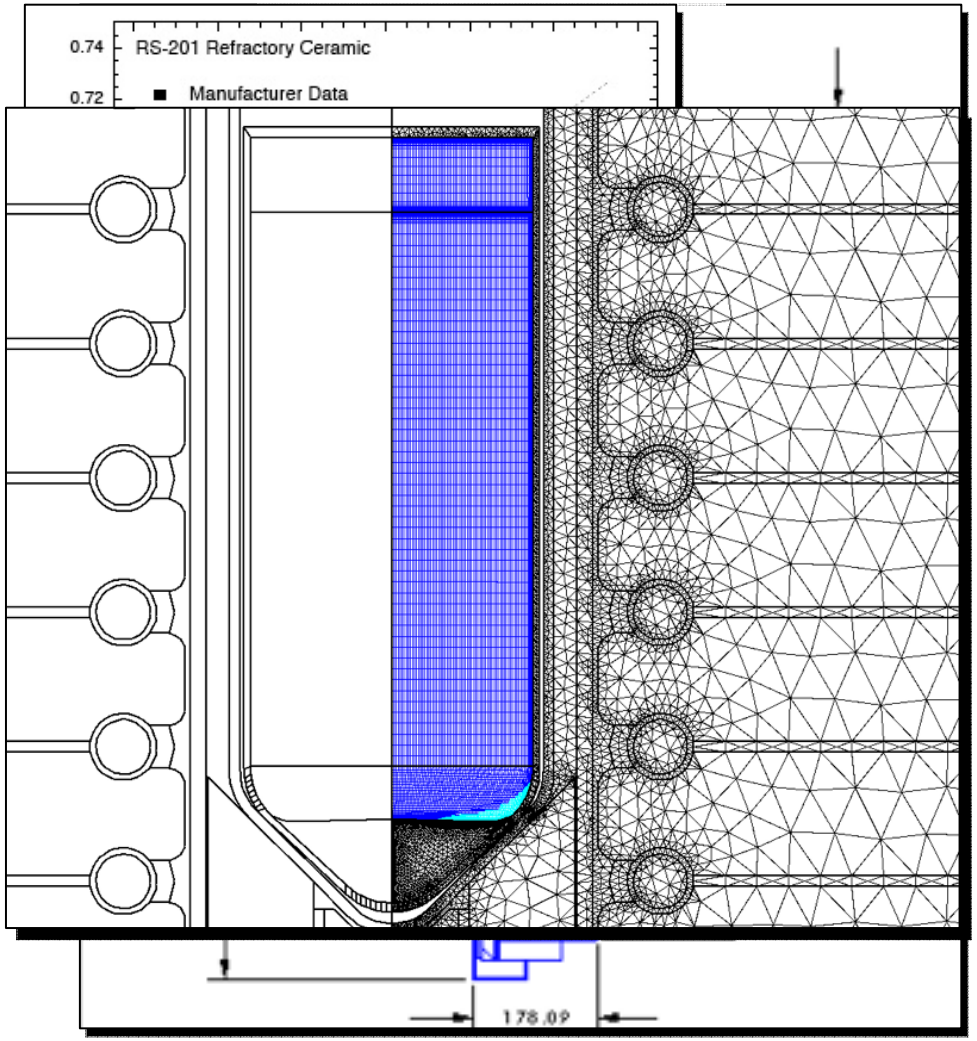

Outline of presentation

QuickTime™ and a
GIF decompressor
are needed to see this picture.

I. Why modeling?

II. CZT crystal growth

III. Modeling and objectives

IV. Results for WSU/PNNL EDG process

V. Future modeling opportunities

VI. Concluding remarks

Validation of WSU/PNNL model

Thermocouple set-points are matched

Cri
zon
gr
cor

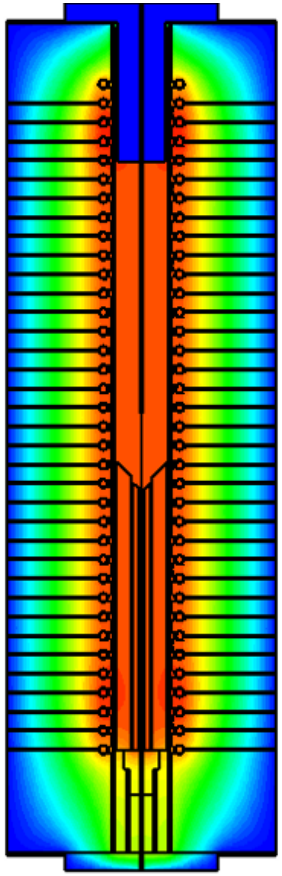

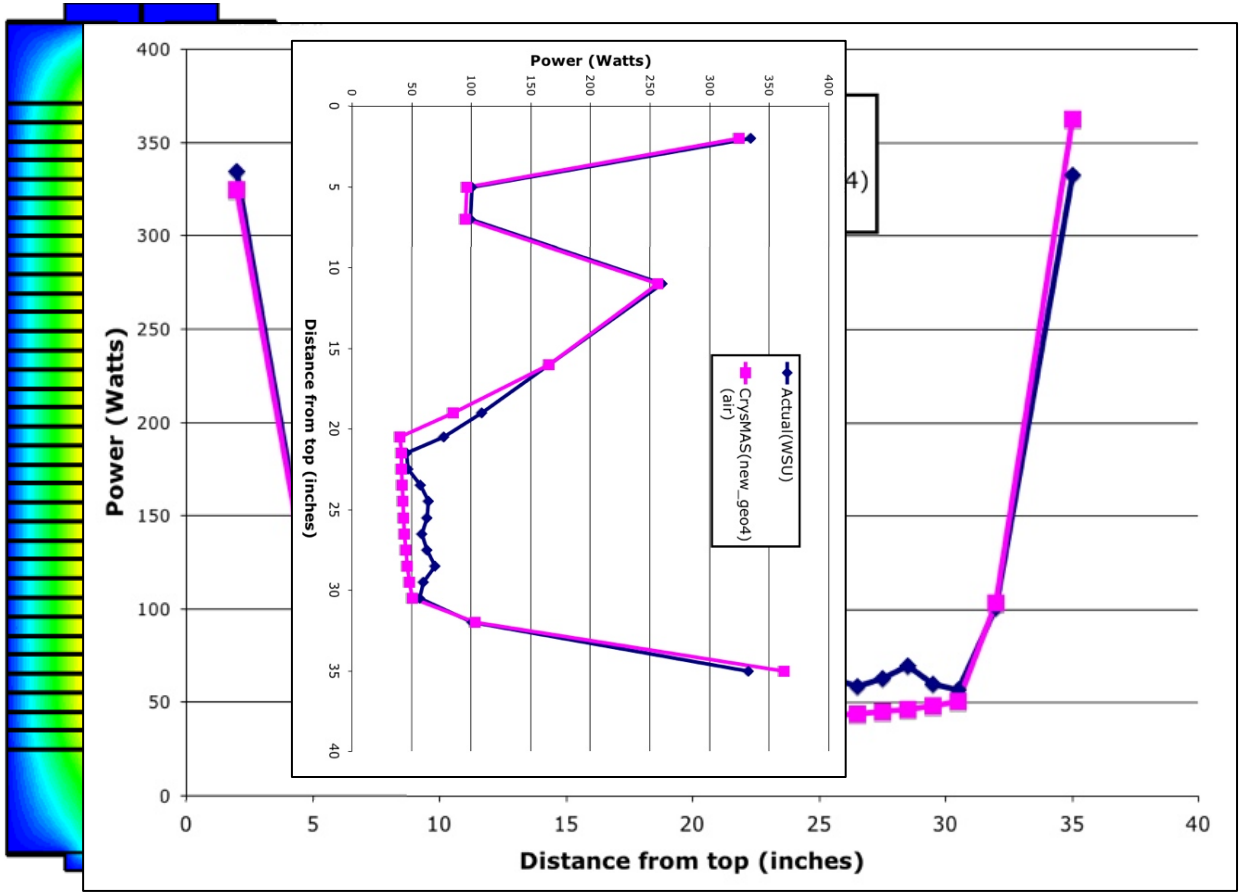

WSU Furnace

Furnace heater power vs. height

Initial PNNL furnace simulations: Comparing crucible materials

Graphite

Pyrolytic Boron Nitride (PBN)

Want to compare:

- intensity and nature of flows within the melt
- heat transfer characteristics
- solid/liquid interface shape

-- using the same temperature profile

Is there a preferred crucible for use in the PNNL furnace with their time-dependent temperature profile?

isotropic thermal conductivity, coated with nonisotropic pyrolytic graphite

Anisotropic thermal conductivity a,b~2.5 W/(m·K) , c~63 W/(m·K)

Significantly different conditions are present near the onset of growth

QuickTime™ and a
GIF decompressor
are needed to see this picture.

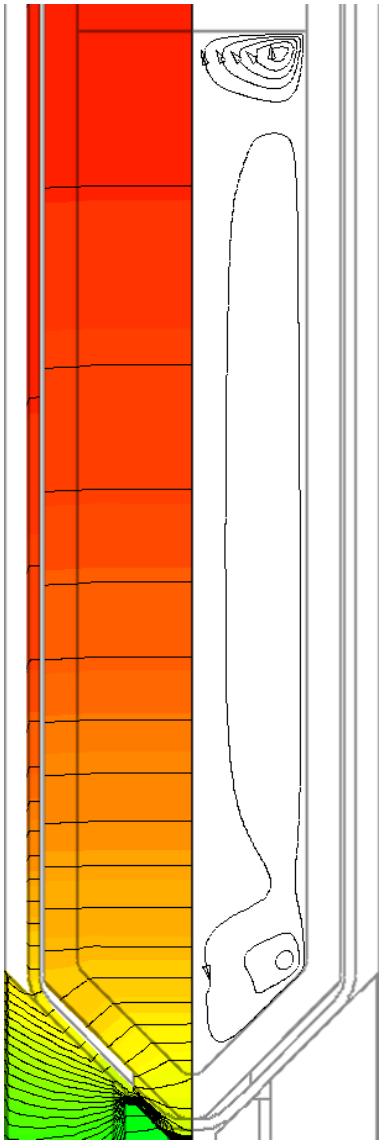

Graphite crucible

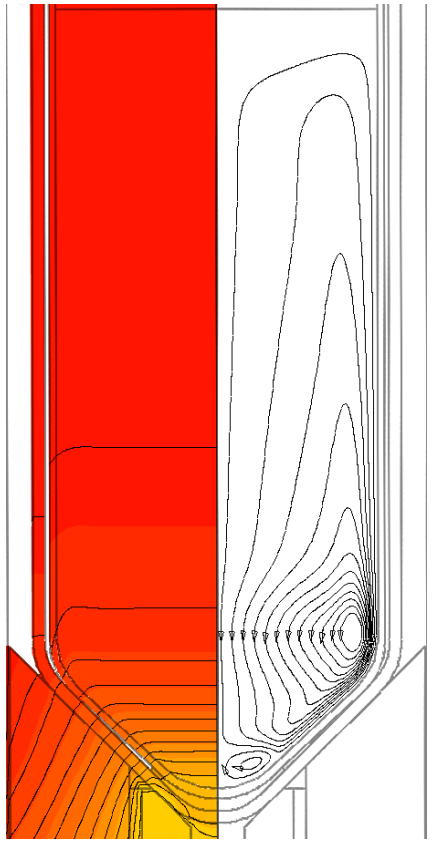

PBN crucible

- Axial thermal gradient is nearly uniform in graphite crucible system
- Axial thermal gradient magnified near PBN crucible tip
- Melt flows are much stronger in PBN crucible system
- The “offset” in axial temperature profile (between crucible contents and furnace bore) is far greater in graphite crucible system

All of these effects are explained by the much greater axial heat flux supported by graphite crucible walls

PBN crucible produces conditions that may favor a more localized nucleation event

QuickTime™ and a
GIF decompressor
are needed to see this picture.

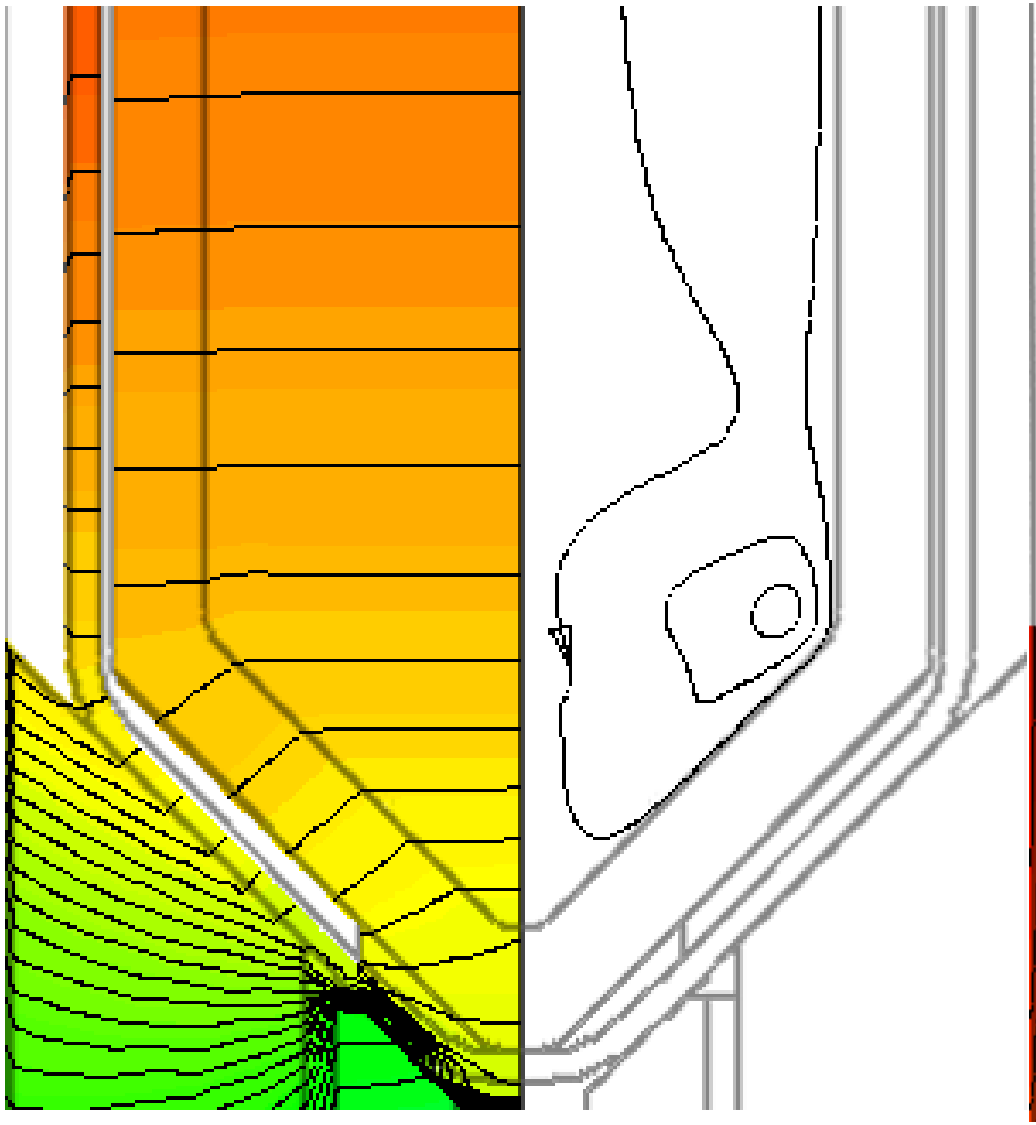

Graphite crucible

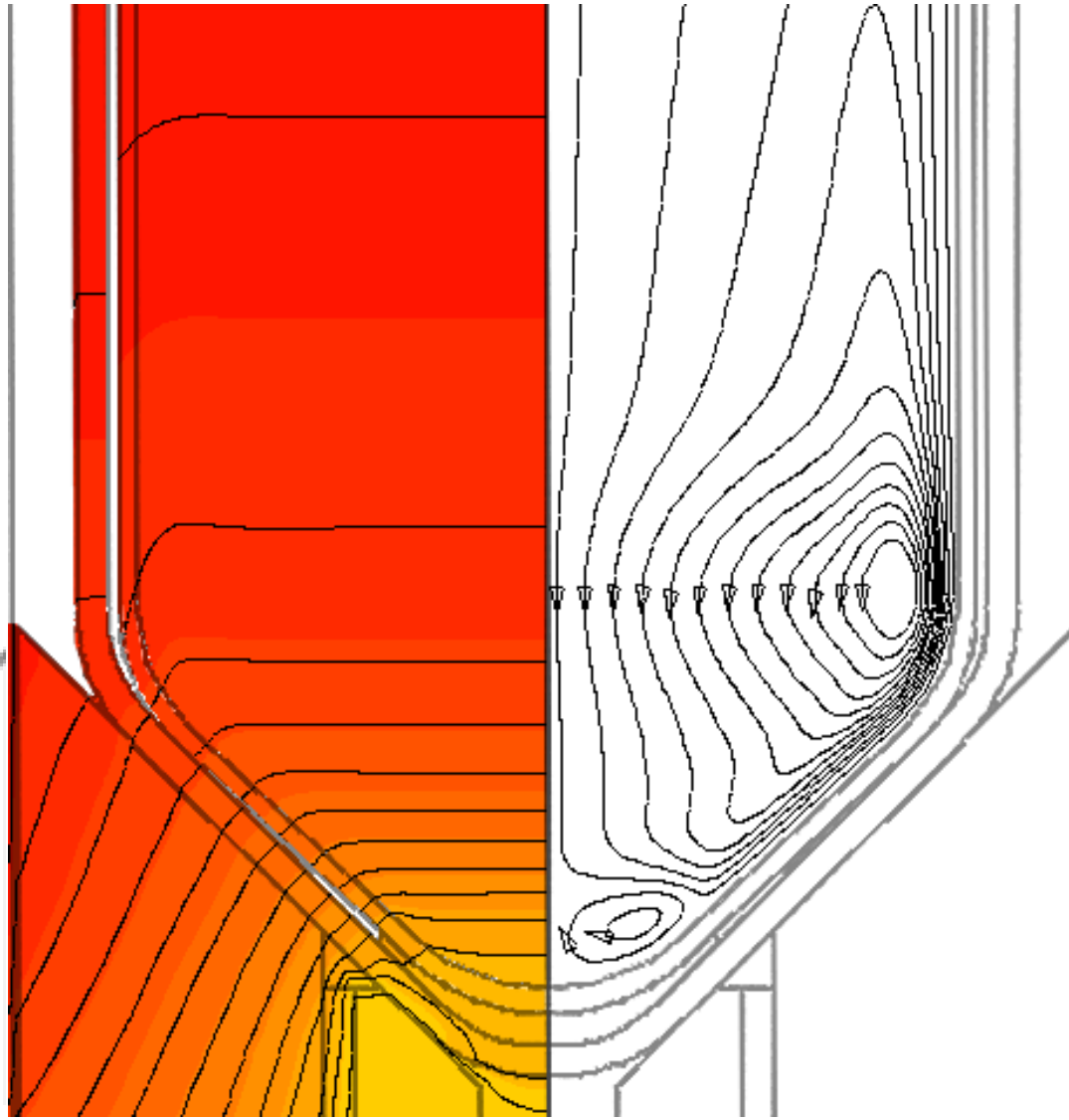

PBN crucible

Quasi-steady growth simulations reveal further differences in system behavior

QuickTime™ and a
GIF decompressor
are needed to see this picture.

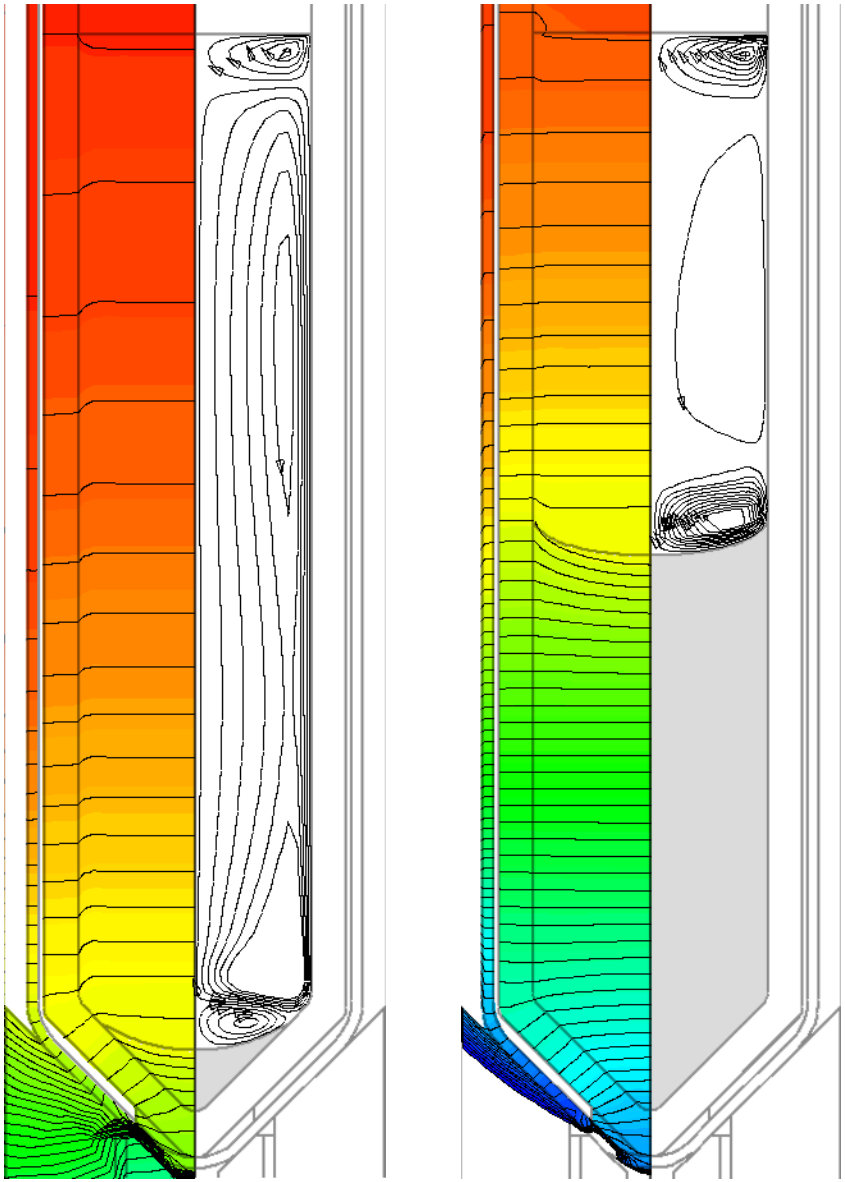

Graphite crucible

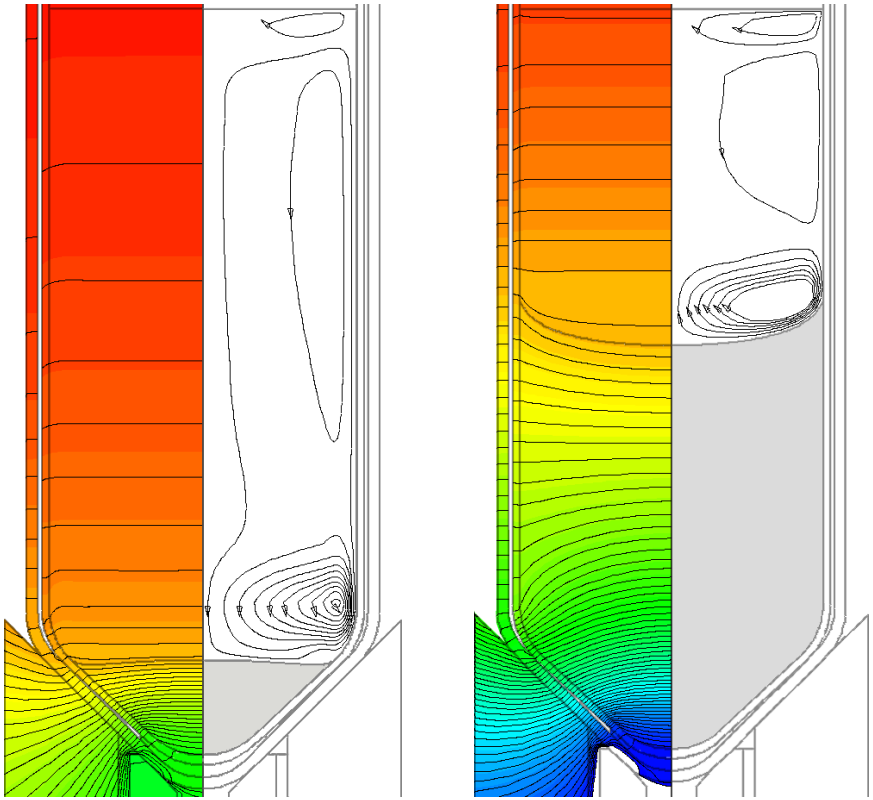

PBN crucible

PBN system promotes more favorable interface shapes during early growth

QuickTime™ and a
GIF decompressor
are needed to see this picture.

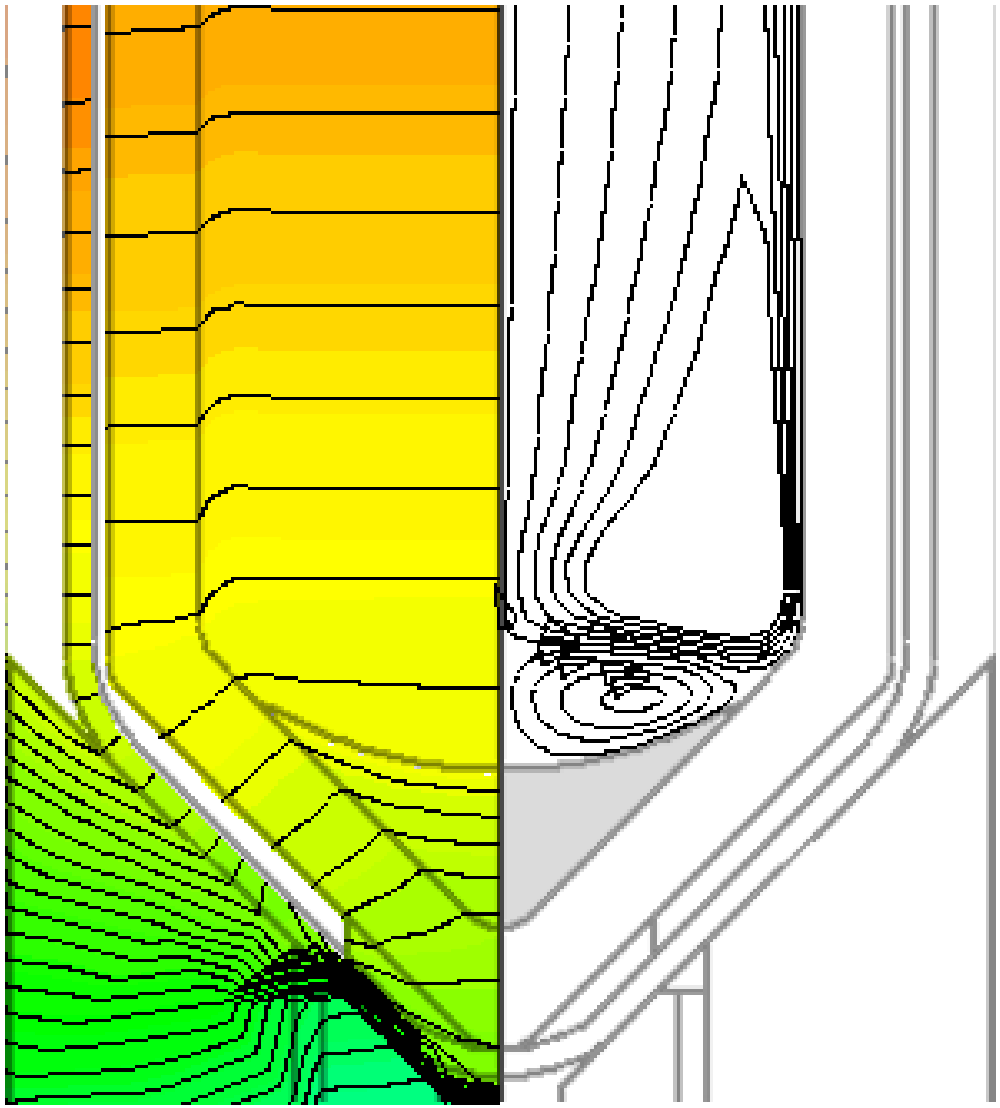

Graphite crucible

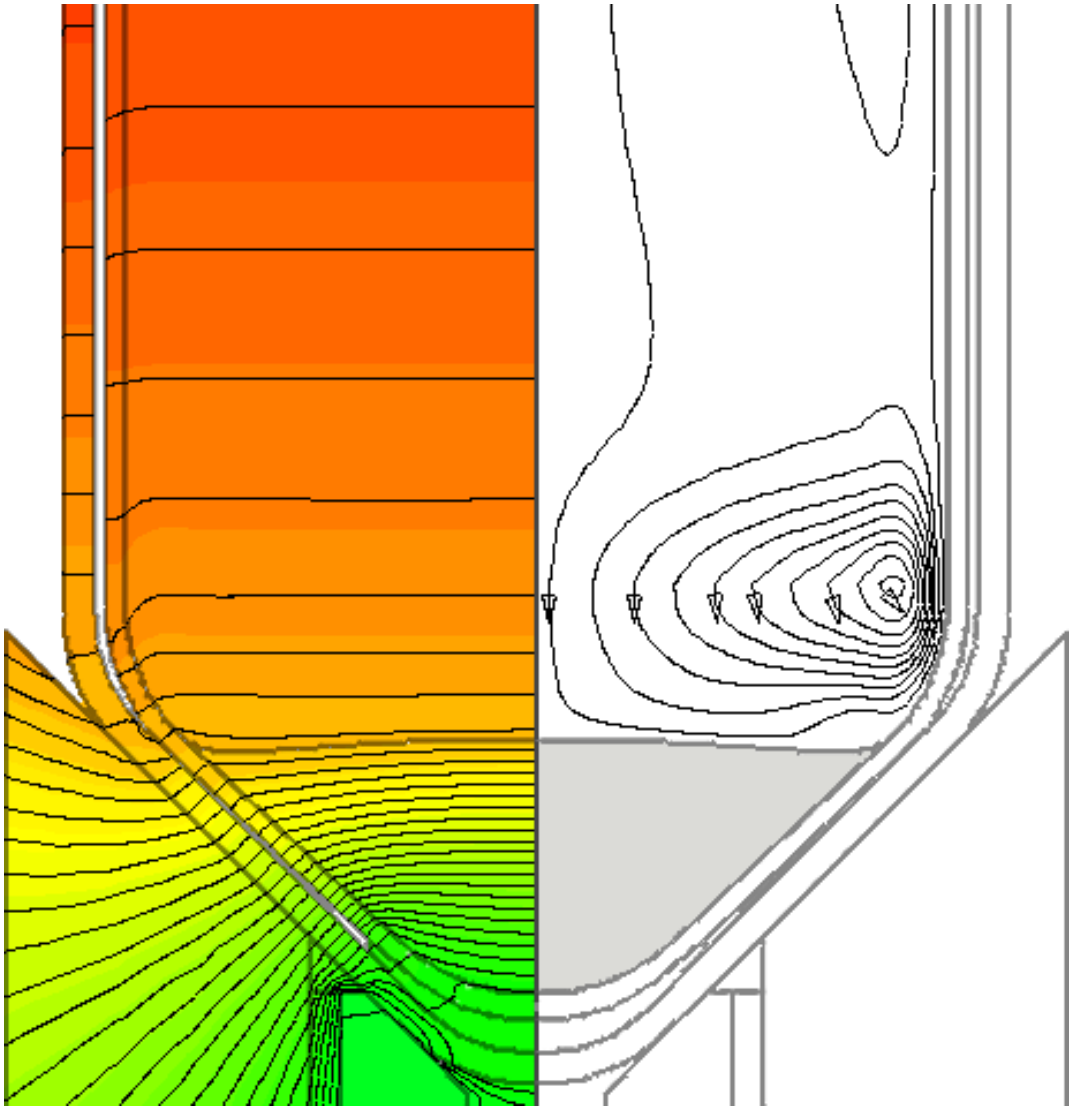

PBN crucible

Interface shapes are similar during later stages of growth

QuickTime™ and a
GIF decompressor
are needed to see this picture.

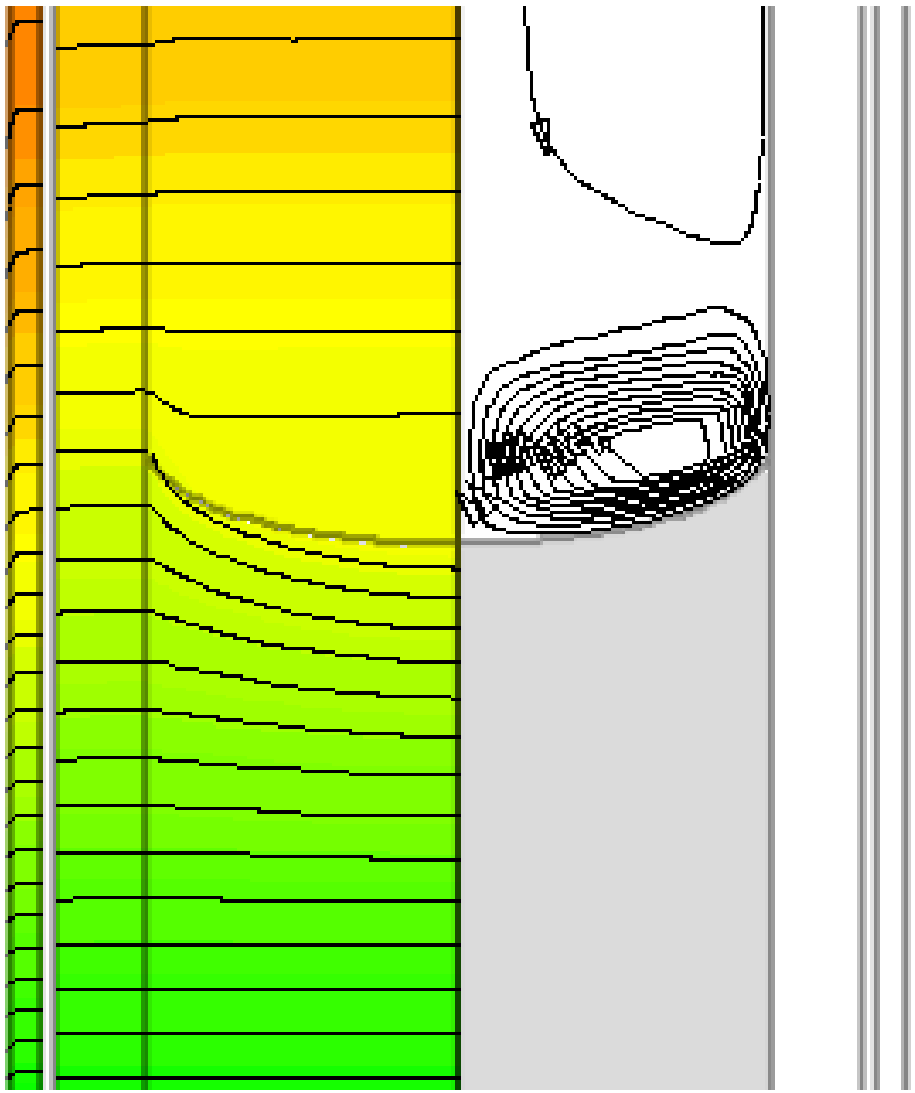

Graphite crucible

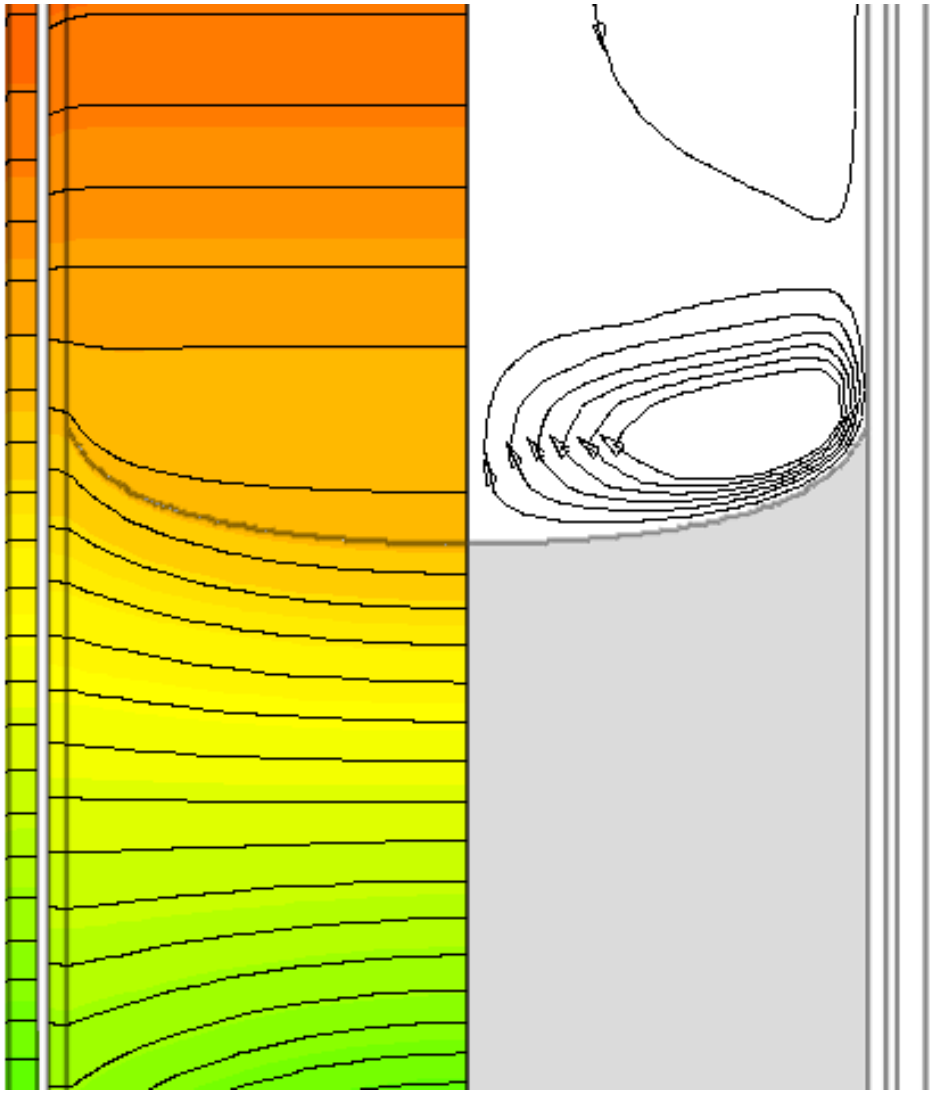

PBN crucible

Simulations suggest that a flat-bottomed, PBN crucible may result in more optimal interface shapes during inital stages of growth

QuickTime™ and a
GIF decompressor
are needed to see this picture.

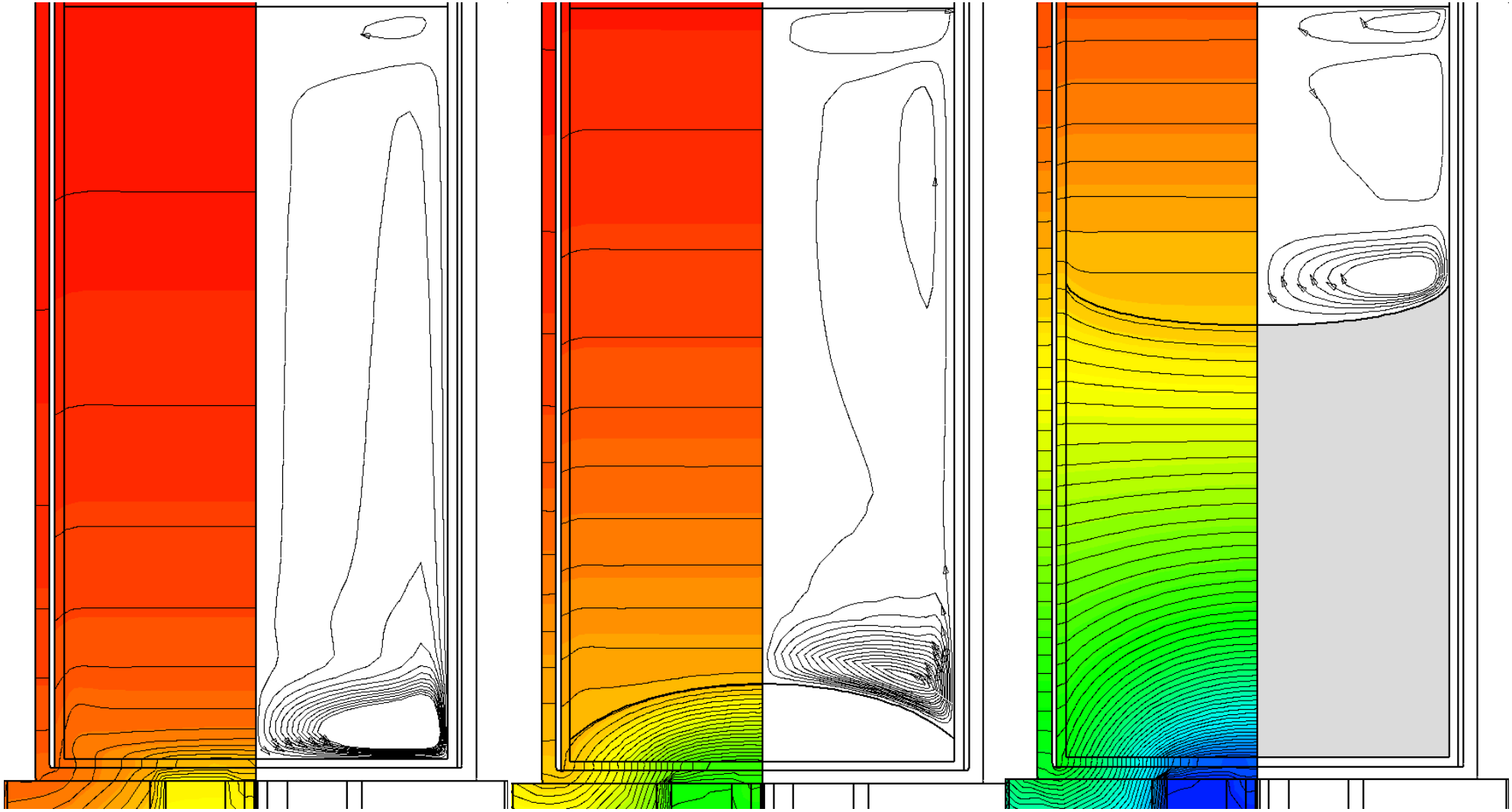

Outline of presentation

QuickTime™ and a
GIF decompressor
are needed to see this picture.

I. Why modeling?

II. CZT crystal growth

III. Modeling and objectives

IV. Results for WSU/PNNL EDG process

V. Future modeling opportunities

VI. Concluding remarks

Continuum crystal growth models need further advances for use in process development

QuickTime™ and a
GIF decompressor
are needed to see this picture.

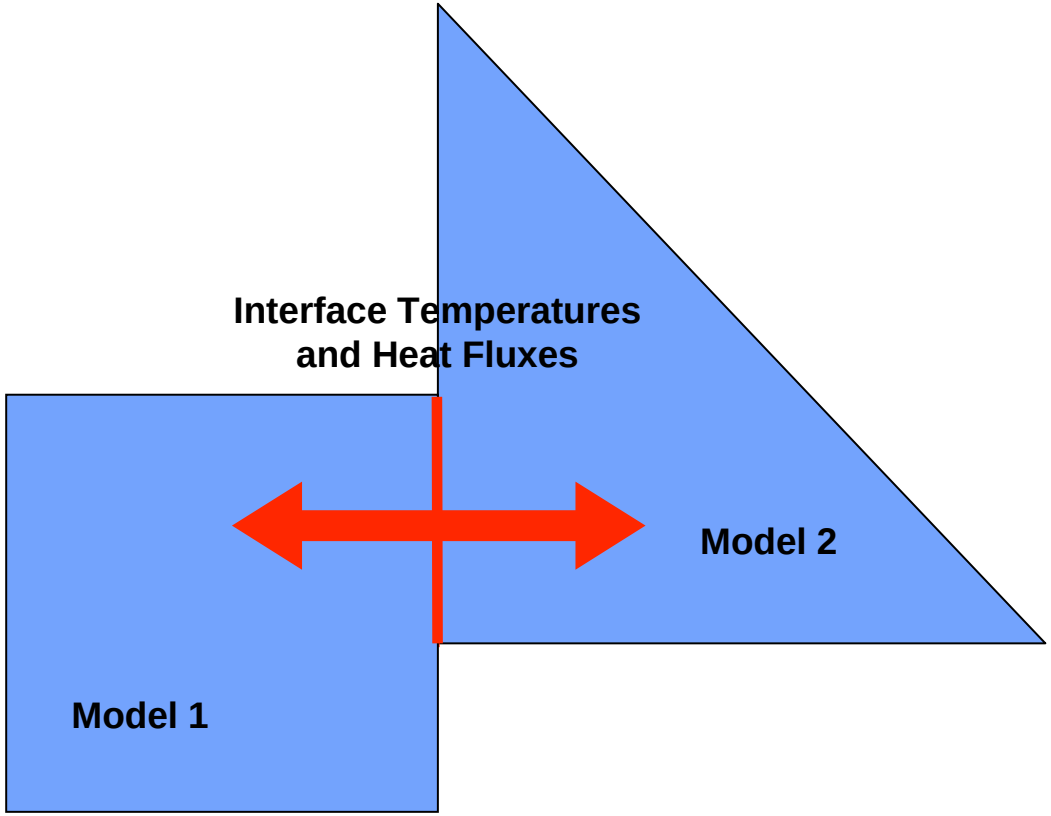

QuickTime™ and a
YUV420 codec decompressor
are needed to see this picture.

**Coupled models
for flexibility and rigor**

**Parallel algorithms
for 3D, time-dependent
simulations**

Advances in crystal growth are typically incremental: Modeling provides a means to assess potential for significant process changes

QuickTime™ and a GIF decompressor are needed to see this picture.

Risk and Difficulty

Modeling c es
feasibility o or

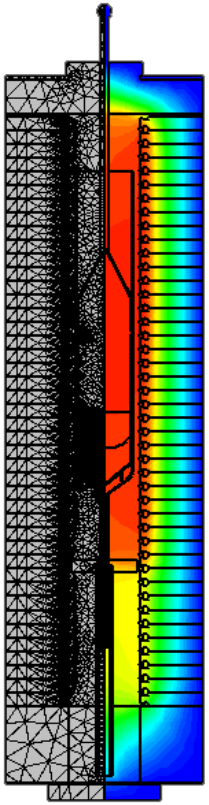

Furnace

Process

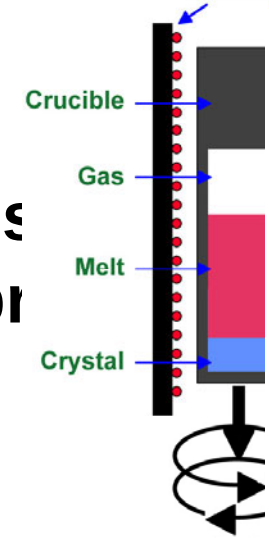

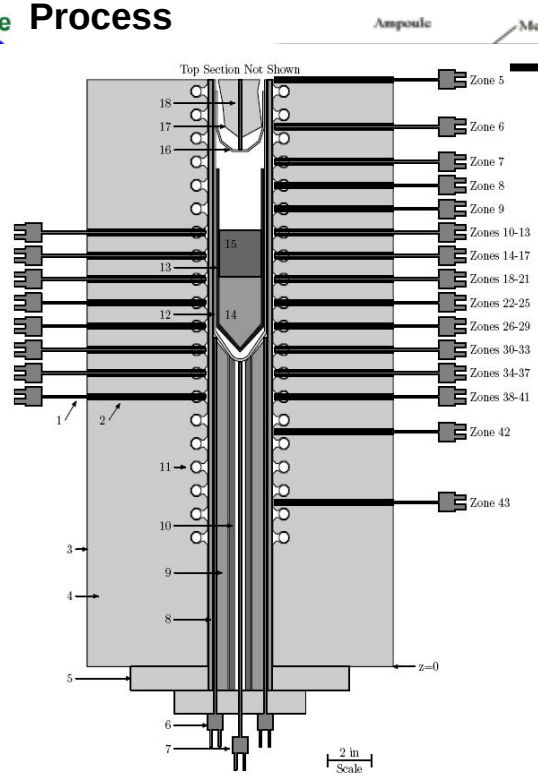

Indirect system measurement

Detached Solidification

and

Model

merged

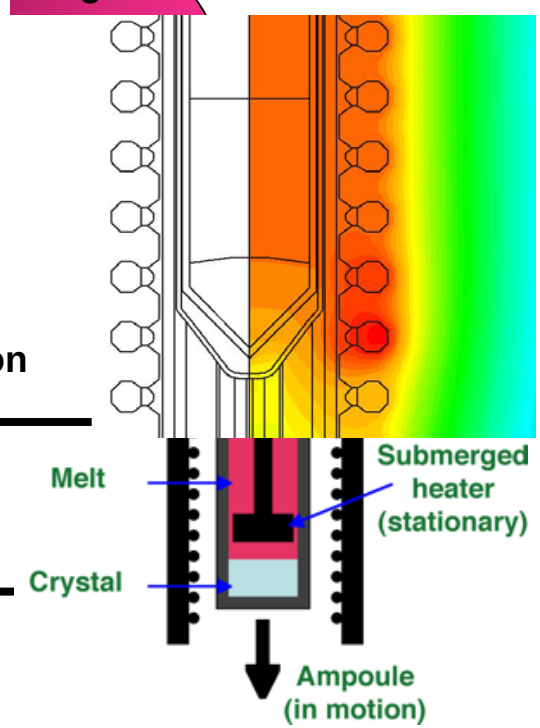

Computed control action

Model-Based Control

Computer-Aided Analysis and Optimization of VB Processes

Potential Reward

Multi-scale, defect dynamics models are needed to connect growth conditions to crystal properties

QuickTime™ and a GIF decompressor are needed to see this picture.

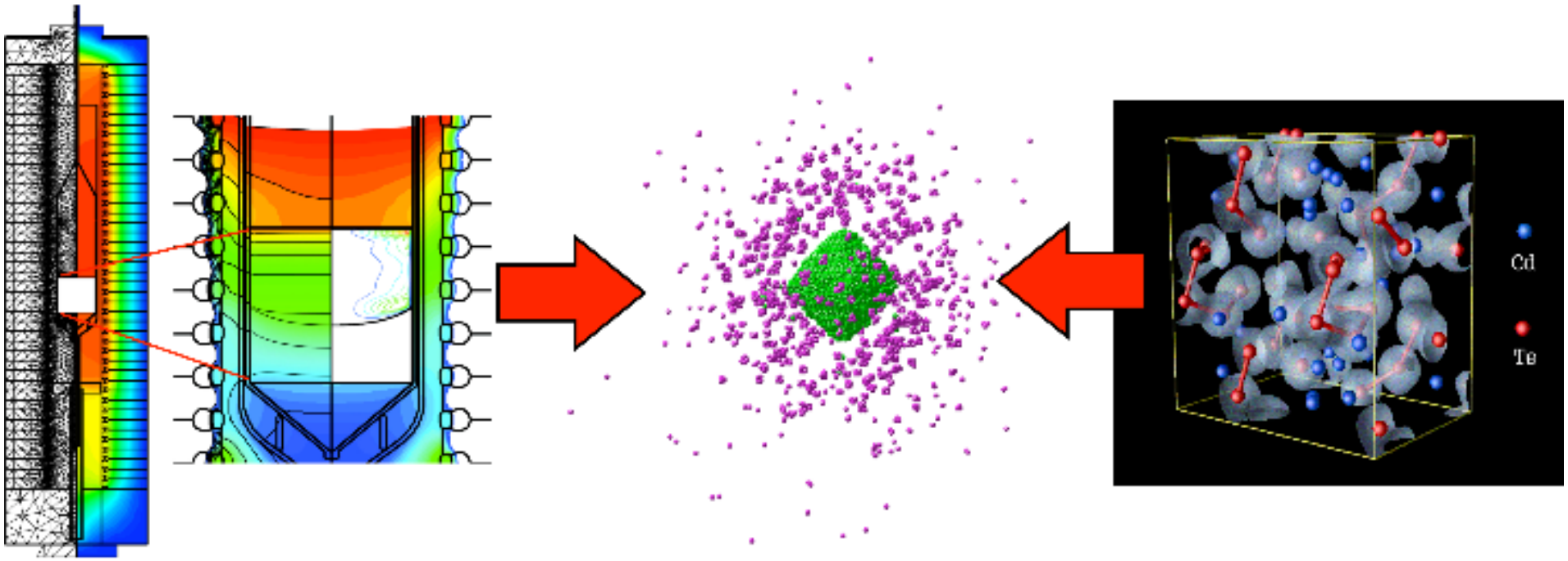

Macroscopic crystal growth model

Mesoscopic defect model

Microscopic ab intio model

Specific challenge for CZT is to understand and control tellurium second-phase inclusions!

Outline of presentation

QuickTime™ and a
GIF decompressor
are needed to see this picture.

I. Why modeling?

II. CZT crystal growth

III. Modeling and objectives

IV. Results for WSU/PNNL EDG process

V. Future modeling opportunities

VI. Concluding remarks

Concluding remarks

QuickTime™ and a
GIF decompressor
are needed to see this picture.

Analysis of PNNL/WSU furnaces indicates PBN crucible with modified mounting base will provide improved conditions at the onset of CZT growth

- **Steeper axial gradient**
- **Better melt mixing**
- **More convex interface shape**

Modeling proves vital to understand subtle heat transfer changes caused by system modification

Future modeling challenges:

- **Flexible, rigorous models (model coupling)**
- **Model-based control**
- **Three-dimensional models (parallel computing)**
- **Design, assessment of novel processes**
- **Defect dynamics**

Theoretical modeling can provide understanding of the growth of crystals to *improve* existing process and material

Ongoing work for WSU/PNNL system...

QuickTime™ and a
GIF decompressor
are needed to see this picture.

- Analysis of thermal environment at nucleation
- Analysis of interface shape evolution during growth
- Analysis of segregation (stoichiometry and dopant packages)
- Analysis of thermal stresses
- Evaluation of possible process changes
  - Furnace set-points
  - Ampoule material
  - Ampoule shape
  - Ampoule mounting and overhead

WASHINGTON STATE UNIVERSITY

World Class. Face to Face.

Crystal Growth and Characterization of $Cd_{1-x}Zn_xTe$ Room Temperature Radiation Detectors

Kelvin Lynn

Kelly Jones

Daniel Trump

Guido Ciampi (now at RMD)

Raji Soundararajan

Santosh Swain

Washington State University

Pullman, Washington

See poster: Kelly Jones for more detail

This research was funded by:

DOE NNSA NA-22 DE-FG07-06IDI4724

$Cd_{(1-x)}Zn_{(x)}Te$ Crystal Growth & Characterization
PI: Dr. Kelvin Lynn

- Project
  - CdZnTe growth for room temp. radiation detectors
  - Low pressure vertical Bridgman crystal growth
  - All fabrication & processes performed at WSU
- Technical Approach
  - Unique co-doping compensation -- **Patent Pending**
- Minimize growth instabilities, control purity and Te inclusions

WSU Crystal Growth Process

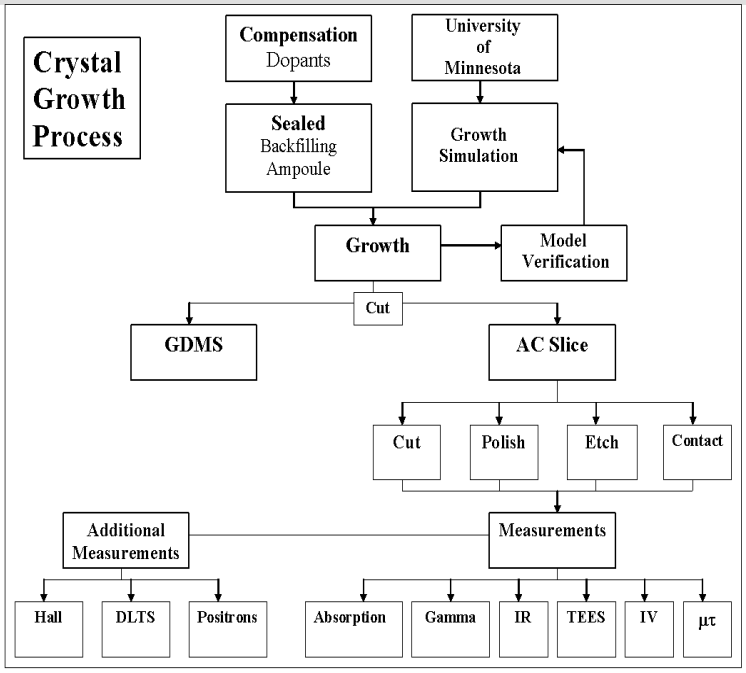

- **Goals**
  - **Grow large single crystal detectors >1cm³**
    - **Fully active detectors**
    - $\mu\tau_e > 1 \times 10^{-3}$ **cm²**
    - **Improved yields**
- **Budget**
  - **<300k per year, pending 3 th year**
  - **Significant costs in materials**
- **Deliverables**
  - **12 ingots per year**
  - **Improved yields**
  - **Large single crystals**
  - **Reproducibility**

Outline

- CZT crystal growth and detector results performed research at WSU
- Overview
- Detector results on various ingots
- Conclusions &growth issues

Linking Purity, Te, Dopants, Growth & Profile to Properties

- IR microscopy on slice
- Crucibles important
  - Impurities are still important
- Te inclusion nucleation
  - *Instabilities during growth*
  - Slower growth rate
- Te (small) inclusions

  Retrograde solubility??

Crystal growth at WSU

CZT

- Reducing the excess Te
- <u>High purity-critical</u>
- EDG Vertical Bridgman Method
- Growth rate varied
- Imposed temperature gradients of 20-50°C per inch

Single Crystal CZT from WSU-Recent result

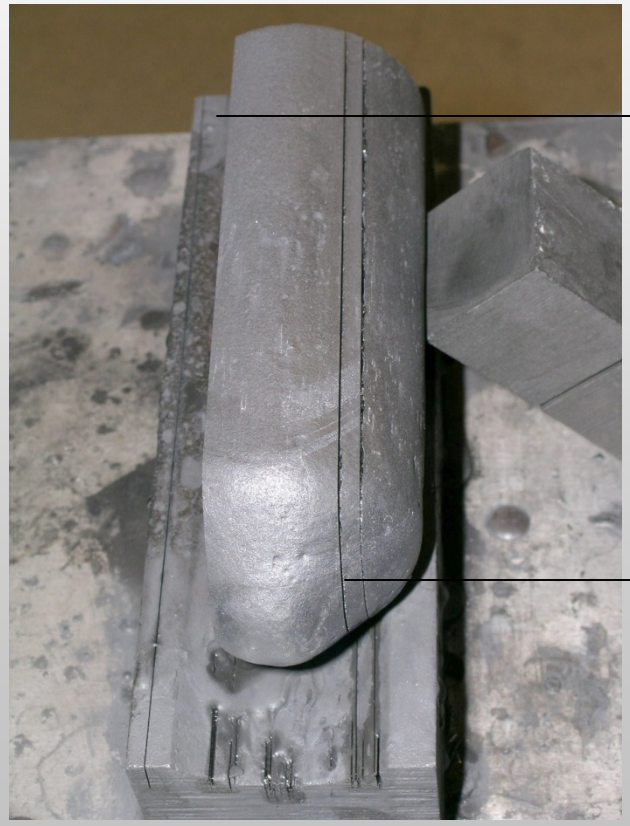

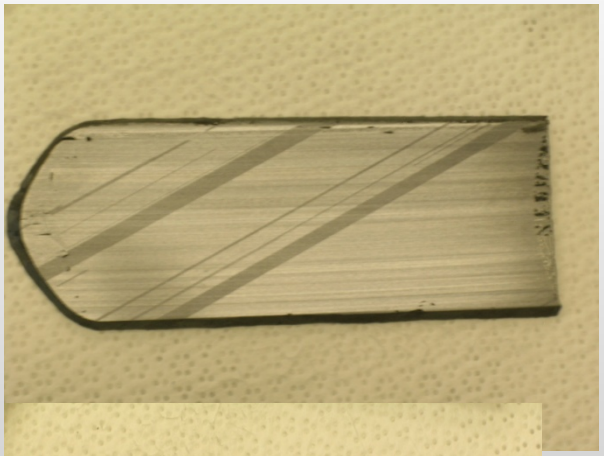

Sample Characterization

10x10mm Samples are cut from vertical slice 3mm thick

Purity and dopant measurements are performed by GDMS analysis taken at the tip, mid and heel

$\mu\tau_e$'s are preformed by fitting the Hecht relation at 0.5μsec shaping

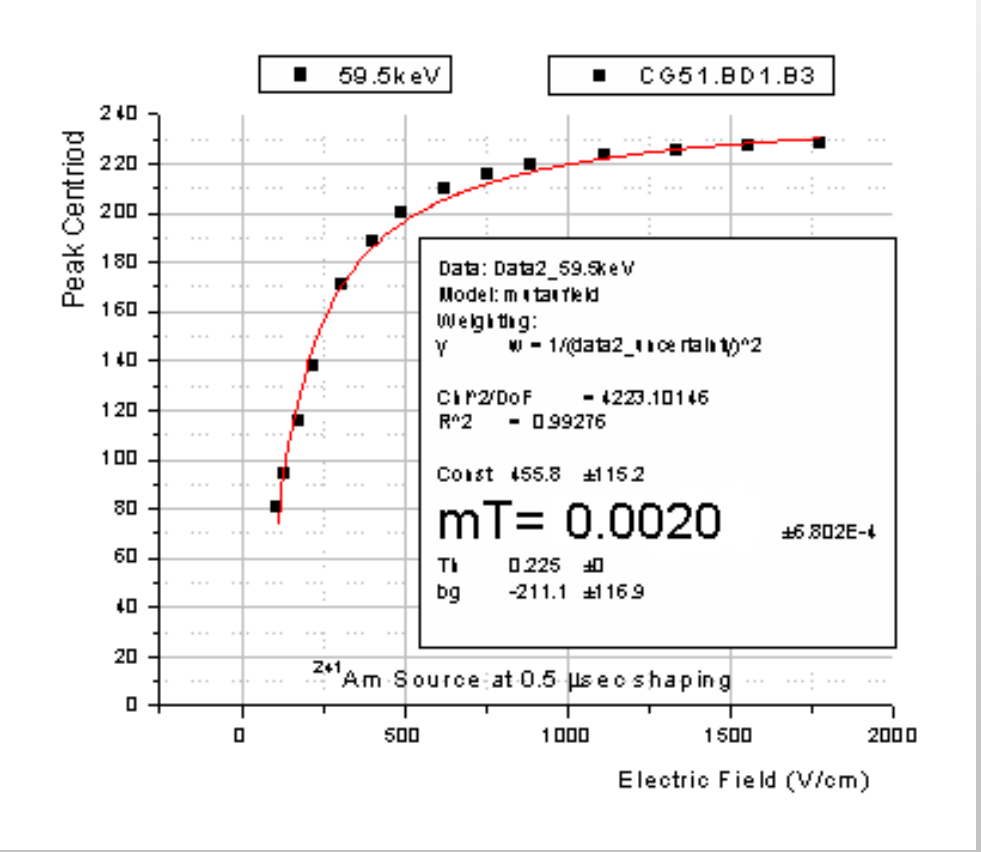

WASHINGTON STATE UNIVERSITY

World Class. Face to Face.

Single Images to a DOF

(top)
Image 1

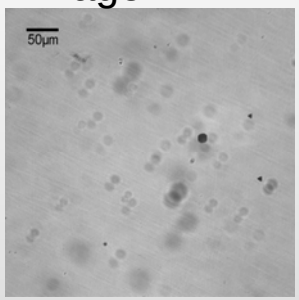

Image 2

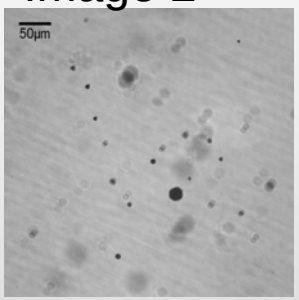

Image 3

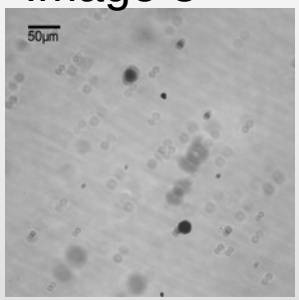

Image 4

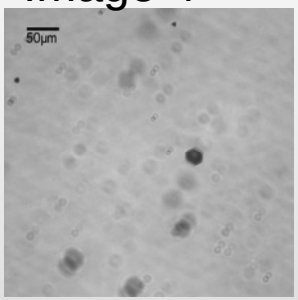

Image 5

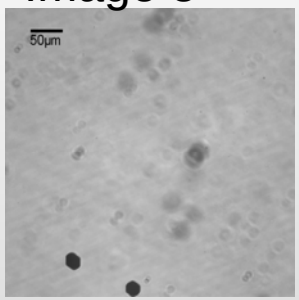

(Bottom)
Image 6

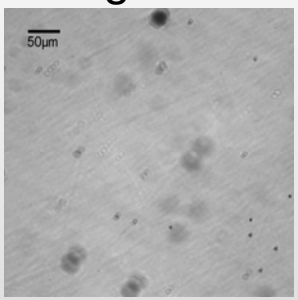

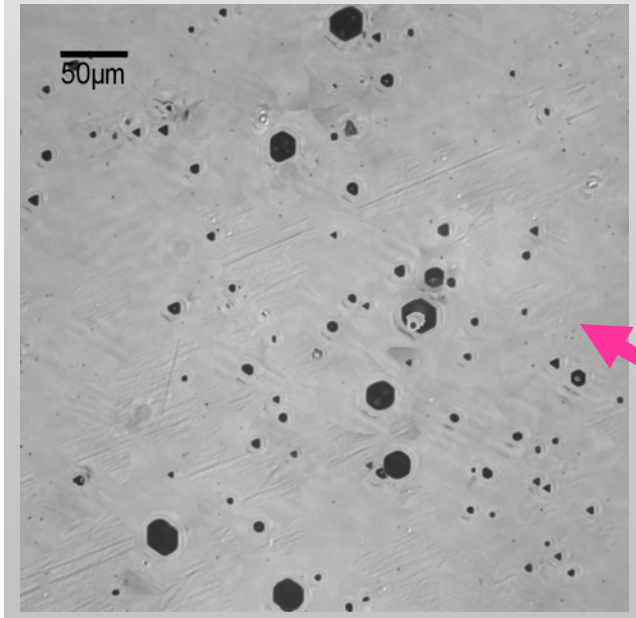

- Depth of Field images is over a detector 2-3 mm thick
- Images 1-6 are spaced in 100um distances.
- **71 Images** were used to generate the DOF image (8um between images)

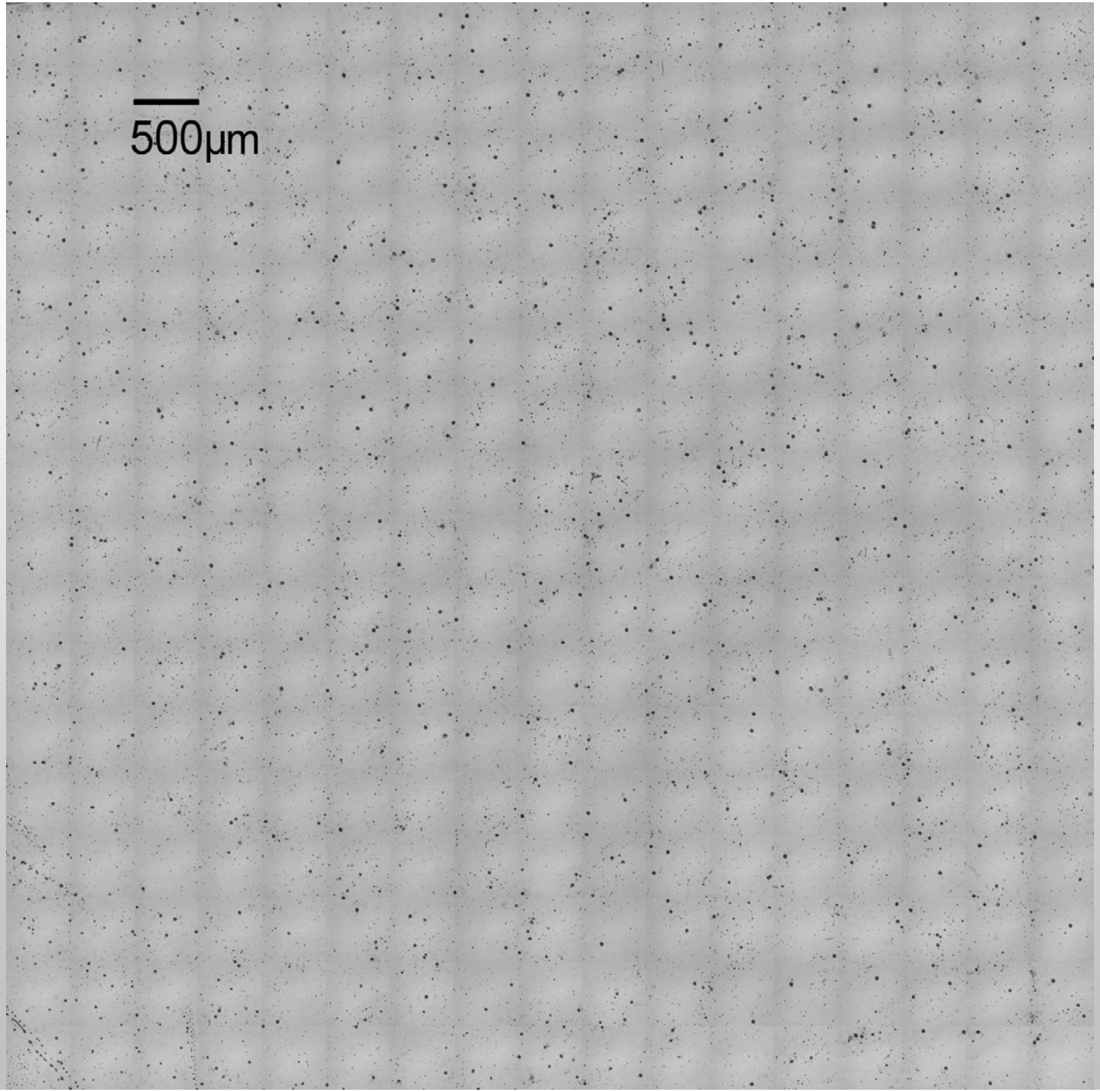
500μm

Sample Characterization

Darker region Zn ⬇

Can estimate Zn composition

Te inclusions affecting $\mu\tau_{\varepsilon}$

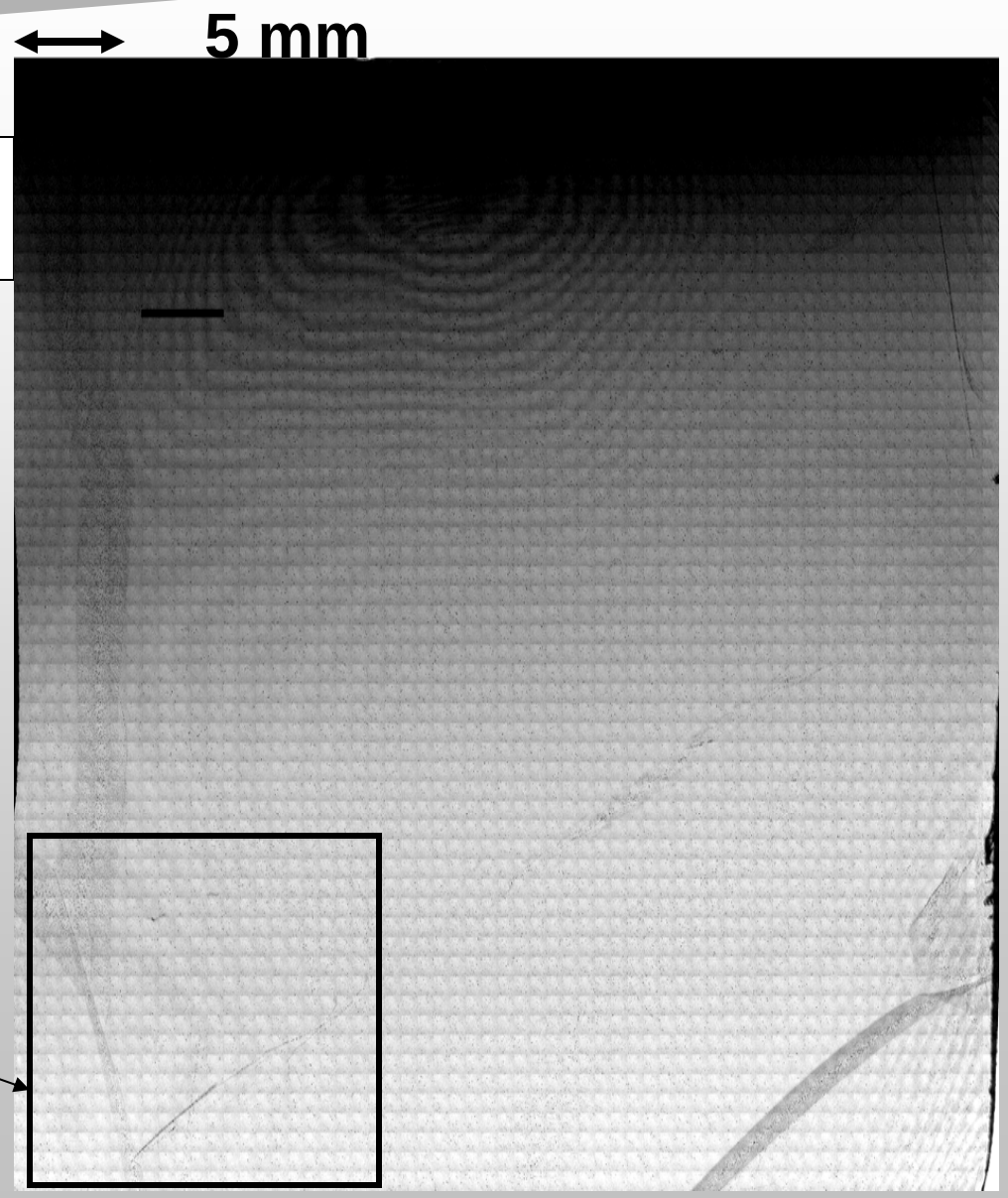

Expanded region
Next slide

Expanded Region of Full Slice Displaying a bad region of Te inclusions

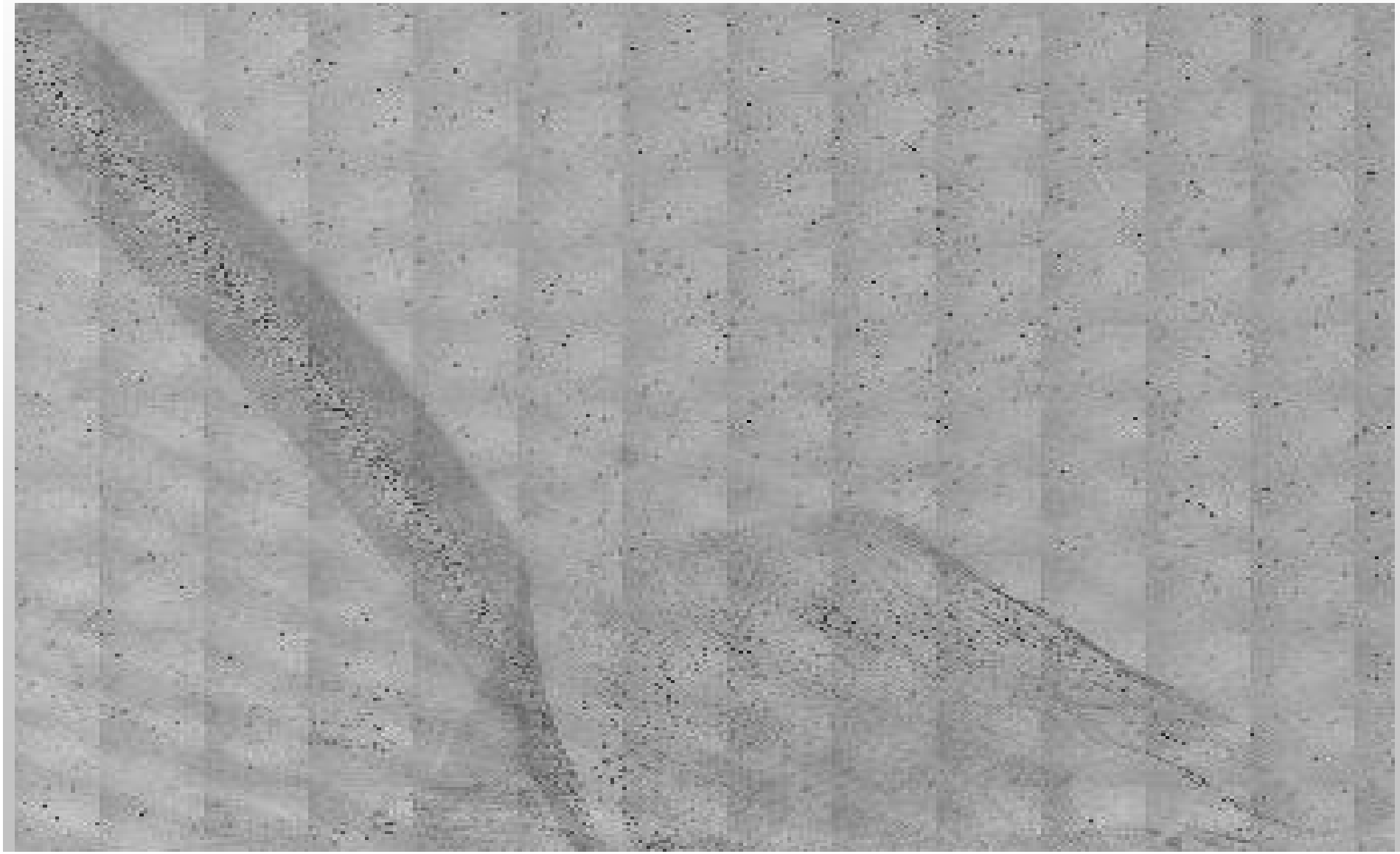

Determining the origin of the Te inclusion is key to removing them in growth.

Note shape:
Triangles
Hexagons
Larger circles

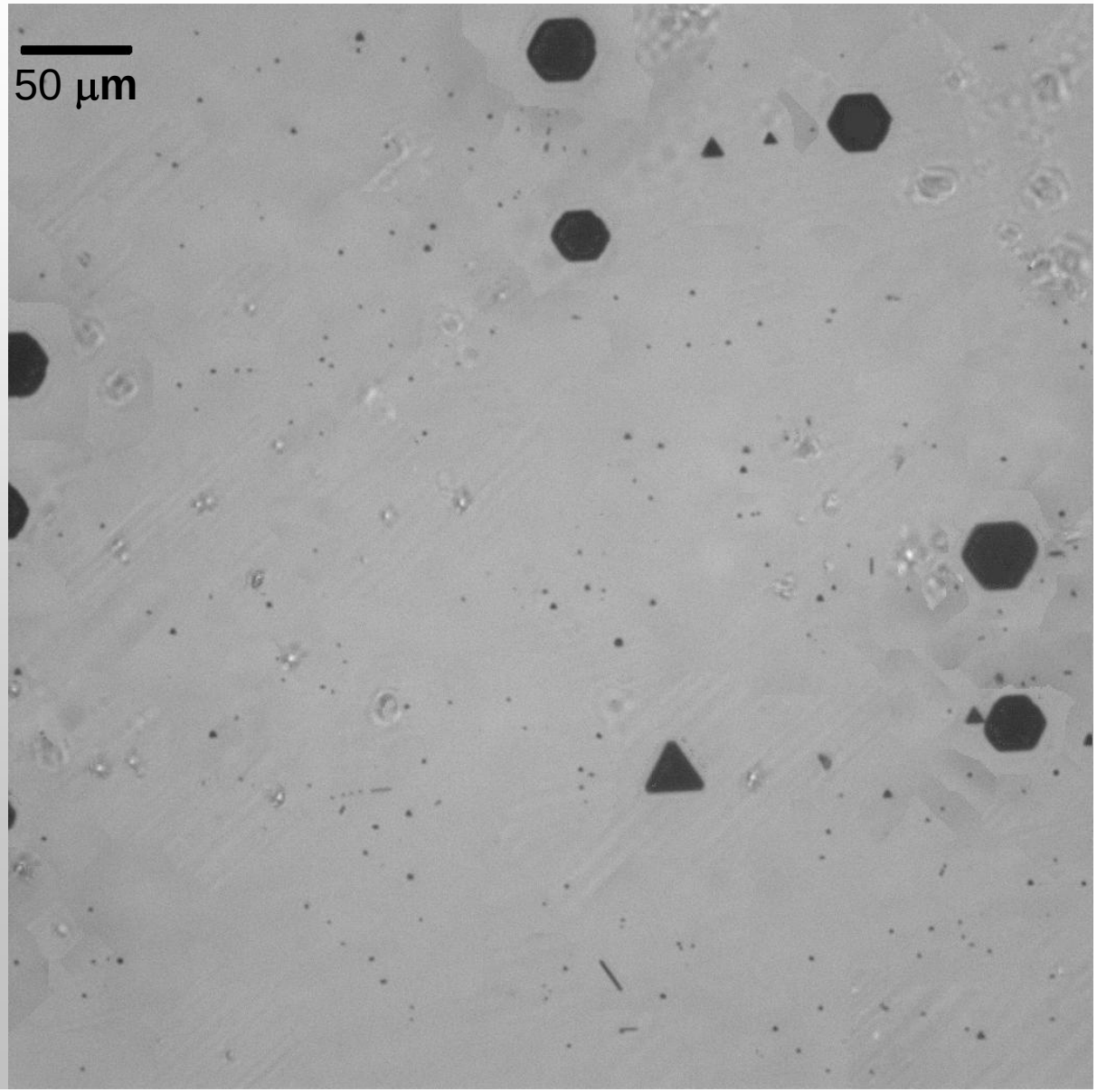

Single Crystal

- CG39 Single Crystal
  - Ave. $\mu\tau_e$ = 2.35x10^{-4} cm^2/V
  - Ave. Bulk resistivity 1.23x10^{10} Ohm*cm
  - Ave. Aluminum concentration 4200 ppb
  - Deep level impurity Chromium 10 ppb

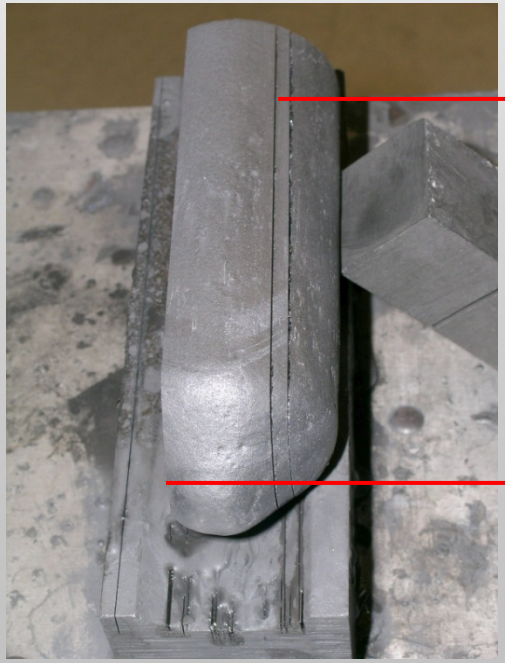

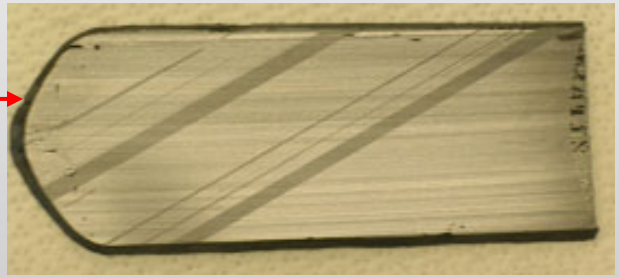

Results

- Graphite Coated Quartz
  - Average Indium Concentration
    - 11000 ppb
  - High resolution planar contacts
  - $\mu\tau'_e$ ave = $1.1 \times 10^{-3} cm^2/V$

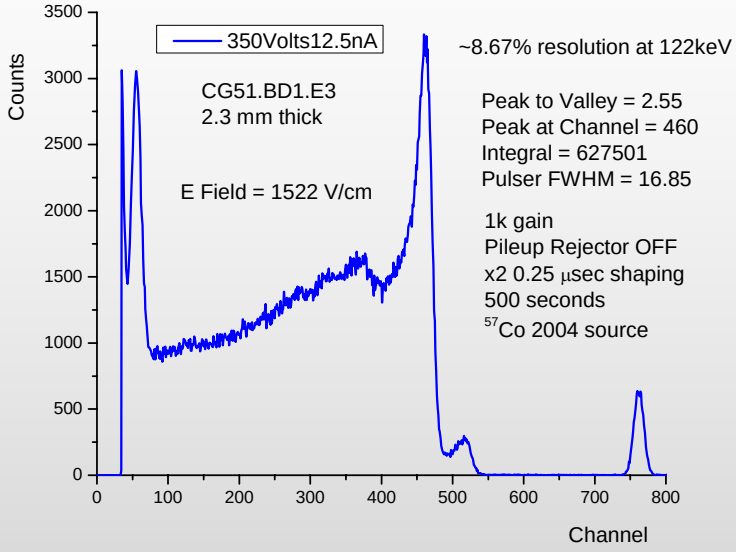

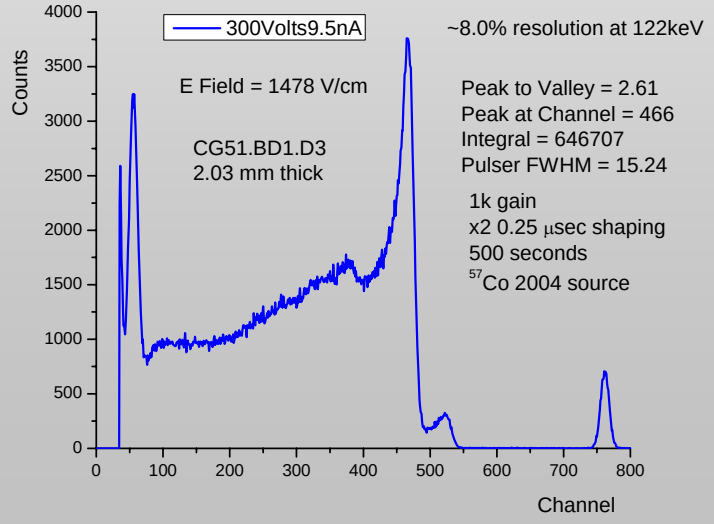

Typical Te inclusion count

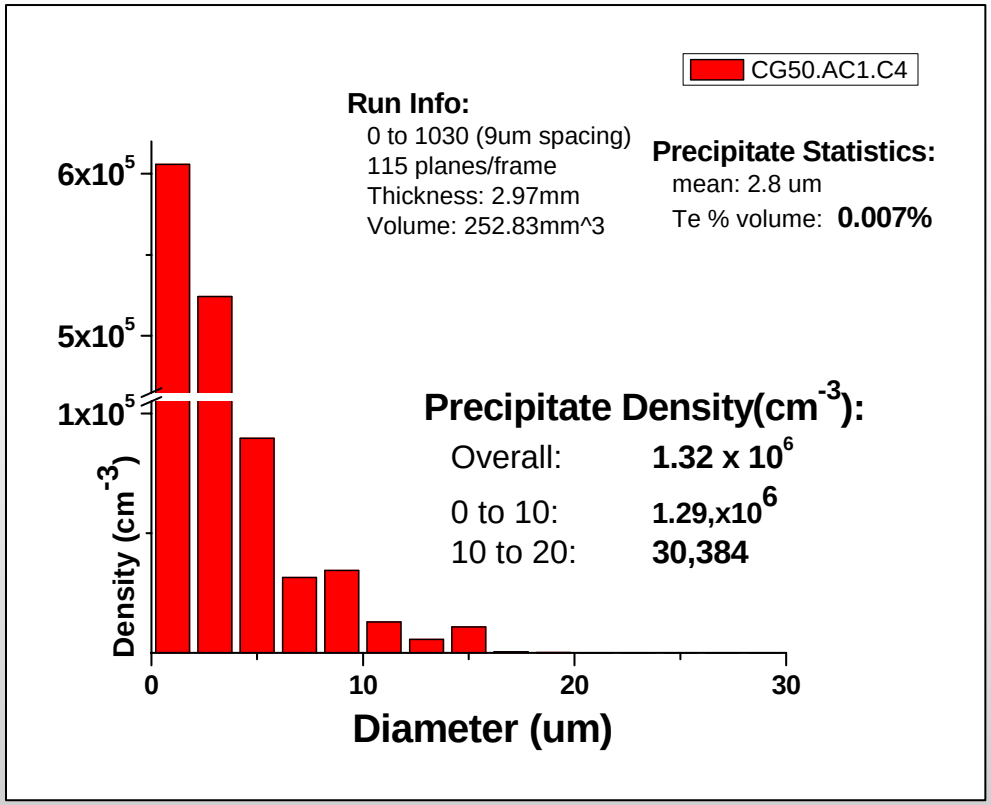

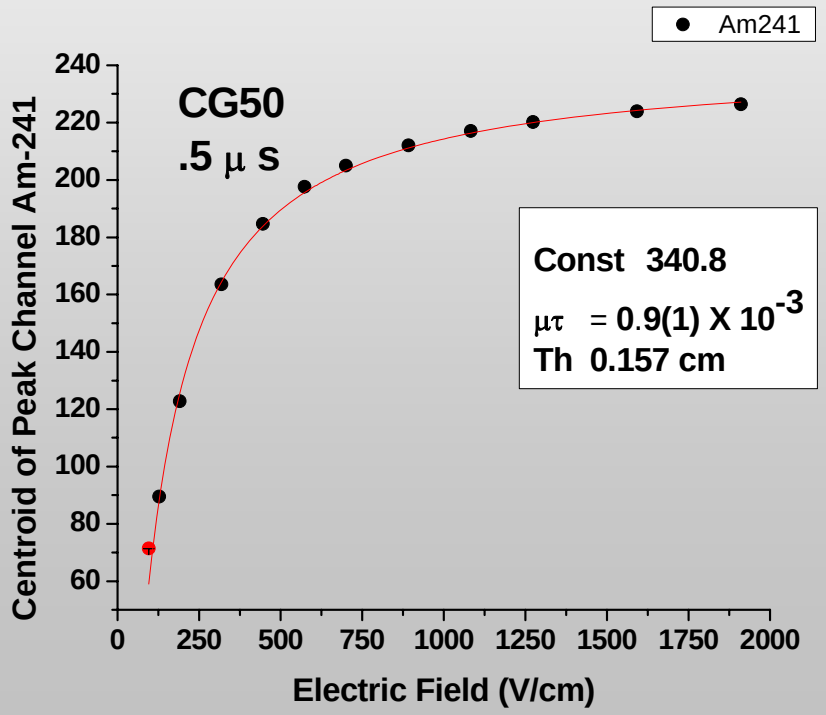

Purity

- Region of $\mu\tau_e = 2x10^{-3}$ cm^2/V
  - GDMS analysis
  - Indium Concentration
    - 1400 ppb
  - High purity
  - Total impurities minus dopants
    - 444 ppb
  - Large grain
  - Tellurium inclusions
    - Smaller near the tip of ingot
  - Excess Tellurium
    - Excess Te/(Cd+Zn) = 0.93 atomic

Element Detected	GDMS (PPB at)
C	110
N	10
O	90
Mg	24
Al	210
Total	**444**
Zn	10%

Four ingots CZT

- High Yield on planar detectors
- Reproducible
  - 4 crystal growths
  - Ave. $\mu\tau_e$'s = 1.74×10^{-3} cm^2/V

Row	Bulk Resistivity (Ohm*cm)	$\mu\tau$ e's (cm^2/V)	CdZnTe AC Slice
G	7.8×10^{9}	0.80E-3	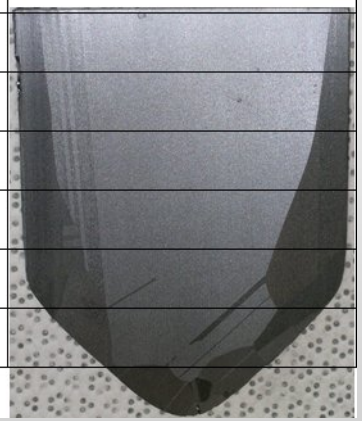
F	1.18×10^{10}	1.87E-3	
E	2.2×10^{10}	1.72E-3	
D	2.5×10^{9}	2.00E-3	
C	2.8×10^{10}	1.54E-3	
B	3.1×10^{10}	0.97E-3	

Scaled to 3 microsecond shaping

Row	Bulk Resistivity (Ohm*cm)	$\mu\tau$ e's (cm^2/V)	CdZnTe AC Slice
F	1.5×10^{10}	0.79E-3	
E	1.9×10^{10}	1.31E-3	
D	3.0×10^{10}	1.14E-3	
C	3.9×10^{10}	1.27E-3	
B	2.7×10^{10}	1.45E-3	

Scaled to 3 microsecond shaping

Row	Bulk Resistivity (Ohm*cm)	$\mu\tau$ e's (cm^2/V)	CdZnTe AC Slice
G	0.8×10^{10}	1.28E-3	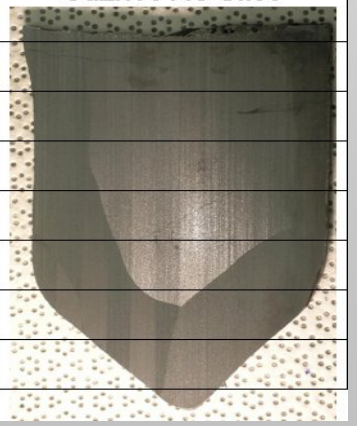
F	1.2×10^{10}	1.65E-3	
E	1.3×10^{10}	1.96E-3	
D	1.2×10^{10}	2.73E-3	
C	2.3×10^{10}	3.09E-3	
B	2.1×10^{10}	4.36E-3	
A	2.0×10^{10}	1.99E-3	

Scaled to 3 microsecond shaping

Row	Bulk Resistivity (Ohm*cm)	$\mu\tau$ e's (cm^2/V)	CdZnTe AC Slice
H	8.3×10^{9}	1.35E-3	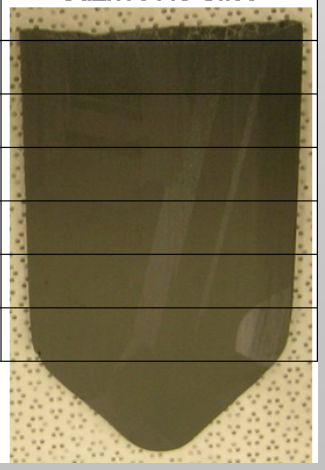
G	2.7×10^{10}	1.39E-3	
F	2.8×10^{10}	1.59E-3	
E	4.4×10^{10}	1.58E-3	
D	2.0×10^{10}	3.67E-3	
C	3.2×10^{10}	1.54E-3	

Scaled to 3 microsecond shaping

Summary

- Ingots produced various detectors with traceable properties and yields
- Consistently reducing impurities and Te inclusions
- Identified intrinsic defect complexes in CdTe & CZT and measured cross sections.
- Some impurities in amounts >10 ppb atomic have changed $\mu\tau_e$ significantly
- Proposed and implemented <u>modifying</u> intrinsic complexes by co-doping in CZT.
- Adjusted temperature gradients & growth conditions and have improved to $\mu\tau_e$ **~3 x 10^{-3}**

Capability improvement:

- **Clean room facilities**
- **Constructed infrared microscopy for Te mapping**
- **Furnace improvements**

Technical challenges:

- **Reproducible single crystal growth**
- **Minimizing Te inclusions & precipitates**
- **Need to develop weighting function for affect of Te**

Future work

- **Implement second furnace-need increased funding**
- **Minimize inclusions and precipitates**
- **Seeded crystal growth**
- **Develop compensation scheme-continued**
- **Large single crystal with high yield and active volume**

- **Thanks to NNSA-DOE Dr. Robert Mayo**

- Collaborators:
  - **Mary Bliss and others at PNNL for charactization**
  - **Su-Huai Wei--*National Renewable Energy Laboratory-Theory***
  - **Paul Luke-UC Berkley**
  - **Kansas State have measured various early samples.**
  - ***Jeff Derby – University of Minnesota***

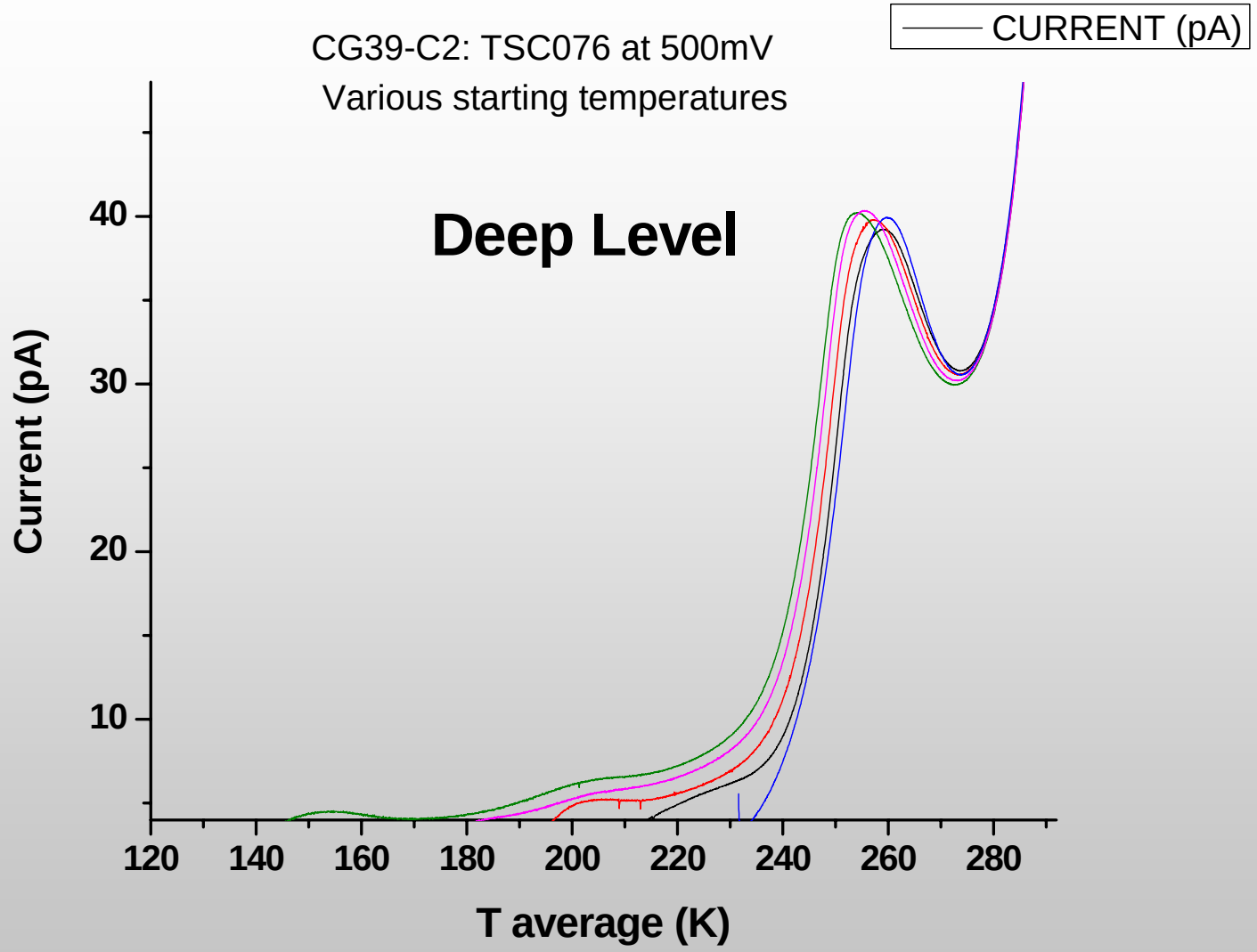

Annealing still good after annealing to 170 C
In the tip showing stable deep level.

WASHINGTON STATE UNIVERSITY
World Class. Face to Face.

Results- Larger dia >37μm Det. B

- Detector A
  - Inclusions: 661,471 cm^{-3}
  - Mean dia: 2.74 um
  - Te Volume: 0.85 $x10^{-2}$ %
  - $\mu\tau$: 8 $x10^{-4}$ cm^2/V
- Detector B
  - Inclusions: 613,753 cm^{-3}
  - Mean size: 2.81 um
  - Te Volume: 1.2 $x10^{-2}$ %
  - $\mu\tau$: 4.5$x10^{-4}$ cm^2/V

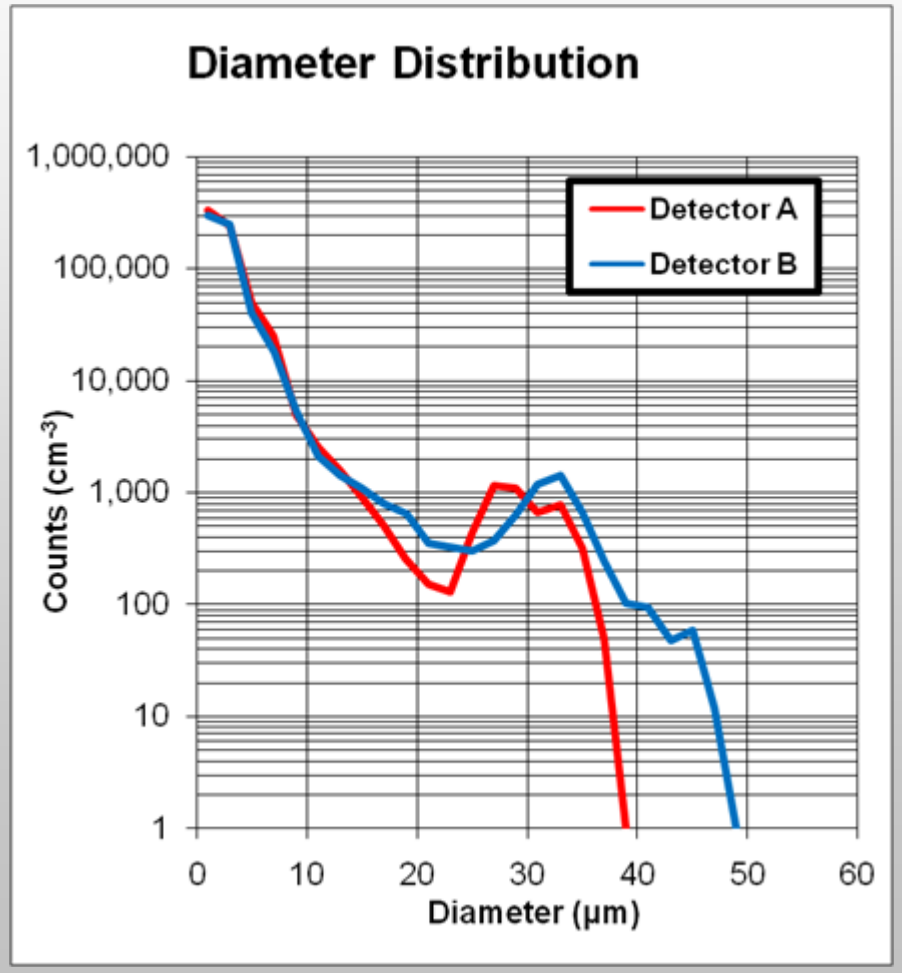

Inclusions are key but only when other parameters are controlled

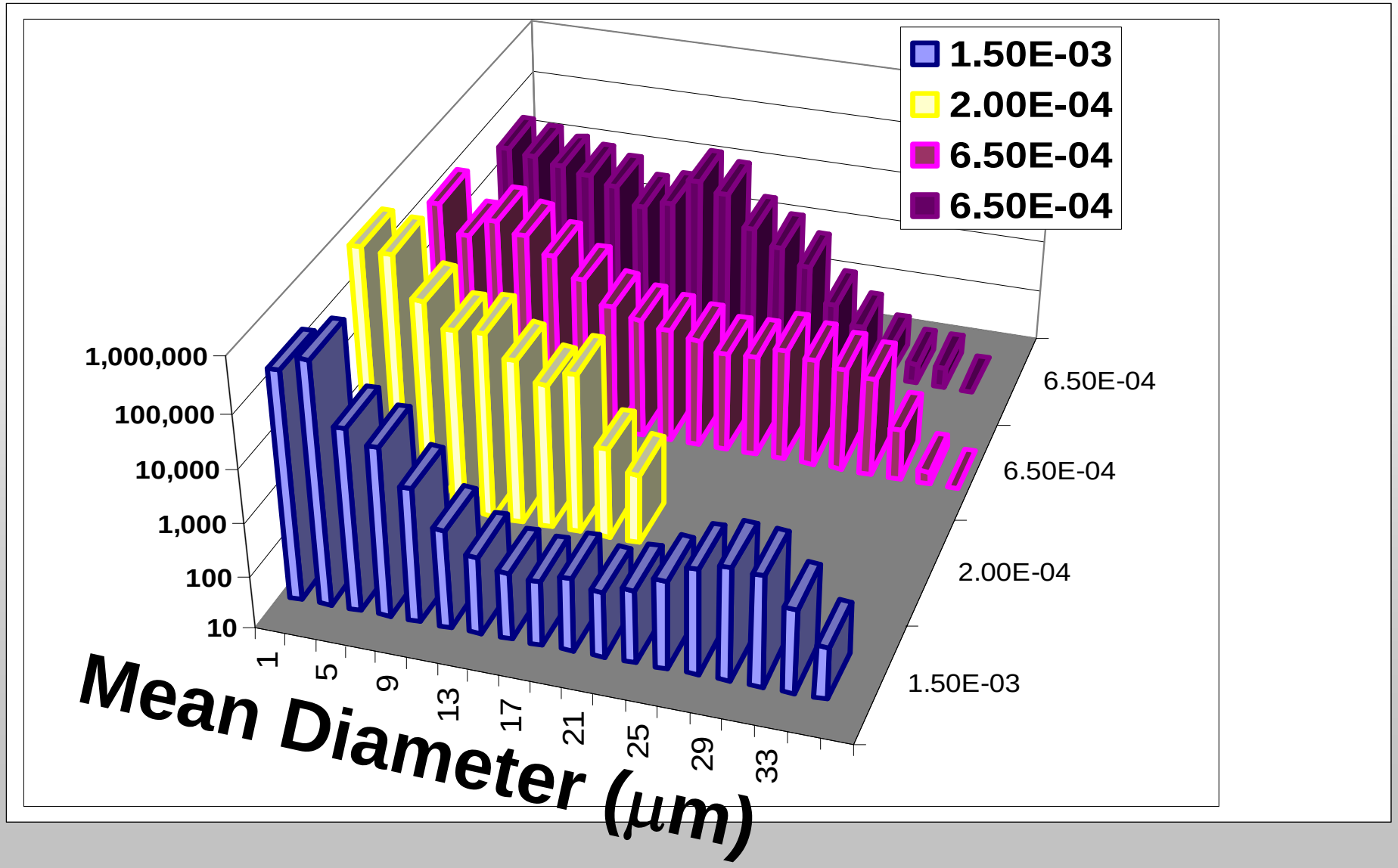

Table of Basic Defect Levels

Trap	Tmax ±1K	Energy (eV)	Trap Cross Section (cm2)	Defect level
1	18 -		-	D: Al Donor
2	33	0.06[05]	$3.6[07]\times10^{-16}$	Iso1 : $(V_{Cd}+O_{Te})^{-/0}$
3	48	0.1[04]	$7.4(5)\times10^{-16}$	V1: $Vcd^{-/0}$
4	60	0.12-0.13	$5(4)\times10^{-16}$	Ac: $(V_{Cd}+Al_{Cd})^{-/0}$
5	92	0.19[05]	$6(4)\times10^{-16}$	Iso2 : $(VCd+O_{Te})^{2-/-}$
6	115	0.23 to 0.25	$5(3)\times10^{-16}$	V2: $VCd^{2-/-}$
7	147	0.39 to 0.43	$4(2)\times10^{-13}$	T: $(TeCd)^{0/+}$
8	180	0.46[03]	$1.1(1)\times10^{-14}$	TV1: $(TeCd + 2VCd)^{2-/-}$
9	245	0.69-0.71	$3.5(2)\times10^{-13}$	TV2: $(TeCd + V\ Cd)^{-/0}$ $(TeCd+2VCd)^{3-/2-}$
10	260	0.79[06]	$1.58[1]\times10^{-12}$	TV3: $(TeCd + VCd)^{2-/-}$)

Materials and Devices for Room Temperature Gamma Ray Spectrometers

NNSA REVIEW

D.S. McGregor, E. Ariesanti, A. Brooks,
A. Hageman, M.J. Harrison, A. Kargar,
T. Krehbiel, R. Lowell, M. Meier, P. Ugorowski, R. White

Semiconductor Materials and Radiological Technologies (SMART) Laboratory

Dept. of Mechanical and Nuclear Engineering Kansas State University, Manhattan, KS 66506

National Nuclear Security Administration

Semiconductor Materials And Radiological Technologies ©

The Semiconductor Materials and Radiological Technologies (S.M.A.R.T.) Laboratory

Radiation Detector Design and Assembly

Crystal Growth
Lapping and Polishing
Semiconductor Processing
Metallization and Coatings
Electronics and Packaging
Testing and Characterization

Over 30 graduate and undergraduate students are working in the SMART Lab!

National Nuclear Security Administration

Semiconductor Materials And Radiological Technologies ©

Project Tasks

1. **$LaBr_3$**
   a) Handling and packaging
   b) Purification
   c) Crystal growth
2. **CdZnTe/CdMnTe**
   a) Vacuum distillation of Cd, Zn, Mn, and Te
   b) Zone melting and zone refining of Cd, Zn, Mn, and Te
   c) Reaction of binaries
   d) Crystal growth
   e) Post-growth annealing
3. **HgI_2**
   a) Purification
   b) Crystal growth
   c) Detector Preparation
4. **CdZnTe Frisch Collars**
   a) Design
   b) Manufacturing
   c) Characterization

National Nuclear Security Administration

Semiconductor Materials And Radiological Technologies

©

Ampoule Enclosure System

We have built a customized ampoule station with five ports for use in all aspects of the crystal growth projects at KSU.

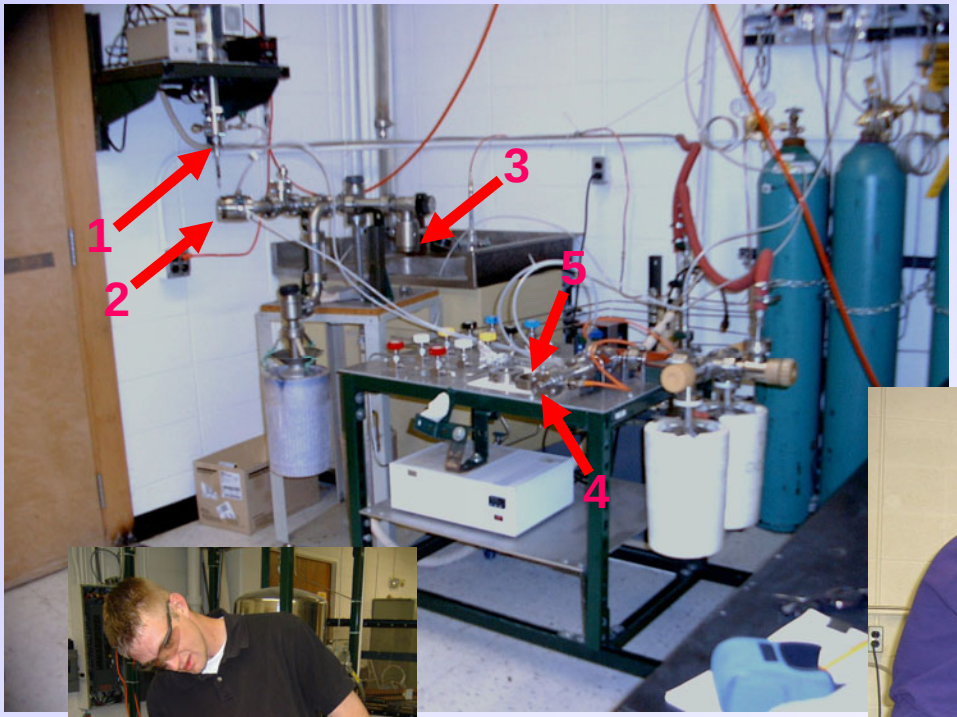

1. Uses oil free sorption pumps for vacuum between 10^{-2}-10^{-4} torr.
2. Uses oil free turbo pump for vacuum between 10^{-4} -10^{-7} torr.
3. Capable of delivering high purity gases into the ampoules for growth processes.

National Nuclear Security Administration

Semiconductor Materials And Radiological Technologies

©

Ampoule Carbon Coating System

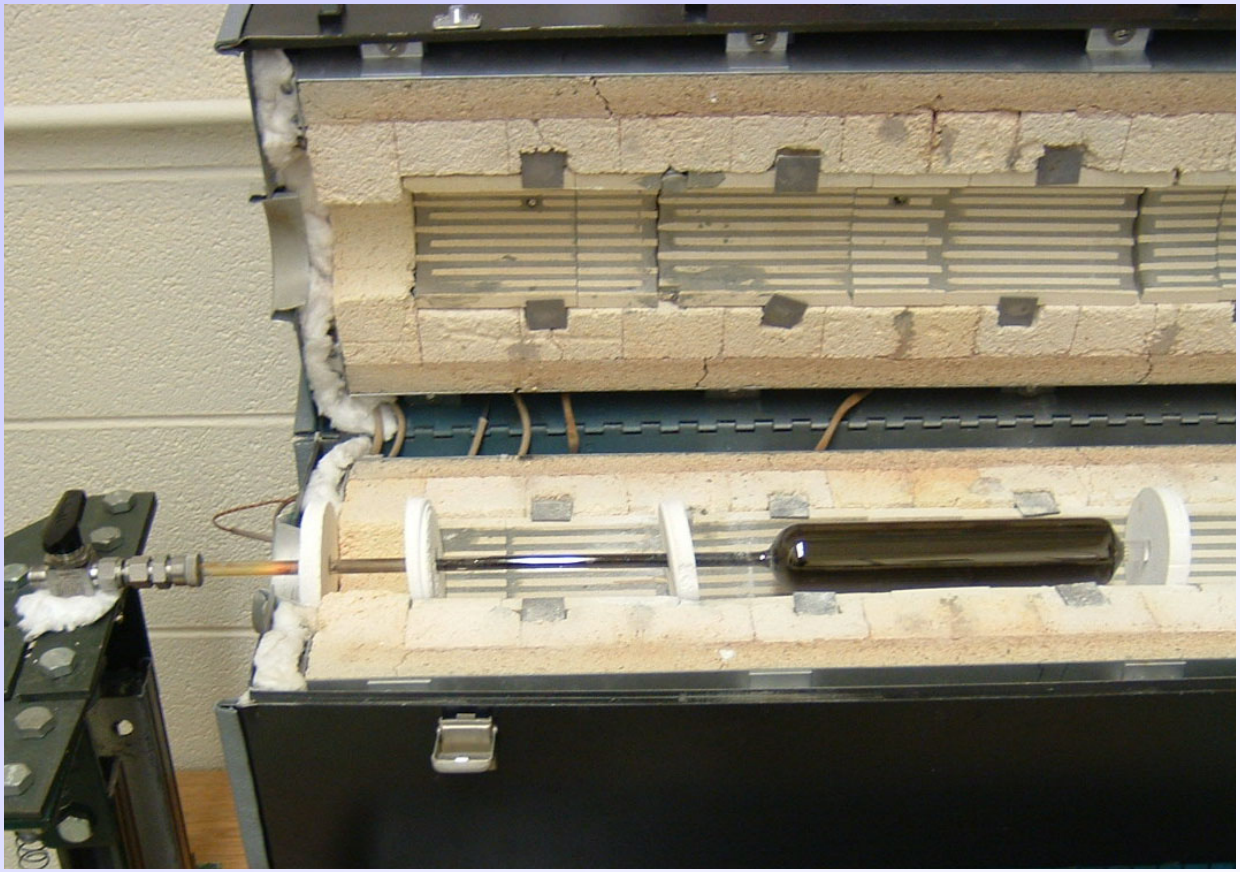

1. Repeatable carbonization and vitrification system.
2. Turnkey operation.

M.J. Harrison, A.P. Graebner, W.J. McNeil, and D.S. McGregor, “Carbon-Coating of Fused Silica Ampoules,” Journal of Crystal Growth, 290 (2006) pp. 597-601.

National Nuclear Security Administration

Semiconductor Materials And Radiological Technologies

©

$LaBr_3$ Handling and Packaging

- Ultra-dry, inert atmosphere glove box installed to handle the hygroscopic $LaBr_3$ material.
- Atmosphere within contains <1ppm H_2O and O_2
- Heat-sealed, metallized bags ensure material does not degrade in shipping.

Ultra-dry glove box for hygroscopic materials.

Ph.D. candidate, Mark Harrison, inspects a $LaBr_3$ ingot grown in the SMART Lab.

National Nuclear Security Administration

Semiconductor Materials And Radiological Technologies

©

$LaBr_3$ Purification

- Careful process design eliminates all exposure of the raw $LaBr_3$ material to atmosphere.
- Sublimation apparatus designed and constructed to remove impurities and filter oxybromides.
- Processing of $LaBr_3$ is in progress.

Mark Harrison operates the custom designed $LaBr_3$ sublimation purification system.

National Nuclear Security Administration

Semiconductor Materials And Radiological Technologies

©

$LaBr_3$ Crystal Growth

- A vertical Bridgman furnace, designed to grow $LaBr_3$ at angles varying from 0° to 30° from vertical, has been characterized.
- Five ingots of $LaBr_3$:Ce have been grown with improving yields.
- Samples of each ingot were sent to SNL for further analysis.

Vertical Growth Method Ingot Number 1

National Nuclear Security Administration

Semiconductor Materials And Radiological Technologies

©

$LaBr_3$ Crystal Growth

- Recently, growth of $LaBr_3$:Ce using the horizontal Bridgman method was trialed.
- Initial results are very promising.
- Two horizontal electro-dynamic gradient (EDG) furnaces committed to further researching the new method.

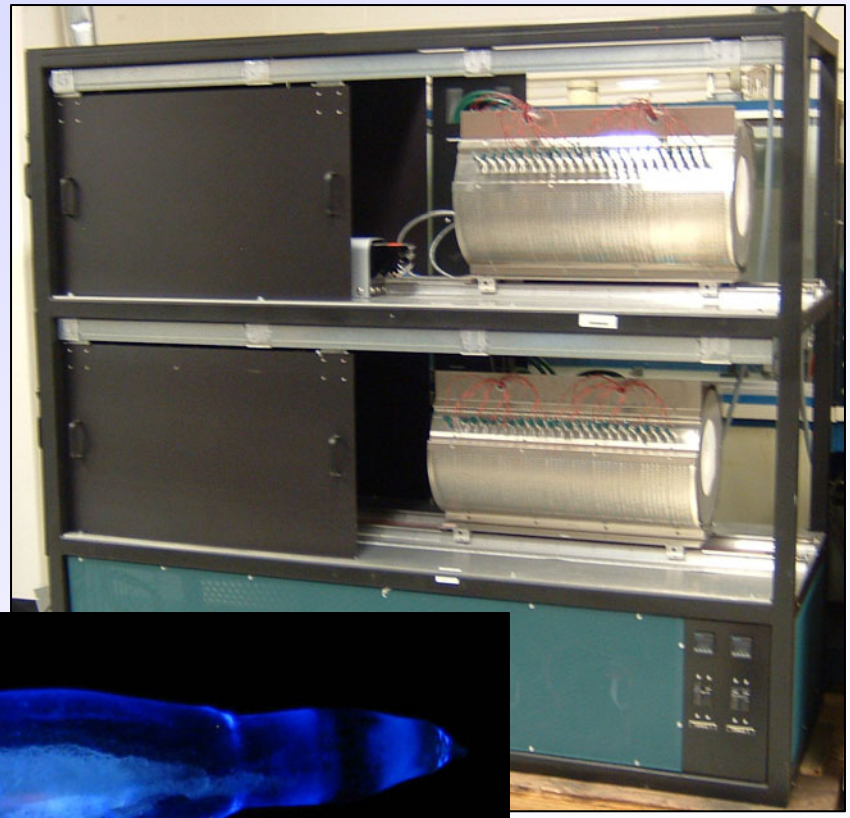

Horizontal Growth Ingot Number 1

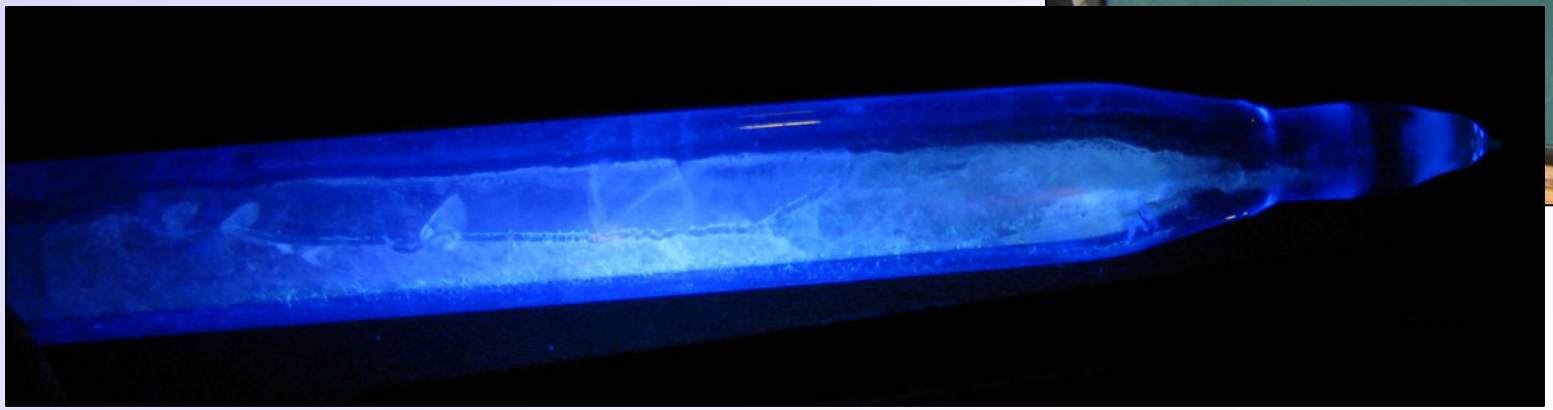

National Nuclear Security Administration

Semiconductor Materials And Radiological Technologies

©

$LaBr_3$ Crystal Handling

- Ability to cut, shape and polish as-grown ingots developed.
- Processing done completely under inert, dry atmosphere (<1ppm O_2 or H_2O).
- New capabilities/equipment:
  - Diamond-wire saw
  - Crystal mounting
  - Grinding
  - Polishing
  - PMT mounting

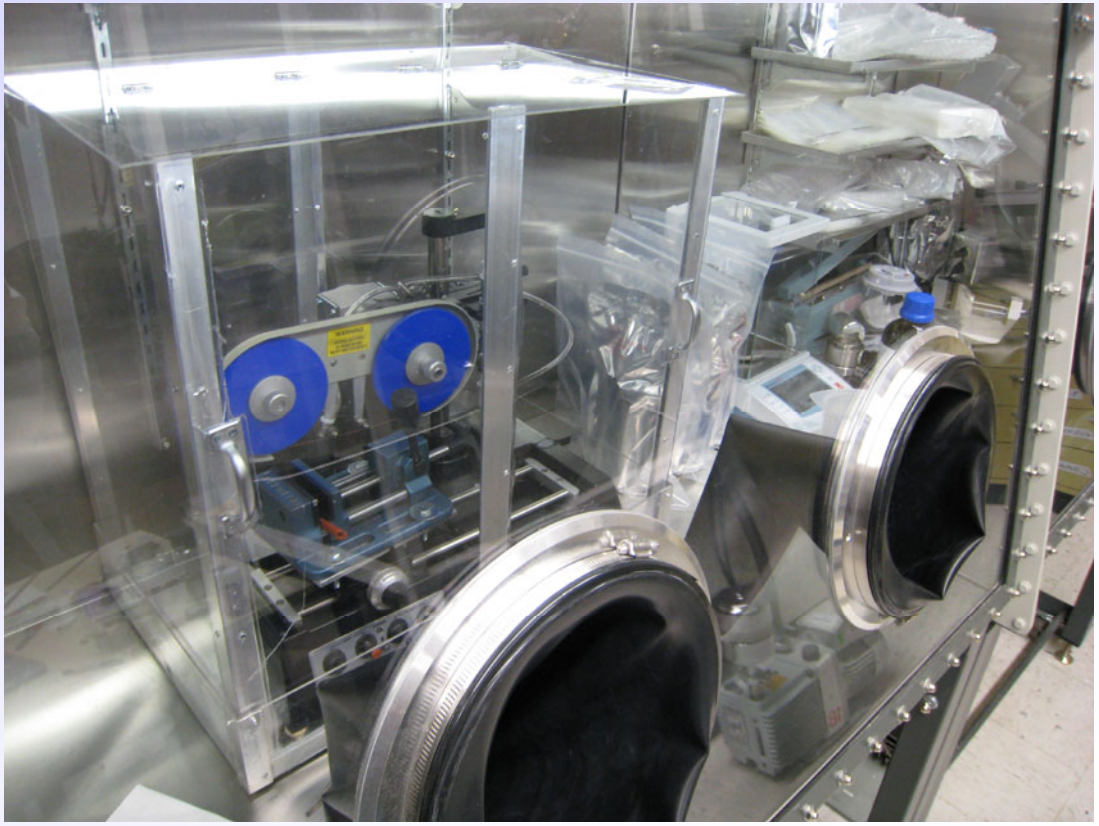

National Nuclear Security Administration

Semiconductor Materials And Radiological Technologies

©

$LaBr_3$ Crystal Analysis

- Several scintillation characterization capabilities added or in progress.
  - Spectroscopy
  - Light proportionality measurement
  - Thomas-Bollinger light decay constant measurement
  - Radioluminescence spectra

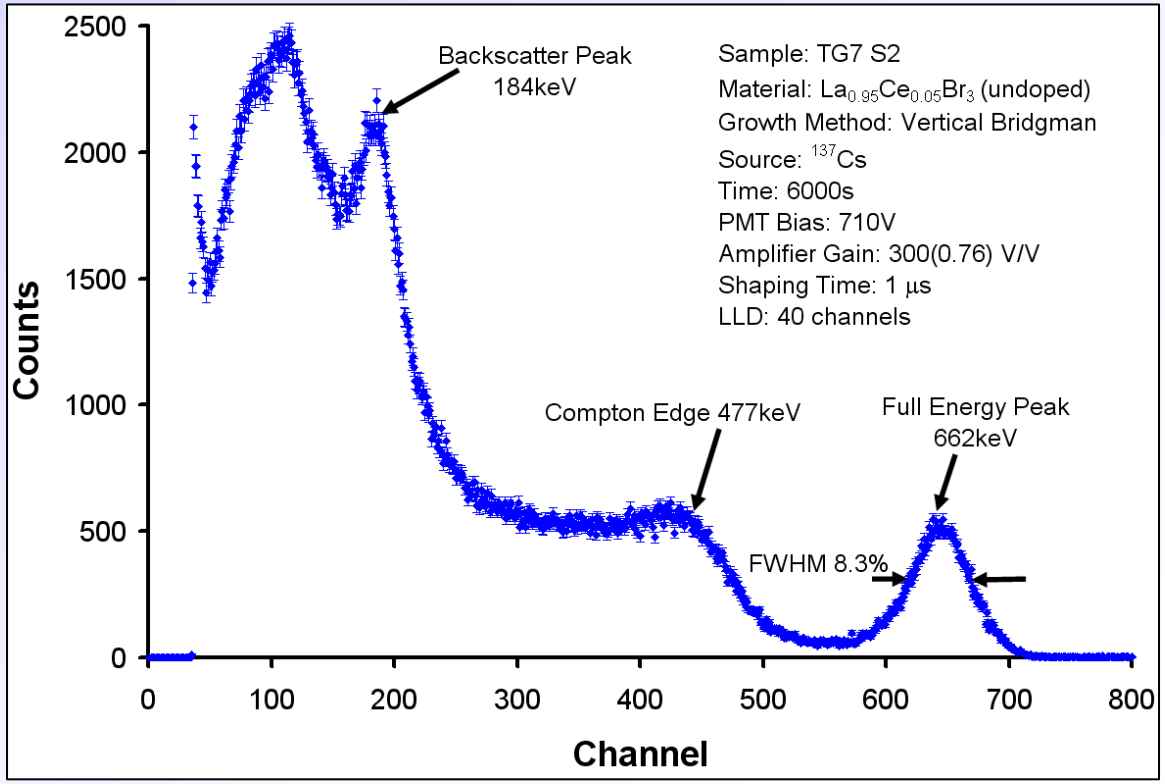

National Nuclear Security Administration

Semiconductor Materials And Radiological Technologies

©

New Scintillator Investigation

- Newly formed collaboration with SNL have yielded several candidate dopants to strengthen lanthanide halide scintillators.
- Expected **10X** increase in strength over current lanthanide halide scintillators.
- Improved strength means more rugged, easier to grow scintillators.

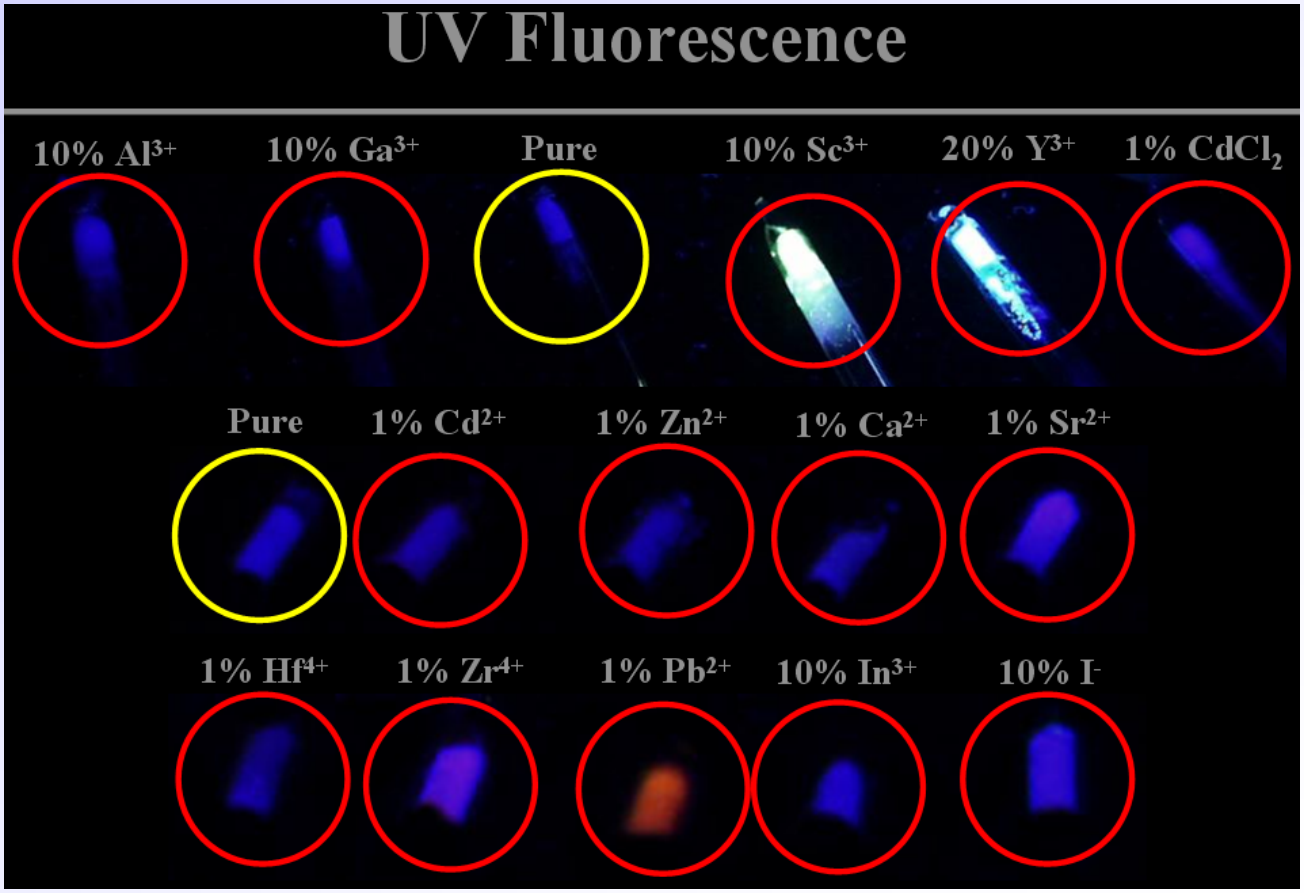

Appearance of doped $CeBr_3$ samples under UV illumination.

National Nuclear Security Administration

Semiconductor Materials And Radiological Technologies

©

Light Yield Characterization

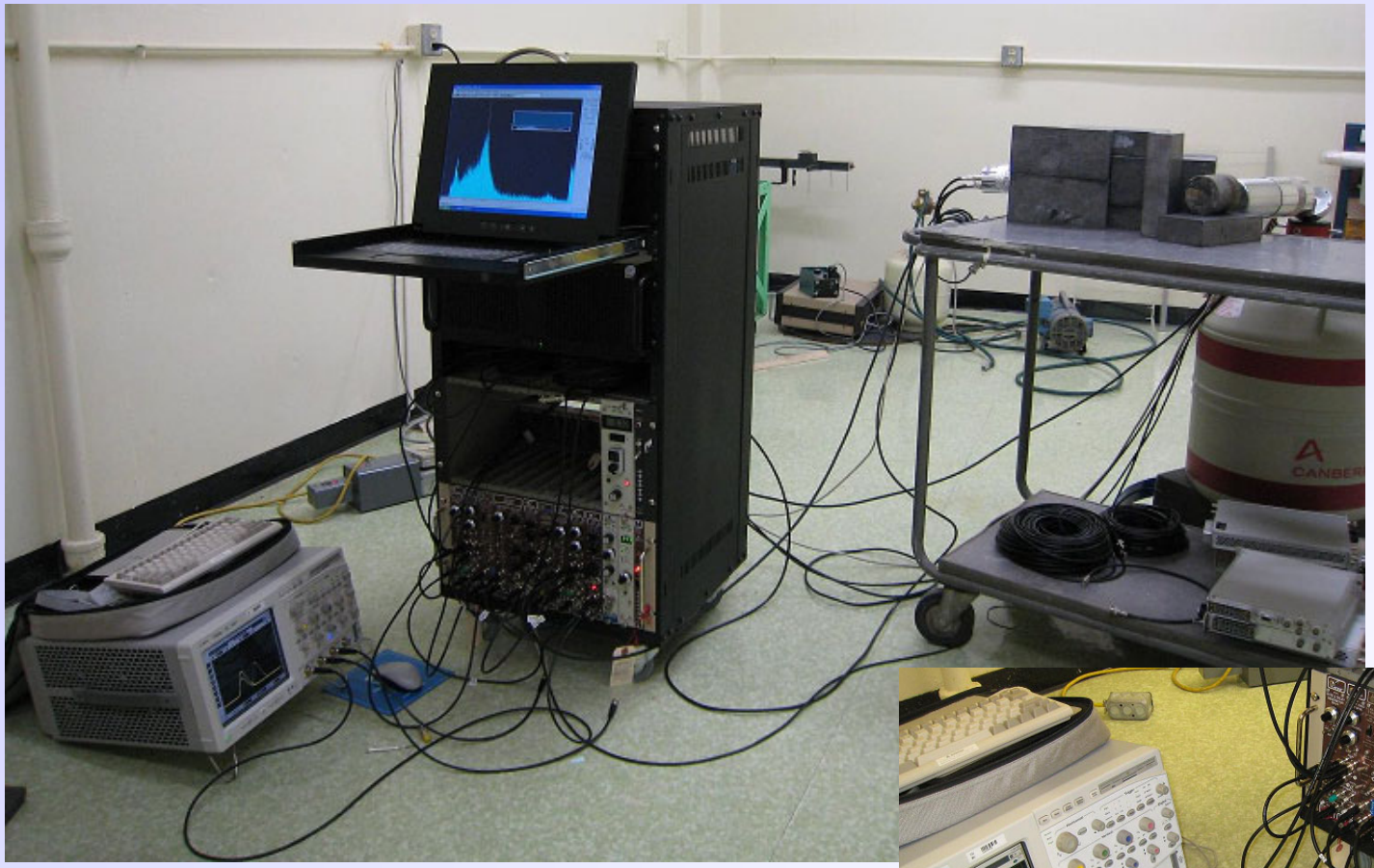

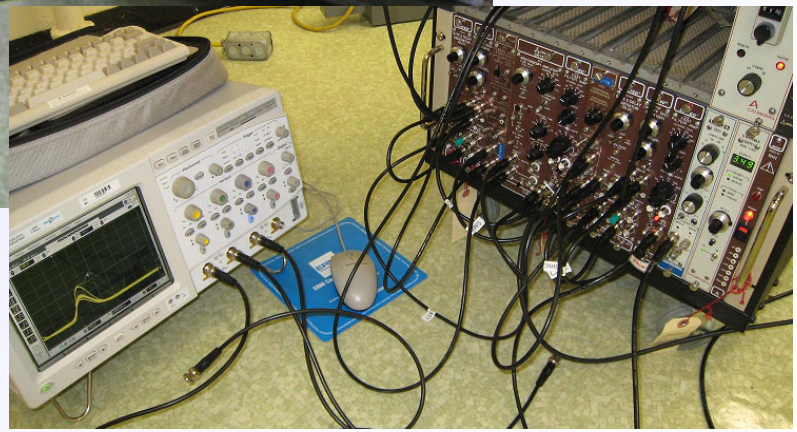

Ge-Scintillator Coincidence Test System

National Nuclear Security Administration

Semiconductor Materials And Radiological Technologies

©

Coincidence System

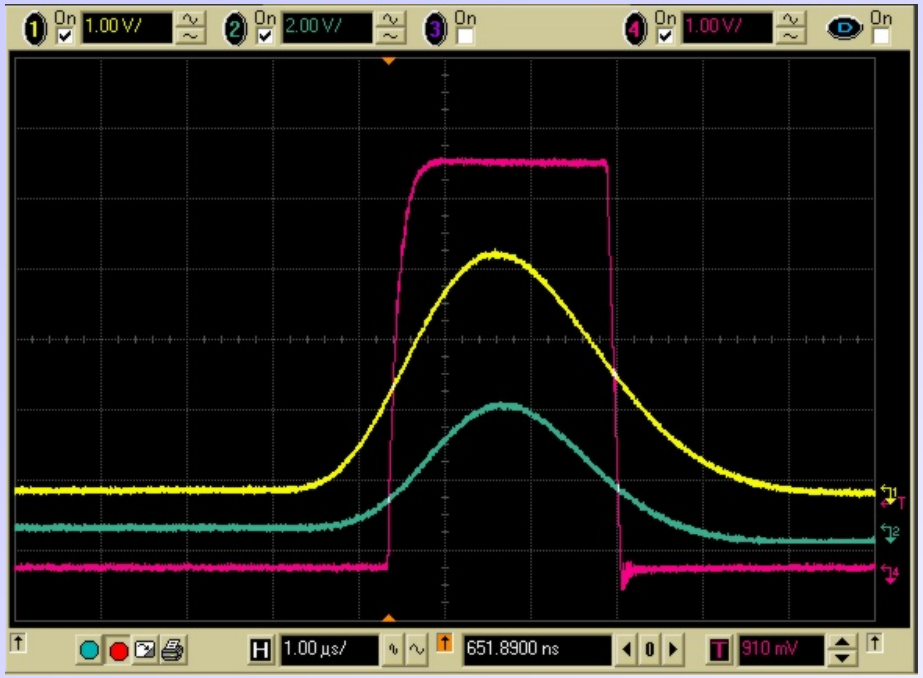

A scope trace showing (from top to bottom), the data-collection GATE signal, a NaI spectroscopic amplifier signal, and a Ge spectroscopic amplifier signal.

A comparison of two coincidence spectra, showing the shift in the main peak when the Compton-scattering angle was changed.

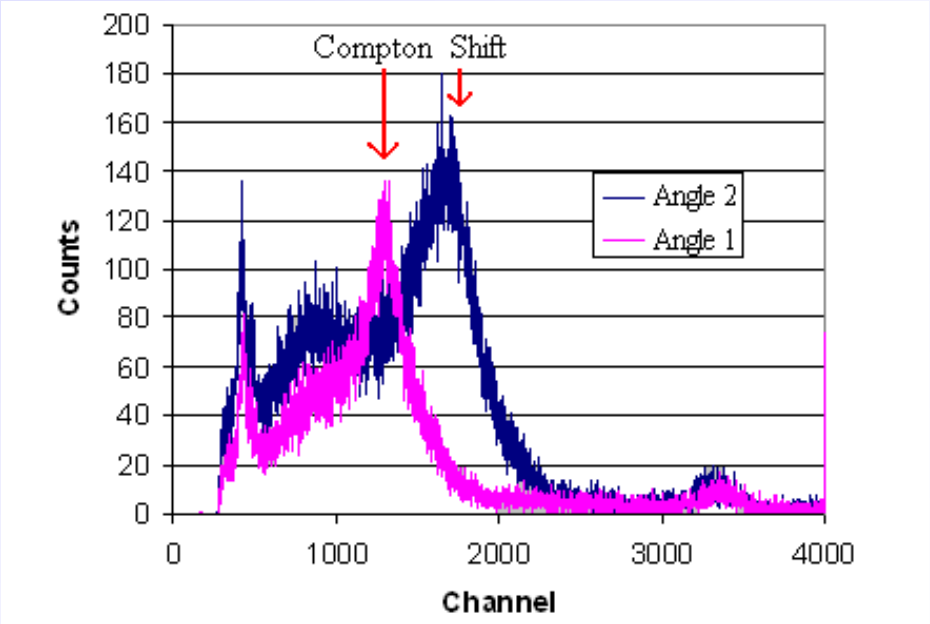

The Compton scattering coincidence setup should provide single-energy input photons of any desired energy, covering the energy range needed to characterize the spectral response of the new scintillators.

National Nuclear Security Administration

Semiconductor Materials And Radiological Technologies

CdZnTe

- CdZnTe materials research covers nearly every aspect of production.
  1. Raw material purification
  2. Compound synthesis and purification
  3. Crystal growth
  4. Post-growth annealing
  5. Device fabrication
- New vacuum distillation methods are being developed and characterized to purify Cd, Zn, and Te to purer levels faster.
- After synthesis of CdTe and ZnTe in a high pressure furnace, compound purification aims to improve purity levels to 8N or better.

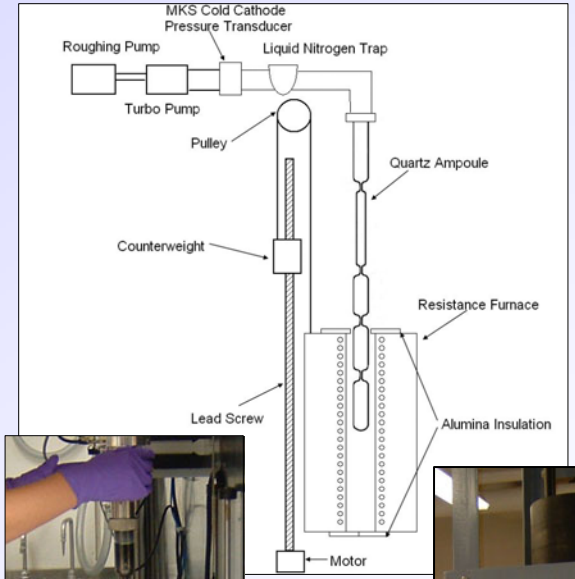

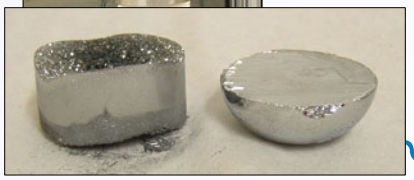

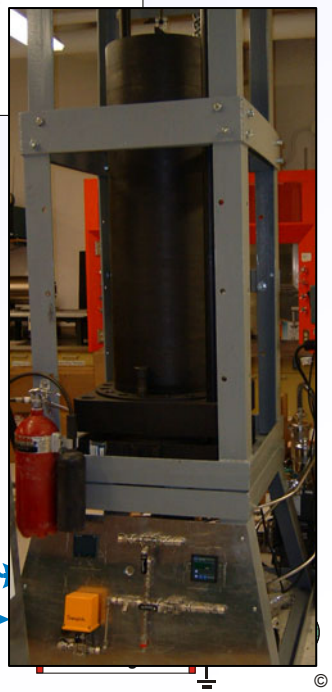

National Nuclear Security Administration

CdZnTe/CdMnTe Vacuum Distillation and Zone Melting

- Two vacuum distillation (VD) columns have been designed and built to purify raw elements Cd, Zn, Mn, and Te from 4N to 6N+ purity.
- System incorporates unique ampoule design to allow multiple distillations to occur without the need for material handling.
- Initial distillation runs with Te have successfully shown proof of concept of the new design.
- Multi-stage distillation process of Te and Zn have been characterized. Cd and Mn have been purified and awaiting impurity analysis

M.S. graduate student, Amy Hageman, and undergraduate researcher, Tyler Krehbiel, are preparing to operate the vacuum distilling system.

National Nuclear Security Administration

Semiconductor Materials And Radiological Technologies

©

Five Stage Ampoule Design Advantages:

- Multi-stage distillation without handling materials
- Removal of residual material after each stage

Ampoule sections containing the thrice-distilled Te and the 3 residues from each stage

Distilled tellurium, after one vacuum distillation stage

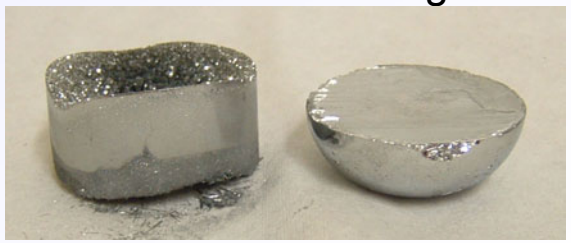

Singly distilled Te | Residue

National Nuclear Security Administration

A.M. Hageman, M.J. Harrison, N. Fritz , T.N. Krehbiel, R. White, J. Patenaude, D.S. McGregor, "Purification of Tellurium to 6N Using a Multistage Vacuum Distillation Method," Proc. SPIE, 6707 (2007) pp. 0Z1-0Z7.

Semiconductor Materials And Radiological Technologies ©

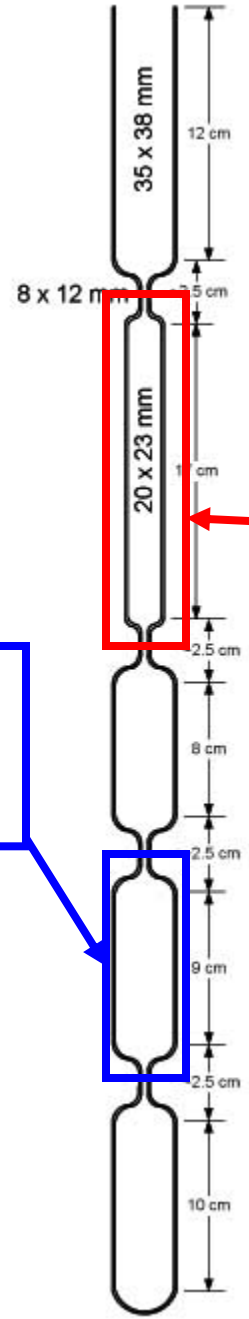

Three Stage Purification (Zinc)

One Stage Purification (Zinc)

Redesign of Ampoule:

- Less volume per successive distillation stage
- Final stage is optimized for zone melting

Tellurium Purification Results

	4N+ Starting Material	One Stage VD	Two Stage VD	Three Stage VD
Na	0.2	0.1	0.02	0.04
Al	0.03	0.009	0.01	0.01
Si	0.02	< 0.005	< 0.005	0.009
Cl	0.2	0.01	0.02	0.02
Ni	0.2	< 0.005	< 0.005	< 0.005
Cu	0.04	< 0.005	0.01	< 0.005
Zn	0.01	< 0.005	< 0.005	< 0.005
Se	0.3	0.25	0.8	0.3
Cd	7	0.05	< 0.005	< 0.005
Pb	0.08	< 0.005	< 0.005	< 0.005
Bi	0.02	< 0.005	< 0.005	< 0.005
Total	8.656	1.03	1.566	0.92
Material Purity Level	99.99913%	99.999989%	99.999843%	99.999908%

Sample	Raw Material, g	Calculated Percent Yield, 1st Stage	Calculated Percent Yield, 2nd Stage	Calculated Percent Yield, 3rd Stage	Amount Recovered, g	Overall Yield
Te-VD-9	308.55	89.37%	n/a	n/a	257.71	83.52%
Te-VD-10	323.704	95.77%	86.69%	n/a	257.756	79.63%
Te-VD-11	326.01	88.75%	99.17%	92.86%	247.07	75.79%

National Nuclear Security Administration

Semiconductor Materials And Radiological Technologies

©

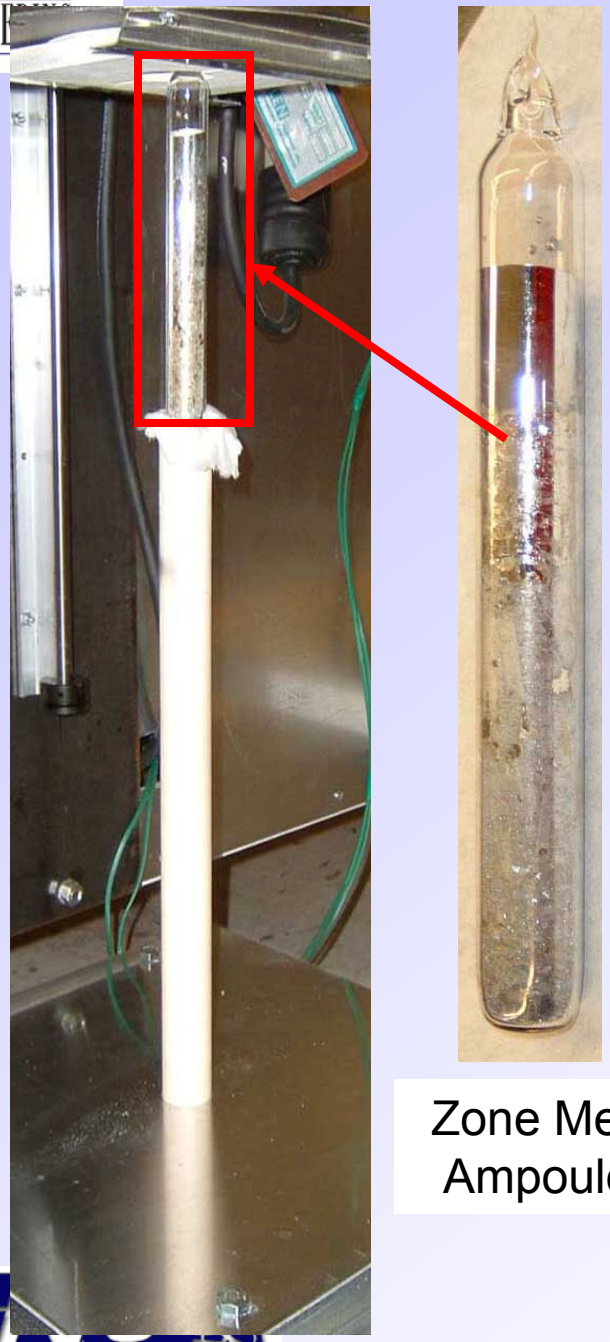

Zone Melt Ampoule

Tellurium Zone Melting (Normal Freeze) Purification Results

Impurity	Raw Material (ppm)	Purified Material (ppm)
Na	0.1	0.01
Al	0.07	< 0.005
Si	0.01	< 0.005
S	0.006	< 0.005
Cl	0.02	< 0.005
K	0.2	< 0.01
Se	0.7	0.45
Cd	0.1	0.4
In	0.01	0.02
Sn	< 0.005	< 0.005
Pb	1	< 0.005
Bi	0.06	0.01
Total	2.281	0.93
	99.9997719	99.999907

National Nuclear Security Administration

Semiconductor Materials And Radiological Technologies

©

Zinc Vacuum Distillation Results

	Zn Raw Mat'l	Zn-VD-1h (1 Stage)	Zn-VD-2c-3 (3 Stage)		Zn Raw Mat'l	Zn-VD-1h (1 Stage)	Zn-VD-2c-3 (3 Stage)
Element	[ppm wt]	[ppm wt]	[ppm wt]				
B	0.01	0.02	0.001	Cu	2.1	0.35	1.3
Na	0.03	0.13	0.007	Mo	0.01	0.38	0.01
Mg	0.01	0.17	0.005	Ag	0.59	0.05	0.05
Al	0.13	0.72	0.004	Cd	3	0.86	0.05
Si	0.28	2.7	0.05	In	0.02	0.005	0.005
P	0.009	0.01	0.005	Sn	0.36	0.2	0.01
S	0.61	0.57	0.05	Sb	0.02	0.01	0.01
Cl	0.18	0.25	0.01	Te	0.64	0.24	0.01
Ca	0.01	0.1	0.01	La	0.001	0.06	0.001
Ti	0.005	0.04	0.005	W	0.18	0.51	0.005
V	0.001	0.002	0.001	Re	0.005	0.08	0.005
Cr	0.04	0.42	0.01	Pt	0.02	0.13	0.008
Mn	0.12	0.13	0.005	Tl	3.9	0.62	0.03
Fe	2	7.2	0.01	Pb	12	0.74	0.05
Co	0.02	0.13	0.005		26.411	18.227	1.732
Ni	0.11	1.4	0.01		99.99736	99.99818	99.99983

National Nuclear Security Administration

Semiconductor Materials And Radiological Technologies

CdZnTe/CdMnTe Binary Reaction

- Two high-pressure vertical Bridgman furnaces were donated to KSU by SAIC.
- Retrofit of 1st high pressure furnace (solely reaction) nearing completion.
  - Construction and testing of pressure controls complete.
  - Design and acquisition of thermal controls and heating elements complete.
  - Installation of heating elements underway.
- Expected operational by January 1, 2008.

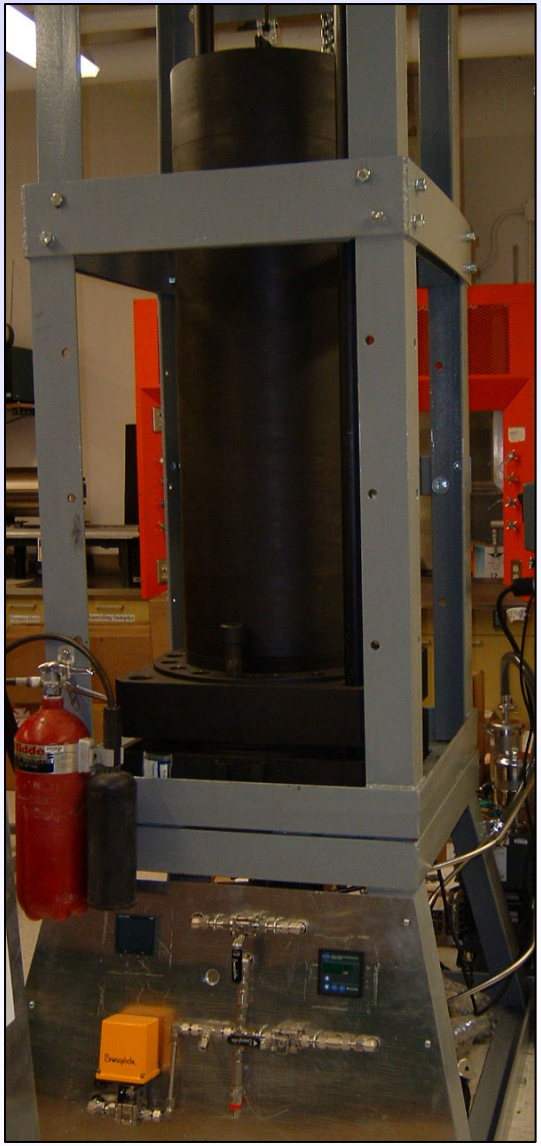

National Nuclear Security Administration

Semiconductor Materials And Radiological Technologies

©

CdZnTe Vertical Bridgman Furnace

- New in-house developed software enables significantly improved data collection and storage as well as improved process control.
- Necessary furnace rebuild completed.

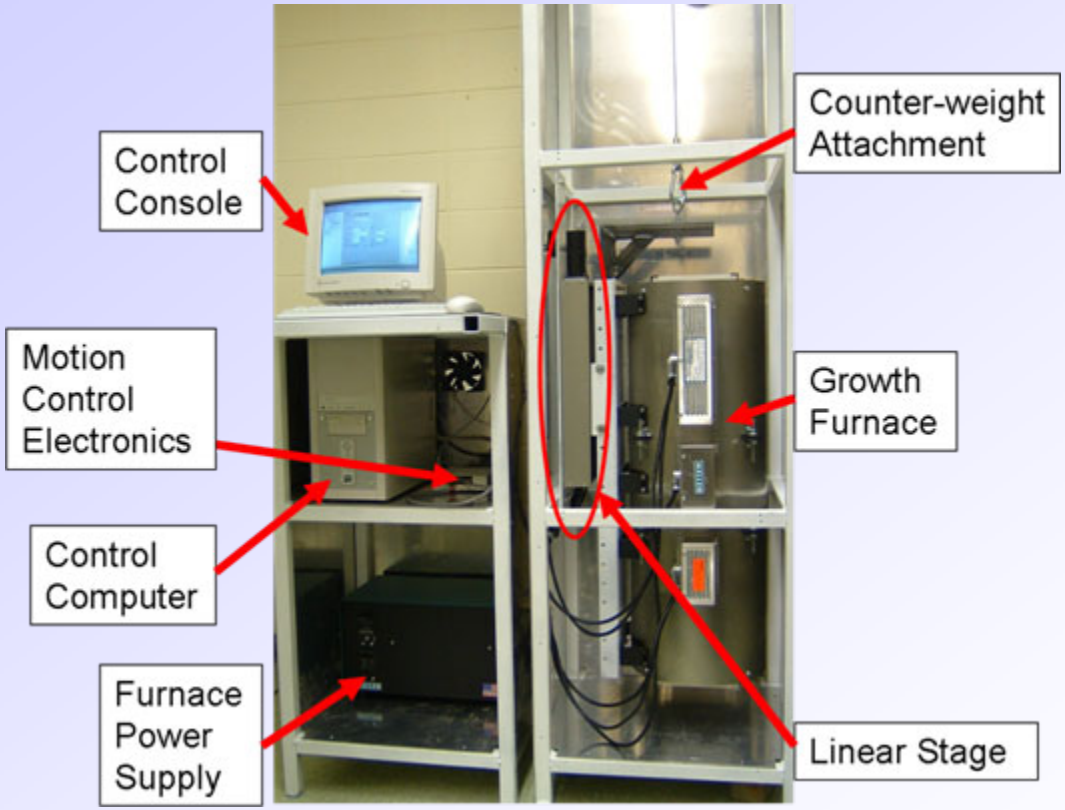

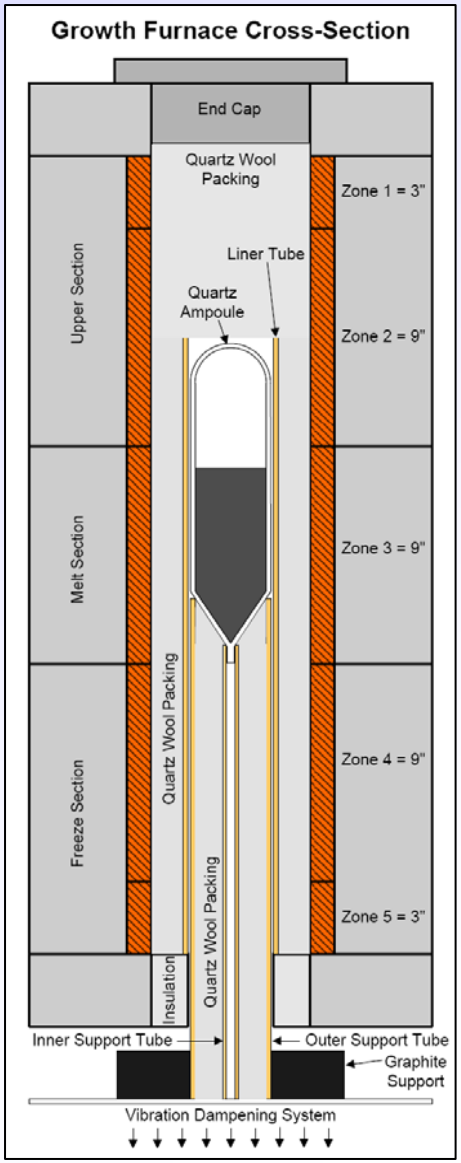

National Nuclear Security Administration

Semiconductor Materials And Radiological Technologies ©

CdZnTe Crystal Growth

- Four ingots of CdZnTe have been grown and characterized in the past year.

Ingot 5 – Year 1

Ingot 8 – Year 2

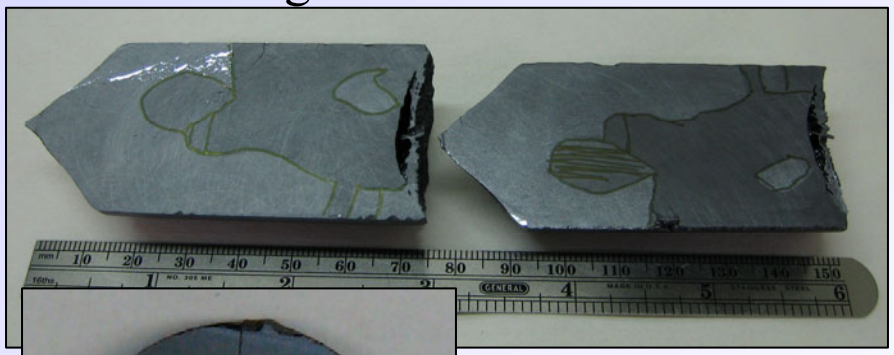

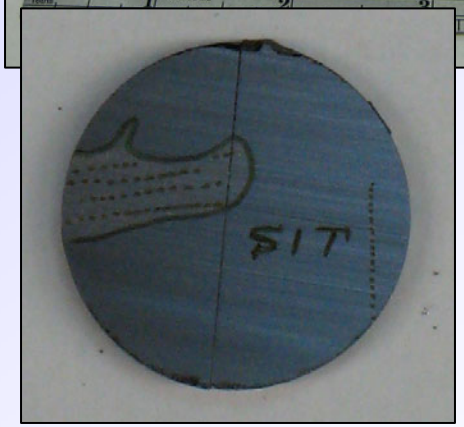

Ingot 9 – Year 2

- Grain structure/yield is improving as the growth process is refined.

National Nuclear Security Administration

Technologies

©

CdZnTe Crystal Growth

- Conversion to 7N pure feedstock has produced significantly improved electronic properties.

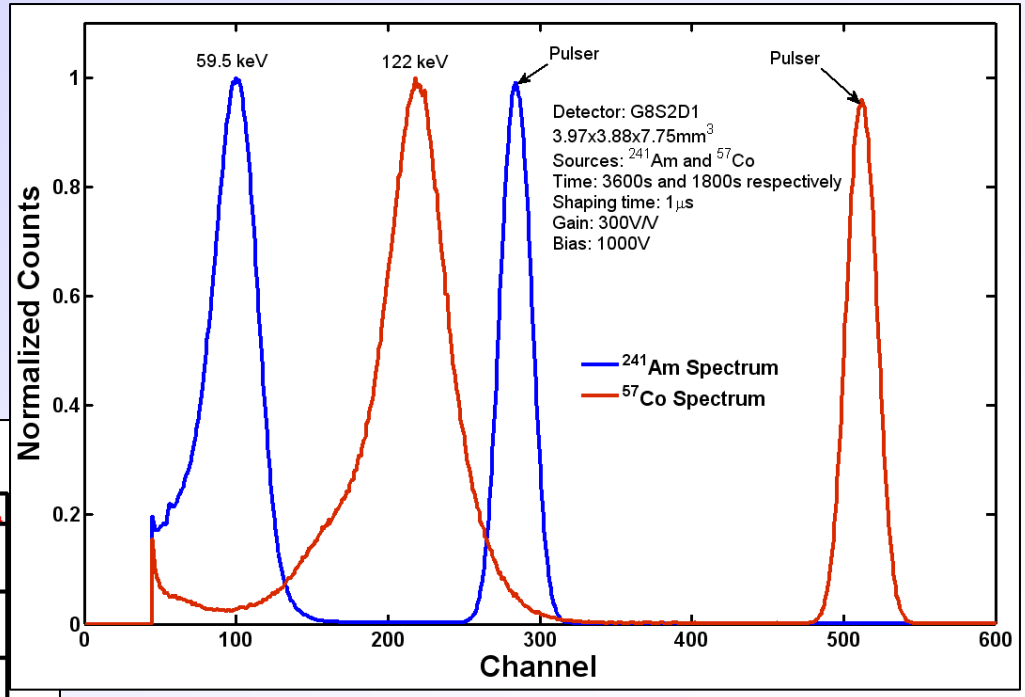

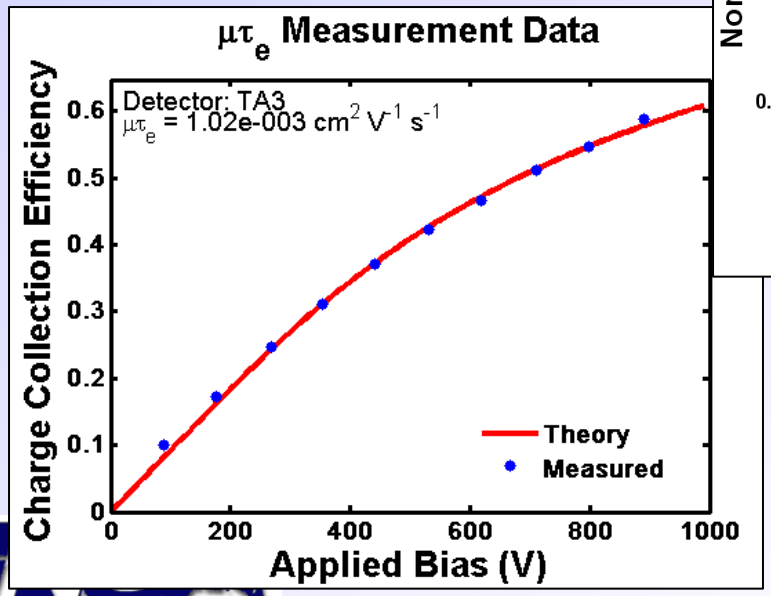

- Three methods will be used to characterize the performance of CdZnTe:
  - $\mu\tau_e$ Measurement
  - Spectral Response
  - I-V Curve Measurement

Semiconductor Materials And Radiological Technologies

National Nuclear Security Administration

CdZnTe Material Characterization

- A fourth method will also be used to characterize CdZnTe, Te precipitate density and size distribution mapping.
- A software program was developed in-house to automatically identify, log, and tally Te precipitates seen under an IR microscope.
- A histogram of Te precipitate size is output for each sample analyzed.
- Addition of program allows for the quantification of Te precipitate density and size distribution throughout entire samples.

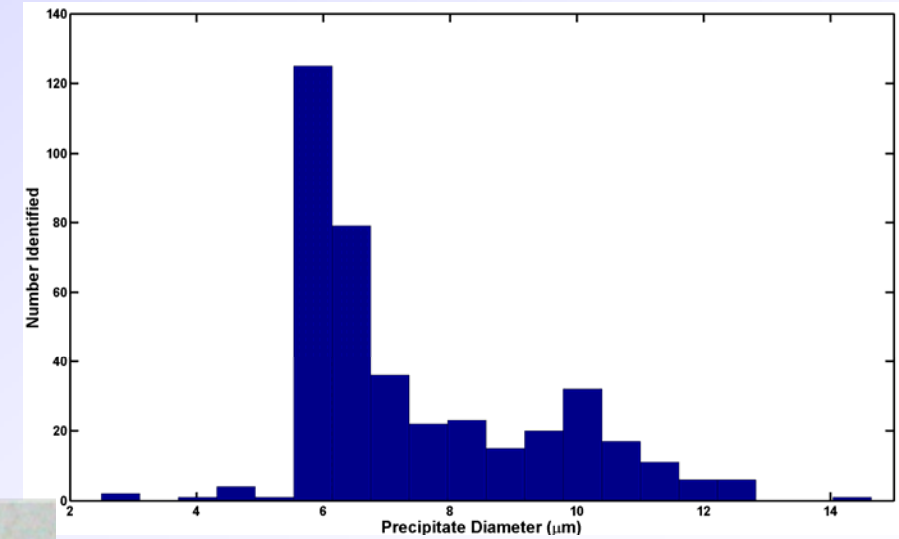

Captured IR Image

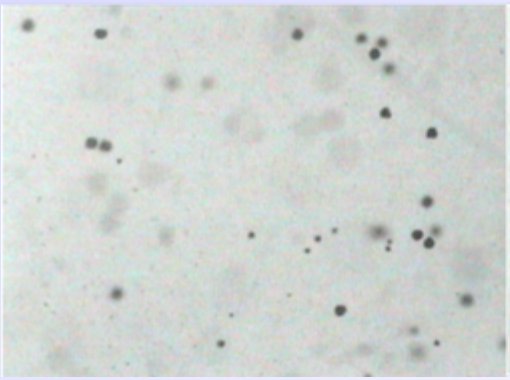

Processed IR Image

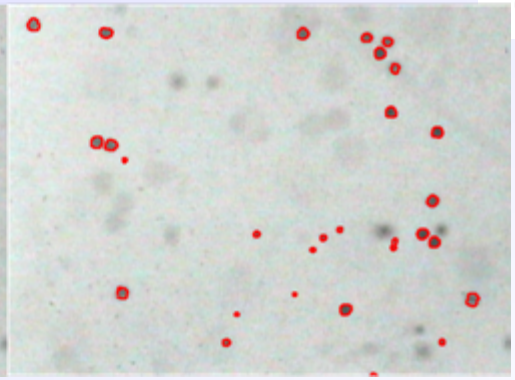

National Nuclear Security Administration

Semiconductor Materials And Radiological Technologies ©

Post Growth Laser Annealing - Scope

- Cadmium Zinc Telluride (CdZnTe) crystals grown via the vertical Bridgman method inherently suffer from the presence of Tellurium precipitates.
- Tellurium precipitates plague device performance in CdZnTe detectors.
- The migration of Te precipitates due to an externally applied thermal gradient has been proven.
- A laser induced thermal gradient annealing method is being investigated as a potentially advantageous approach.

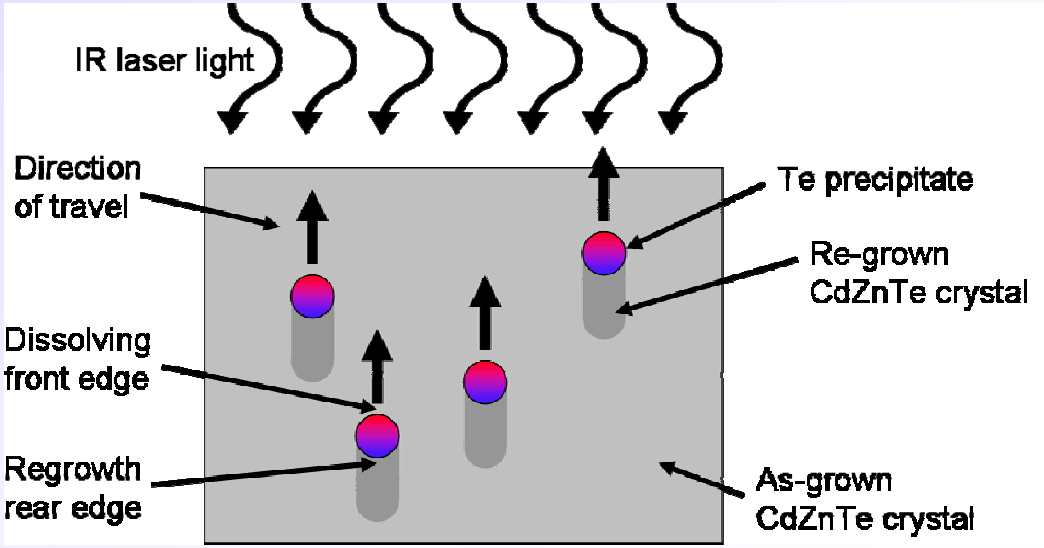

National Nuclear Security Administration

Semiconductor Materials And Radiological Technologies

Laser Annealing - Numerical Simulation

- Te and CdZnTe both are transparent to the CO_2 (λ=10.6μm) laser light.
- It is believed that the interface energy states at the surface of the precipitates are largely responsible for the heat absorption.
- Matlab finite difference thermal simulations suggest that pulsed laser power leads to steep temperature gradients at the neighborhood of the precipitate.
- The steep gradient leads to increased conduction such that longer laser exposure does not increase the gradient but heats up the entire crystal
- Intermittent laser power however leads to rapid local cooling which prevents local crystal melting.

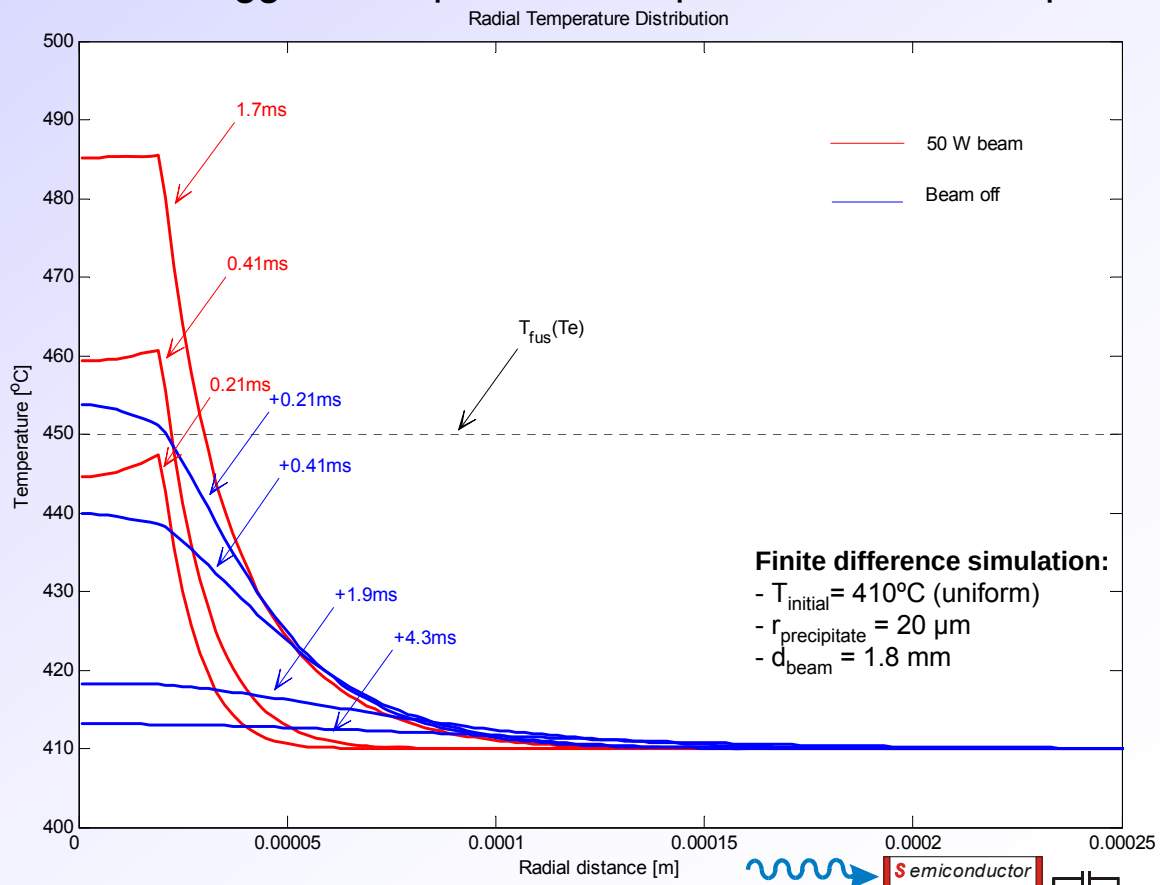

Semiconductor Materials And Radiological Technologies

National Nuclear Security Administration

©

Laser Annealing - Experimental Setup

- In initial trials, heat loss due to natural convection prevented the bulk crystal from reaching appropriate annealing temperatures
- In the modified setup, the crystal is placed in a single zone furnace which provides supplementary heat and a constant thermal environment.
- First experiments with the shown setup are underway.

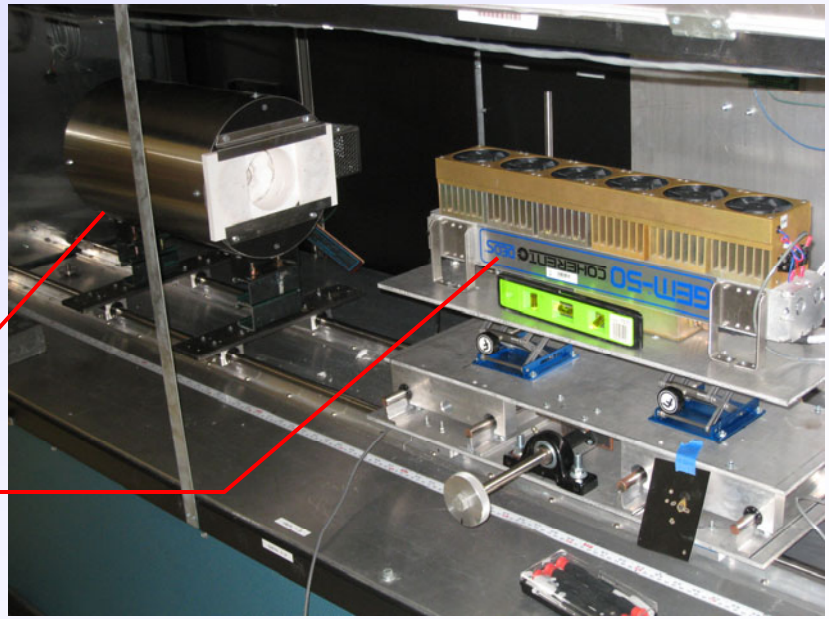

Single zone furnace

CO_2 laser mounted on translation stage

Semiconductor Materials And Radiological Technologies

National Nuclear Security Administration

Growth of HgI_2 Platelets

Procedure

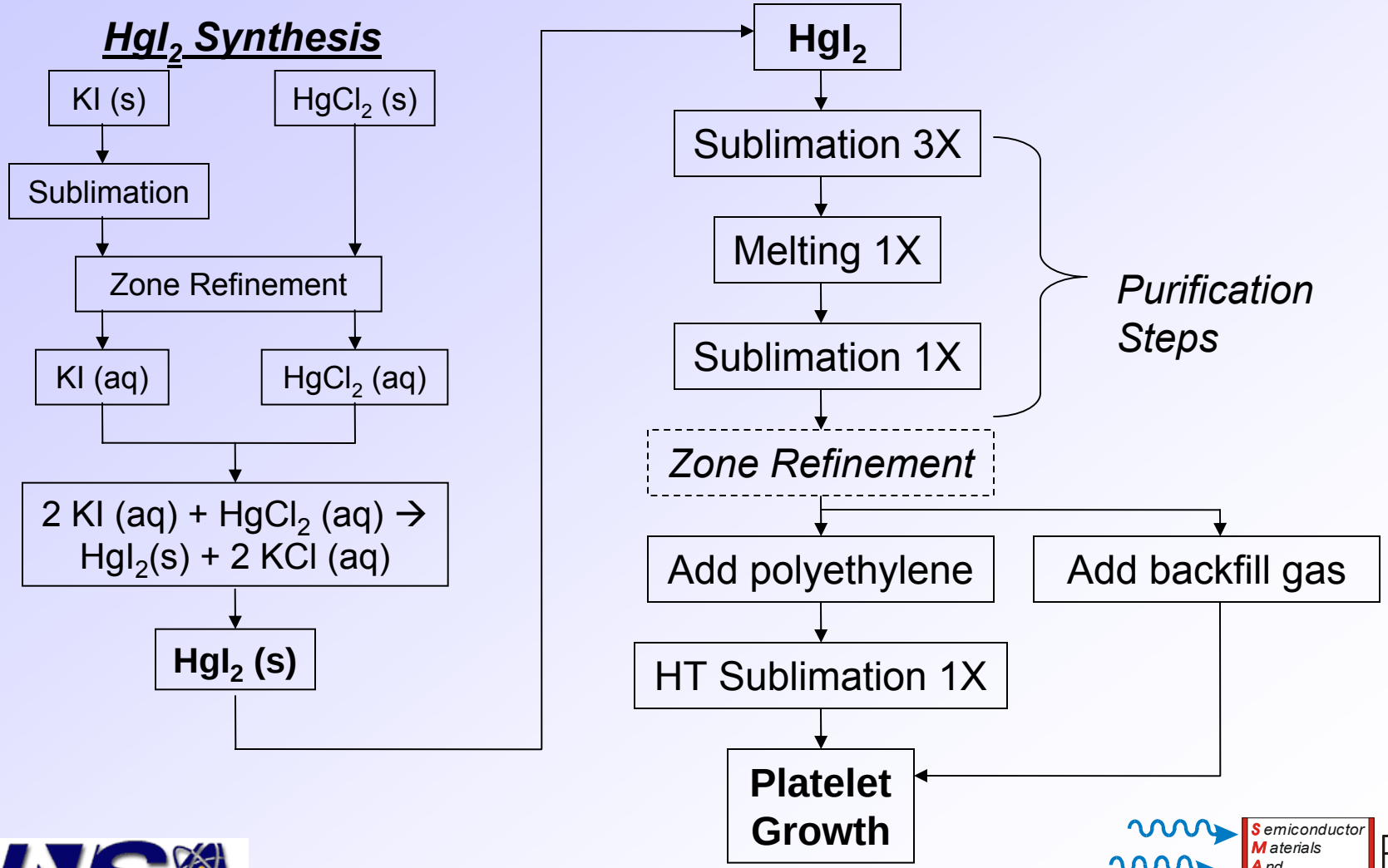

National Nuclear Security Administration

Semiconductor Materials And Radiological Technologies

HgI_2 Purification

Sublimation in Dynamic Vacuum

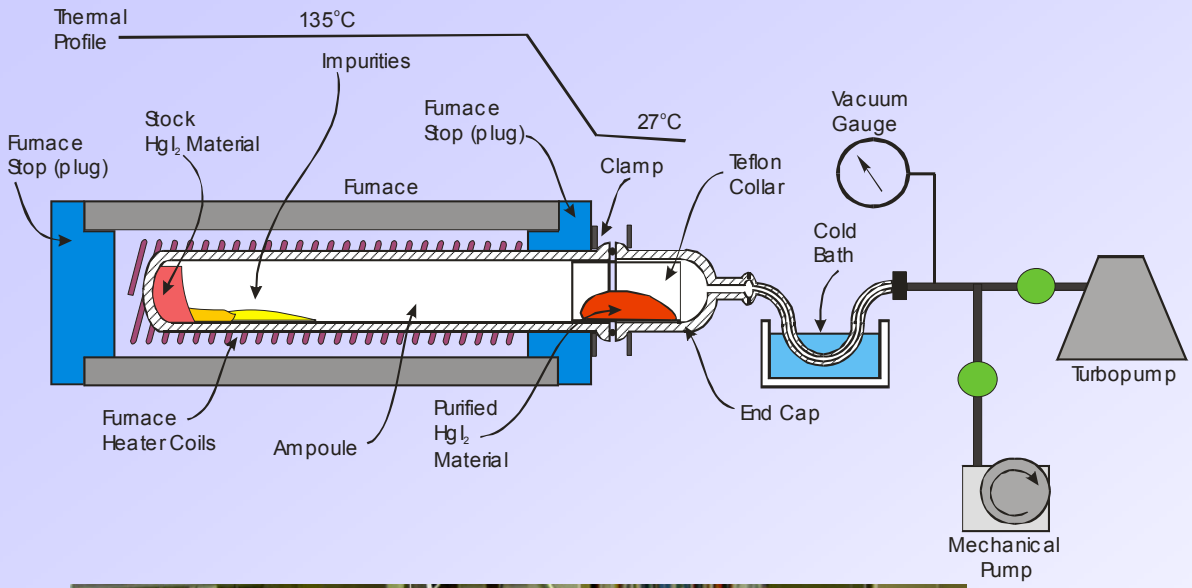

- One-zone furnace (hot zone; T = 140°C) and water-LN_2 cold trap
- Dynamic vacuum with $P < 10^{-5}$ Torr
- Average time period per run: two days
- Total three sublimation runs

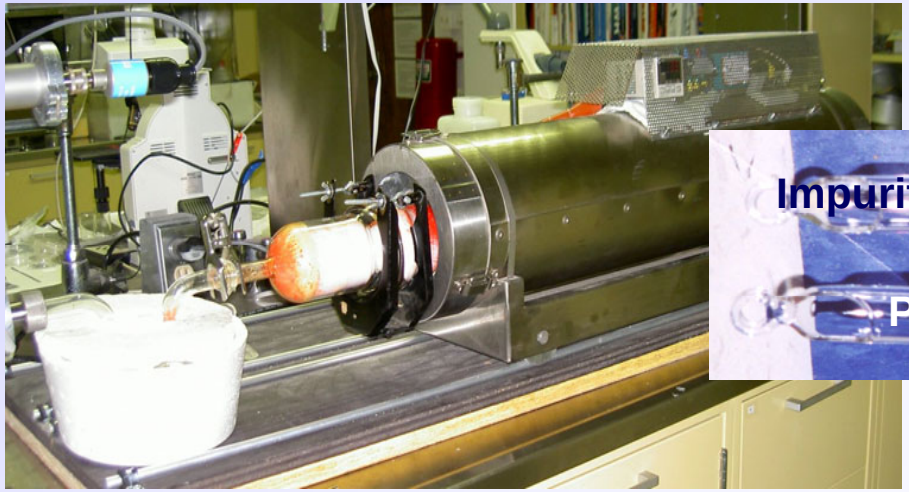

National Nuclear Security Administration

Semiconductor Materials And Radiological Technologies ©

HgI_2 Purification

Melting and Sublimation in Static Vacuum

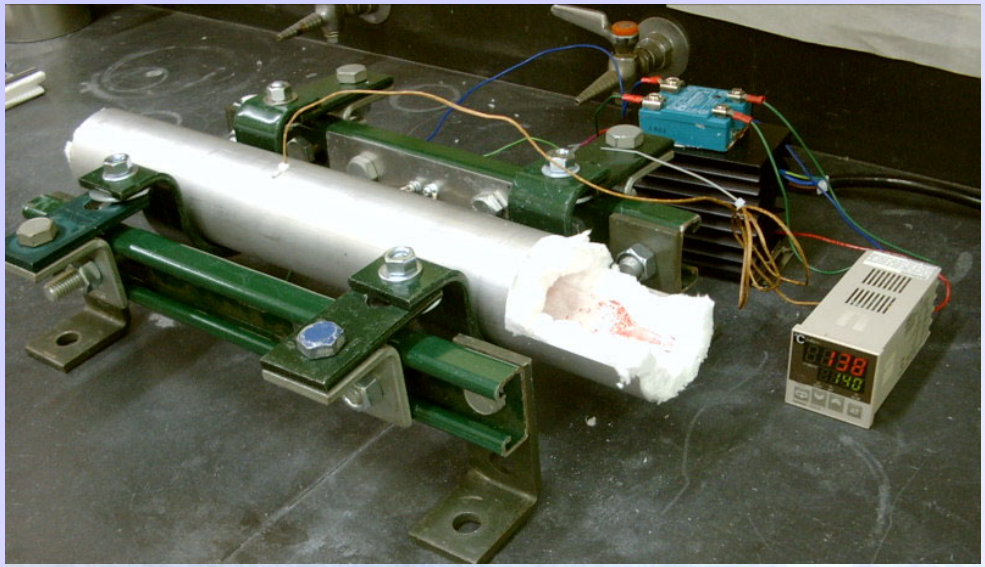

Two-chamber melting ampoule:

A small static transport furnace was built to move the purified material (in the 1st chamber) to a holding chamber (2nd chamber).

National Nuclear Security Administration

Semiconductor Materials And Radiological Technologies

©

HgI_2 Purification

GDMS Results (in ppm)

element	source	sublimation	melting
B	0.02	0.18	0.04
C	~ 12	~ 2	~ 15
N	~ 200	~ 25	~ 20
O	~ 20	~ 2	~ 2
Na	0.15	0.05	3
Mg	0.04	< 0.005	0.01
Al	0.48	0.35	0.28
Si	2	1.8	0.38
P	0.02	< 0.005	< 0.005
S	8	0.35	0.35
Cl	35	14	2
K	20	< 0.05	0.15
Ca	0.5	< 0.05	< 0.05

element	source	sublimation	melting
Sc	< 0.001	< 0.001	< 0.001
Ti	0.75	0.17	0.03
V	< 0.005	< 0.005	< 0.005
Cr	0.02	0.02	< 0.01
Mn	< 0.005	< 0.005	< 0.005
Fe	1.7	0.28	0.28
Co	< 0.005	< 0.005	< 0.005
Ni	0.06	< 0.01	< 0.01
As	0.18	0.22	0.08
Se	< 0.5	< 0.5	< 0.5
Br	1.8	1.2	0.45
Ag	=< 30	=< 2	=< 0.7
In	0.15	< 0.005	< 0.005
Sn	0.2	< 0.01	< 0.01
Sb	0.75	< 0.01	< 0.01

Elements in red show an increase in contents in the melted material, possibly due to recontamination.

National Nuclear Security Administration

Semiconductor Materials And Radiological Technologies

©

HgI_2 Platelet Growth

Platelet Growth Furnaces

(40 now in operation)

National Nuclear Security Administration

Semiconductor Materials And Radiological Technologies ©

HgI_2 Platelet Growth

Without polyethylene

Twinned prismatic crystals (faces with higher indices still grow)

With polyethylene addition

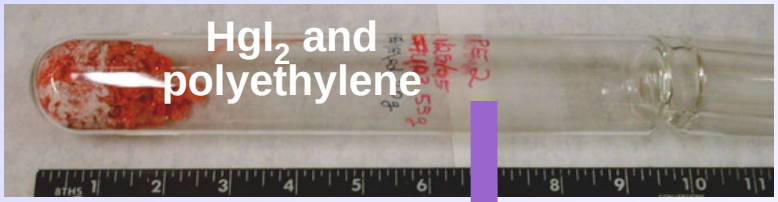

Sublimated material is retrieved and sealed in a new growth ampoule

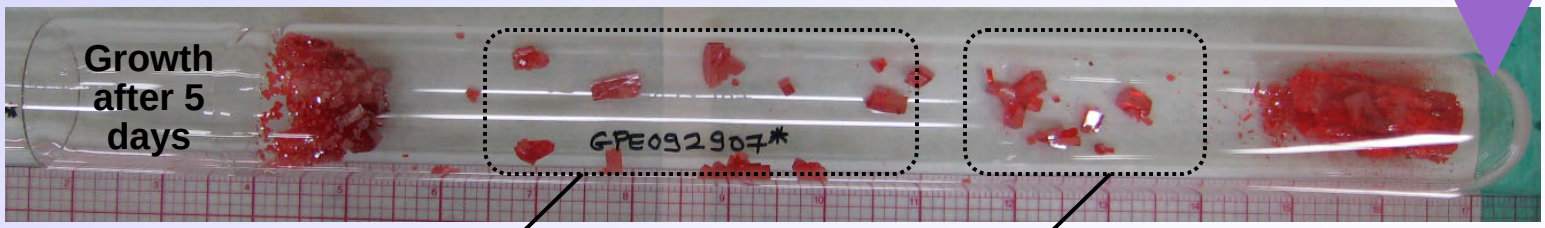

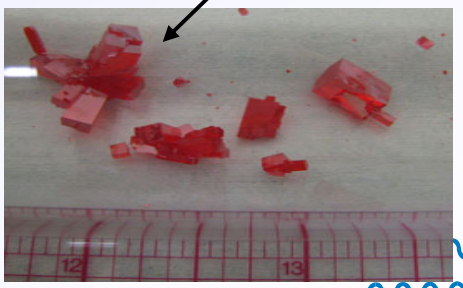

Twinned platelets (faces with lower indices prevail)

National Nuclear Security Administration

Semiconductor Materials And Radiological Technologies ©

Vertical Growth Furnaces

(10 now operating)

Seeded Crystal

Completed Crystal

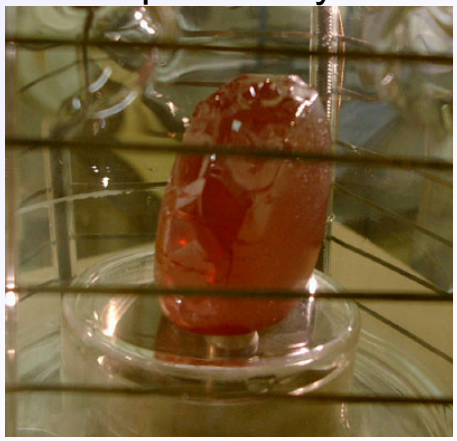

National Nuclear Security Administration

Semiconductor Materials And Radiological Technologies ©

HgI_2 Detector Fabrication and Testing System

The following systems have been constructed:

- KI-solution string saw
- Measurement system for simultaneous testing of numerous detectors.

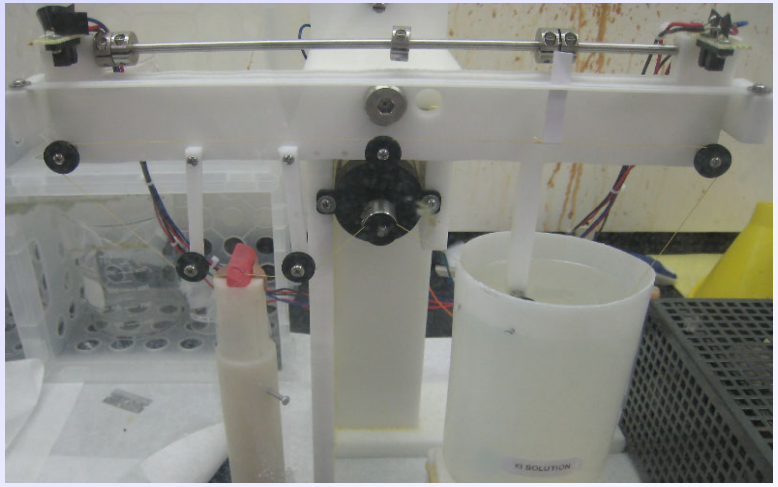

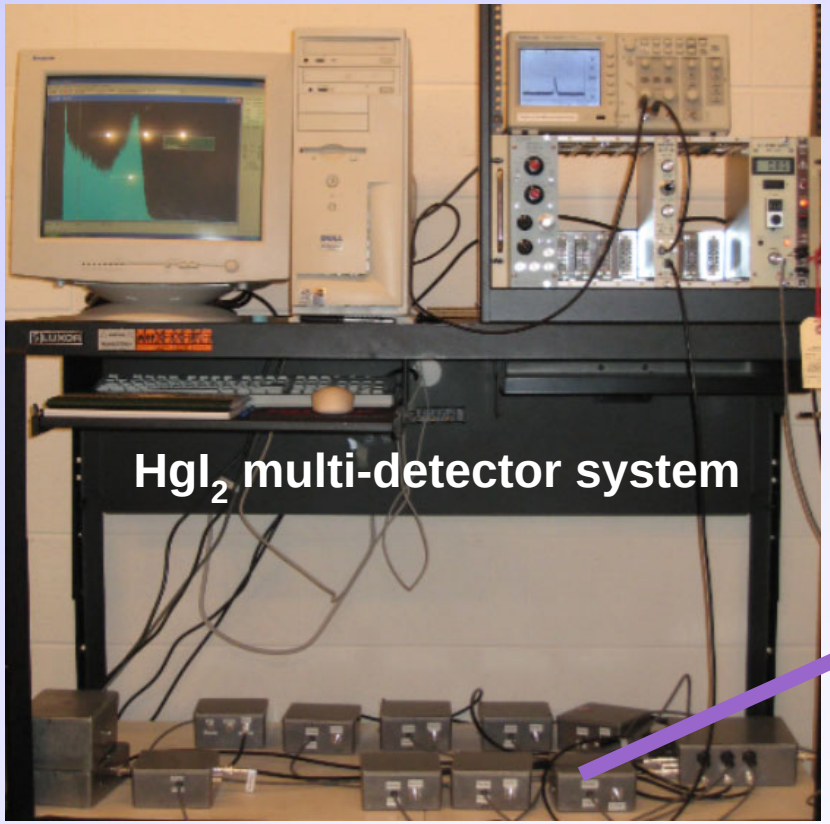

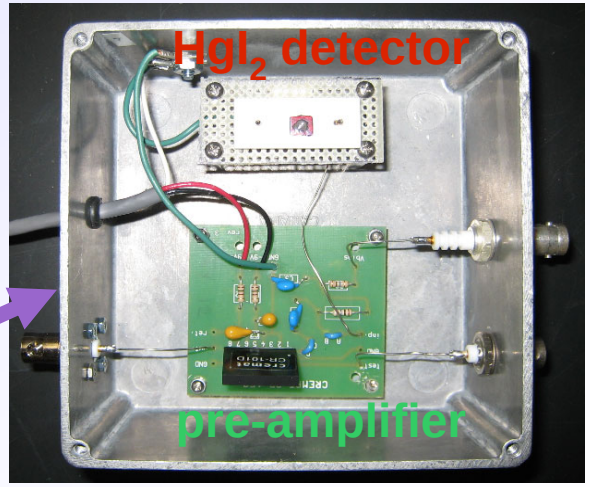

National Nuclear Security Administration

Semiconductor Materials And Radiological Technologies ©

Frisch Collar Devices

- Signal output-due to *e* motion
- Eliminates hole trapping effect
- NO leakage current between grid and anode.

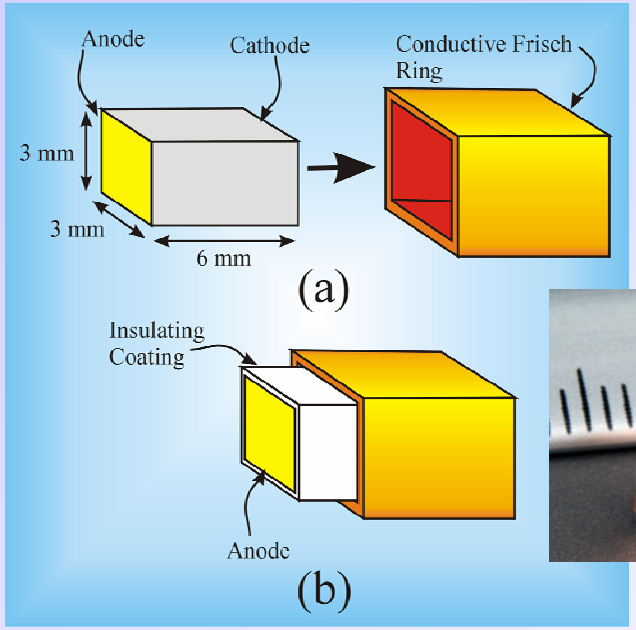

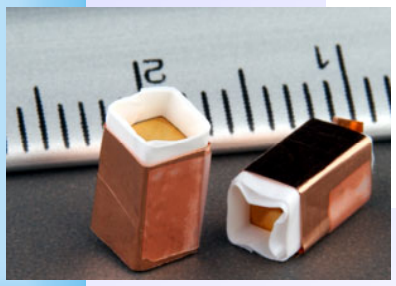

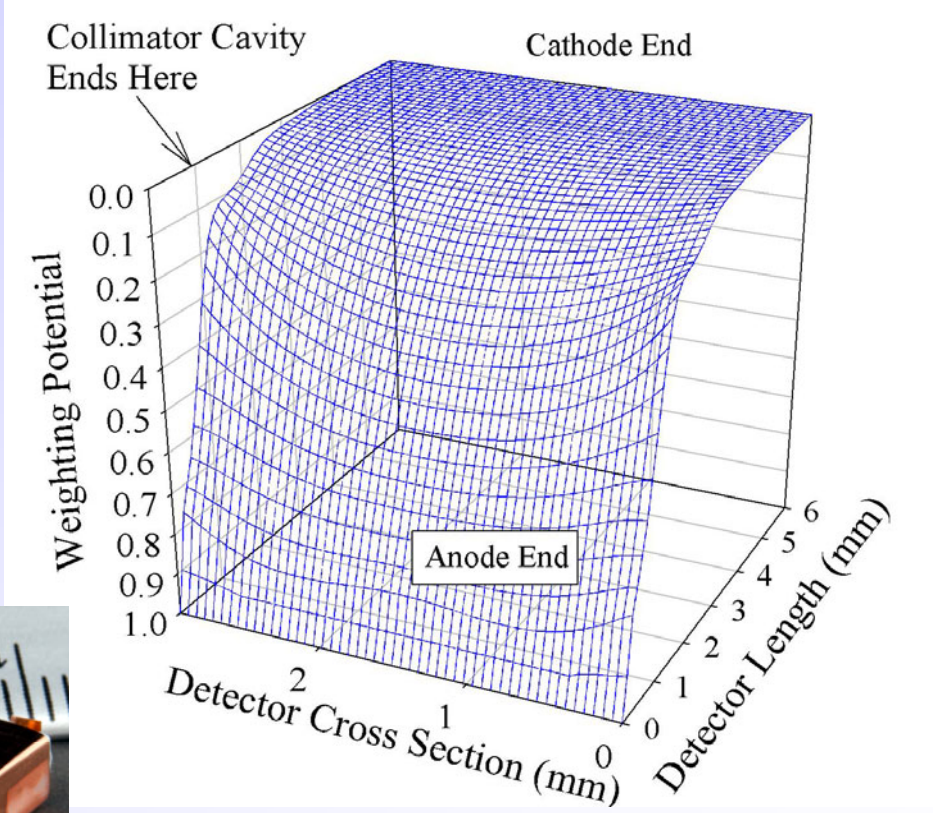

weighting potential

McGregor, Rojeski, US Patent 6,175,120
McGregor, US Patent 6,781,132

W.J. McNeil, D.S. McGregor, A.E. Bolotnikov, G.W. Wright, R.B. James, Appl. Phys. Lett., 84 (2004) pp. 1988-1990.

National Nuclear Security Administration

Semiconductor Materials And Radiological Technologies

©

Frisch Collar Geometry Effect

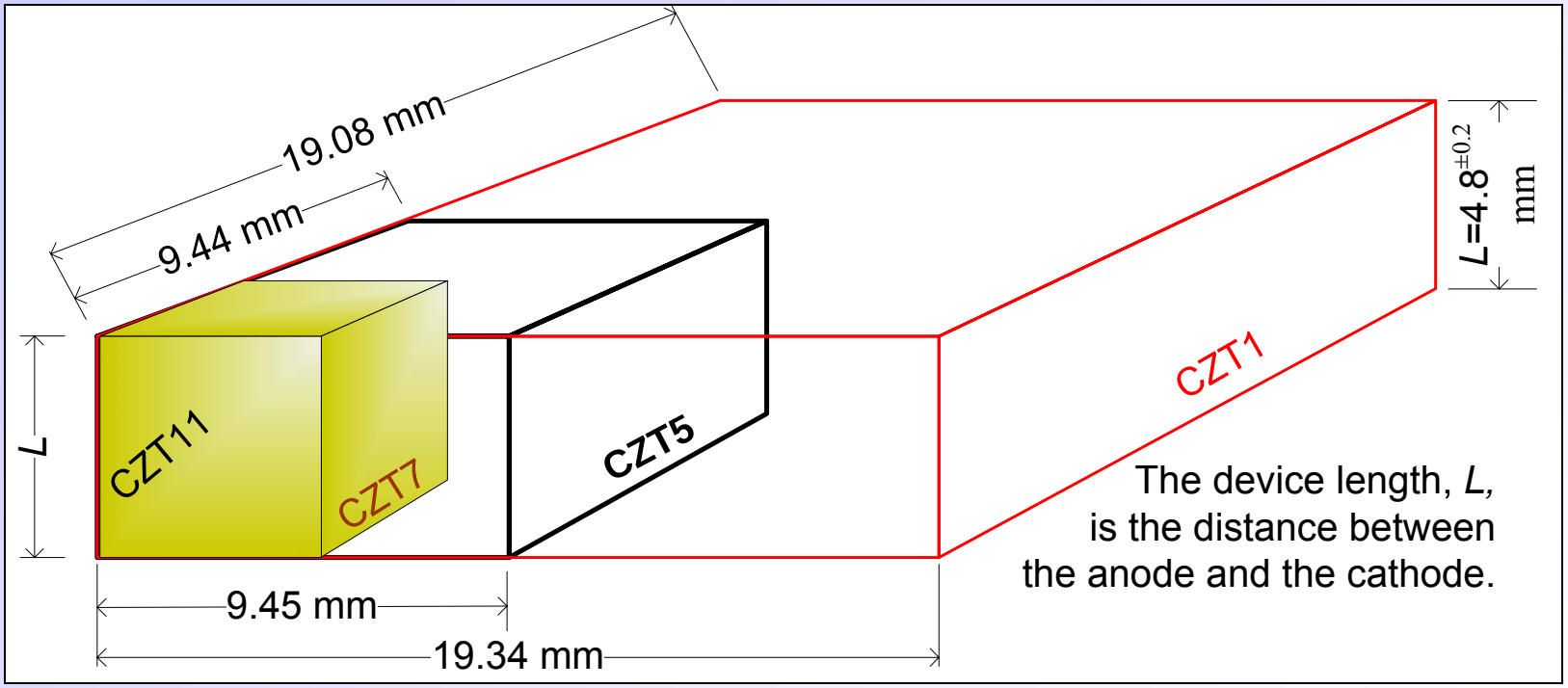

- The effect of crystal geometry were investigated, experimentally and numerically.
- Eight different aspect ratios (AR) were fabricated from the starting material, and then modeled (AR=0.25 to 2.0).

National Nuclear Security Administration

Semiconductor Materials And Radiological Technologies

Frisch Collar Geometry Effect

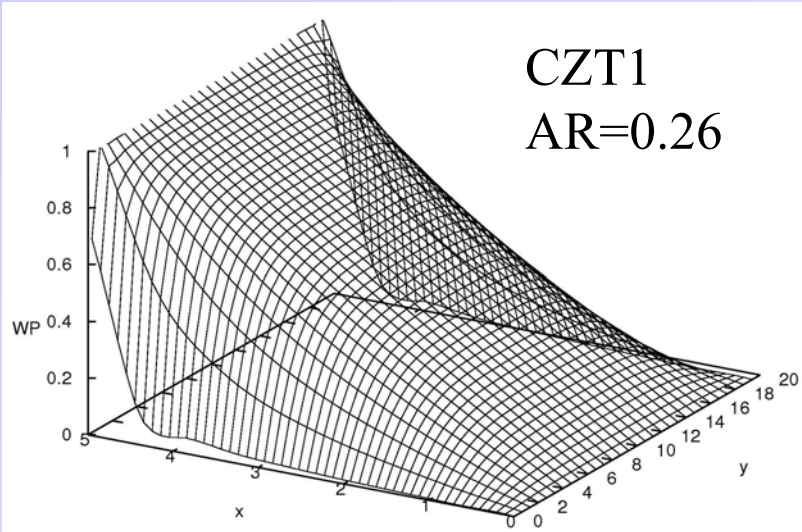

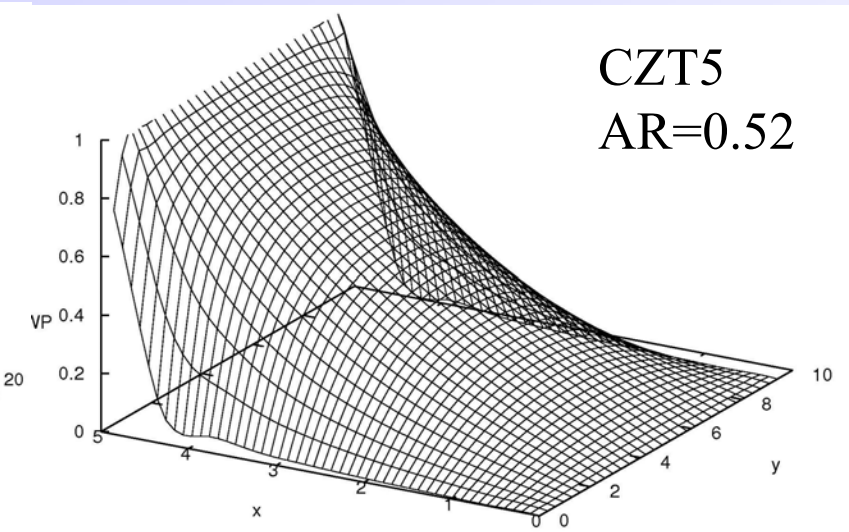

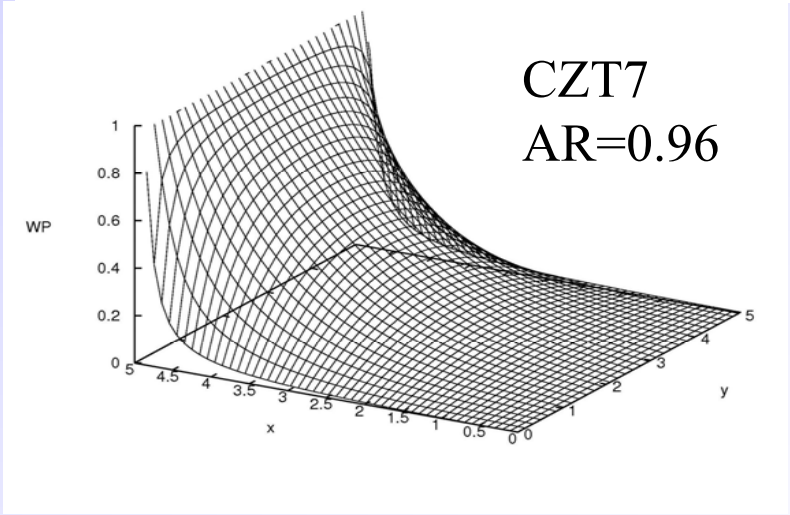

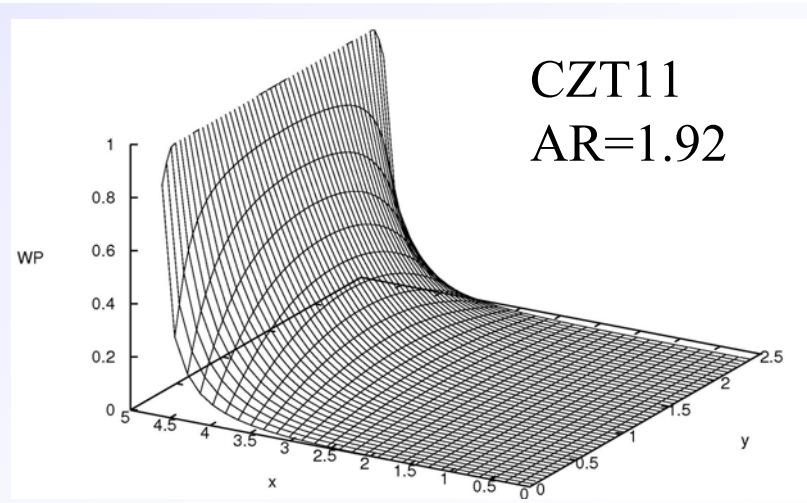

A. Kargar, R.B. Lowell, M.J. Harrison and D.S. McGregor, "The Crystal Geometry and the Aspect Ratio Effects on Spectral Performance of CdZnTe Frisch Collar Device," Proc. SPIE, 6706 (2007) pp. 1J1-1J17.

National Nuclear Security Administration

Semiconductor Materials And Radiological Technologies

©

Frisch Collar Geometry Effect

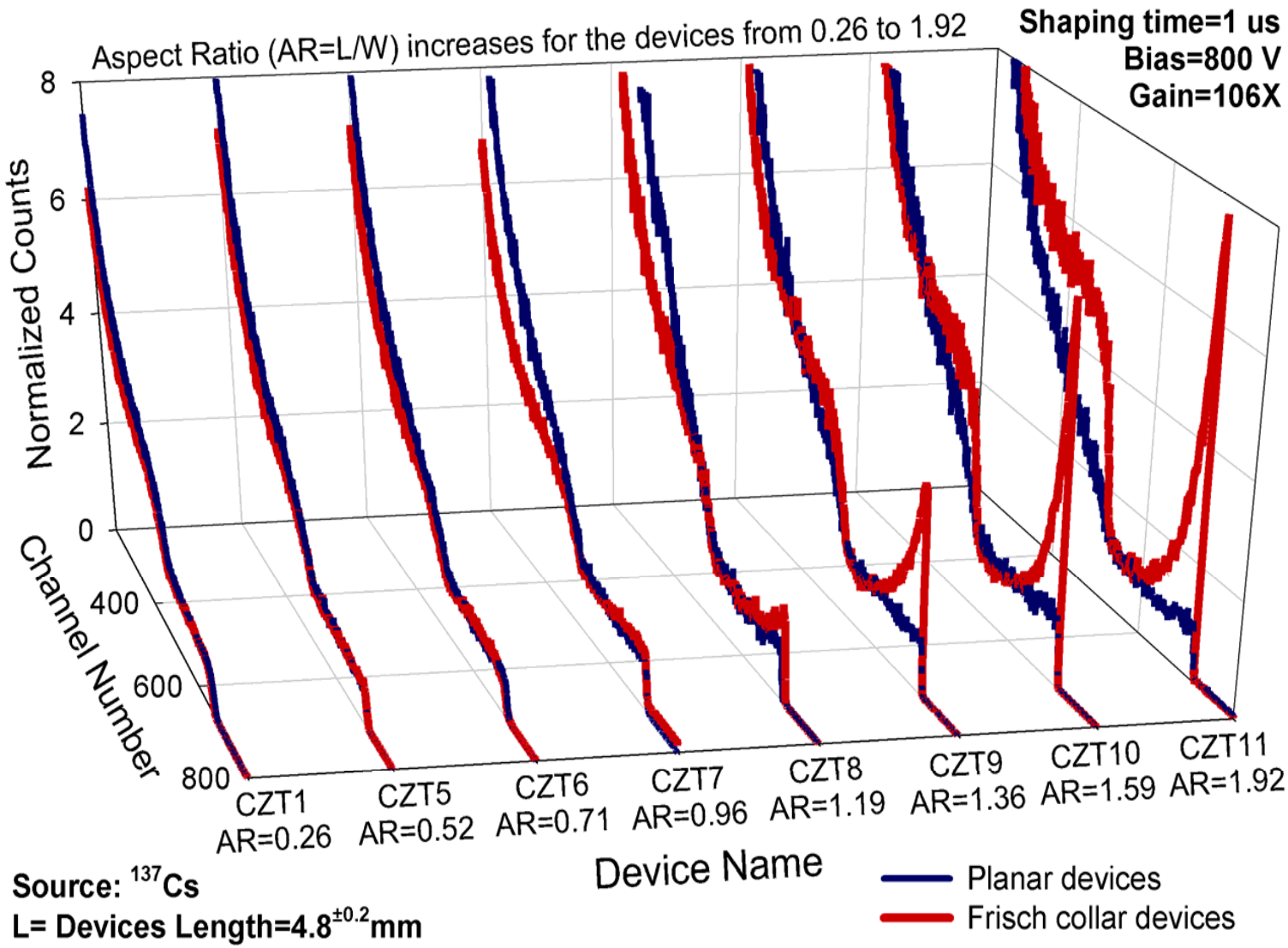

Source: ^{137}Cs

L= Devices Length=4.8$^{\pm 0.2}$mm

National Nuclear Security Administration

Semiconductor Materials And Radiological Technologies

©

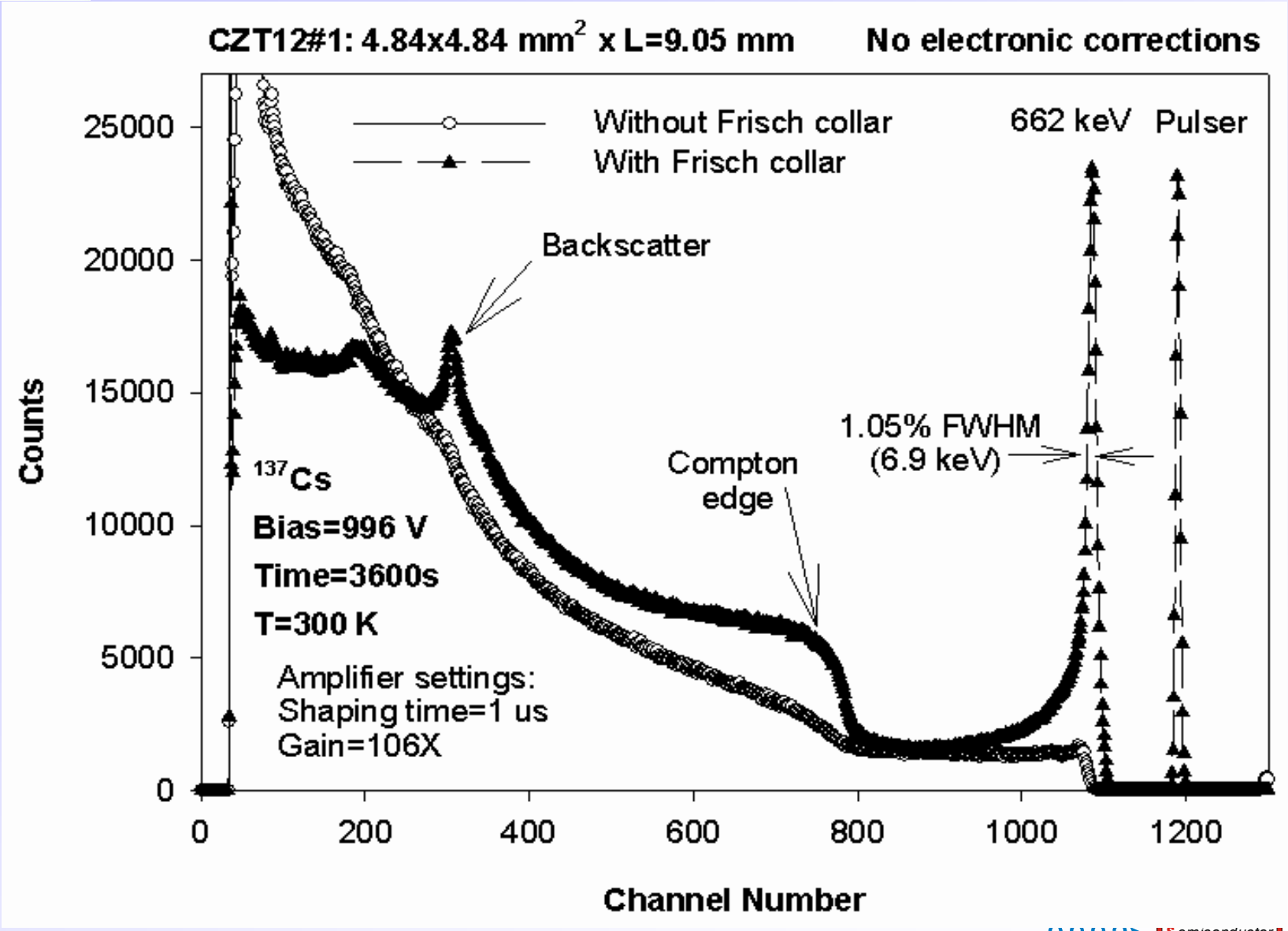

National Nuclear Security Administration

Semiconductor Materials And Radiological Technologies

The insulating layer serves to eliminate leakage current between the grid and anode and decouple the operating potential from the weighting potential.

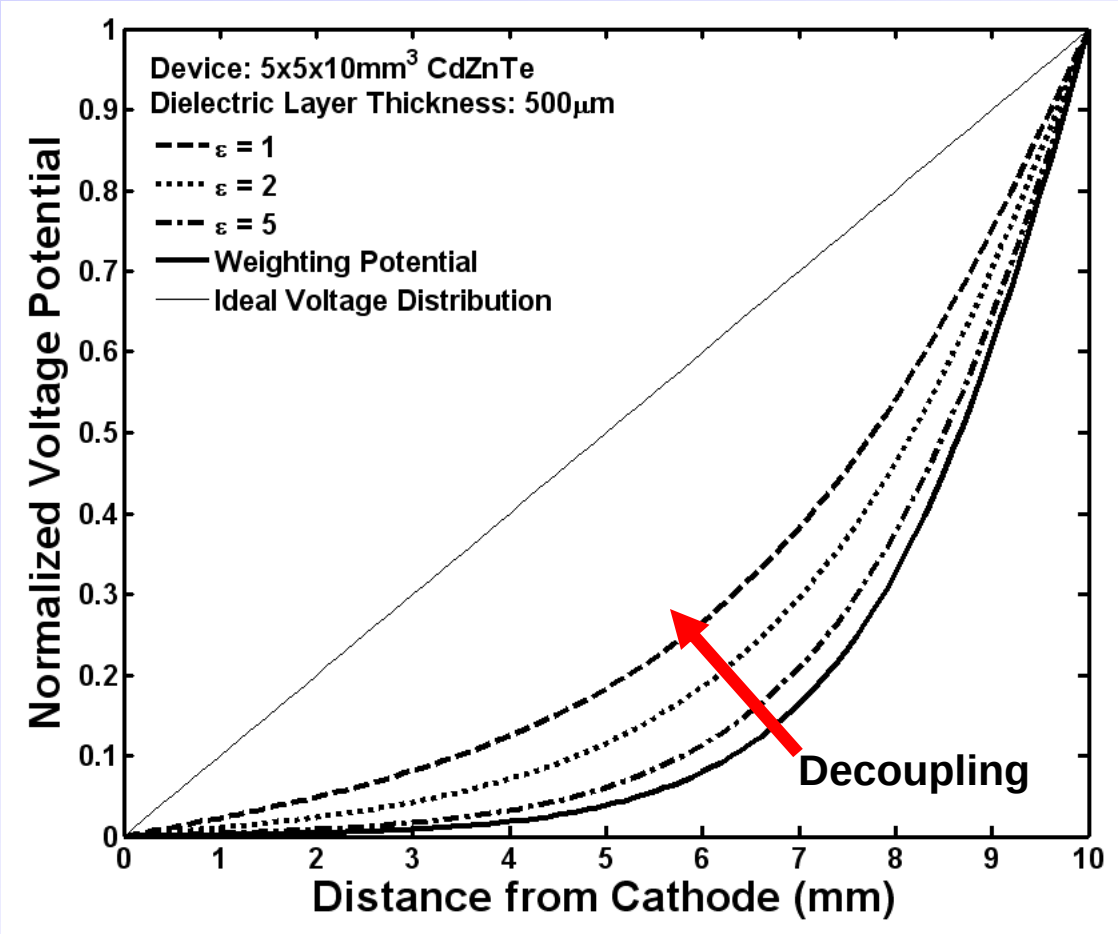

National Nuclear Security Administration

Semiconductor Materials And Radiological Technologies ©

Alternative Fabrication Method

- Previous Method
  - Teflon tape/Copper shim
- New Method
  - Parylene N/Conductive paint

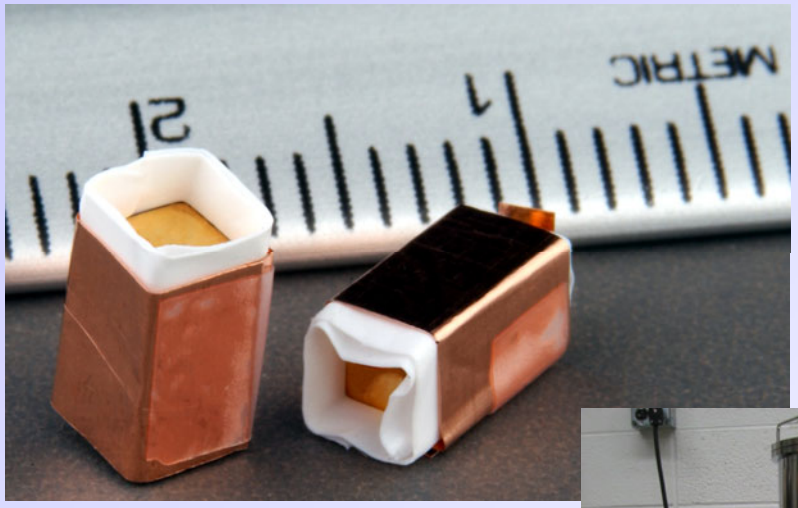

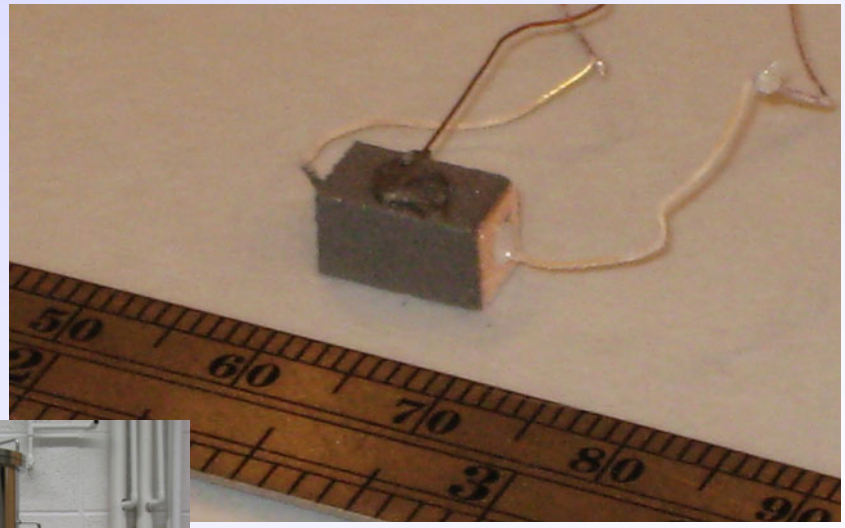

Right:
Parylene coater from (SCS)
Specialty Coating Systems

- Three conductive coatings
  - Silverdag (brush)
  - Silver paint (brush)
  - Nickel paint (spray)

National Nuclear Security Administration

Semiconductor Materials and Radiological Technologies ©

A repeatable inexpensive process is under development.
Parylene is used for the insulator and the metal is deposited afterwards.

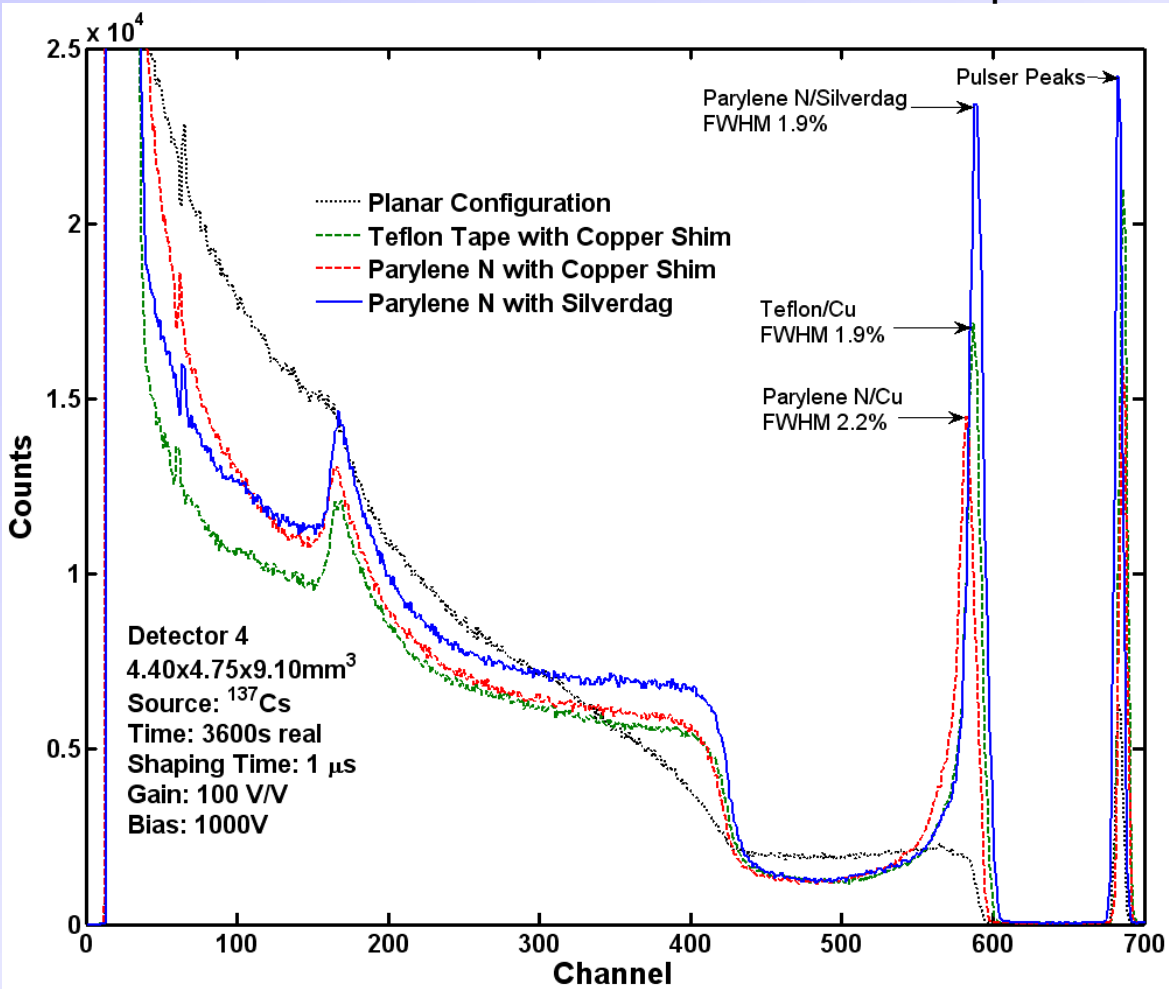

Spectra from a CdZnTe Frisch ring device. The best performance is from a parylene coated device with Ag paint as the Frisch ring.

M.J. Harrison, A. Kargar, D.S. McGregor, "Improved Fabrication of Frisch Collar CdZnTe Gamma Ray Spectrometers," IEEE Nuclear Science Symposium, Waikiki, Hawaii, Oct. 28-Nov. 3, 2007.

National Nuclear Security Administration

Semiconductor Materials And Radiological Technologies

©

Sinusoidal Trench High Efficiency Neutron Detectors (backfilled with ^{6}LiF material)

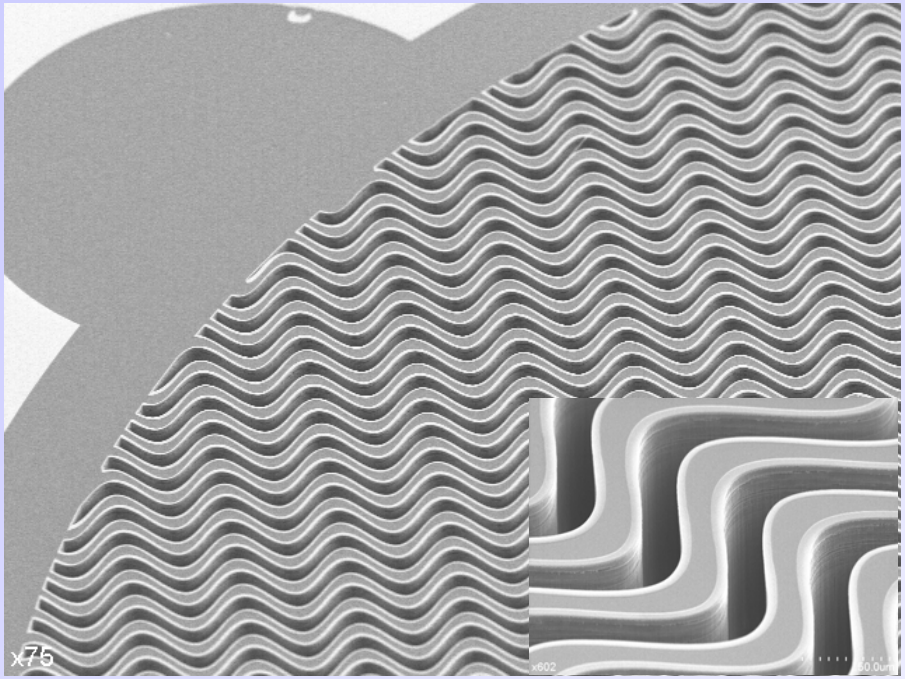

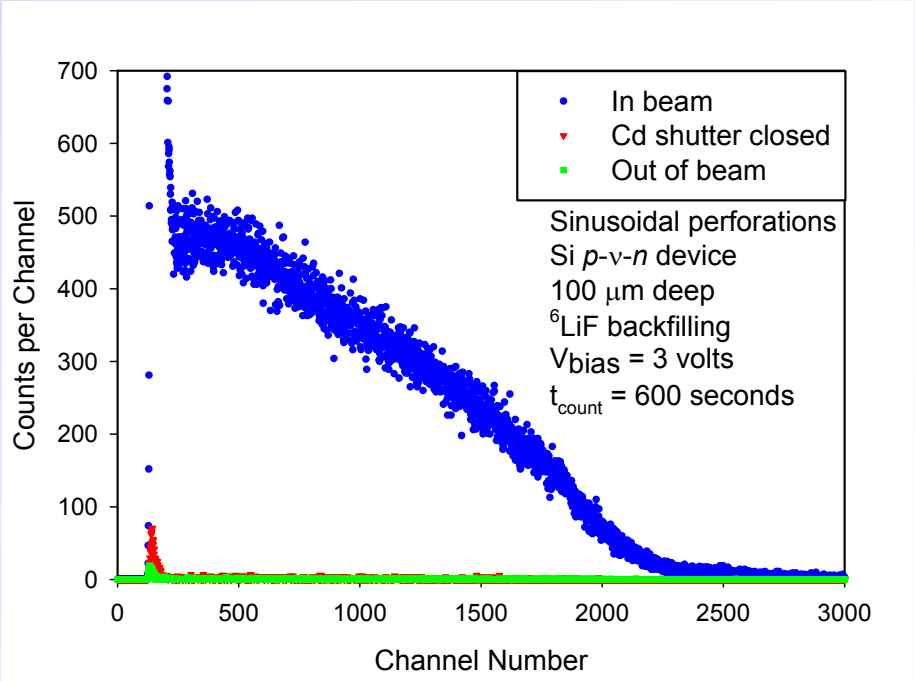

McGregor et al., US Patent Pending, 2007.

Eliminates neutron streaming dependence.
Flattens the neutron response of perforated detectors.
Increases thermal neutron detection efficiency.

Neutron beam normal to surface. Experimentally measured **35%** intrinsic neutron detection efficiency as compared to a ^{3}He tube.

S.L. Bellinger, W.J. McNeil, T.C. Unruh, D.S. McGregor, "Angular Response of Perforated Silicon Diode High Efficiency Neutron Detectors," IEEE Nuclear Science Symposium, Waikiki, Hawaii, Oct. 28-Nov. 3, 2007.

Semiconductor Materials And Radiological Technologies ©

Low-power readout electronics for a small dosimeter/detector package

The low power detectors need very little voltage to operate (<10 volts), hence compact electronics with low power needs can be used.

Detector/Preamplifier/ Amplifier

Detector Bias Supply

Dosimeter Module

McGregor et al., US Patent Pending, 2007.

D.S. McGregor, S.L. Bellinger, D. Bruno, W.J. McNeil, E. Patterson, J.K. Shultis, C.J. Solomon, T. Unruh, "Perforated Semiconductor Neutron Detectors for Battery Operated Portable Modules," Proc. SPIE, 6706 (2007) pp. 0N1-0N12.

National Nuclear Security Administration

Semiconductor Materials And Radiological Technologies ©

Transmitter and receiver modules for the prototype wireless neutron detector network

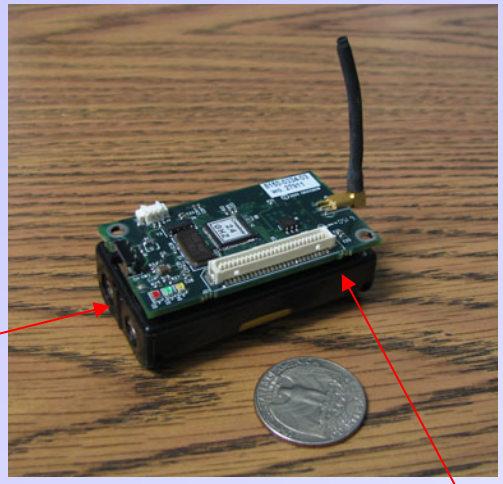

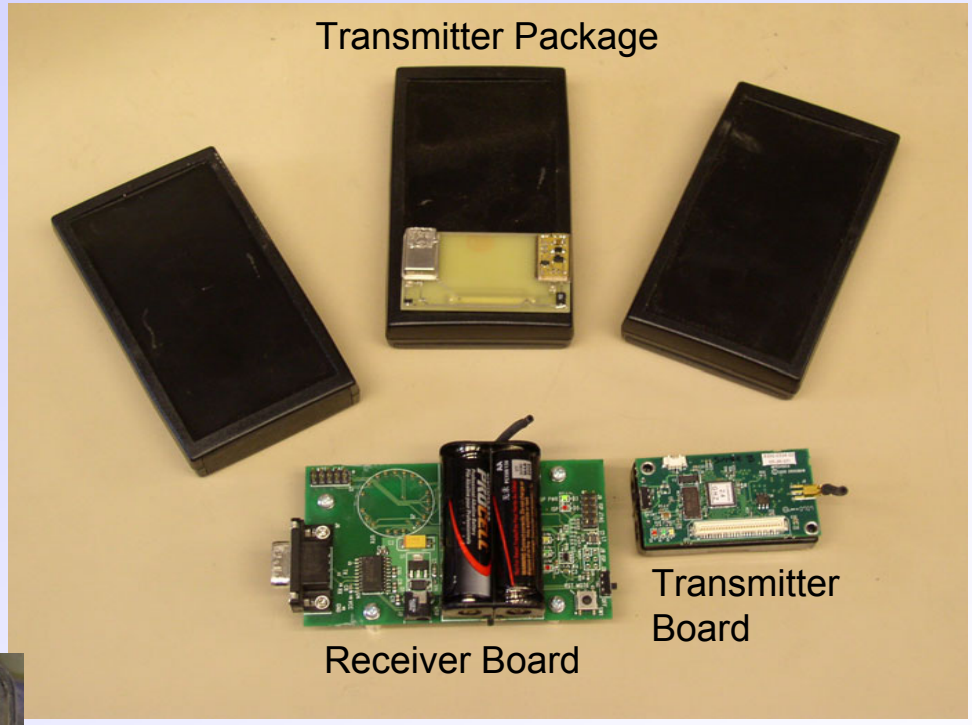

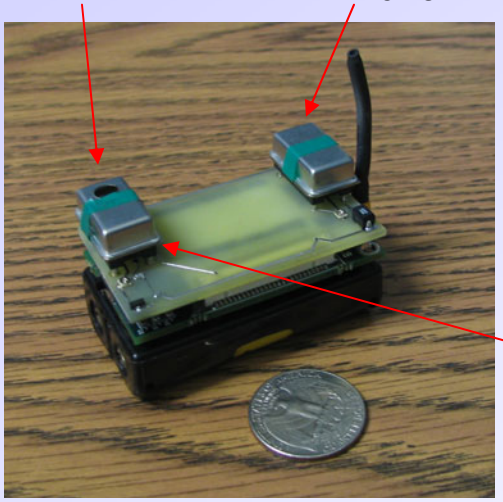

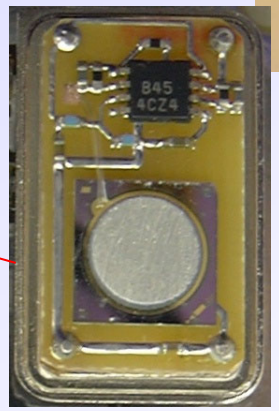

- Wireless Sensor Network
  - IEEE 802.15.4 compliant
  - Onboard Atmel 128 processor
  - Modular and expandable
  - 50,000 cps
  - 20-30m indoor range
  - 70-100m outdoor range

D.S. McGregor, S.L. Bellinger, D. Bruno, S. Cowley, W.L. Dunn, M. Elazegui, W.J. McNeil, H. Oyenan, E. Patterson, J.K. Shultis, G. Singh, C.J. Solomon, A. Kargar, T. Unruh, "Wireless Neutron and Gamma Ray Detector Modules for Dosimetry and Remote Monitoring," IEEE Nuclear Science Symposium, Waikiki, Hawaii, Oct. 28-Nov. 3, 2007.

National Nuclear Security Administration

Semiconductor Materials And Radiological Technologies

©

Wireless Network

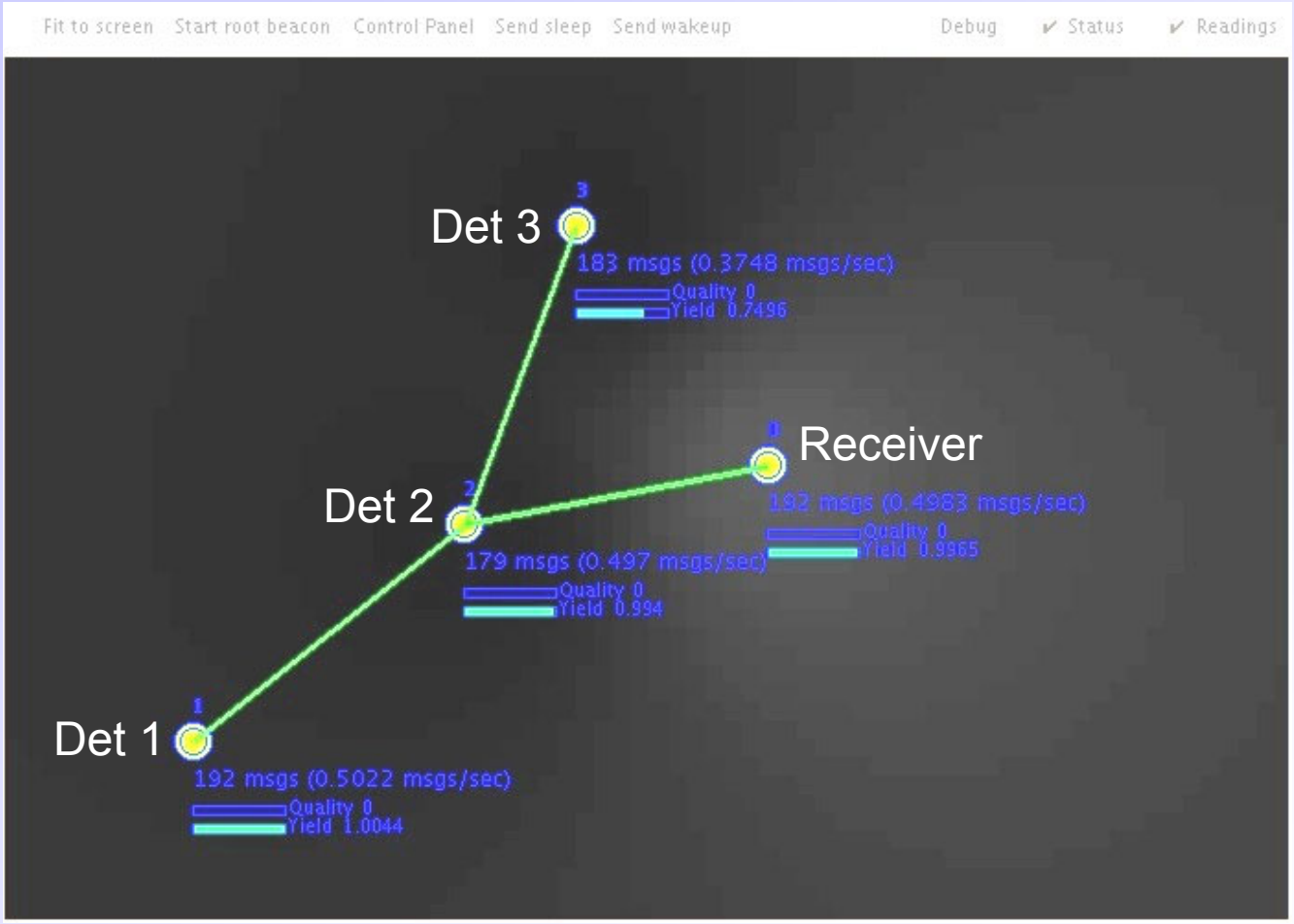

A three detector system, showing Det 1 and Det 3 communicating to the receiver through Det 2.

National Nuclear Security Administration

Semiconductor Materials And Radiological Technologies ©

Wireless Gamma Spectrometer

- Side by side with neutron detectors
- Base computer analyzes spectrum
- CZT and preamplifier in crystal package
- Returns raw spectrum
- Utilizes tiny HV supply

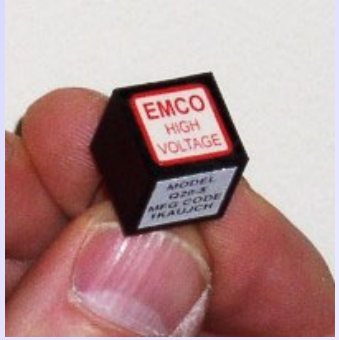

Miniature power supply

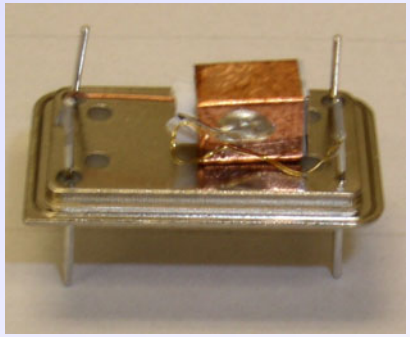

CdZnTe Frisch ring spectrometer

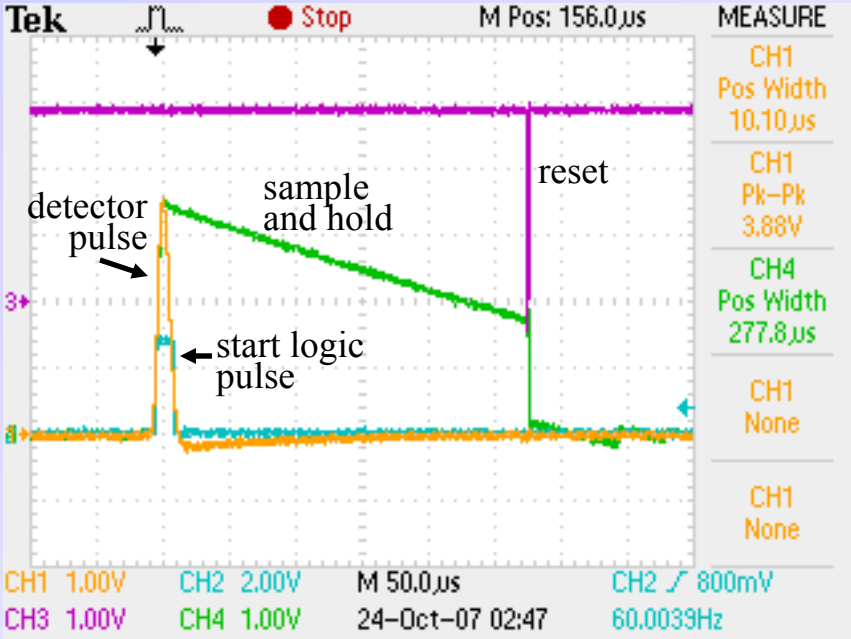

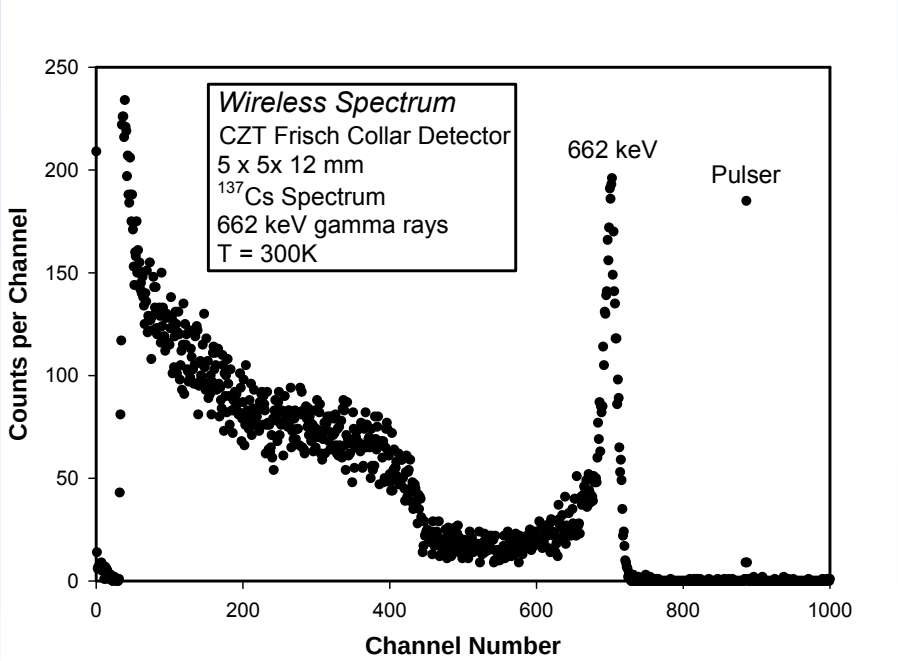

National Nuclear Security Administration

D.S. McGregor, et al., "Wireless Neutron and Gamma Ray Detector Modules for Dosimetry and Remote Monitoring," IEEE Nuclear Science Symposium, Waikiki, Hawaii, Oct. 28-Nov. 3, 2007.

Semiconductor Materials And Radiological Technologies ©

Summary

1. An ampoule sealing station for $LaBr_3$, HgI_2 and CdZnTe processing and growth has been built and is operating.
2. An ampoule carbon coating system has been built and is operating.
3. A slant Bridgman furnace has been designed, built and is now operating.
4. An ultra-dry glove box has been acquired, installed and is now operating.
5. A vertical vacuum distillation/zone melt purification system has been designed, built, and is now operating.
6. Distillations:
   a. Te: 1,2 and 3 stage distillations complete and material is tested.
   b. Zn: 1 and 3 stage distillations complete and material is tested.
   c. Mn and Cd: Initial trial runs are complete.
7. Zone Melting: Initial trials are complete for Cd, Zn, and Te. Te samples have been analyzed.
8. A horizontal $LaBr_3$ sublimation purification system has been designed, built, and is under test.

National Nuclear Security Administration

Semiconductor Materials And Radiological Technologies

©

Summary

9. We have grown CdZnTe and $LaBr_3$ ingots in our multizone vertical Bridgman furnace.
10. A dual electro-dynamic gradient freeze system has been retrofitted for horizontal $LaBr_3$ growth and ingots have been grown.
11. A laser assisted post growth annealing system has been built and is under test.
12. We have retrofitted 40 horizontal ampoule furnaces for HgI_2 growth and they are now in operation.
13. We have rebuilt 10 vertical furnaces for HgI_2 growth and they are now in operation.
14. We have purified HgI_2 using sublimation, melting, and post sublimation methods with encouraging results.
15. We have grown HgI_2 platelets and bulk crystals.
16. We have constructed a KI-solution string saw for detector fabrication.
17. We have constructed a multi-detector system for simultaneous measurement of many detectors.

Summary

17. We have built numerous CdZnTe Frisch collar devices from inferior grade material with outstanding results.
18. We are now building the first CdZnTe frisch collar collimated array for imaging and spectroscopy applications.
19. We have installed Frisch ring detectors onto wireless spectroscopy platforms combined with high-efficiency semiconductor neutron detectors.

This work has been funded in part through NNSA contract number DE-FG07-06ID14725

National Nuclear Security Administration

Semiconductor Materials And Radiological Technologies

©

Summary – Year 1
FY07

Year 1; *Initiate Growth Processes* - In the first year, we will:

1. Procure/install/construct the furnaces for $LaBr_3$, CdZnTe and CdMnTe growth.
2. Construct the purification equipment for the materials.
3. Outfit the high-pressure vertical Bridgman furnaces (donated by SAIC) with controls so as to aid in the synthesis of compounds.
4. Complete first purification by sublimation runs for the elements needed for growth.
5. Grow 1" diameter $LaBr_3$ crystals by vertical Bridgman method.
6. Grow 1" diameter CdZnTe crystals by vertical Bridgman method.
7. Grow 1" diameter CdMnTe crystals by vertical Bridgman method.
8. Completely outfit the remaining 25 HgI_2 horizontal furnaces with controllers.
9. Complete a reliable method to grow detector grade HgI_2 crystals in the horizontal furnaces.
10. Manufacture CdZnTe Frisch ring detectors.
11. Ship materials to Sandia National Laboratory and SAIC for analysis and feedback.

National Nuclear Security Administration

Semiconductor Materials And Radiological Technologies

©

Summary – Year 2
FY08

1. Grow 1.5” $LaBr_3$, CdZnTe and CdMnTe diameter crystals by vertical Bridgman method.
2. Grow 1.5” $LaBr_3$ and CdZnTe diameter crystals using ACRT.
3. Grow 1.5” $LaBr_3$ and CdZnTe diameter crystals under tilted conditions.
4. Observe effects of ACRT and tilting vs. vertical, non-ACRT growth (e.g. Ce distribution, crystal quality & size).
5. Study the effects of Ce and its distribution in $LaBr_3$ crystals.
6. Optimize polymer doped horizontal growth of HgI_2 crystals.
7. Ship materials to Sandia National Laboratory for analysis and feedback.
8. Manufacture CdZnTe and HgI_2 Frisch ring detectors.

National Nuclear Security Administration

Semiconductor Materials And Radiological Technologies

Summary – Year 3
FY09

1. Grow 2" $LaBr_3$, CdZnTe and CdMnTe diameter crystals by vertical Bridgman method.
2. Grow 2" $LaBr_3$ and CdZnTe diameter crystals using ACRT.
3. Grow 2" $LaBr_3$ and CdZnTe diameter crystals under tilted conditions.
4. Observe effects of ACRT and tilting vs. vertical, non-ACRT growth (e.g. Ce distribution, crystal quality & size).
5. Study the effects of Ce and its distribution in $LaBr_3$ crystals.
6. Optimize polymer doped horizontal growth of HgI_2 crystals.
7. Ship materials to Sandia National Laboratory and SAIC for analysis and feedback.
8. Manufacture CdZnTe and HgI_2 Frisch ring detectors.

This work has been funded in part through NNSA contract number DE-FG07-06ID14725

National Nuclear Security Administration

Semiconductor Materials And Radiological Technologies

©

Additional Slides

Imaging Array

- RENA3 board
- Developed by Nova R&D Inc
- Two detectors mounted
- Spectra taken from the two devices simultaneously

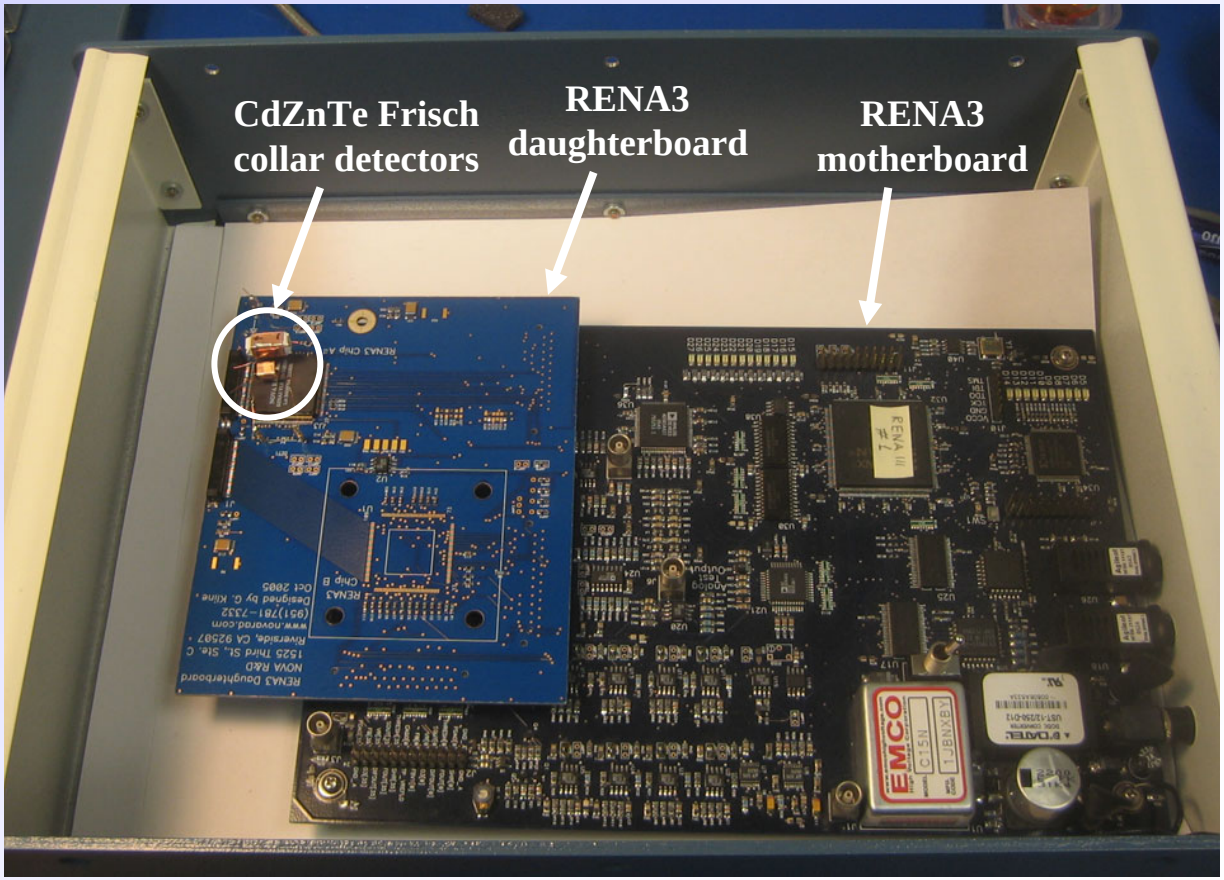

National Nuclear Security Administration

Semiconductor Materials And Radiological Technologies

©

Imaging Array

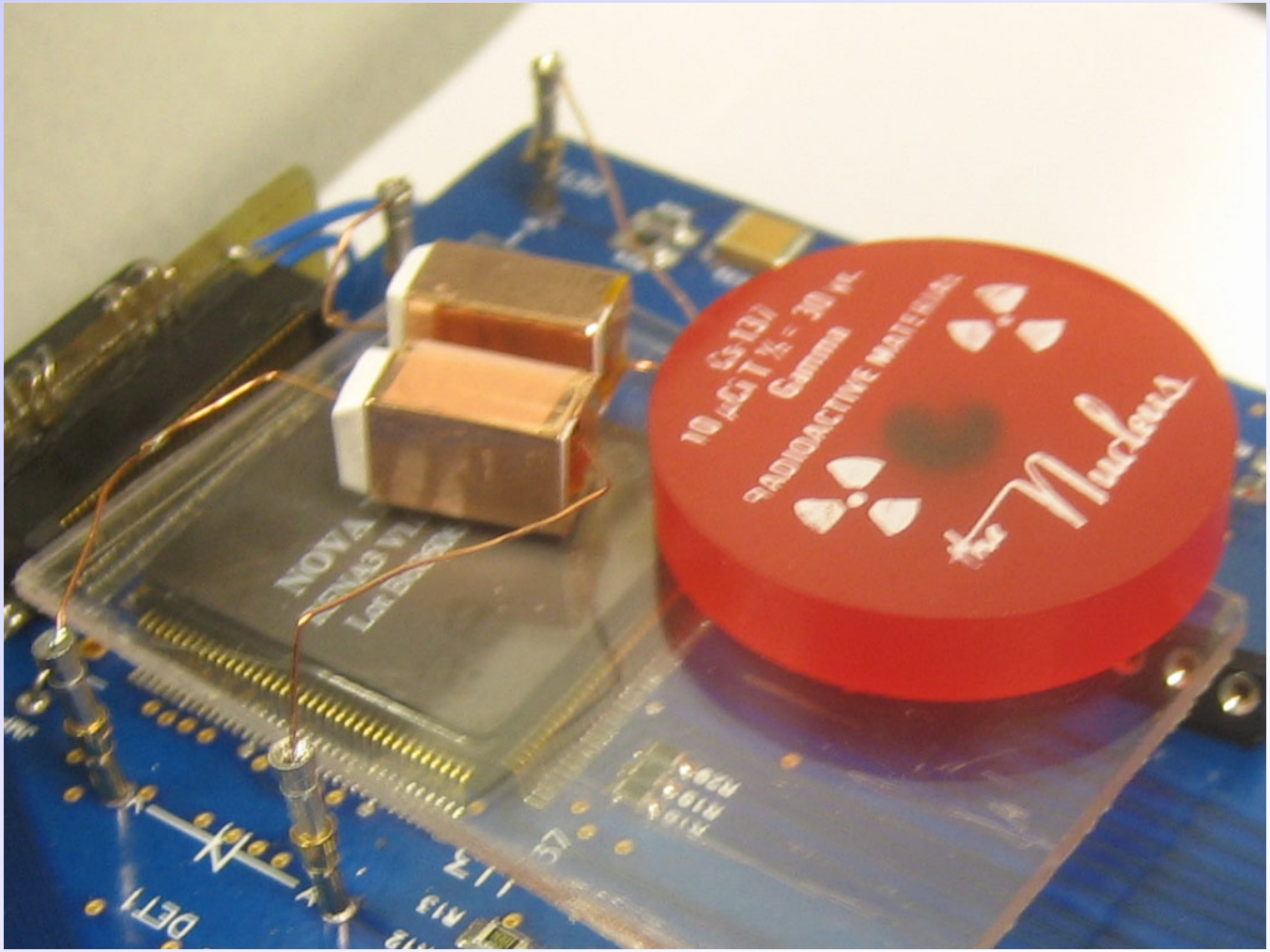

National Nuclear Security Administration

Semiconductor Materials And Radiological Technologies

©

Imaging Array

- Comparing the spectra from one of CdZnTe Frisch collar devices.

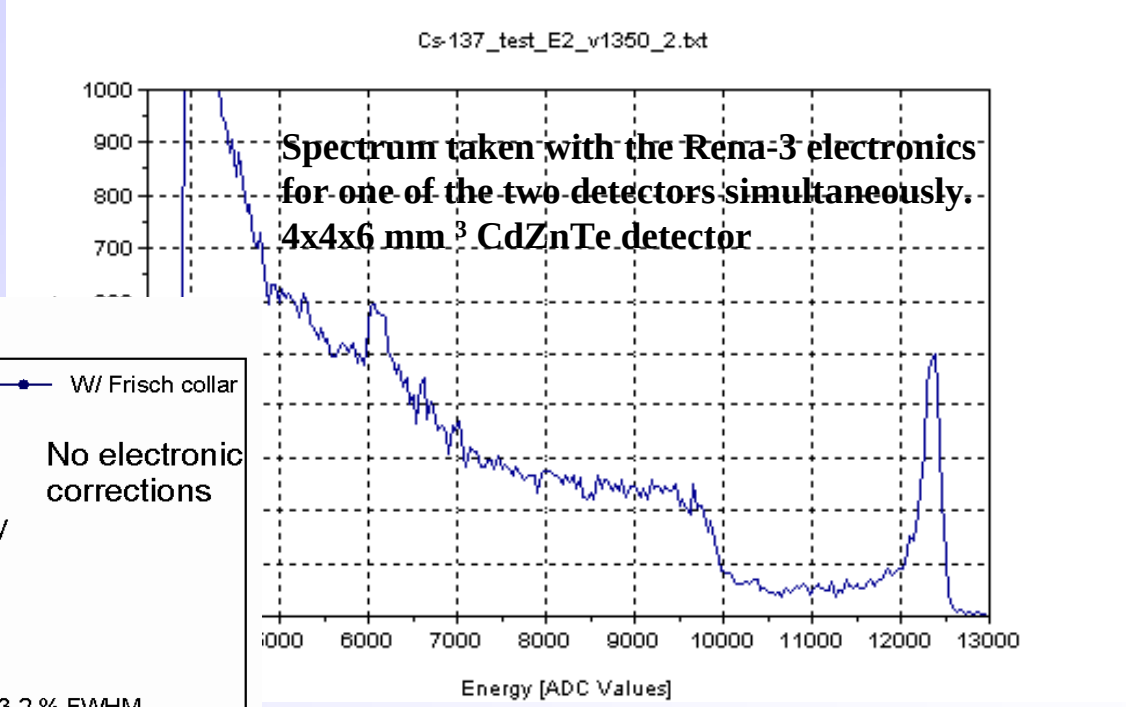

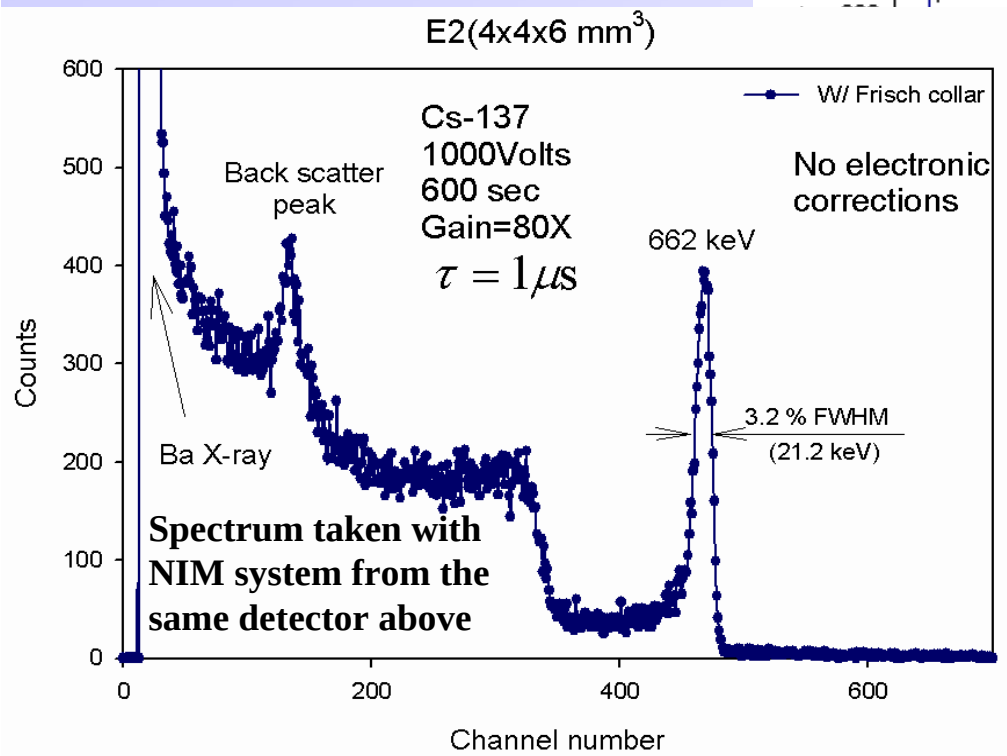

- Top-taken with RENA3 board
- Left-taken with standard 142A preamplifier and NIM

National Nuclear Security Administration

Semiconductor Materials And Radiological Technologies ©

Optical Processing of Chalcogenide Glasses for Remote Sensing Applications

Institution: University of Arizona

Principal Investigator: Prof. Pierre Lucas

Budget: $540K ($180K/year)

Duration: 3 years

Main Milestones:

- Provide advanced method for photorefractive processing of chalcogenide glass infrared photonics.
- Provide technique for characterization of refractive index patterns with sub-micron spatial resolution.

Program Goal:

Technology development for the early detection of nuclear proliferation.

This Project Goals:

Technology development for enabling the detection of infrared signatures of effluent associated with the nuclear fuel cycle.

Technical Scope (Dual):

- Enable direct LASER writing of complex optical device and circuits in infrared glass.
- Characterization of refractive index patterns with sub-micron spatial resolution.

Chalcogenide glasses

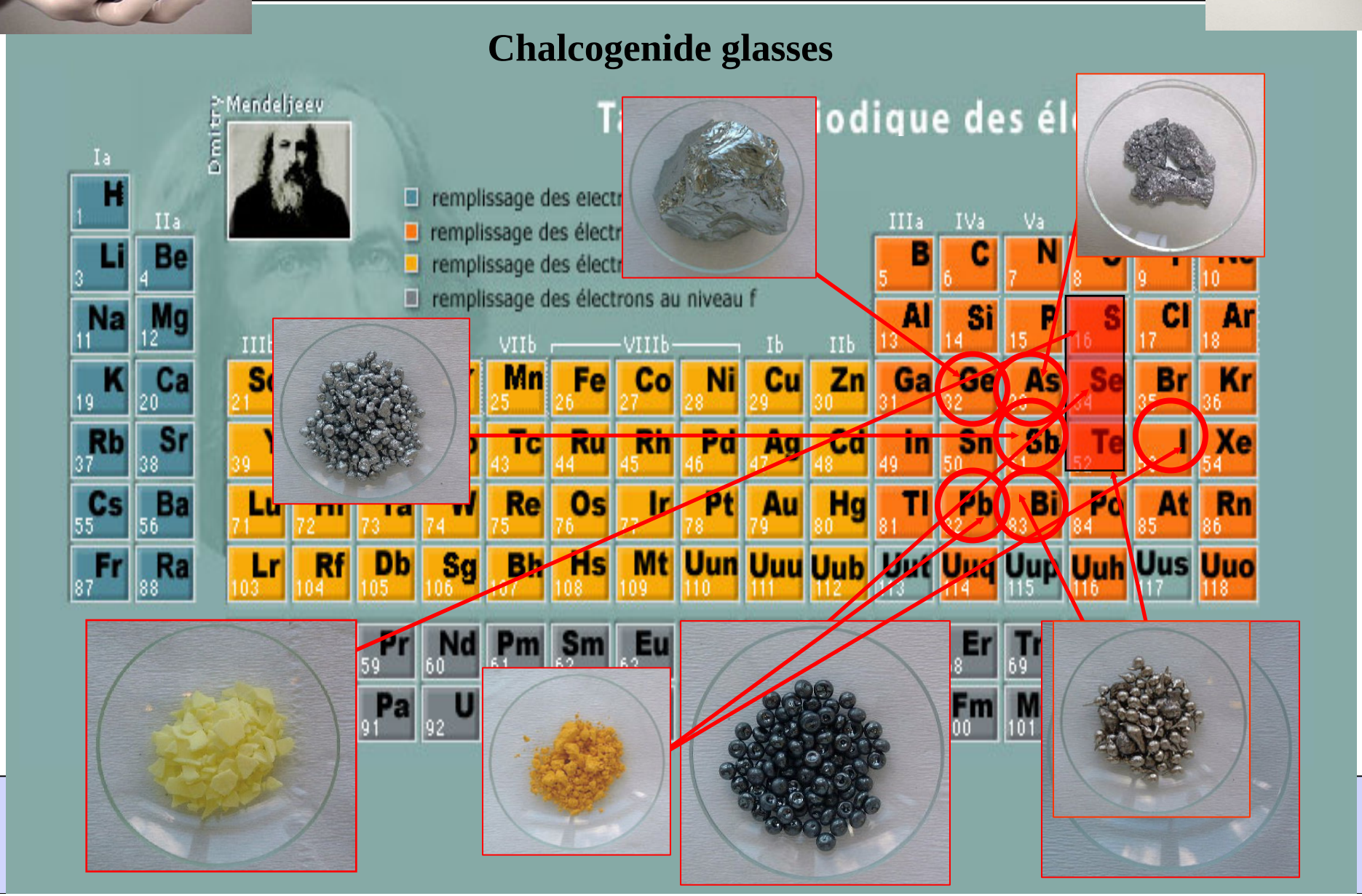

IR Transmission of Chalcogenide glasses

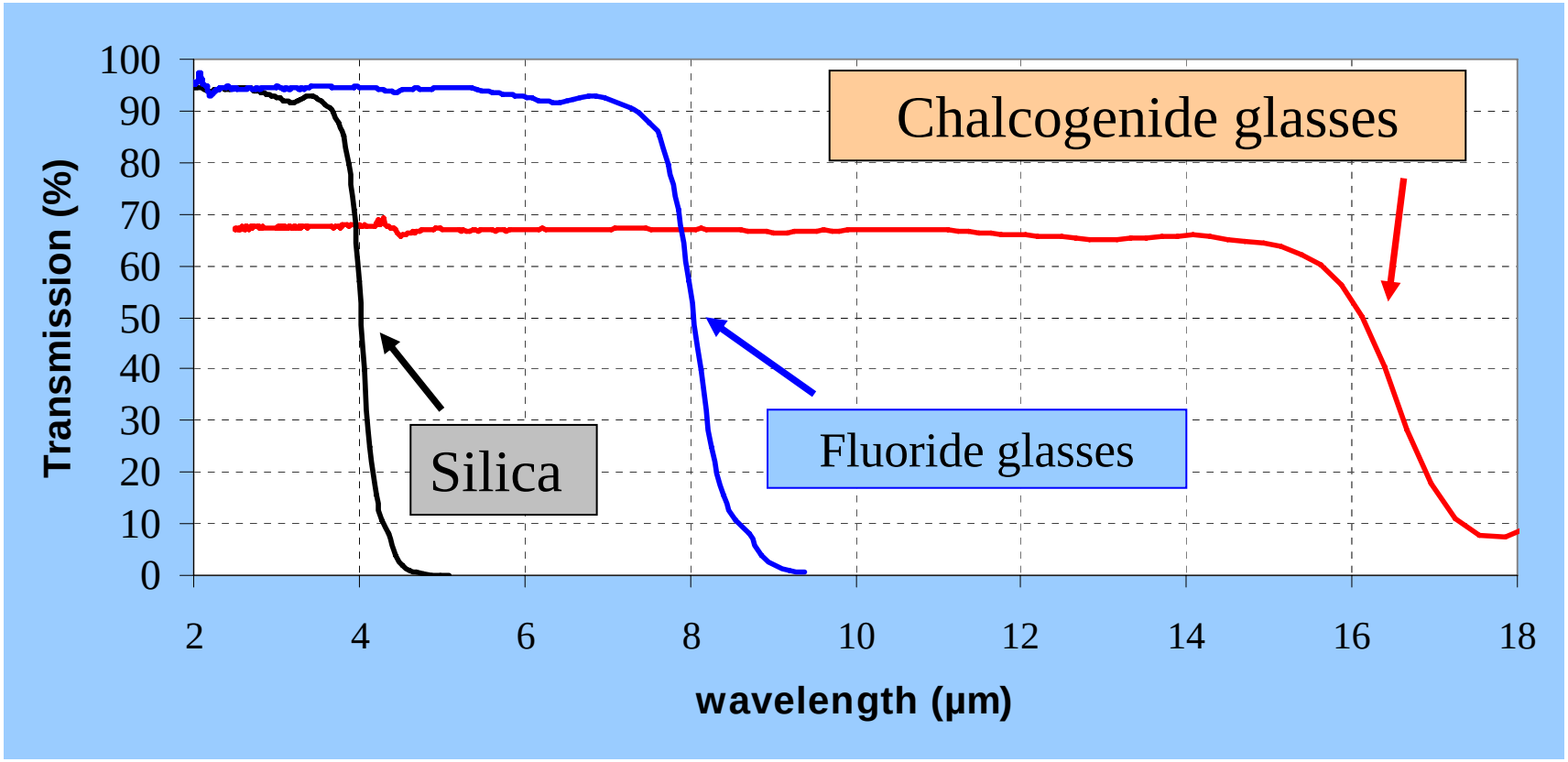

Application of Infrared Glasses

Medical Imaging

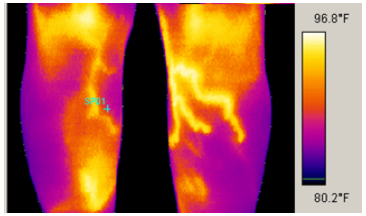

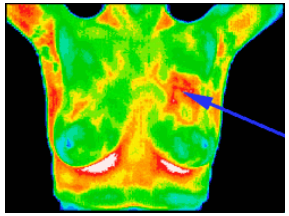

Night Vision

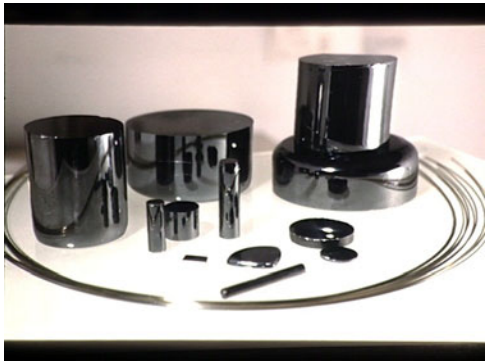

Infrared Spectroscopy

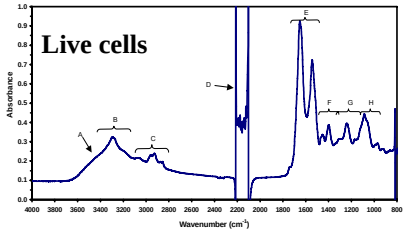

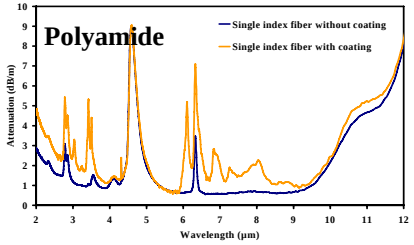

Thermal Imaging

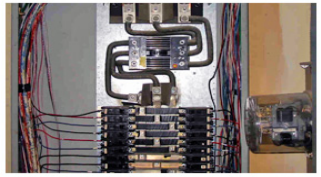

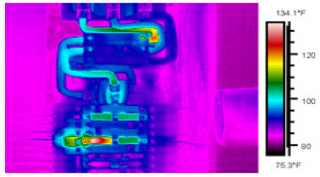

Photoinduced structural change:
Two main type: Volume and Index changes

Photodarkening (photorefraction)

Waveguides

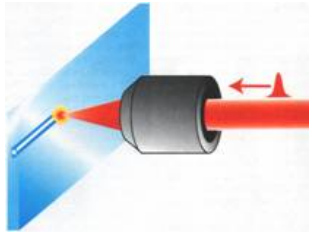

Gratings

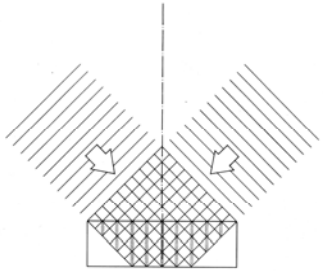

Index pattern

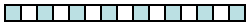

Photoexpansion

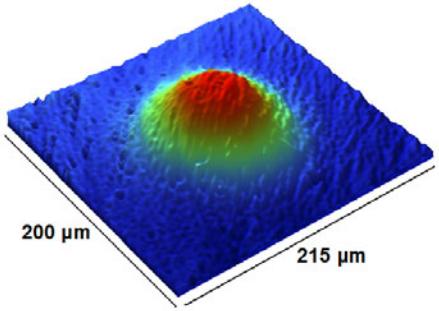

Microlenses

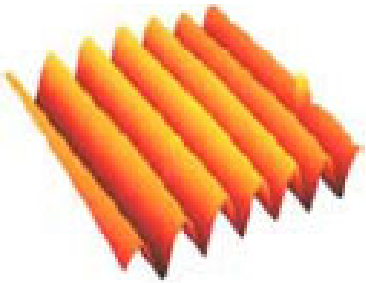

Relief Gratings

Index Mapping

Index patterns offer great potentials for IR photonics devices

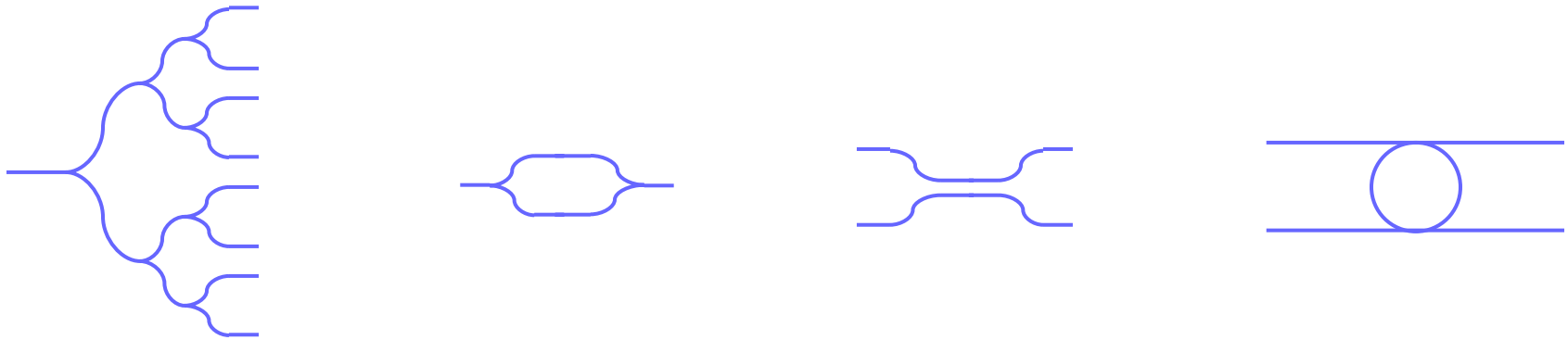

multiplexer interferometer coupler ring resonator

- Also 1D, 2D, 3D photonic bandgap structures

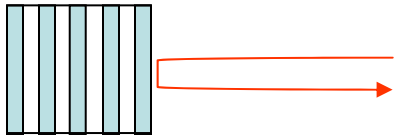

Interest in imaging these features for quality check

• Near-field Scanning Optical Microscopy (NSOM)

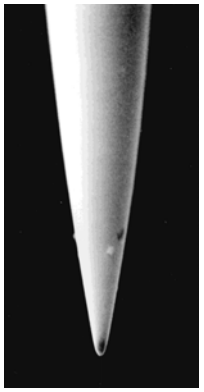

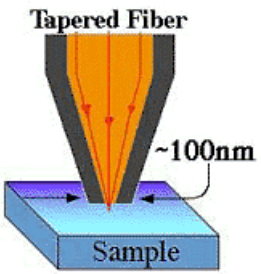

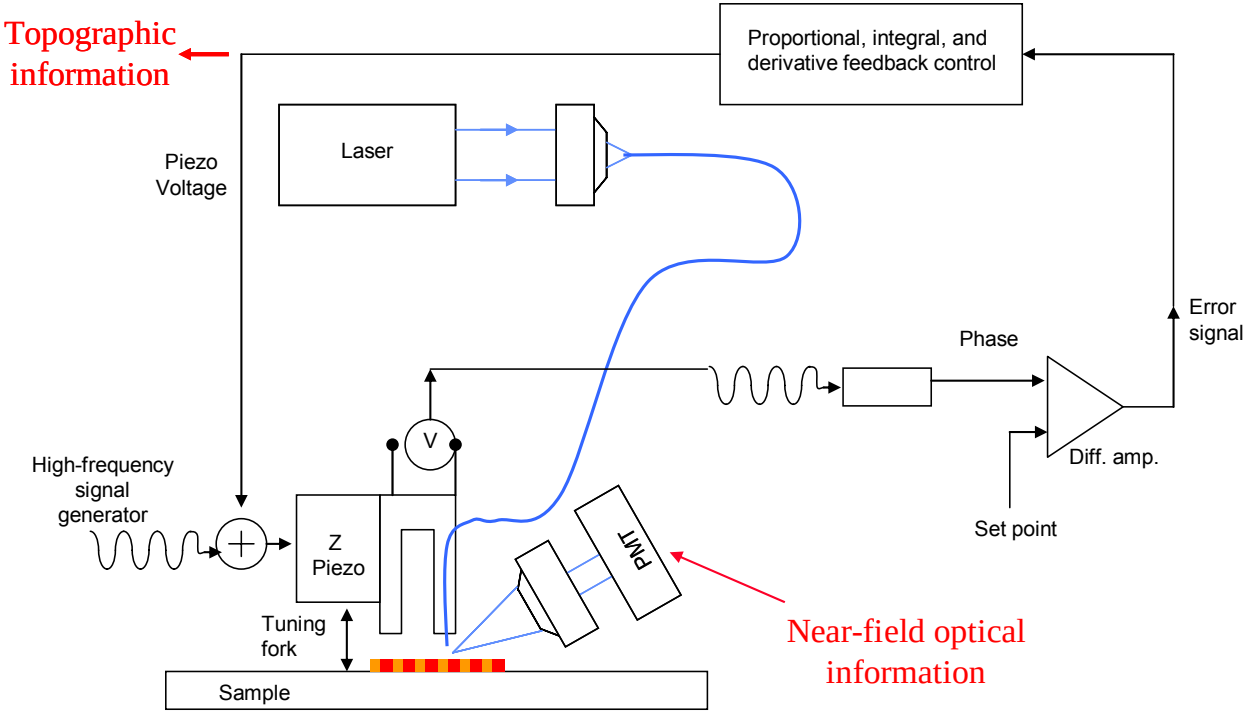

• Variation in index n results in change in reflection: image n.

• Scanning probe technology

• **Advantage**: Provide simultaneous topography and optical image.

• Provide an index pattern image (photorefraction) as well as surface elevation (photoexpansion) **simultaneously**.

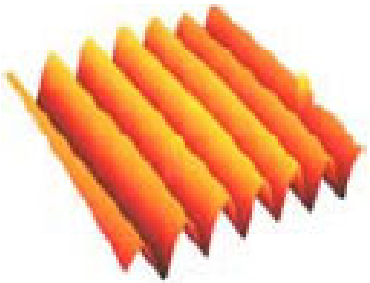

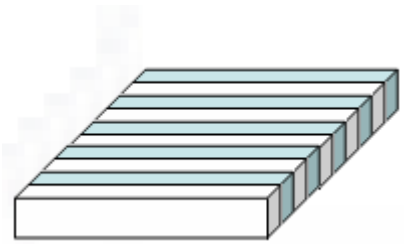

• Can help resolve relative effects of PE and PD during holographic printing of gratings

NSOM TEST IN REFLECTION at 785 nm

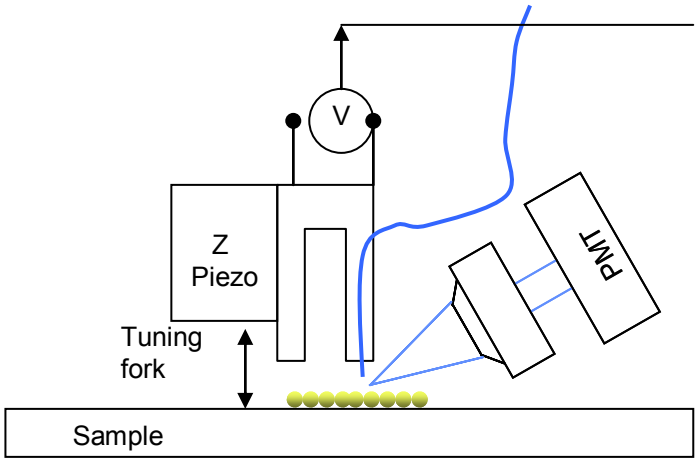

STANDARD:

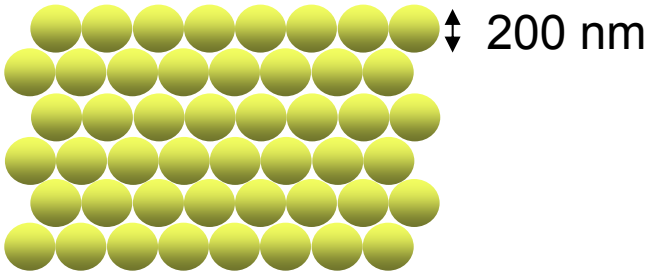

Gold colloid 200 nm in diameter in order to demonstrate sub-diffraction limit resolution

Feature < $\lambda/3$

NSOM TEST IN TRANSMISSION

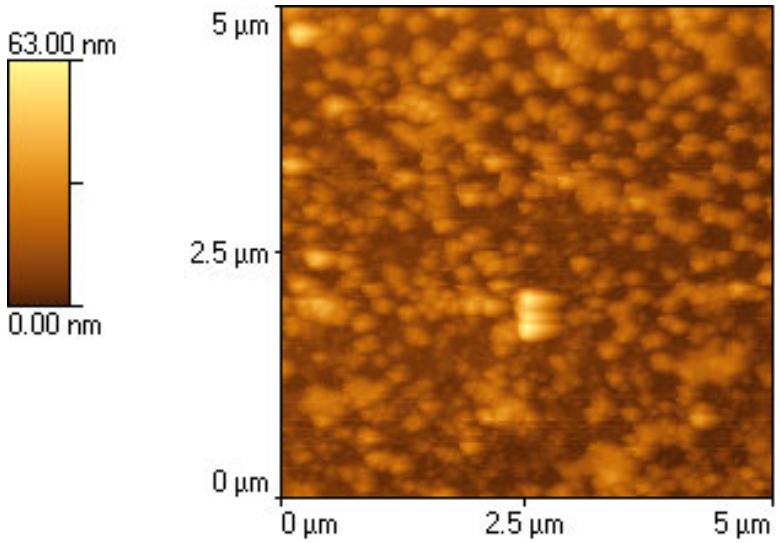

Topography image

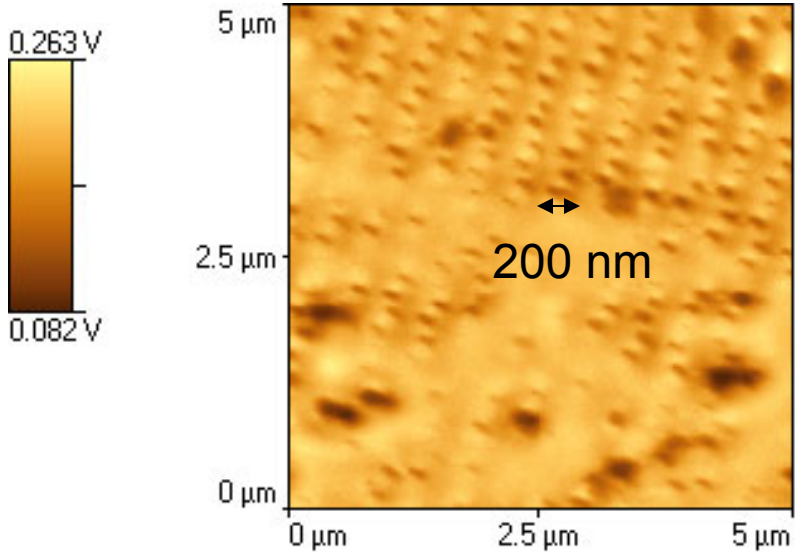

NSOM Transmission image

Demonstration of sub-wavelength resolution in NIR

NSOM TEST IN REFLECTION

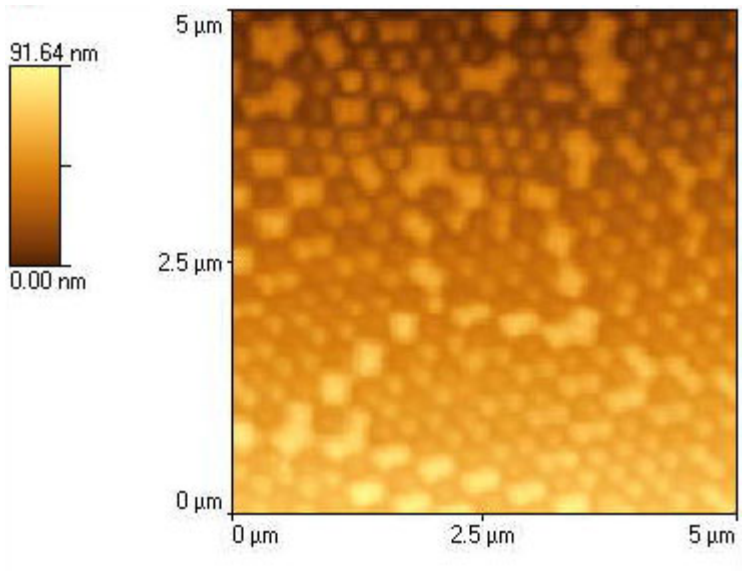

Topography image

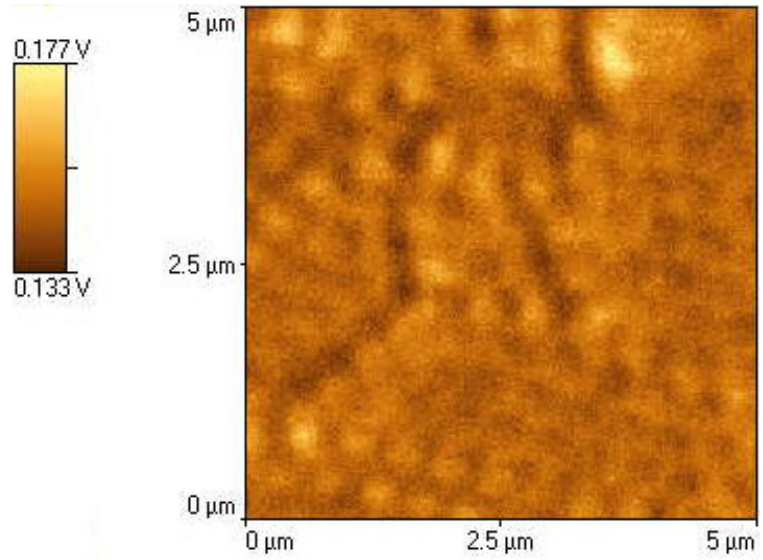

NSOM reflection image

NSOM INDEX MAPPING

NSOM: topography

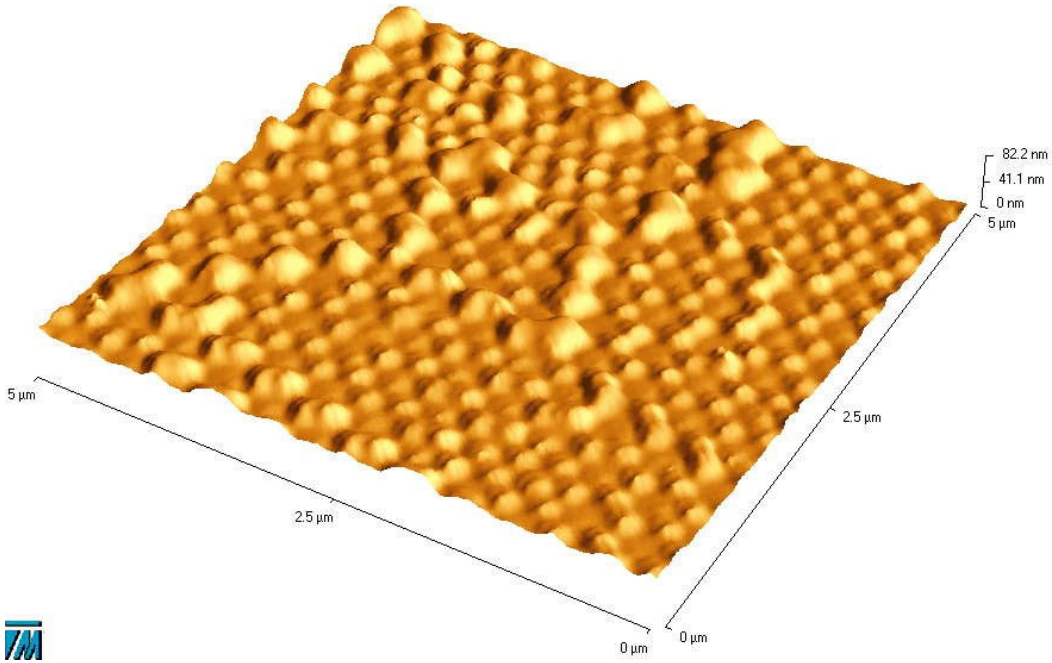

Topography after 3D imaging treatment

FUTURE PLANS

Image photoinduced refractive index pattern

- Produce gratings by holographic printing on As_2S_3 (U of A and PNNL)
- Collect index pattern image at 785 nm.

Simultaneous Optic-Topographic imaging:

- Measure relative magnitude of PE and PD on As_2S_3 gratings.
- Measure relative PE/PD as a function of irradiation time, Intensity, λ.

Laser writing with NSOM:

- Test writing by doing line scans with 514 nm source.
- Image the resulting channel waveguide with 785 nm source.

Mechanism of Photostructural changes

GLASS SYNTHESIS:

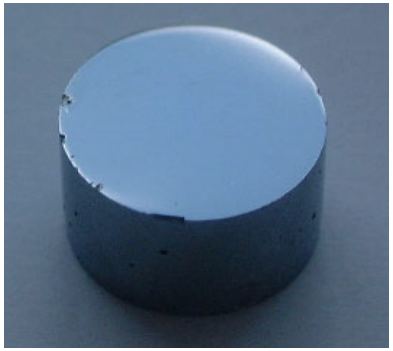

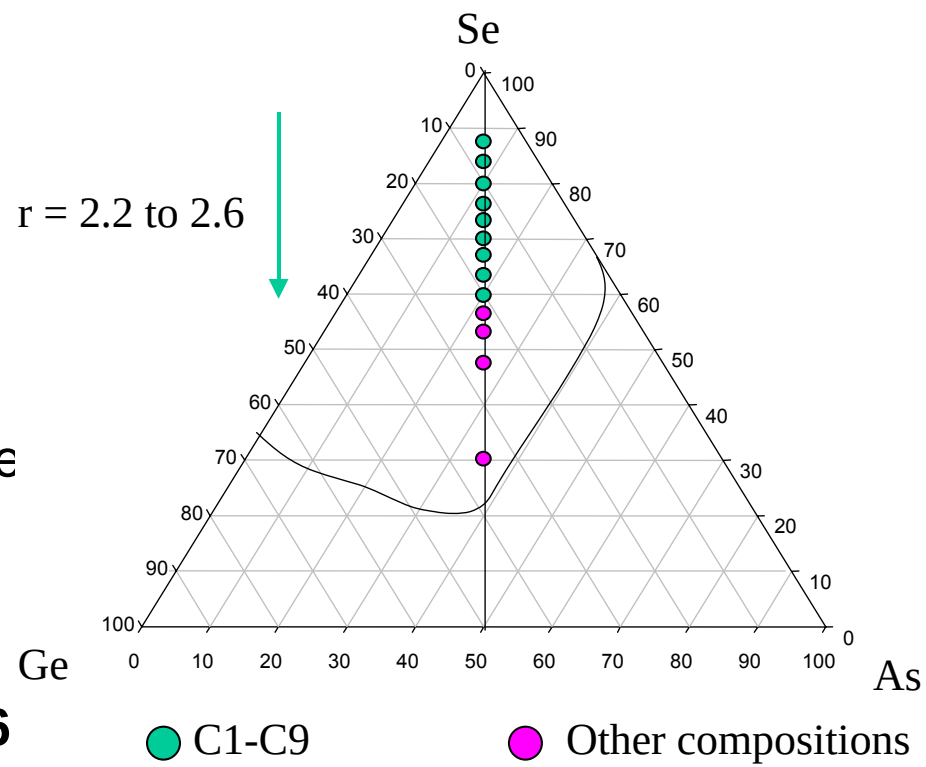

- Identify, synthesize and characterize series of sample that simultaneously:
  - **Are all good glassformers**
  - **Cover wide range of <r>: 2.2 - 2.6**
  - **Have bandgap between 700-900 nm**

PHOTOSTRUCTURAL CHANGES

- **PHOTODARKENING:**

EX-SITU:

- **Irradiate through constant aperture**
- **UV-Vis before and after.**

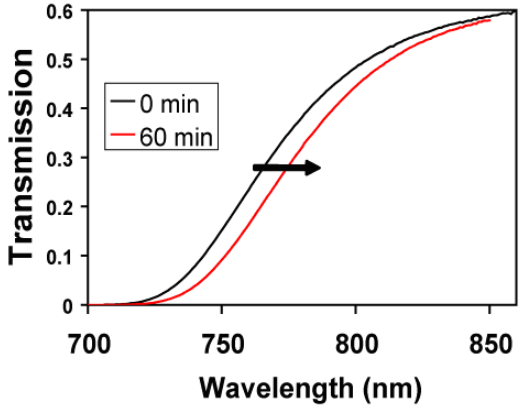

IN-SITU:

- **Continuous irradiation and collection through the sample**

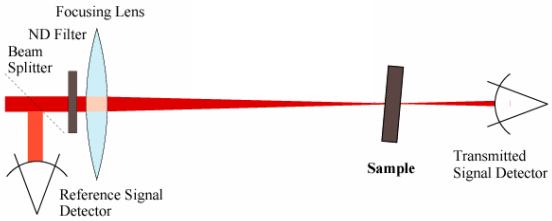

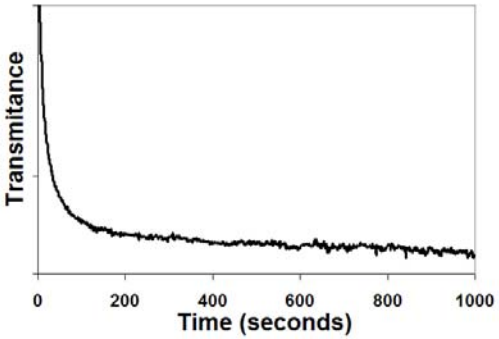

PHOTOSTRUCTURAL CHANGES

- **PHOTOEXPANSION:**
  - **Irradiate through 5X objective**
  - **Change focus (intensity, size)**

  - **Characterize expansion by profilometry**
  - **2D or 3D**

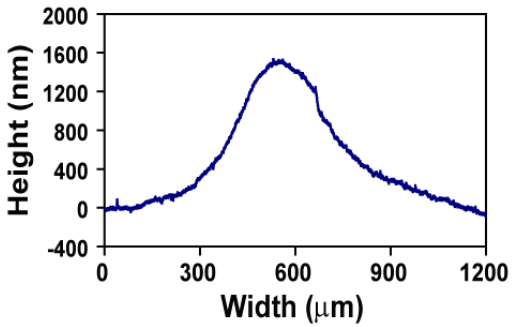

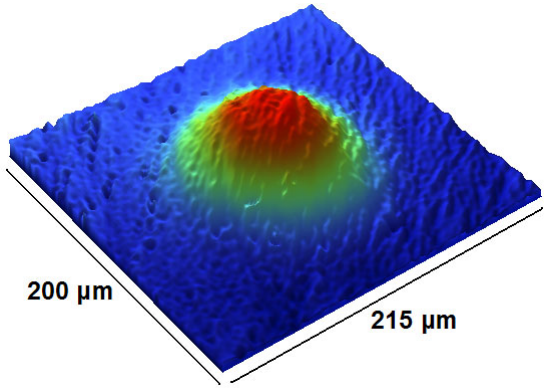

PHOTOSTRUCTURAL CHANGES

- **PHOTORELAXATION:**
  - **Erase thermal history: DSC 10 C/min up/down**
  - **Irradiate bulk of glass**
  - **Measure resulting enthalpy relaxation (DSC)**

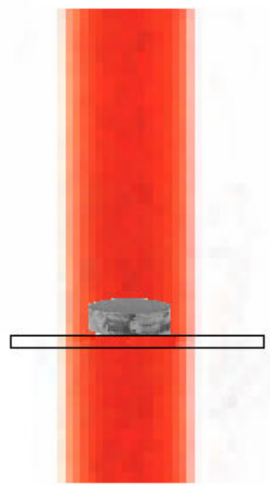

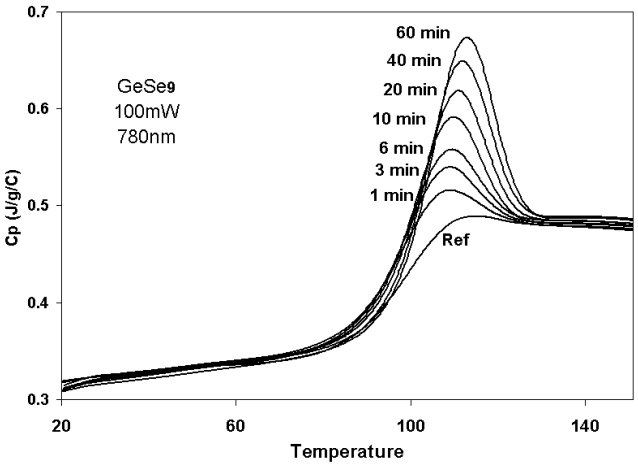

Photosensitivity Ge-As-Se system

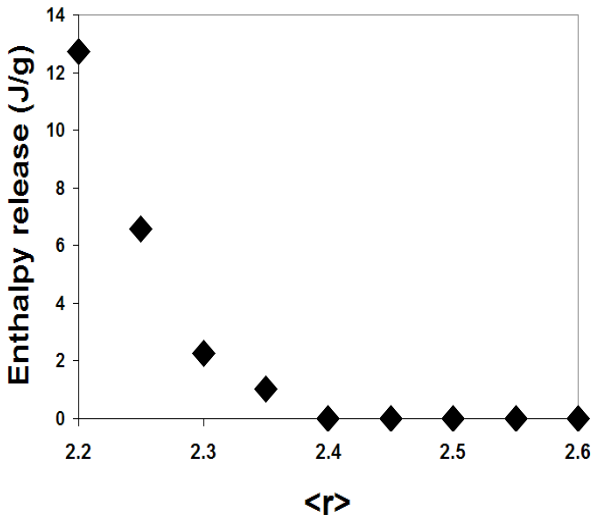

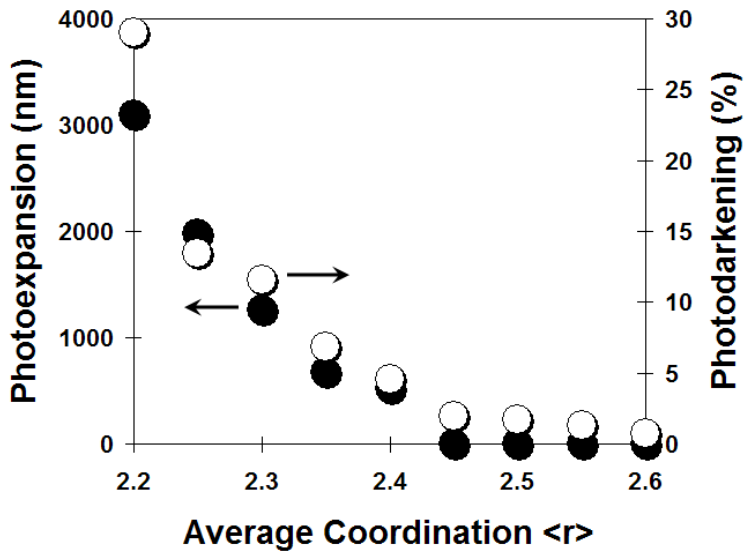

Photostructural effects are suppressed in overcoordinated network glasses.

Photosensitivity Ge-As-Se system

- **Control photosensitivity in fragile (low coordination) glass.**

<r> = 2.2 glass was selected for investigation of photosensitivity control.

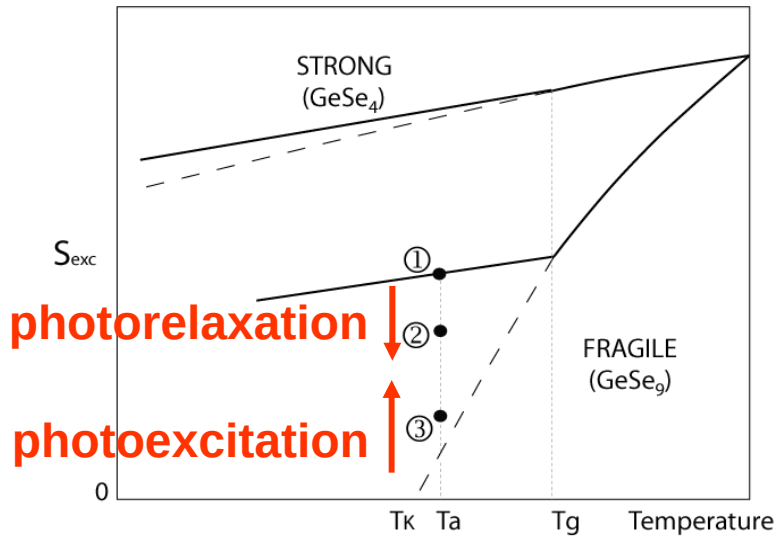

- **Control photosensitivity in fragile (low coordination) glass.**

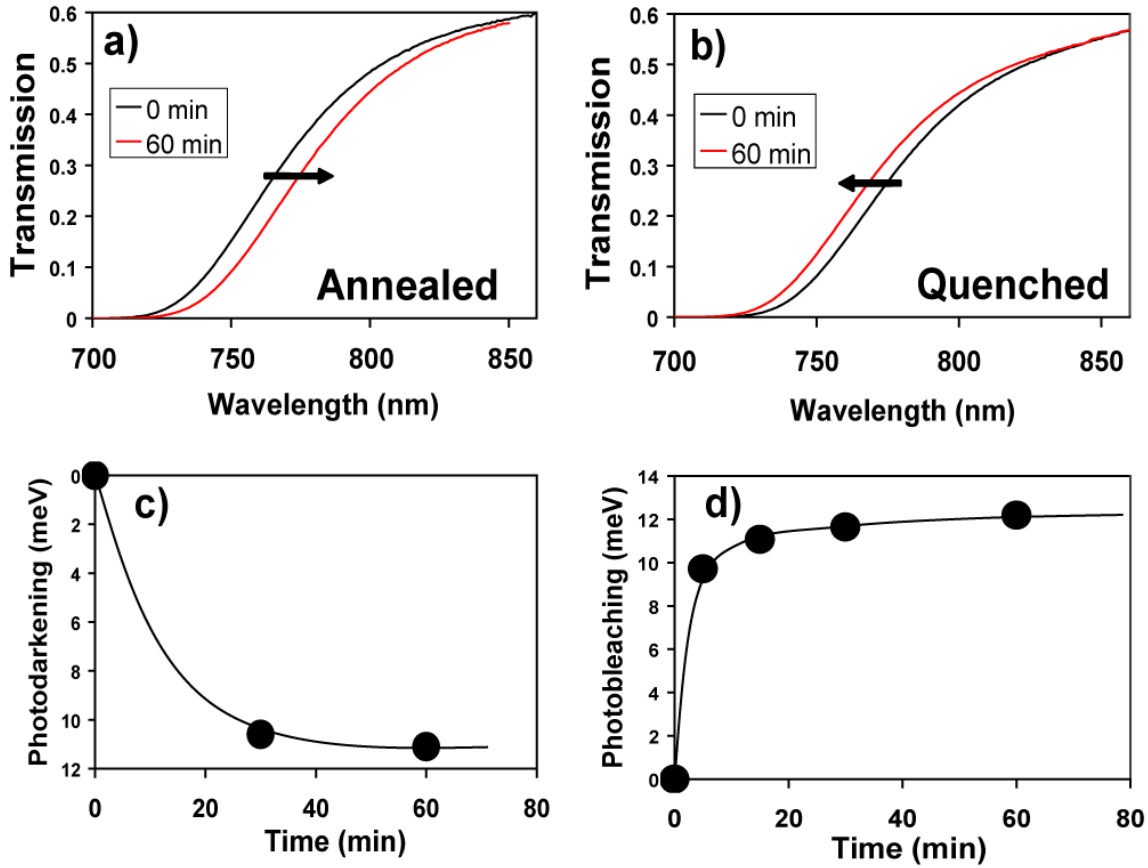

- **Control photosensitivity in fragile (low coordination) glass.**

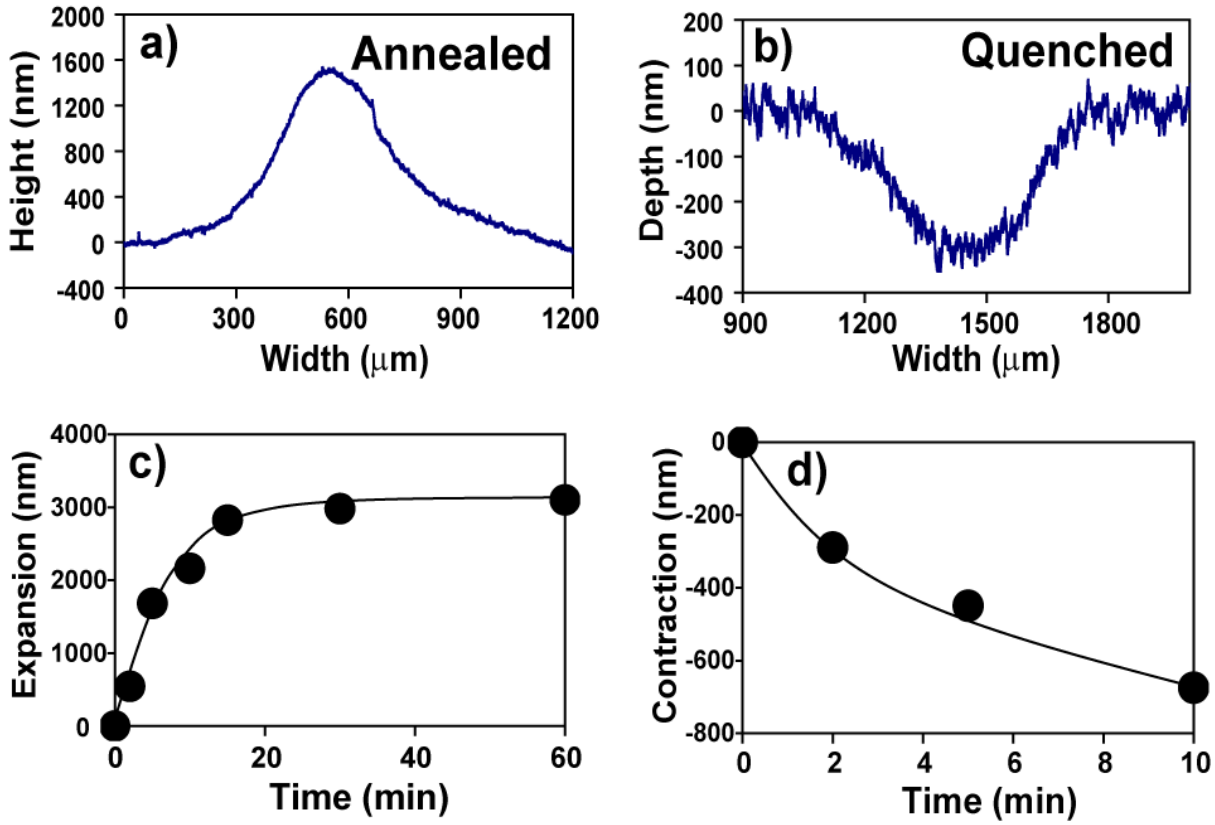

FABRICATION OF COMPLEX OPTICS

- Possibility of inducing contraction and expansion subsequently in the same sample.

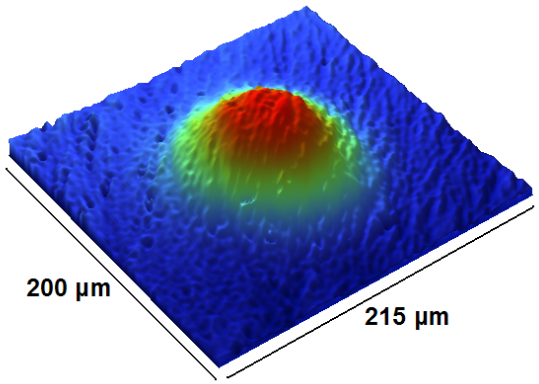

Convex Photoexpansion

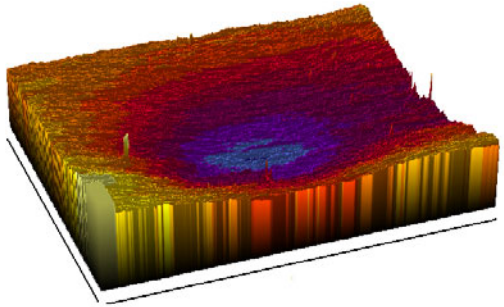

Concave Photocontraction

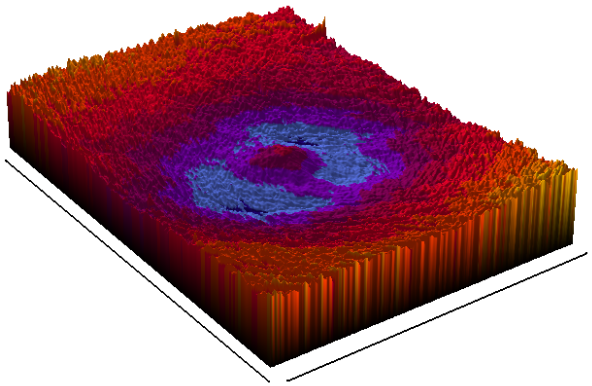

Combined Convex-concave

FUTURE PLANS

Thermal stability of photo effects

- Study as a function of <r>
- Calorimetric characterization in relation to PE and PD.

Wavelength dependence of photosensitivity

- Wavelength dependence of photostructural change
- Dependence of PE vs PD (can we separate effects)

Effect of Intensity in over-constrained glasses

- Comparison of dependence between over and under-constrained
- Max power before optical damage.

Optical Microsensor Array for Remote Sensing of Chemicals

Dr. Kathleen Richardson, PI
Glass Processing and Characterization Laboratory (GPCL)
COMSET
School of Materials Science and Engineering
Clemson University
richar3@clemson.edu

Dr. Anu Agarwal
Electronic Materials Laboratory
Materials Science and Engineering
Massachusetts Institute of Technology
anu@mit.edu

List of participating organizations

- Clemson University
- Massachusetts Institute of Technology
- University of Central Florida
- Lockheed Martin Corporation

PI's and Co-investigators

- Clemson University
  - Prof. Kathleen Richardson, PI
  - Dr. Laeticia Petit, Mr. Nathan Carlie
  - Prof. Igor Luzinov, Dr. Bogdan Zdyrko
- Massachusetts Institute of Technology
  - Prof. L. Kimerling, co-PI
  - Dr. Anu Agarwal, Mr. JJ Hu
- University of Central Florida
  - Prof. Martin Richardson, co-PI
  - Mr. Troy Anderson
- Lockheed Martin Corporation
  - Ms. Patricia Sharek-Evans, co-PI

Budget

- Annual budget - $290K/year
- Clemson - $160K/yr
- MIT subcontract - $120K/yr
- LMCO subcontract
  - Years 2, 3 partial funds for intern support (<$10K)

Project objectives, findings to date

- **The program objectives aim to** improve the performance characteristics of optical sensor systems by developing and characterizing ***robust, highly sensitive and specific, planar multi-chemical sensors, by capitalizing on optical resonance enhanced sensitivity***. The **novelty** of our sensor design is three-fold:
  - **use of chalcogenide materials** for chemical sensing, which serves both to extend the operating wavelength range from UV to visible to far infrared, and to enable a low temperature process to fabricate an ultra-high-Q optical resonant cavity with an atomically smooth surface; and
  - **use of a planar optical resonant cavity** to enhance the device sensitivity; and
  - fabrication based on **CMOS-compatible processing** allowing for integration with other key components of a system-compatible structure

Findings to date

- Year I (from Sept. 06 to Aug. 07) of this project has focused on ***material identification and the fabrication of chalcogenide-based evanescent field waveguide structures*** for sensing a target species in a fluid analyte:
  - Chalcogenide glass (ChG) design and synthesis for 2-inch sputter targets for film deposition as well as bulk material for evaporation; characterization of bulk glass/glassy film properties
  - Chalcogenide waveguide fabrication by lithography; evaluation of post-processed structure and properties (thermal, structural and optical)
  - Evaluation of polymer coated chalcogenide film waveguide surfaces, chemical durability and analyte interaction behavior
  - Investigation of laser processing conditions for trench and buried waveguide fabrication

Technical Presentation Outline

- Glass development and characterization
  - Synthesis, photo-induced structural changes
- Polymer coatings for enhanced sensitivity
- Laser – material interaction
- Device fabrication and performance
  - CMOS compatibility, device fabrication and performance

Glass processing and film deposition

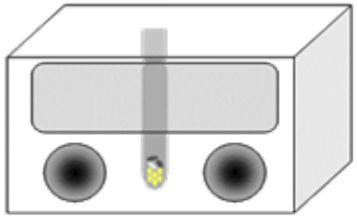

Weigh in Glove Box

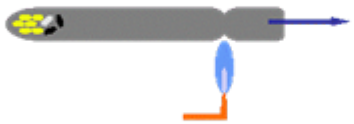

Vacuum @ 110 °C ~ 4 hrs
Seal with torch

Melting ~ 12 Hrs

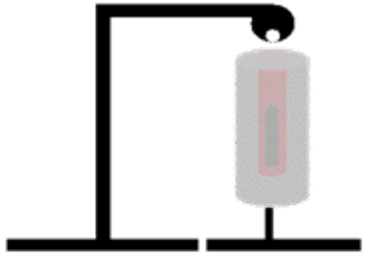

Air quenching

Annealing

Thermal Evaporation (TE)

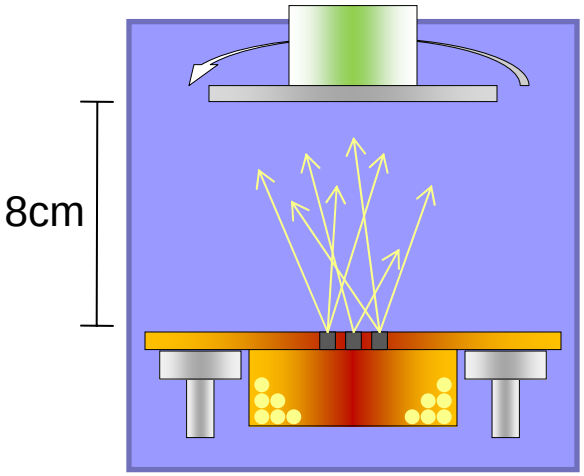

Ar Pressure	5.0 x 10^{-7} Torr

Pulsed Laser Deposition (PLD)

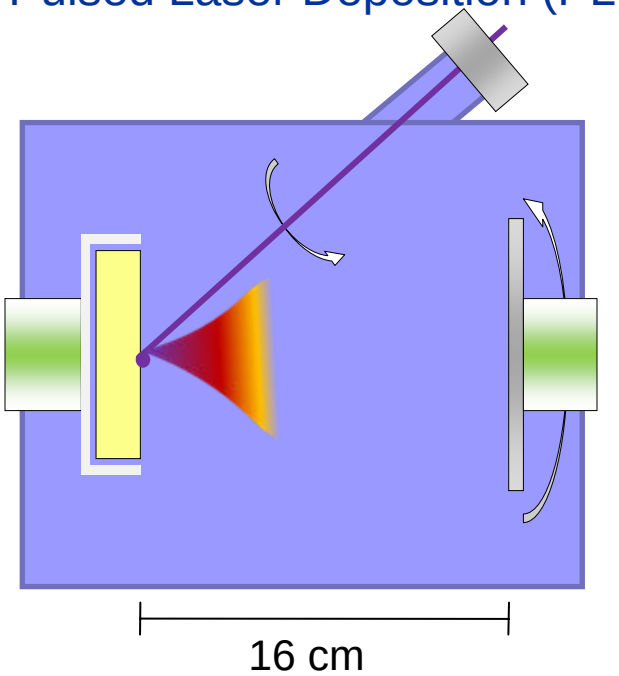

Ar Pressure	5.0 x 10^{-7} Torr

PLD Laser parameters

Wavelength	355 nm
Average Power	5 W
Pulse Duration	12 ps
Repetition Rate	28 MHz
Focal spot dia.	15 μm
Peak Intensity	10 GW/cm^2

Scanning Electron Microscopy (SEM) with Energy Dispersive Spectroscopy (EDS)

TE Film

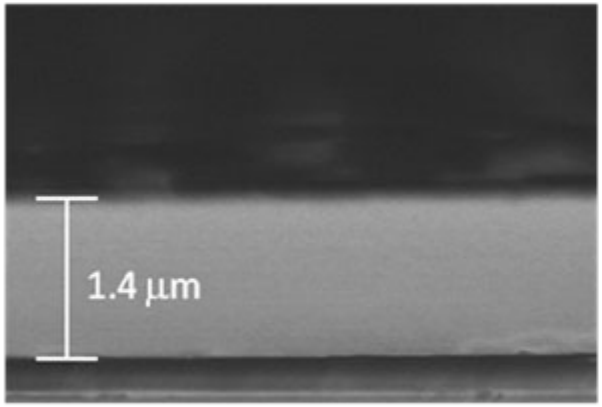

PLD Film

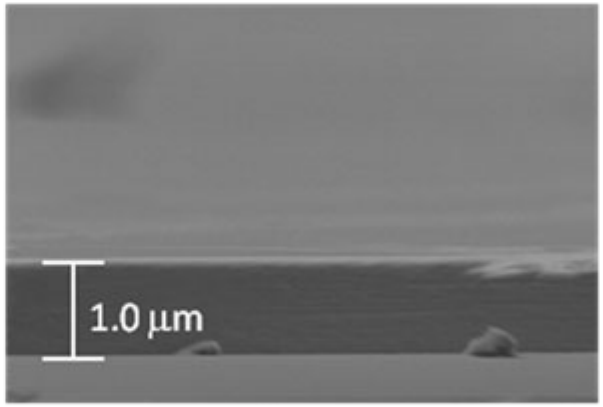

2.0kV x20.0k 2.00 µm

Deposition Method	Target	Thickness by SEM* (± 10nm)	Composition by EDS (± 2 at. %)**		
			% Ge	% Sb	% S
Thermal Evaporation	$Ge_{23}Sb_7S_{70}$	1400 nm	23	11	66
PLD	$Ge_{23}Sb_7S_{70}$	1000 nm	23	7	70

** Thickness confirmed using Zygo white light interferometer and AFM*
*** Composition by difference*

- PLD films appears to have a composition identical to that of the bulk target
- Composition difference for TE is close to limit of error for the measurement (@ ±2%)
- Both films appear to have a uniform structure through the thickness

Optical property determination

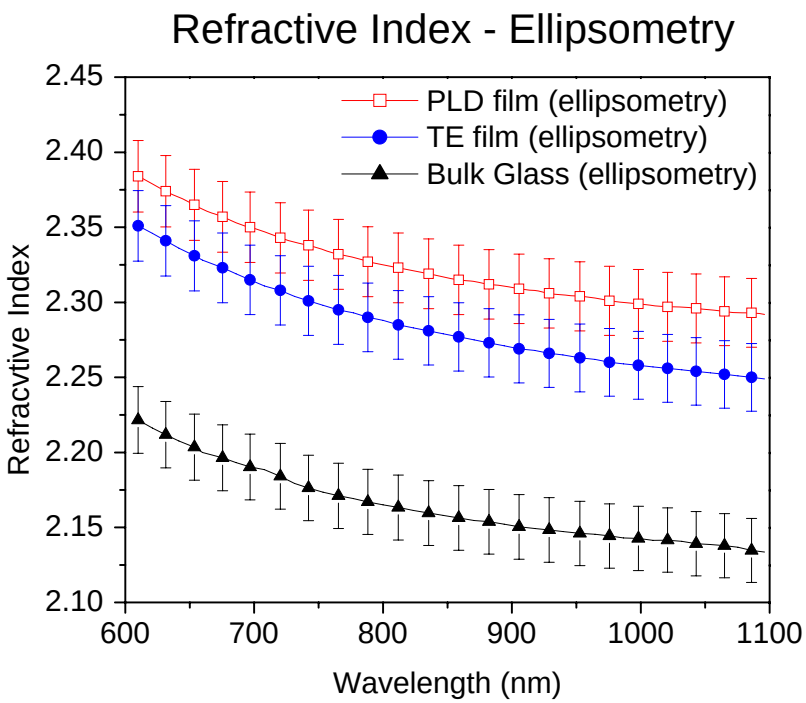

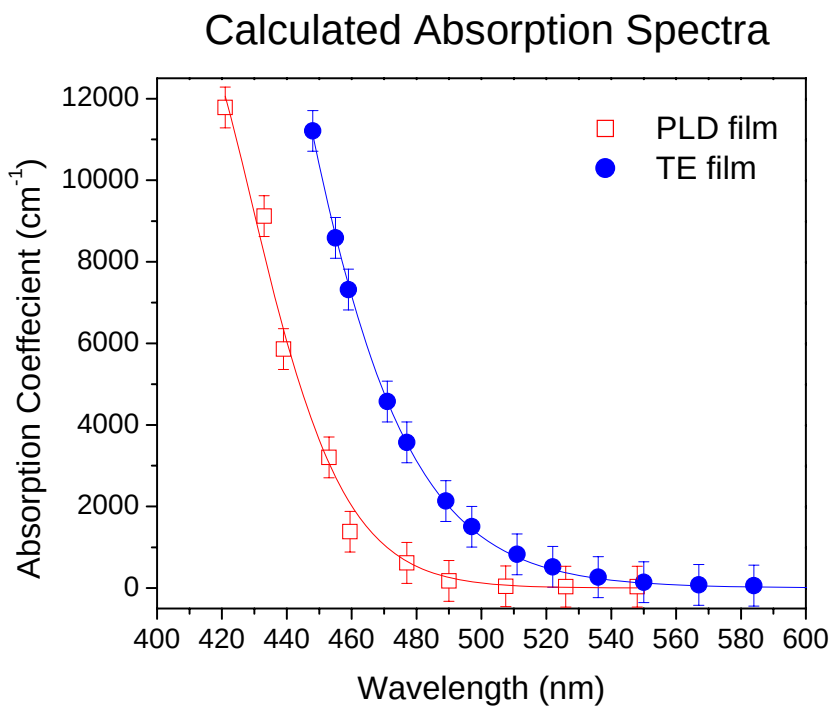

Films share similar refractive index, which is higher (proportional to density) than that of parent bulk glass

Film deposition process impacts density, refractive index

Cannot compare absolute values due to bulk ⇒ thickness difference

Band gap of TE film red shifted from PLD

Deposition method influences band gap of film

Micro-Raman Spectroscopy

PLD film versus TE film

GeS_4 (isolated)

$GeS_{4/2}$ (corner sharing) **$Ge_2S_4S_{2/2}$** (edge sharing)

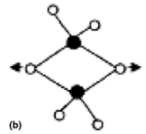

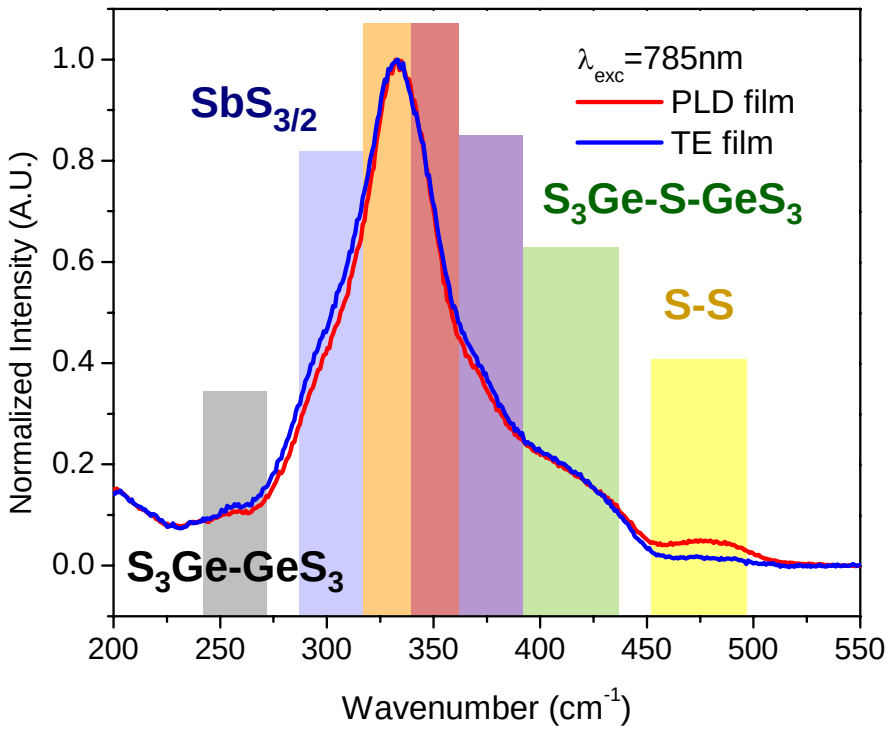

Shift to higher wavenumber & narrower band

$\Rightarrow \uparrow GeS_4$, $\downarrow GeS_{4/2}$ & $Ge_2S_4S_{2/2}$

$\uparrow$ S-S, $\downarrow$Ge-Ge

$\Rightarrow$ Less interconnected structure in PLD film

PLD film versus bulk glass

$GeS_{4/2}$ **GeS_4** **$Ge_2S_4S_{2/2}$**

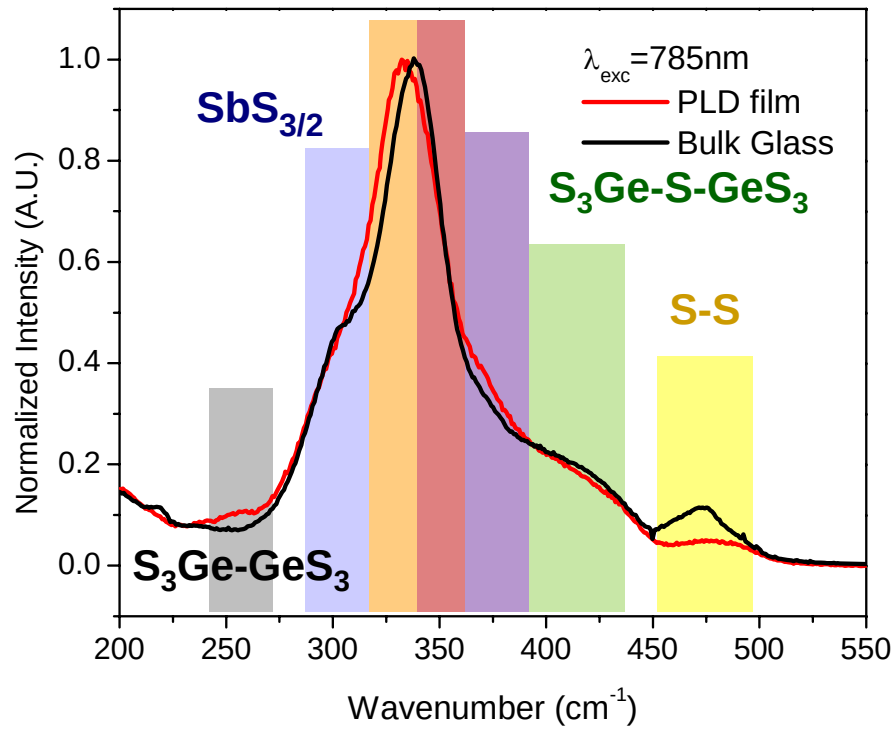

Shift to higher wavenumber & narrower band

$\Rightarrow \uparrow$Isolated units, $\downarrow$Edge & Corner Sharing

$\uparrow$ S-S, $\downarrow$Ge-Ge

$\Rightarrow$ Least interconnected structure in bulk

Polymer Coatings for Chalcogenide Glasses

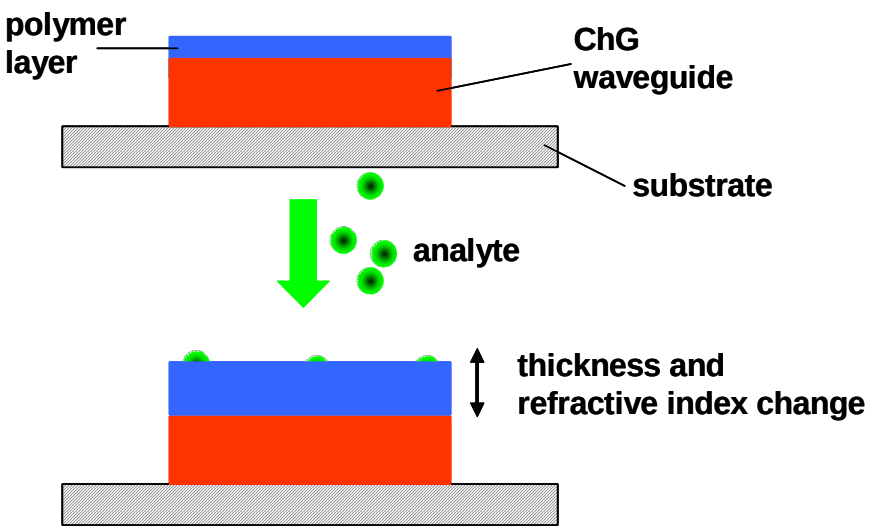

Objective:

Enhance evanescent wave sensor response to target analyte (N-methylaniline)

Strategy:

Create a polymer layer on top of chalcogenide glass waveguide able to selectively bind analyte of interest

Approach:

Grafting of the polymer layer bearing carboxylic moieties able to react reversibly with amine group of the analyte

Two carboxyl group containing compounds were chemically attached to the ChG surface:

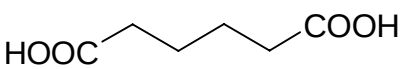

Adipic acid:
approach #1

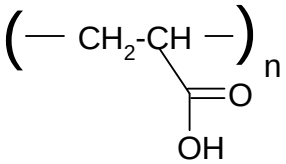

Poly(acrylic acid):
approach #2

Approach #1: *adipic acid grafting*

1. PGMA dip coating from 5% MEK solution
2. Thermal PGMA cross-linking
3. Adipic acid grafting from vapor phase
4. Test of the samples to analyte exposure

Image size 10x10 μm; vertical scale – 10 nm

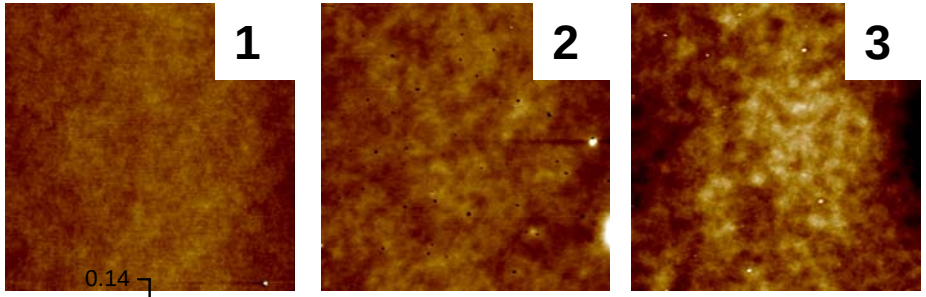

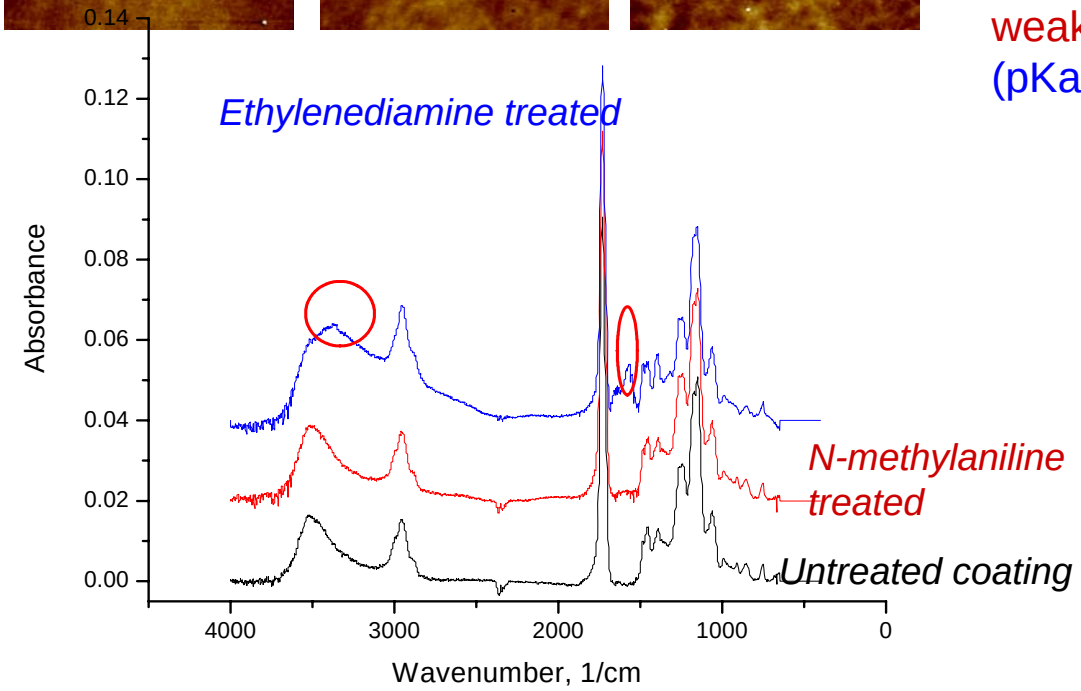

✓Model Si wafer surface and ChG were modified

✓Coatings are permanent and stable against treatment with solvents

✓AFM imaging revealed uniformity and smoothness of the coatings

✓Binding properties of the coatings were tested with N-methylaniline (pKa=4.85, weak base) and Ethylenediamine (pKa=9.92, strong base)

FT-IR

Weak Ethylenediamine binding

Not detectable N-methylaniline binding

Approach #2: *poly(acrylic acid) grafting*

- ✓ **Less cross-linked and more swell-able coating**
- ✓ **Sequential layer-by-layer deposition of PGMA and PAA**
- ✓ **Number of layers and thickness of the coating can be easily tuned**

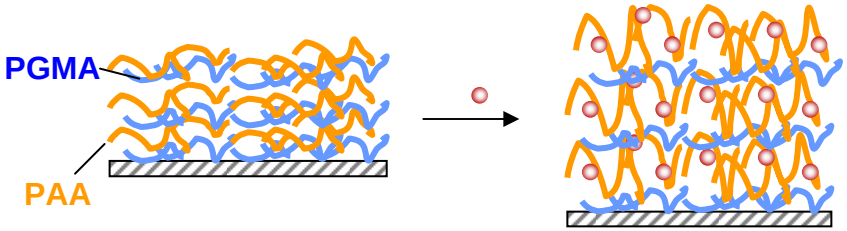

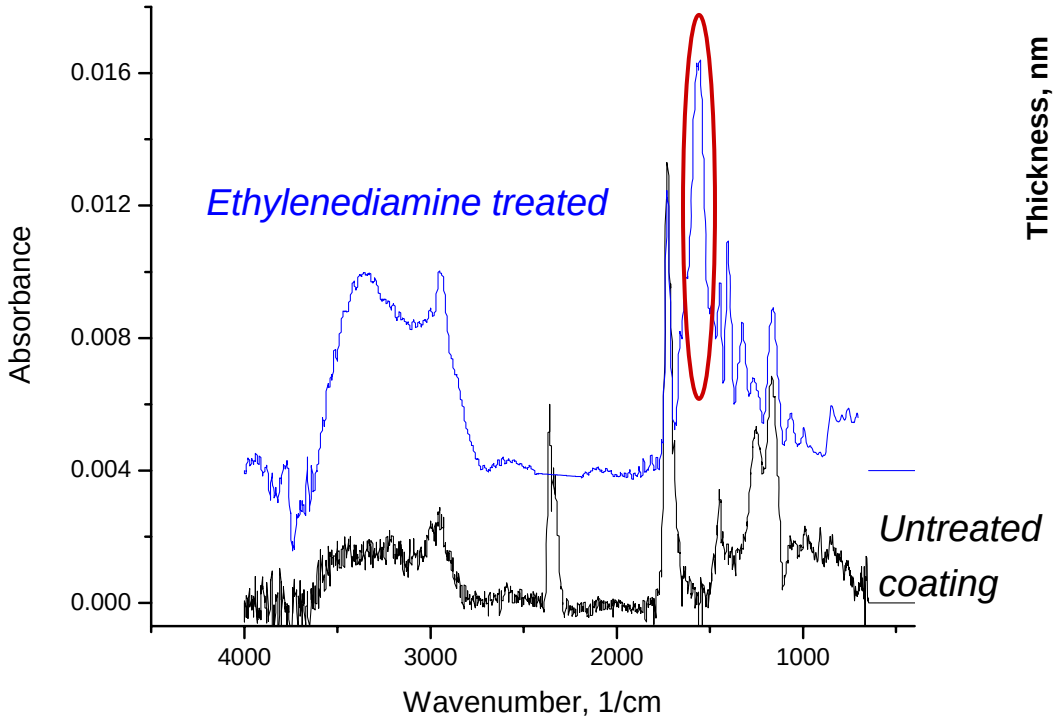

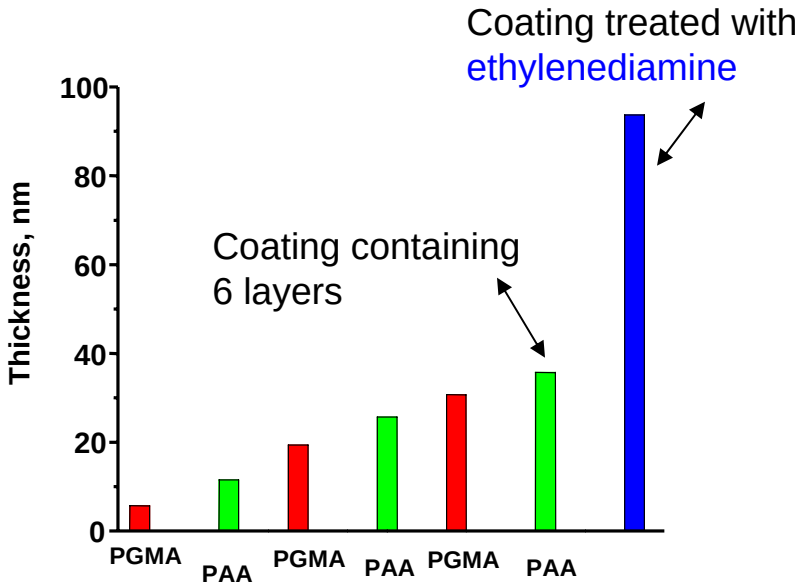

FT-IR

Layered system exhibits large capacity towards ethylenediamine

Femtosecond Direct Laser Writing

Flexible fabrication method for the machining of chemical sensors in transparent media

- Femtosecond regime allows 3-D volumetric processing and **minimizes thermally induced defects**

- Fabrication of multiple elements with single laser:
  - Microfluidic Channel: Laser Ablation
  - Optical Waveguide: Irradiation below ablation threshold

- Fabrication of many transparent materials in both bulk/film form
  - Chalcogenide Glass
  - Oxide Glass
  - Polymer
  - Crystal

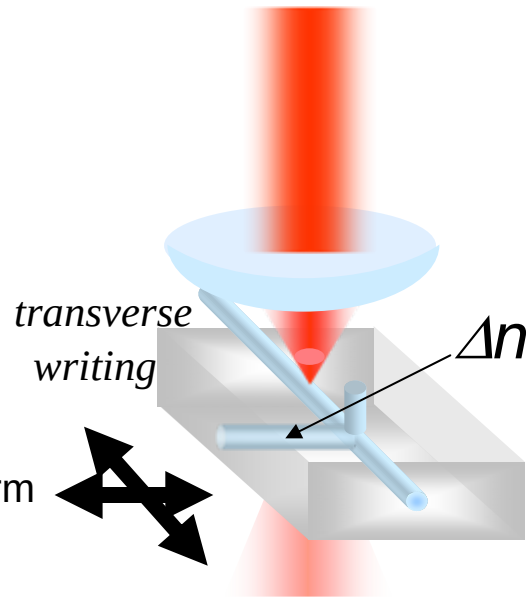

ns or other "conventional" exposure

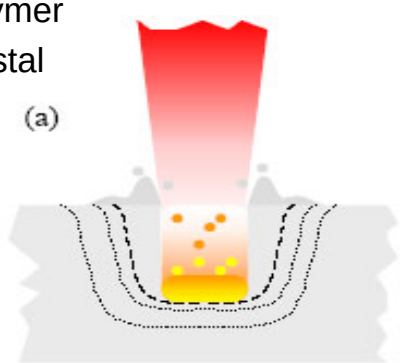

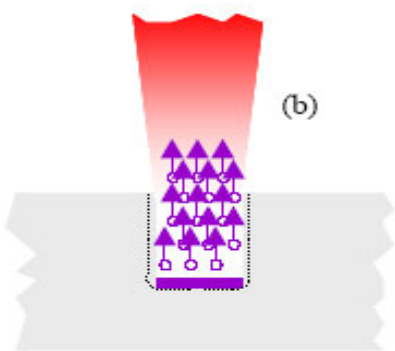

fs exposure with minimal debris and thermal effect

Dependence of Ablation Threshold on Repetition Rate

Logarithmic dependence on number of pulses relates to nonlinear absorption of the fs irradiation

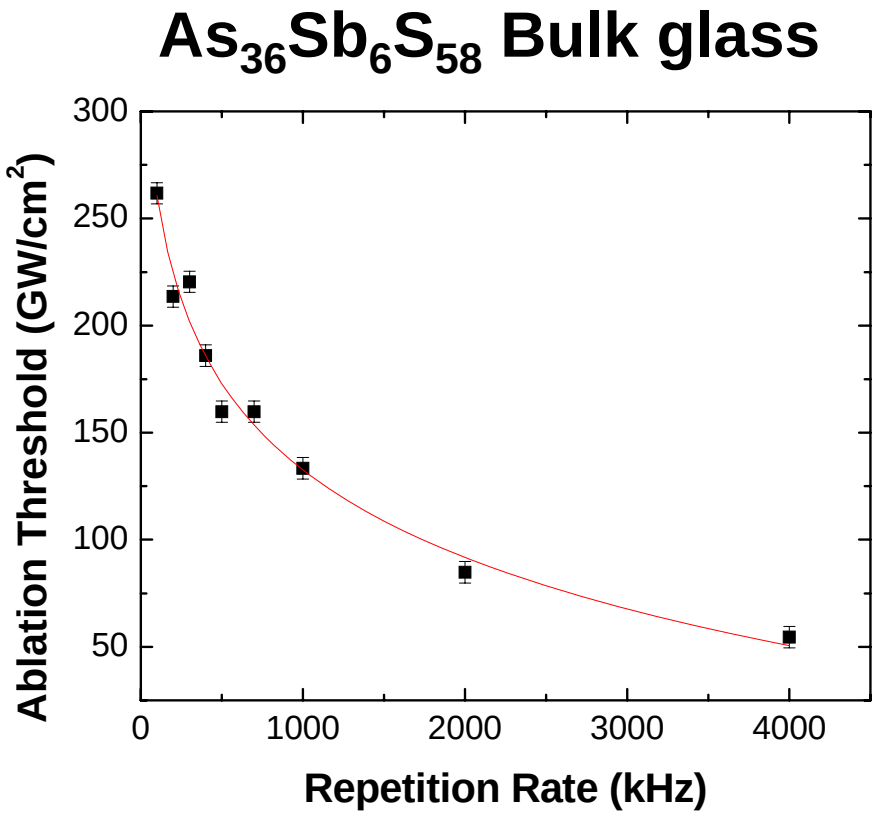

- λ = 1048 nm
- τ = 400fs

↑ Repetition Rate ⇒ ↓ Ablation Threshold

More pulses per focal spot lower the maximum pulse energy needed to induce ablation

Refractive Index Modifications in Thin-Film $Ge_{23}Sb_7S_{70}$

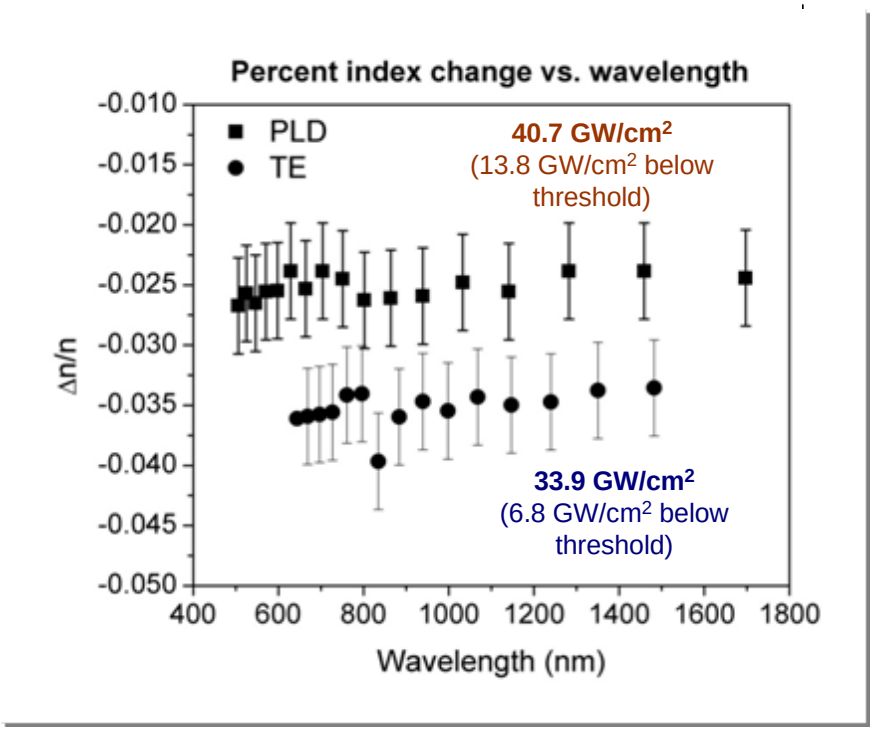

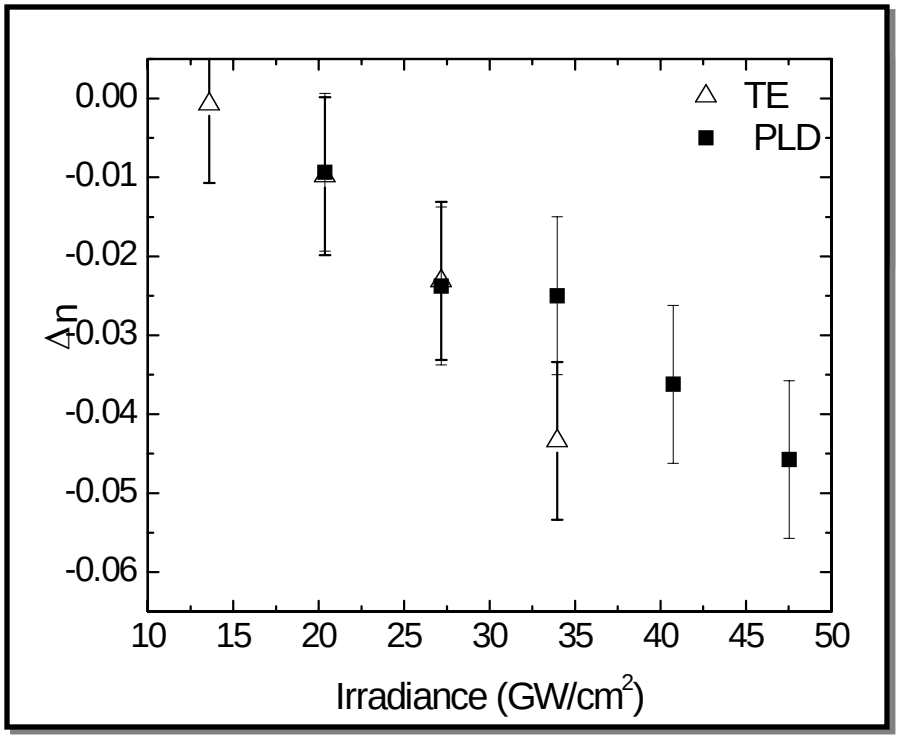

Constant Δn over the transmission spectrum of the glass

Dynamically tunable refractive index modifications possible with fs direct writing

Developing CMOS-compatible processes for devices using chalcogenide materials

<u>Why CMOS-compatibility is important:</u>

- Cost reduction
  - ✓ Leverage on existing infrastructures
  - ✓ High volume production
  - ✓ Take advantage of the scaling law
- Performance improvement
  - ✓ Improved processing capabilities
  - ✓ Integration with other planar optoelectronic devices

Chalcogenides are NOT yet considered CMOS-compatible materials!

Developing CMOS-compatible processes for devices using chalcogenide materials

CMOS-compatible fabrication processes demonstrated for:

- Waveguide device
- Integrated microfluidic sensor device
- GRIN cladding device

Waveguide fabrication process: Etching vs. Lift-off

Plasma etching

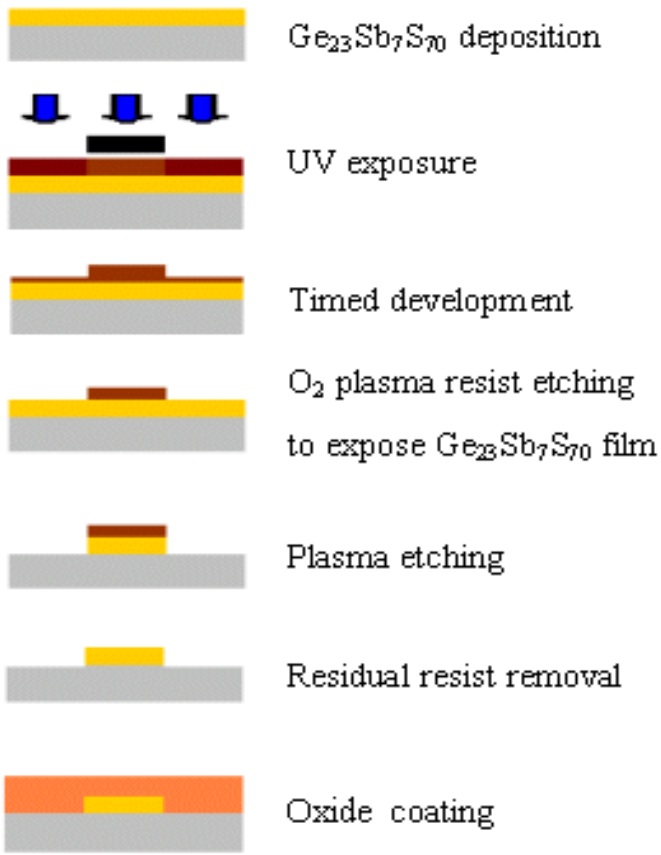

Lift-off

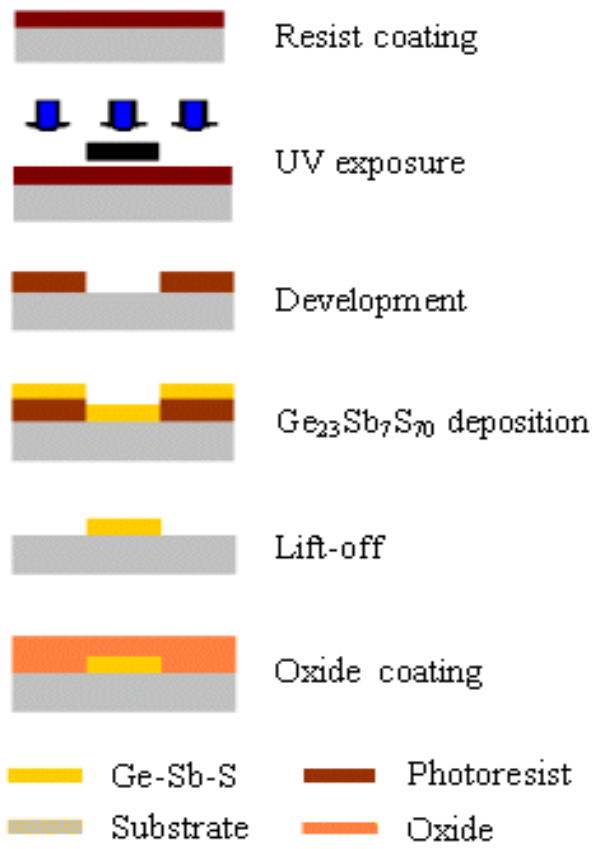

"Subtractive process"

"Additive process"

Waveguide fabrication process: Non-CMOS material in a CMOS process

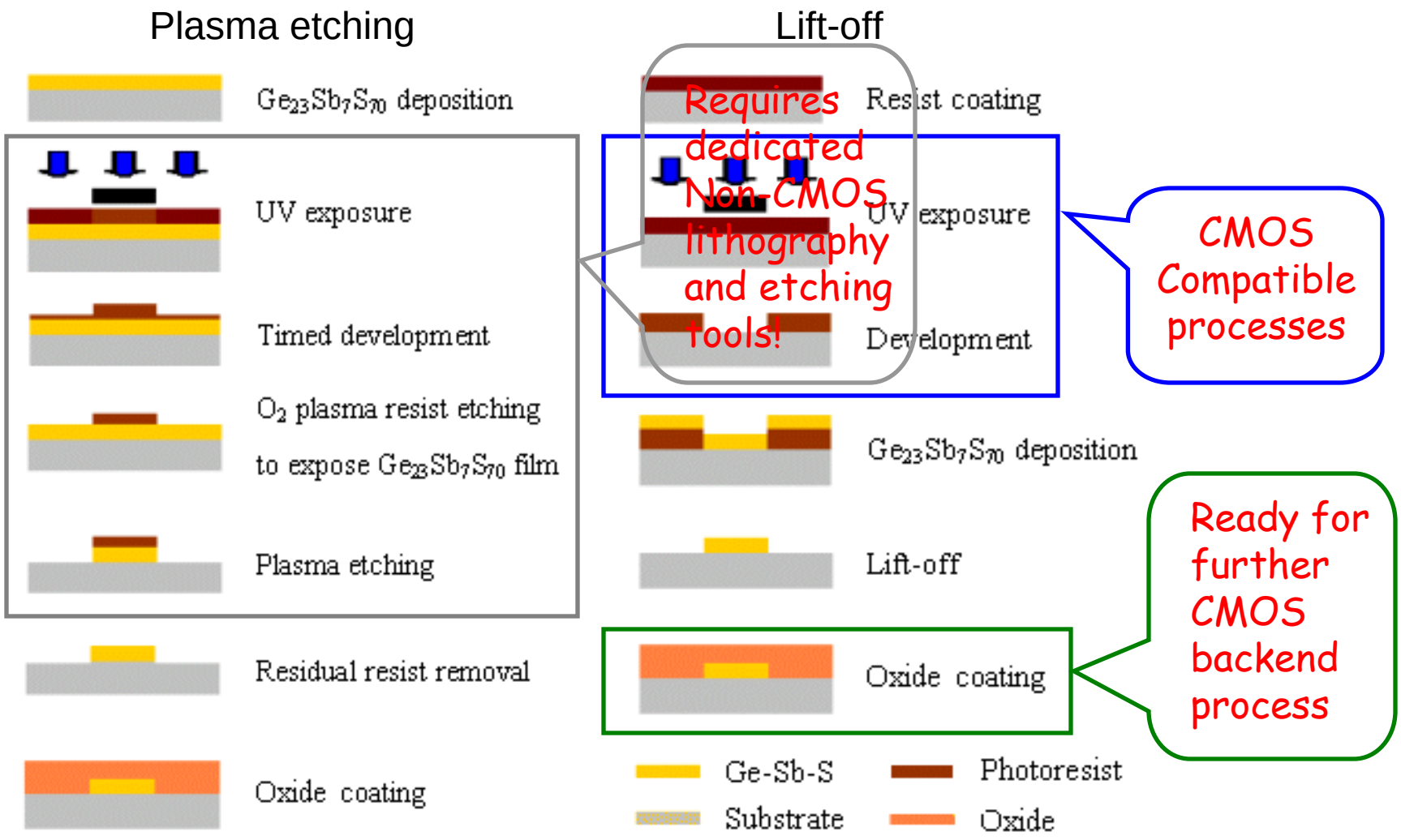

Waveguide fabrication process: Waveguide morphology

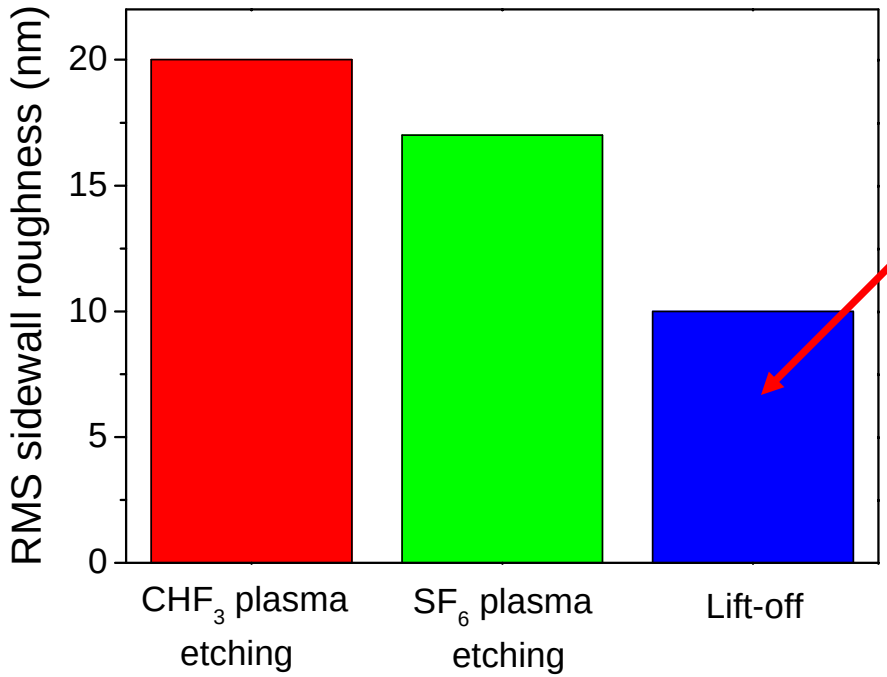

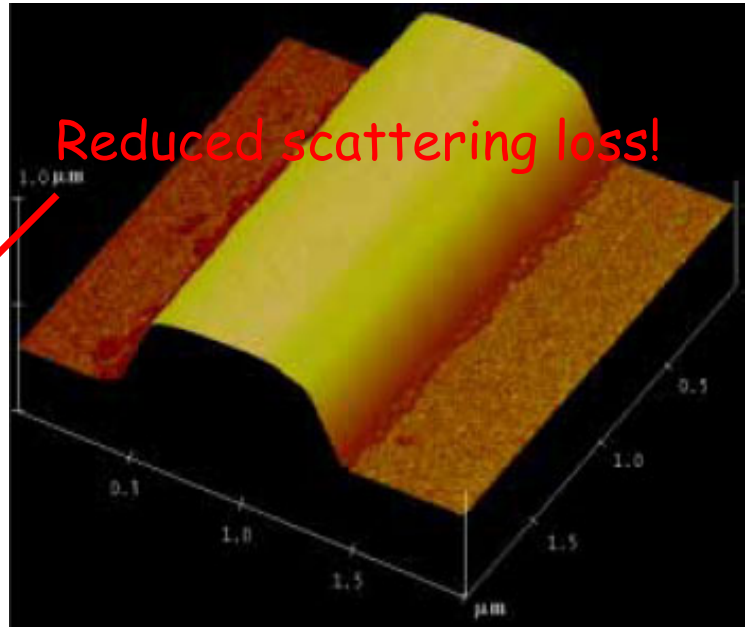

- Lift-off leads to slanted sidewall profile and rounded corners
- Lift-off patterned waveguides exhibit lower sidewall roughness
  - Sidewall defined during the deposition process rather than etching
  - Reduced scattering loss from sidewall roughness

Waveguide fabrication process: Lift-off Waveguide Characterization

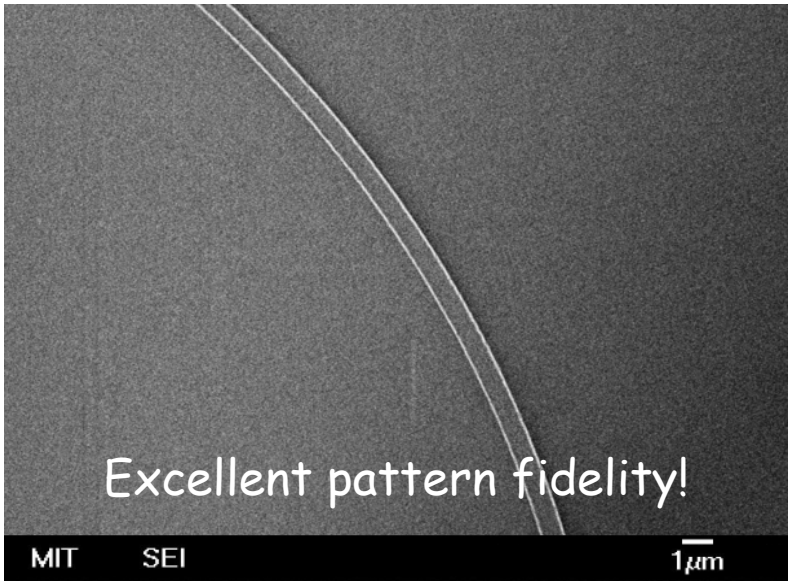

Single-mode submicron Ge-Sb-S strip waveguide patterned using lift-off on a 500-nm CMOS line

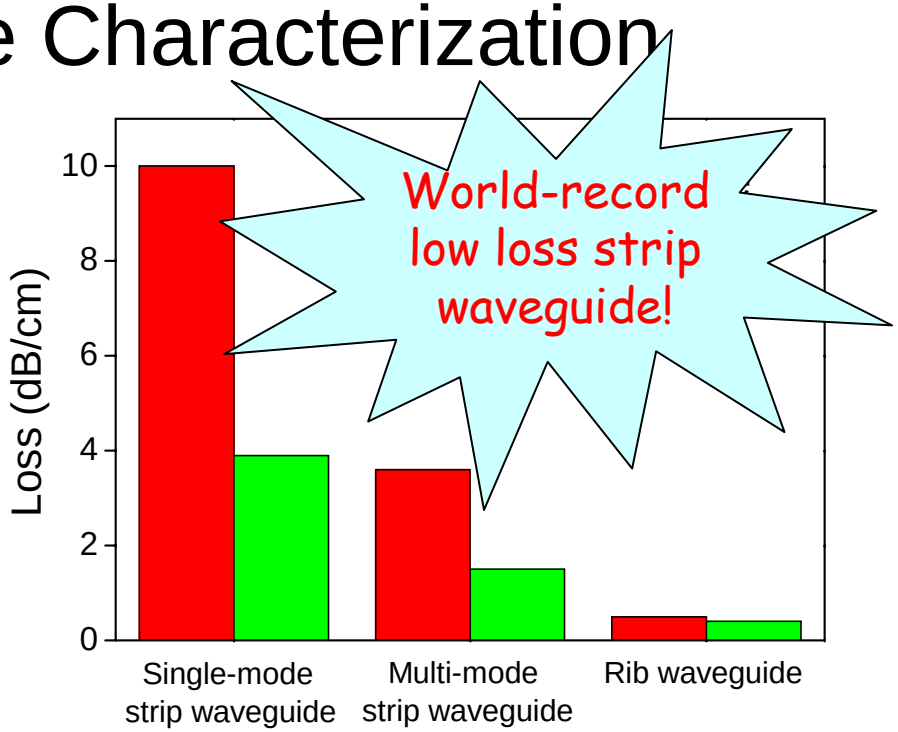

Measured waveguide loss

Rib waveguide loss: ***< 0.5 dB/cm***

Waveguide fabrication process: Lift-off Waveguide Characterization

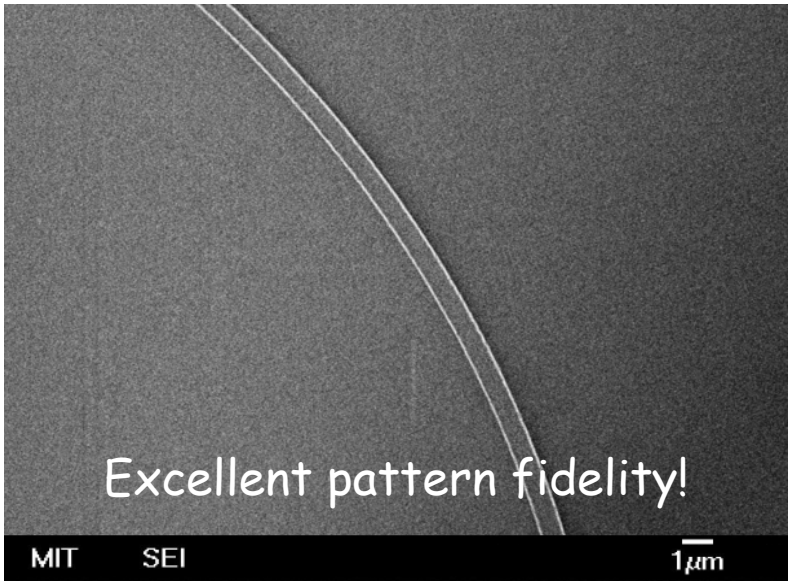

Single-mode submicron Ge-Sb-S strip waveguide patterned using lift-off on a 500-nm CMOS line

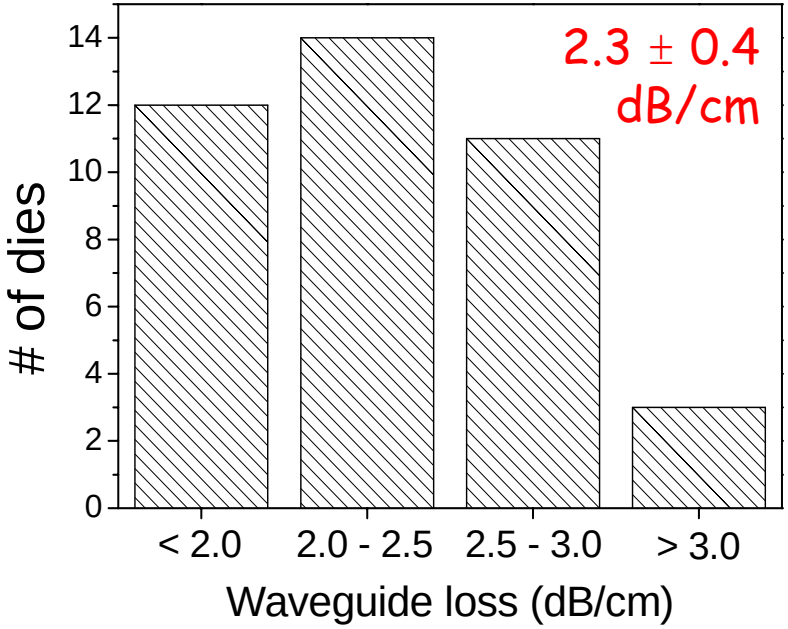

Uniform wafer-scale process for high-volume production

- We choose lift-off over plasma etching because of:
  - ✓ CMOS process compatibility
  - ✓ Superior sidewall quality of lift-off patterned waveguides

Integrated Microfluidic Sensor

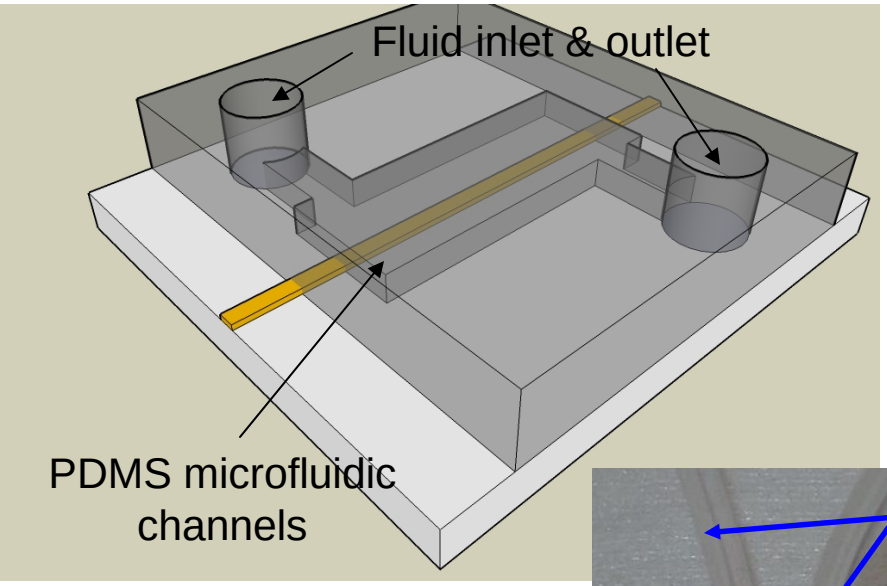

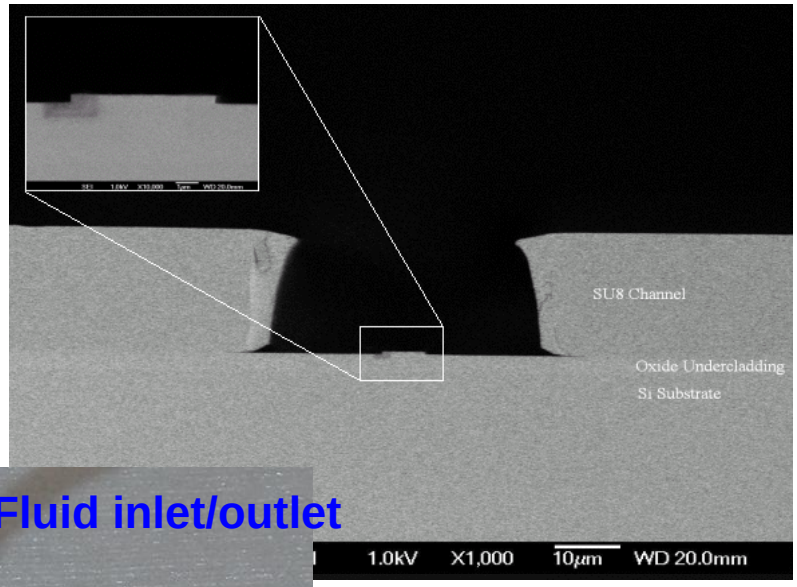

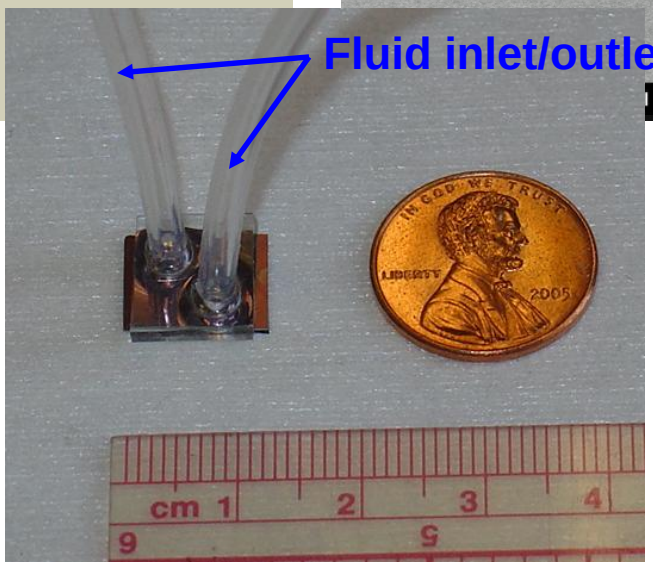

Integrated Microfluidic Sensor

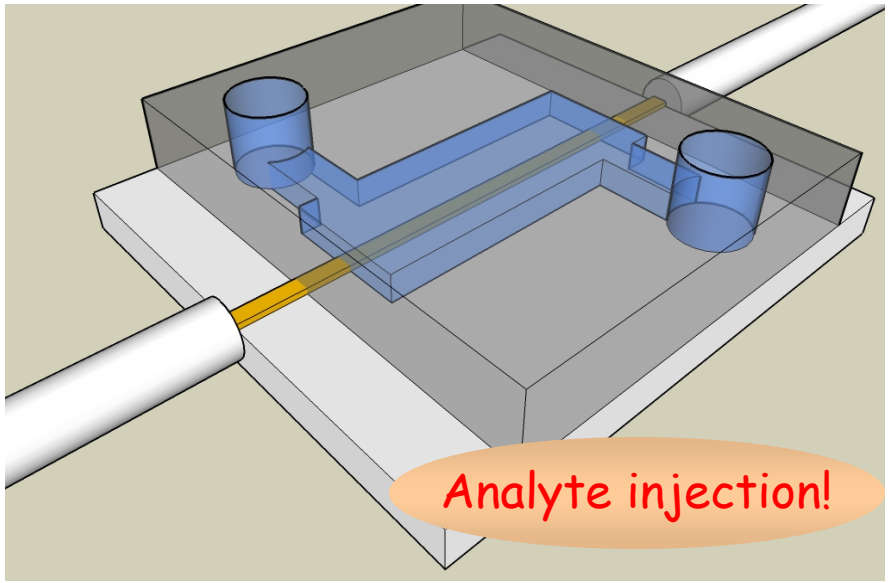

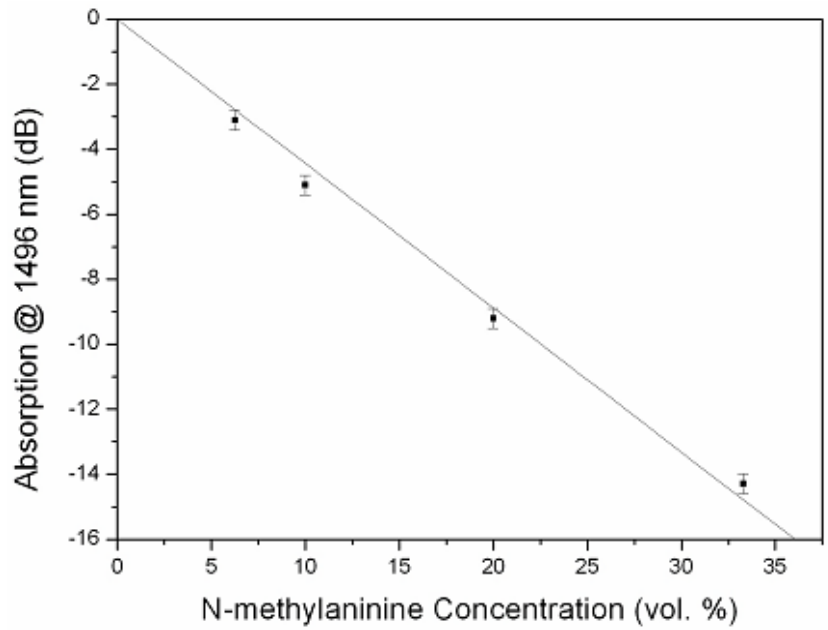

- ✓ Demonstrate monolithically integrated microfluidic sensor
- ✓ Linear response: suitable for quantitative measurement
- ✓ Sensitivity: ~ 0.7 vol. %
  - ➢ Change operation wavelength: mid-IR absorption is 100x stronger
  - ➢ Increase interaction length: loss reduction & resonant enhancement

Graded-Index (GRIN) Claddings: Loss reduction

- Incremental addition of GRIN claddings effectively reduces loss
- Oxide coating improves chemical stability and biocompatibility
- A wealth of chem-bio functionalization available on oxide surface

Kills three birds with one stone!

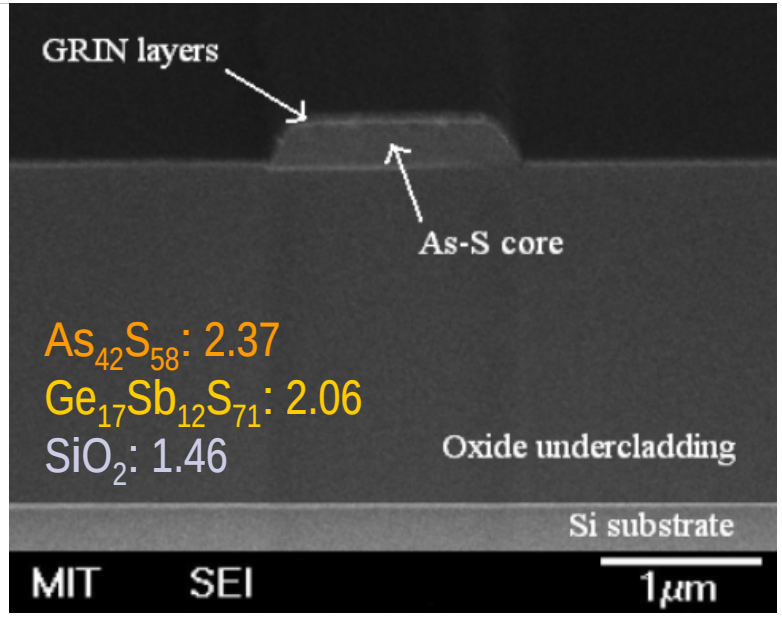

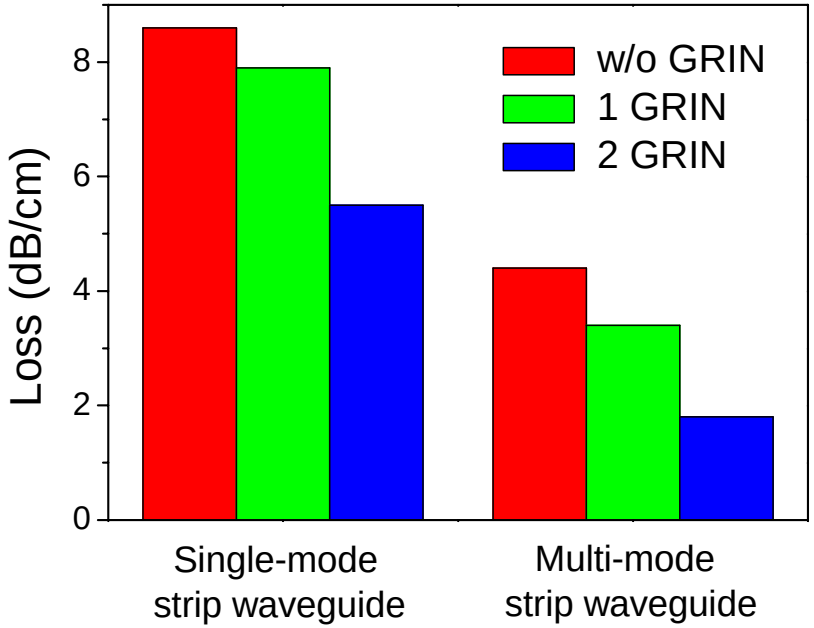

Waveguide Loss Measurement

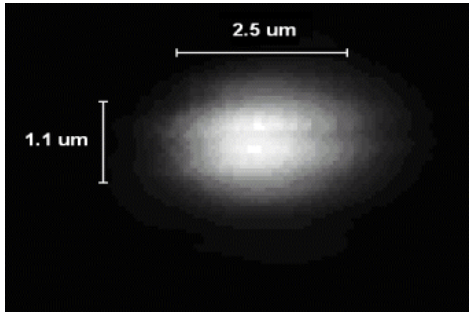

Top View Example of a Waveguide Chip

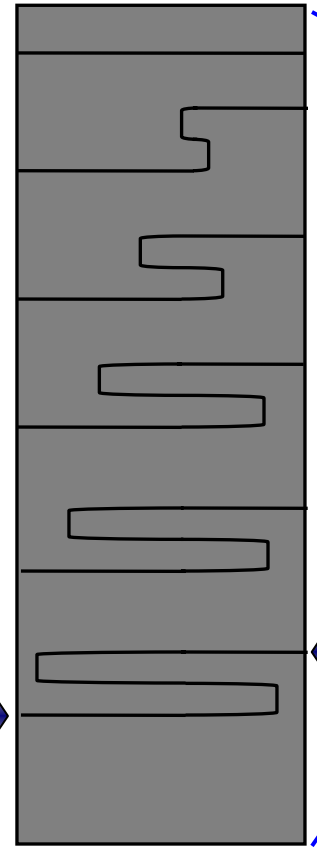

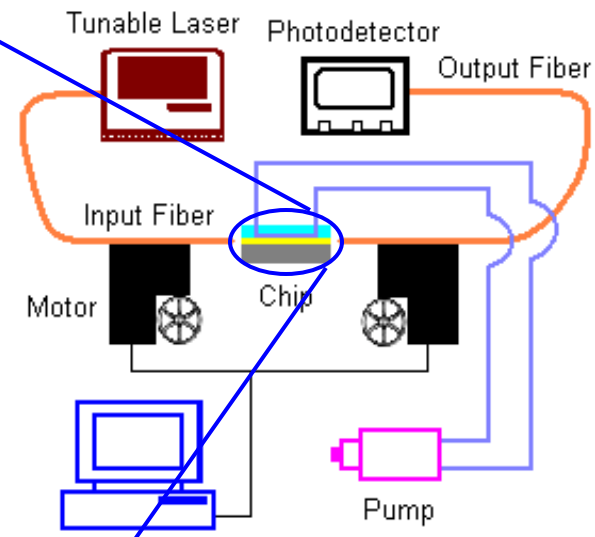

Input/Output

JDS Uniphase Swept Wavelength System

Tunable Laser and Broadband Detector

PDL and Insertion Loss Measurements

3 pm wavelength resolution

Output

Input

Alignment

Newport-Autoalign Station

50 nm spatial resolution

Fibers

Nanonics Lens-Tipped Fibers

1.7 um Modal Field Diameter (MFD)

Waveguide Loss Measurement

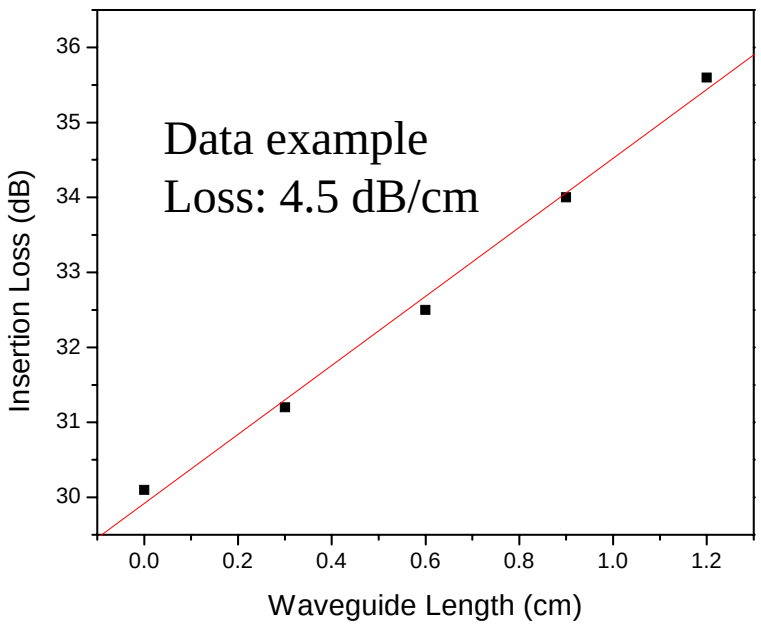

Example of Waveguide Layout

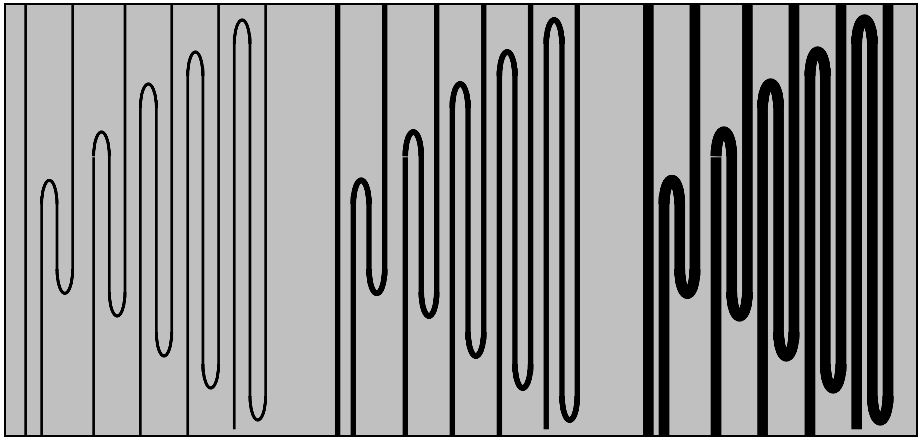

We use different length waveguides (as shown above) to ascertain waveguide loss.

- Loss (dB/cm) is slope of Insertion Loss (dB) versus waveguide length (cm)
- Example above is for a single wavelength (λ = 1550 nm)

Future work for the remainder of the project

- Year II (from Sept. 07 to Aug. 08) of the project will be focused on material identification and the fabrication of chalcogenide-based evanescent field waveguide structures for sensing a specific target species in a fluid analyte:
  - Evaluation and testing of materials compatibility, including with CMOS processing materials and conditions (CU/ MIT) and for direct write trench and waveguide structures (CU/UCF)
  - Optimization of ChG material for structuring; assessment of material/property changes associated with process parameters (CU/MIT, CU/UCF – parallel approaches)
  - Lateral coupling to resonator (MIT)
  - Initial evaluation of polymer coated ChG performance: durability and optical impact (CU/MIT/UCF)
  - Smoothing process for sensitivity enhancement (MIT)

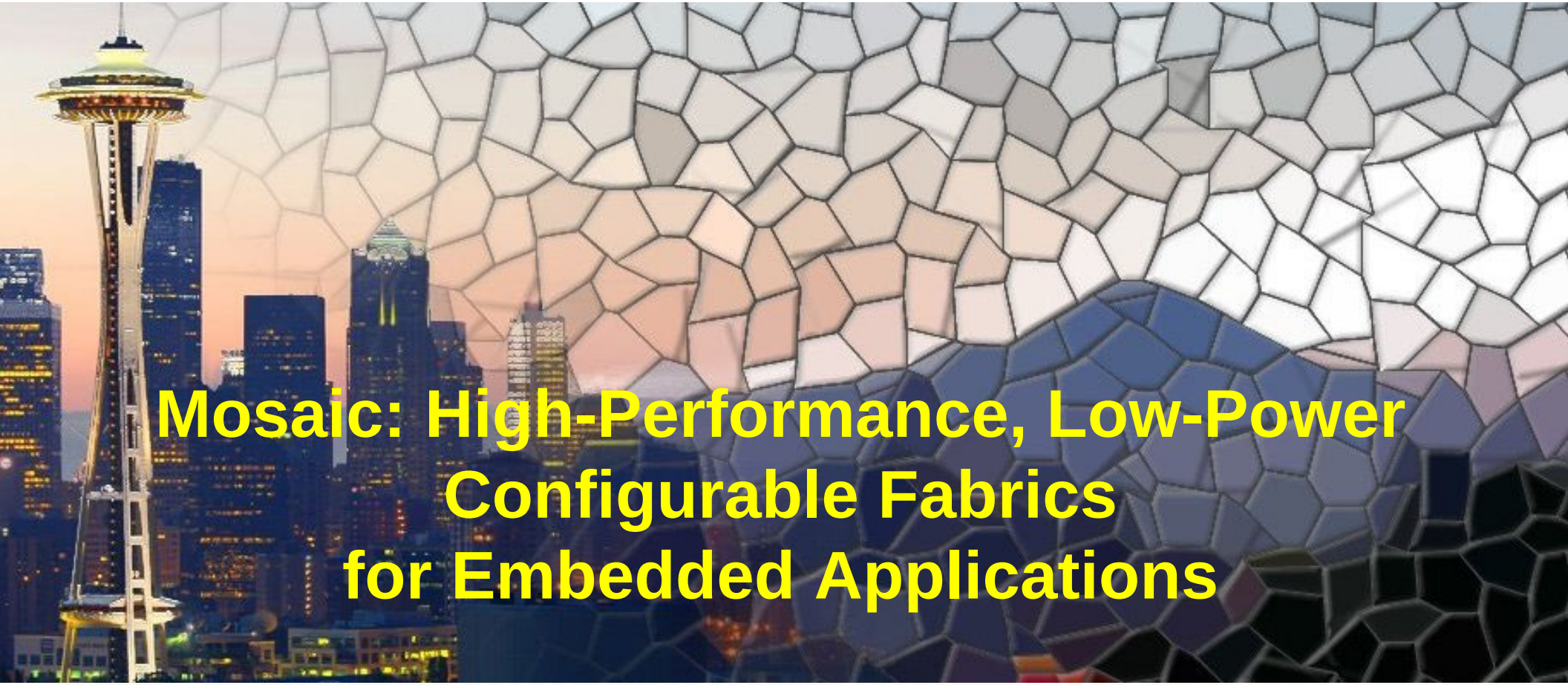

Mosaic: High-Performance, Low-Power Configurable Fabrics for Embedded Applications

PIs: Carl Ebeling, Maya Gokhale*, Scott Hauck

Co-Investigators: Allan Carroll, Jon Cohen*, Ken Eguro, Stephen Friedman, Robin Panda, Brian Van Essen, Aaron Wood, Benjamin Ylvisaker

University of Washington

* Lawrence Livermore National Lab

Accelerating DSP & Scientific Computing

- DoE-specific DSP
  - Principle Component Analysis
  - Match Filter
  - Hyperspectral Image Compression
  - Multispectral Image Classification
  - K-Means Clustering

- General DSP, Scientific Computing
  - Video
  - Networking
  - Encryption
  - DNA sequencing
  - Protein Folding

- Large, repetitive, computations
- Power, cost, and performance requirements
- Want flexibility within commodity devices

CPUs

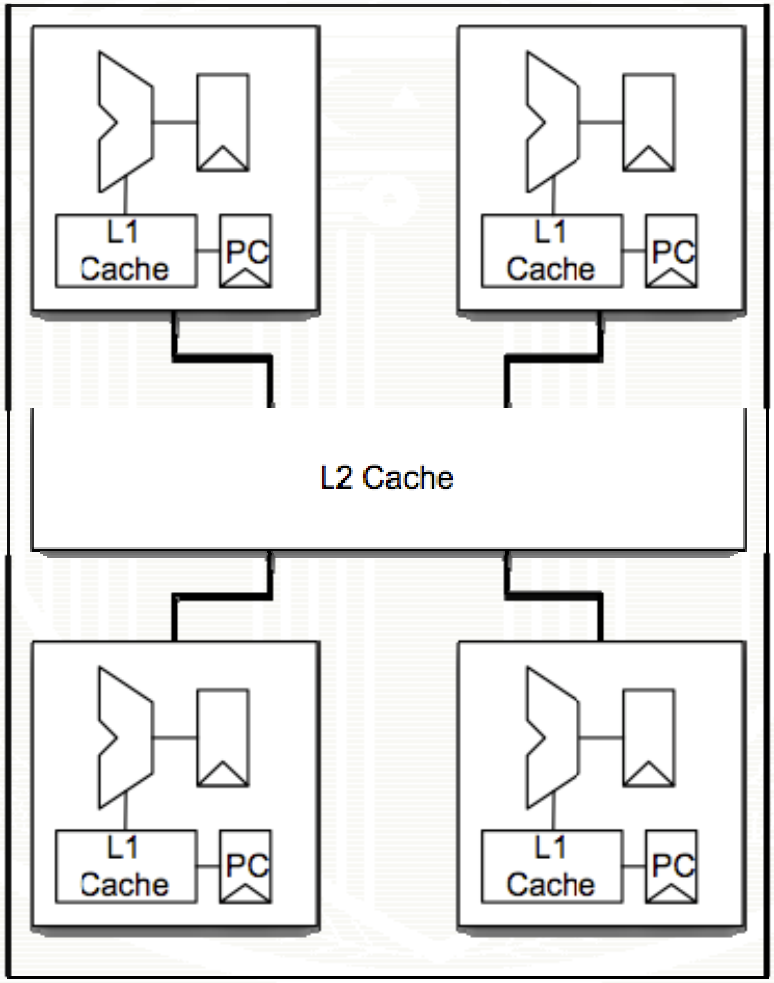

+ general purpose - doesn't exploit regularity

ASIC

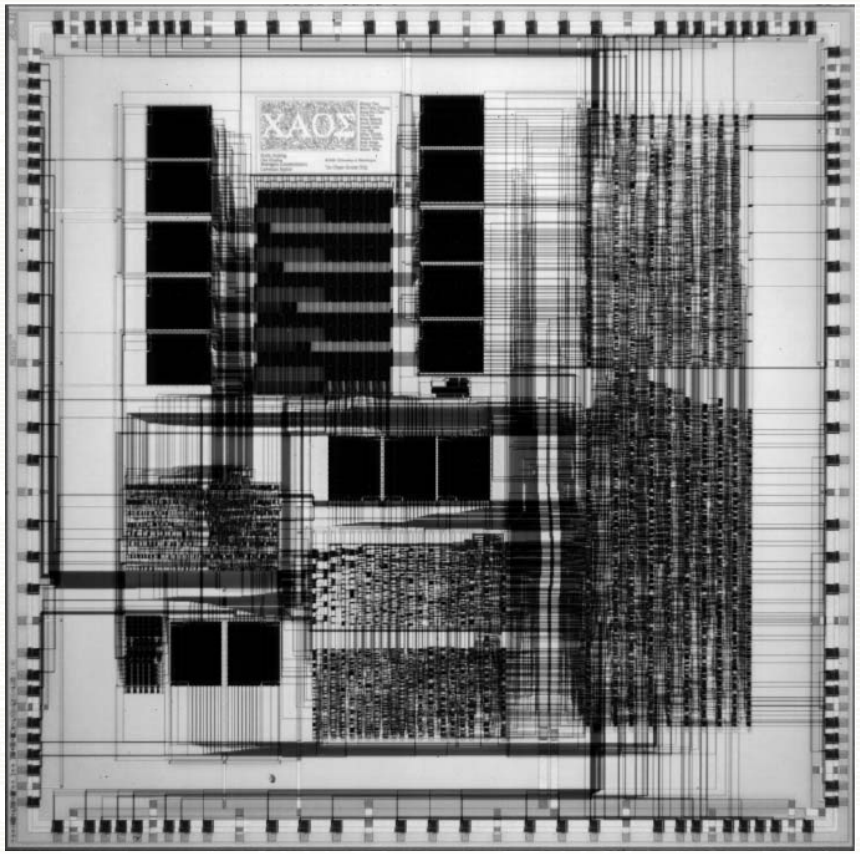

+ high performance

- high cost

FPGA

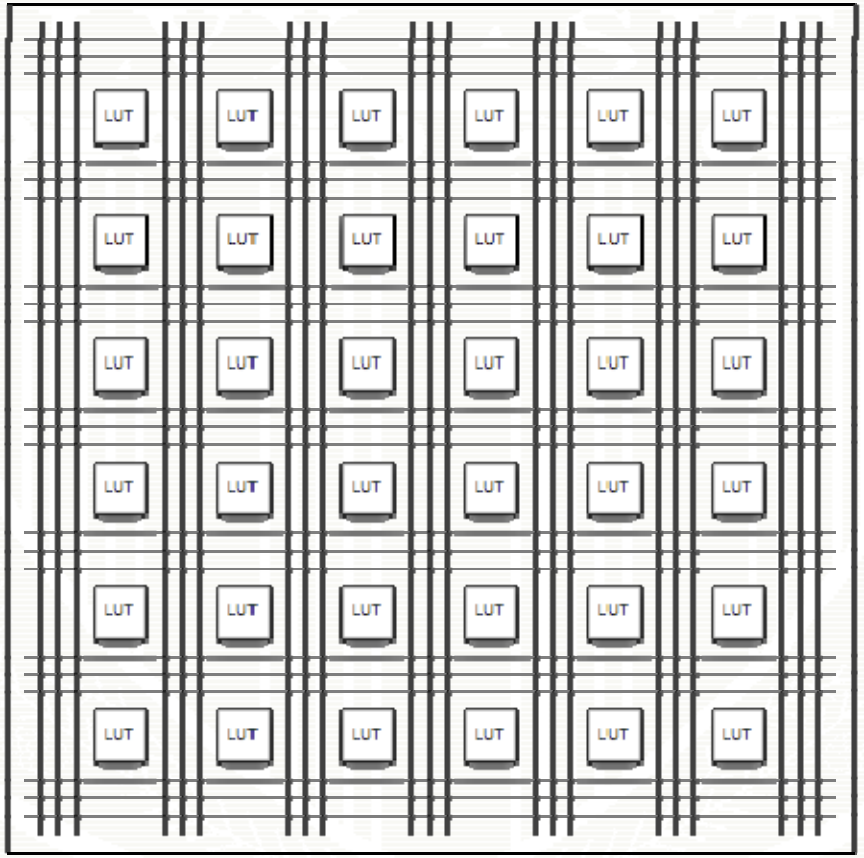

+ flexibility

- inefficient

Coarse-Grained Reconfigurable Arrays

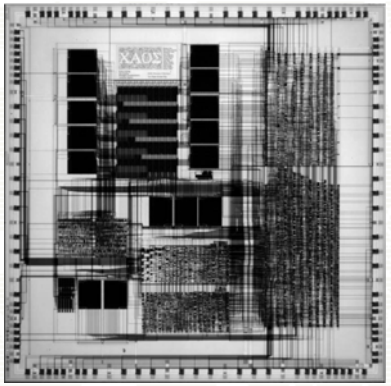

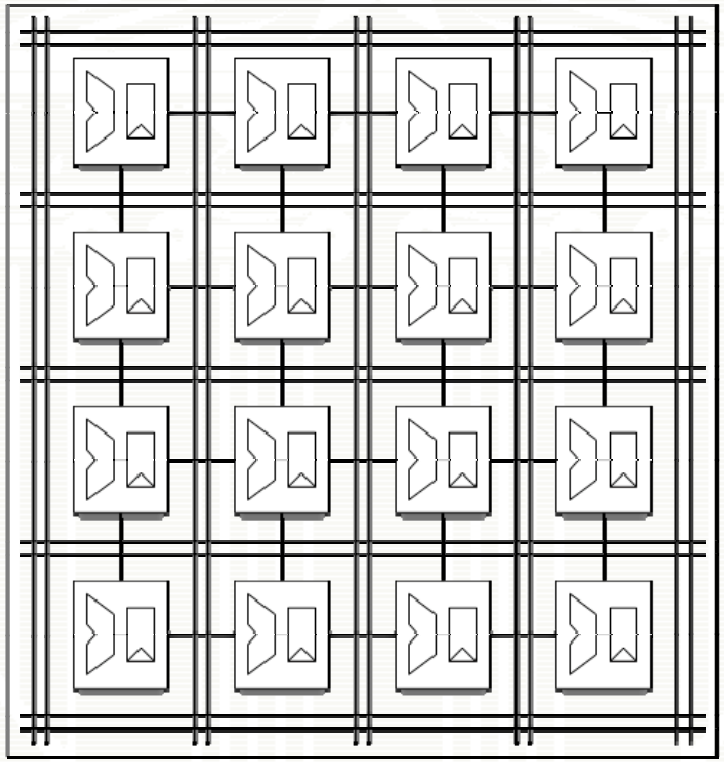

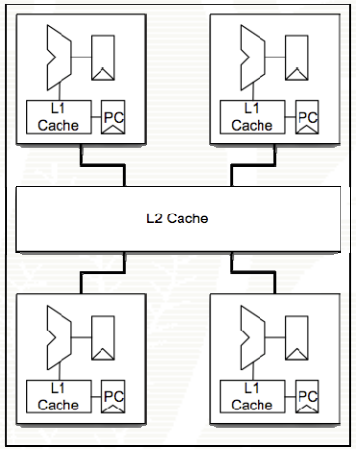

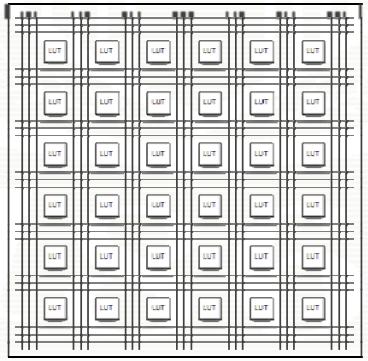

CGRA Architecture

- Lots of ALUs
  - Spatial parallelism
- Small program per ALU
  - Pipelined, multi-cycle
  - Time multiplexing
- Embedded memories
  - Close-coupled to ALUs
- Scheduled interconnect
- Streaming I/O

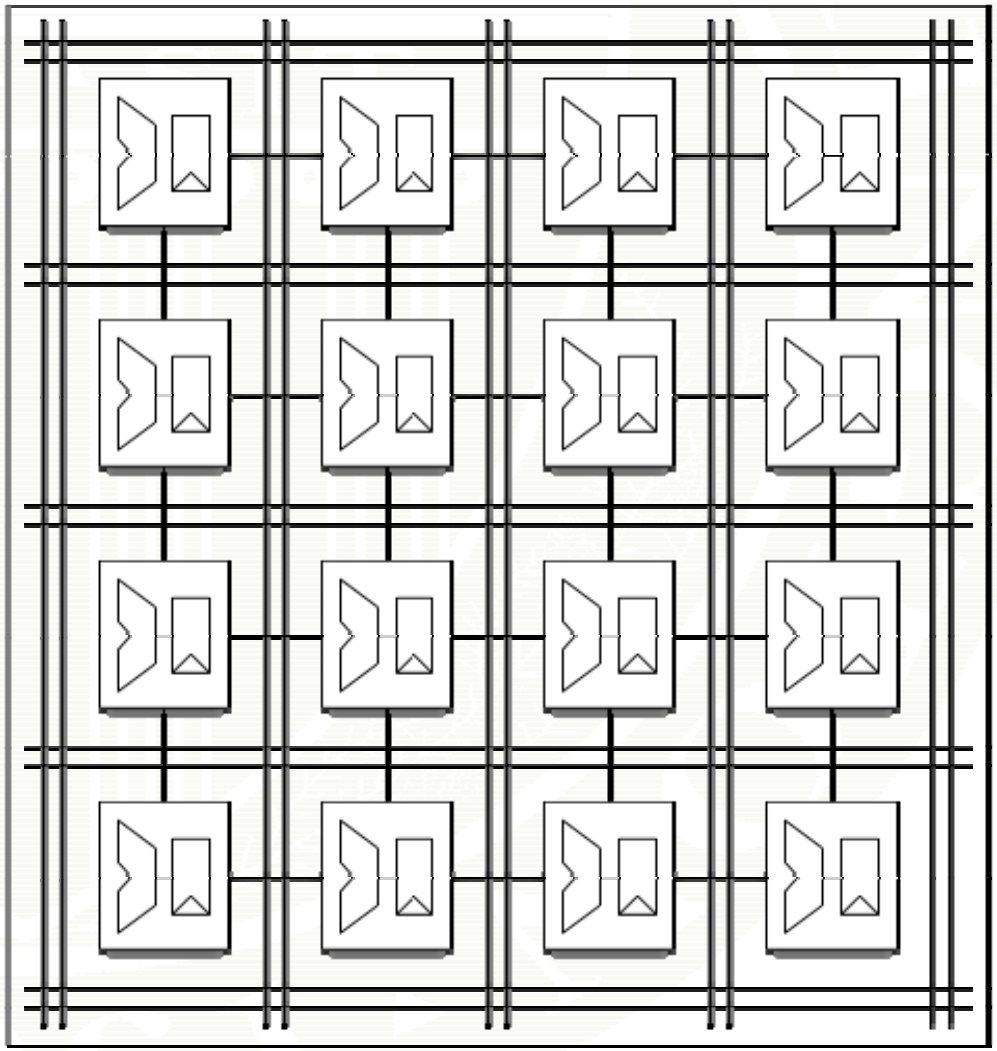

CGRA Usage – FFT8

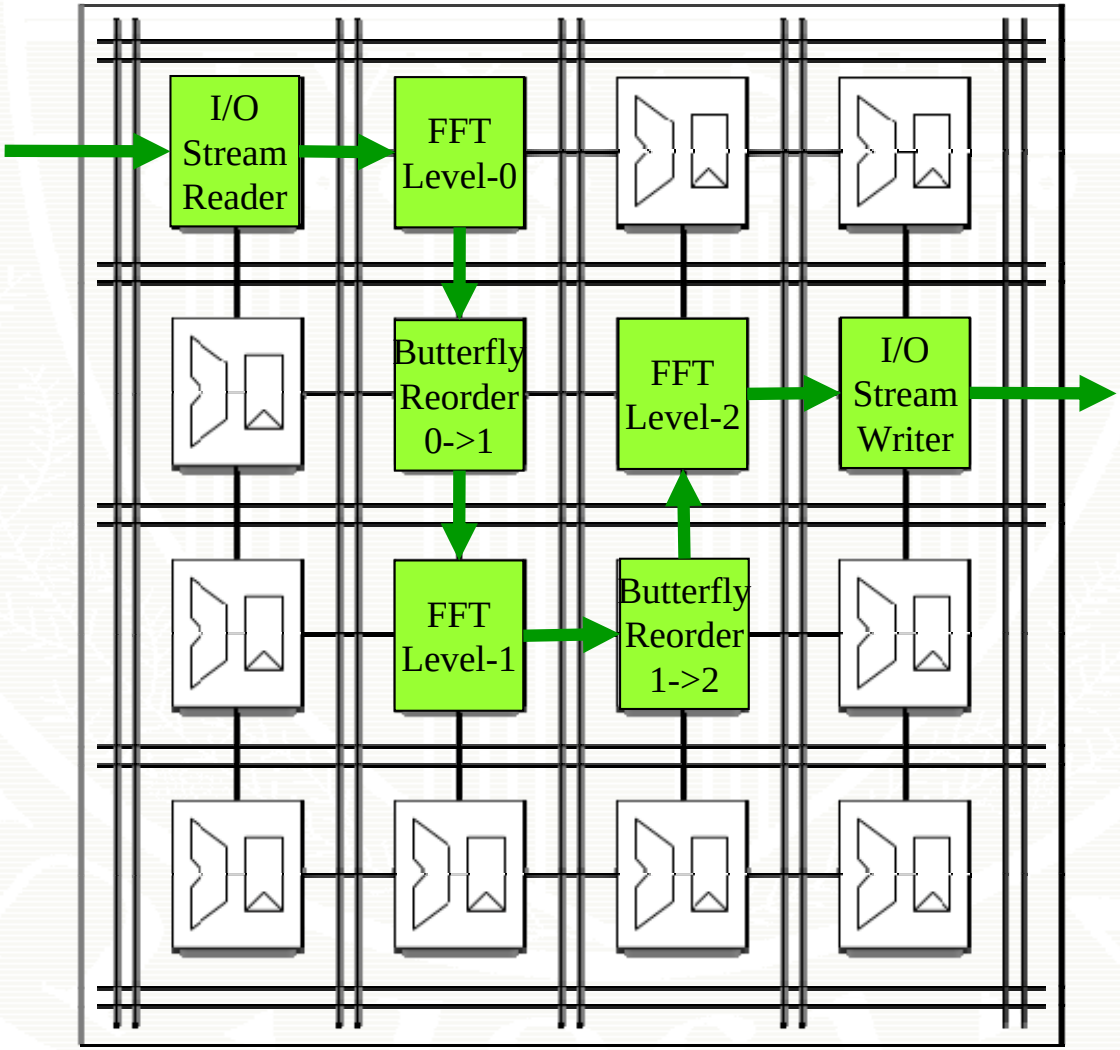

CGRA Usage – PNN Image Classifier

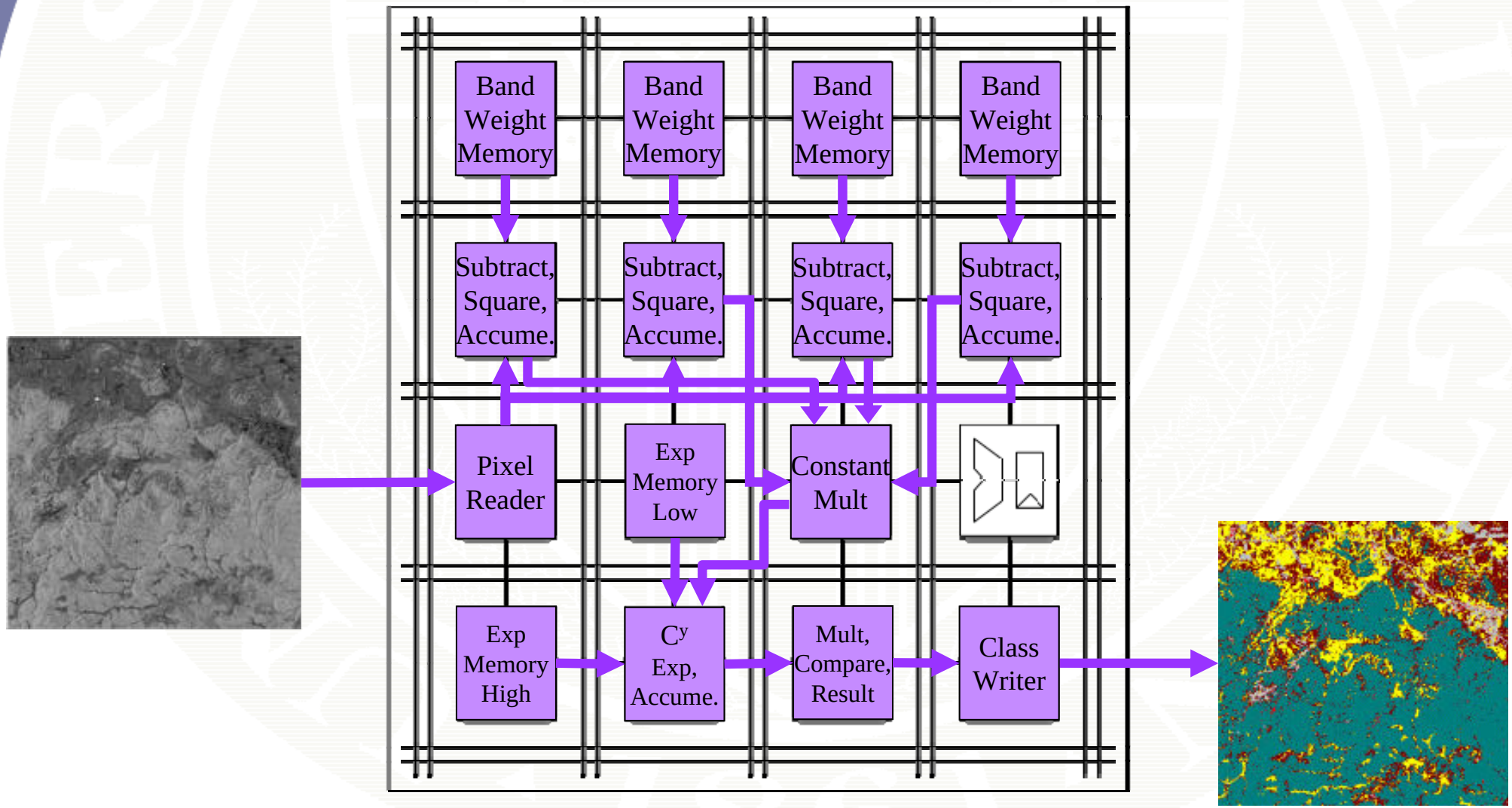

CGRA Usage – Combined

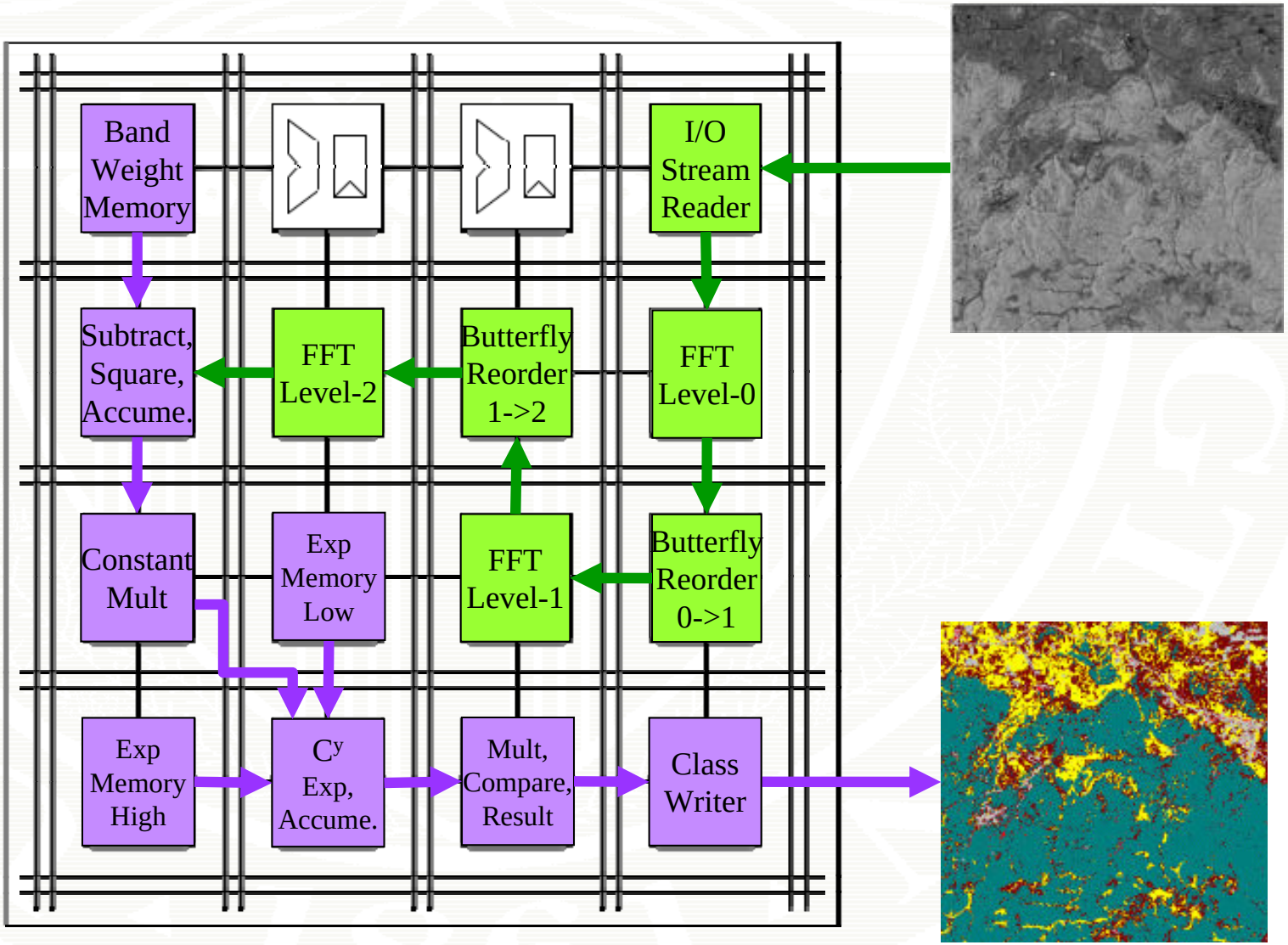

Project Goals

- Create benchmarks for CGRAs
- Develop compilation/mapping flow for CGRAs
- Determine “best” CGRA architecture

Mosaic System Diagram

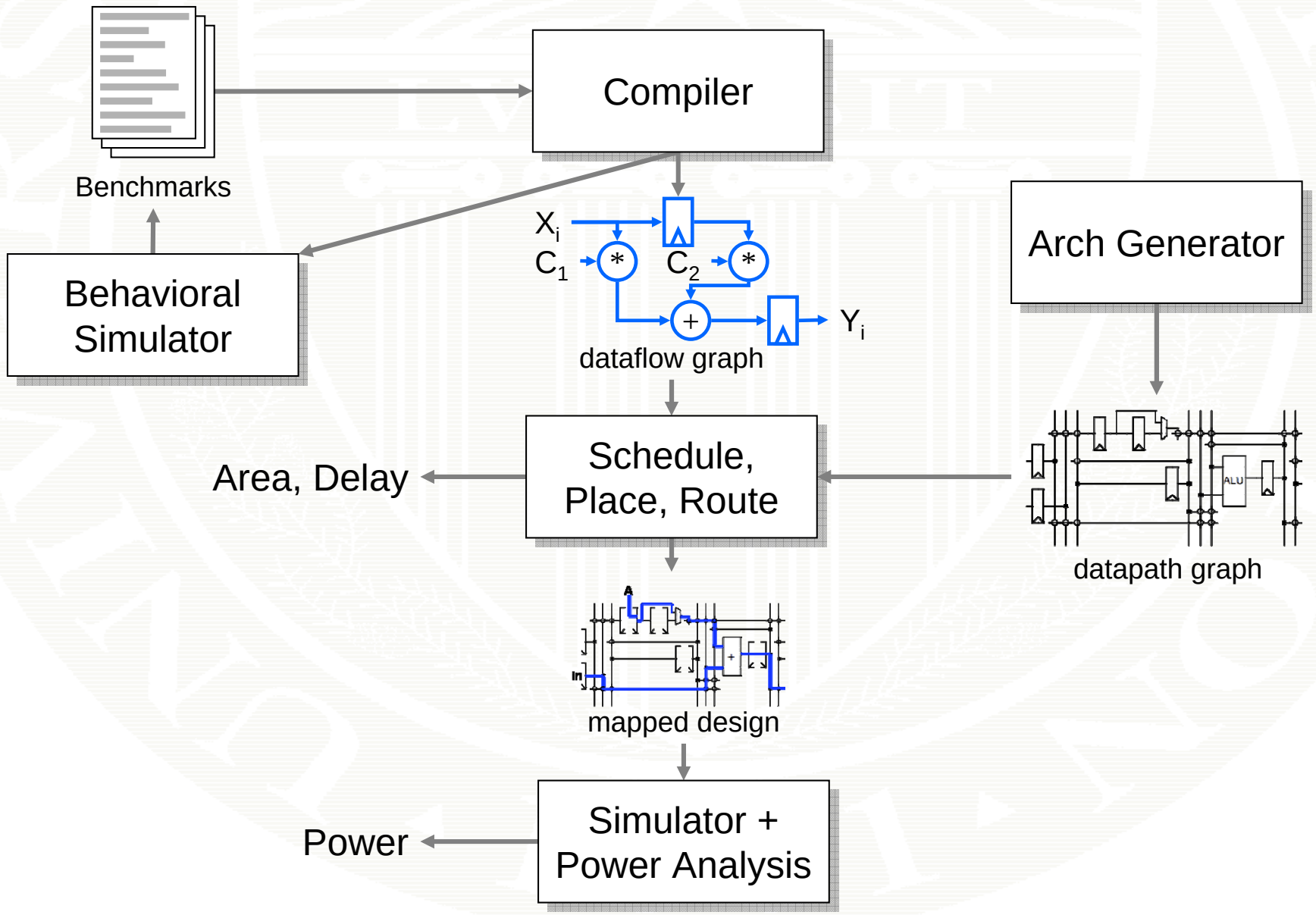

Mosaic System Diagram

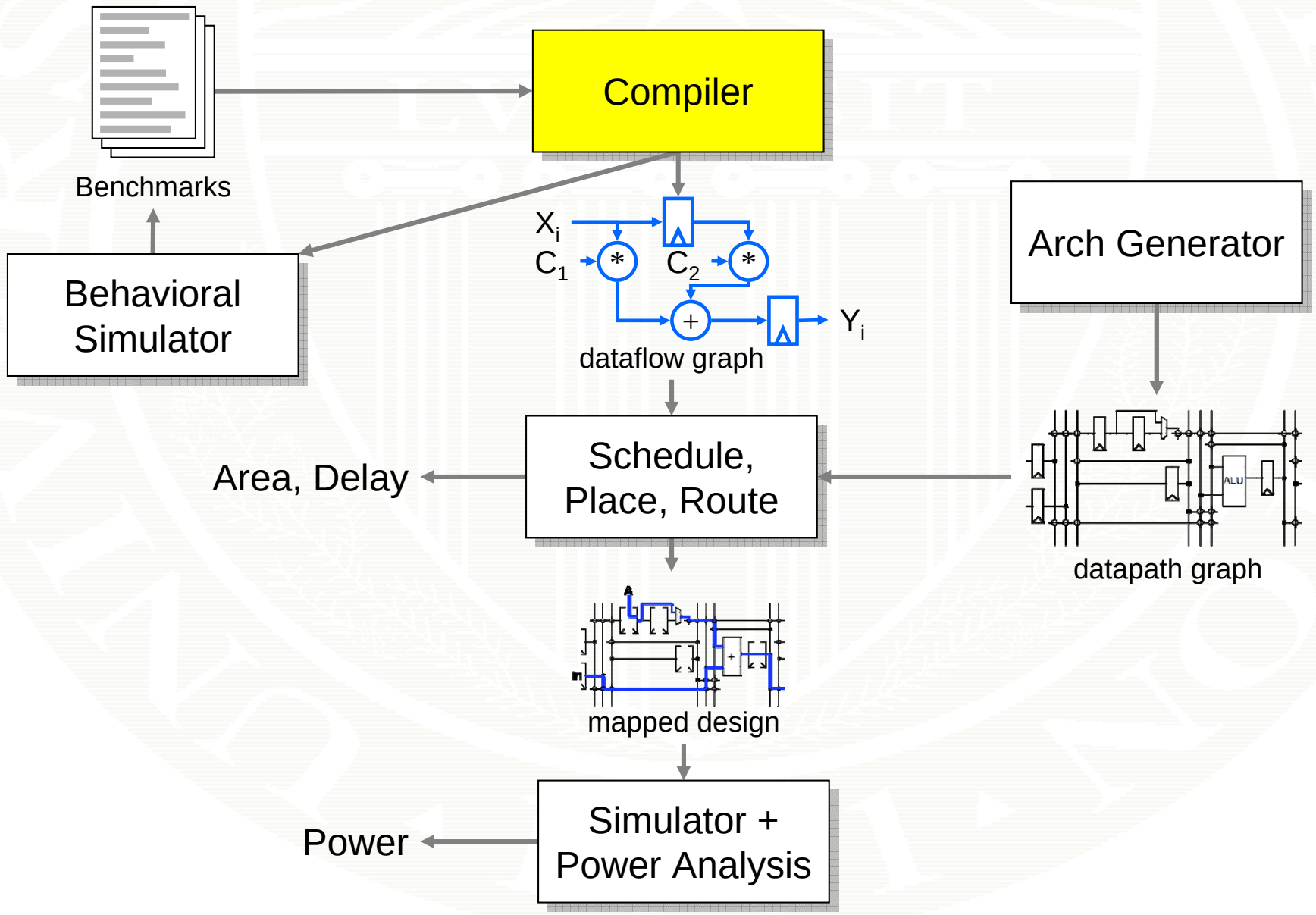

Macah: 2D Convolution

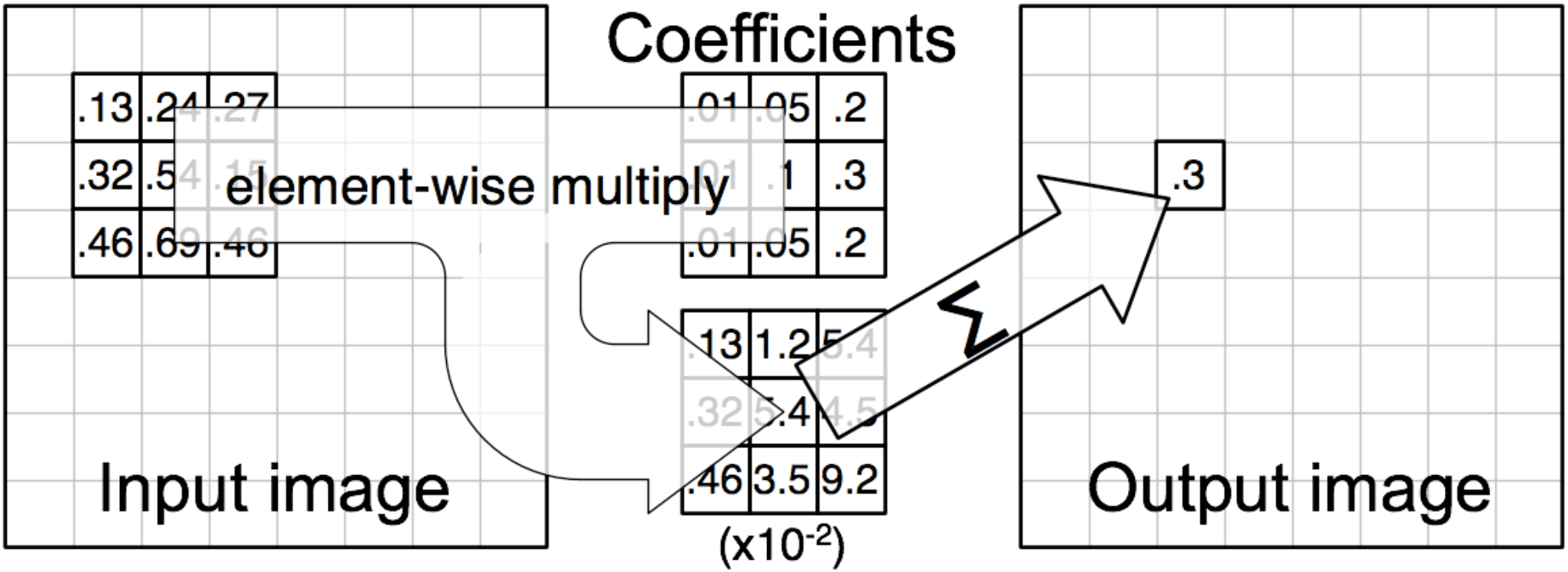

Compute Mults. And Additions

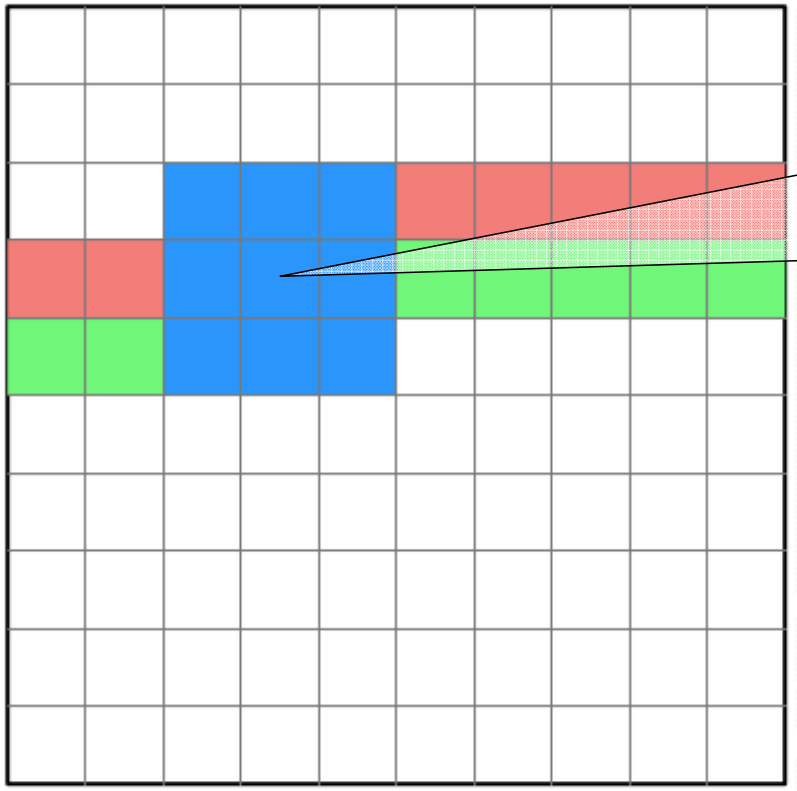

```
o=0;
FOR (ky = 0; ky < Kd; ky++) {
  FOR (kx = 0; kx < Kd; kx++) {
    o+=window[ky][kx]*coef[ky][kx];
  }
}
```

Move the Window

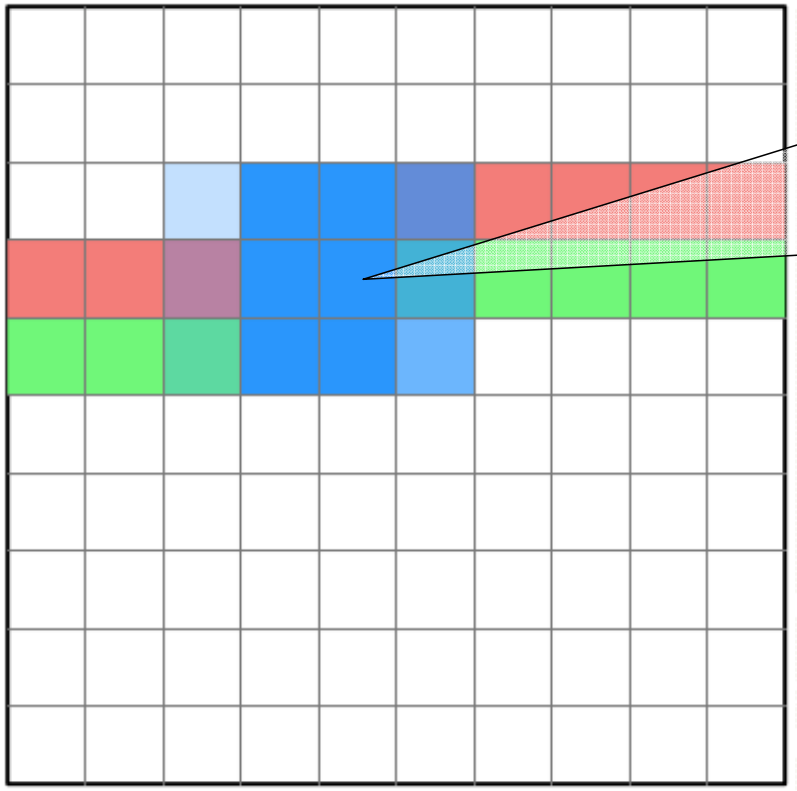

```
FOR (ky = 0; ky < Kd - 1; ky++) {
  shift_left_fill(temp, buffers[ky],
                  window[ky + 1][0]);
  shift_left_fill(temp, window[ky],
                  temp);
}
window[Kd - 1] <<= 1;
window[Kd - 1][^Kd - 1^] = ...;
```

Stream in from Main Memory

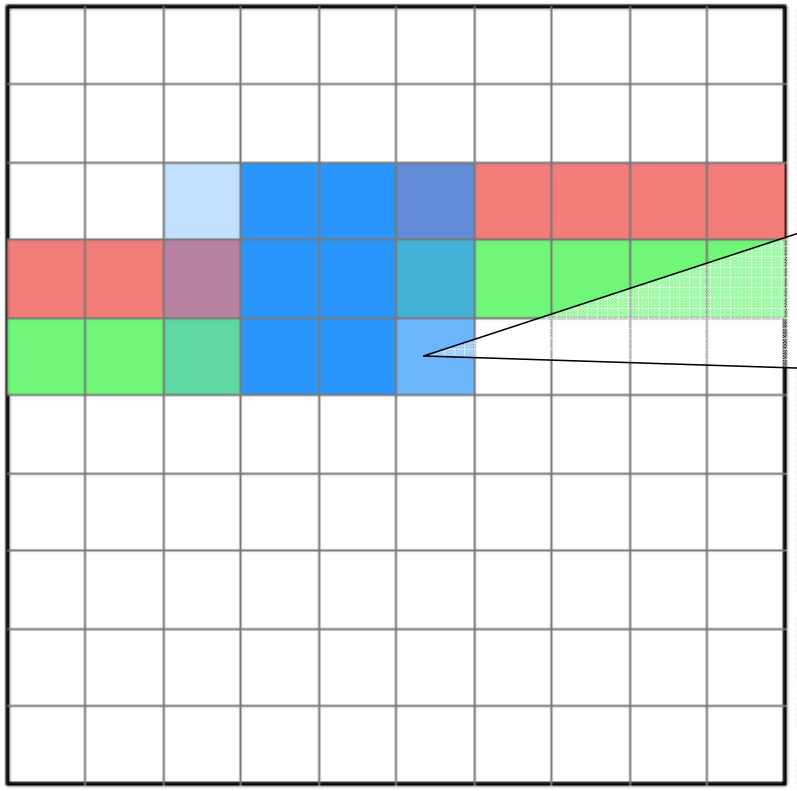

```
window[2][^2^] <? rdStr;

void convolution_reader (stream str)
  {
    for (i = 0; i < height; i++) {
      for (j = 0; j < width; j++) {
        str <! img[i][j];
      }
    }
  }
```

Possible Benchmarks

- Match Filter
- Principle Component Analysis (PCA)
- K-Means Clustering
- Image Resampling/Source Detection
- PNN-Based Multi-spectral Image Classifier
- Smith-Waterman/BLAST
- FFT
- CORDIC
- …

- <Yours here?>

Mosaic System Diagram

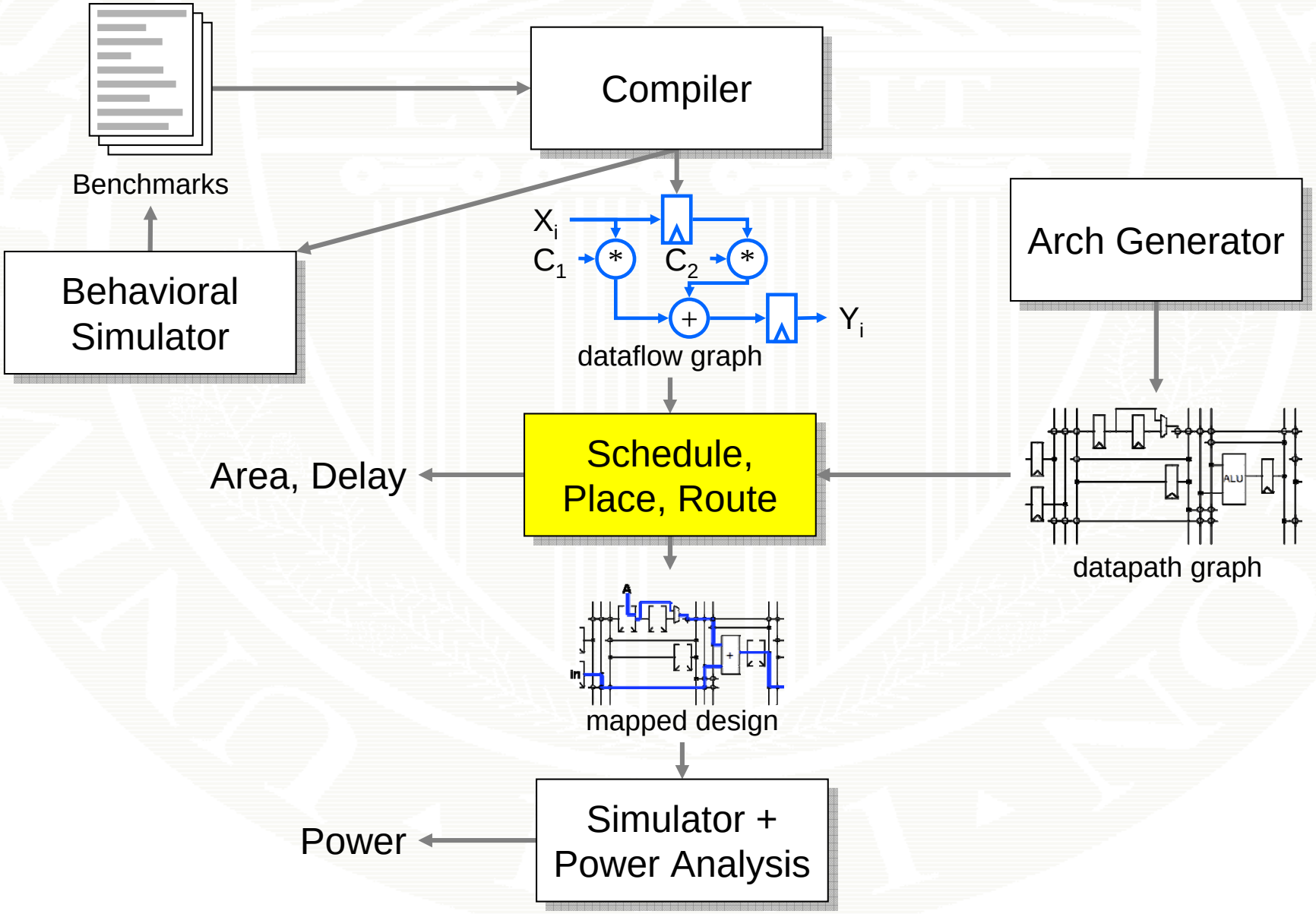

Schedule, Place and Route

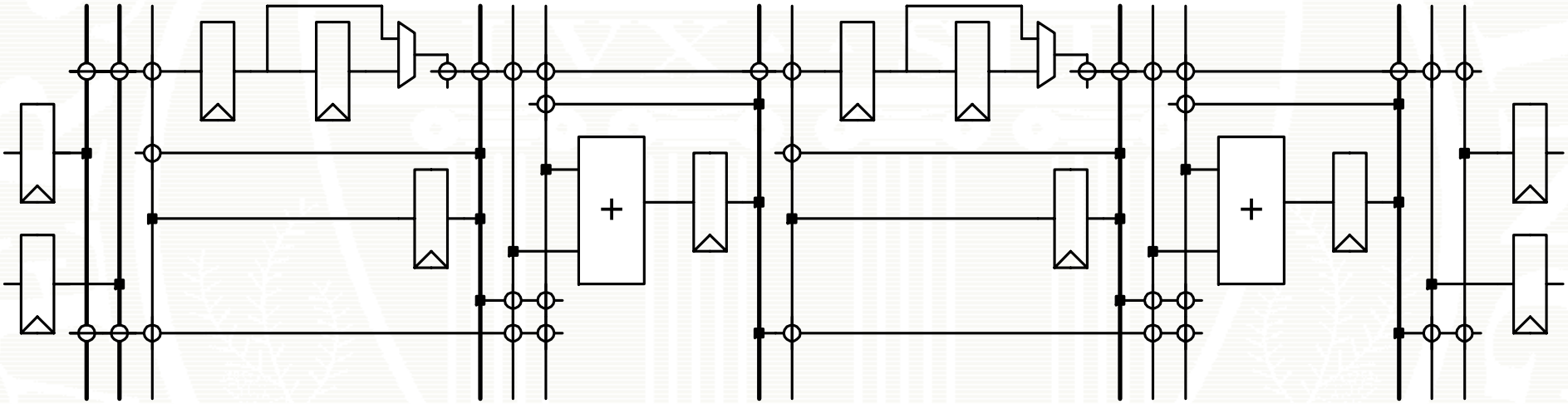

Space/Time Execution: Virtual Fabric

Cycle 1

Cycle 2

Cycle 3

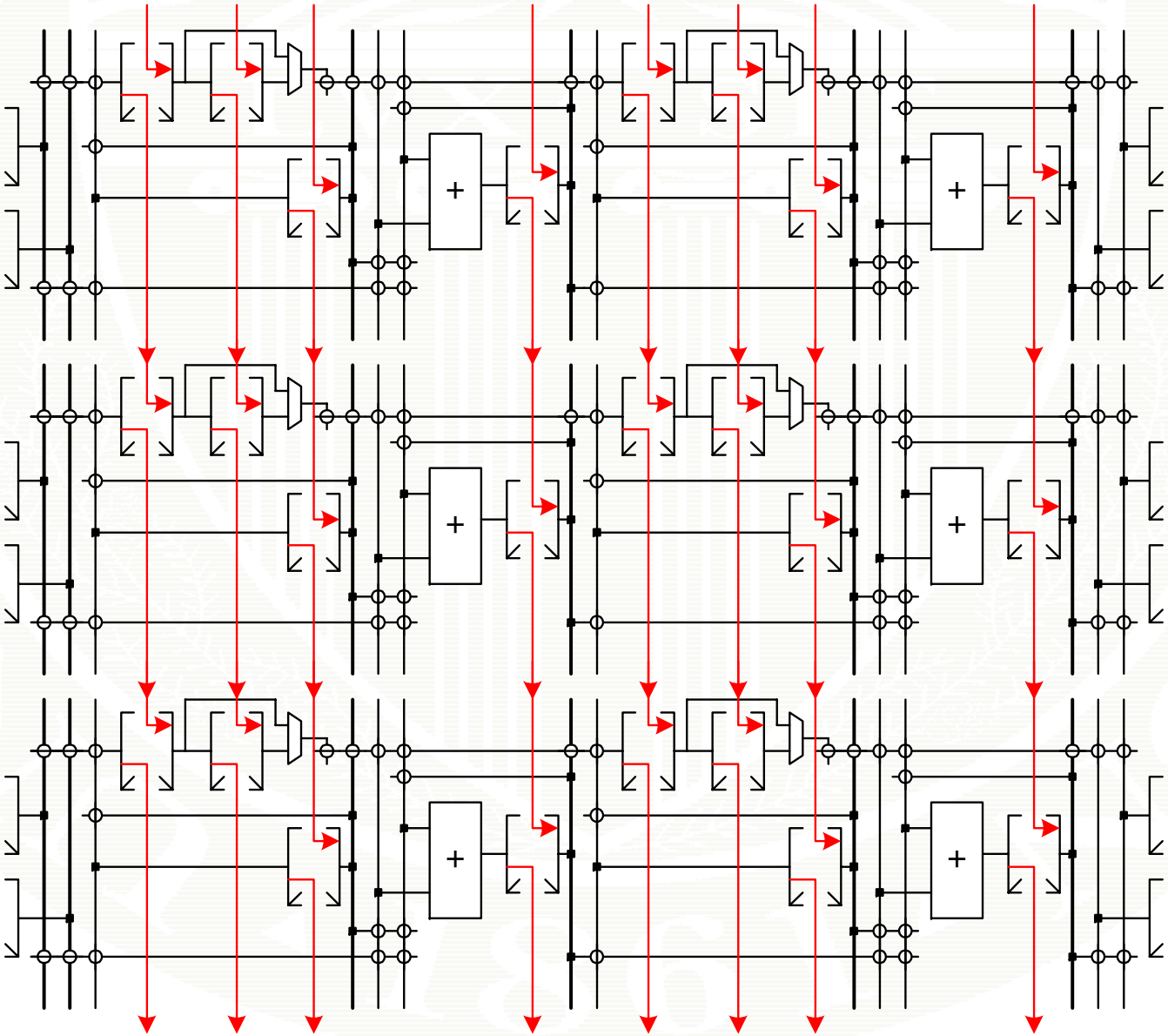

Dataflow Graph Execution

Cycle 1

Cycle 2

Cycle 3

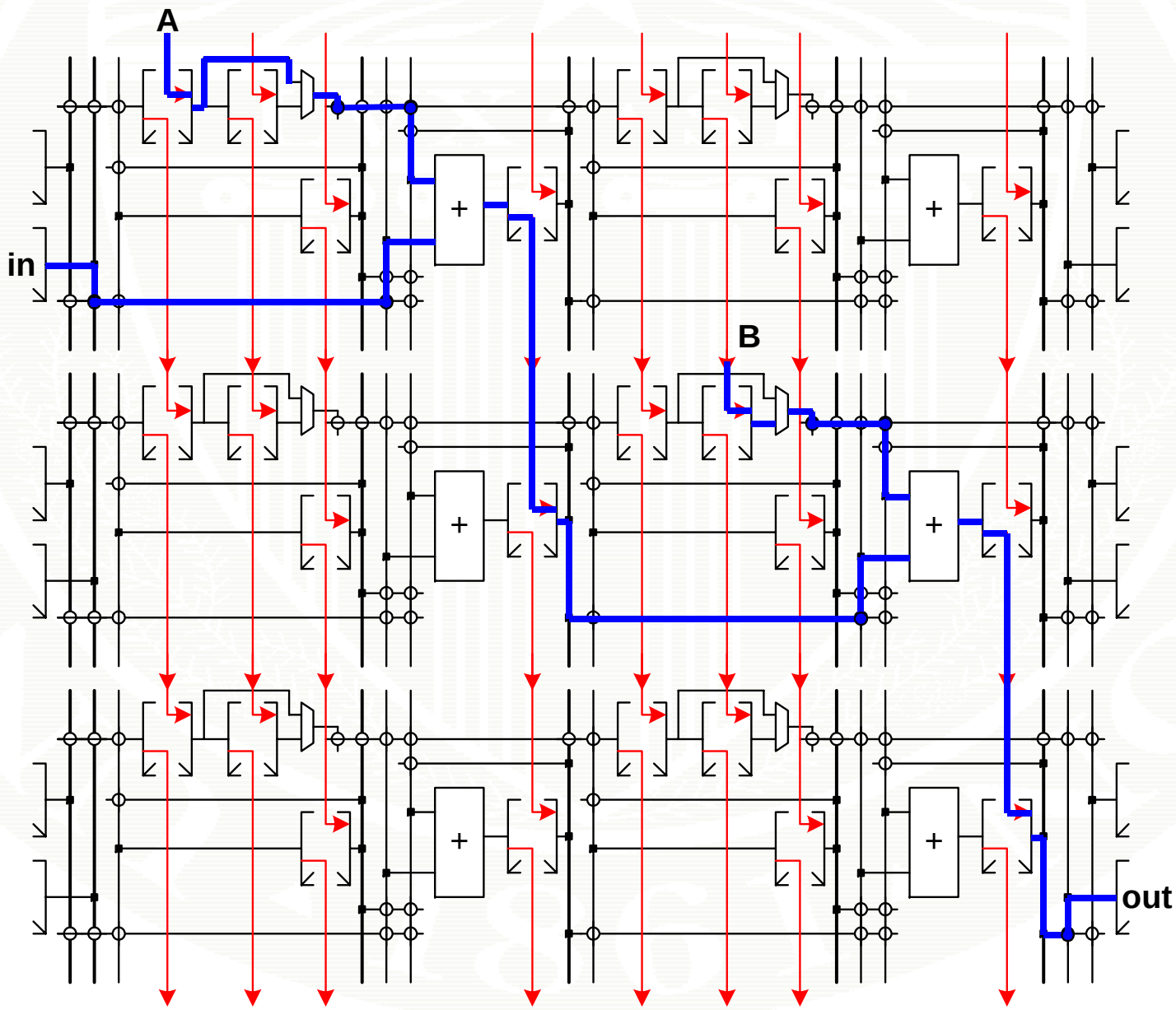

Interleave Multiple Cycles

Cycle 1

Cycle 2

Cycle 3

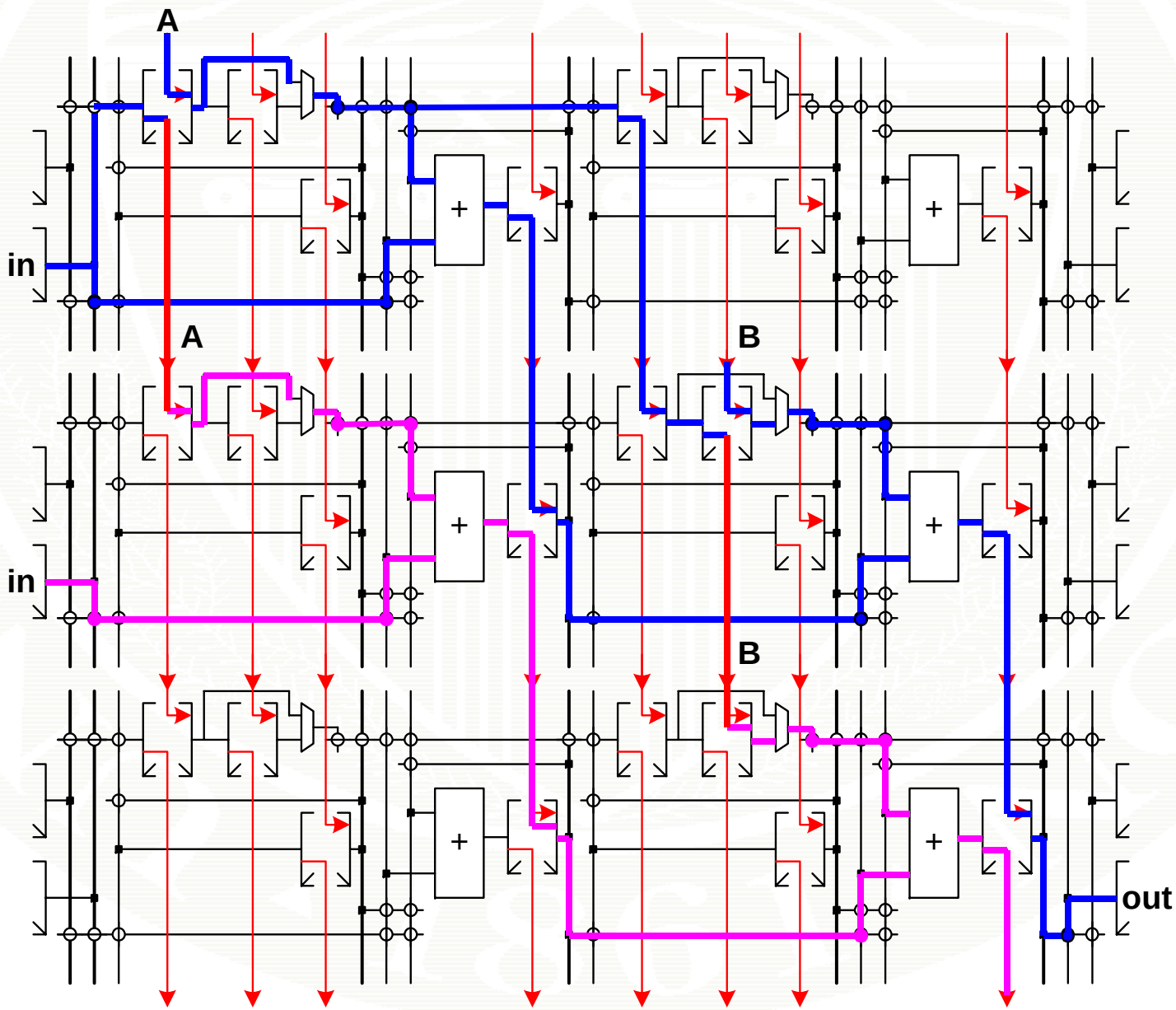

Mosaic System Diagram

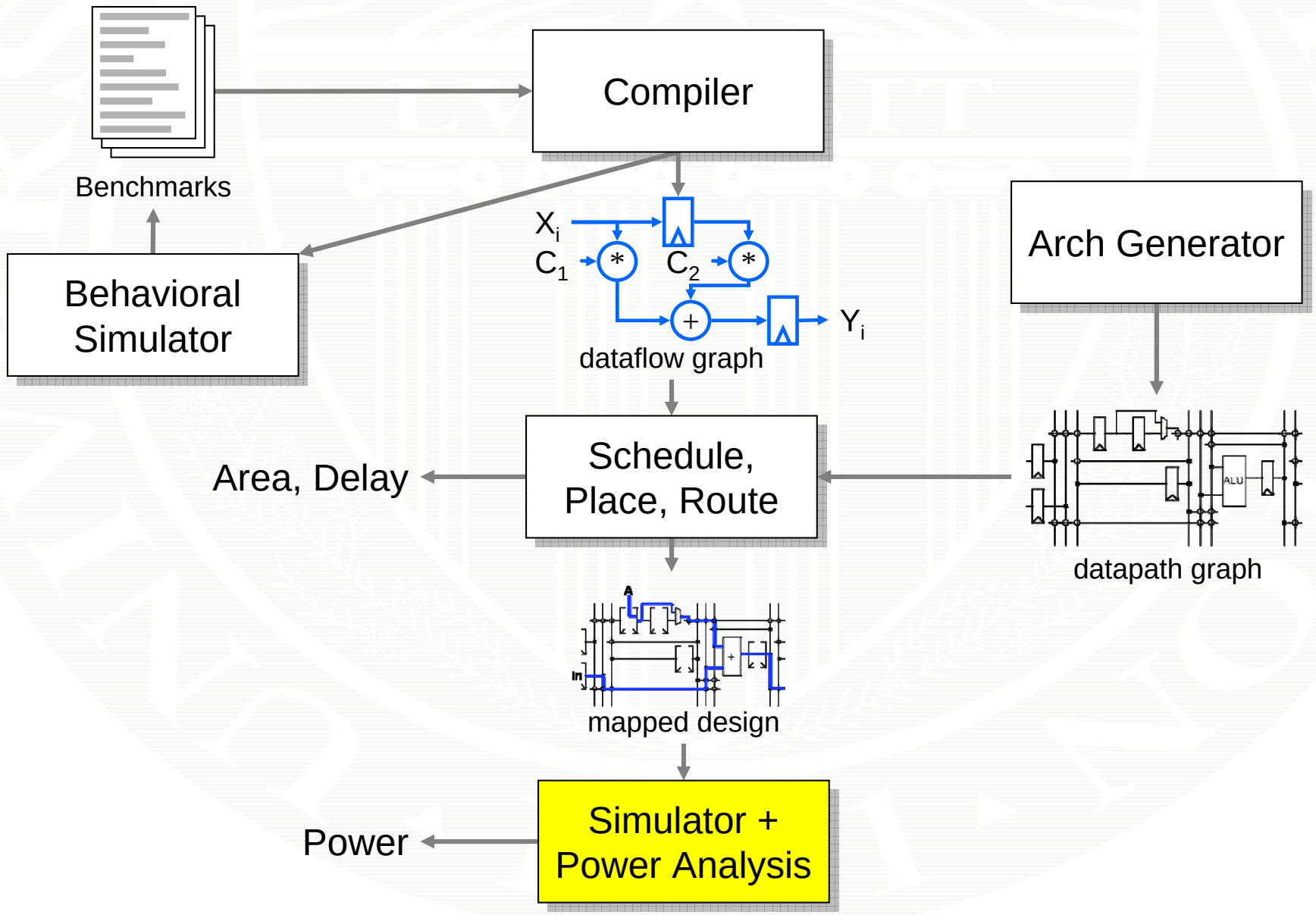

Power Analysis

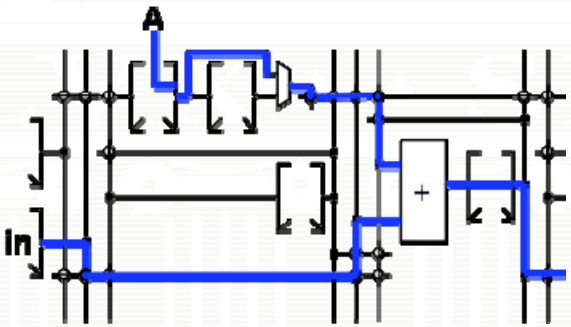

mapped design

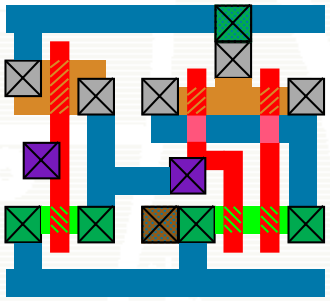

component layouts

Cycle	A	B	C	D
0	FFFF	0001	0000	00E1
1	0000	0001	0001	FF01
2	FFFF	0001	0002	00E1
3	FFFE	0001	0004	FF00
4	FFFA	0001	0008	00E1
5	FFE0	0001	0010	FFF1
6	FE91	0001	0020	00E0
…				

simulation input data

Verilog Simulator

Power

```
Dyn_pwr_inv1(L,D,M)
  = 1450*L+11900*M+9140*D-.0053*L²
    +1.07*L*M-7.4*L*D+6560
Static_pwr_inv1 = 21.9
Delay_inv1(L,D,M)
  = 2440*L+13100*M+10300*D-.0026*L²
    +3.45*L*M-.23*L*D+20500
…
```

area, delay, power models

Mosaic System Diagram

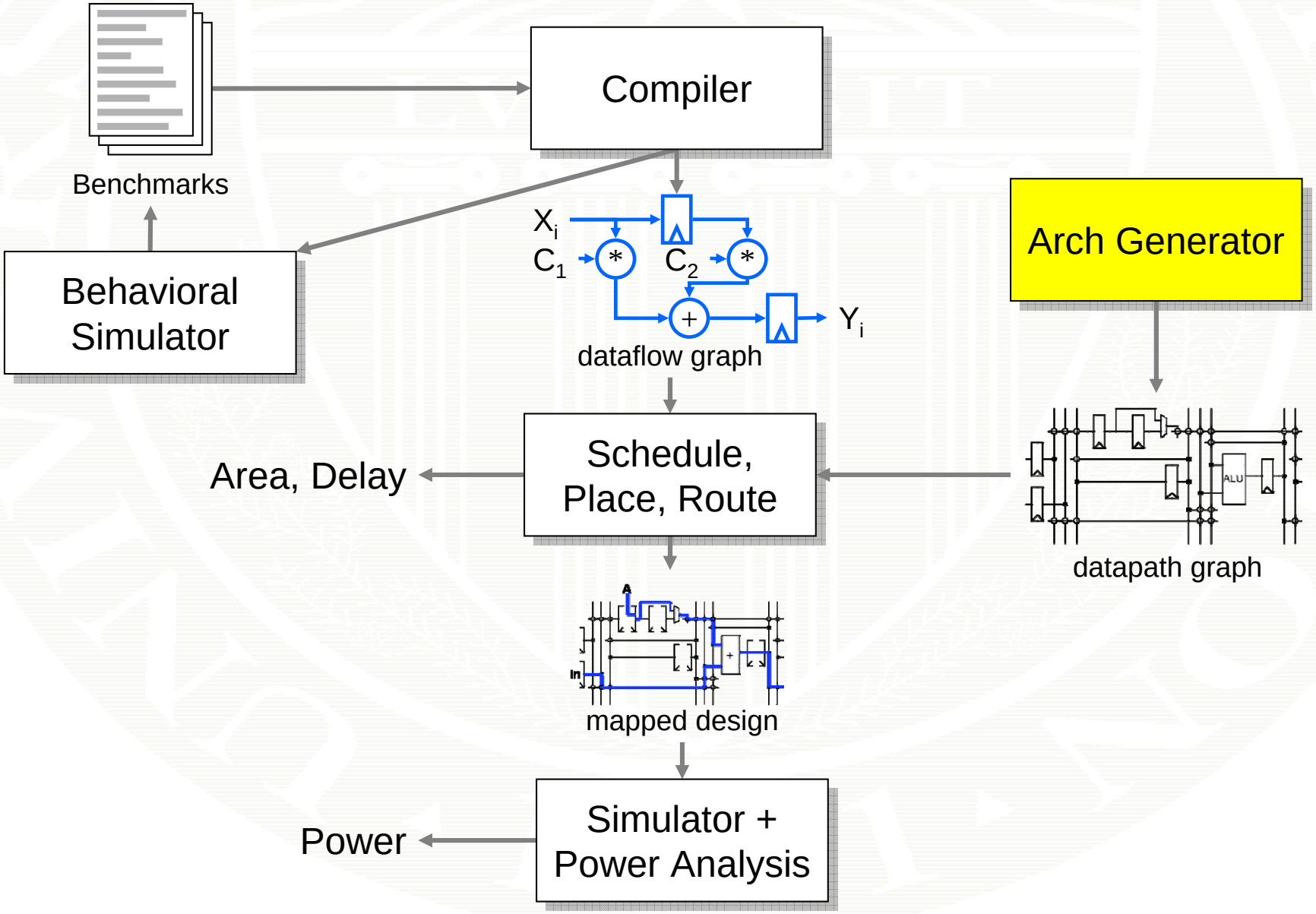

Representing prototype architectures

- Datapath graph
  - computing resources
  - storage
  - interconnect

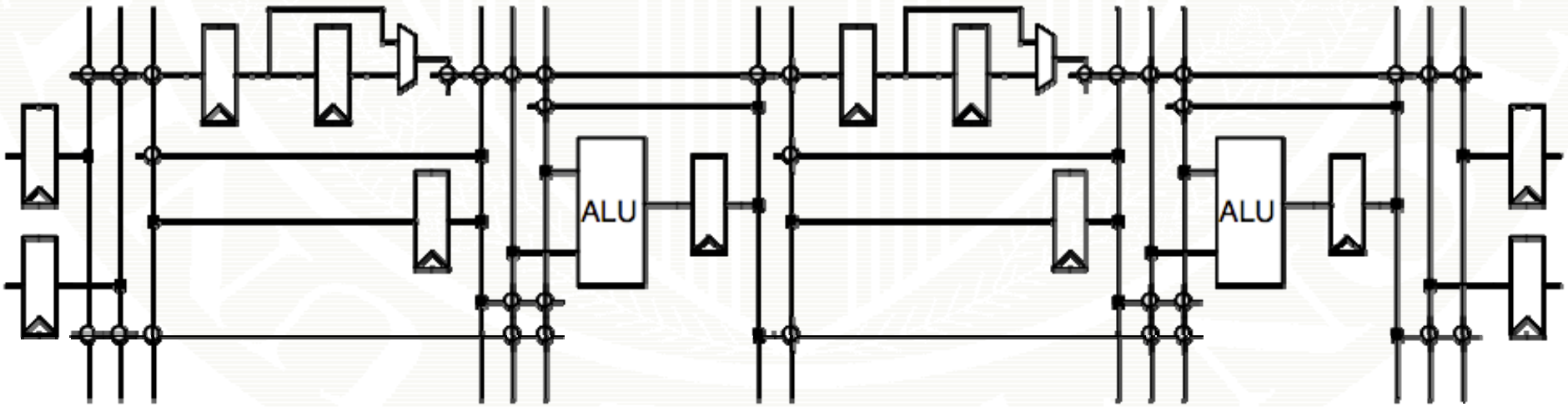

Example: Interconnect topology

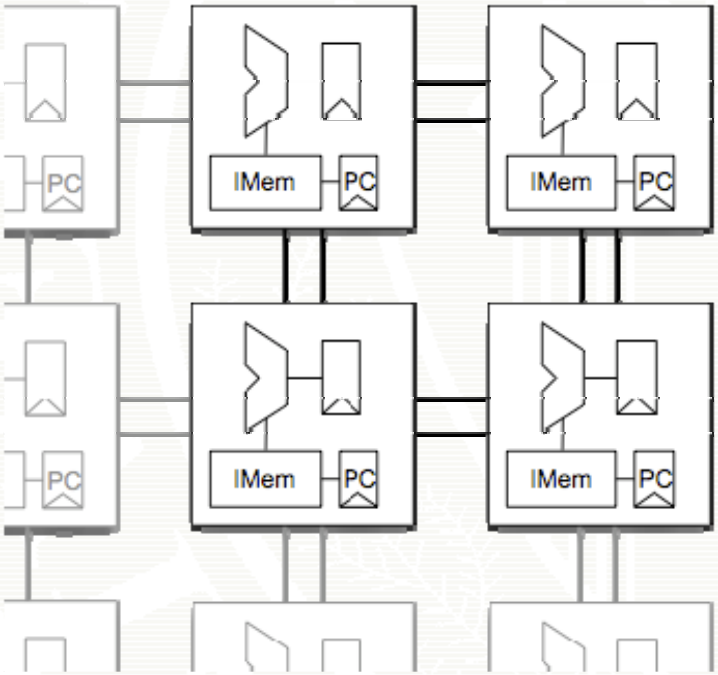

nearest neighbor

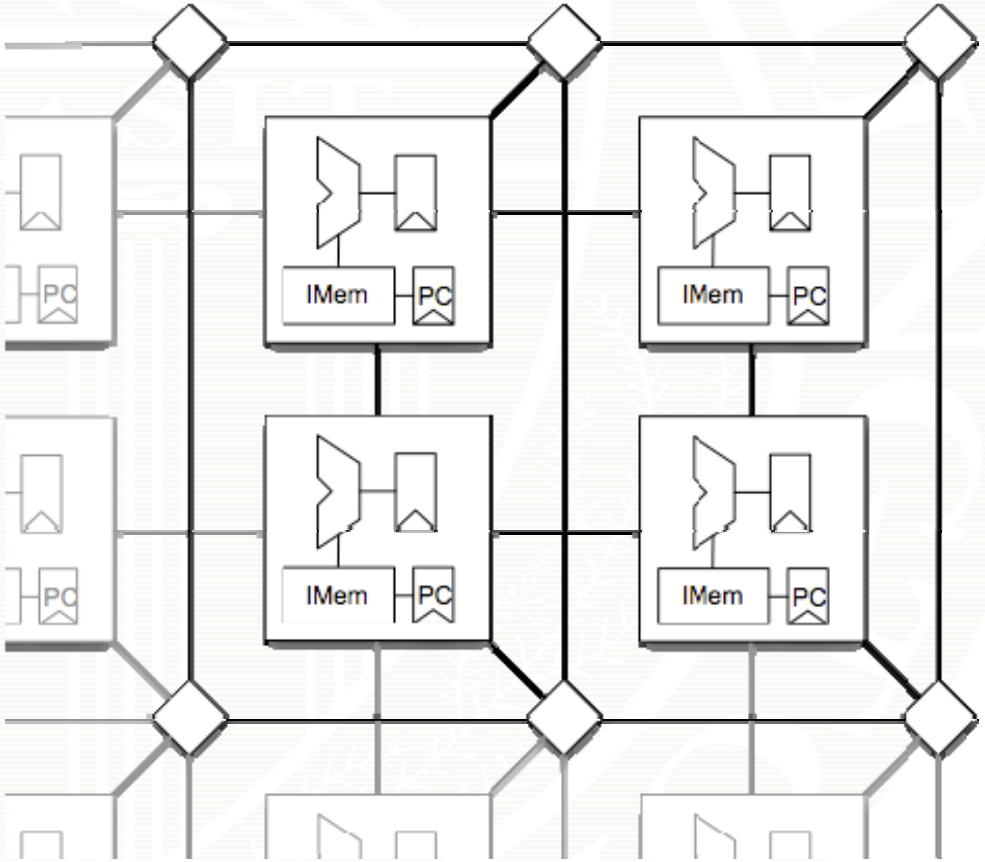

nearest neighbor + switched network

Architectural Exploration

- Interconnect
  - Topology
  - Static vs. Scheduled Interconnect
  - Control vs. Datapath networks
- Logic Blocks
  - ALU-everywhere vs. (some) dedicated units
  - Richer units: mult, divide, barrel-shift…
- Memory organization & distribution
  - # of instructions per ALU
  - Data memory size, location
- Low-power optimizations
  - Clock gating
  - Crosstalk-aware, value-aware place & route

Mosaic System Diagram

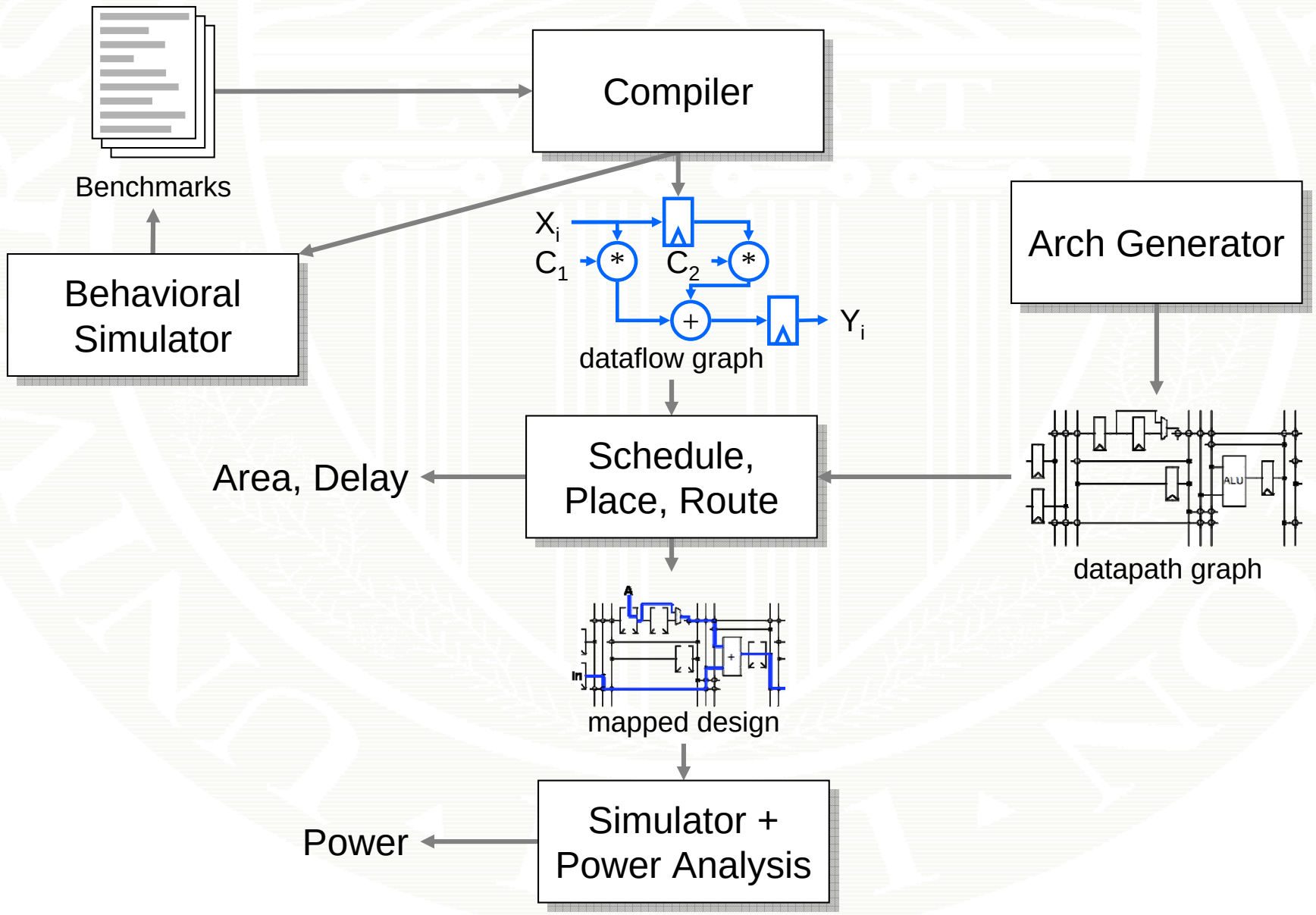

Budget & Timeline

- Total Budget: $730,000
- As of 11/8/07, spent $220,722.90 (30%)
- Project runs 10/1/06 – 9/30/09
  - 11/8/07 is 36% of project period

Milestones

- **Year 1**
- Identify benchmark applications
- Generate initial power/delay models, logic
- Generate initial architecture templates
- Import Trident compiler, adapt to SPR
- **Deliverables**
- Benchmark and kernel definitions
- Initial power/delay estimates for benchmarks
- Initial set of CGRA architecture alternatives

- **Year 2**
- Generate initial power/delay models, routing
- Generate, analyze alternative CGRA archs
- Perform initial exploration of CGRA archs
- Develop infrastructure for emulating CGRA architectures on multi-FPGA system
- Emulate a complete example CGRA arch.
- **Deliverables**
- Parameterized power and delay model
- Emulate one benchmark on example CGRA

- **Year 3**
- Final power and delay models for CGRA
- Identify best CGRA arch for benchmarks
- Emulation of target app on optimized CGRA
- Complete generator for CGRAs
- **Deliverables**
- Complete spec of final optimized CGRA
- Complete characterization of performance, cost and power of final CGRA
- Emulate benchmark apps on final CGRA
- Measured power/performance of emulated benchmark

Mosaic Project Goals

- CGRA benchmarks
- Compiler/Mapper
- Design “best” CGRA arch.

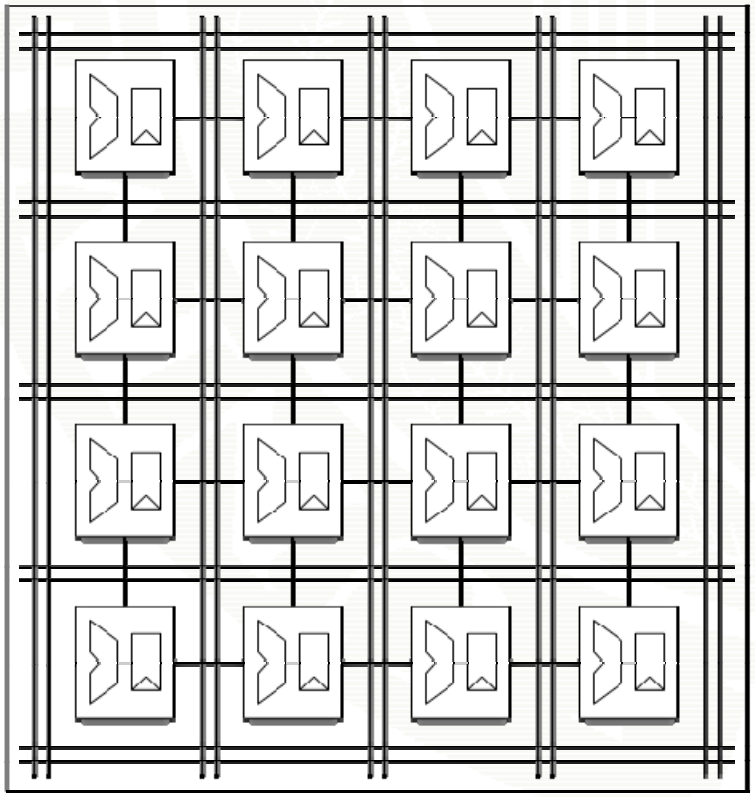

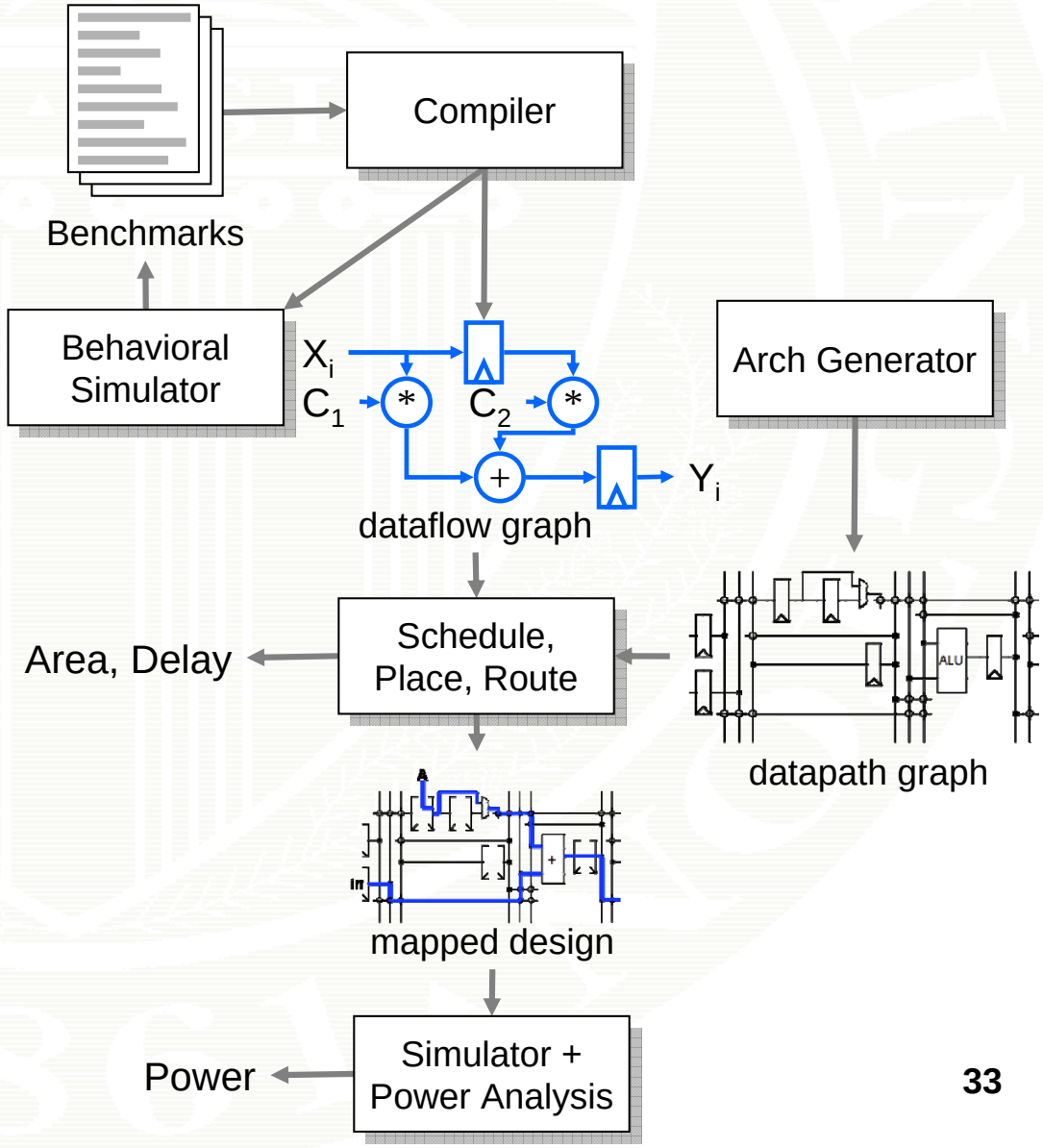

Ultra-Small Imaging and Spectroscopic Elements with Subwavelength Performance

Kevin J. Webb, Shivanand, and Huikan Liu

School of Electrical and Computer Engineering
Purdue University
West Lafayette, IN 47907, USA
webb@purdue.edu

PURDUE
UNIVERSITY

Outline

- Anisotropic Slab Lens
- Irregular Diffractive Elements

Negative Refractive Index

- ►Naturally-occurring media we know have a positive refractive index (RH)
- ►Negative refractive index media have $\mu' < 0$ and $\varepsilon' < 0$ (LH)[1]
- ►A matched and lossless negative index slab can act as a perfect lens[2]
- ►Metamaterial implementation has been achieved in the microwave range[3]
- ►Even small loss limits the resolution and imposes a near-field requirement[4,5]
- ►Kramers-Kronig relations provide information on causal resonant systems

[1] V. G. Veselago, *Sov. Phys. Uspekhi*, **10**, 509 (1968)

[2] J. B. Pendry, *Phys. Rev. Lett.*, **85**, 3966 (2000)

[3] R. A. Shelby, D. R. Smith, and S. Schultz, *Science*, **292**, 77 (2001)

[4] M. Yang and K. J. Webb, *Opt. Lett.*, **20**, 2382 (2005)

[5] K. J. Webb, M. Yang, D. W. Ward, and K. A. Nelson, *Phys. Rev. E*, **70**, 035602 (2004)

Planar Uniaxial Slab

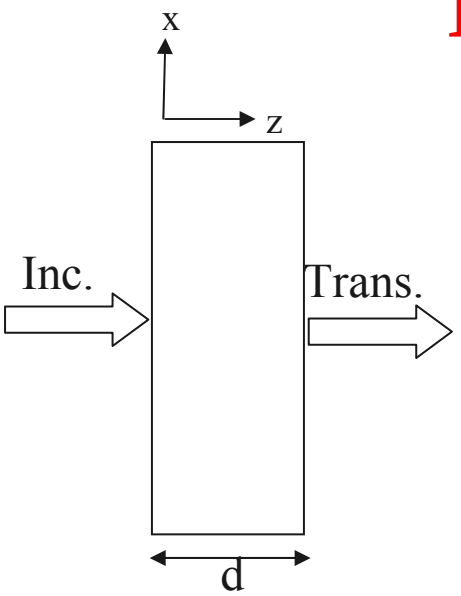

$$\varepsilon_x = \varepsilon_x' + j\varepsilon_x'' \qquad \varepsilon_z = \varepsilon_z' + j\varepsilon_z''$$

TM field (H_y, E_x, E_z) dispersion relation:

$$k_z = \sqrt{\varepsilon_x k_0^2 - \frac{\varepsilon_x}{\varepsilon_z} k_x^2} \qquad k_0^2 = k_x^2 + k_{z0}^2$$

$$r = \frac{Z_0 - Z_s}{Z_0 + Z_s} \qquad Z_0 = \frac{k_{z0}}{\omega\varepsilon_0} \qquad Z_s = \frac{k_z}{\omega\varepsilon_0\varepsilon_x}$$

Transfer function: $$T(k_x) = \frac{(1-r^2)\exp(-jk_z d)}{1 - r^2\exp(-j2k_z d)}$$

For $\varepsilon_z \to \infty$,

$$T(k_x) = \left\{\cos\left(\sqrt{\varepsilon_x}k_0 d\right) + \frac{j}{2}\left(\sqrt{\frac{\varepsilon_x\left(k_0^2 - k_x^2\right)}{k_0^2}} + \sqrt{\frac{k_0^2}{\varepsilon_x\left(k_0^2 - k_x^2\right)}}\right)\sin\left(\sqrt{\varepsilon_x}k_0 d\right)\right\}^{-1}$$

When $k_z d = \sqrt{\varepsilon_x}k_0 d = n\pi, \quad n = 1,2\ldots \quad T(k_x) = \cos(n\pi)$

Anisotropic Slab Transmission Spectrum

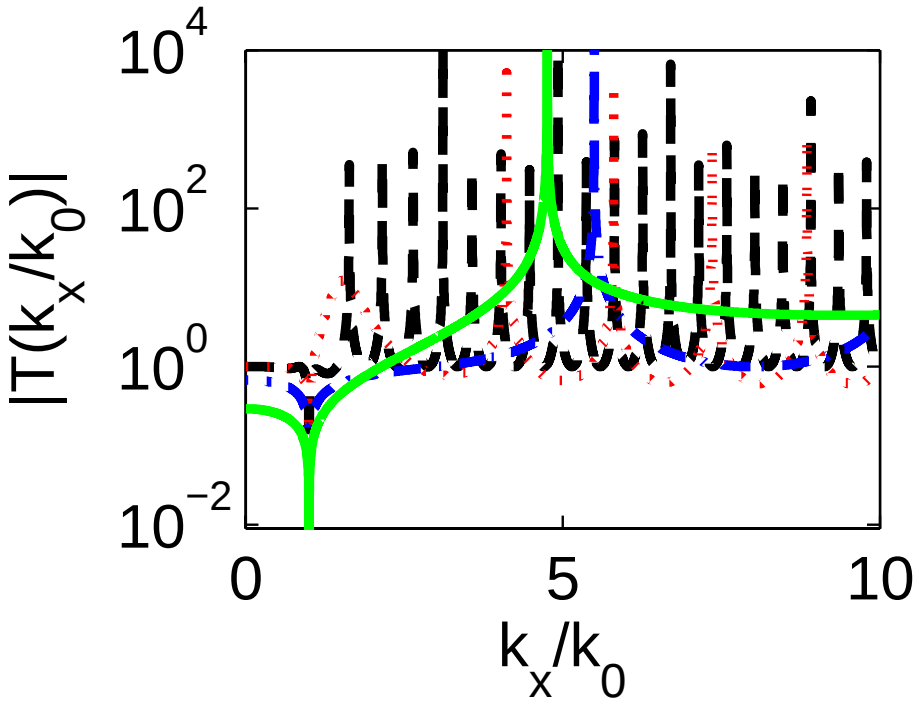

Black, dashed: ε_x=1, ε_z=-1
Red, dotted: ε_x=1, ε_z=-10
Green, solid: ε_x=0.01, ε_z=-100
Blue, dash-dotted: ε_x=0.1, ε_z=-10

λ = 700nm, d = 800nm

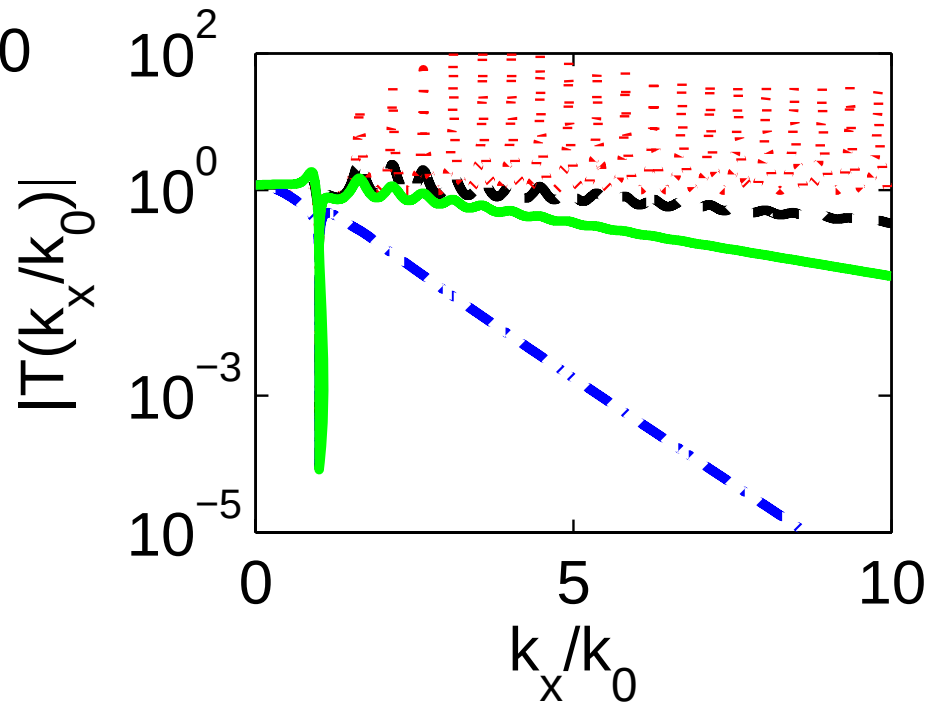

Black, dashed: ε_z=-1
Red, dotted: ε_z=-1-j0.05
Green, solid: ε_z= =-1+j0.05
Blue, dash-dot: ε_z= =-1-j0.5

ε_x=1+j0.05

Anisotropic Slab Transmission Spectrum

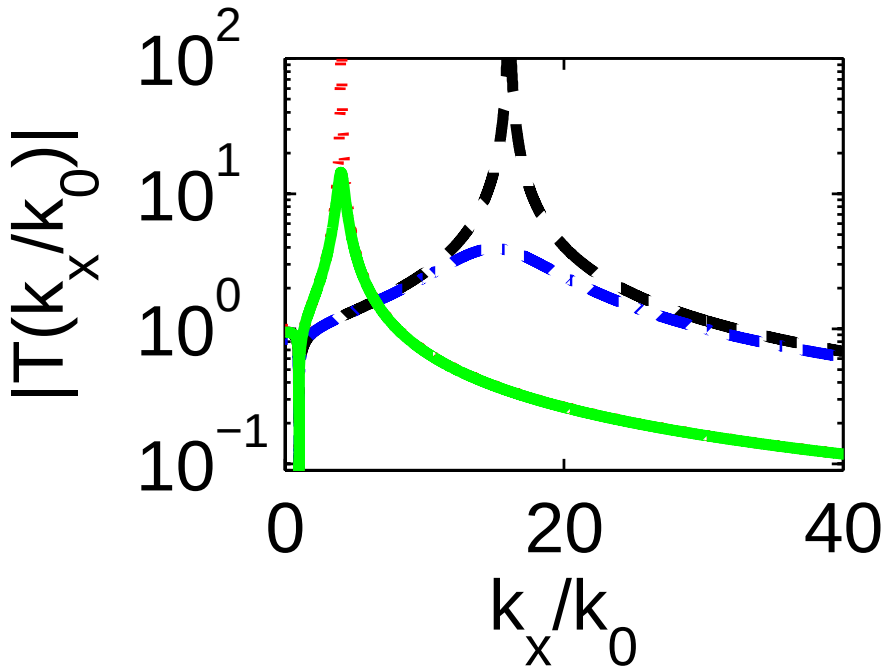

Black, dashed: $k_z d$=0.9π, lossless
Red, dotted: $k_z d$=1.8π, lossless
Blue, dash-dot: Re[$k_z d$]=0.9π, Im[ε_x]=-0.01
Green, solid: Re[$k_z d$]=1.8π, Im[ε_x]=-0.01

λ = 700nm, d = 800nm, $\varepsilon_z \rightarrow \infty$

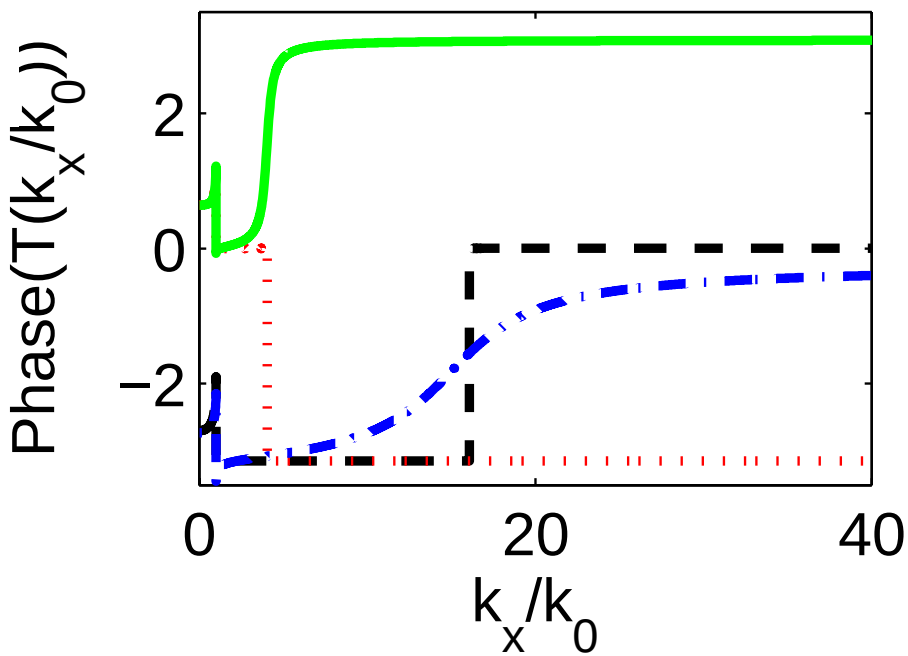

Imaging Example: Anisotropic Slab

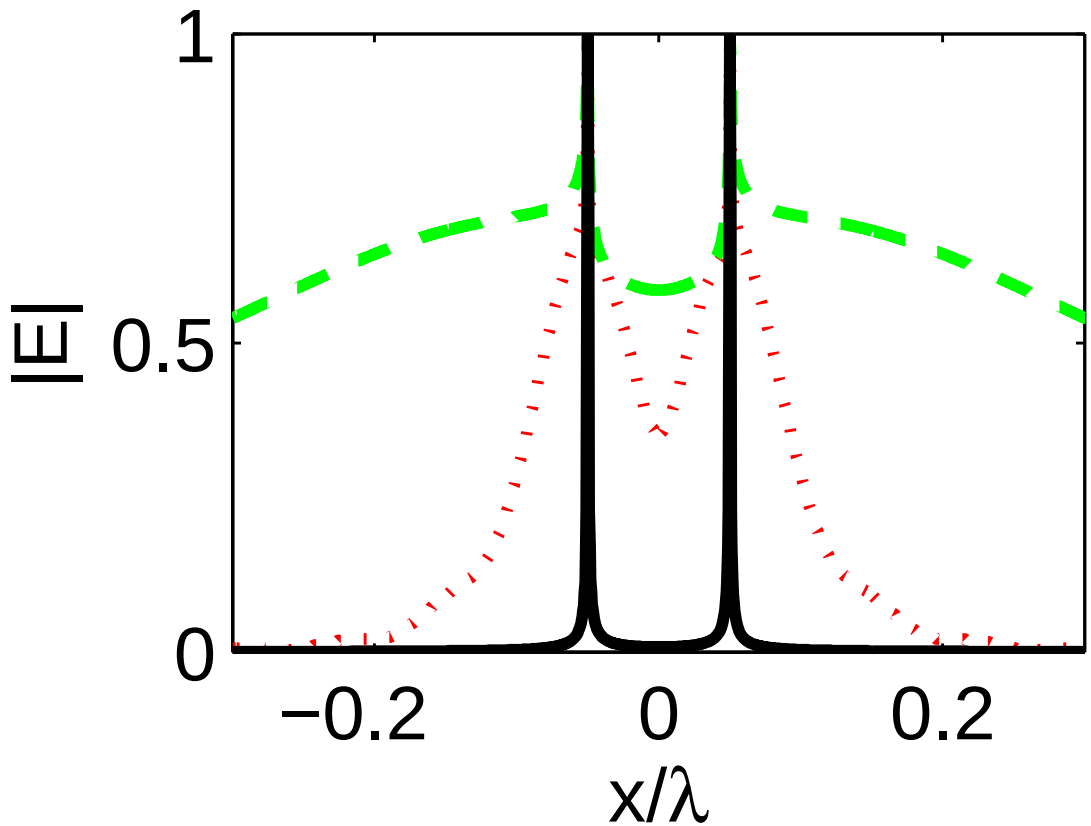

Simulation parameters:
λ=700nm, d=800nm

$\varepsilon_z = -10^7$

Red, dotted line: $k_0 d\sqrt{\varepsilon_x'} = 0.9\pi$

Green, dashed line: $k_0 d\sqrt{\varepsilon_x'} = 1.8\pi$

Black, solid line: 0.1λ wide object

Imaging Example: Anisotropic Slab

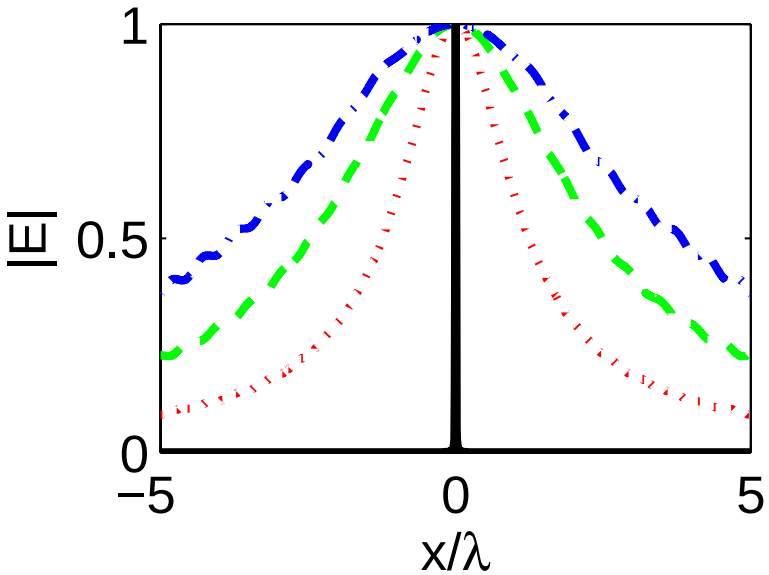

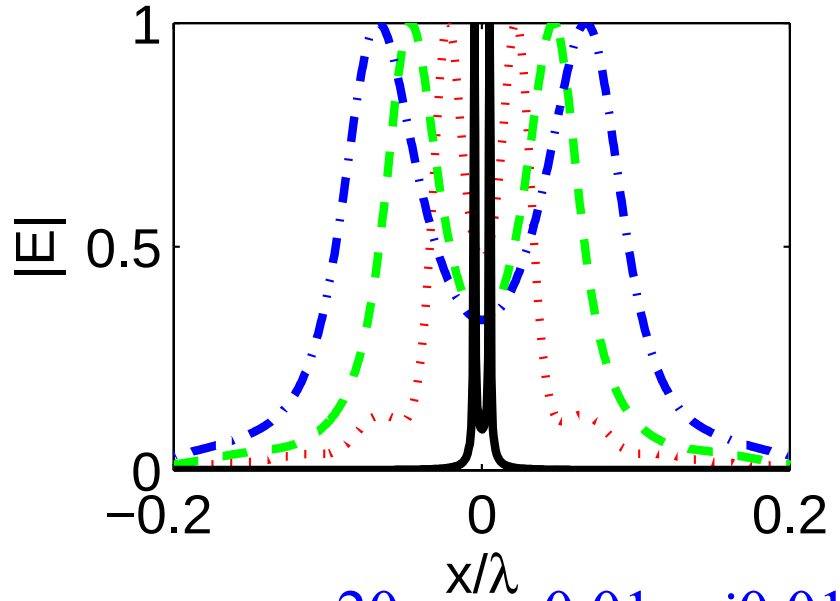

Free space propagation

λ=700nm $\varepsilon_z = -20, \varepsilon_x = 0.01 - j0.01$

Simulation parameters

Red, dotted line:

Green, dashed line:

Blue, dash-dotted line:

Black, solid line: object (0.01λ)

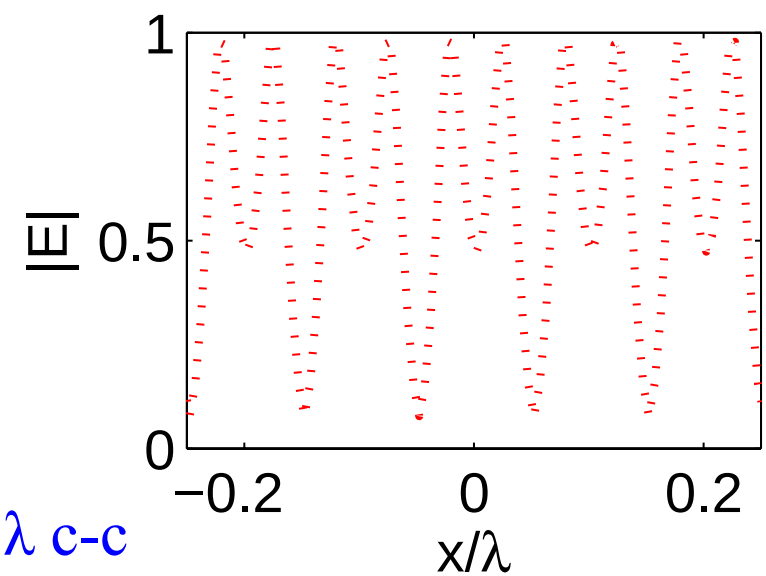

Multiple objects 0.1λ c-c

Multilayer Metal Film[1]

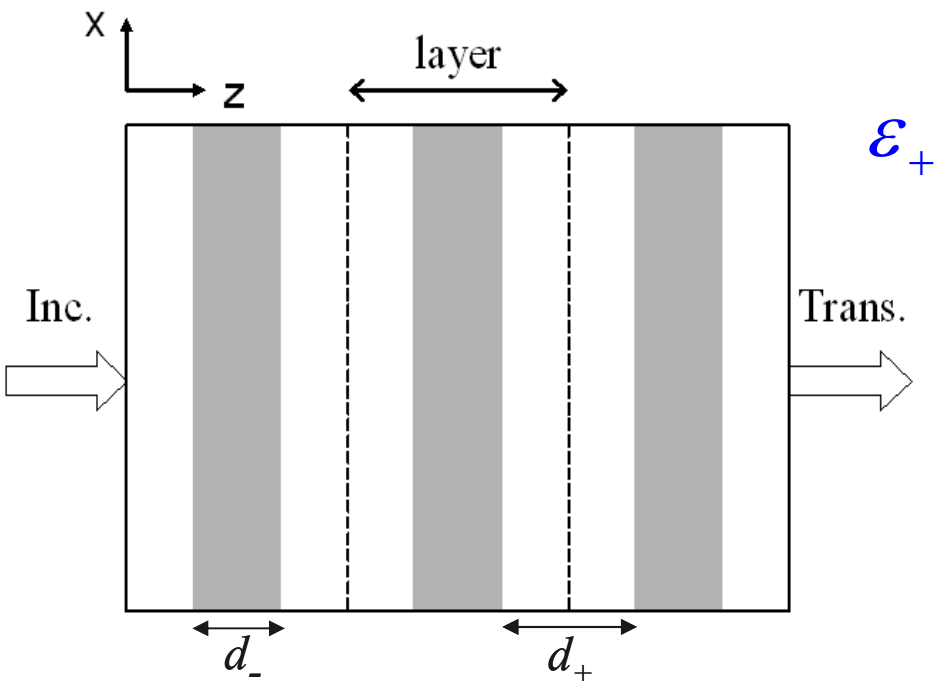

$$\varepsilon_+ = \varepsilon_+' + j\varepsilon_+'' \qquad \varepsilon_- = \varepsilon_-' + j\varepsilon_-''$$

Spatial average:

$$\left.\begin{aligned} \hat{n}\times\left({}_+ - {}_-\right) &= 0 \\ \hat{n}\cdot\left(\varepsilon_+ {}_+ - \varepsilon_- {}_-\right) &= 0 \end{aligned}\right\}$$

$$\varepsilon_x = \varepsilon_- D + \varepsilon_+ (1-D)$$

$$\frac{1}{\varepsilon_z} = \frac{D}{\varepsilon_-} + \frac{(1-D)}{\varepsilon_+}$$

Duty cycle $\quad D = \dfrac{d_-}{d_- + d_+}$

[1] K. J. Webb and M. Yang, *Opt. Lett.*, **31**, 2130 (2006)

Multilayer Metal Film Transmission Spectrum[1]

Transmission spectrum with varying number of layers for a 400 nm thick Ag/SiO_2 slab having duty cycle D=0.1

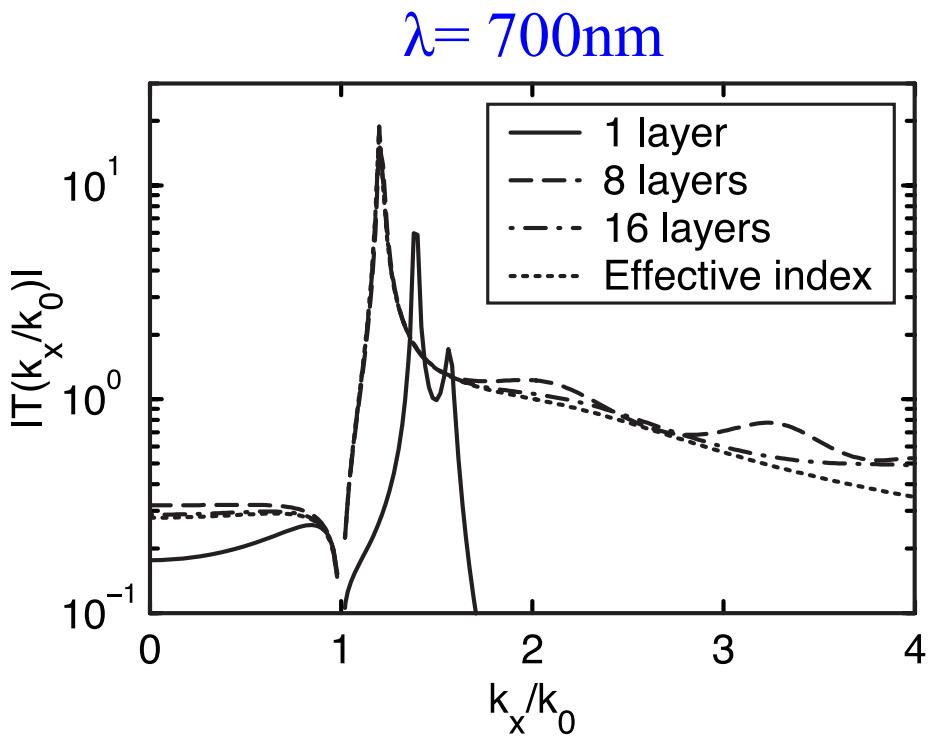

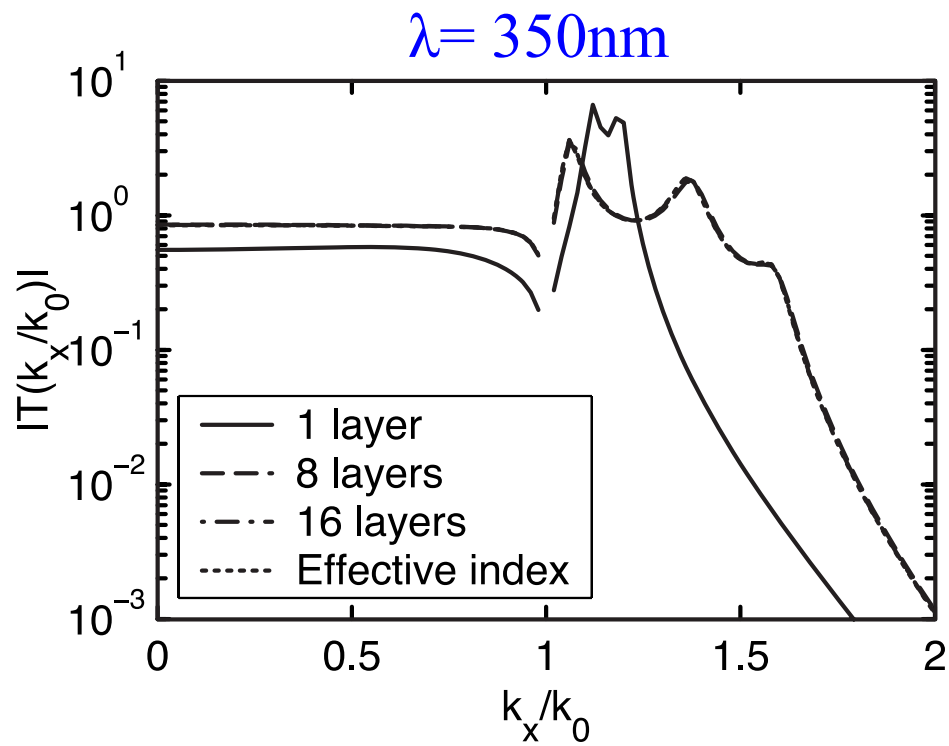

[1] K. J. Webb and M. Yang, *Opt. Lett.*, **31**, 2130 (2006)

Multilayer Metal Film Transmission Spectrum[1]

Transmission spectrum with varying duty cycle *D* for a 400 nm thick Ag/SiO_2 slab having 8 layers:

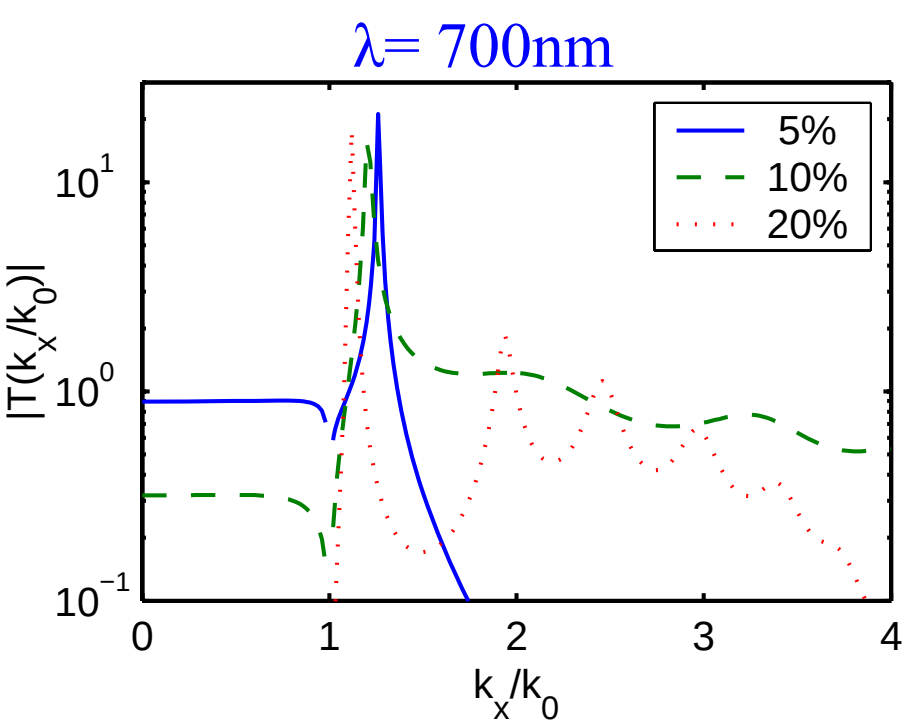

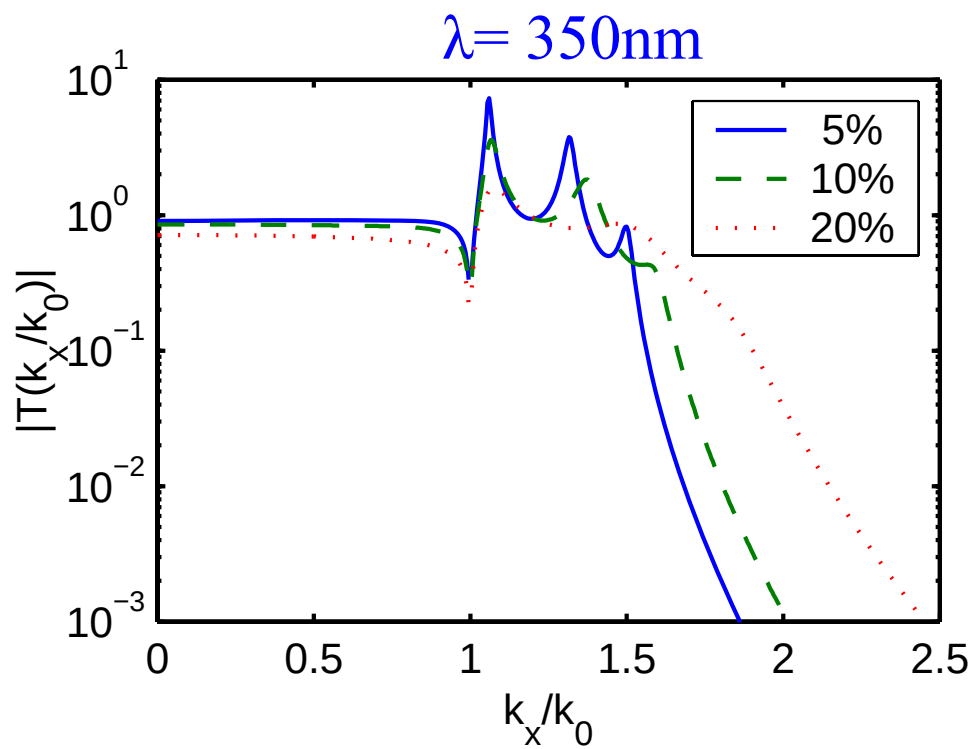

[1] K. J. Webb and M. Yang, *Opt. Lett.*, **31**, 2130 (2006)

Anisotropic Slab: Possible Geometry

$$\varepsilon_+ = \varepsilon_+' + j\varepsilon_+'' \qquad \varepsilon_- = \varepsilon_-' + j\varepsilon_-''$$

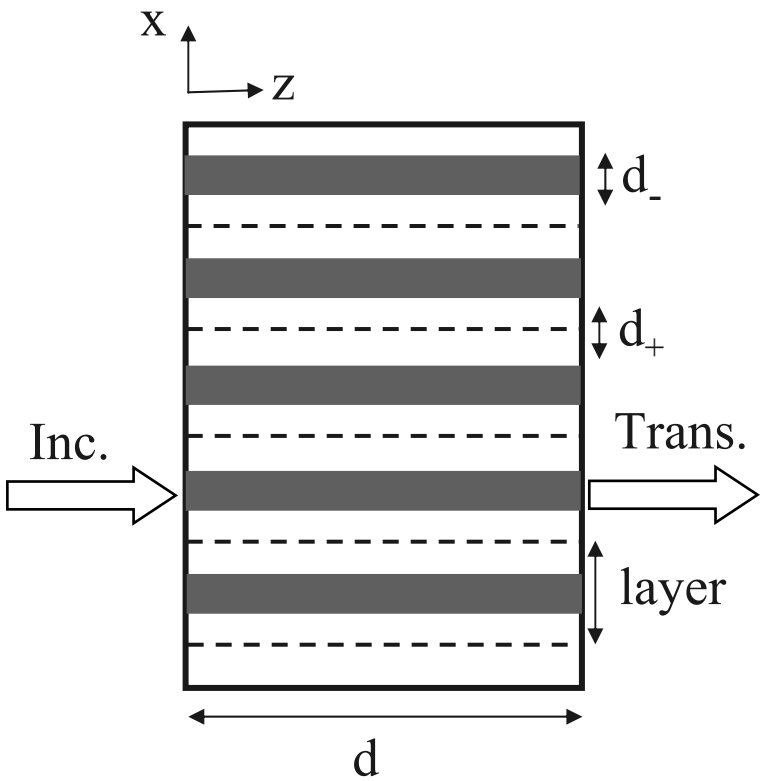

$$\frac{1}{\varepsilon_x} = \frac{D}{\varepsilon_-} + \frac{(1-D)}{\varepsilon_+}$$

$$\varepsilon_z = \varepsilon_- D + \varepsilon_+ (1-D)$$

Duty cycle

$$D = \frac{d_-}{d_- + d_+}$$

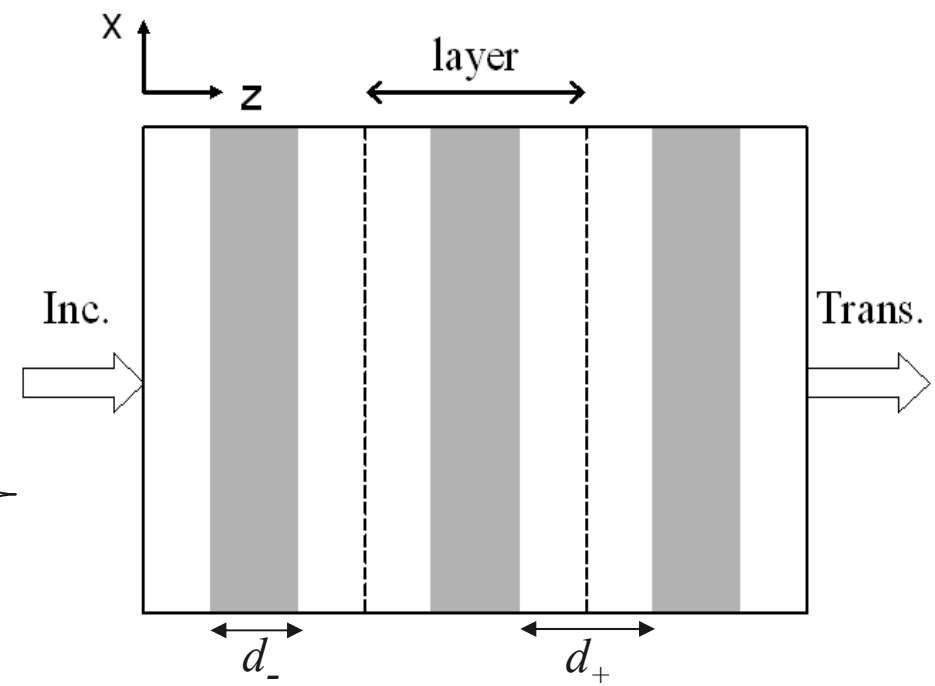

$$\varepsilon_x = \varepsilon_- D + \varepsilon_+ (1-D)$$

$$\frac{1}{\varepsilon_z} = \frac{D}{\varepsilon_-} + \frac{(1-D)}{\varepsilon_+}$$

[1] K. J. Webb and M. Yang, *Opt. Lett.*, **31**, 2130 (2006)

Multilayer Metal Film Image

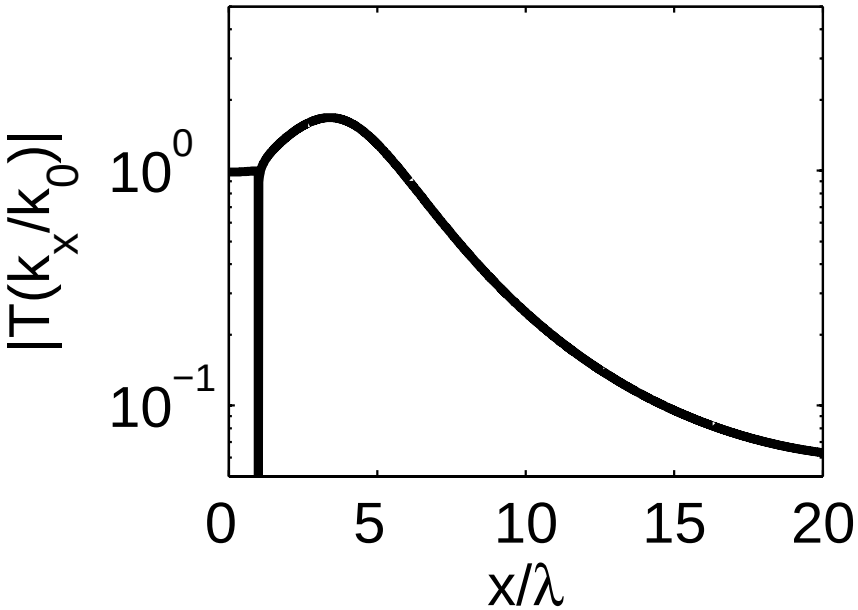

$$\varepsilon_{Ag} = -587.887 - j109.334$$

$$\varepsilon_{SiO_2} = 2.792$$

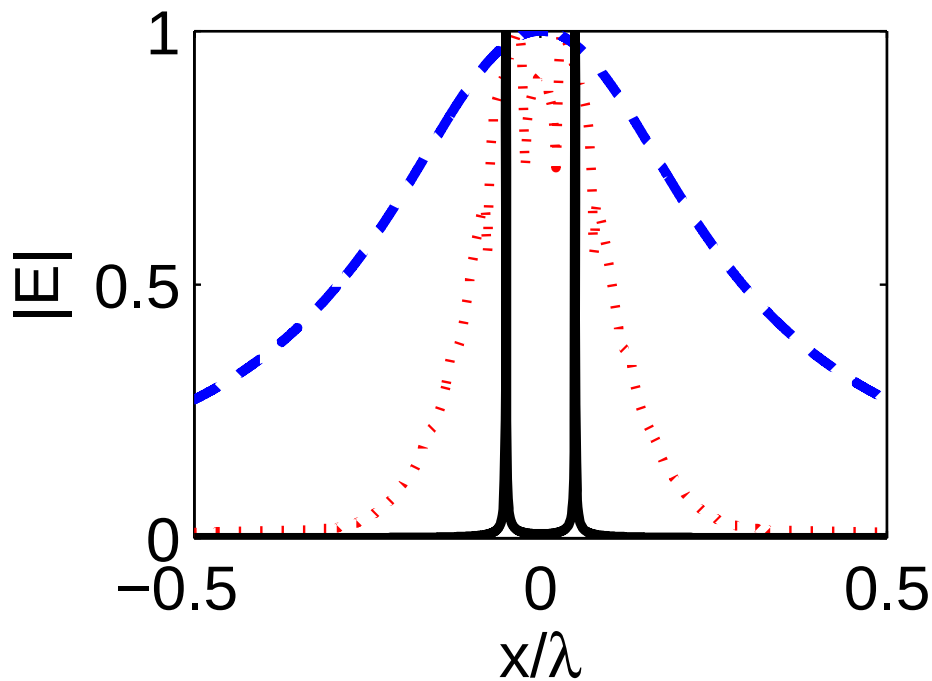

Simulation parameters:

λ=4μm, d=0.8μm

$D = 0.5$

Dotted, red line: image

Solid, black line: 0.1λ wide object

Dashed, blue line: free space propagation

Isotropic Negative Dielectric Constant Slab

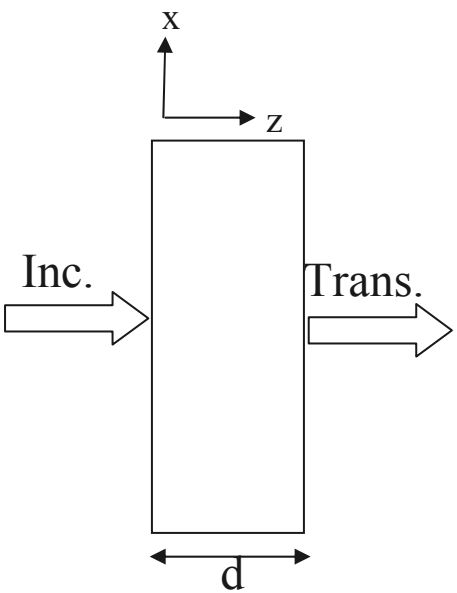

$$\varepsilon = \varepsilon' + j\varepsilon''$$

Reflection coefficient: $$r = \frac{Z_0 - Z_s}{Z_0 + Z_s}$$

$$Z_0 = \frac{k_{z0}}{\omega\varepsilon_0} \qquad Z_s = \frac{k_z}{\omega\varepsilon_0\varepsilon}$$

Transfer function: $$T(k_x) = \frac{(1-r^2)\exp(-jk_z d)}{1 - r^2\exp(-j2k_z d)}$$

For real ε, the poles are given by: $$r^2 = \exp\left(2k_0 d\sqrt{\left(\frac{k_x}{k_0}\right)^2 + |\varepsilon|}\right)$$

Transmission Spect.: Lossless Isotropic Slab

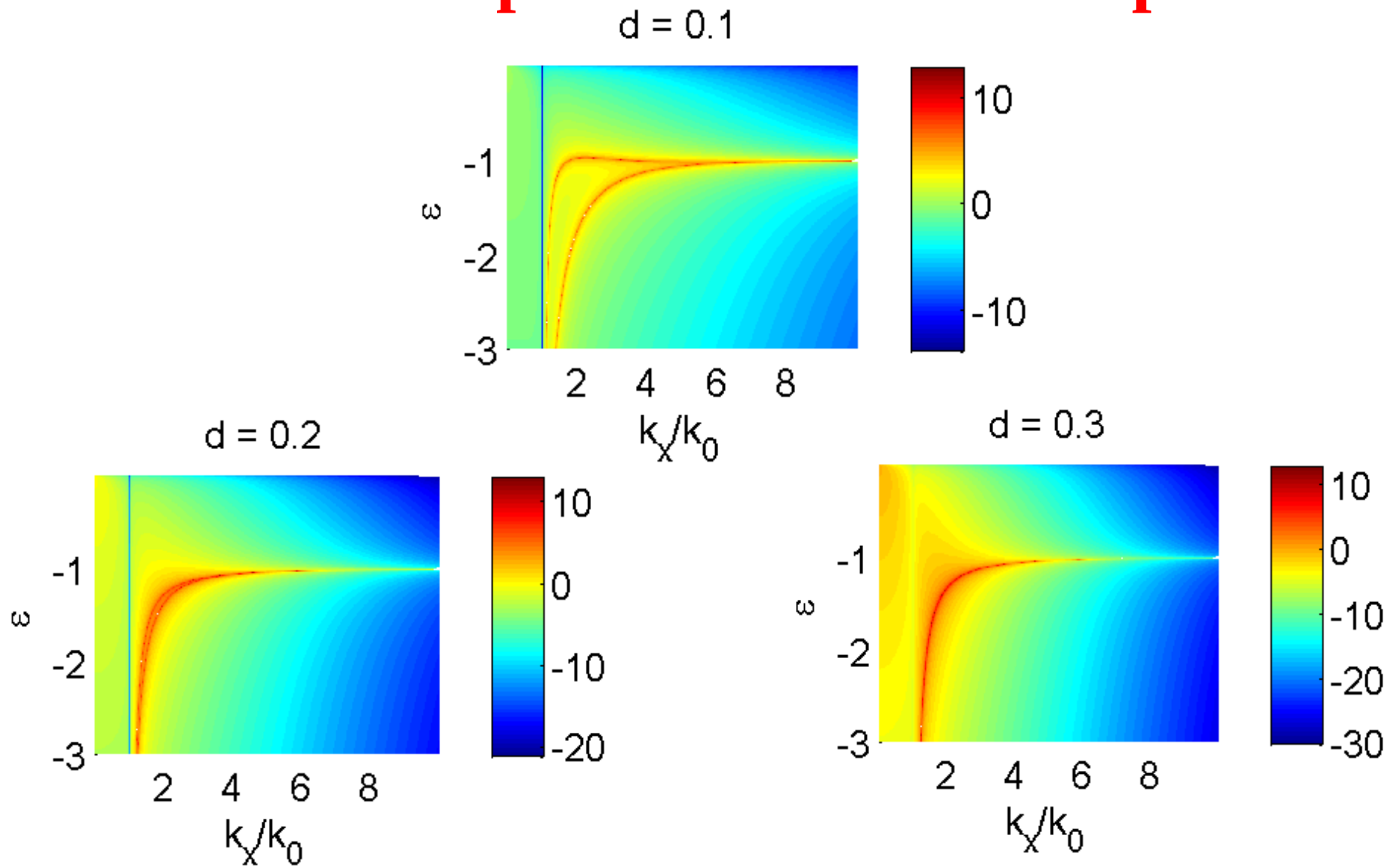

Simulation parameters: λ=700nm, slab thickness d in μm

Transmission Spectrum: Isotropic Slab

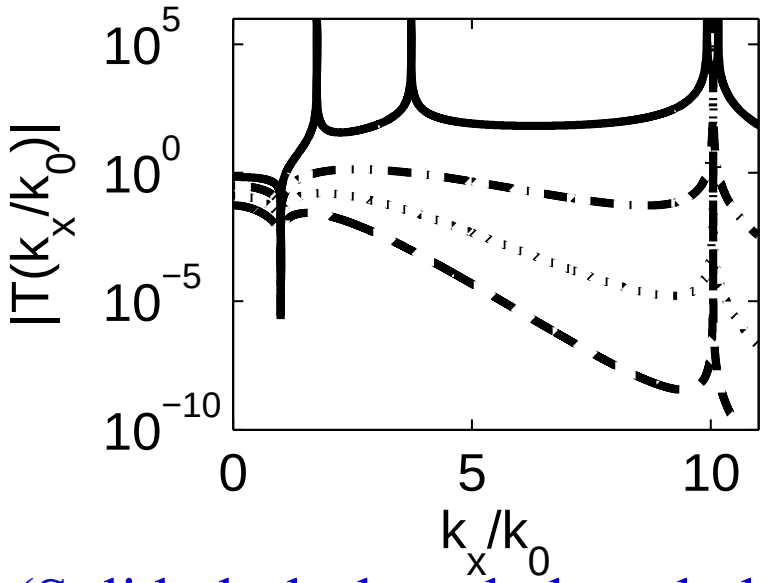

← $\varepsilon' = -1.01$
$\varepsilon'' = 0$

$\varepsilon' = -1.1$ →
$\varepsilon'' = 0$

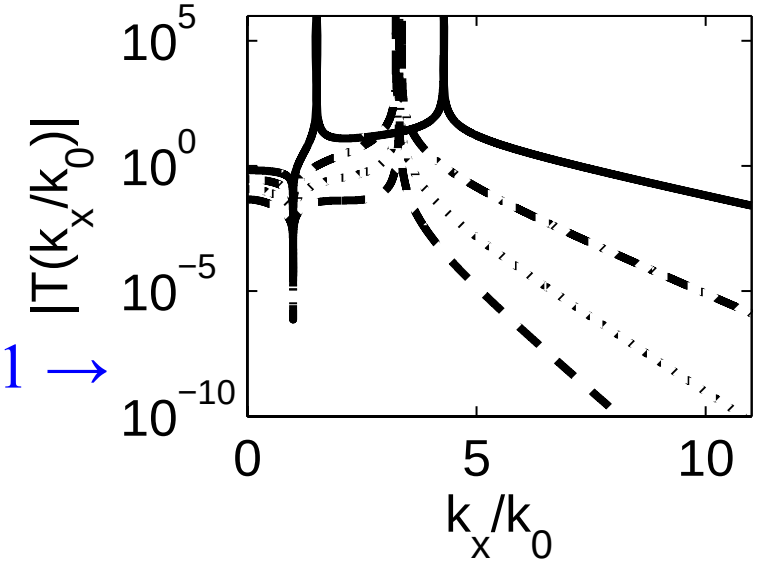

(Solid, dash-dotted, dotted, dashed) lines → d = (0.1, 0.2, 0.3, 0.4) μm

λ=700nm

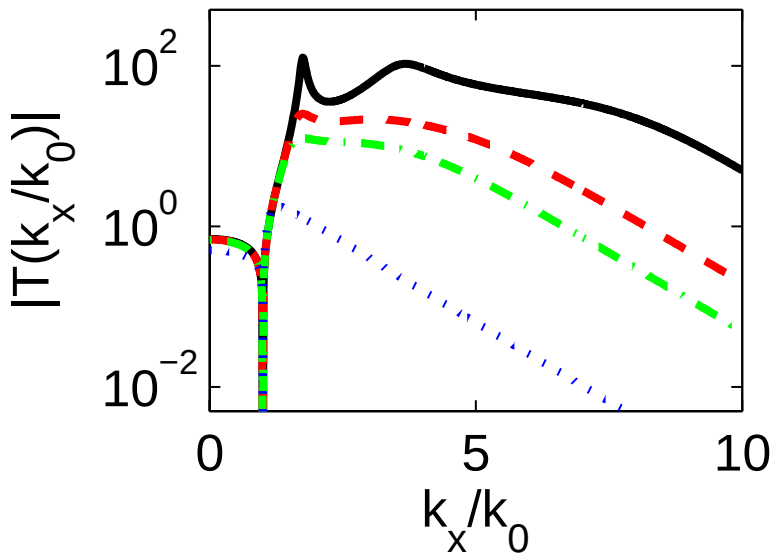

Slab thickness d=0.1μm
ε'=-1.01
Solid: ε'' = -0.01
Dashed: ε'' = -0.05
Dash-dotted: ε'' = -0.1
Dotted: ε'' = -1.0

Imaging Example: Isotropic Slab

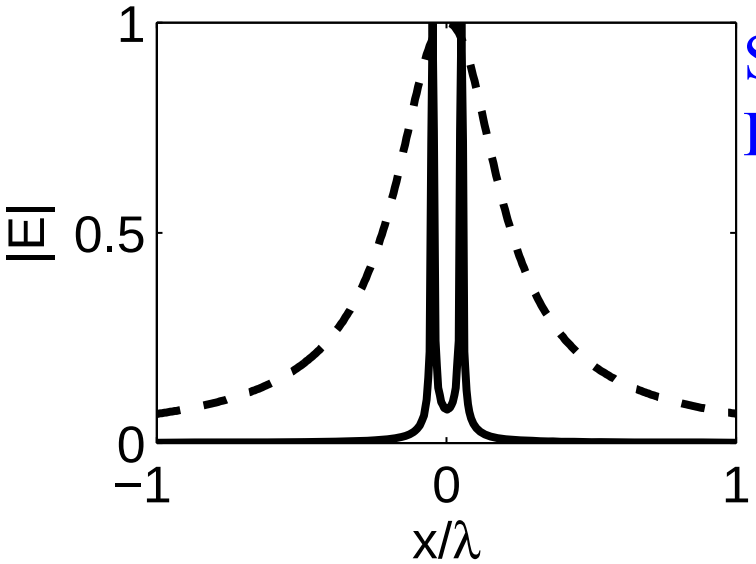

Solid: object
Dashed: ε=1

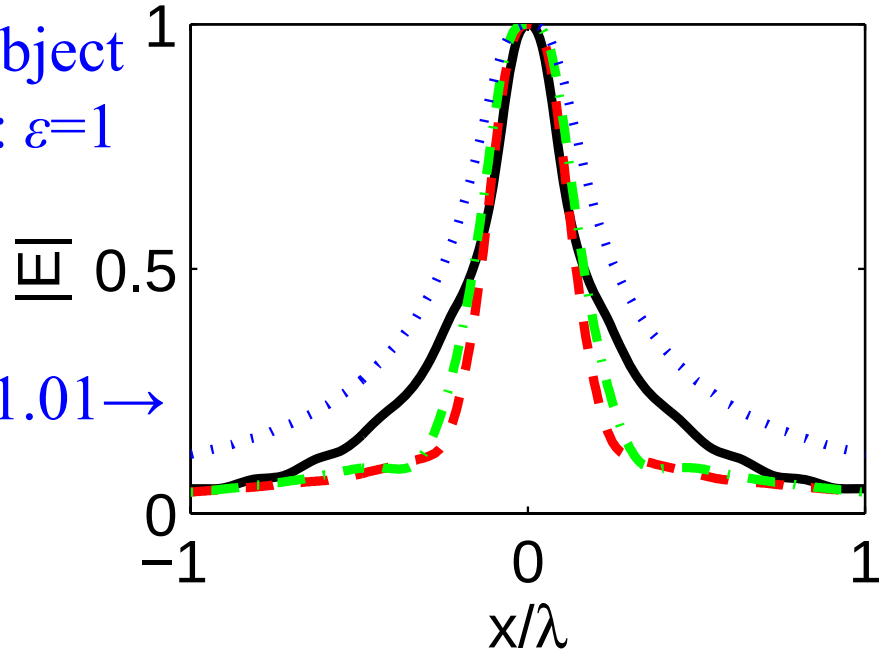

ε'=-1.01→

(Solid, dashed, dash-dotted, dotted) lines → ε''=(-0.01, -0.05, -0.1, -1)

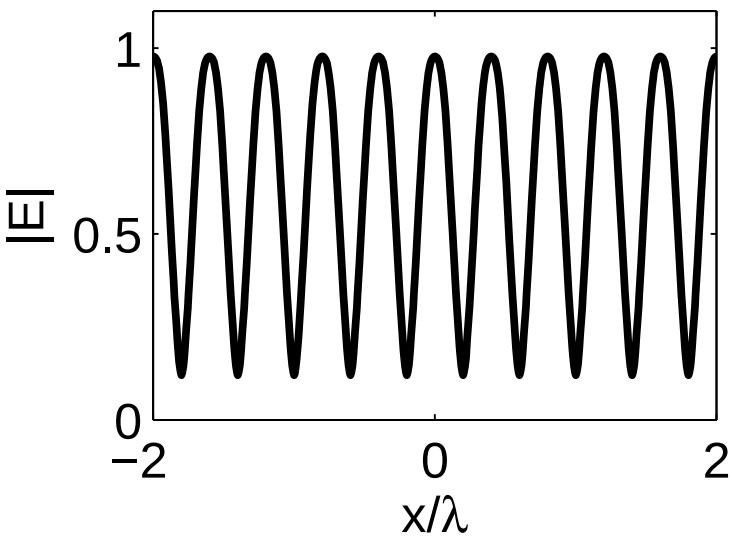

Multiple objects: 0.5λ c-c
ε=-1.01-j0.05

Parameters: λ=700nm, d = 0.1μm, single object width = 0.1λ

Outline

- Anisotropic Slab Lens
- Irregular Diffractive Elements

Field Transformation and Mode Control

Multi-Mode Interference [1]

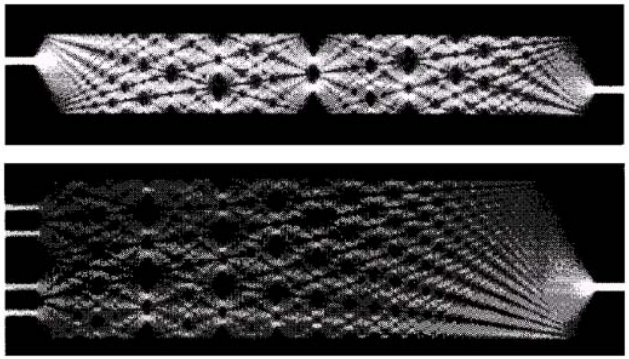

Phased Array Waveguide [2]

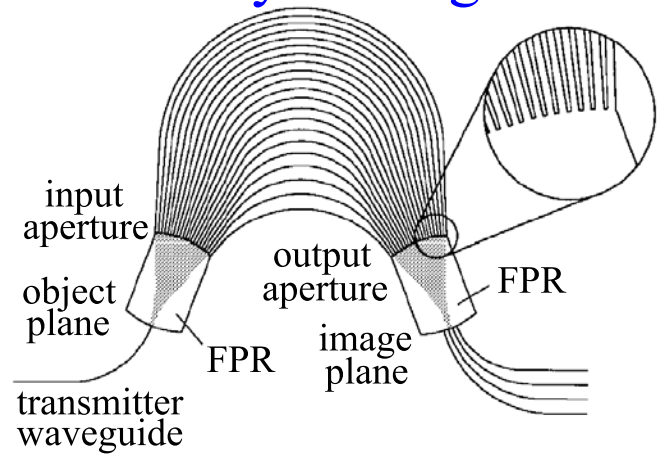

Multi-Mode Interference [1]

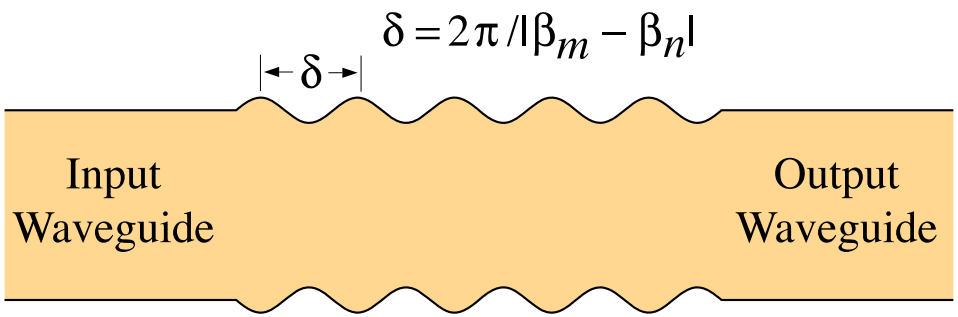

Photonic Crystal Waveguide [4]

[1] L. B. Solando and E. C. M. Pennings, *J Lightwave Technol.*, **13**, 615 (1995)
[2] M. K. Smit and C. Dam, *IEEE J. Select. Topics Quantum Electron.,* **2**, 236 (1996)
[3] J. S. Levine, *Int. J. Infrared and Millimeter Waves*, **5**, 937 (1984)
[4] S. Y. Lin *et al.*, *Science,* **282**, 274 (1998)

Irregular Diffractive Elem: Direct Binary Search

Multiresolution optimization
Si scatterers
λ_0=1.55μm
TE (E out of screen)
3dB spot size of 0.16 λ_0

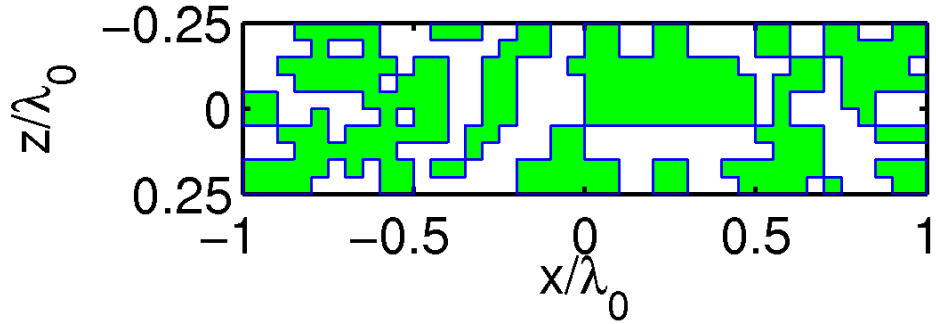

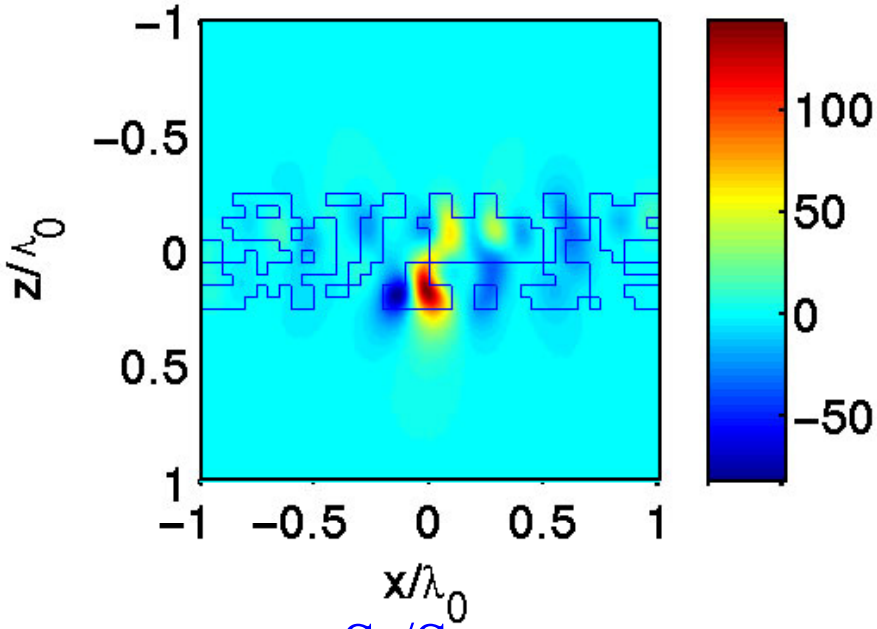

S_z/S_i

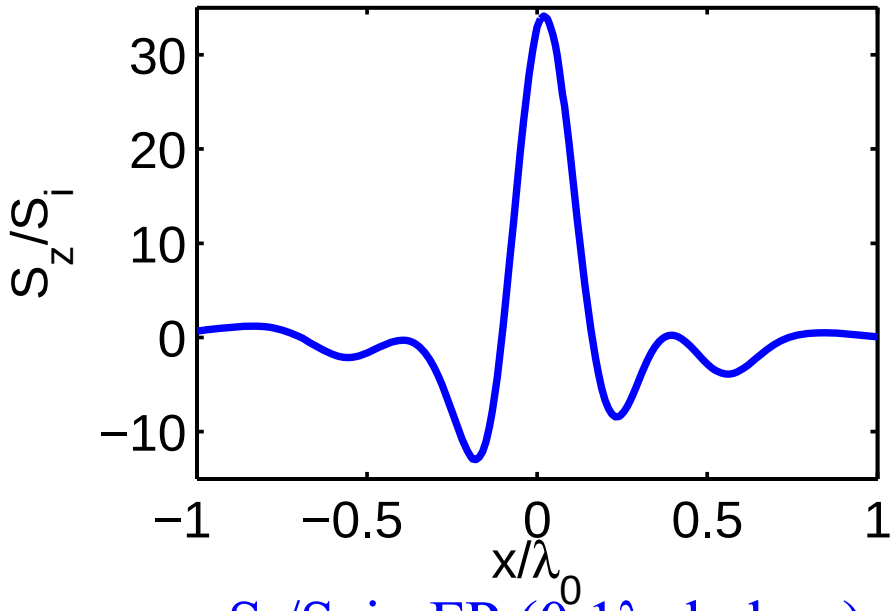

S_z/S_i in FP ($0.1\lambda_0$ below)

[1] J. Li, G. J. Burke, D. A. White, C. A. Thompson, and K. J. Webb, *Opt. Lett.*, **31**, 1181 (2006)

Spectrometry/WDM: Si in Free Space

S_z/S_i at λ_0

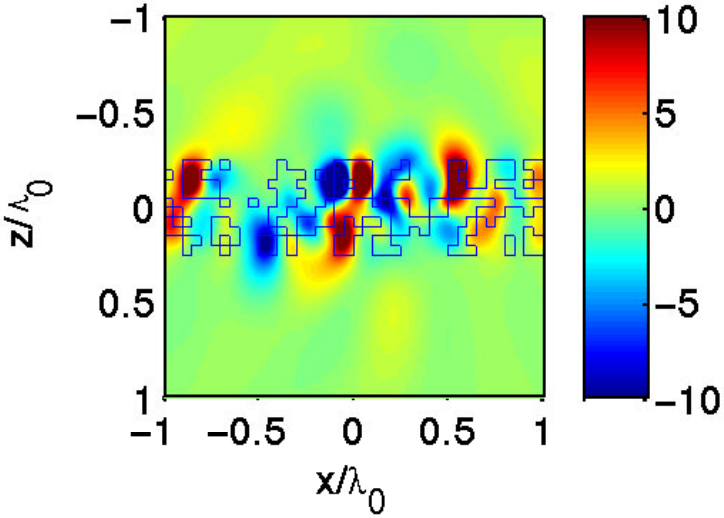

S_z/S_i 1.001λ_0

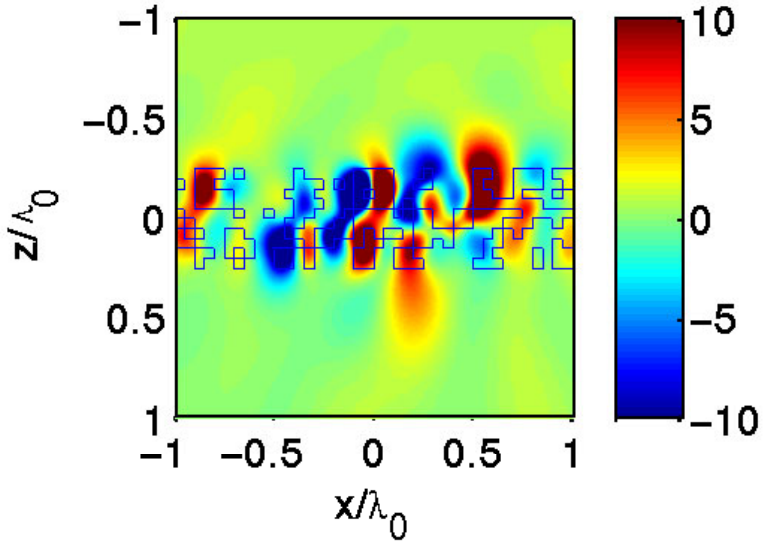

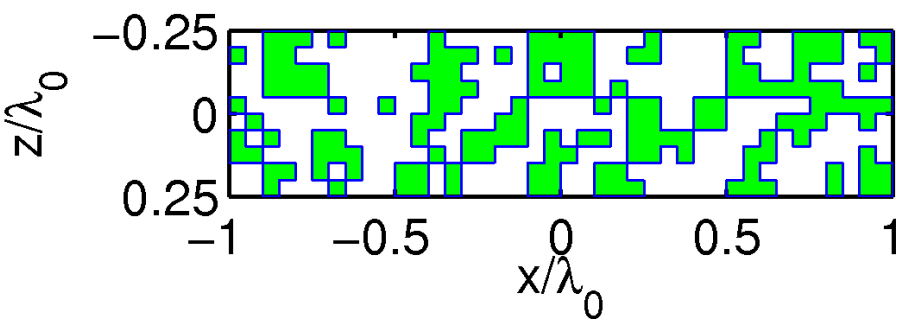

S_z/S_i in focal plane

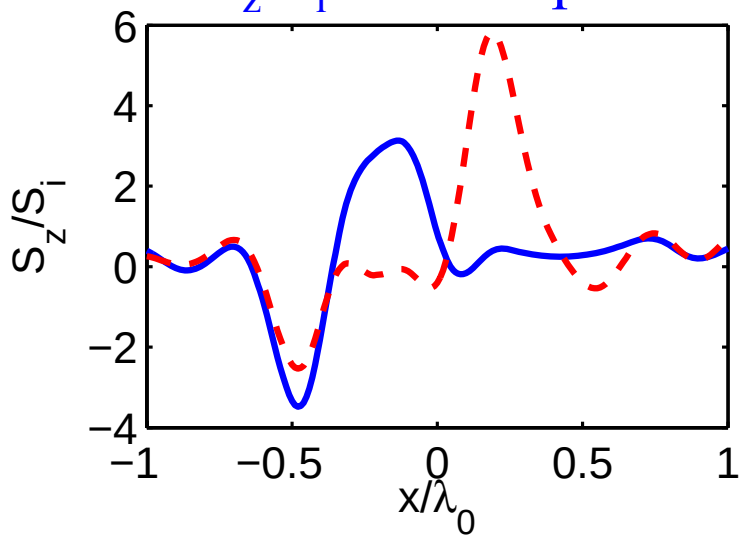

Waveguide Mode Converter Synthesis

- Coarse-to-fine procedure: $TE_{10} \rightarrow TE_{30}$ example

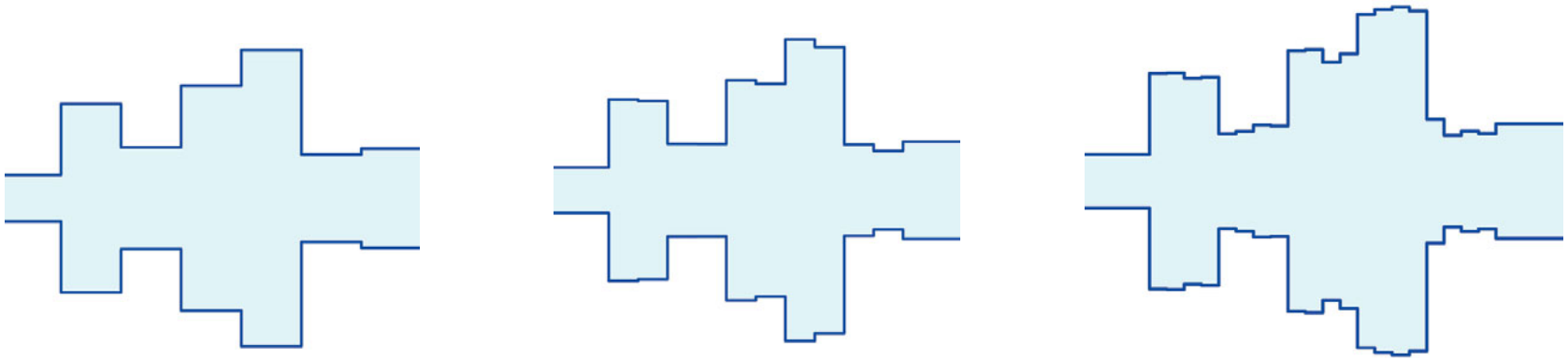

- Optimization starting from a random initial guess

- Generalized scattering matrix serving as forward solver

$$c(W) = -P_{\text{mode}_1,\lambda_1} P_{\text{mode}_2,\lambda_2} \ldots\ldots\ldots P_{\text{mode}_M,\lambda_M}(W)$$

$$W = [w_1, w_2, \ldots\ldots]^T$$

[1] M. Yang J. Li, and K. J. Webb, *Appl. Phys. Lett.*, **83**, 2736 (2003)

Mode-Selective Reflector

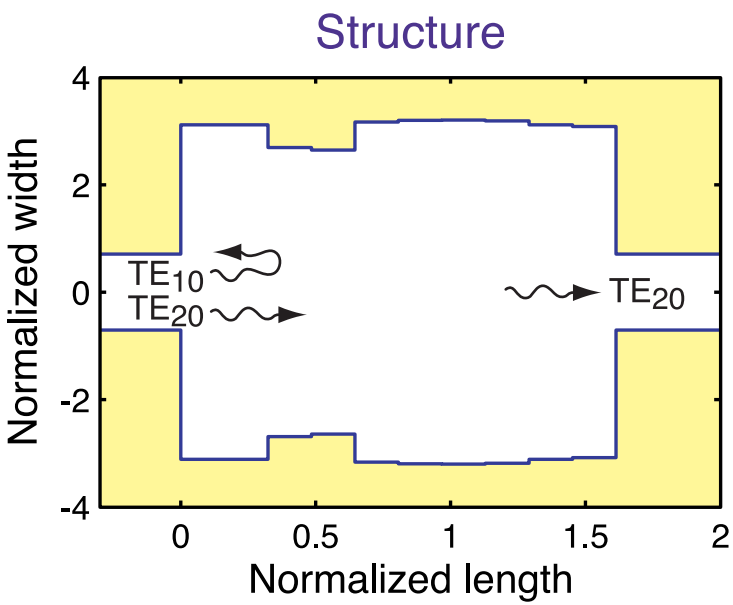

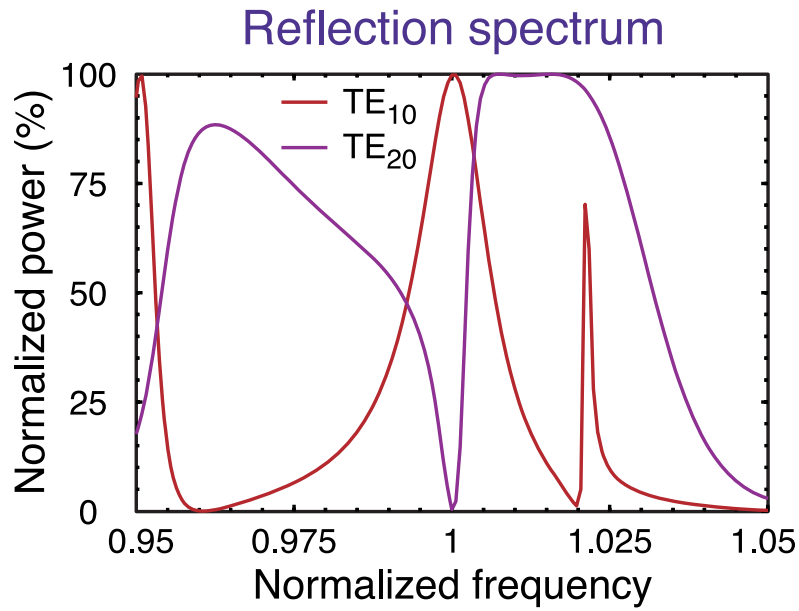

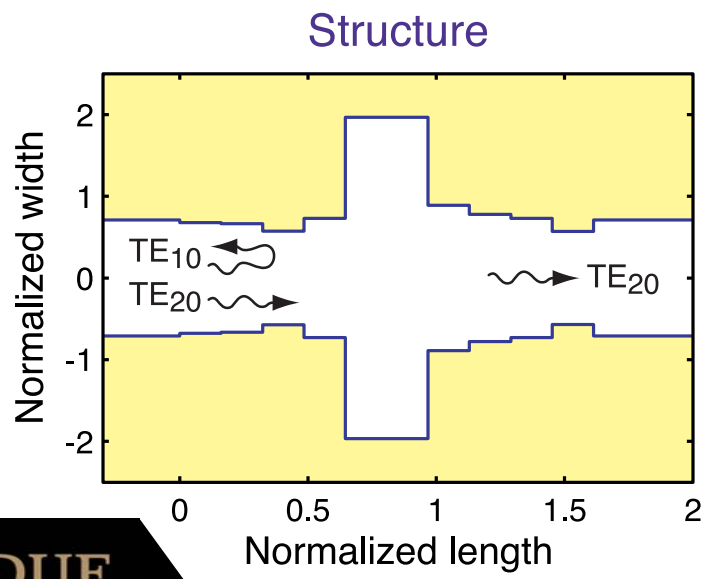

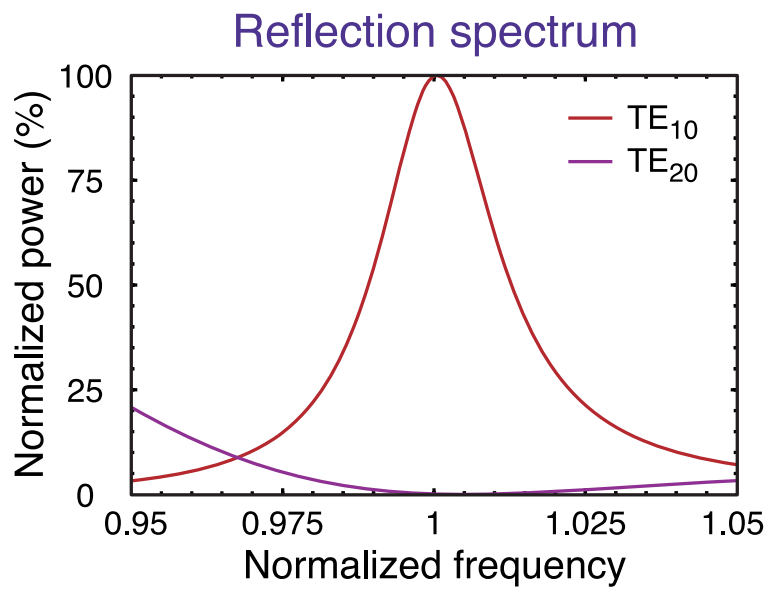

Microwave Verification

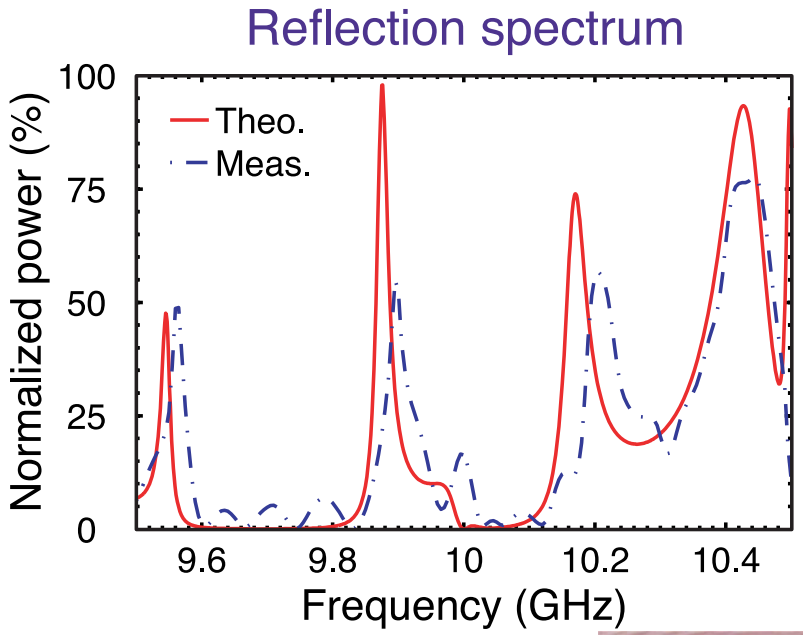

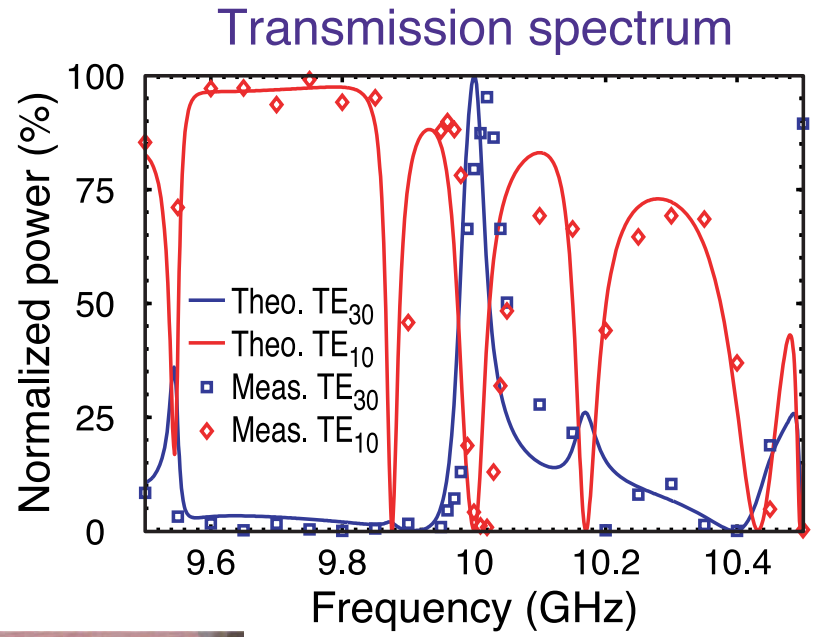

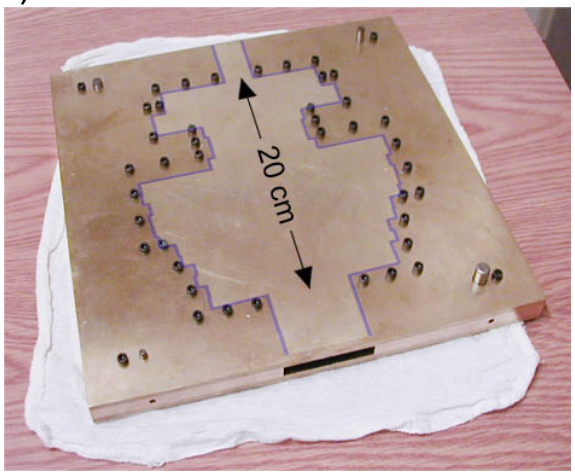

[1] M. Yang, J. Li, and K. J. Webb,
IEEE Trans. Microwave Theory Tech., **52**, 161 (2004)

Optical Device

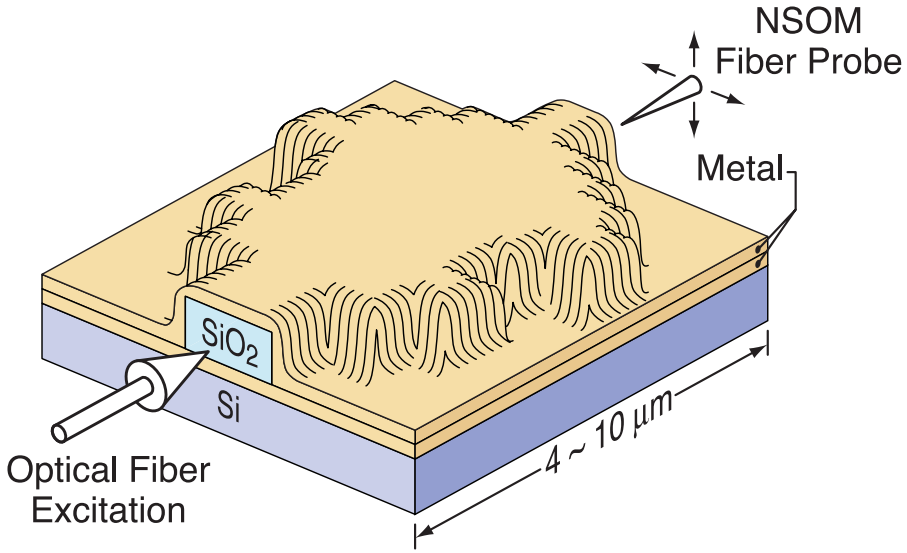

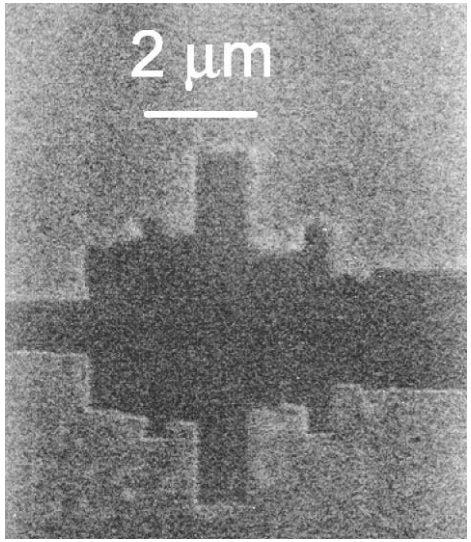

Microscope View

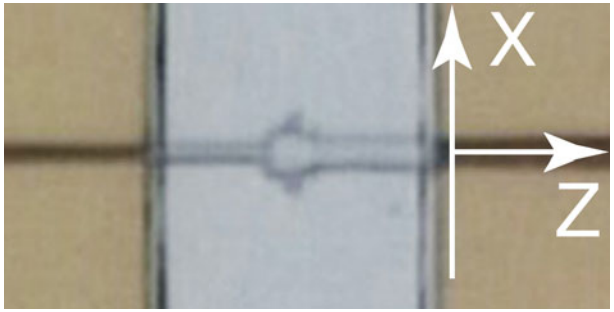

λ=1.565μm, $TE_{10} \rightarrow TE_{30}$

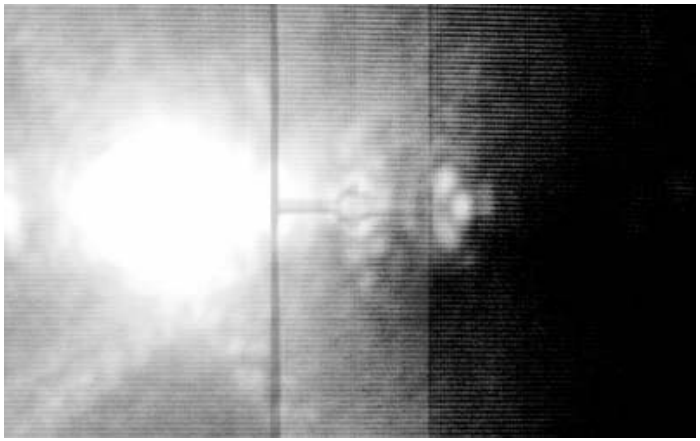

[1] M. Yang, H. Chen, K. J. Webb, S. Minin, S. L. Chuang, and G. R. Cueva, *Opt. Lett,* **31**, 383 (2006)

Optical Experiment

Measured (crosses)
Simulated (dashed)
λ_0=1550 nm

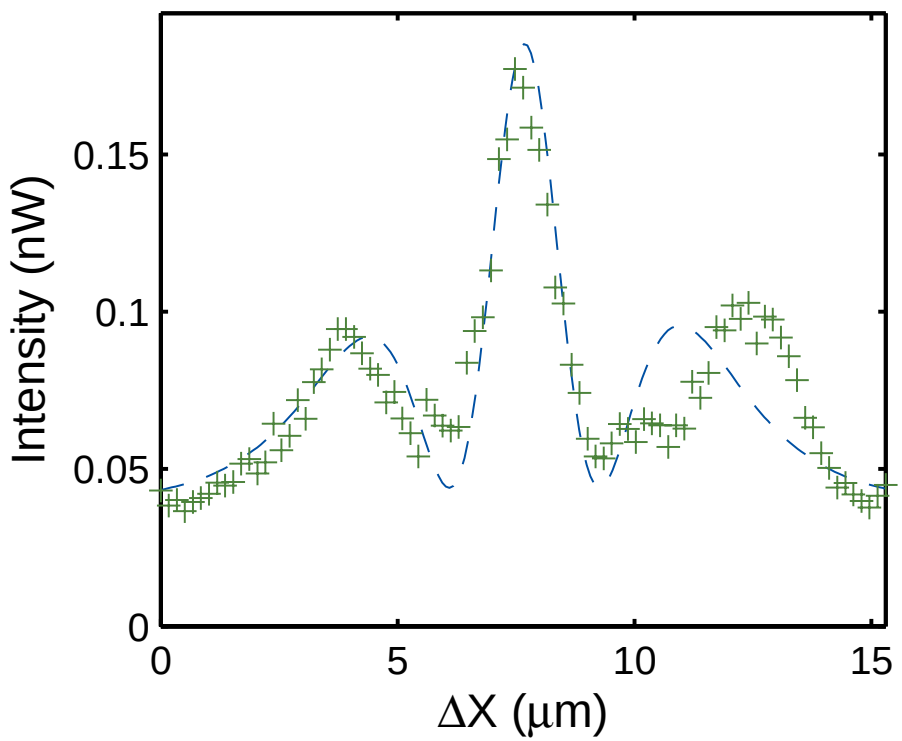

TE_{30}: simul (solid), meas (crosses)
TE_{10}: simul (dashed), meas (circles)

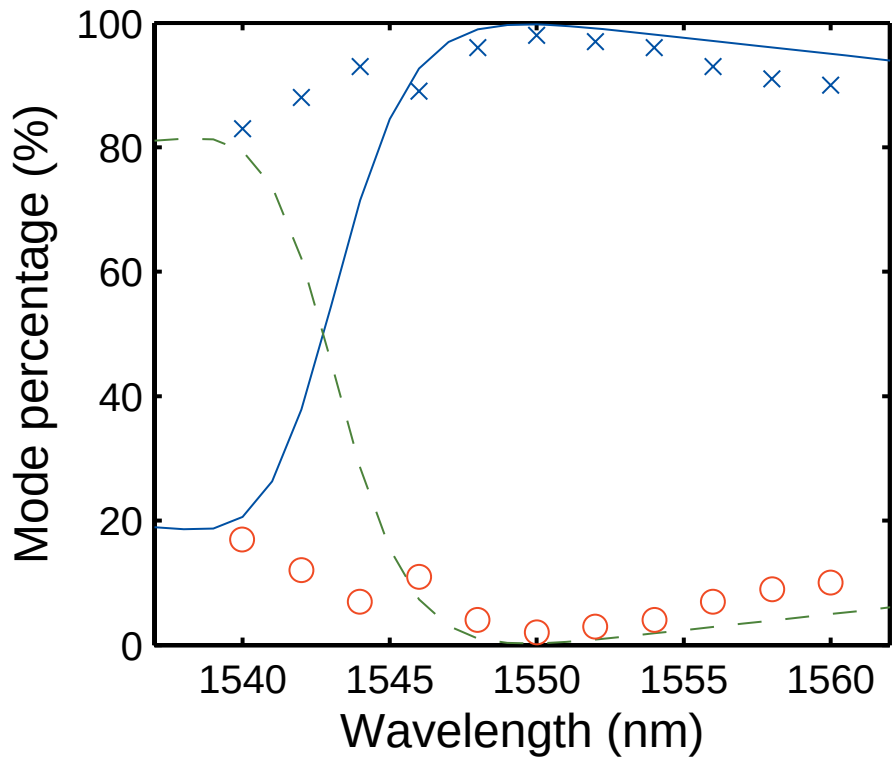

Detection of Ammonia

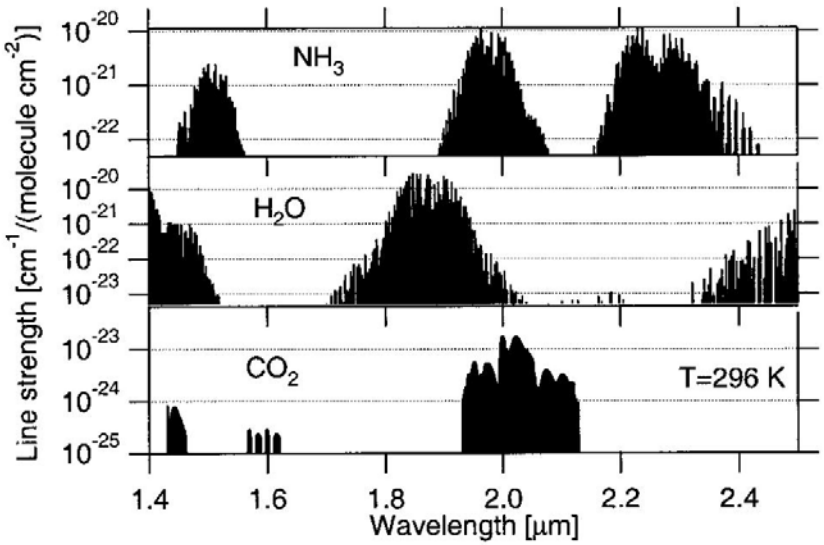

Ammonia, water and carbon dioxide line strengths in near IR[1]

Major atmospheric gases:

N_2 (78%) and O_2(21%)

N_2 and O_2 are transparent around 1.5µm and 2.3µm

Major interfering gases:

H_2O vapor (0 to 3%)

CO_2(~0.04%)

Line Strength (cm^{-1}/molecule cm^{-2})

λ→	1.5317µm	1.5270µm	1.5224µm	1.5160µm	1.5152µm	1.4974µm
NH_3[1]	9.2×10^{-22}	1.3×10^{-21}	1.6×10^{-21}	6.4×10^{-22}	8.5×10^{-23}	5.6×10^{-23}
H_2O[2]	3×10^{-25}	9×10^{-26}	7×10^{-27}	-	-	5×10^{-25}
CO_2[2]	9×10^{-26}	1×10^{-24}	1.9×10^{-25}	-	3×10^{-26}	6.5×10^{-26}

[1] M. E. Webber, D. S. Baer, and M. Yang, Appl. Opt., **40**, 2031 (2001)

[2] Hitran Database (http://cfa-www.harvard.edu/hitran/)

Detection of Ammonia: Simulation Model

Mathematical model for experimental data: $y = Ax + e$

Cost function: $C(x) = \|y - Ax\|^2$

$$\hat{x} = \underset{x}{argmin} \|y - Ax\|^2$$

$y_i \rightarrow$ Experimental data at i^{th} wavelength
$x_j \rightarrow$ Actual percentage of jth gas
$A_{ij} \rightarrow$ Absorption for j^{th} gas at i^{th} wavelength
$e \rightarrow$ Shot noise

$S_{ij} \rightarrow$ Line strength for j^{th} gas at i^{th} wavelength

$A_{ij} = S_{ij} \times f \times C \times L \times x_j$ at P=1atm, T=296K and L = 50cm

Concentration: $C = \frac{N_A}{V_M} = 2.47 \times 10^{19}\ molecules/cm^3$

N_A is Avogadro's number
V_M is molar volume

Line shape function $f \sim$ 1cm

Detection of Ammonia: Simulation Results

$\lambda \rightarrow$	1.5317μm	1.5224μm	1.4974μm
NH_3	9.2×10^{-22}	1.6×10^{-21}	5.6×10^{-23}
H_2O	3×10^{-25}	7×10^{-27}	5×10^{-25}
CO_2	9×10^{-26}	1.9×10^{-25}	6.5×10^{-26}

Simulation parameters
Laser power: 2mW
Integration time: 1sec

	x	$\hat{x}$
NH_3	0.04%	0.0400%
H_2O	2.00%	2.0013%
CO_2	0.96%	0.9623%

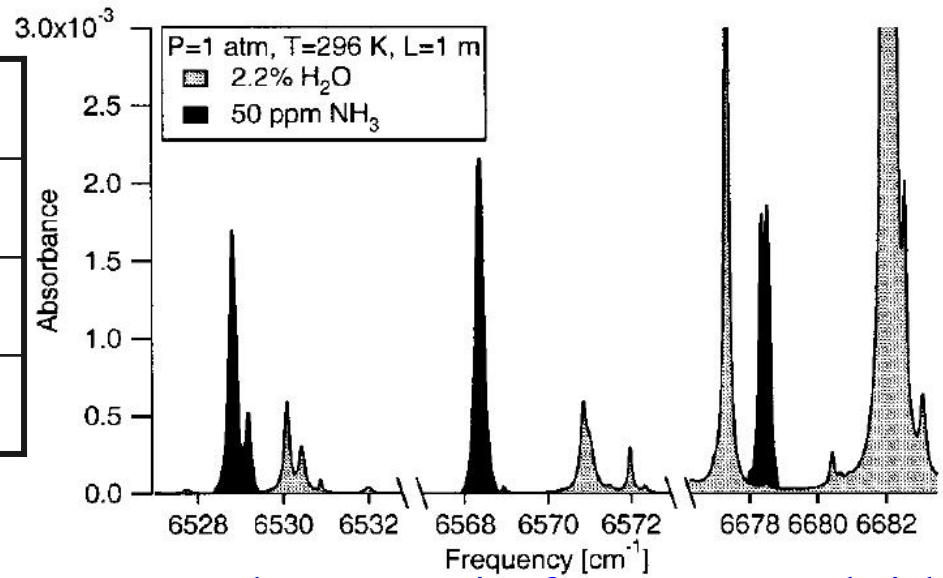

Measured ammonia feature overlaid with absorbance of water in near IR[1]

[1] M. E. Webber, D. S. Baer, and M. Yang, *Appl. Opt.*, **40**, 2031 (2001)

Conclusions

- Anisotropic slab lens is promising for effective sub-wavelength performance
- A small set of absorption lines should allow detection of ammonia
- Implementation of λ-dependent irregular diffractive element in silicon-on-insulator waveguide [1]

[1] H. Chen and K. J. Webb, *Opt. Lett.*, 31, 2145 (2006)

Purdue Team

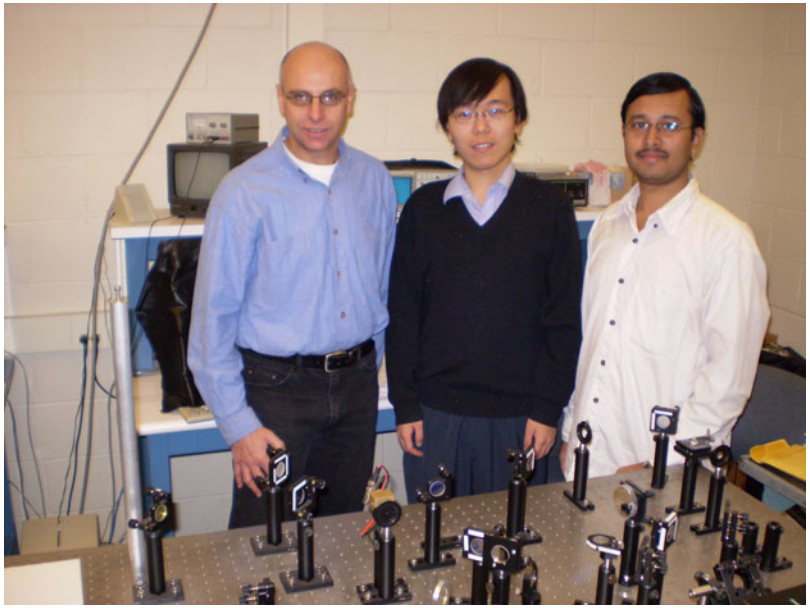

- Shivanand (Ph.D. student)
- Huikan Liu (Ph.D. student)
- Alon Ludwig (Post-doc) – will join us from the Technion in March
- Kevin Webb

DoE UITI 2007 Workshop

Optical Stand-off Detection

Martin Richardson

S. Palanco, C. Brown M. Fisher, , R. Bernath

Townes Laser Institute,

College of Optics & Photonics, UCF

M. Sigman

Nat. Inst. for Forensic Science & Dept. of Chem, UCF,

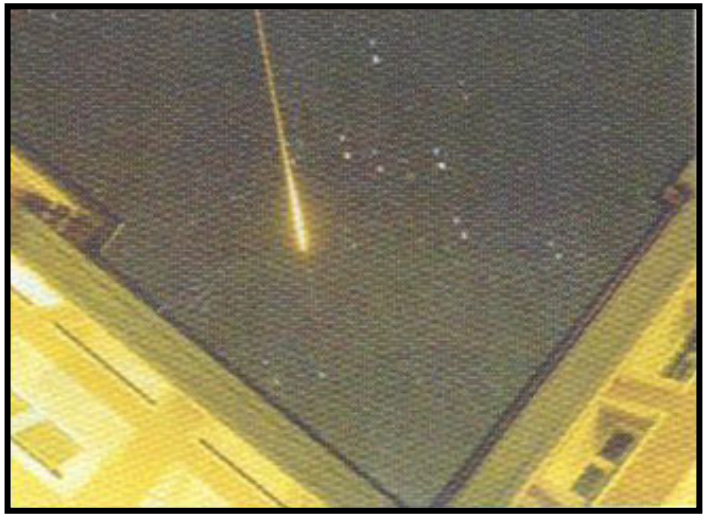

Nov 27 , 2007

Orlando 2007

Optical methods of stand-off detection of materials

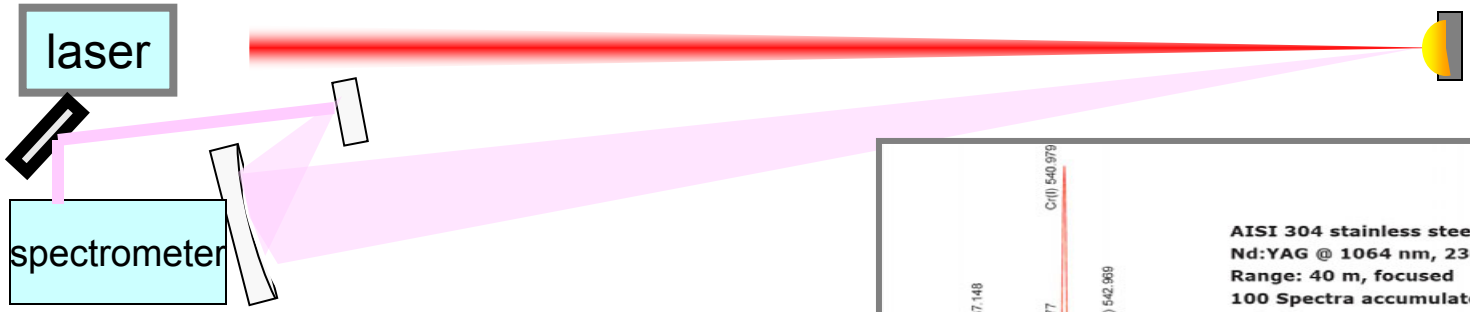

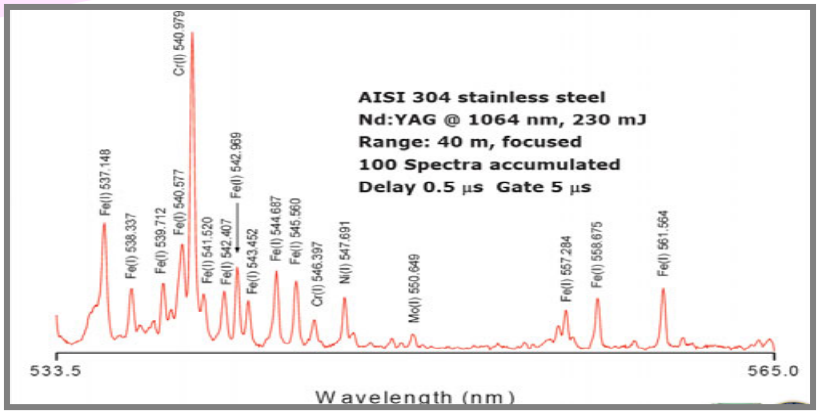

Spectrochim Acta B 57 (2002) 591-599

SPECTROSCOPIC TECHNIQUES

- **Fluorescence**
- **Raman spectroscopy**
- **Multiphoton absorption induced fluorescence**
- **Laser-induced breakdown spectroscopy**

LASER TECHNOLOGIES

- **ns and fs lasers; multi-pulse and self-filamentation modalities**

STAND-OFF DETECTION TECHNOLOGIES

- **trace elements of explosives, biological agents, aerosols**
- **commercial monitoring systems**
- **Stand-off detection of radioactive materials**

FY06 MURI Topic 25
Army Office of Research
Ultrafast, Non-Equilibrium Laser-Material Interactions

ULTRAFAST LASER INTERACTION PROCESSES FOR LIBS AND OTHER SENSING TECHNOLOGIES

Martin Richardson

LPL, College of Optics & Photonics, CREOL, UCF

Dennis R. Alexander,	*Dept Electrical Eng., University of Nebraska,*
Valeri I. Babushok,	*NIST, Gaithersburg MD,*
Paul J. Dagdigian,	*Dept Chemistry, Johns Hopkins University*
Lewis E. Johnson,	*Dept. Physics, Florida A&M University,*
Samuel S. Mao,	*Dept. Mech. Eng, Univ. of California, Berkeley,*
Costas Grigoropoulos	*Dept. Mech. Eng, Univ. of California, Berkeley*
Michael E. Sigman	*Dept. Chem Natl. Ctr for Forensic Science UCF*
	and
Michael J Nusca,	*ARL, Aberdeen Proving Ground, MD*
Richard E. Russo,	*LBNL, Berkeley CA*
Robert Fedosejevs,	*Dept Electr. Eng, Univ. Alberta, Edmonton,*
Roy Walters	*Winter Park, FL*

LIBS is material non-specific detection regime

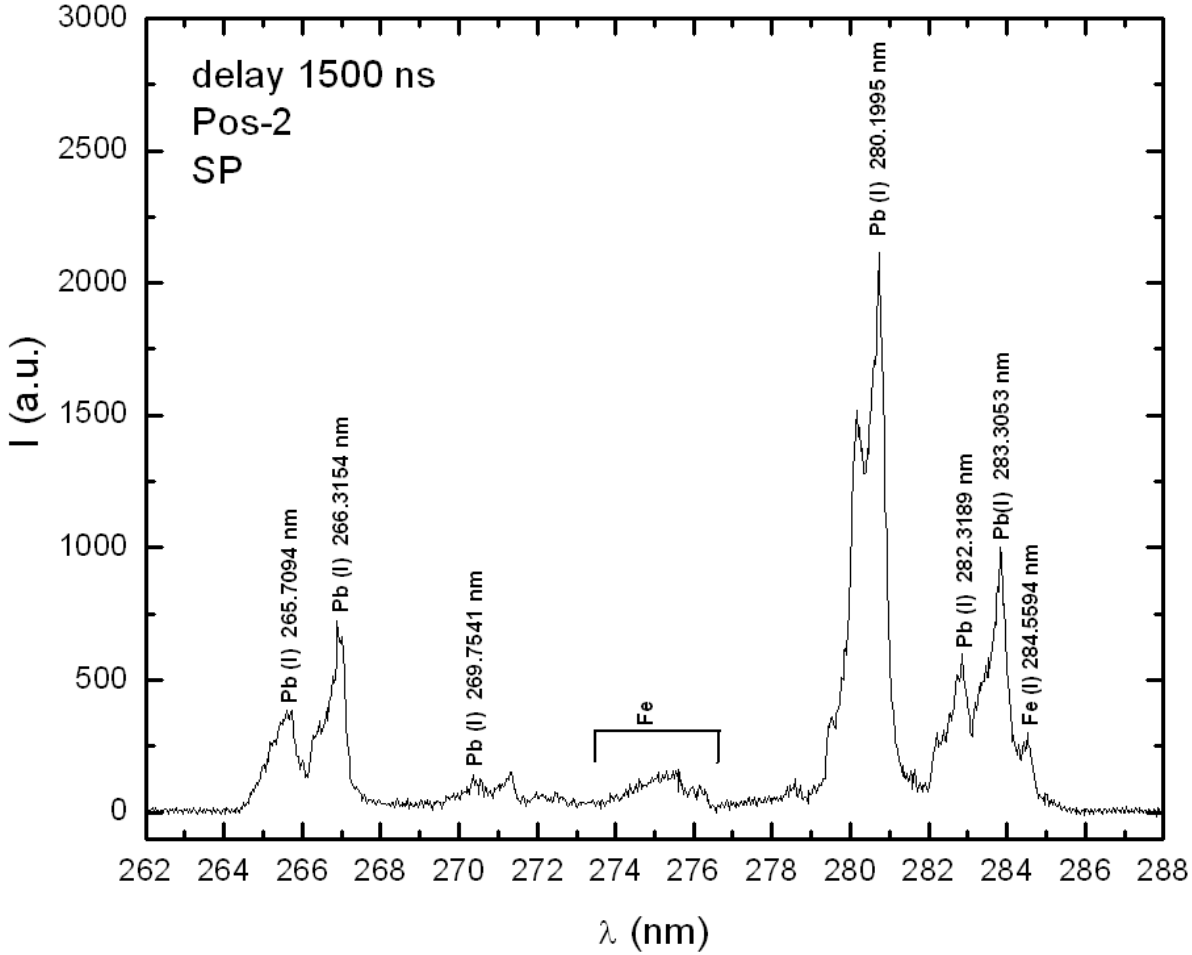

Combined experimental & theoretical study
Atomic and molecular signature modeling
High Z materials currently under study

Atmospheric propagation of fs laser pulses

A. Braun et al., Opt. Lett. 20, 73 (1995).

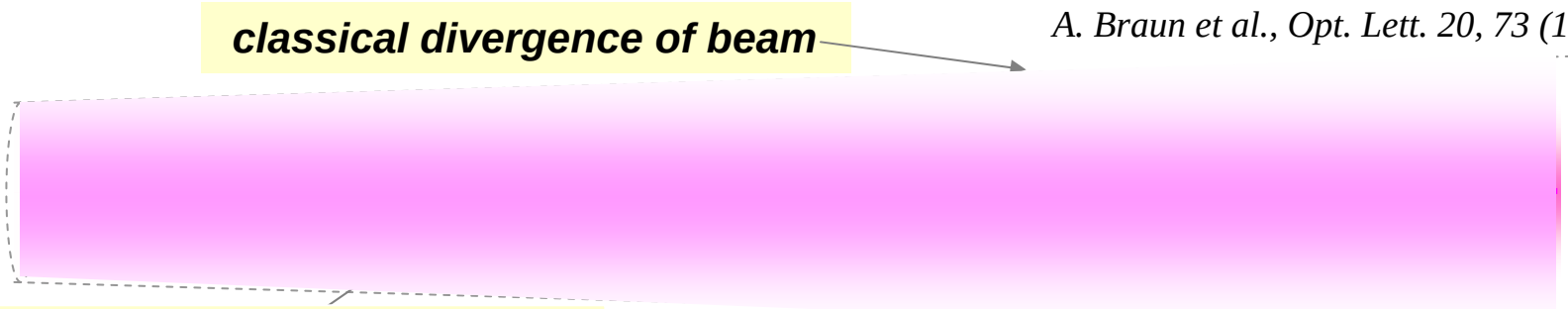

At sufficiently high intensities (10^{12} W), the second-order, intensity-dependent refractive index n_2 of the air comes into play, increasing the overall refractive index of the air through which the beam propagates, according to the relation,

$$n = n_0 + n_2 I$$

$$n_2 = 5\times10^{-19}\, cm^2 / W$$

When the intensity of the light within the focusing beam reaches a threshold (about 10^{14} W/cm^2 at atmospheric pressure), weak ionization of the air begins to occur by multi-photon ionization. Free electrons are created from the molecules of the air by the intense oscillating electric fields within the laser pulse. Since free electrons provide a negative contribution to the total refractive index, they produce a counteracting weakly defocusing effect.

$$n_e \sim 1\times10^{17}\, cm^{-3} \qquad I \sim 200 mA$$

$$\eta < 1.2\Omega$$

Beam collapse with increasing energy

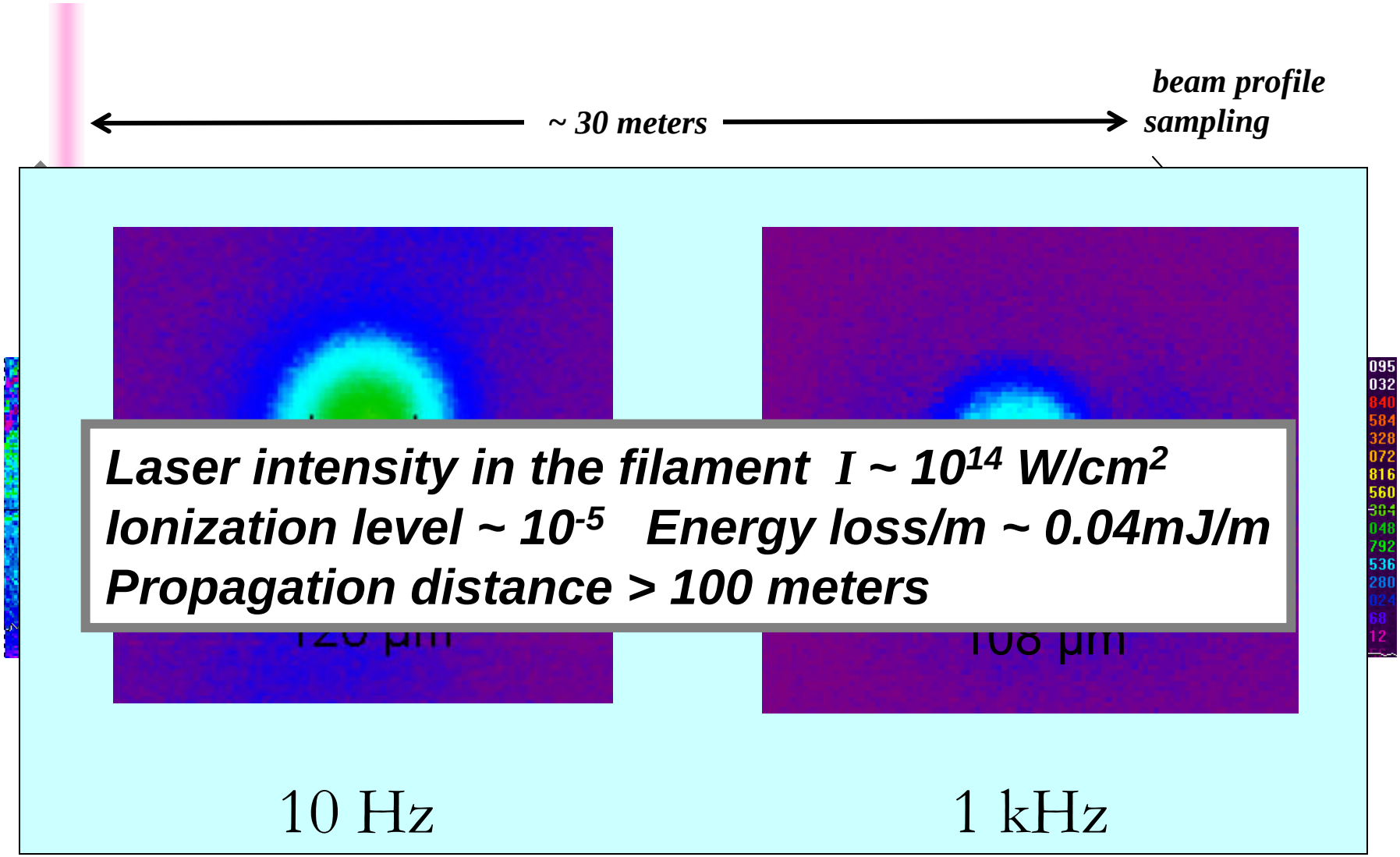

Laser intensity in the filament $I \sim 10^{14}$ W/cm^2
Ionization level ~ 10^{-5} Energy loss/m ~ 0.04mJ/m
Propagation distance > 100 meters

Creating the filament at any desired range

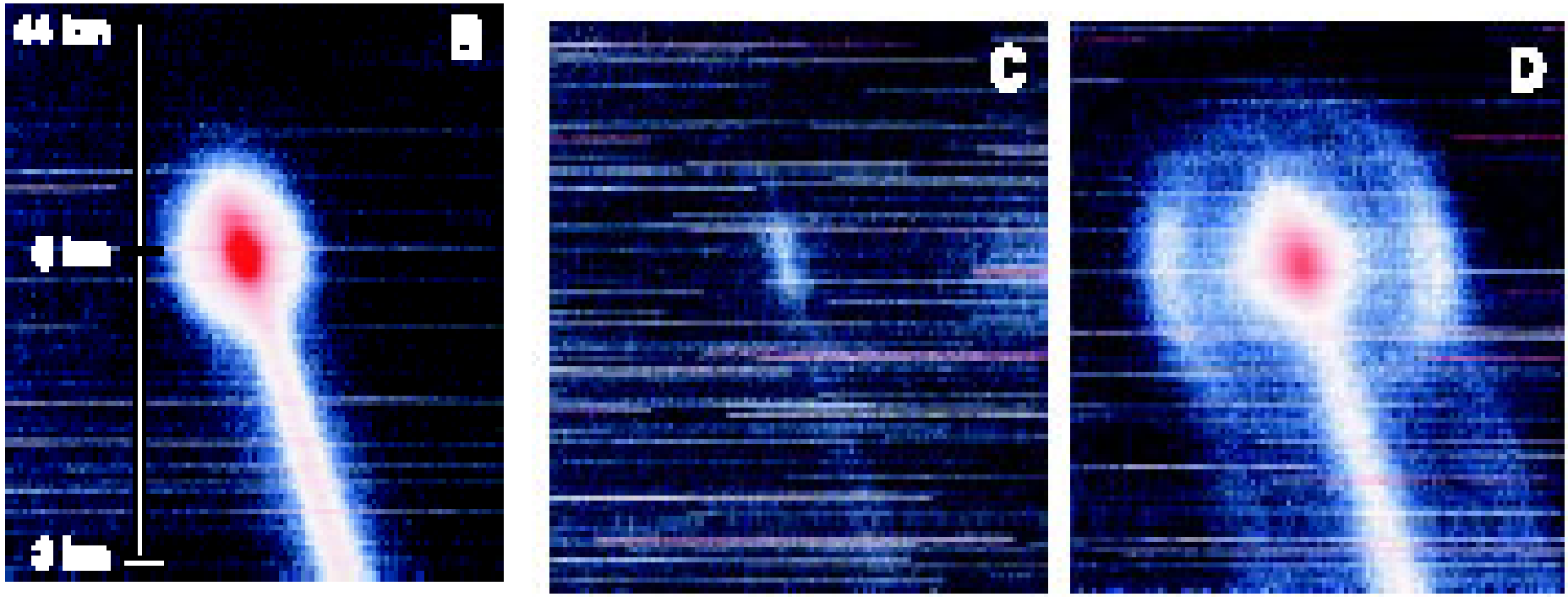

Compensating for self-phase modulation and GVD, with negative pre-chirp creates white light at different altitudes *Kasparian Science 301, 61-64 (2003).*

White light is produced in the filament

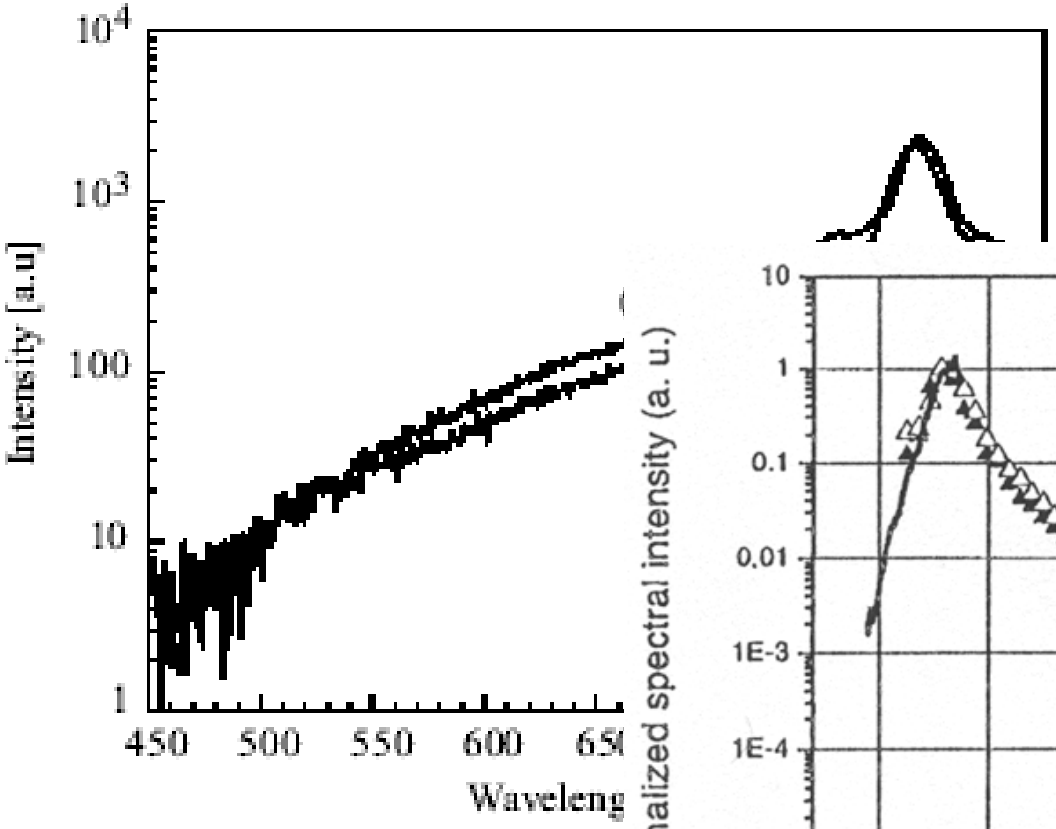

R Rairoux et al., Appl. Phys B 7

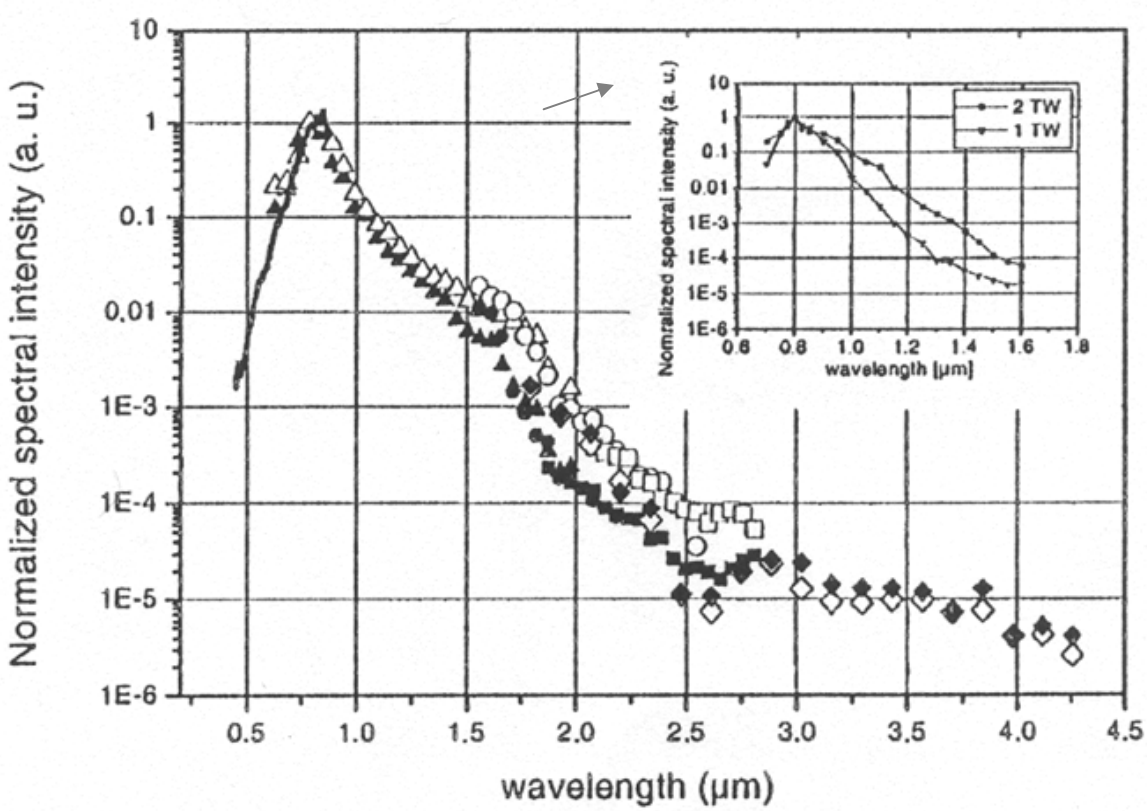

Kasparian etal., Opt. Lett. 25, 1397 (2000)

LIBS Spectra - solid TNT

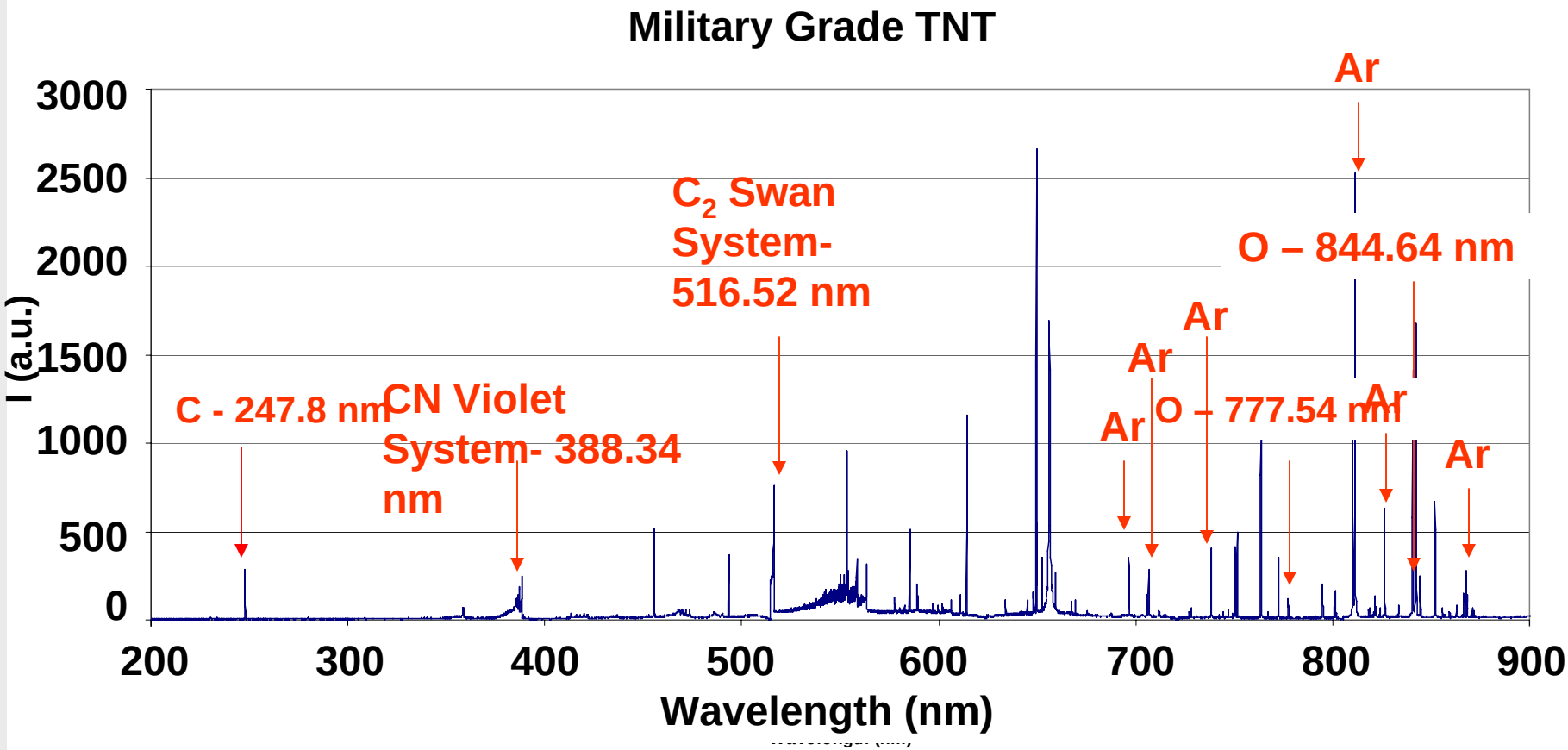

Single Pulse Nanosecond LIBS, 1064 nm, 100 mJ/pulse
Argon atmosphere

Setup of Standoff LIBS Sensor (next to U-Haul Truck) and Test Vehicle

Andrzej Miziolek – ARL

C4, single shots, 30 m LIBS

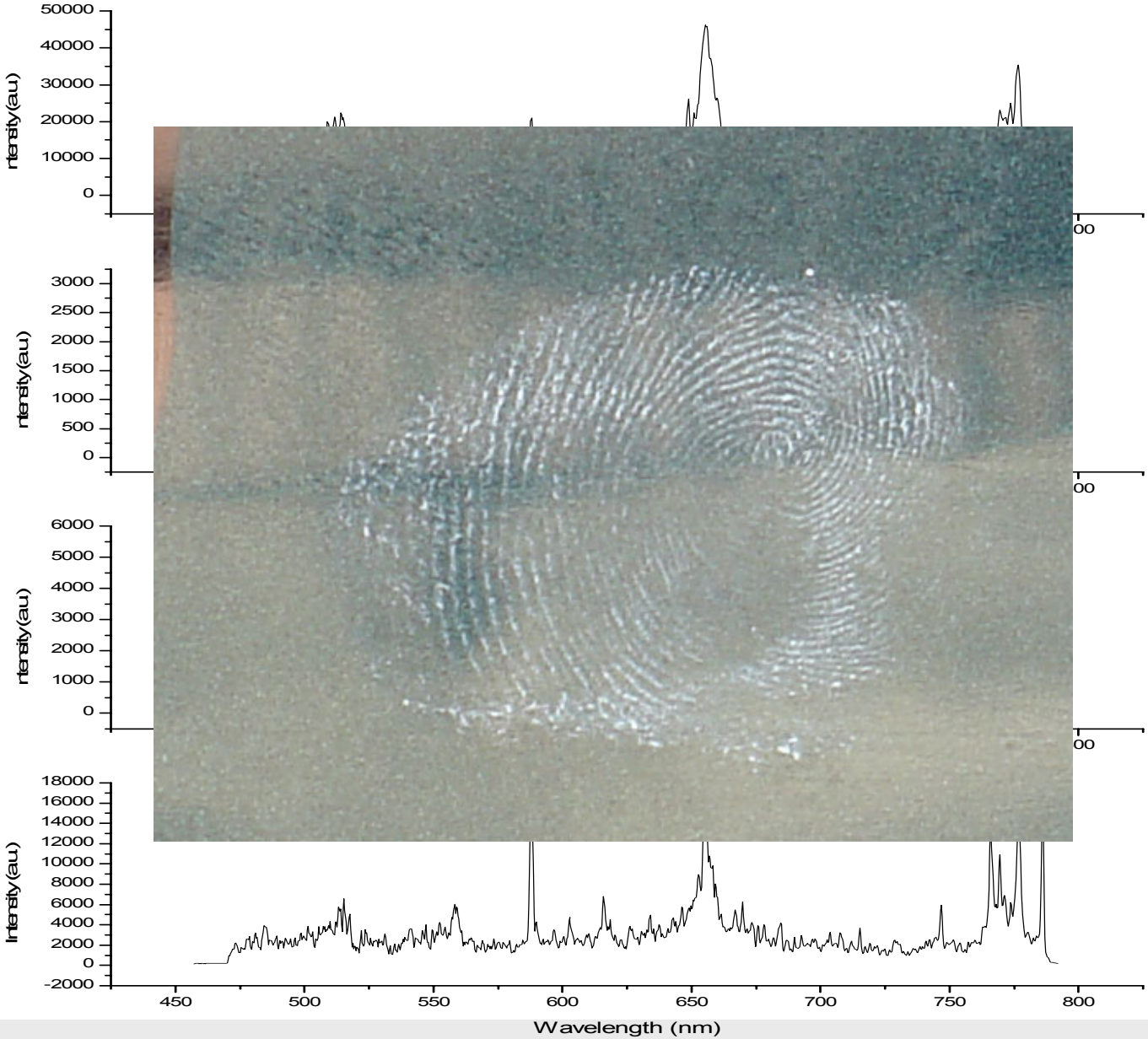

Blind Test Spectra

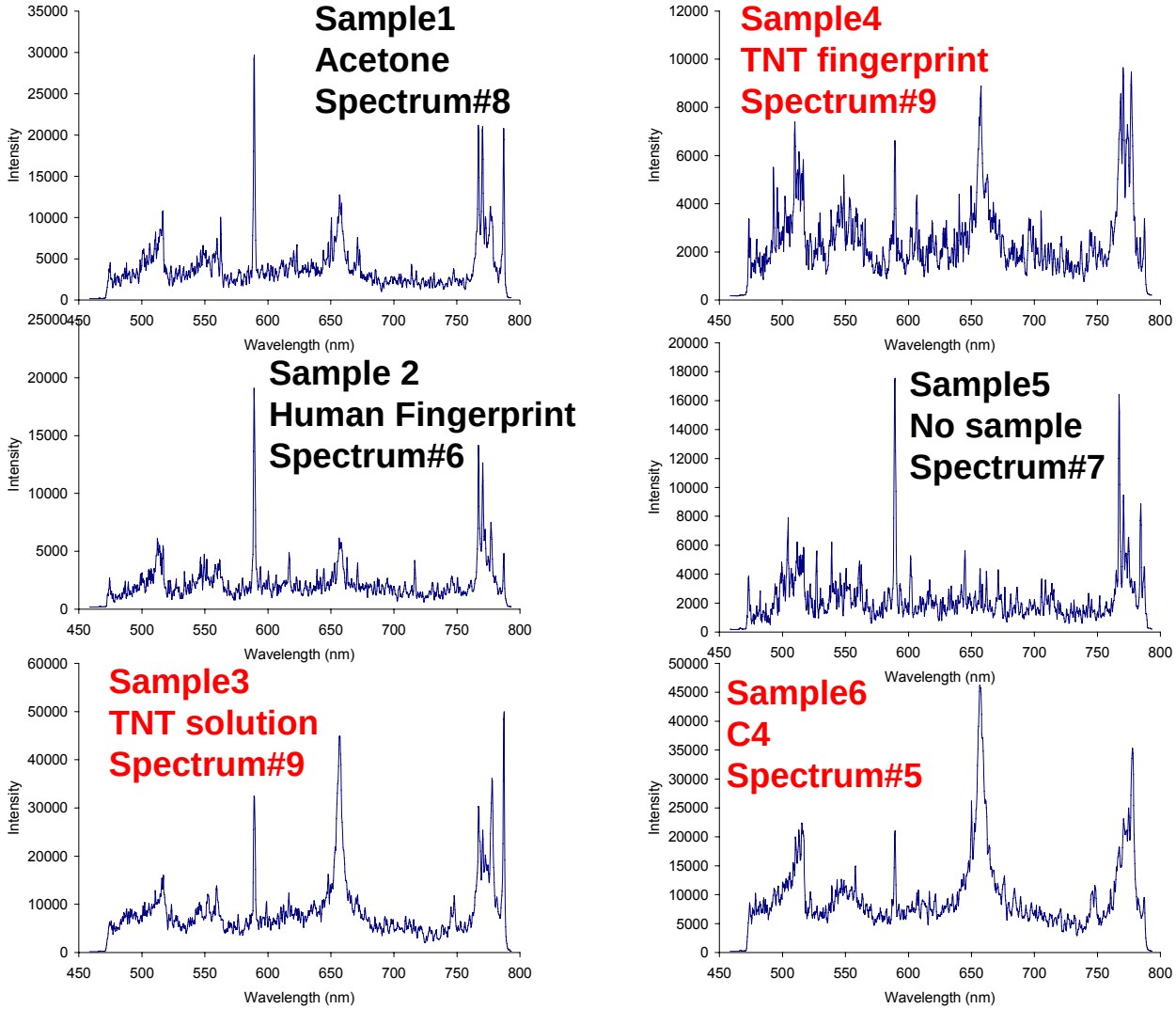

LPL - UCF femtosecond laser facilities

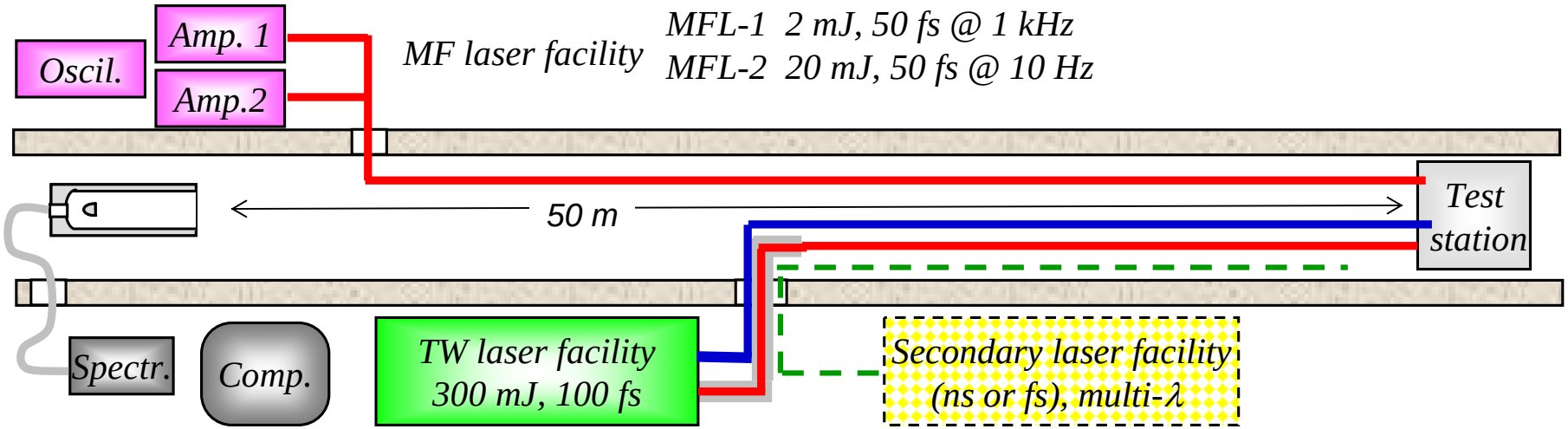

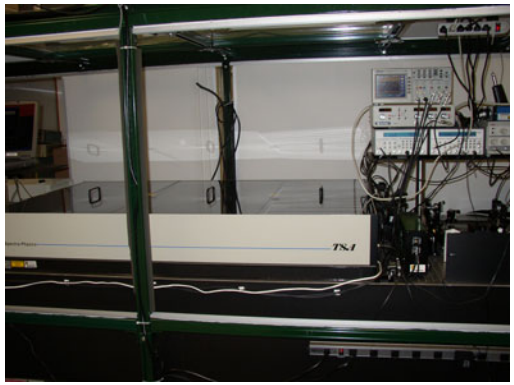

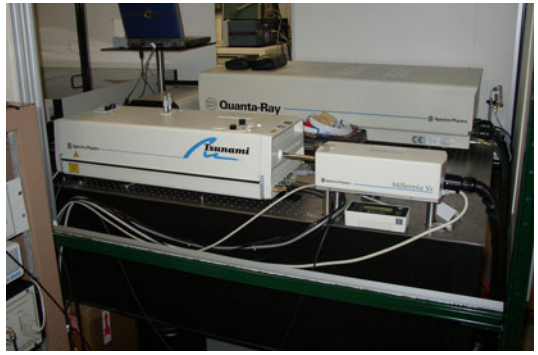

The MDA ISTEF Laser ranging facility on Merritt Island

A fully equipped laser ranging facility on Merritt Island
Full laser and telemetry support.
1 km, (fully secure) range
5 km and 10 km ranges
Many different receivers
Cooperative arrangements with NASA, USAF

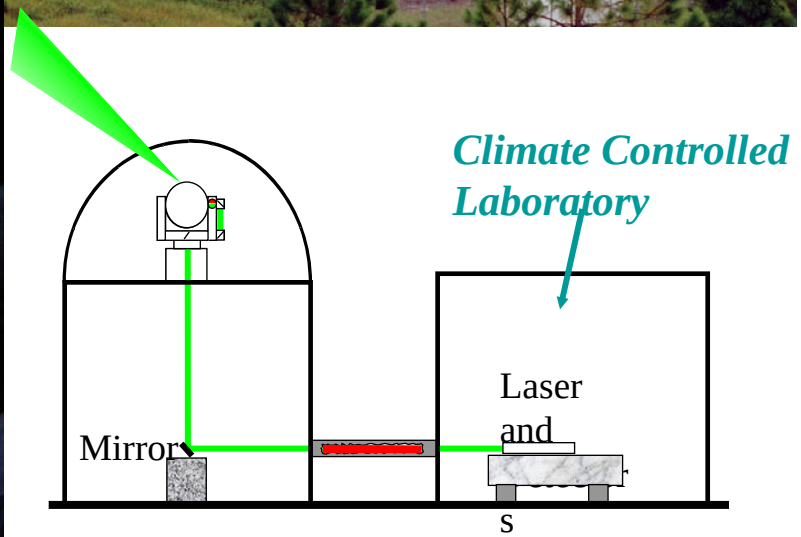

High rep-rate LIBS for scanning/mapping

High repetition scanning
1 -100 kHz
1 m^2/10s
1 mm separation

Yb fiber laser
1 uJ /pulse, < 100fs
100 kHz, 100W

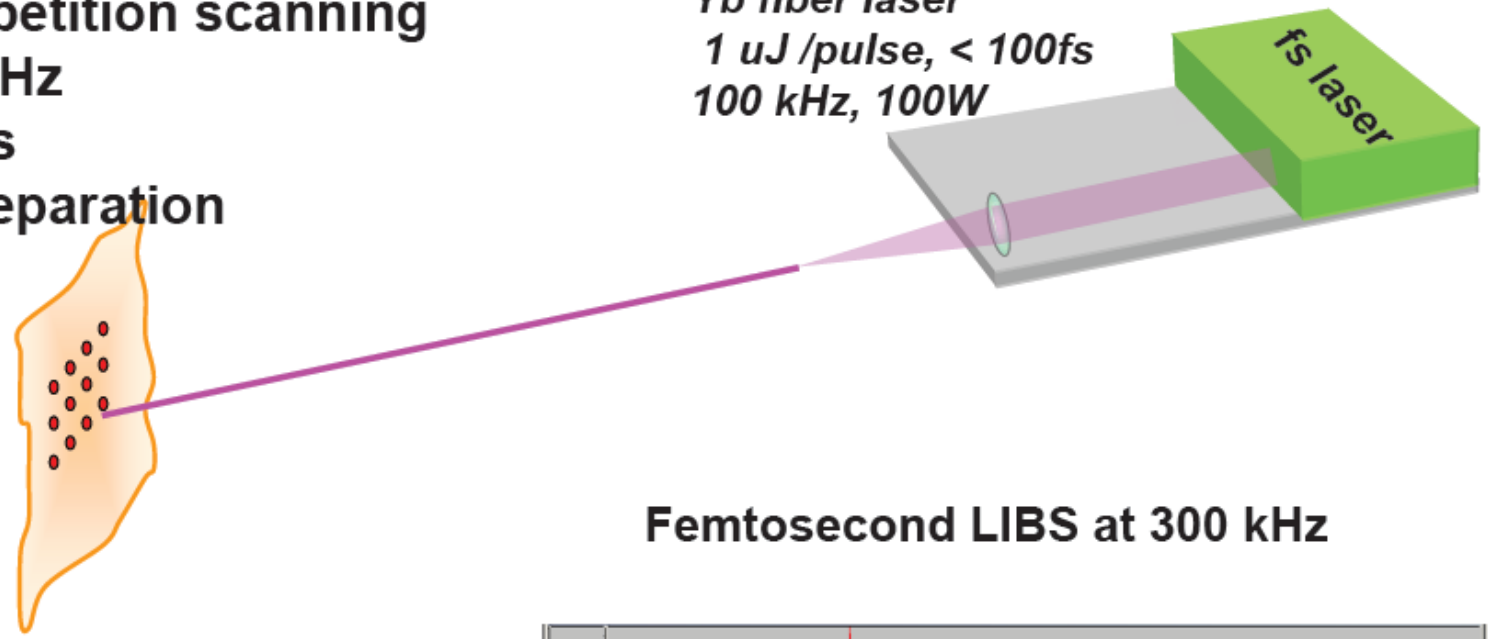

Femtosecond LIBS at 300 kHz

50 uJ, 400 fs, 1060 nm
50 kHz
Doped water target
0.1% NaCl

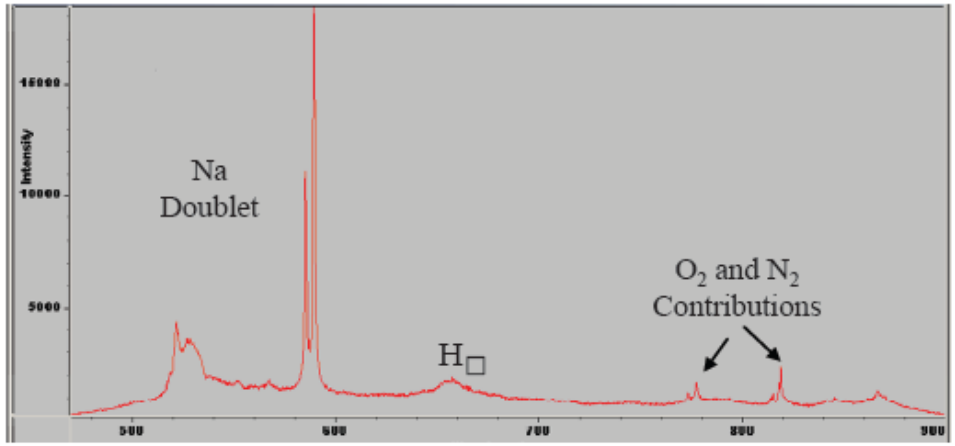

New spatial and temporal irradiation modalities

Diffractive optical elements - beam engineering

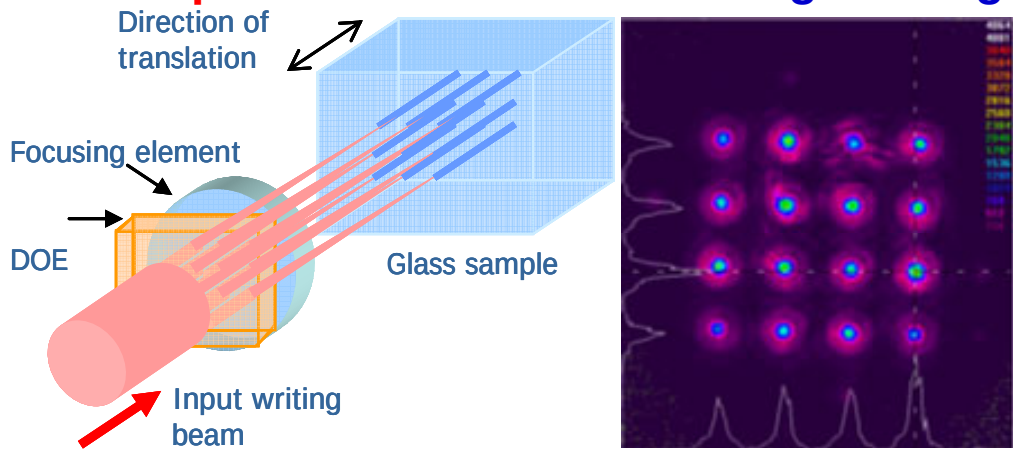

Multiple pulse modality - Burst-mode

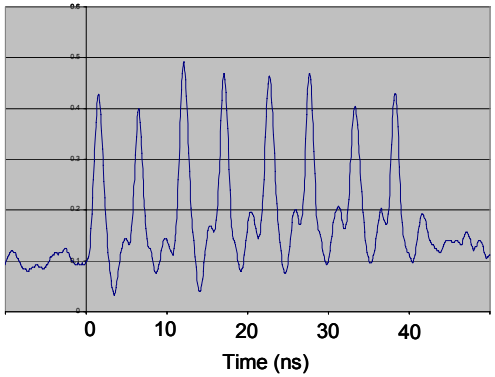

Eight-pulse train

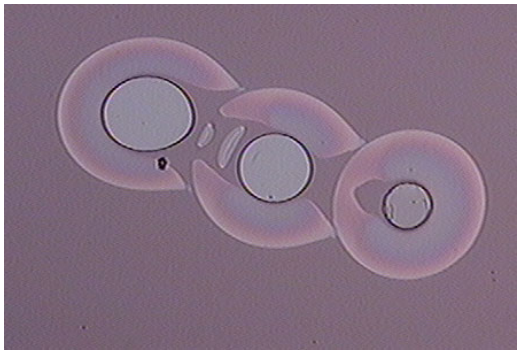

Integrating LIBS and Raman techniques

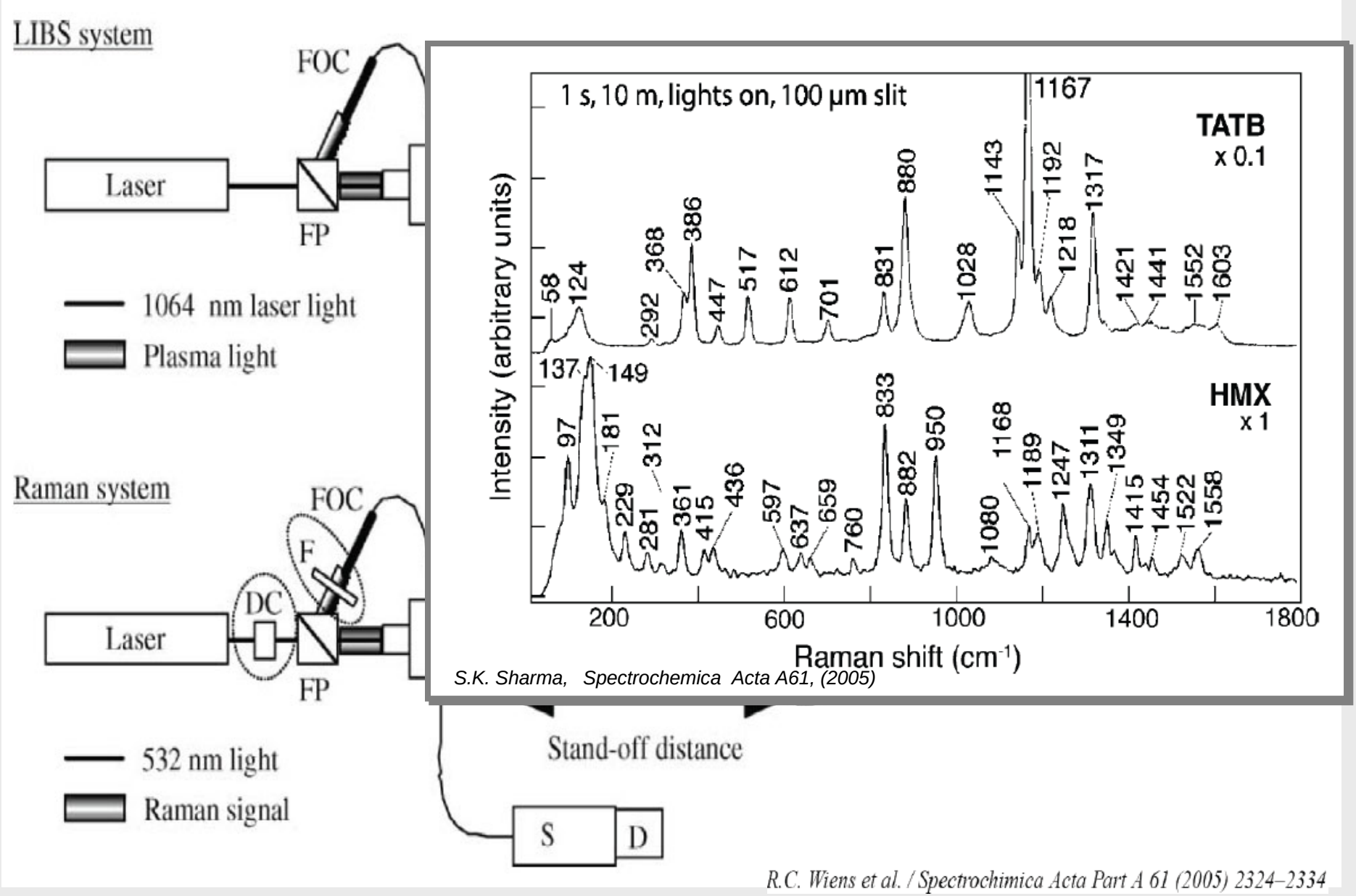

S.K. Sharma, Spectrochemica Acta A61, (2005)

R.C. Wiens et al. / Spectrochimica Acta Part A 61 (2005) 2324–2334

Remote LIBS detection of radio-active materials

Remote Detection of uranyl fluoride in Sea Water and Ice

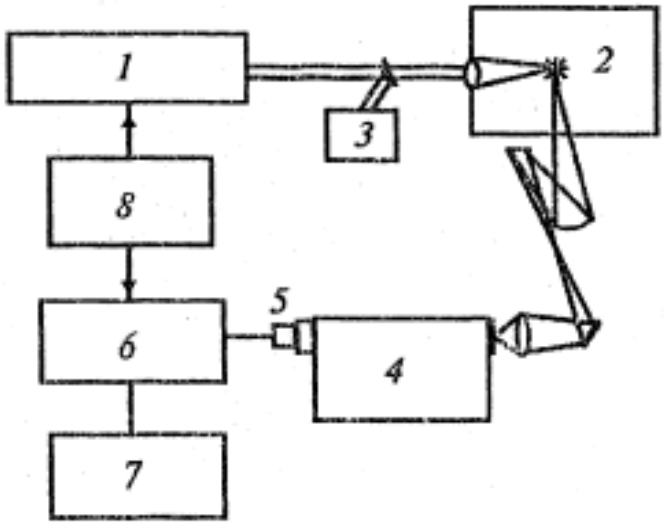

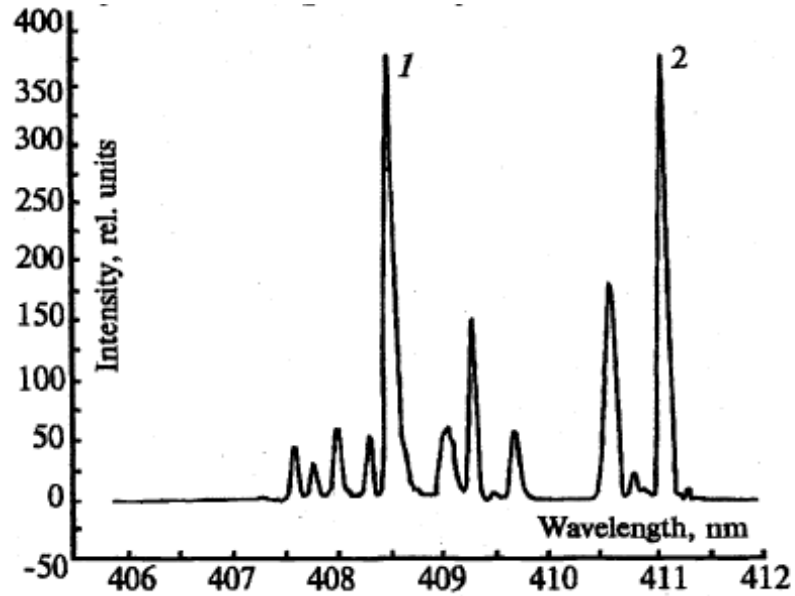

Fig. 1. The diagram of the experimental setup for spectrochemical analysis of the aerosols by breakdown plasma emissions spectra: CO_2 laser 1, hermetically sealed cell 2, IMO-2 power meter 3, MDR-6 monochromator 4, TV camera 5, graphics digitizer 6, computer 7, and block of synchronization 8.

Chrisyakova, et al.
Institute of Atmospheric Optics, Russian Academy of Sciences, Tomsk, Russia
SPIE Vol. 3222. 508 -511 (1997)

High resolution LIBS of Pu isotope ratios

Pu-239Pu-240 isotope ratios determined using high resolution emission spectroscopy

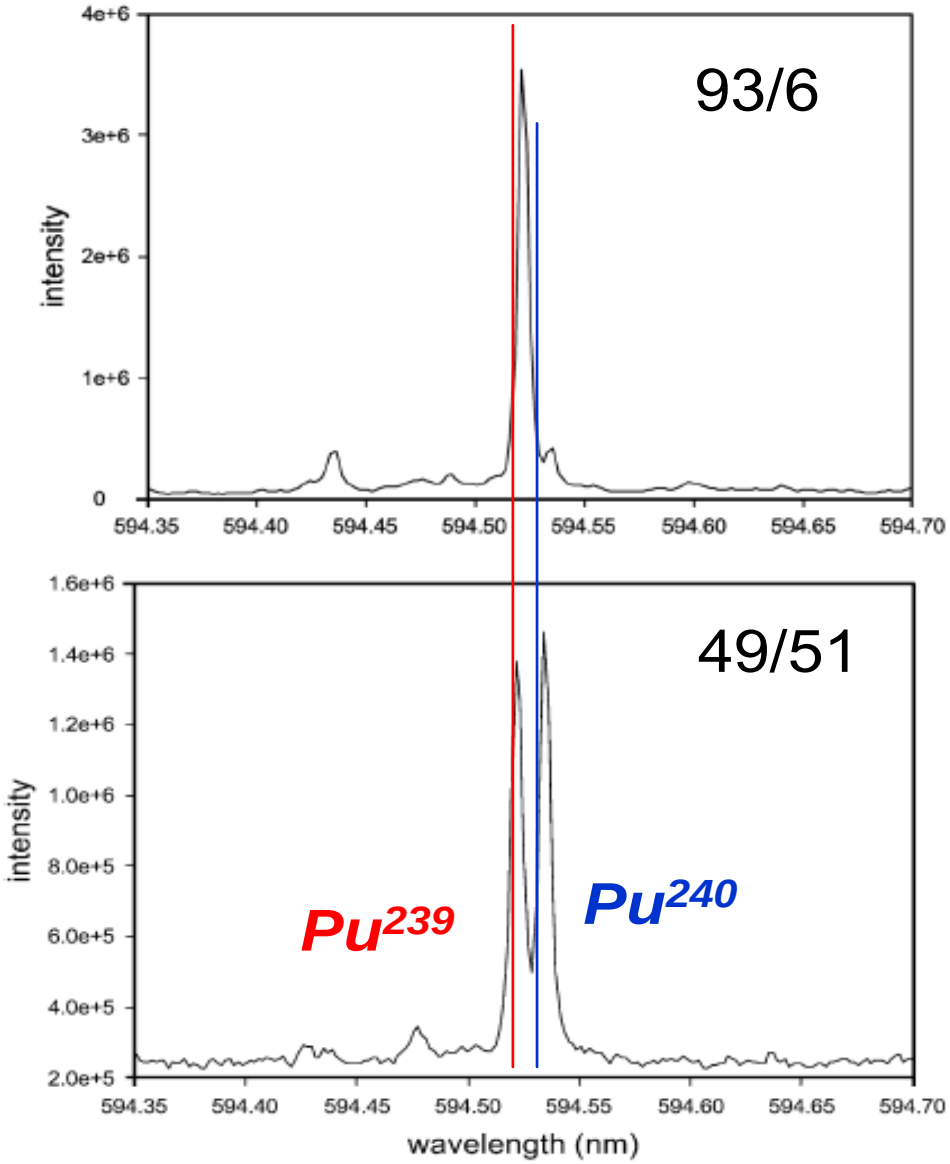

Coleman A. Smith, et al, Spectrochimica Acta Part B 57 (2002) 929–937

Summary

No concentrated research effort on optical stand-off detection of radio-active materials, trace elements, for civilian and military protection.

New laser technologies, hyper-spectral detection techniques and illumination modalities offer increased options for radio-active material detection

Opportunities for new development of stand-off detection technologies specific to radio-active materials for Nonproliferation objectives.

PNNL-SA-57841

PNNL Program Overview

Steven Sharpe

Nuclear Nonproliferation Research & Development Program

Pacific Northwest National Laboratory

November, 2007

Battelle

Pacific Northwest National Laboratory
Operated by Battelle for the U.S. Department of Energy

DOE Laboratory System

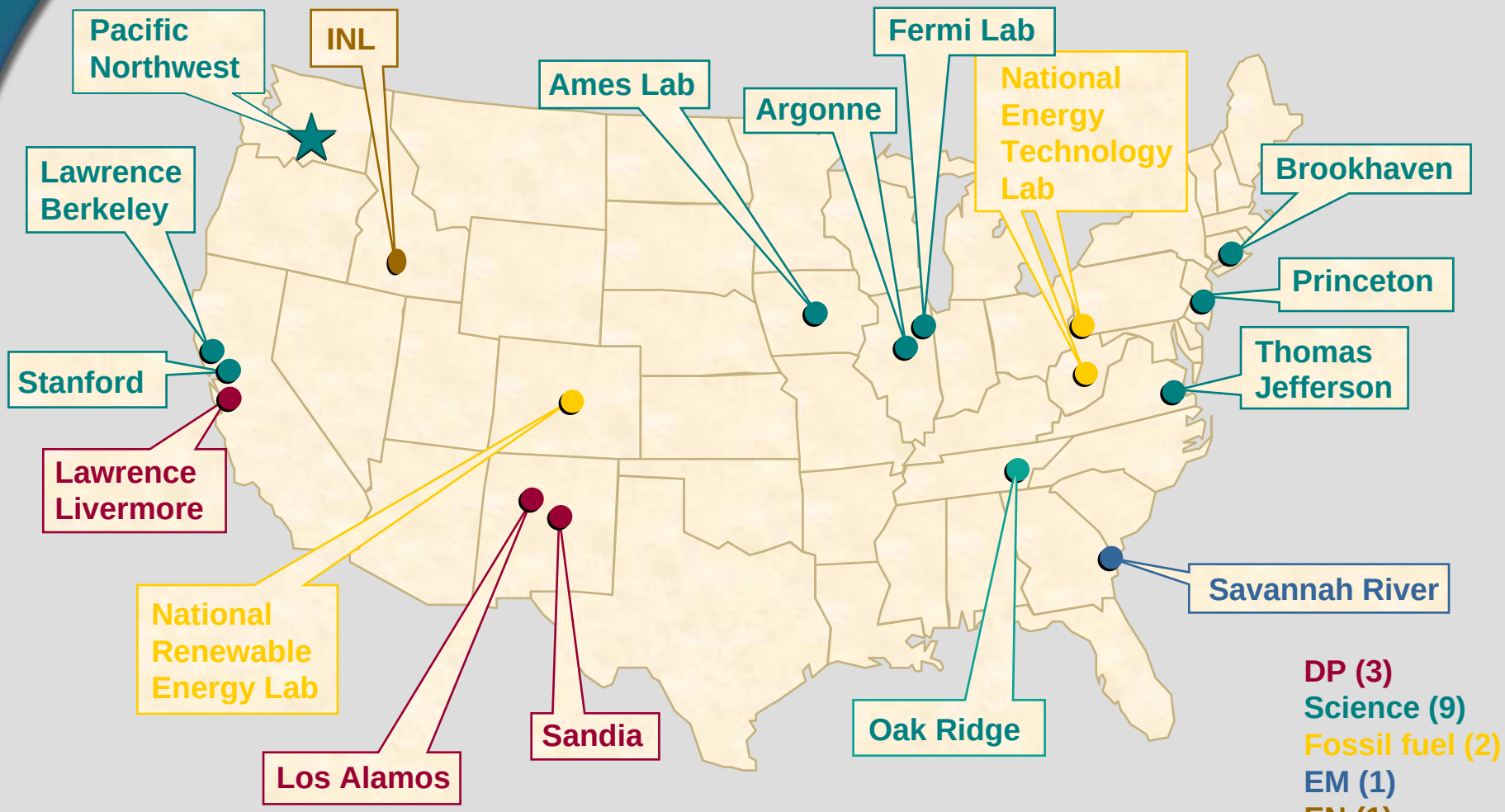

DP (3)
Science (9)
Fossil fuel (2)
EM (1)
EN (1)

PNNL is 1 of 9 Office of Science Labs

Hanford's Original Mission Plutonium Production

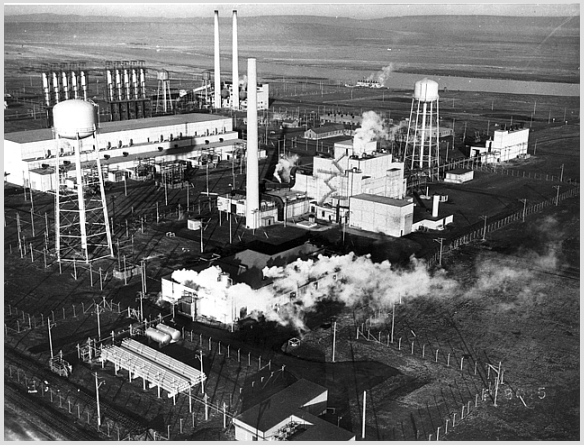

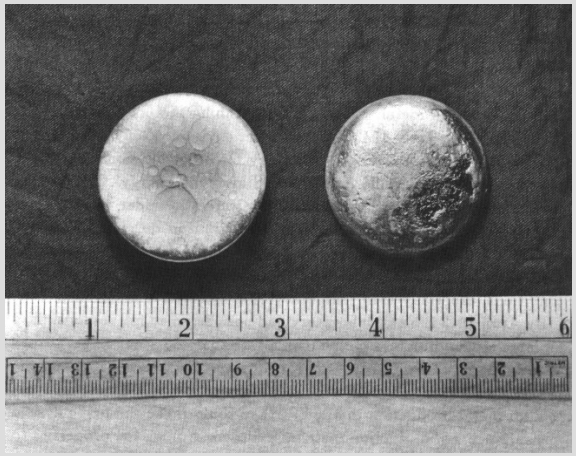

Battelle

Missions at Hanford

Science & Technology

Pacific Northwest National Laboratory

Hanford Cleanup DOE Richland

Management & Integration
Fluor Daniel + Subcontractors

Environmental Restoration
Bechtel

Hanford Cleanup Office of River Protection

CH2M HILL Hanford Group, Inc.

PNNL at a glance

Mission:

PNNL performs basic and applied research to deliver energy, environmental, and national security for our Nation.

- **4,200 staff**
- **$750 million budget**
- **71 R&D 100 awards since 1969**
- **More than 1,100 patents and 200 active licenses**
- **Two national user facilities**

Atmospheric Radiation Measurement Program

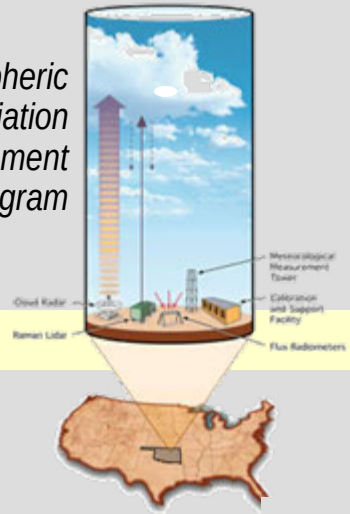

PNNL FY07 Client Base

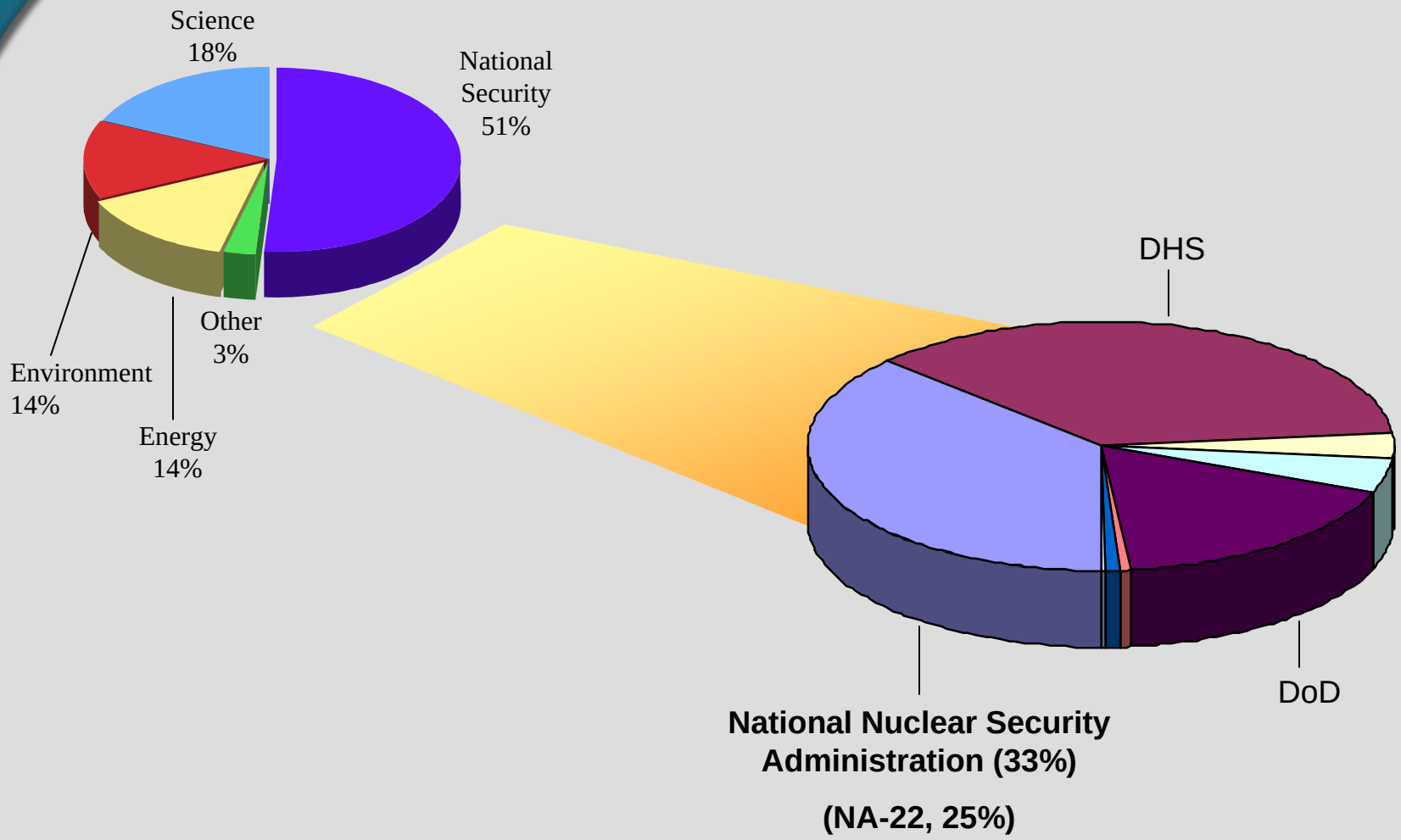

PNNL's support to NNSA is derived from Hanford mission

- Historical expertise
  - Nuclear fuel cycle expertise
  - Actinide chemistry
  - Radionuclide fate and transport
  - Low background radiation detection
  - Nuclear materials safeguards and security

NA-22's structure

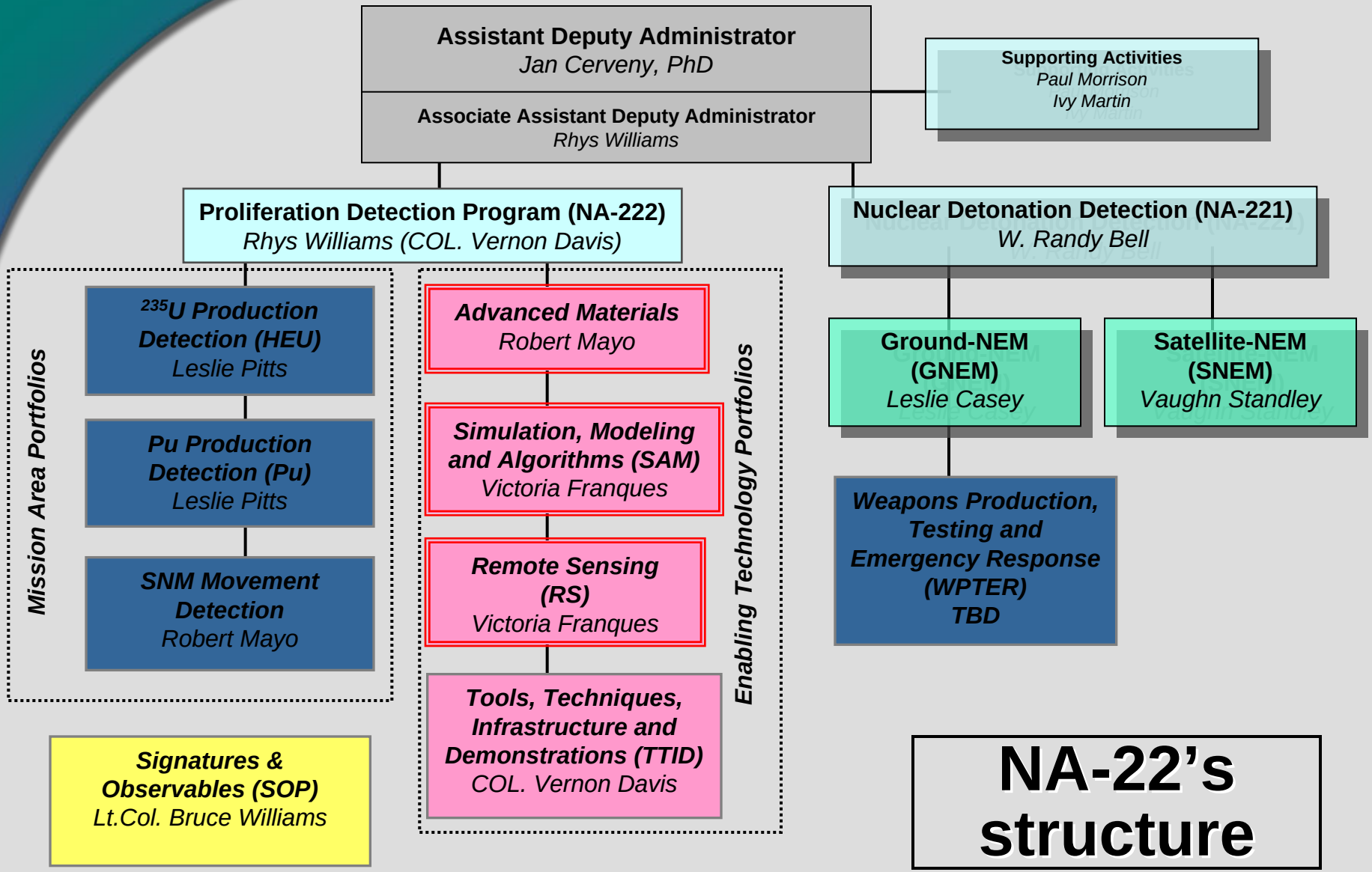

PNNL Proliferation Detection Program

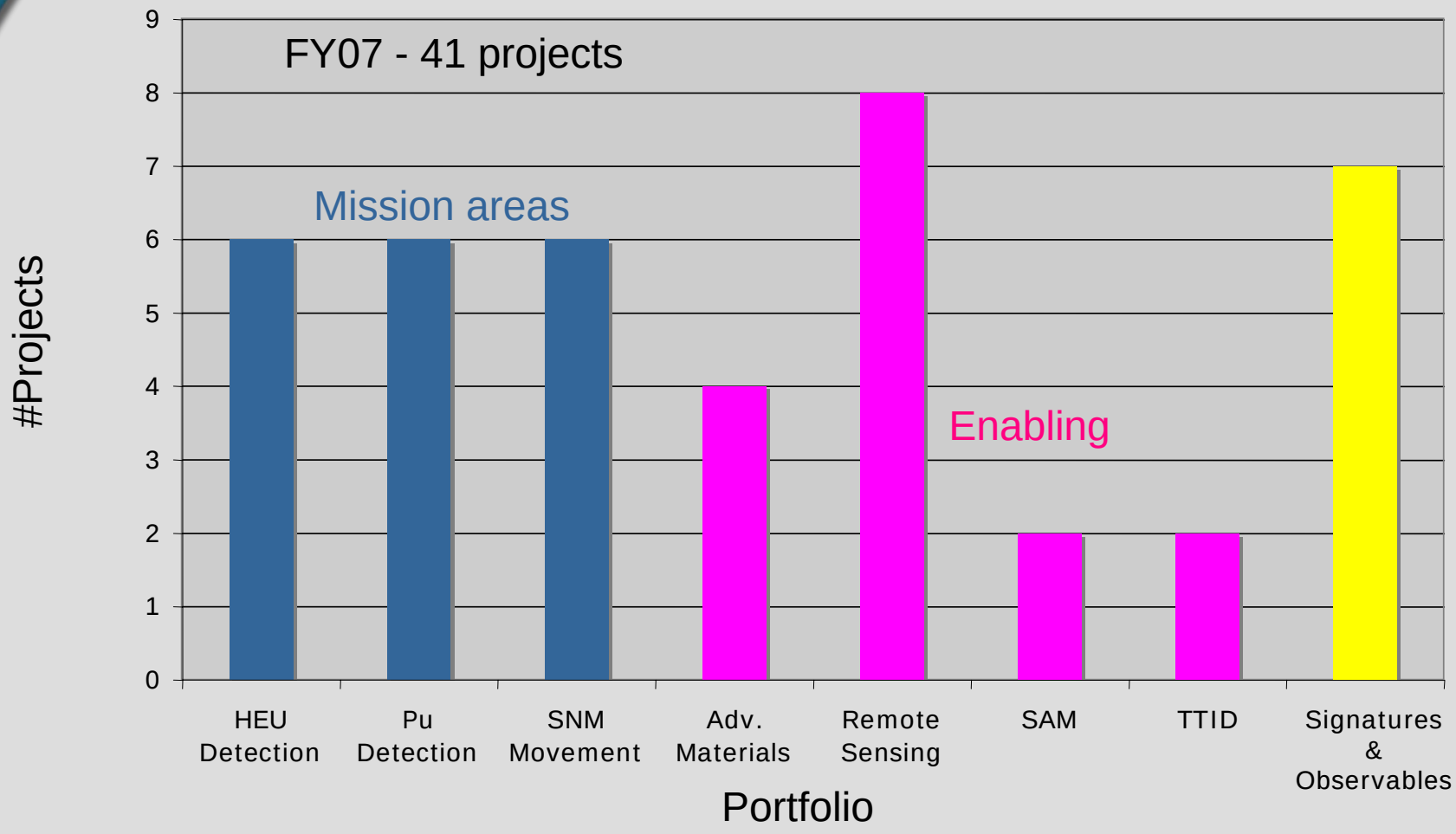

University BAAs and Collaborations

- Universities have unique resources including equipment and bright, creative people
- Research is often cutting-edge and high-risk/high-payoff
- Investment in future scientists and engineers
- Allows students a preview of USG/DOE labs- recruiting opportunity

Remote Sensing

- Bayesian spatial-temporal algorithms
- Multi-spectral imaging S&T (MIST)
- Infrared signatures reference library
- Spectral library statistical analysis

- Miniature spherical retroreflectors
- IR photonics integration and point sensing
- Calibration systems
- Active standoff detection of organics

Bayesian Spatial-Temporal Algorithms

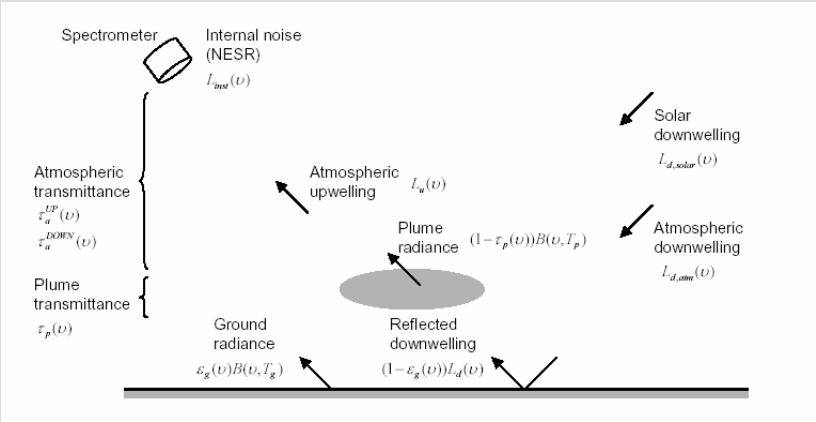

Research Team:

Principal Investigators: Lawrence K. Chilton

Supporting Investigators:
Kevin K. Anderson
Patrick G. Heasler, Kristin H. Jarman,
Sandra E. Thompson


Larry Chilton

Technical Challenges:

- Embed nonlinear physics of remote sensing (RS) into Bayesian mathematics. Provides analysis with mathematical integration of 1) a priori physical basis, 2) a priori intelligence and 3) other signatures.
- Develop mathematics of spatial dependence across RS image. Provides rigorous confirmation of ROI.
- Develop mathematics of temporal ROI behavior from UAV data. Provides rigorous confirmation of a target and micro forecast of ROI evolution.

University:

Prof. Lawrence Carin, Duke University
Applications of machine learning to HSI.
Identifying and classifying background clutter.

Multi-Spectral Imaging Science and Technology (MIST)

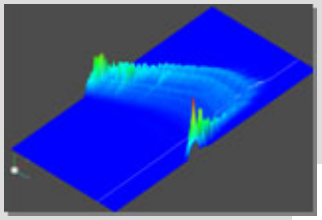

Entropy

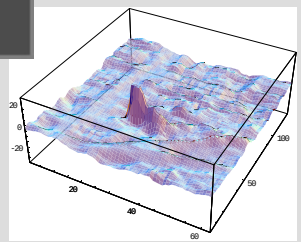

3-D FFT

Research Team:

Principal Investigator: Mike Lind

Supporting Investigators:
Mike Foley, Harlan Foote,
Larry Gerhardstein, Pat Heasler,
Randy Kirkham, Pat Medvick,
Lisa Nuffer, Sandy Thompson

Mike Lind

Technical Challenges:

- Optimizing performance of Whitened Matched Filtering (WMF) in real-world non-Gaussian statistics (Higher-order Statistics, HOS), using Independent Component Analysis (ICA), preceding the normal Principle Component Analysis (PCA) approaches.
- Automating the ROI signature location as a preprocessor to the human selection of “ON-ROI pixels,” to avoid contaminating the Cov-1 function used in whitening.
- Improving the incoherent, “super-pixel” averaging in 1D WMF detection, by forming a 3D WMF and using FFT-domain whitening.
- Assess the utility of Precision Registration of images to spectrally-classified 3D site models based on historic data cube analysis for coherent subtraction of clutter contamination.
- Optimally combining the linear (3D WMF) and nonlinear (ICA) algorithms.

University :

Prof. Gus Williams, Brigham Young University
Incorporation of geometric information into independent component analysis (ICA)

Miniature Spherical Retroreflectors for Remote Sensing

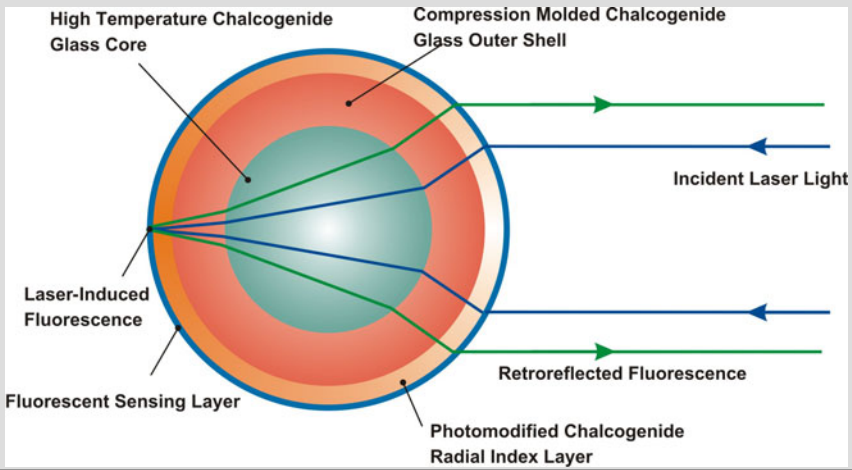

Research Team:

Principal Investigator: Norm Anheier

Supporting Investigators:
Bruce Bernacki, Kannan Krishnaswami, Steven Miller


Norm Anheier

Technical Challenges:

- Resolve sphere fabrication bottleneck by using multilayered chalcogenide glass and compression molding.
- Develop optical designs needed to minimize both spherical and chromatic aberrations and improve the optical retroreflection efficiency.
- Generate required spherical optical index profile needed to fine tune retroreflection performance.
- Develop a miniature spherical retroreflector incorporating sensing layers to enable large standoff radiation and chemical detection
- Explore active modulation to enable IR Comms

University focus:

Prof. Kathleen Richardson, Clemson Univ.
Synthesis and characterization of novel glass and glass ceramic materials for optical applications.

Simulation, Algorithm and Modeling

- Radiation detection scenario (RADSAT)
- Advance decision making for low-count spectra

Rafiation Detection Scenario Analysis Toolbox (RADSAT)

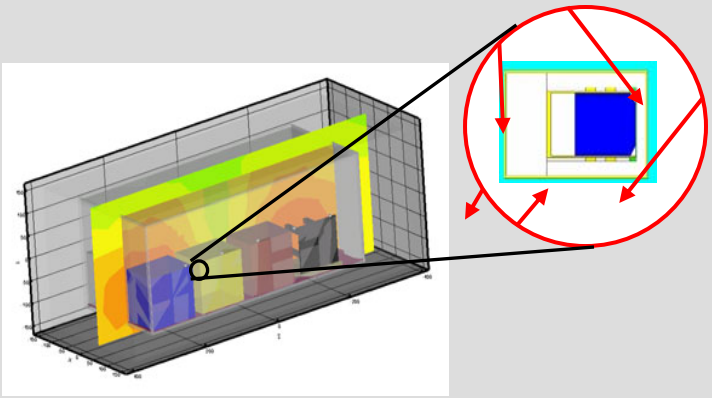

Research Team:

Principal Investigator: Eric Smith

Supporting Investigators:
Christopher Gesh, Erin Miller,
Richard Pagh, Mark Shaver, Edward Ellis

Partners:
Sandia National Laboratories (Dean Mitchell)
Transpire, Inc. (Todd Wareing)


Eric Smith

Technical Challenges:

- Modify, augment Transpire's 3-D deterministic transport code, called Attila, to support detection scenario analysis, for both gamma-ray spectroscopy and neutron detection.
- Develop front-end methods to rapidly and automatically create a problem-specific energy group structure, and the corresponding multi-group cross-sections and source terms.
- Develop back-end methods to port the deterministic angular flux to Monte Carlo and GADRAS for detector response function calculations.
- Validate new methods and implement in a user-friendly software package

University:

Prof. Todd Palmer, Oregon State University
Detector response function calculations

Advanced Materials

- Synthesis and characterization of amorphous semiconductors
- Ambient Temperature Gamma Ray Detectors
- Solid-state neutron detection
- Materials discovery tool for radiation detection materials

Amorphous Semiconductors for Gamma Radiation Detection (ASGRAD)

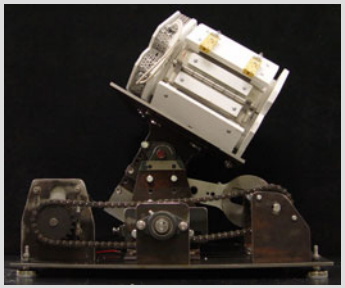

Research Team:

Principal Investigator: Bradley R. Johnson

Supporting Investigators:
S. K. Sundaram
Charles Henager
Yanwen Zhang

Brad Johnson

Technical Challenges:

- Develop improved synthesis methods to minimize chemical impurities that could interfere with electrical properties of detector.
- Develop suitable compositions adjustments to enhance and expand glass formation region of nominally crystalline compounds without adversely impacting their electrical properties.
- Integrate bulk amorphous semiconducting materials into state of the art electronic detection circuitry.

University :

Prof. Angus Rockett (Univ. of Illinois Urbana-Champaign)

Develop, characterize and test electrical contacts on amorphous materials (Cd-Ge-As & Ag-Ga-Te).

Ambient Temperature Gamma Ray Detectors

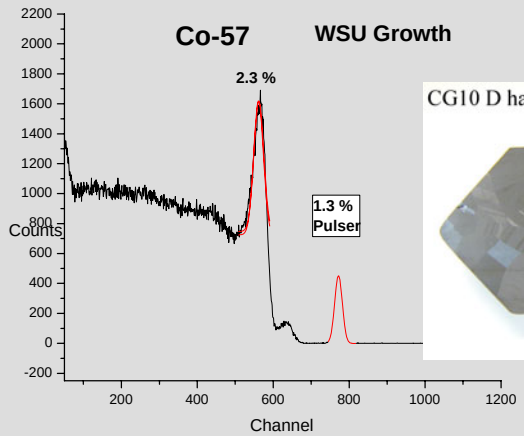

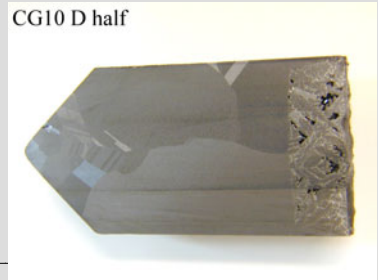

Research Team

Principal Investigator: Dr. Mary Bliss

Technical Challenges:

- Determine the robustness of the new ternary doping scheme
- Increase the yield of large crystals
- Develop optimized detector designs to take full advantage of material properties
- Establish the processing parameters for the new ternary doping scheme.
- Determine composition tolerances and impact on detector performance.
- Develop advanced thermal models of the growth process to increase large crystal yield and ingot uniformity.
- Determine optimal detector designs and signal readout for material produced by this process and doping scheme.

University:

- Prof. Kelvin Lynn - Washington State University
  Systematic doping studies in CZT, to improve material
- Prof. Zhong He - University of Michigan
- Prof. Jeffery Derby - University of Minnesota

Contacting PNNL






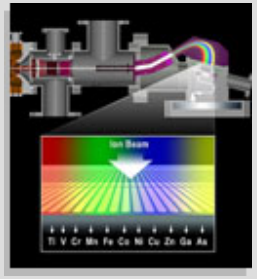

Steven Sharpe
(509) 372-4740
sw.sharpe@pnl.gov

Advanced Wavelet-Based Analysis of Hyperspectral Imagery

Lawrence Carin
Department of Electrical & Computer Engineering
Duke University
Durham, NC
www.ece.duke.edu/~lcarin

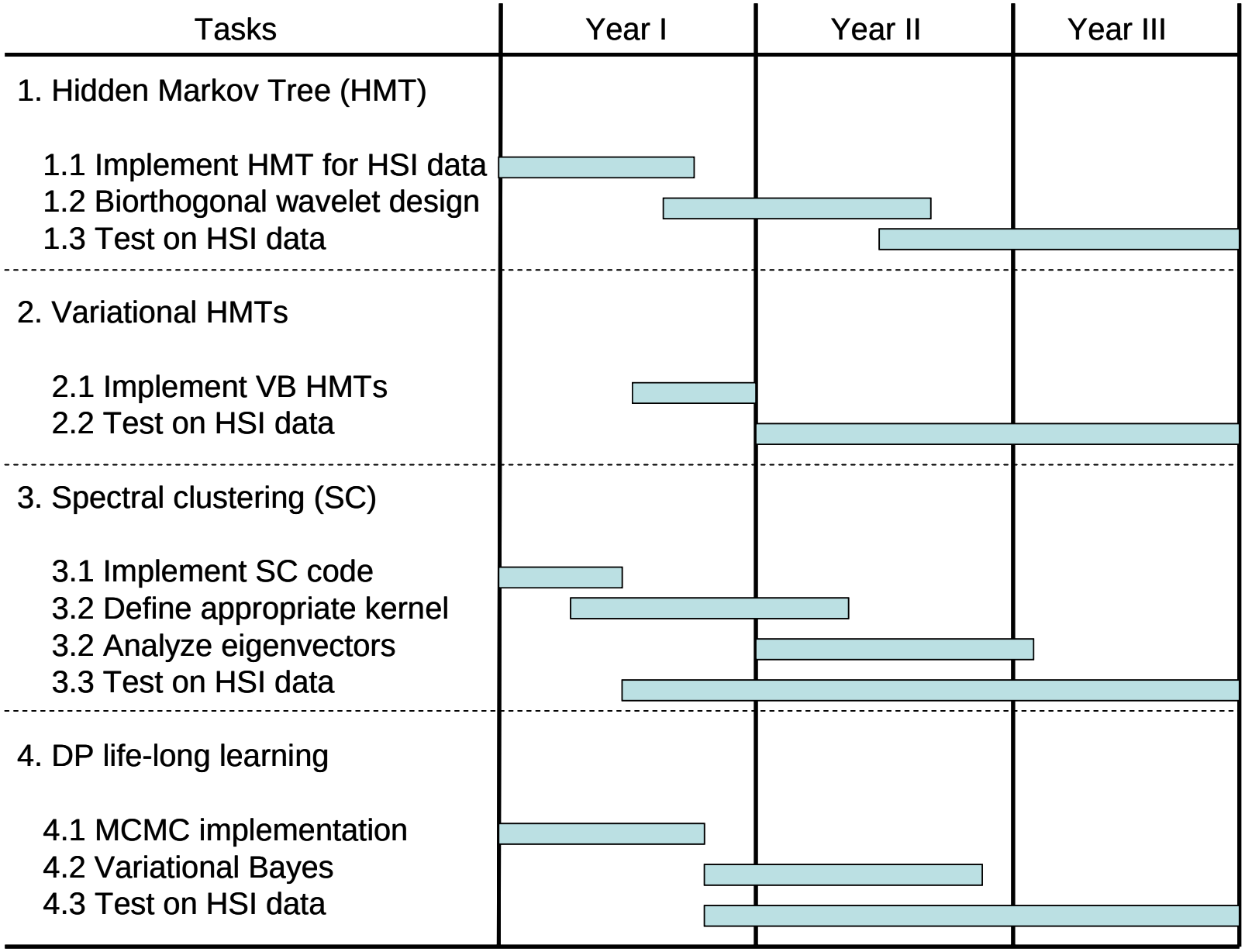

Funding Level: $190K/yr

Overview & Goals

- Statistical methods are needed to analyze the large volume of imagery collected by the DOE, to aid the analyst

- Particular need in the context of hyperspectral imagery, due to high data dimensionality

- Dimensionality reduction via graph-diffusion technology

- Inferring statistical inter-relationships between large data sets via hierarchical Bayesian methods, with computationally efficient inference

- Close linkage to DOE labs: Dr. Lawrence Chilton, PNNL

    - Analyzing PNNL-provided hyperspectral imagery

Technical Presentation

- Intra-scene context: random walk on a graph
- Inter-scene context: Dirichlet process technology
- Application to airborne radar and hyperspectral DOE data
- Future research plans

Intra-Scene Context

Single Band in Hyperspectral Image

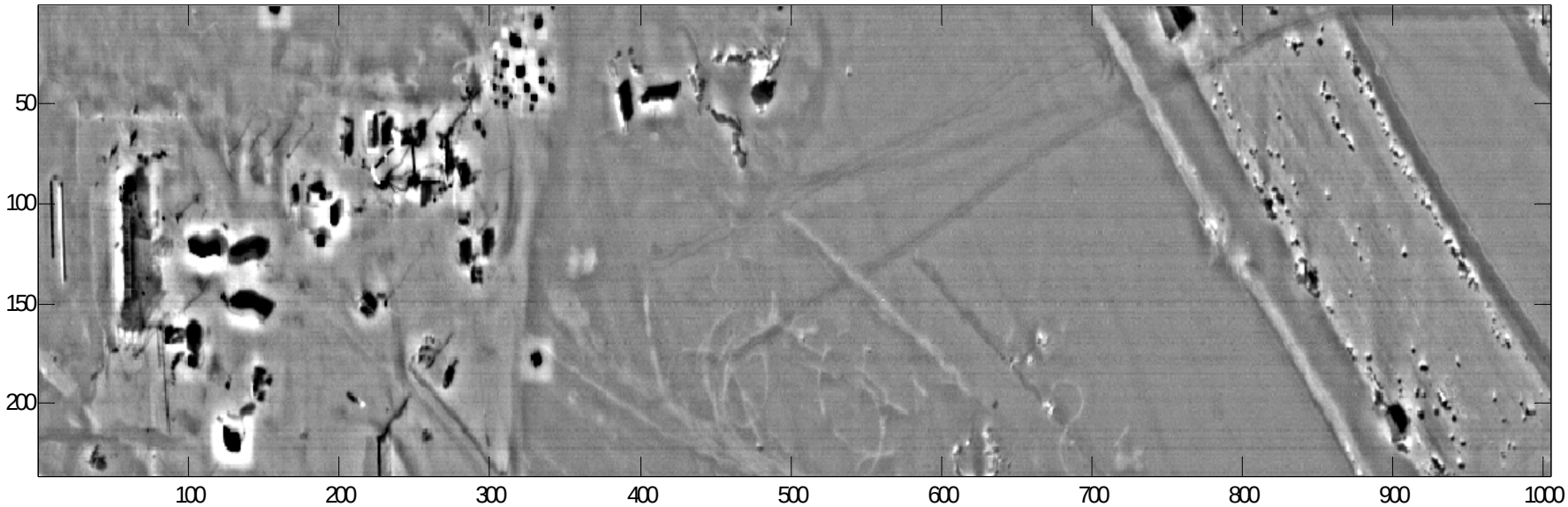

One of 258 Spectral Bands

Data provided by PNNL

What Analyst Processes:

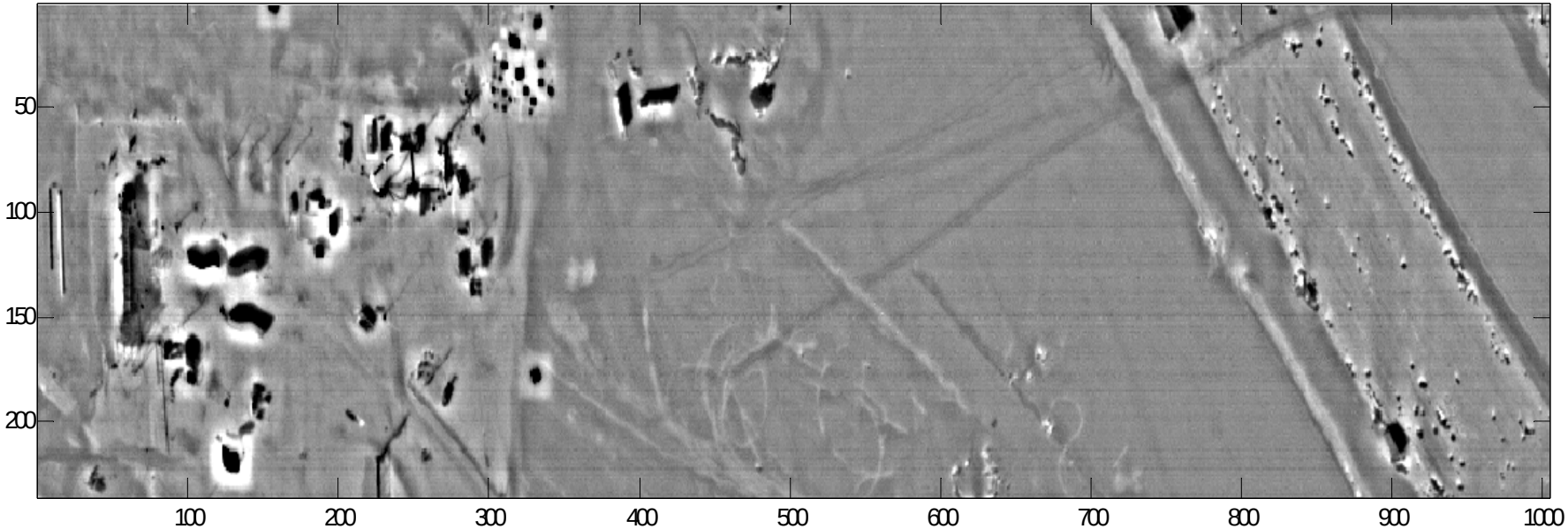

What Supervised Algorithm Processes:

Decision surface based on labeled data (supervised)

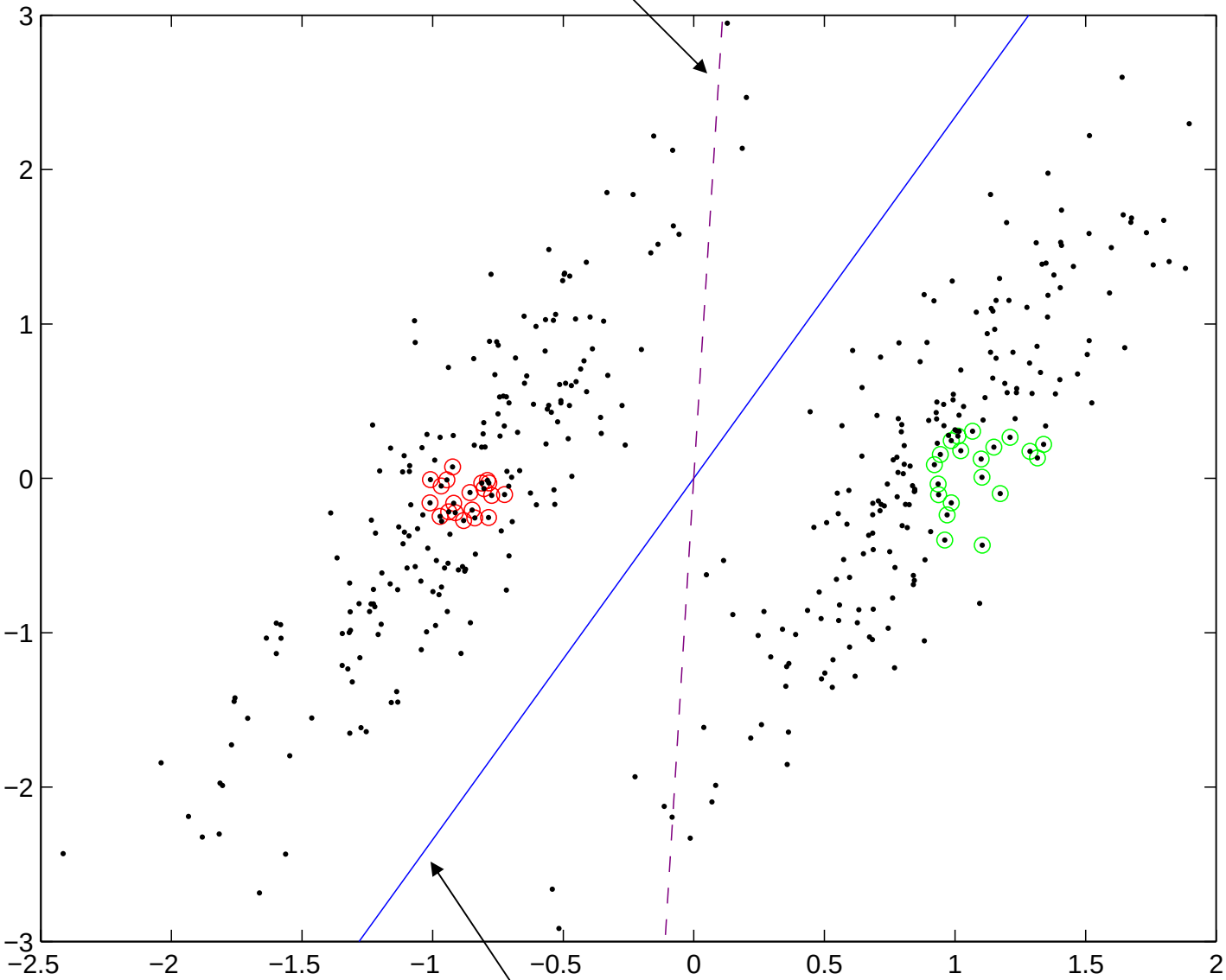

Decision surface based on labeled &
Unlabeled data (semi-supervised)

Inter-Scene Context

Environments Encountered Over “Lifetime”

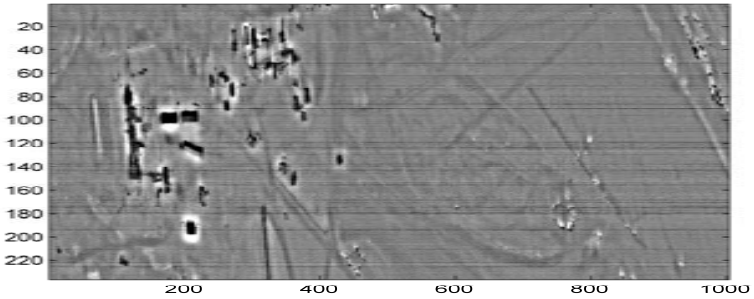

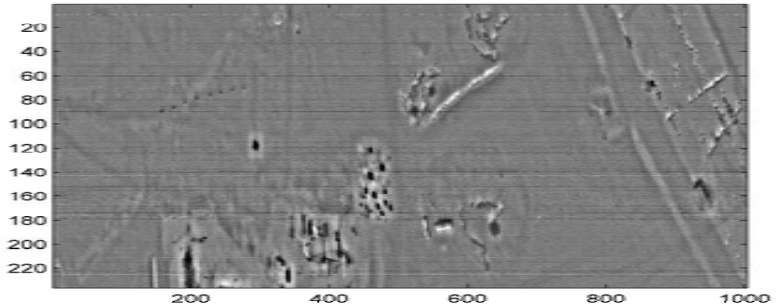

…

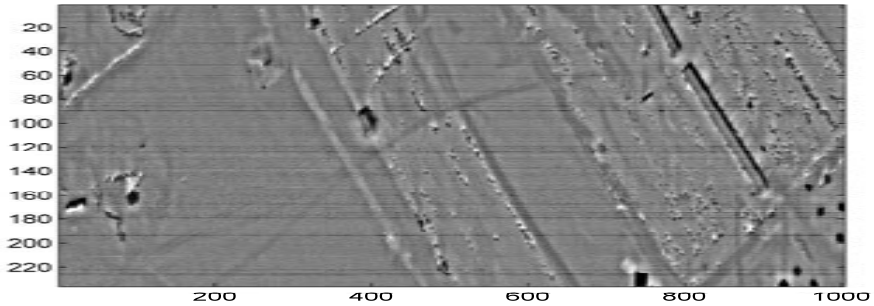

We Now Encounter a New Environment ….

New Environment:

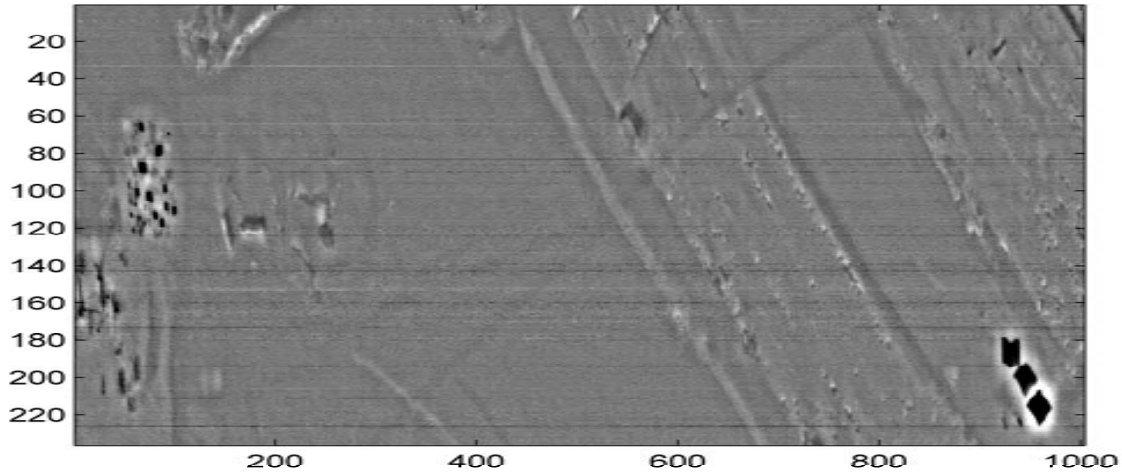

- People are very good at placing a new environment in the context of environments observed previously

- Infer what environments from past are and are not relevant to interactions with new environment

Message

- Humans are very good at exploiting *context*, both within a given scene and across multiple scenes
- Intra-scene context: semi-supervised learning
- Inter-scene context: multi-task and transfer learning
- New and promising directions in sensor signal processing
- A major focus of machine learning currently

Data Manifold Representation Based on Markov Random Walks (1/2)

- Given $X=\{x_1, \ldots, x_N\}$, first construct a graph G=(X,W), with the affinity matrix W, where the (i, j)-th element of W is defined by a Gaussian kernel:

$$w_{ij} = \exp(-\|x_i - x_j\|^2 / 2\sigma_i^2)$$

- we consider a Markov transition matrix A, which defines a Markov random walk, where the (i, j)-th element:

$$a_{ij} = \frac{w_{ij}}{\sum_{k=1}^{N} w_{ik}}$$

gives the probability of walking from x_i to x_j by a single step.

- The one-step Markov random work provides a local similarity measure between data points.

Data Manifold Representation Based on Markov Random Walks (2/2)

- **A *t*-step Markov random walk**, however, would result in **a volume of paths** connecting the data points instead of the shortest paths[3]; thus it permits us to incorporate **global manifold structure** in the training data set.

$$\mathbf{A}^t = [a_{ij}^{(t)}]_{N \times N}$$

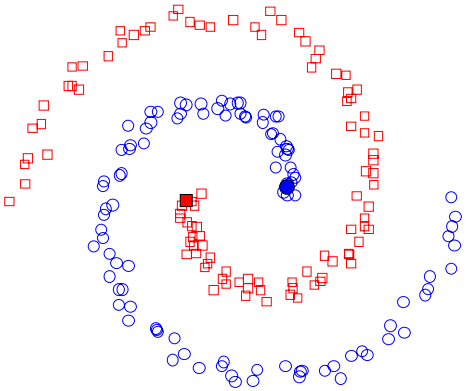

Data manifold

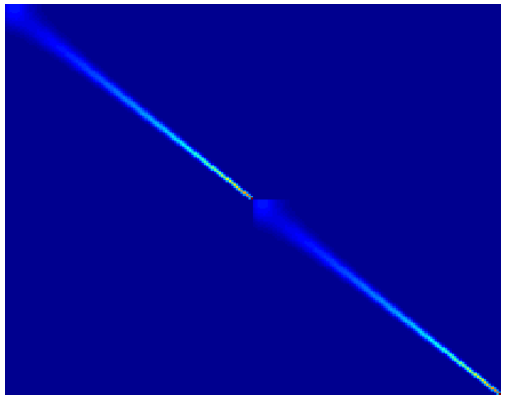

Transition matrix with t

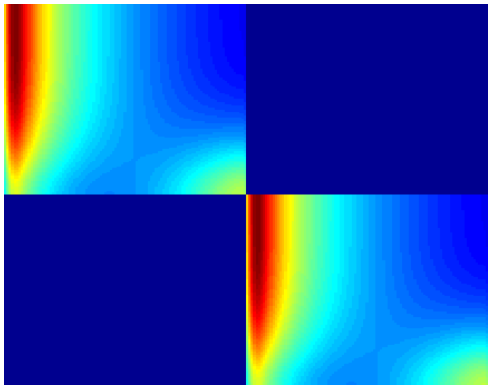

Transition matrix with t 100

- **t-step neighborhood of x_i: defined as the set of data points x_j with $a_{ij}^{(t)} > 0$ and denoted as $\mathcal{N}_t(x_i)$.**

Semi-supervised Learning Algorithm: NeBC (1/2)

- **Parameterized Neighborhood-based classification(PNBC): Define the probability of label y_i given the t-step neighborhood of x_i as:**

$$p(y_i \mid \boldsymbol{N}_t(x_i), \theta) = \sum_{j=1}^{N} a_{ij}^{(t)} p(y_i \mid x_j, \theta)$$

- In order for x_i to be labeled y_i, each point x_j in its neighborhood must be labeled consistently with y_i,
- **The contribution of x_j to the label of x_i is proportional to the global similarity between x_i and x_j .**
- y_i implicitly propagates over the neighborhood.
- It is possible to learn a classifier with only a few labels present and yet the is much less subject to over-fitting than when ignoring the neighborhood.

Semi-Supervised Learning Algorithm: NeBC (2/2)

- For binary classification problems with $y \in \{\pm 1\}$, we **choose** the form of the base classifier as standard logistic regression classifier:

$$p(y_i \mid x_j) = \frac{1}{1 + \exp(-y_i \theta^T x_j)}$$

Sigmoid function:

$$p(t) = \frac{1}{1 + e^{-t}}$$

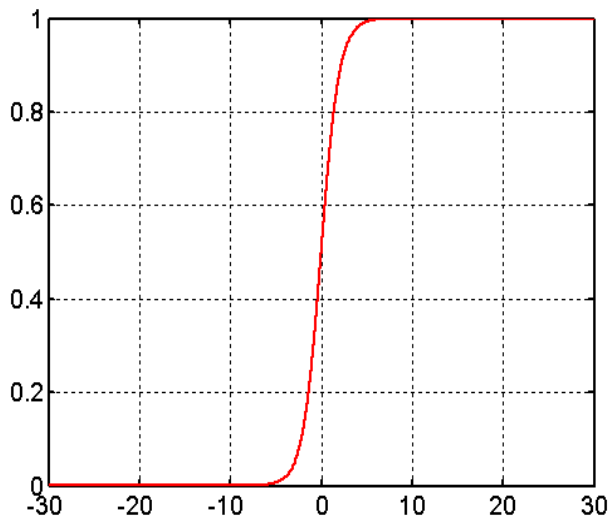

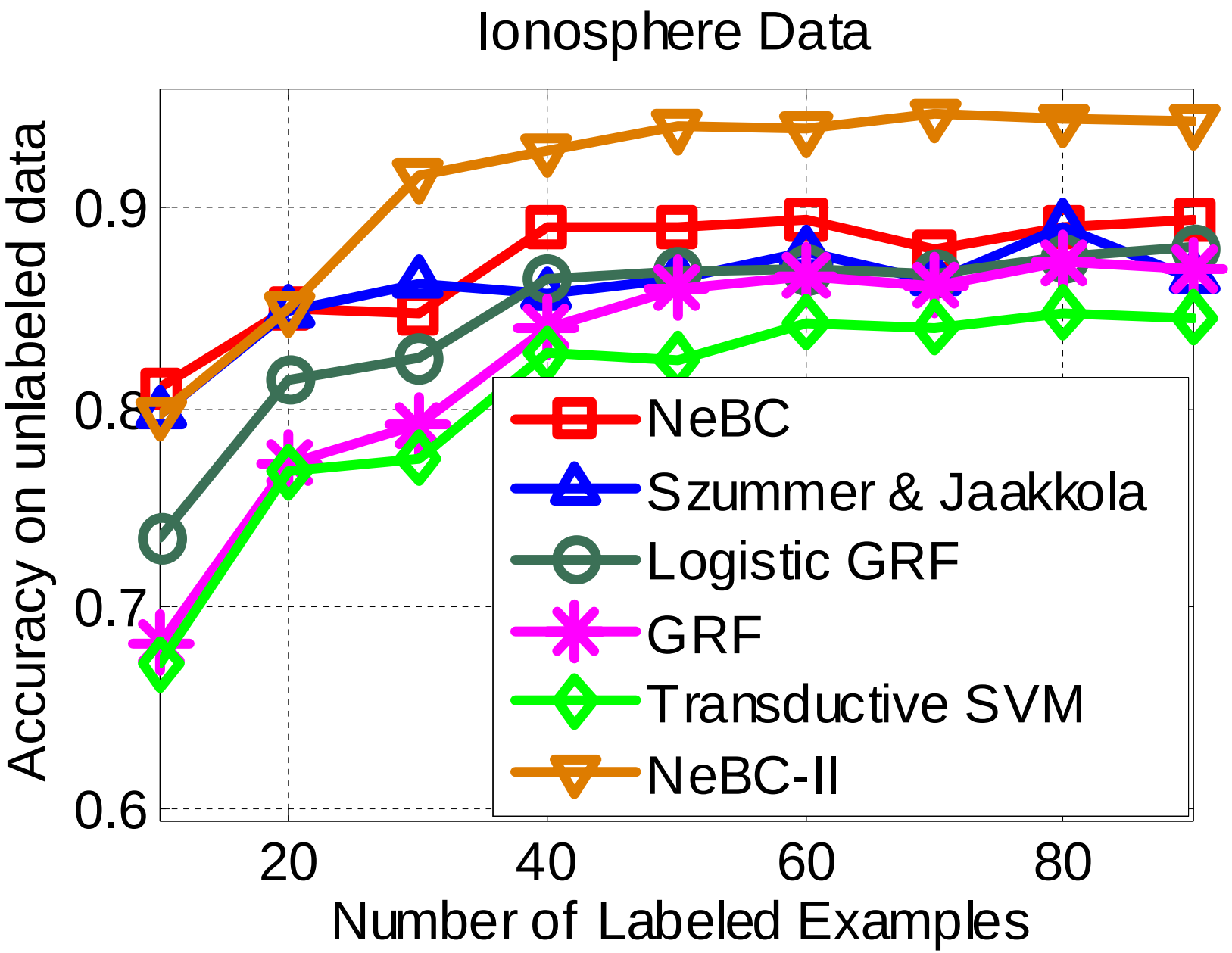
Ionosphere Data
Accuracy on unlabeled data
0.9
0.8
0.7
0.6
20
40
60
80
Number of Labeled Examples
NeBC
Szummer & Jaakkola
Logistic GRF
GRF
Transductive SVM
NeBC-II

Technical Presentation

- Intra-scene context: random walk on a graph

➢ Inter-scene context: Dirichlet process technology

- Application to airborne radar and hyperspectral DOE data

- Future research plans

Semi-Supervised Multitask Learning (1/2)

- **Semi-supervised MTL**: Given M partially labeled data manifolds, each defining a classification task, we propose a unified sharing structure to learn the M classifiers simultaneously.
- **The Sharing Prior**:

  We consider M **NeBC** classifiers, parameterized by θ_m, $m = 1,2...,M$. **The M classifiers are not independent but coupled by a joint prior distribution:**

$$p(\theta_1,..,\theta_M) = \prod_{m=1}^{M} p(\theta_m \mid \theta_1,..,\theta_{m-1})$$

Semi-Supervised Multitask Learning (2/2)

$$p(\theta_m \mid \theta_1,..,\theta_{m-1}) = \frac{1}{\underbrace{\alpha}_{\text{Balance parameter}} + m - 1}\left[\alpha \underbrace{p(\theta_m \mid \boldsymbol{\gamma})}_{\text{Baseline prior}} + \sum_{l=1}^{m-1} \underbrace{N(\theta_m;\theta_l,\eta_{ml}^2\mathbf{I})}_{\text{Prior transferred from previous tasks}}\right]$$

- The normal distributions indicates the meta-knowledge indicating how the present task should be learned, based on the experience with a previous task.
- When there are no previous tasks, only the baseline prior is used by setting m=1 =>NeBC.
- Sharing tasks to have similar $\theta's$, not exactly the same (advantages over the Dirac delta function used in previous MTL work).

Experimental Results

- Illustrative toy example

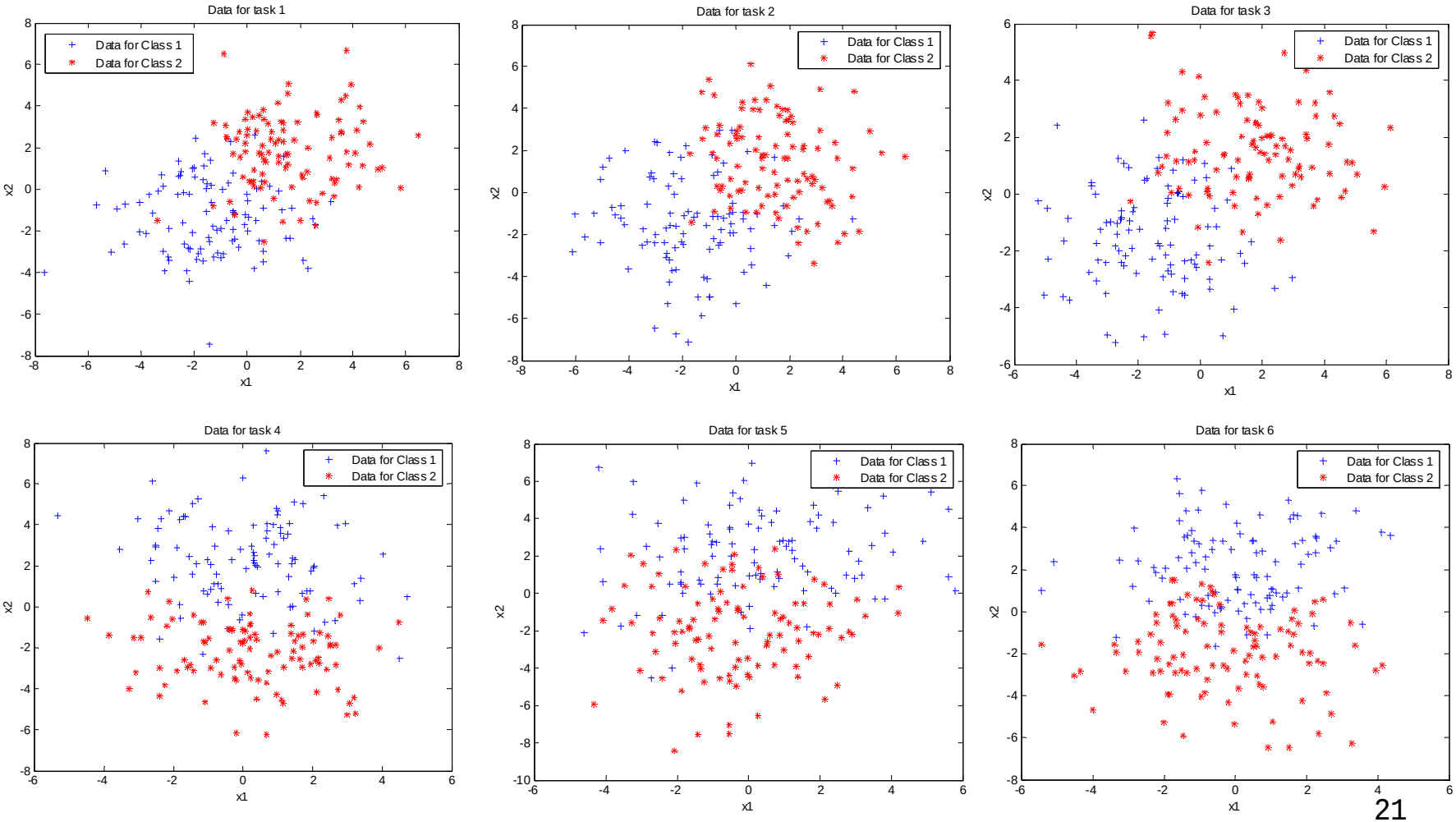

Data Pooling

Pooling task 1-3

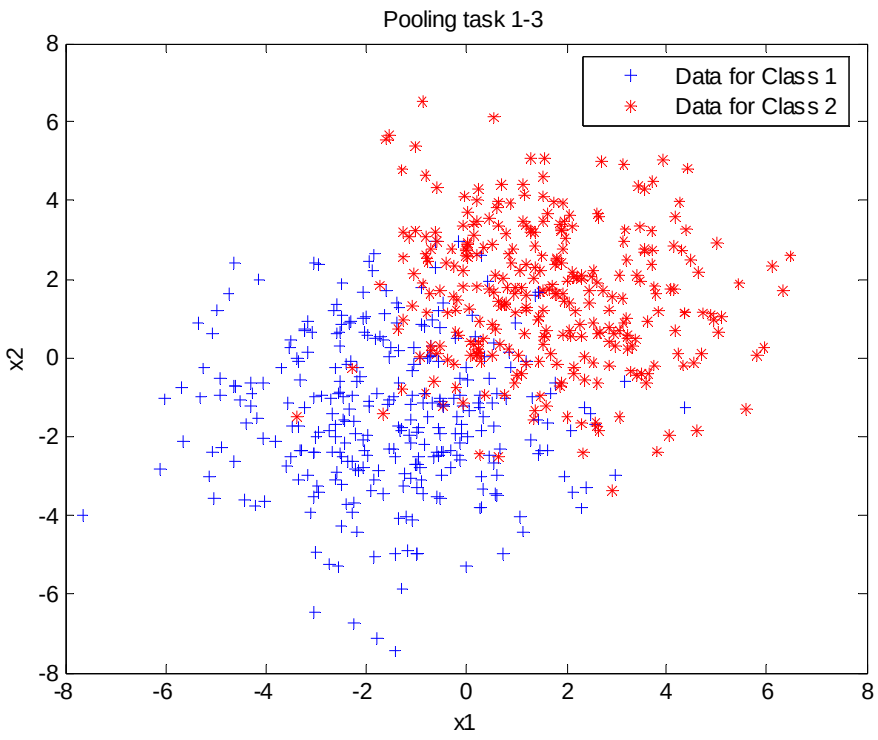

Pooling task 1-6

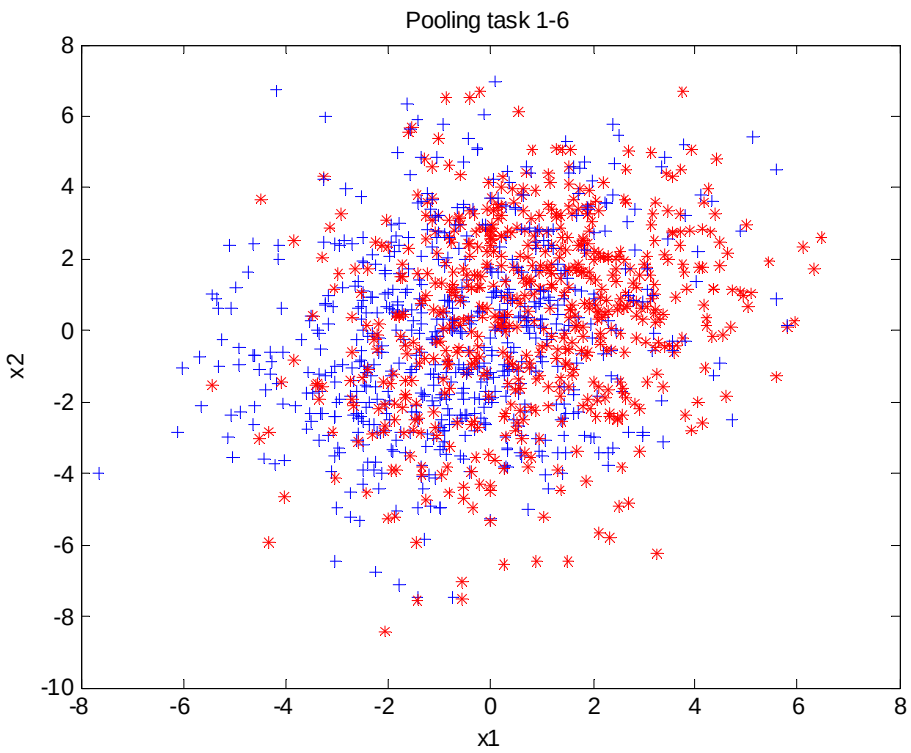

Hinton Diagram of Between-Task Similarity:

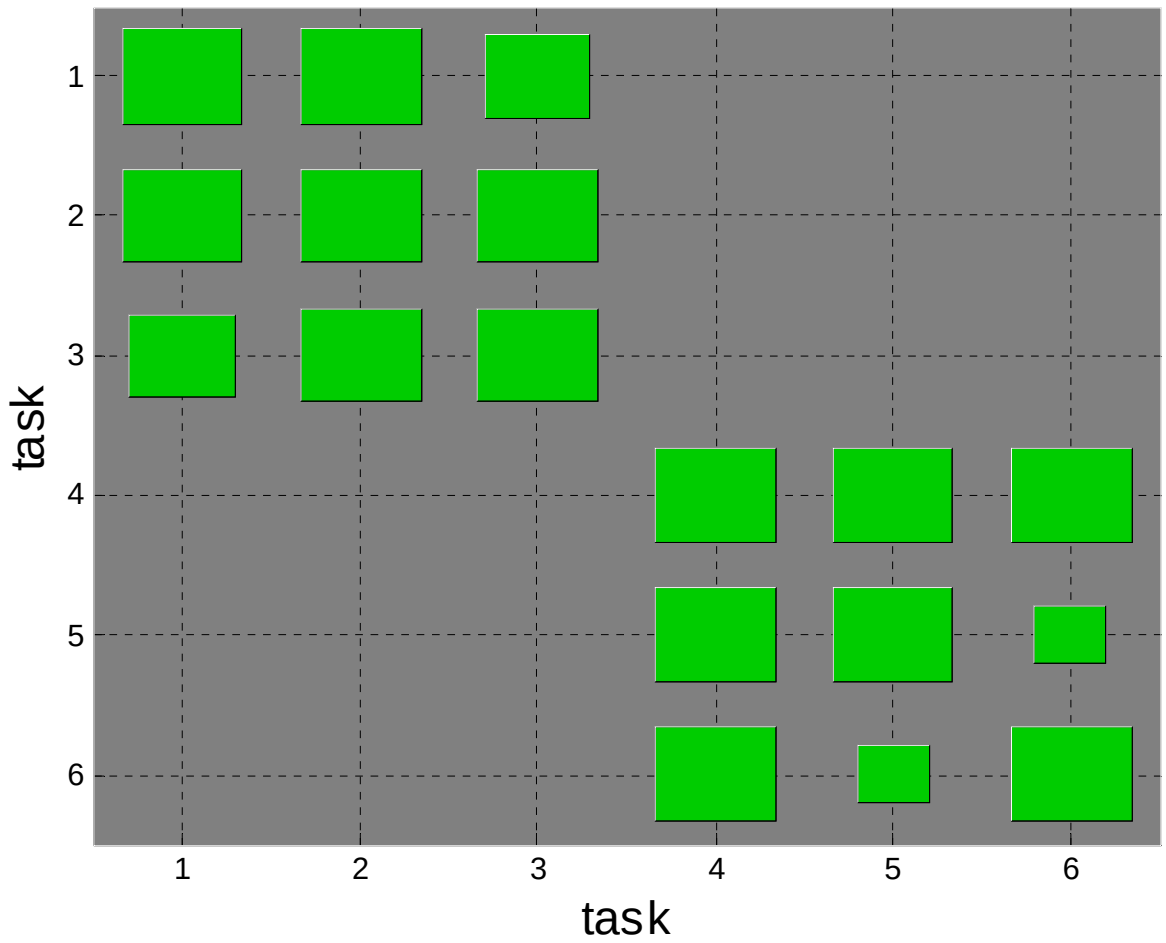

Technical Presentation

- Intra-scene context: random walk on a graph

- Inter-scene context: Dirichlet process technology

➢ Application to airborne radar and hyperspectral DOE data

- Future research plans

Airborne Radar Data

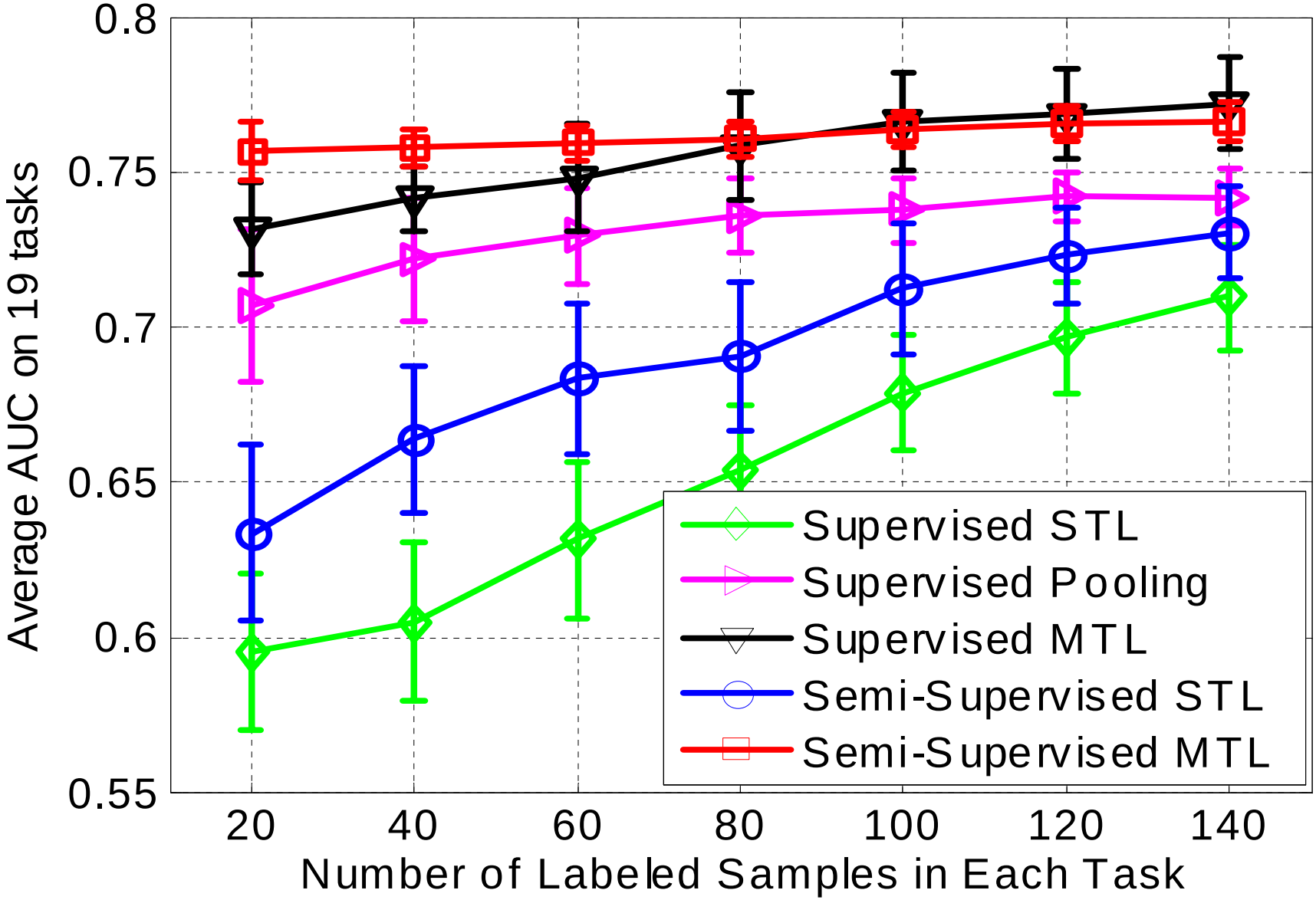

Between-Task Similarity

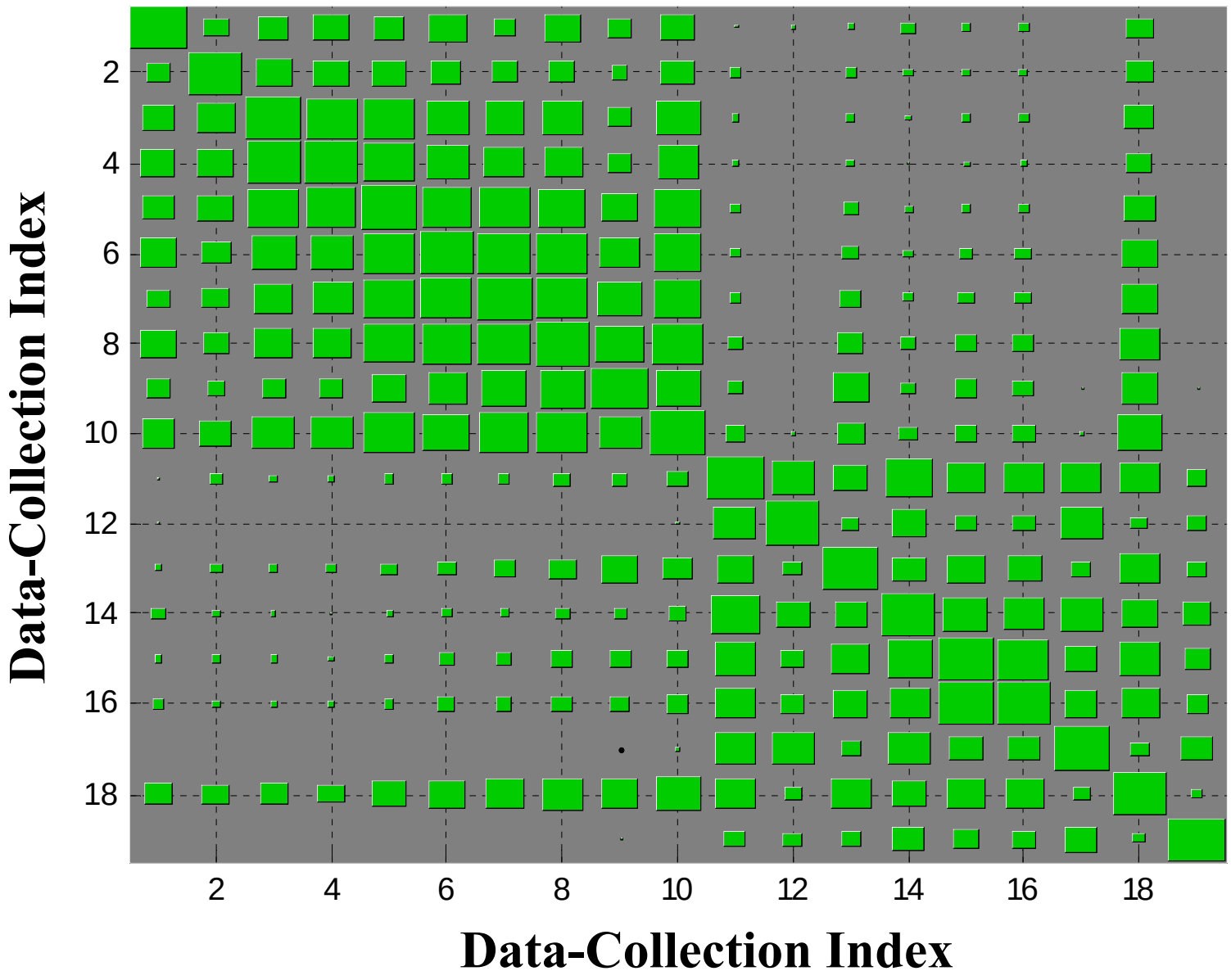

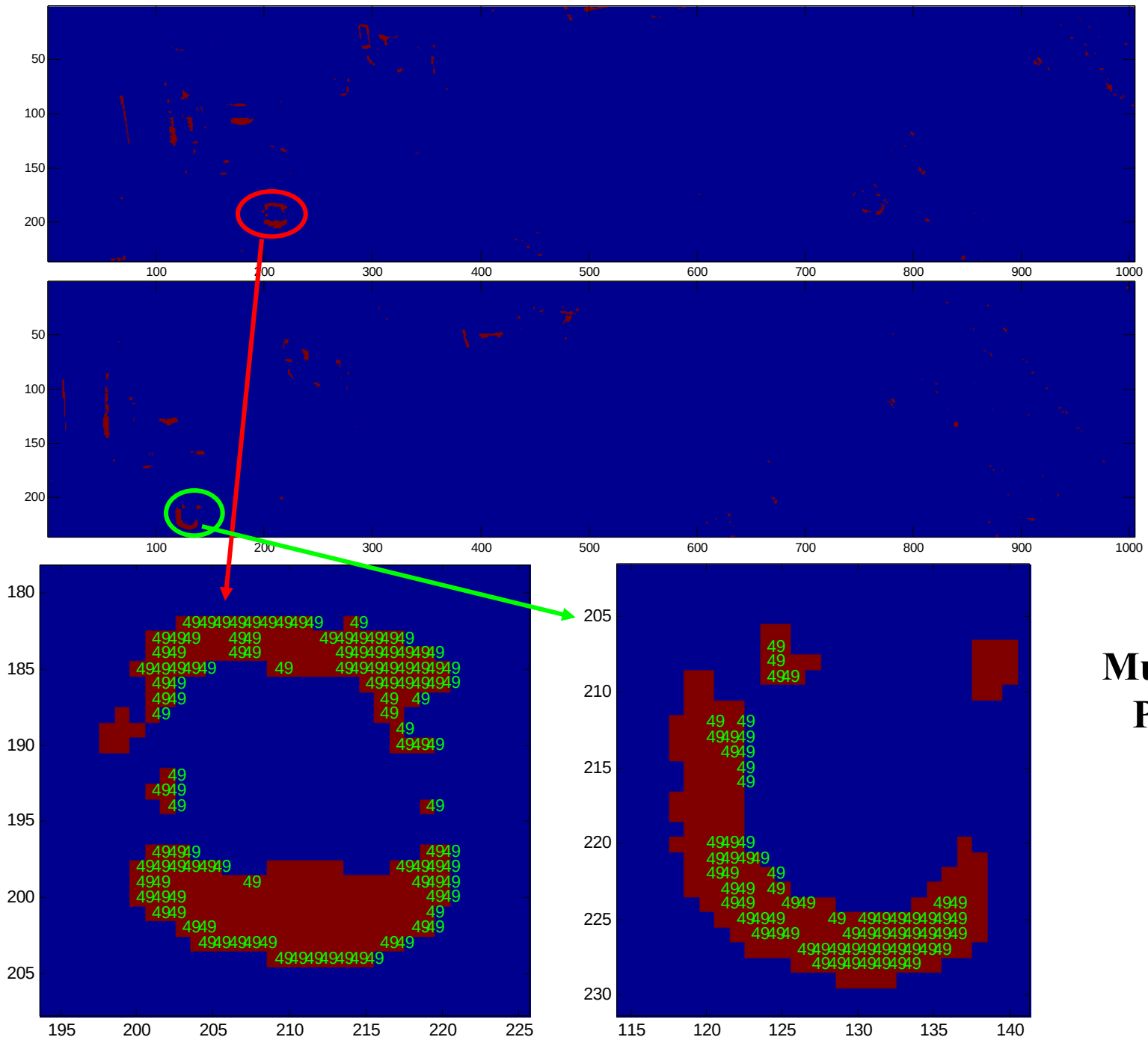

Multi-Pass HSI PNNL Data

Technical Presentation

- Intra-scene context: random walk on a graph

- Inter-scene context: Dirichlet process technology

- Application to airborne radar data and to hyperspectral DOE data

➢ Future research plans

- Hierarchical Bayesian image analysis for background characterization
- Transition technology to PNNL for testing on operational data
- Hybrid spatial-spectral image segmentation

“A paper is an advertisement for software”

Prof. David Donoho, Stanford Statistics Department

“A talk is an advertisement for a paper”

Lawrence Carin, 11/28/07

Related Papers

Q. Liu, X. Liao and L. Carin, “Semi-supervised multitask learning”, *Neural and Information Processing Systems* (NIPS), 2007

Y. Xue, X. Liao, L. Carin and B. Krishnapuram, “Multi-task learning for classification with Dirichlet priors,” *J. Mach. Learning Res.*, vol. 8, pp. 35-63, Jan. 2007

GEOM-ICA: Incorporating Geometric and Other Information into Hyperspectral Independent Component Analysis

J. Gunther[1], T. Moon[1], G. Williams[2], M. Stites[1], J. Pearson[2]

[1]Department of Electrical and Computer Engineering
Utah State University

[2]Department of Civil Engineering
Brigham Young University

UITI Review Meeting 2007

Research Grant Status

- Two years (of potential 3 year project)
  - Grant Start date: Oct. 1, 2006
  - Grant End date: Sept. 30, 2008
- 54% of time expended (13 of 24 months)
- 45% of funds expended (on track)
- All milestones are on track and on budget
- Publications
  - M. Stites, T. Moon, J. Gunther, and G. Williams, "A Bayesian Framework for Hyperspectral Estimation using Markov Random Fields," Asilomar Conference on Signals, Systems, and Computers, IEEE Signal Processing Society, Monterey, CA, November 4-7, 2007.

Goals of the Project

- Many hyperspectral image processing algorithms focus exclusively on spectral processing, neglecting spatial information.
- There is a need for a more holistic approach, which exploits spatial, morphological (i.e. shape), and spectral information jointly.
- Incorporate other constraints such as positivity, sparseness, advection, diffusion, etc.
- Hoped-for gains: more sensitivity and fewer false alarms.

Talk Overview

- Independent component analysis
- Quasi-Bayesian framework
- Future work

Hyperspectral Data Model

- Linear mixing model is assumed:

$$x(\lambda, m, n) = \sum_{k=1}^{K} s(\lambda, k) a(k, m, n) + v(m, n, \lambda)$$

$$1 \leq m \leq M, \qquad 1 \leq n \leq N, \qquad 1 \leq \lambda \leq L$$

  - $s(\lambda, k)$ ("spectrum",radiance,...) of material k in band λ
  - $a(k, m, n)$ fractional abundance of material k in $(m, n)^{\text{th}}$ pixel
  - $x(\lambda, m, n)$ measurement in band λ in $(m, n)^{\text{th}}$ pixel
  - $v(\lambda, m, n)$ Gaussian measurement noise

- Stack over λ

$$\mathbf{x}(m, n) = \mathbf{S}\mathbf{a}(m, n) + \mathbf{v}(m, n) \quad \longrightarrow \quad \mathbf{x}(t) = \mathbf{S}\mathbf{a}(t) + \mathbf{v}(t)$$

  - view each spectral band as a "sensor"
  - view each material as a "signal"

Independent Component Analysis

Independent Component Analysis

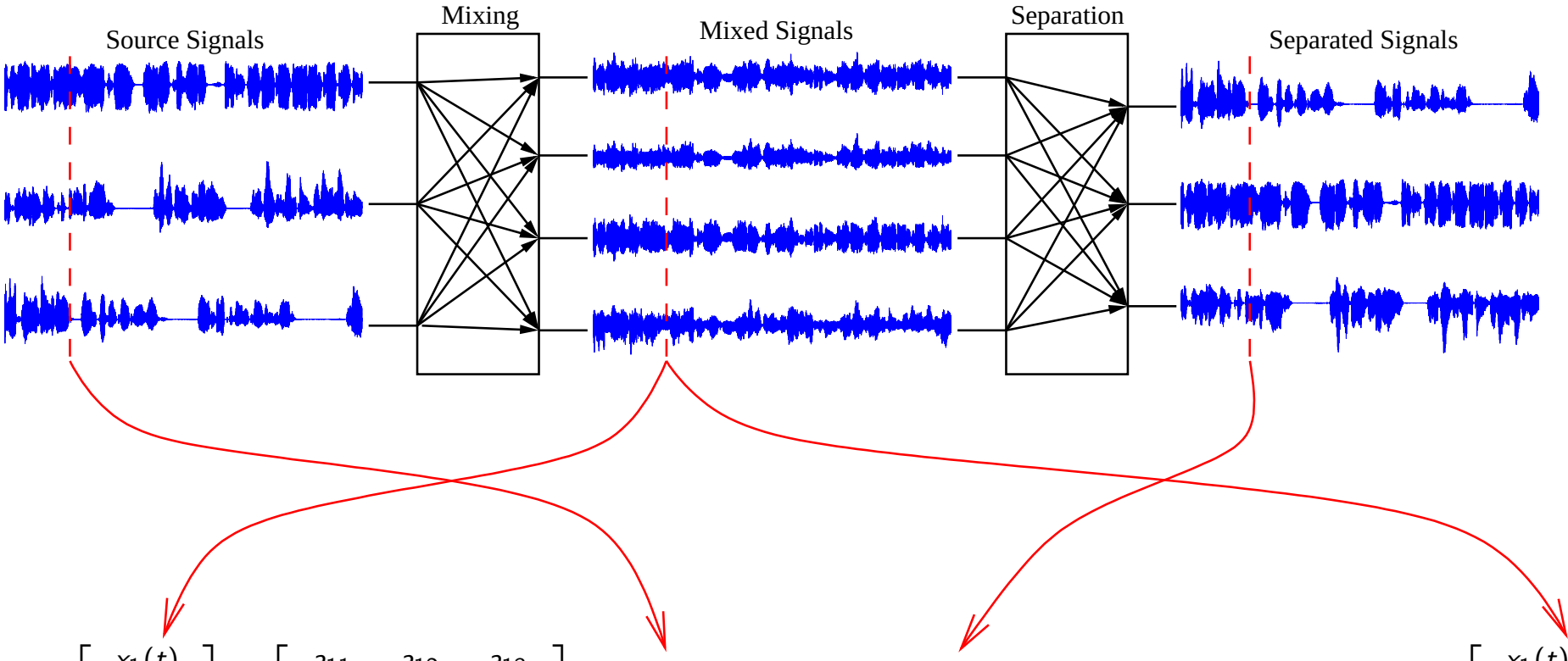

$$\begin{bmatrix} x_1(t) \\ x_2(t) \\ x_3(t) \\ x_4(t) \end{bmatrix} = \begin{bmatrix} a_{11} & a_{12} & a_{13} \\ a_{21} & a_{22} & a_{23} \\ a_{31} & a_{32} & a_{33} \\ a_{41} & a_{42} & a_{43} \end{bmatrix} \begin{bmatrix} s_1(t) \\ s_2(t) \\ s_3(t) \end{bmatrix}$$

$$\begin{bmatrix} y_1(t) \\ y_2(t) \\ y_3(t) \end{bmatrix} = \begin{bmatrix} w_{11} & w_{12} & w_{13} & w_{14} \\ w_{21} & w_{22} & w_{23} & w_{24} \\ w_{31} & w_{32} & w_{33} & w_{34} \end{bmatrix} \begin{bmatrix} x_1(t) \\ x_2(t) \\ x_3(t) \\ x_4(t) \end{bmatrix}$$

$\mathbf{x}(t) = \mathbf{A}\mathbf{s}(t)$

$\mathbf{y}(t) = \mathbf{W}\mathbf{x}(t)$

$\mathbf{X} = \mathbf{A}\mathbf{S}$

$\mathbf{Y} = \mathbf{W}\mathbf{X}$

Independent Component Analysis

- Given the linear mixing model,

$$\mathbf{x}(t) = \mathbf{S}\mathbf{a}(t) + \mathbf{v}(t)$$

  Process the data by a linear transformation

$$\mathbf{y}(t) = \mathbf{W}\mathbf{x}(t) \approx \mathbf{a}(t) \qquad \text{or} \qquad y(t) = \mathbf{w}^T\mathbf{x}(t) \approx a(t)$$

- Look for a transformation that:
  - exposes spatial structure in $\mathbf{y}(t)$
  - produces statistically independent components in $\mathbf{y}(t)$
- Assumptions:
  - Unknown spectra. (How do we incorporate spectra for known materials?)
  - Spatial distributions of materials (i.e. abundances) are unknown and independent.

Exploiting Spatial Structure

- Covariance of "sources", "measurements", and "outputs"

$$\begin{aligned}\mathbf{\Lambda_a}(t,\tau) &= E\{\mathbf{a}(t)\mathbf{a}^T(t+\tau)\} \\ &= \mathrm{diag}\{\cdots, E\{a(k,t)a(k,t+\tau)\}, \cdots\}\end{aligned}$$

$$\begin{aligned}\mathbf{R_x}(t,\tau) &= E\{\mathbf{x}(t)\mathbf{x}^T(t+\tau)\} \\ &= \mathbf{S}\mathbf{\Lambda_a}(t,\tau)\mathbf{S}^T\end{aligned}$$

$$\begin{aligned}\mathbf{R_y}(t,\tau) &= E\{\mathbf{y}(t)\mathbf{y}^T(t+\tau)\} \\ &= \mathbf{W}\mathbf{R_x}(t,\tau)\mathbf{W}^T = (\mathbf{WS})\mathbf{\Lambda_a}(t,\tau)(\mathbf{WS})^T\end{aligned}$$

- Transform to restore diagonality to output covariances: Only possible with $\mathbf{W} = \mathbf{S}^{-1}$.
- Note that diagonalizing a single covariance matrix amounts to eigendecomposition and is insufficient to achieve $\mathbf{W} = \mathbf{S}^{-1}$.

Exploiting Spatial Non-stationarity

- Let $\tau = 0$ and choose $t \in \{t_1, t_2, \cdots, t_P\}$, then jointly diagonalize $\mathbf{R_y}(t_1, 0), \mathbf{R_y}(t_2, 0), \cdots, \mathbf{R_y}(t_P, 0)$
- Materials appear in different concentrations in different locations
- Material distributions can be spatially uncorrelated

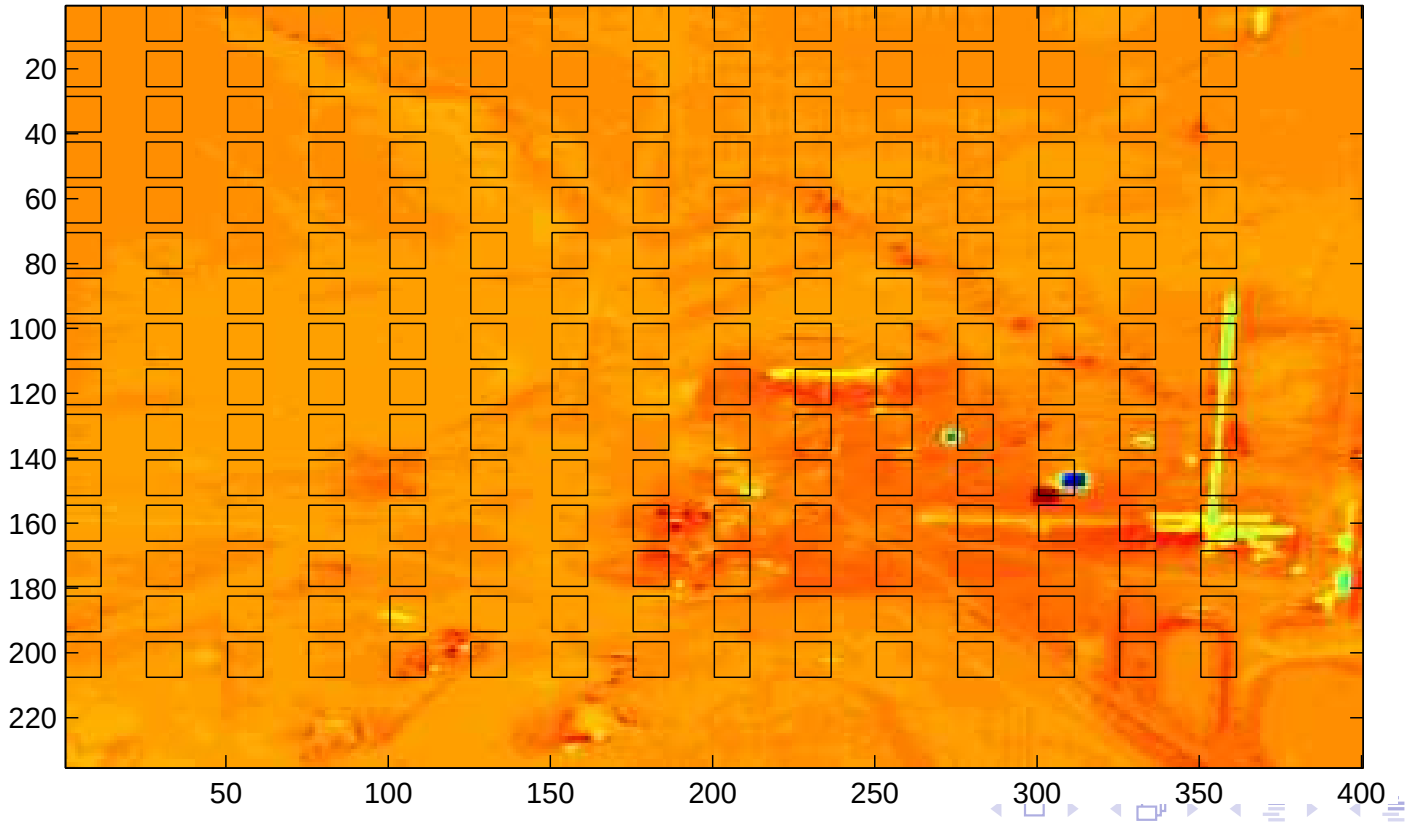

Non-stationary Based Separation Example

ICA (PC 50)

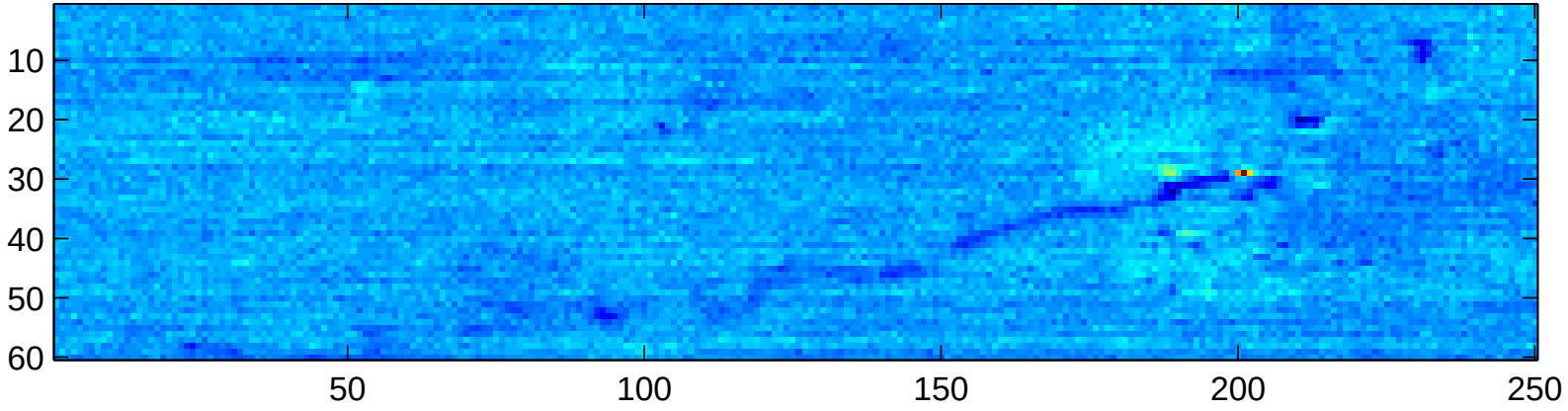

MF (PC 50)

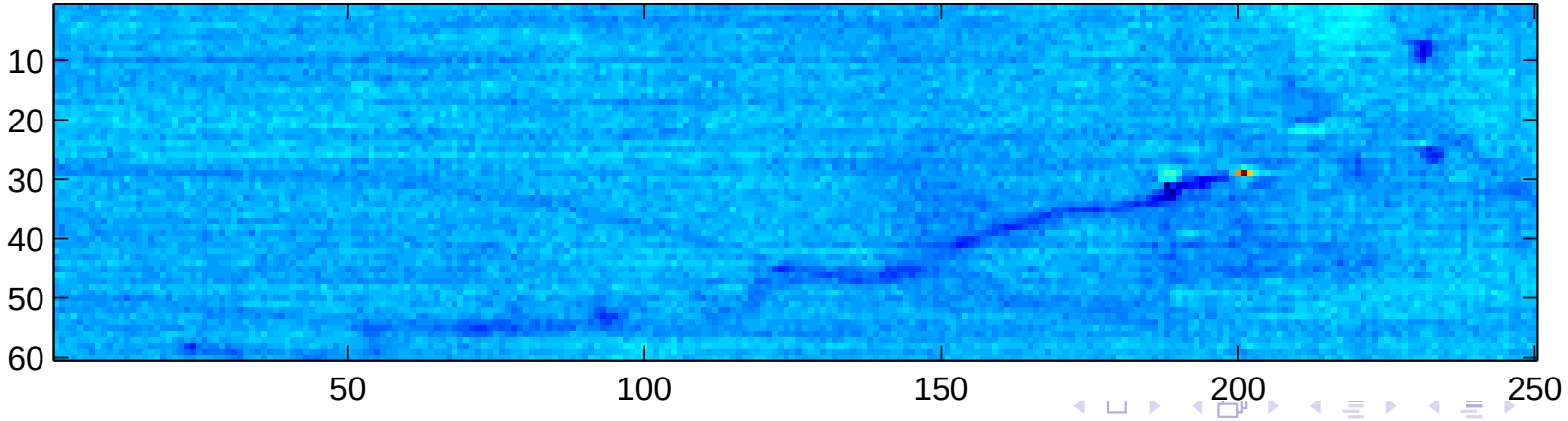

Exploiting Local Correlation Structure

- Let $t = t_0$ and choose $\tau \in \{\tau_1, \tau_2, \cdots, \tau_P\}$, then jointly diagonalize $\mathbf{R_y}(t_0, \tau_1), \mathbf{R_y}(t_0, \tau_2), \cdots, \mathbf{R_y}(t_0, \tau_P)$
- Materials are spatially locally correlated
- If a material is present in a given location, then the same material may also be found close by
- Signals can be uniformly distributed or sparse
- Currently developing an algorithm to jointly diagonalize a set of non-symmetric, indefinite matrices

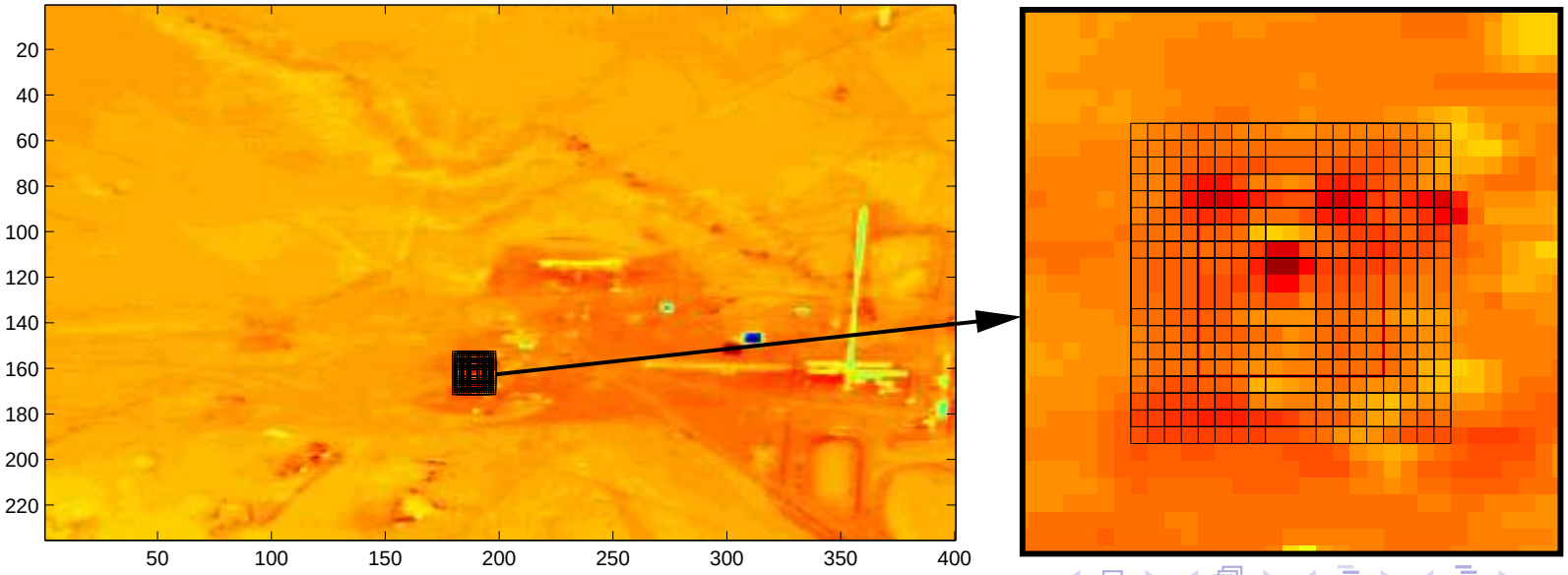

Exploiting Sparsity

$$y(t) = \mathbf{w}^T \mathbf{x}(t)$$

$$\mathbf{w}' = \mathbf{w} - \mu \frac{\partial}{\partial \mathbf{w}} \varphi(y(t)), \qquad \mathbf{w} \leftarrow \frac{\mathbf{w}}{\|\mathbf{w}\|}$$

φ

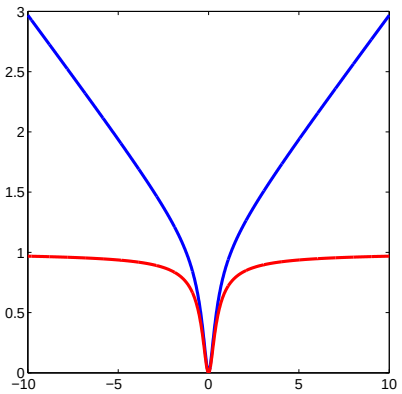

- Gradient descent
- Initialized with matched filter
- Smoothed with non-local mean
- Thresholded to enhance contrast

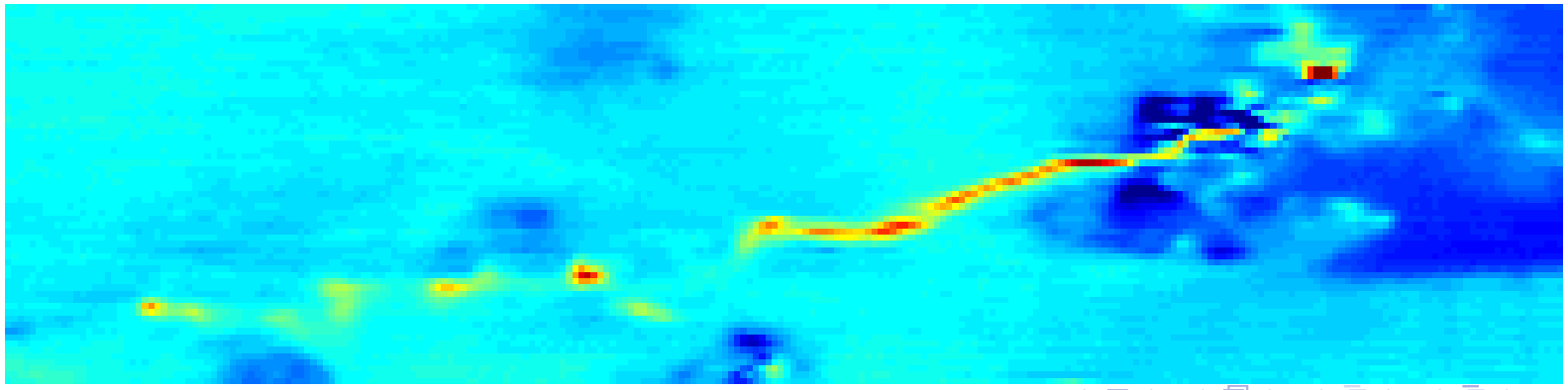

Likelihood Function

- It is assumed that a library of reference spectra is available

$$\mathbf{S} = \begin{bmatrix} \mathbf{s}_1 & \mathbf{s}_2 & \cdots & \mathbf{s}_M \end{bmatrix} \in \mathbb{R}^{L \times M}$$

- Assumed, for a starting point, a linear mixing model: $\mathbf{x}_t = \mathbf{S}\mathbf{a}_t + \boldsymbol{\nu}_t$
- The noise, $\boldsymbol{\nu}$, is assumed to be Gaussian with mean 0 and covariance $\sigma_n^2 I$
- The likelihood of a measured pixel is

$$p(\mathbf{x}_t | \mathbf{a}_t) = \mathcal{N}(\mathbf{x}_t; \mathbf{S}\mathbf{a}_t, \sigma_n^2 I)$$

Bayesian Framework

- **Neighborhood model:** $p(\mathbf{a}_t|\{\mathbf{a}_{t'}, t' \in \text{nbd}(t)\})$ denotes the information pixels in the neighborhood of t provide about $\mathbf{a}_t$
- **Image formation model:** Given $\mathbf{a}_t$, $\mathbf{x}_t$ is independent of $\{\mathbf{a}_{t'}, t' \in \text{nbd}(t)\}$, $\quad p_{\mathbf{x}}(\mathbf{x}_t|\mathbf{a}_t, \{\mathbf{a}_{t'}, t' \in \text{nbd}(t)\}) = p(\mathbf{x}_t|\mathbf{a}_t)$
- These assumptions imply that

$$p(\mathbf{x}_t, \mathbf{a}_t|\{\mathbf{a}_{t'}, t' \in \text{nbd}(t)\}) = p_{\mathbf{x}}(\mathbf{x}_t|\mathbf{a}_t)p(\mathbf{a}_t|\{\mathbf{a}_{t'}, t' \in \text{nbd}(t)\})$$

- **Bayes rule:**

$$p(\mathbf{a}_t|\mathbf{x}_t, \{\mathbf{a}_{t'}, t' \in \text{nbd}(t)\}) = \frac{p_{\mathbf{x}}(\mathbf{x}_t|\mathbf{a}_t)p(\mathbf{a}_t|\{\mathbf{a}_{t'}, t' \in \text{nbd}(t)\})}{\int p(\mathbf{x}_t, \mathbf{a}|\{\mathbf{a}_{t'}, t' \in \text{nbd}(t)\})d\mathbf{a}}$$

- **MMSE estimate:** can be obtained as

$$\hat{\mathbf{a}}_t = E[\mathbf{a}_t|\mathbf{x}_t, \{\mathbf{a}_{t'}, t' \in \text{nbd}(t)\}]$$

Markov Random Field—A General Model

- A general predictive model, M, can be defined such that

$$\mathbf{a}_t = M(\{\mathbf{a}_{t'}, t' \in \text{nbd}(t)\}, \mathbf{c}) + \boldsymbol{\nu}(t)$$

  where $\mathbf{c}$ is a vector of model parameters and $\boldsymbol{\nu}(t)$ represents model noise

- One example is a linear predictive model:

$$\mathbf{a}_t = \sum_{t' \in \text{nbd}(t)} c_{t'} \mathbf{a}_{t'} + \boldsymbol{\nu}(t)$$

- From this model an energy function can be formulated as

$$E(\mathbf{a}; J) = \sum_t J_t \left| \mathbf{a}_t - M(\{\mathbf{a}_{t'}, t' \in \text{nbd}(t)\}) \right|^2$$

Markov Random Field—A Smoothing Model

- Using a model for smoothing, the dependence among the variables in $\mathbf{a}_\rho$ is given by the energy function

$$E(\mathbf{a}_\rho; J) = \frac{1}{2} \sum_{t,t'} J_{t,t'} (a_{\rho,t} - a_{\rho,t'})^2$$

  where $J_{t,t'}$ is called the connection weight
- One approach is to let

$$J_{t,t'} = \begin{cases} J > 0 & t \text{ and } t' \text{ are in the same neighborhood} \\ 0 & \text{otherwise} \end{cases}$$

- From this energy function, a probability density is formed as

$$p(\mathbf{a}_\rho) = \frac{\exp\left[-\beta E(\mathbf{a}_\rho; J)\right]}{Z(\beta, J)}$$

  where

$$Z(\beta, J) = \int_{\mathbb{R}^T} \exp\left[-\beta E(\mathbf{a}; J)\right] d^T \mathbf{a}$$

Results—Testing Setup

- To demonstrate the validity of the Bayesian framework, initial testing was performed using an artificial $100 \times 100 \times 10$ data cube.
- An artificial 10×5 library, S, was also created
- The image has a uniform background and a single ellipsoidal region with abundances

$$\mathbf{a}_{\text{background}} = \begin{bmatrix} 0.51 \\ 0.22 \\ 0.94 \\ -1.6 \\ 0.80 \end{bmatrix} \qquad \mathbf{a}_{\text{blob}} = \begin{bmatrix} 1.5 \\ 0.18 \\ 1.16 \\ 0.16 \\ -0.96 \end{bmatrix}$$

- Added noise with $\sigma_n^2 = 1$

Results—Simple Neighborhoods

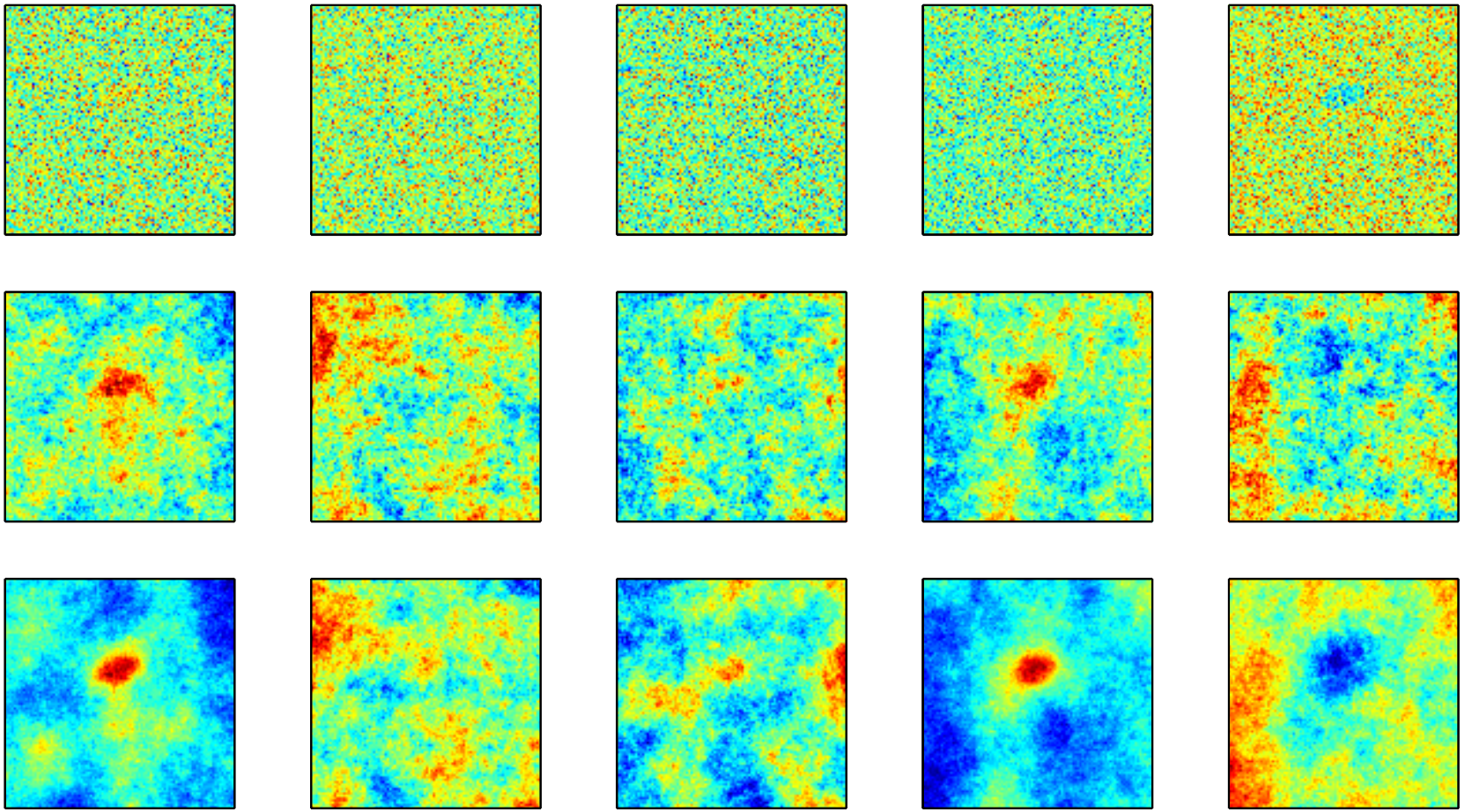

Results—Simple Neighborhoods

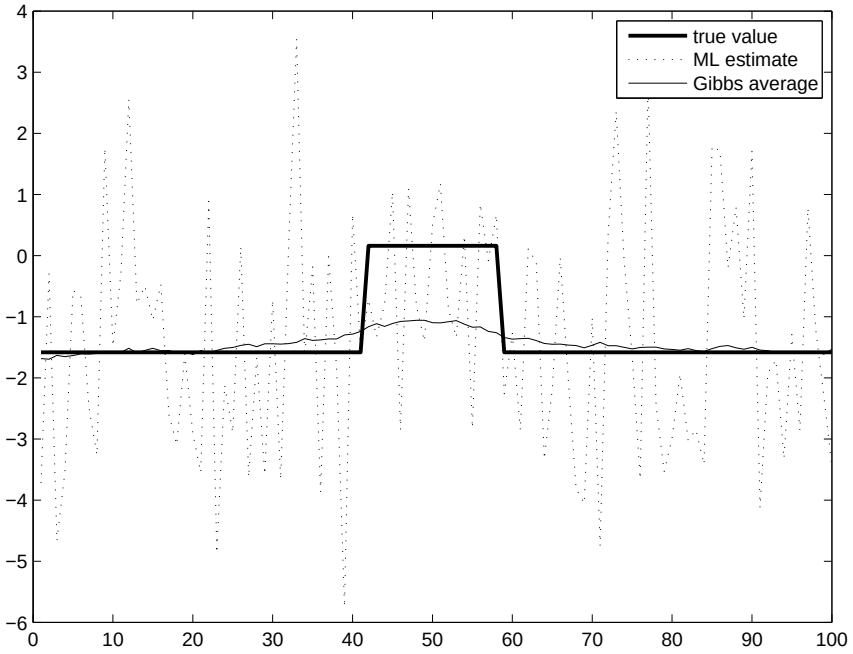

- noise is suppressed
- blob region is enhanced
- edges are blurred

Modifying Neighborhoods

- To allow for sharper transitions in the abundance images, more effort was put into improving the contribution of the prior
- Before each iteration of the Gibbs sampling the abundance images from the previous iteration were partitioned into two regions
- The partitioning was accomplished using a simple cost function:

$$R_t = \|\mathbf{m}(W_{t,r}) - \mathbf{m}_{\mathrm{bg}}\|$$

- Simple neighborhoods were restricted to those pixels that were in the same class as the pixel being considered

Results—Modified Neighborhoods

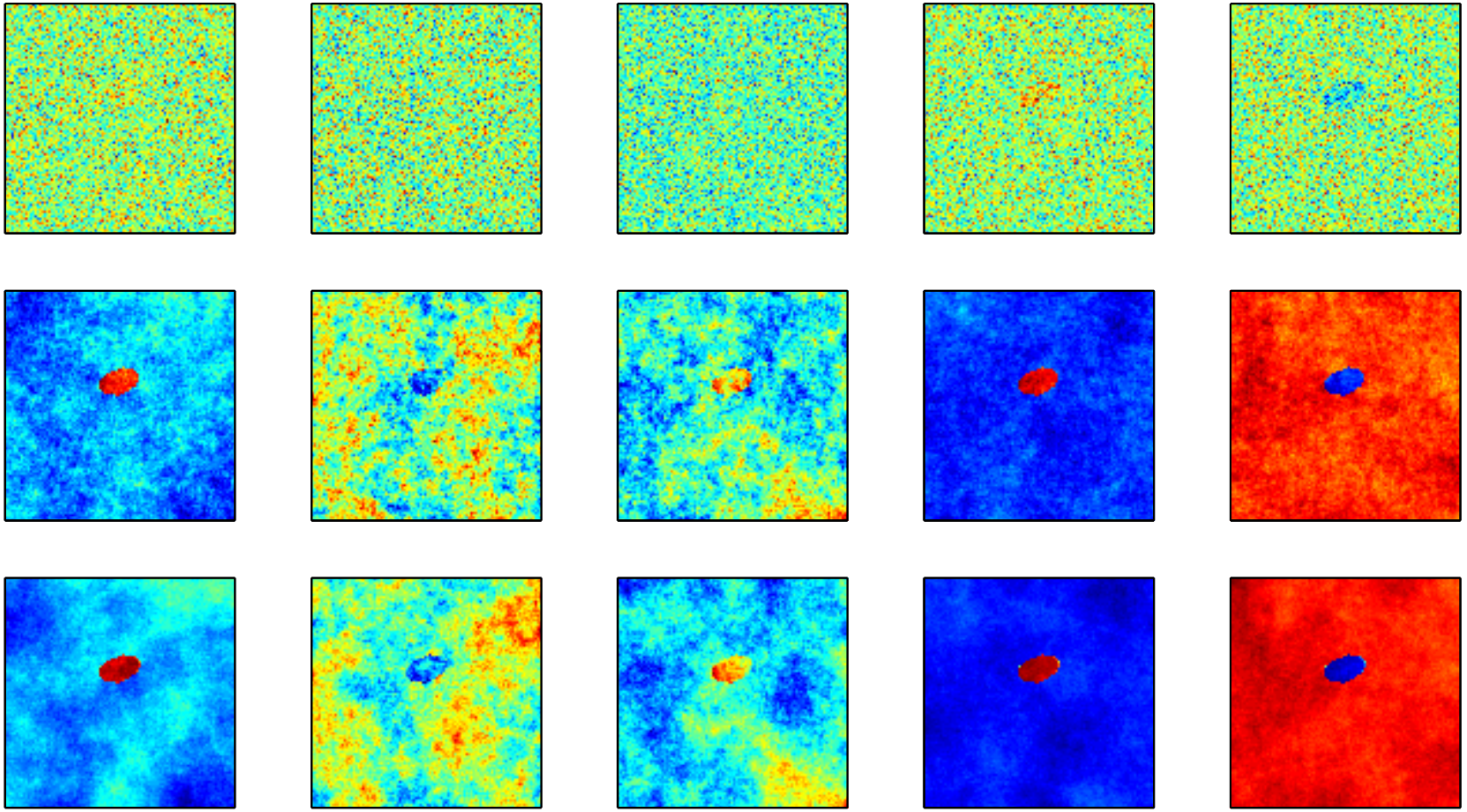

Results—Modified Neighborhoods

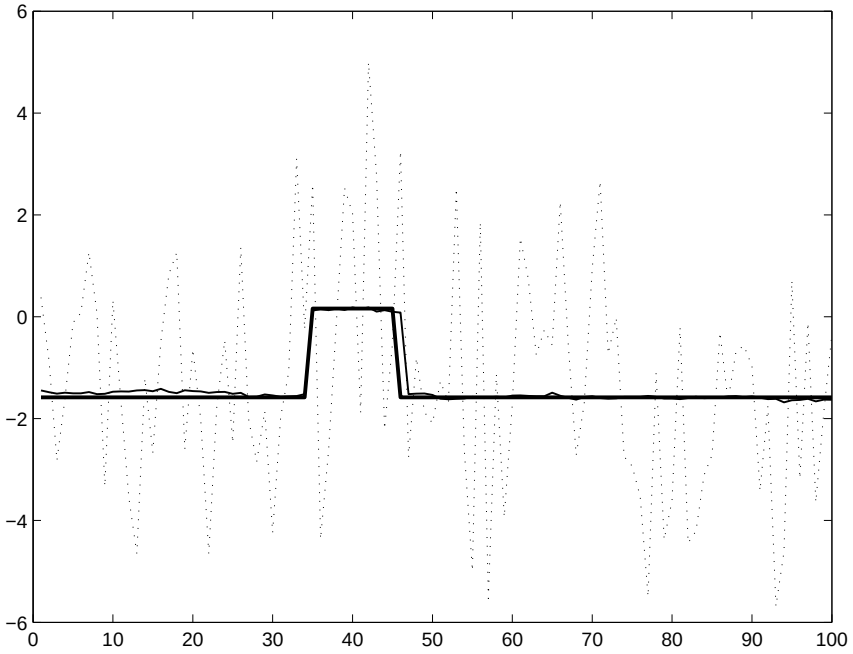

- noise suppression is still very good
- blob enhancement is more dramatic
- edges are sharper

Results on Real Data

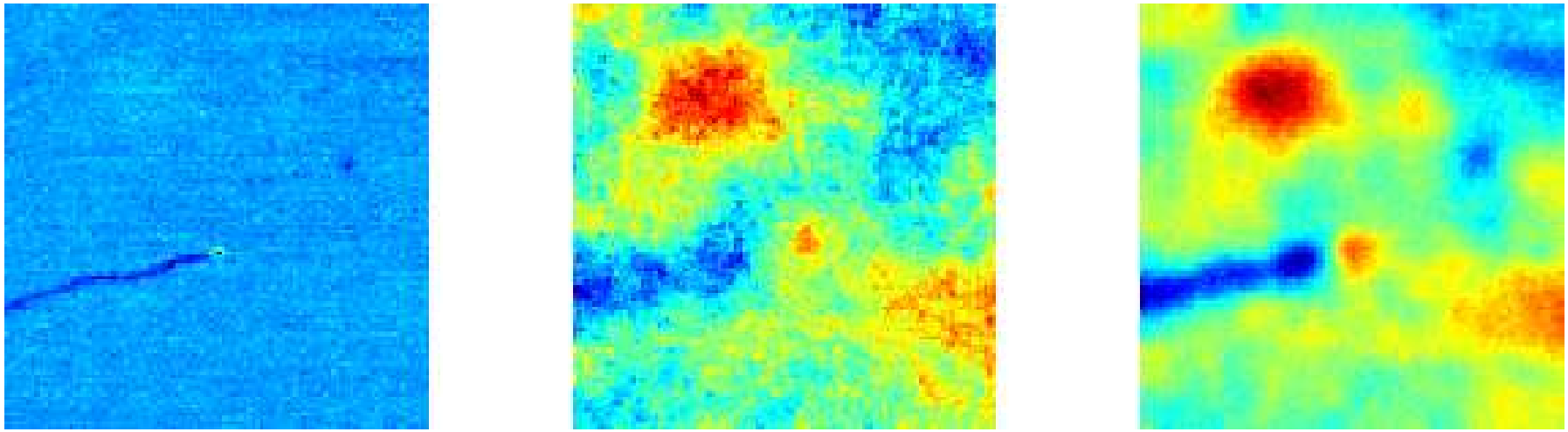

- Matched filter (left)
- Quasi-Bayes, 1 iteration (middle)
- Quasi-Bayes, average of 5 iterations (right)

Future Work

- Incorporate advection and diffusion into prior model in Bayesian formulation.
- Plumelets and sparse reconstruction, plumelet transformation.
- Explore alternative data models. How accurate is the linear mixing model?
- Processing using non-local means.

Project title: **Image Recognition and Classification Based on Object Parts**

PI: Longin Jan Latecki (Temple Univ.)

Co-PI: Rolf Lakaemper (Temple Univ.)
Co-PI: Zygmunt Pizlo (Purdue Univ.)

Budget: $360,000

Duration: 3 years

	Milestones and Deliverables
Phase 1: Year 1	D1, D2 with a static shape space, and D1.1, D2.1
Phase 2: Year 2	D3 and D1, D2 with a dynamic shape space, and D3.1
Phase 3: Year 3	D4, D5 and a final project report

1. Grouping of line segments to contour parts

   D1. Software **D1.1.** Rules of perceptual grouping

2. Grouping evaluation with particle filters

   D2. Software **D2.1.** Shape related grouping constraints

3. Shape familiarity (database of familiar parts)

   D3. Software **D3.1.** Perceptually based shape similarity metric

4. Recognition of 2D objects based on shape and texture of parts

   D4. Software

5. Reconstruction and recognition of 3D objects

   D5. Software

Project overview and goals

We have completed the work on

1. Grouping of line segments to contour parts.
2. Grouping evaluation with particle filters

It will be presented in part 1 of the technical presentation.
Part 2 of the technical presentation will also present

4. Recognition of 2D objects based on shape and texture of parts (symmetry recognition)
5. Reconstruction of 3D objects

Project overview and goals

We are currently working on

3. Shape familiarity (database of familiar parts)

   D3. Software **D3.1.** Perceptually based shape similarity metric

4. Recognition of 2D objects based on shape and texture of parts

5. Recognition of 3D objects; detection of 3D symmetries

   D5. Software

Technical presentation, part 1: Contour Grouping Based on Local Symmetry

Object recognition process:

Source:
2D image of a 3D object

Object Segmentation

Contour Extraction

Contour Cleaning, e.g., Evolution

Contour Segmentation

Matching: Correspondence of Visual Parts

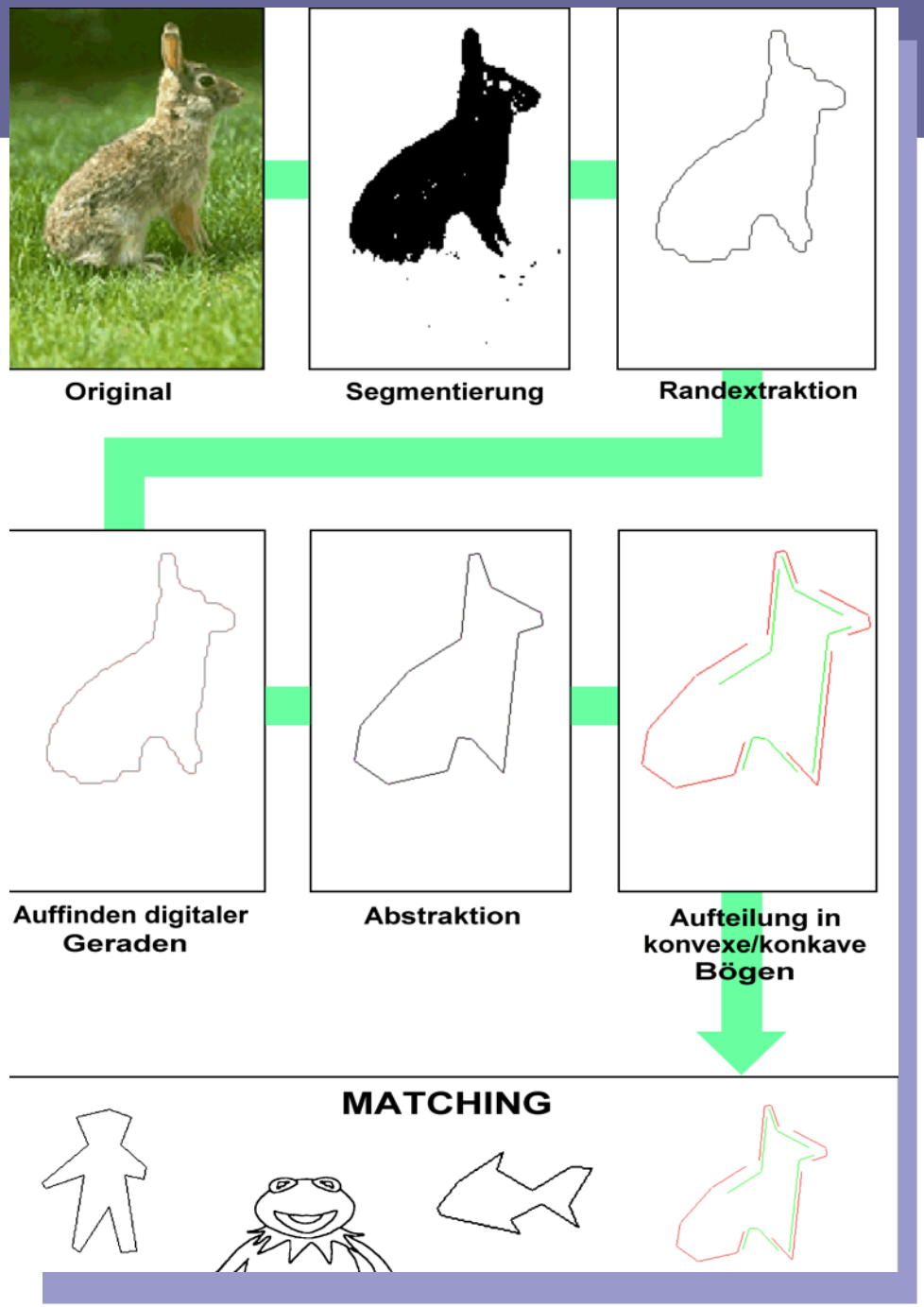

How to find contours in images?

In an edge image, here is uncertainty:
which contour parts belong together to form a contour?
Our approach is to use probabilistic grouping
based on local symmetry.

Skeletons capture local symmetry in all planar shapes

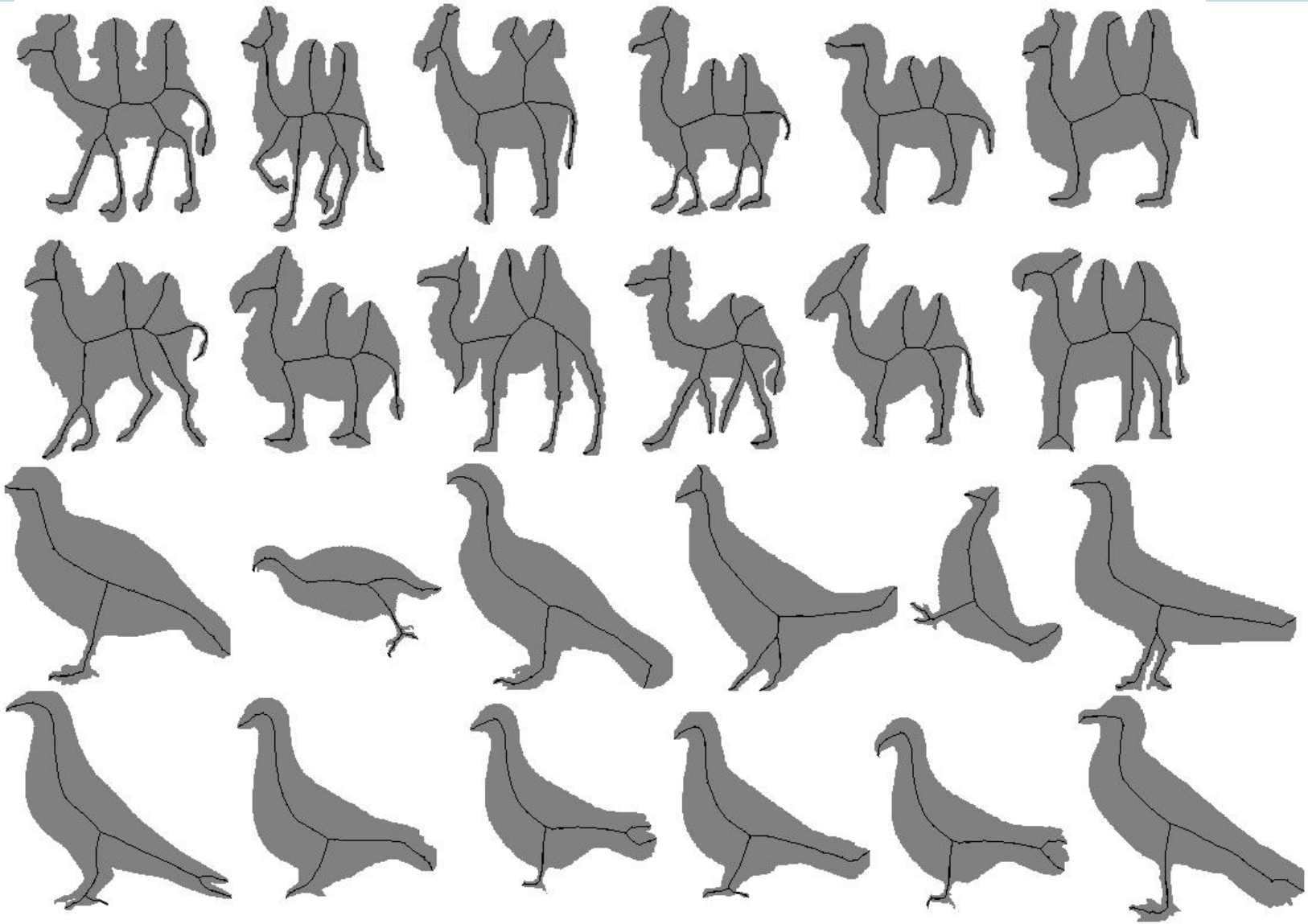

Algorithmic flow

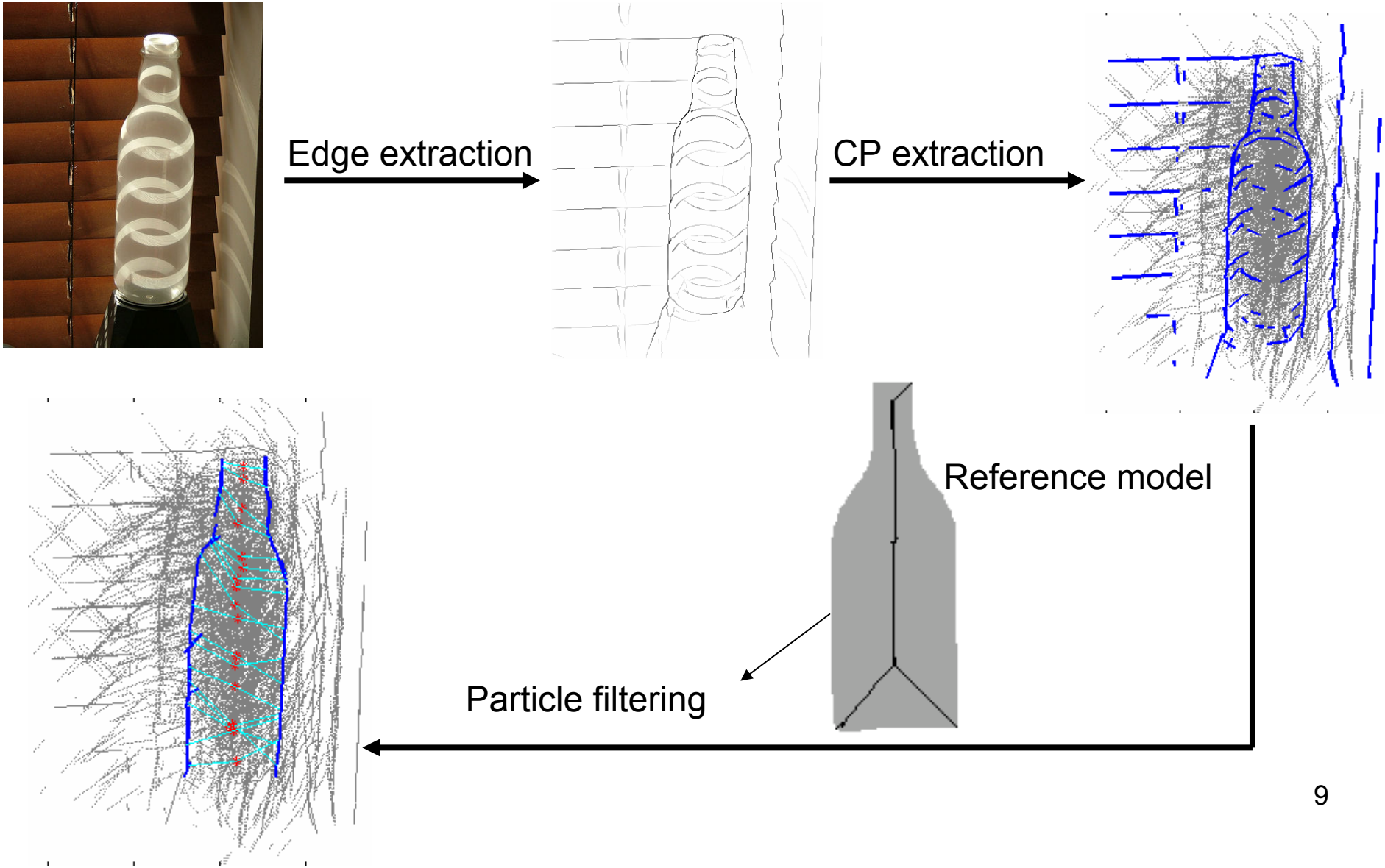

What does contour grouping have to do with robotics?

- Very similar to map-acquisition problem in robotics.
- Hence we formulate contour grouping as map-acquisition of a virtual robot.
- The virtual robot walks around “acquiring the contour”.

Contour acquisition using virtual robot

- The virtual robot walks along “center points” constructed from segments on edge image.
- The contour is a sequence of segment-pairs associated with the center points on the edge image.
- A reference shape model guides the robot’s motion and gives sensor information of what to look for.

Reference shape model

- Contour grouping has been a low-level vision problem.
- By using a reference model, we cast it as a high-level vision problem.
- Our reference model is based on skeletal paths. Each path is a sequence of skeleton points and the associated radii of the maximal discs.

Sensor information from reference model

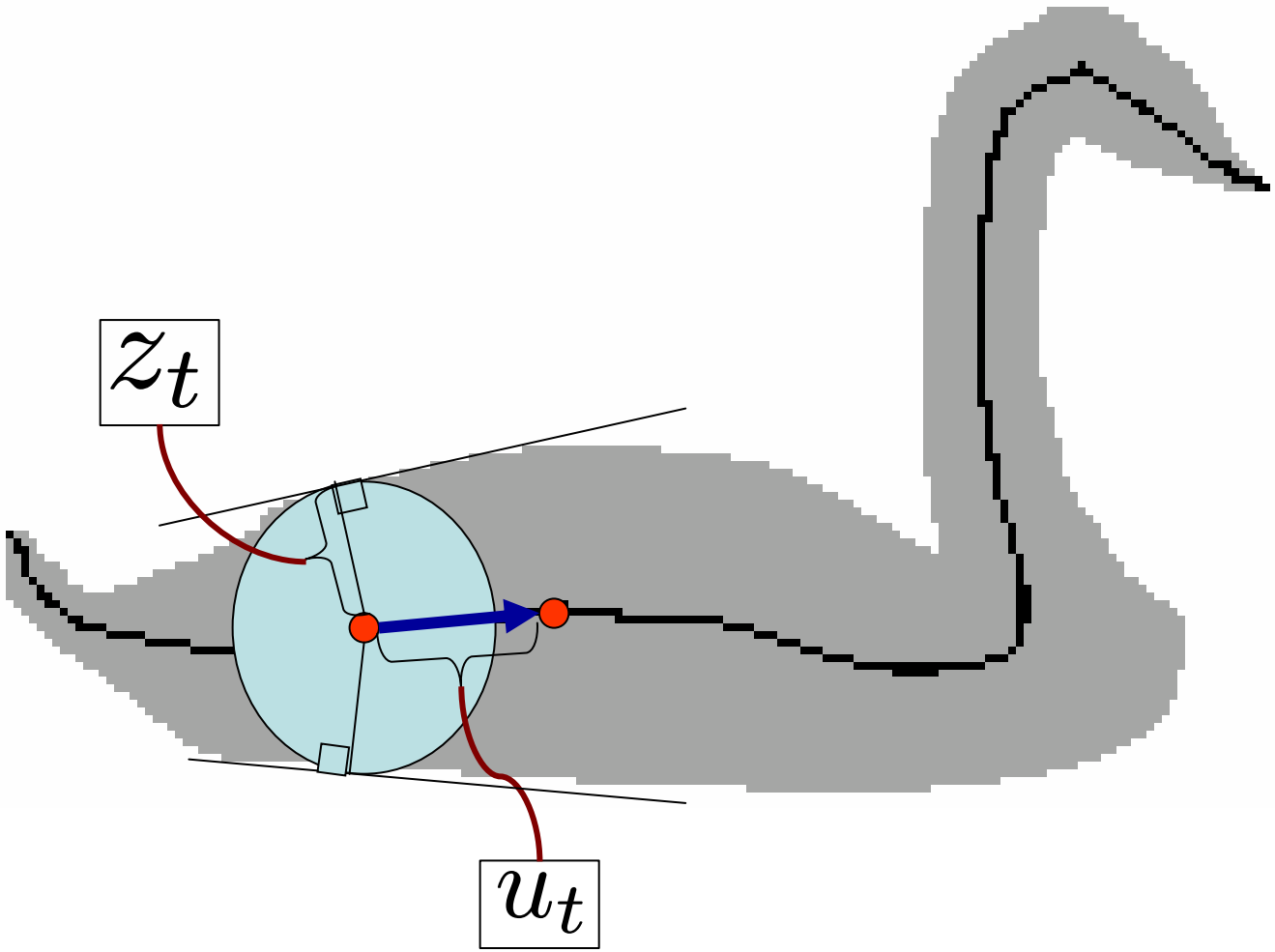

Probabilistic map/contour acquisition

- Map acquisition problem is called SLAM in robotics community.
- Any solution to that problem *has* to deal with uncertainties in sensor information.
- Rao-Blackwellized particle filtering has been successfully applied for the problem in practice.
- Hence we adopt that approach for contour grouping.

Formal definition of the problem

- We estimate the posterior:

$$p(x_{1:t}, m_t | z_{1:t}, u_{1:t})$$

- Where
  - $x_{1:t}$ is the trajectory of the robot.
  - m_t is the contour grouped.
  - $z_{1:t}$ is the sequence of observations.
  - $u_{1:t}$ is the sequence of motion control.

Rao-Blackwellized Sampling Importance Resampling (SIR) particle filter

- The posterior is estimated *sequentially* using a particle filter.
- Rao-Blackwellization allows the following factorization by conditional independence:

$$\boxed{p(x_{1:t}, m_t | z_{1:t}, u_{1:t}) = p(x_{1:t} | z_{1:t}, u_{1:t}) p(m_t | x_{1:t}, z_{1:t})}$$

- The SIR has four main steps
  1. Sampling
  2. Imortance weighting
  3. Resampling
  4. Contour estimating

Sampling (from proposal) (1)

- A new set of poses $\{x_t\}$ is sampled from a proposal distribution $\pi(x_{1:t}|z_{1:t}, u_{1:t})$ which is assumed to satisfy the following recursion:

$$\pi(x_{1:t}|z_{1:t}, u_{1:t}) = \pi(x_t|x_{1:t-1}, z_{1:t}, u_{1:t})\pi(x_{1:t-1}|z_{1:t-1}, u_{1:t-1})$$

- Therefore the new set of sampled trajectories is: $x_{1:t} =< x_t, x_{1:t-1} >$.
- A follower pose is sampled for each particle.

Sampling (from proposal) (2)

- The choice of π is a very crucial design issue and usually depends on the application.
- Since we use a weak reference model, we use "prior boosting" i.e. sample many followers for each particle.
- We choose a simple proposal based on the motion control i.e. $p(x_t|x_{t-1}, u_t)$.
- Since we sample a lot of followers, before evaluating the particles we cull obviously bad particles by restricting huge jumps and those that do not extend the contour.

Importance weighting (particle evaluation) (1) Basics

- The new particles $\{x_{1:t}\}$ are assigned the following importance weights:

$$\boxed{w_t(x_{1:t}) = \frac{p(x_{1:t}|z_{1:t},u_{1:t})}{\pi(x_{1:t}|z_{1:t},u_{1:t})}}$$

- Using Bayes rule, Markov assumption and observational independence the weights can be recursively estimated as:

$$w_t = w_{t-1}\frac{p(z_t|x_t,m_{t-1})\boxed{p(x_t|x_{t-1},u_t)}}{\boxed{p(x_t|x_{t-1},z_{1:t},u_{1:t})}}$$

- Using the motion-based proposal the weights can be recursively estimated as

$$\boxed{w_t = w_{t-1}p(z_t|x_t,m_{t-1})}$$

Importance weighting (particle evaluation) (2) Likelihood computation

$$p(z_t|x_t, m_{t-1}) = M(\hat{z}_t)C(m_{loc}, m_{t-1})$$

- where
  - $\hat{z}_t$ is the radius of the center point.
  - z_t is the expected radius given by the shape model.
  - $M(\hat{z}_t) = \mathcal{N}(z_t - \hat{z}_t, 0, \sigma_M)$measures how well the extension fits the reference model.
  - The weaker the reference model the larger σ_M is.
  - m_{loc} is the segment-pair intending x_t.
  - $C(m_{loc}, m_{t-1})$ measures local smoothness.

Importance weighting (particle evaluation)
(2) An example of $M(\hat{z}_t)$ with $z_t = 10$

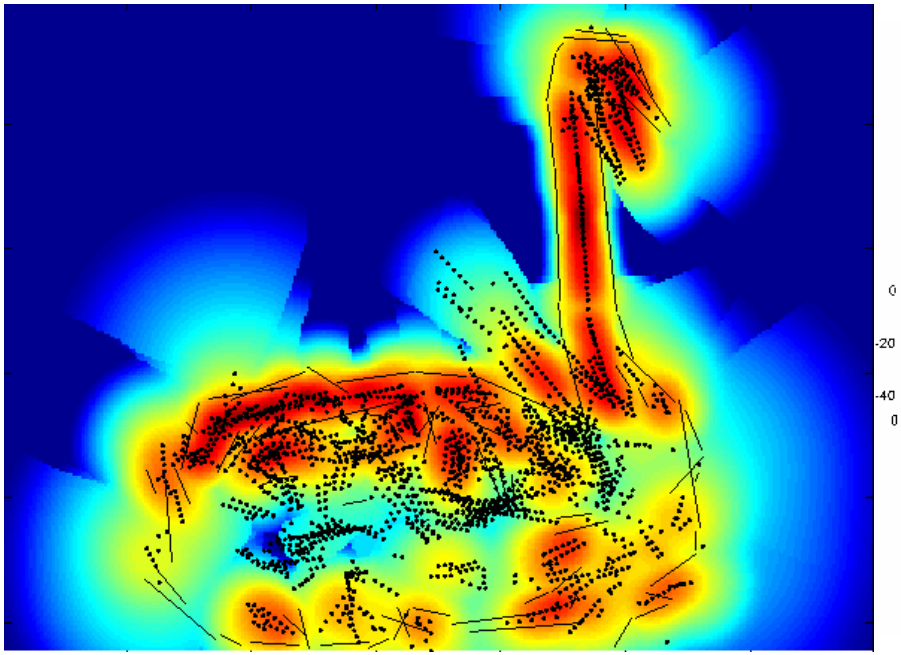

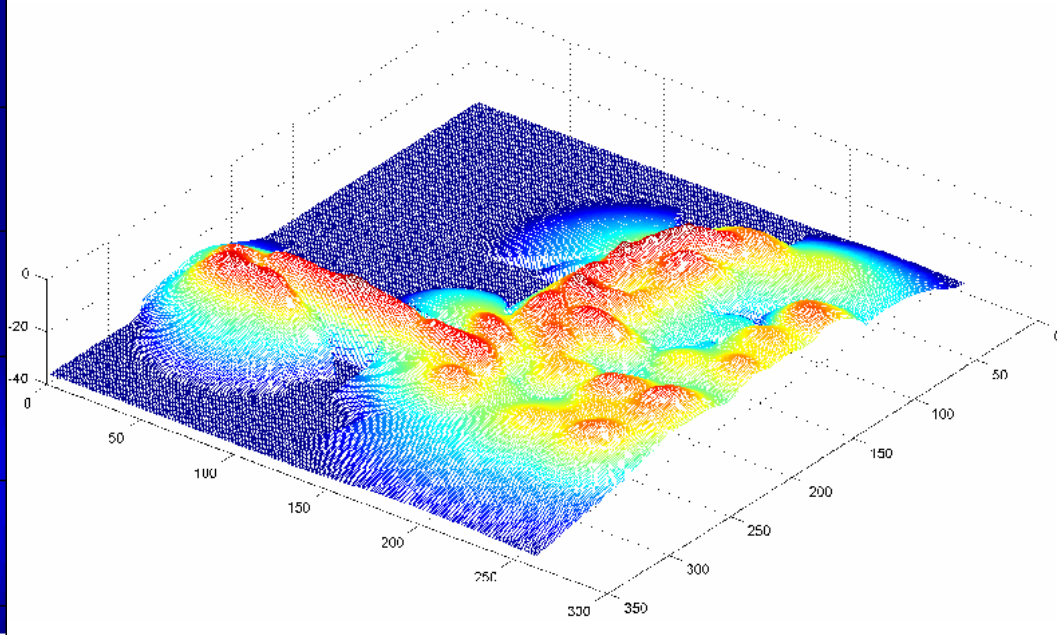

Example set of center points

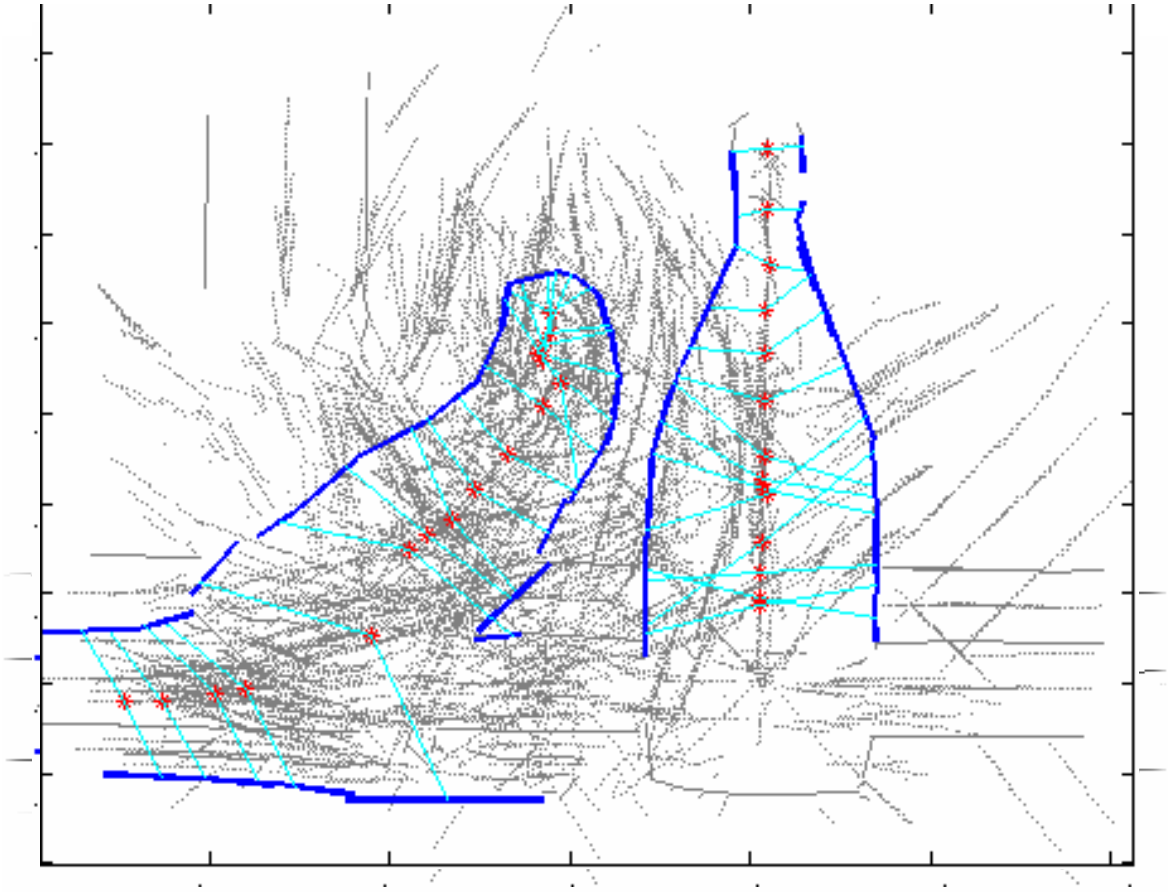

Sample evolution of particles

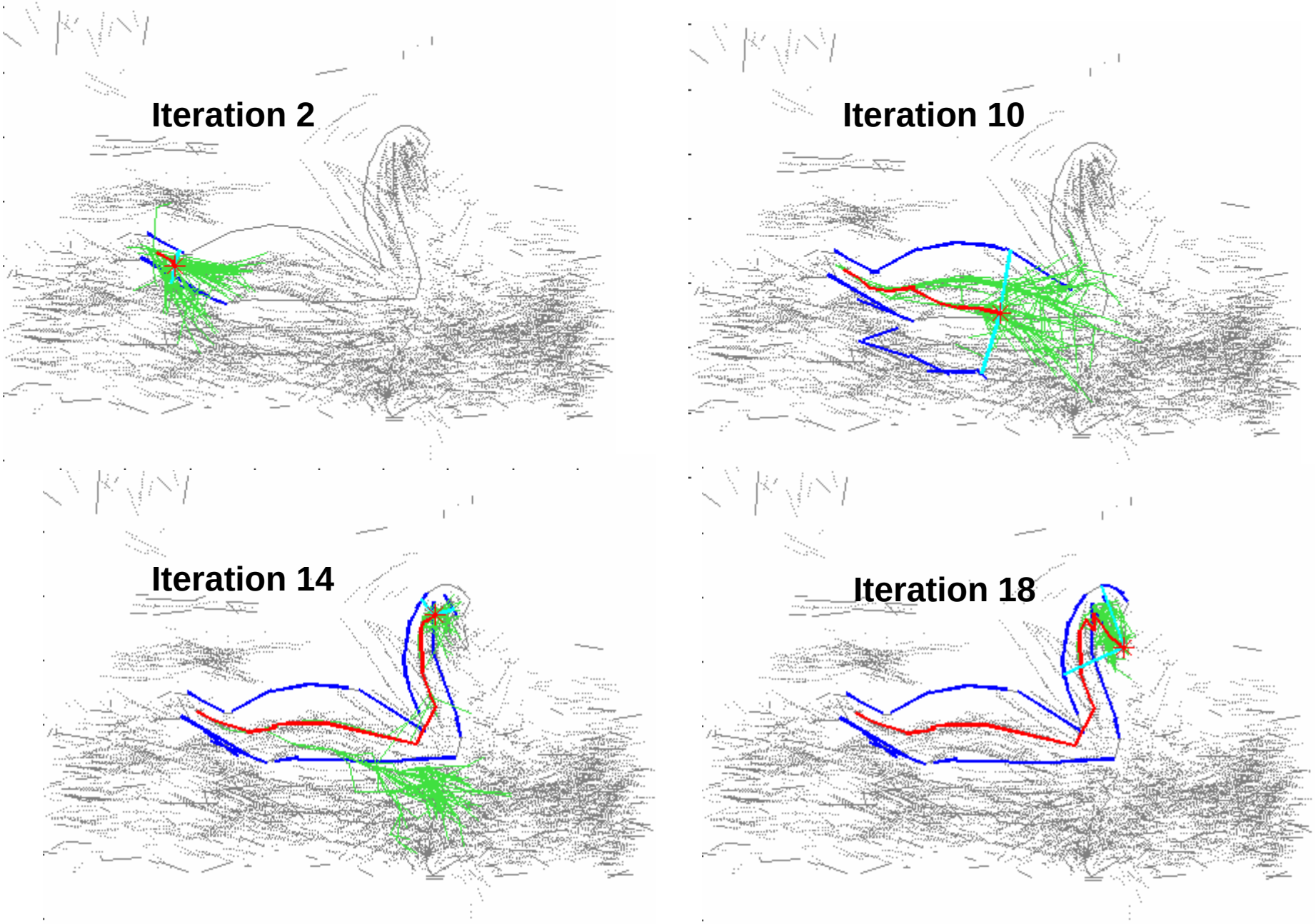

Experimental results
Reference models

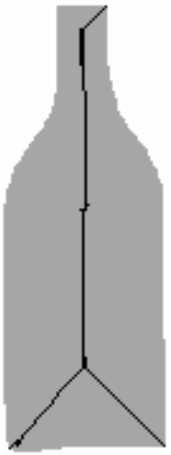

Bottle model

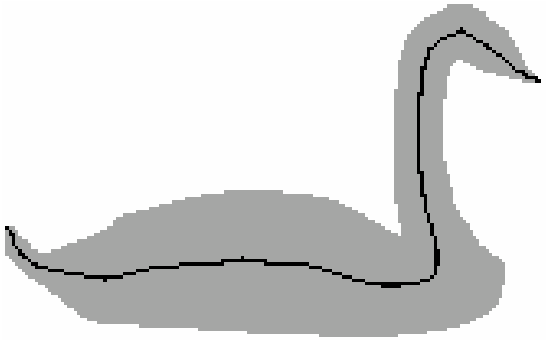

Swan model

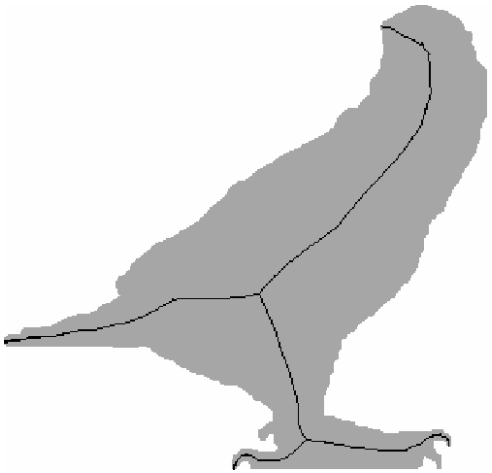

Bird model

Experimental results
Grouping

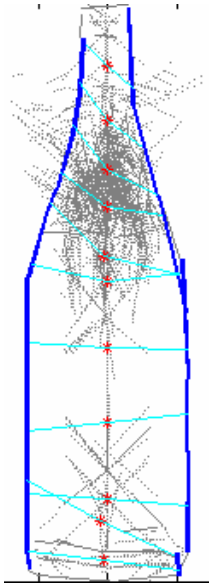

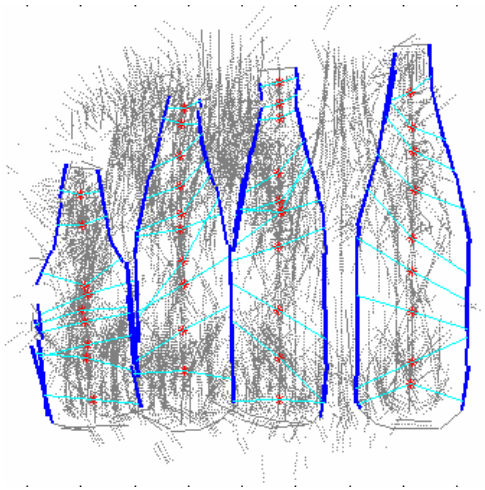

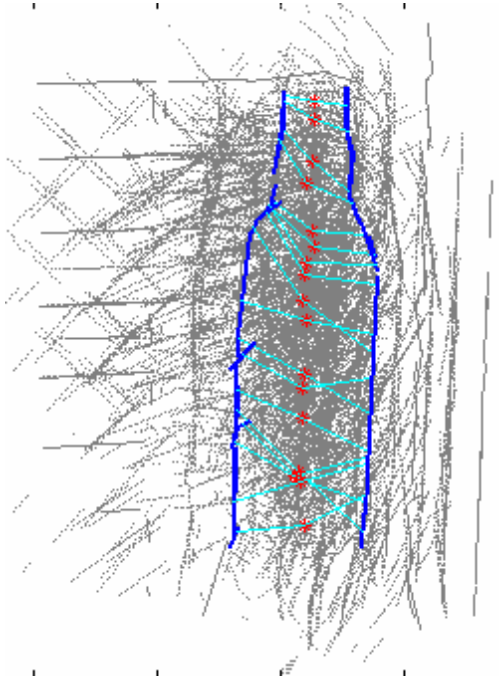


Arbor Mist
© Tom Philo
www.taphilo.com

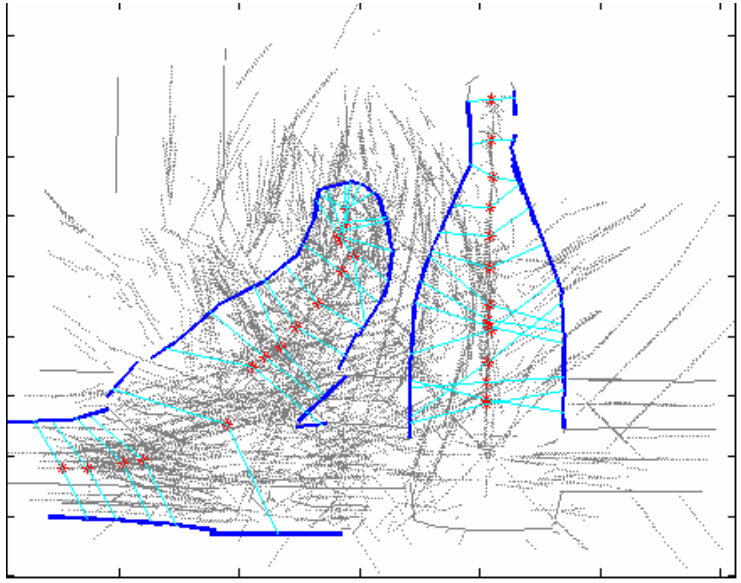

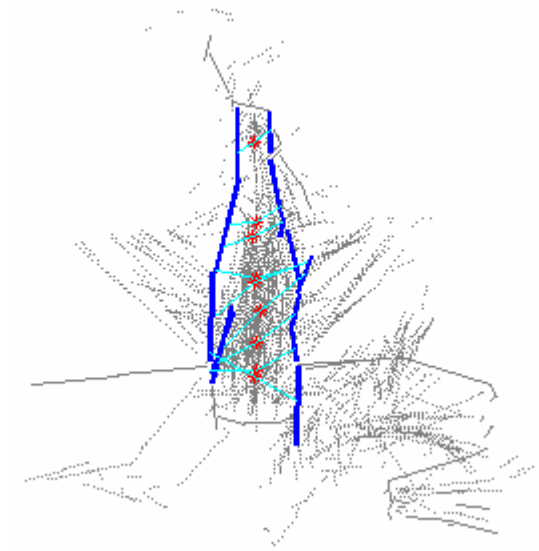


PALE

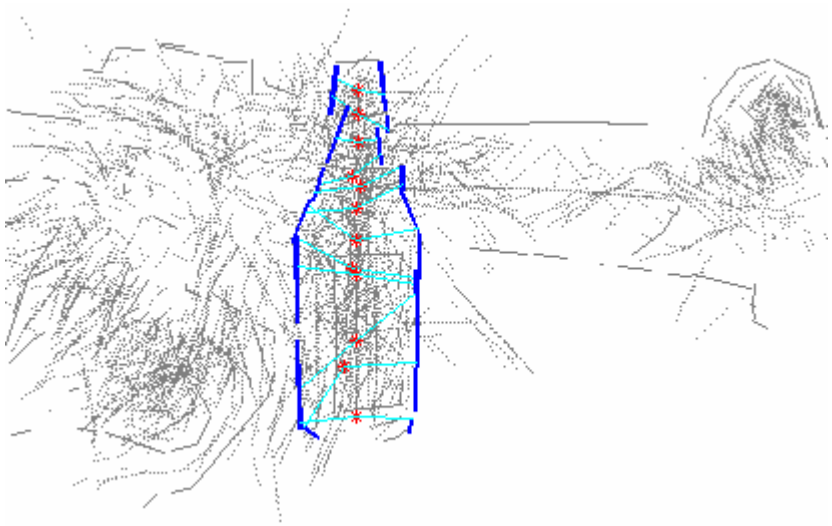

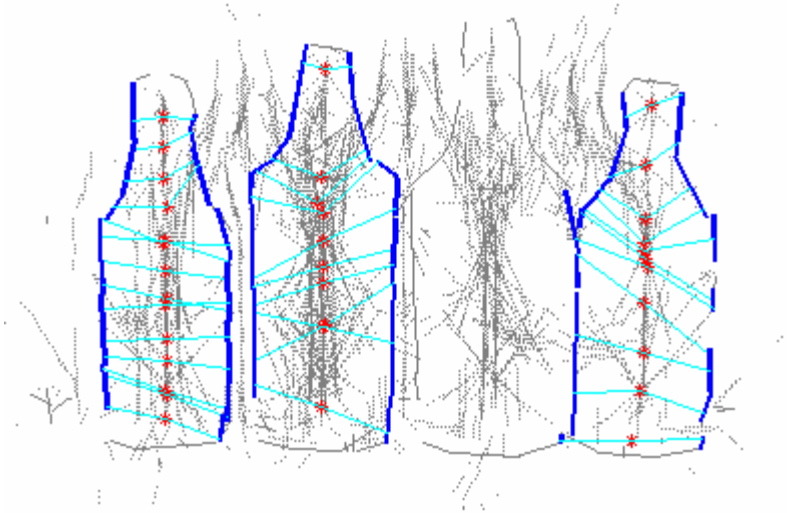


Sanginvere

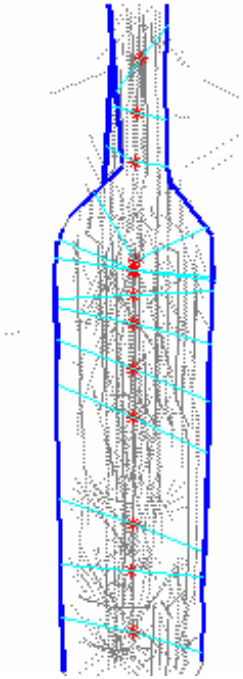


©Silvia Ganora

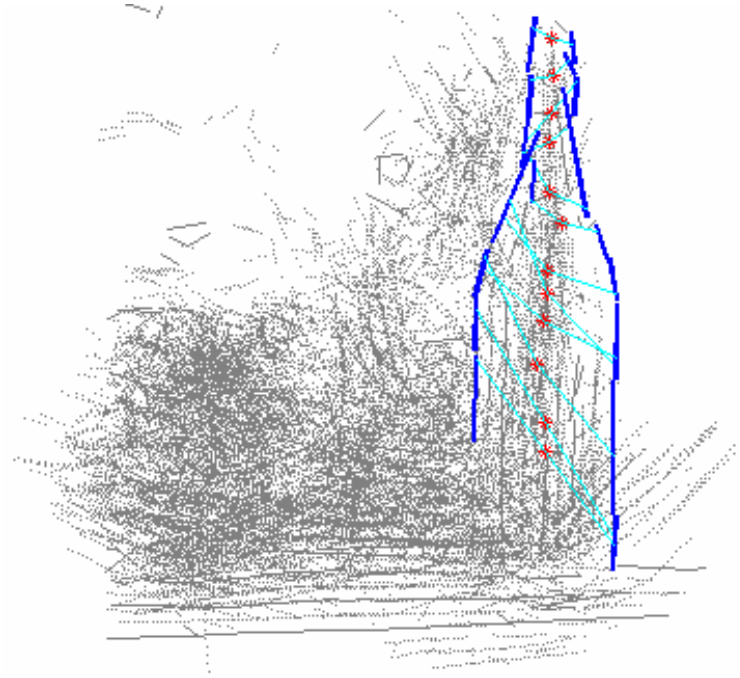

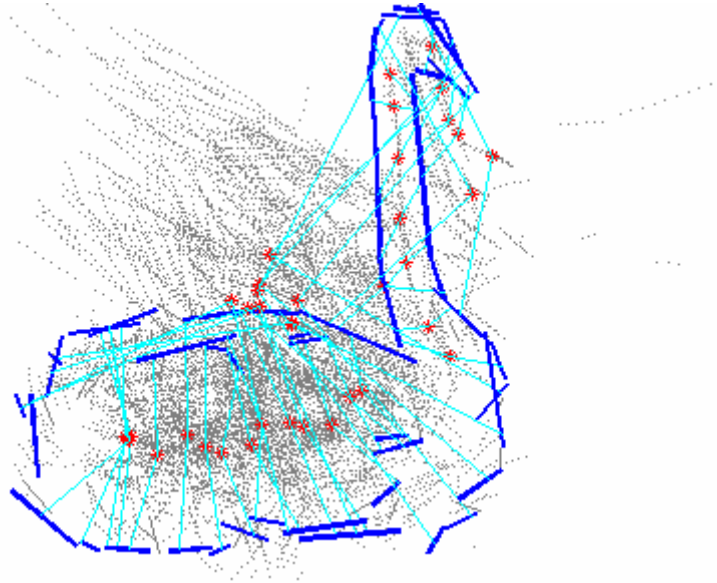

Experimental results

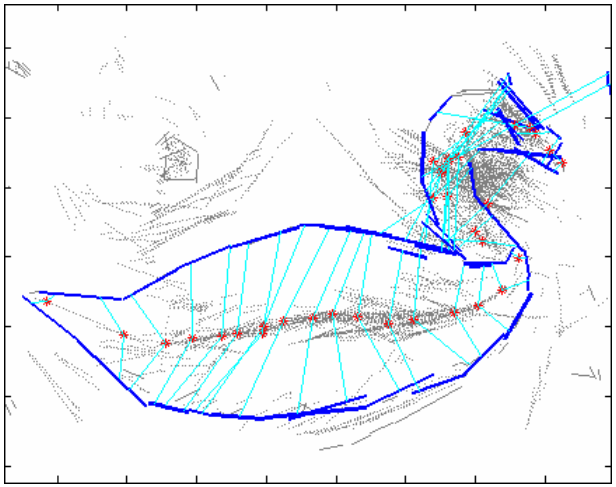

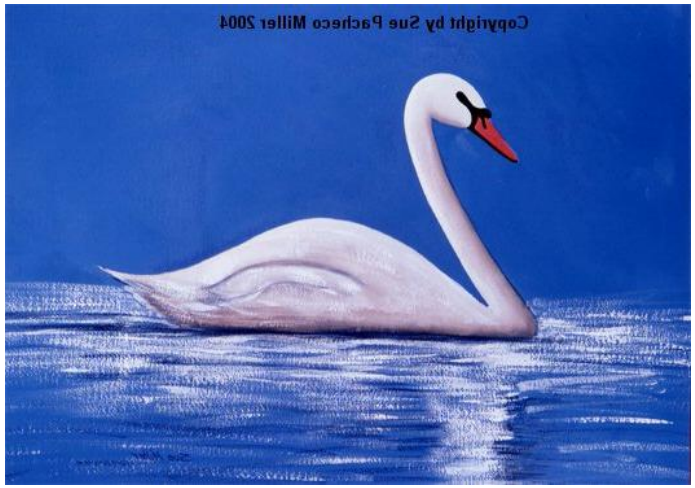

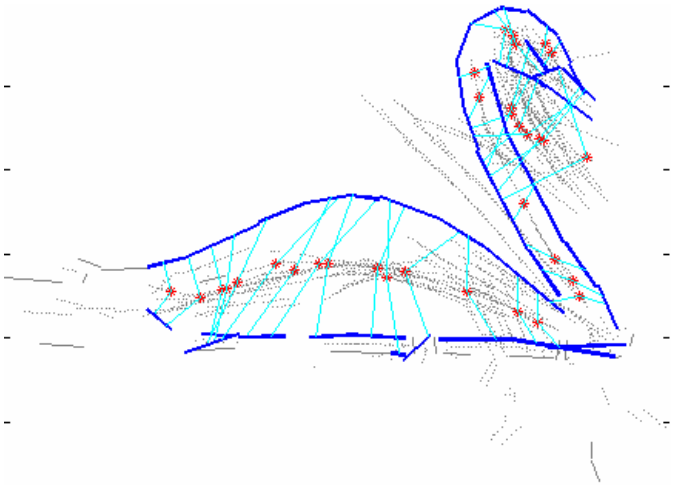

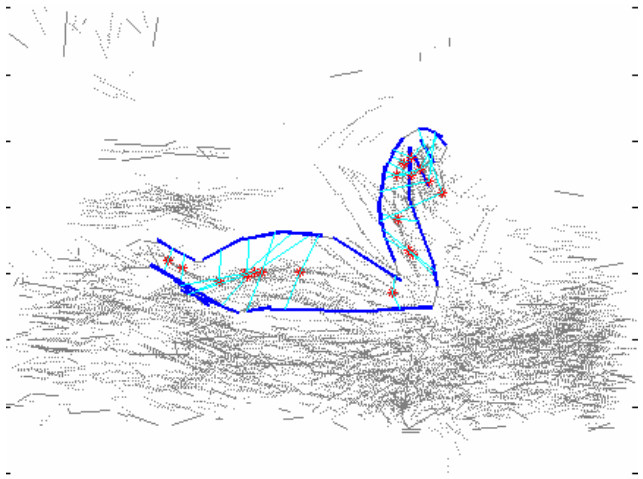

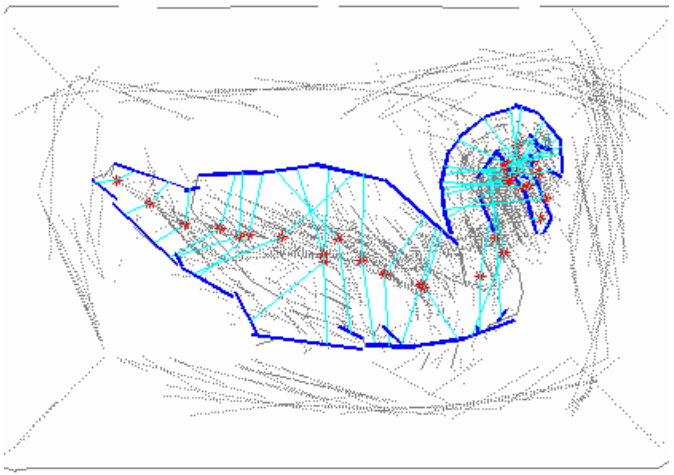

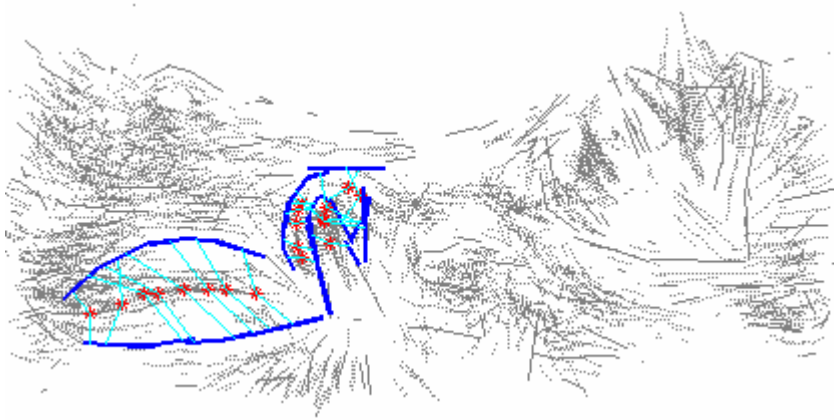

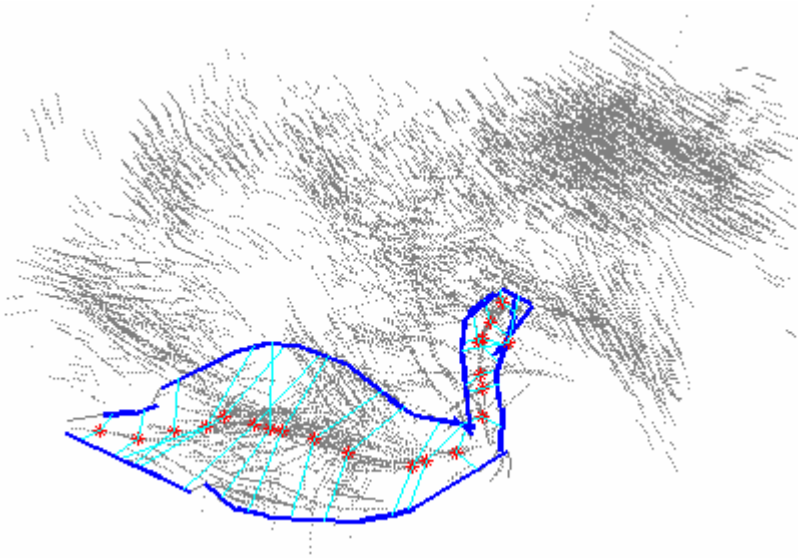

Experimental results
Filtering process in action

<play movie>
http://www.cis.temple.edu/~latecki/Talks/CGLS_0001.wmv

Experimental results
Some technical details

- 100 particles were used for filtering.
- On average about 200 followers were chosen for each particle as prior boosting. If there is lot of clutter more followers were chosen. This is automatically done in our program by our proposal.
- The parameters used for particle evaluation were pretty stable and one set worked for almost all images.

Technical presentation, part 2: Psychophysics of Shape Perception

Motivation: The Role of Contour Information

- In the absence of reliable contour information, the human visual system may fail to extract shapes of objects, including their properties such as symmetry
- Examples…

2D Symmetrical Shapes

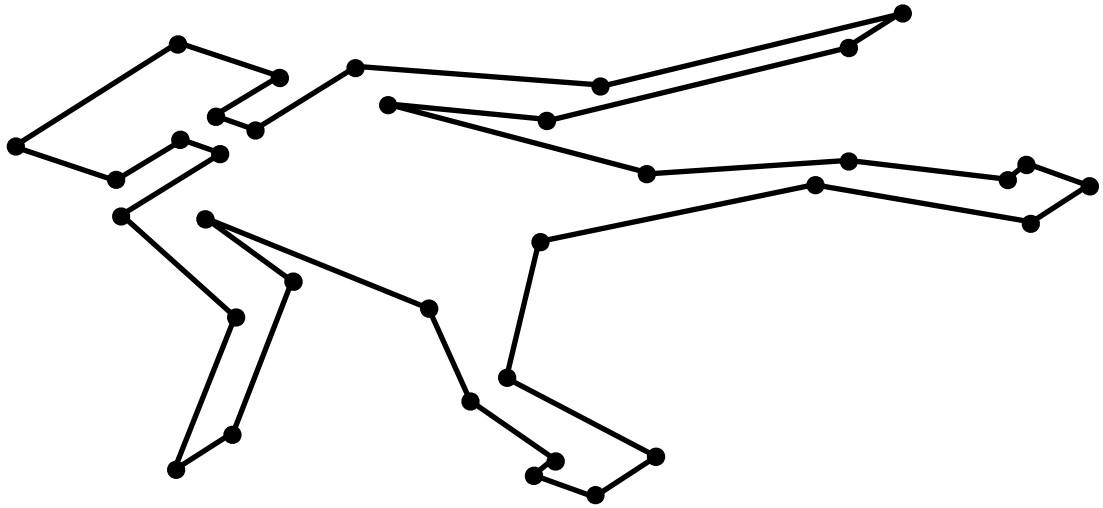

3D Symmetrical Shapes

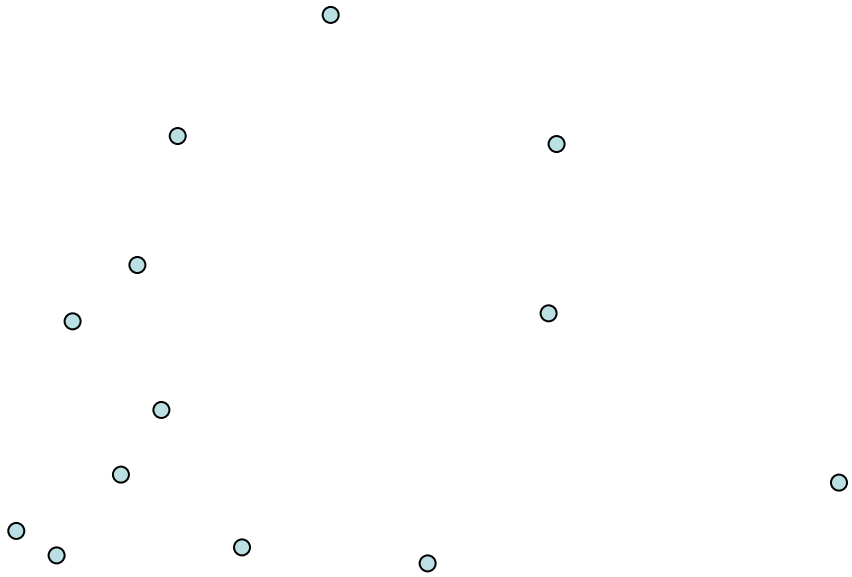

3D Symmetrical Shapes

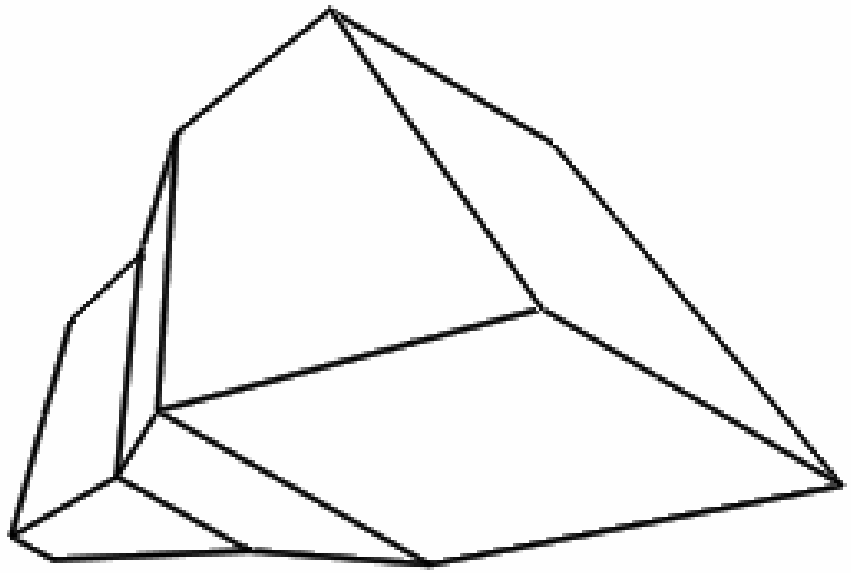

The Role of Shape Parts

Fragmented (camouflaged) objects can be detected after one part is recognized

Study 1: Detection of 2D Mirror Symmetry

- Psychophysical experiment using signal detection method
- Computational model

Stimuli

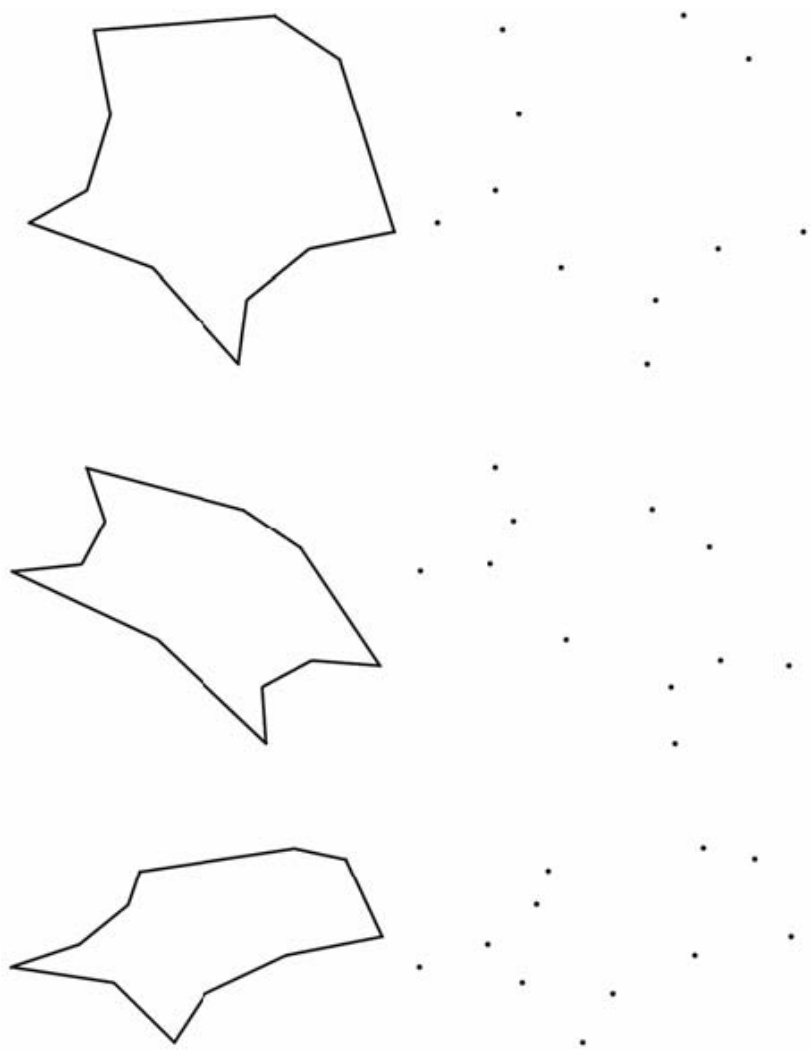

- Discrimination between symmetrical and asymmetrical figures
- The retinal image of a symmetrical figure was not necessarily symmetrical
- Dotted figures vs. polygons
- Orthographic vs. perspective projection

Results (dots vs. polygons)

- Higher d′ represents better performance. d′=0 represents chance performance.
- The retinal image of a symmetrical figure was symmetrical only in the 0 deg condition

Results (orthographic vs. perspective projection)

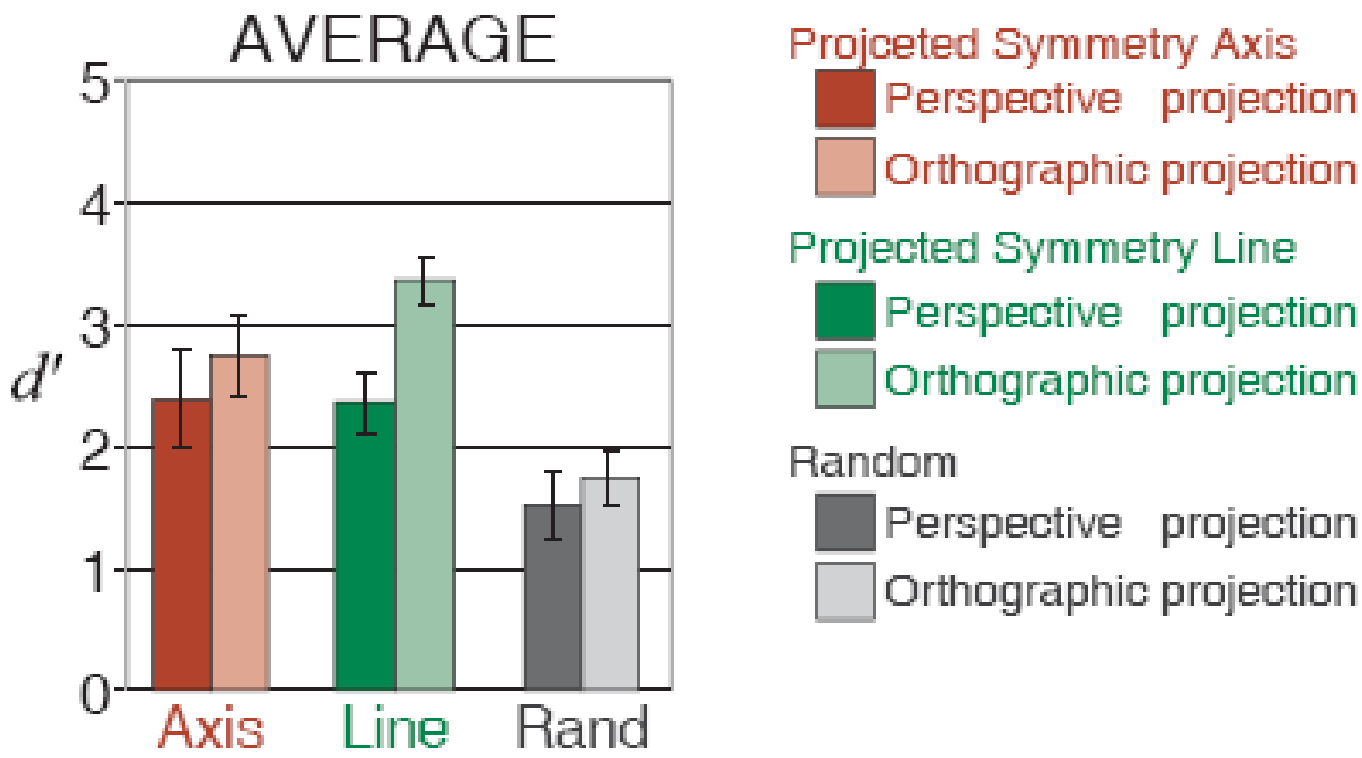

Summary of the Results

- Skewed symmetry can be detected reliably only in the case of polygons.
- The knowledge of the orientation of the projected symmetry lines or symmetry axis improves performance.
- Visual system uses the rules of orthographic projection and perspective projection is treated as an approximation.

How to detect symmetry from a skewed-symmetric image?

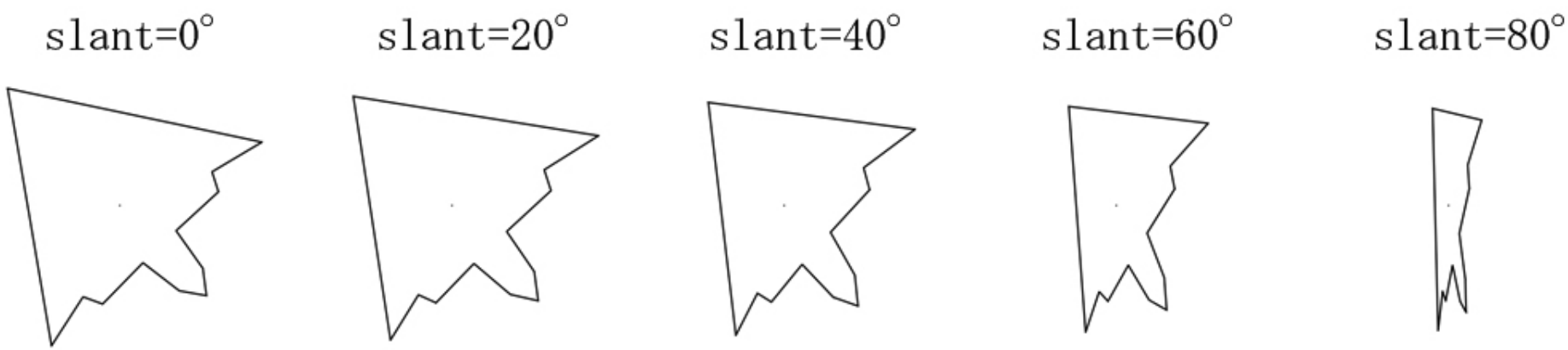

Two invariants of skewed symmetry

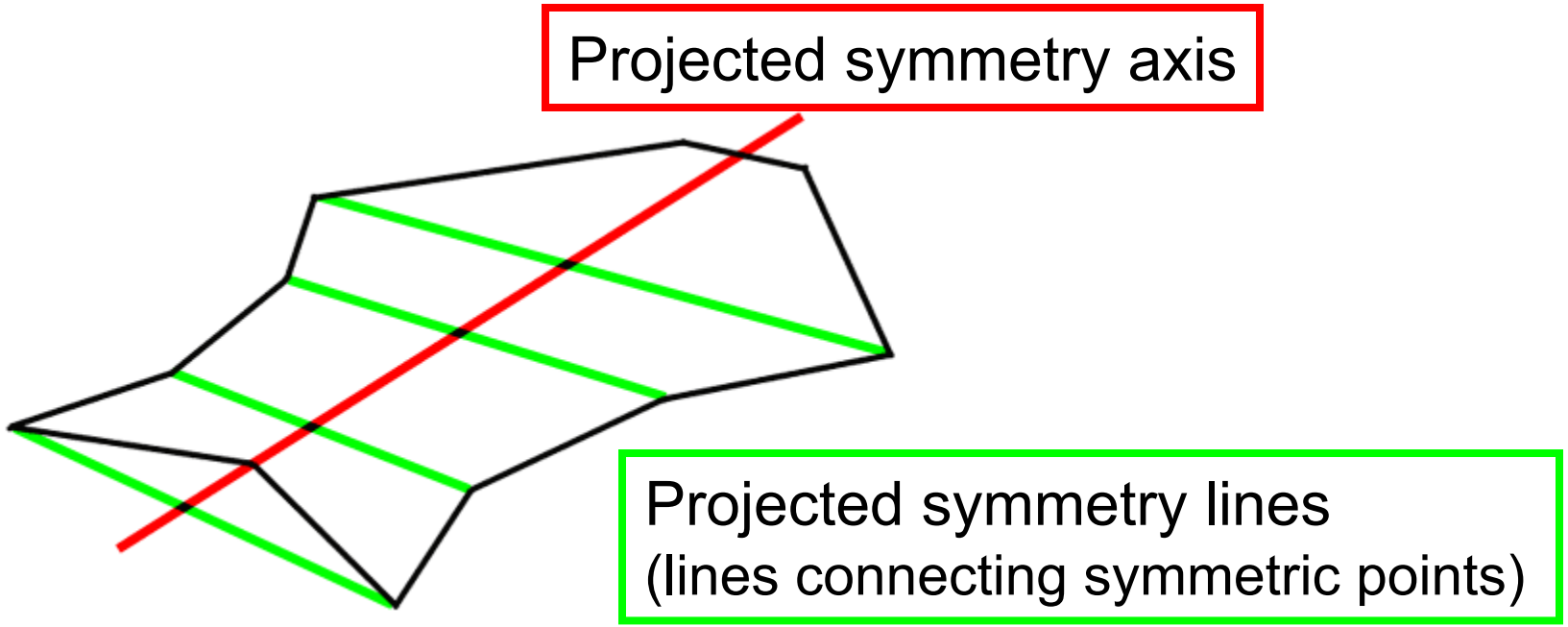

Symmetry lines are parallel and their midpoints are collinear (the midpoints are on the line which is a projected symmetry axis).

Results of the Simulation Model

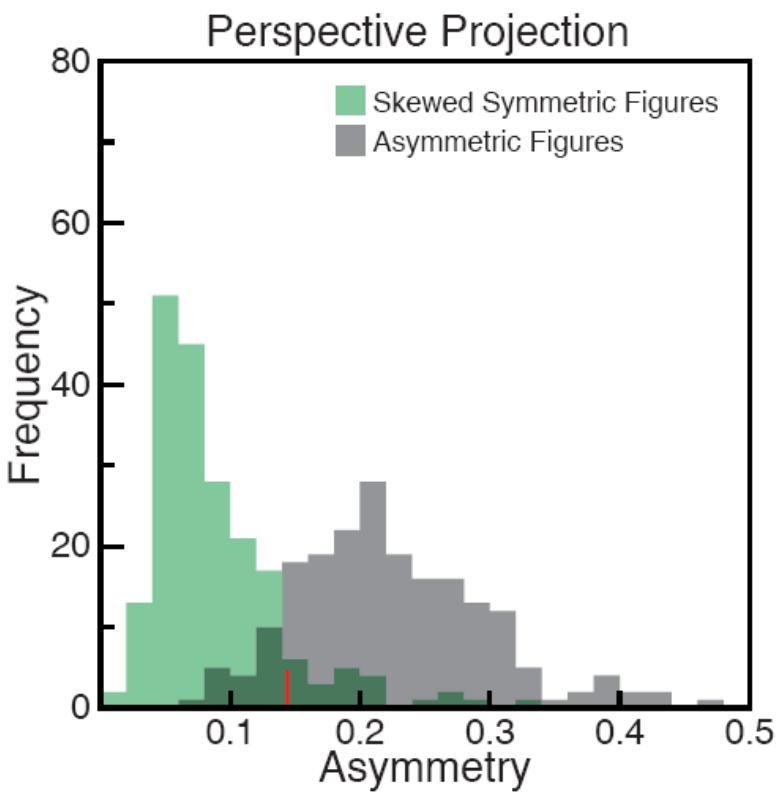

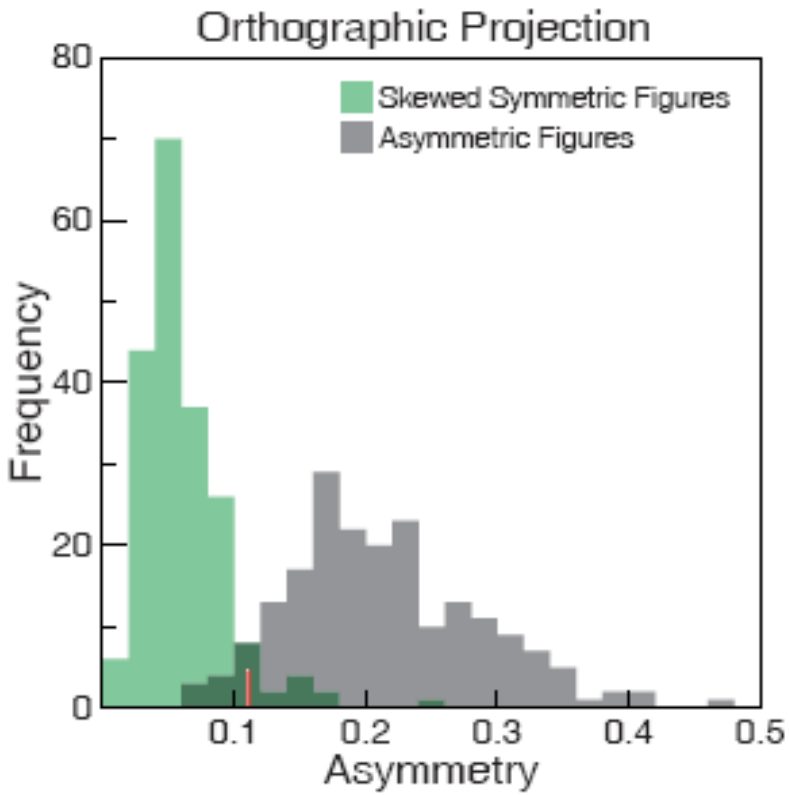

The model measures the asymmetry of a polygon. Discrimination performance is the same as that of human subjects.

The Model an also be Applied to Smoothly Curved Shapes

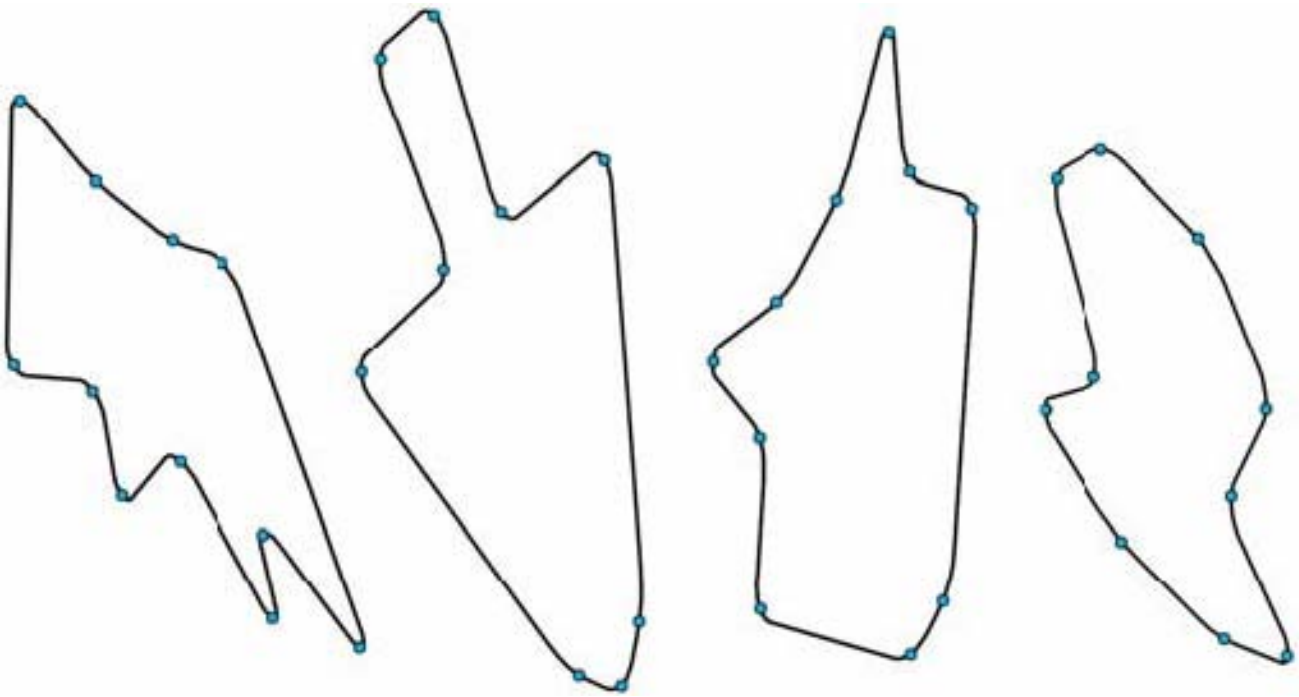

Study 2: Recovery of 3D Shapes

- Motivation derived from human vision
- Computational model

3D Space Perception

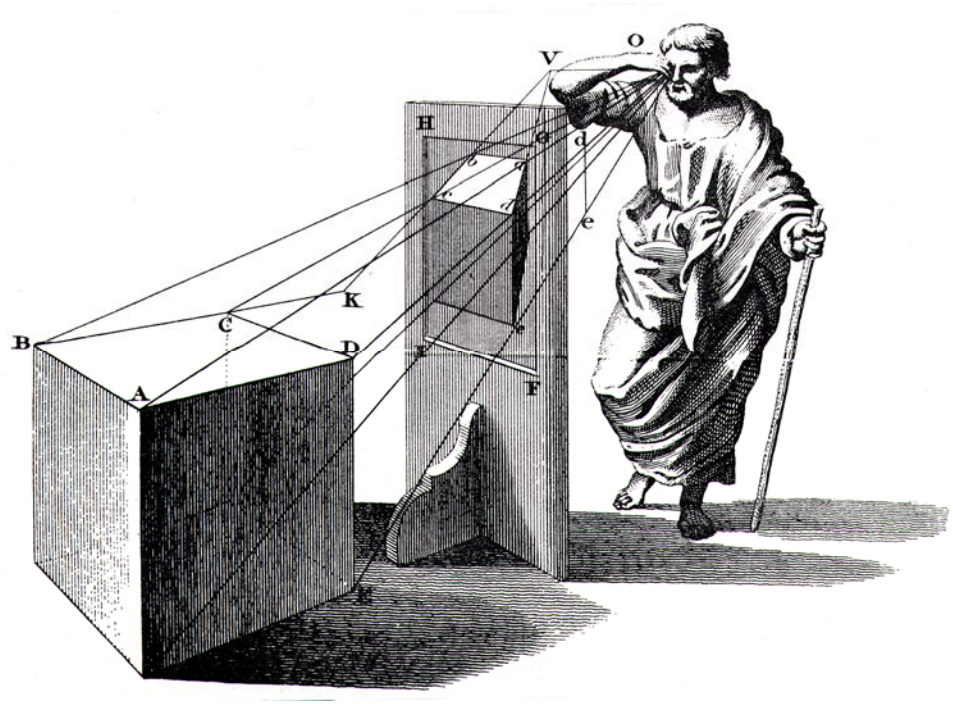

How to recover 3D shapes from a single 2D image?

3D Space Perception

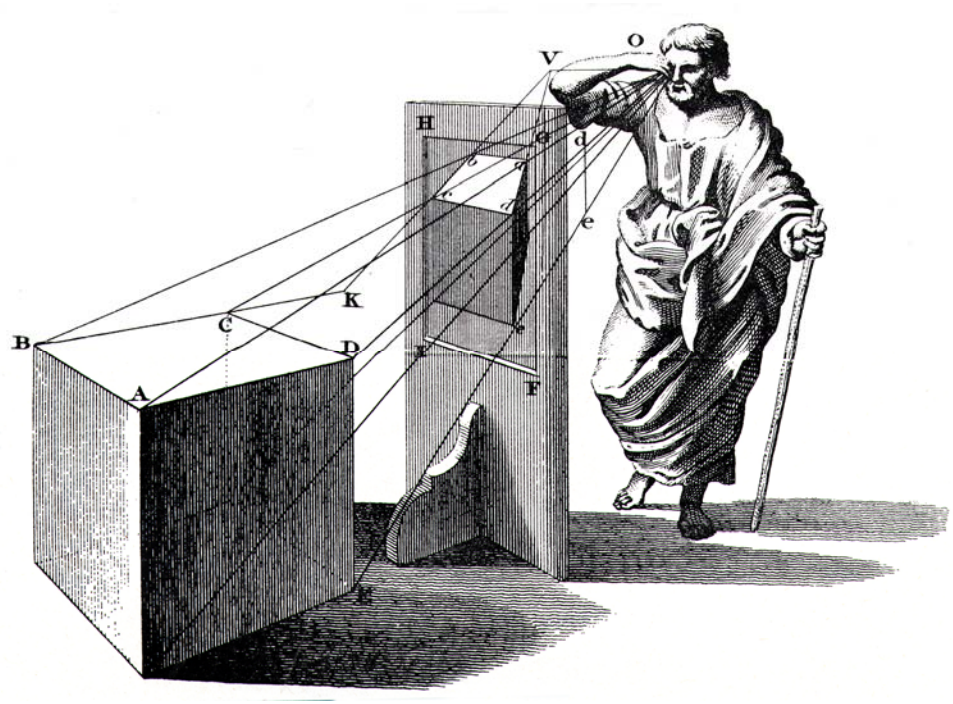

Humans do it very well.

Humans do it very well because:

- 3D shapes are *complex*
- 3D shapes are *regular*

Different 3D objects almost never produce the same 2D retinal shape because 3D shapes are complex.

Different 3D objects almost never produce the same 2D retinal shape because 3D shapes are complex.

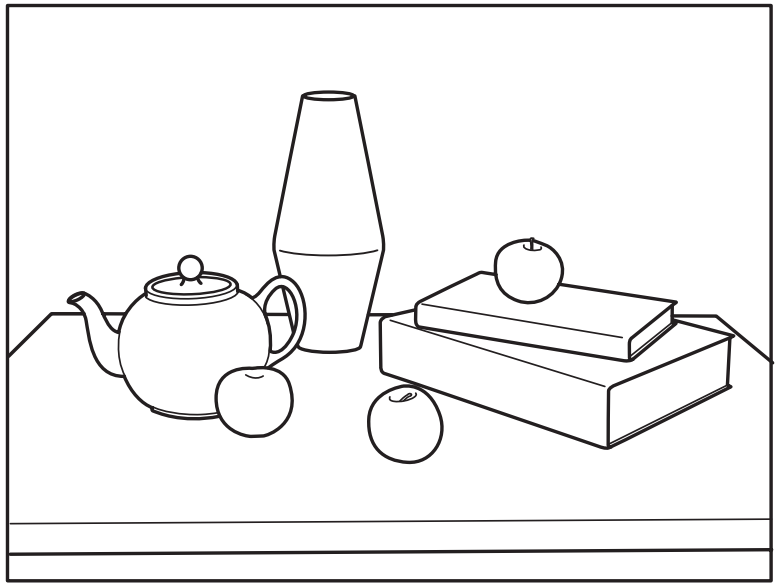

Applying regularity constraints to 2D retinal shape, should lead to correct 3D recovery.

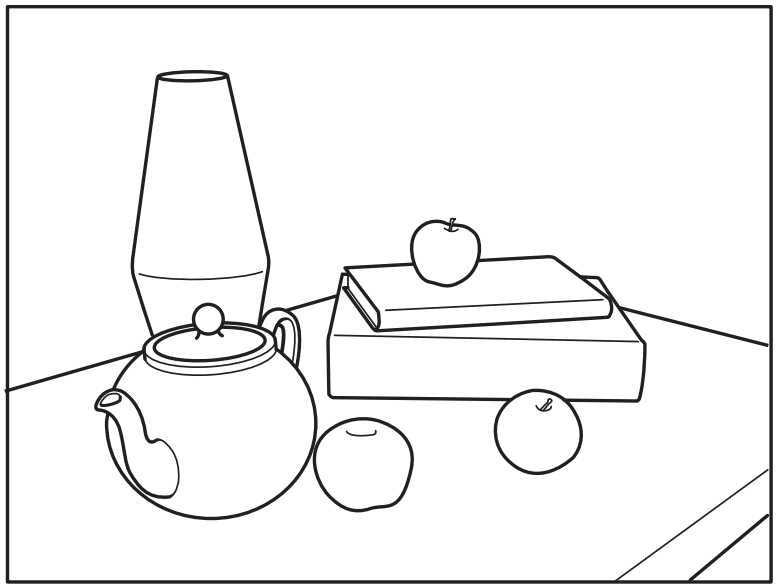

The role of regularity

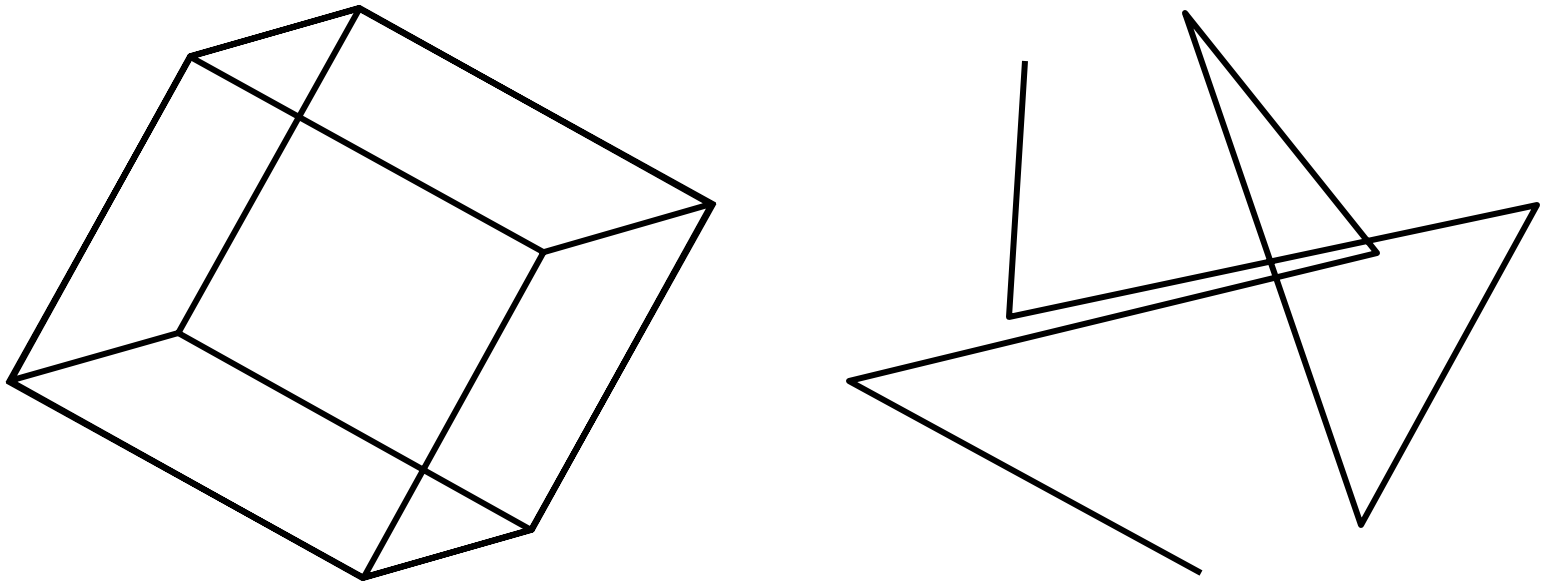

Percept is not 3D when all symmetry is removed and topology is trivial

Symmetry and Volume

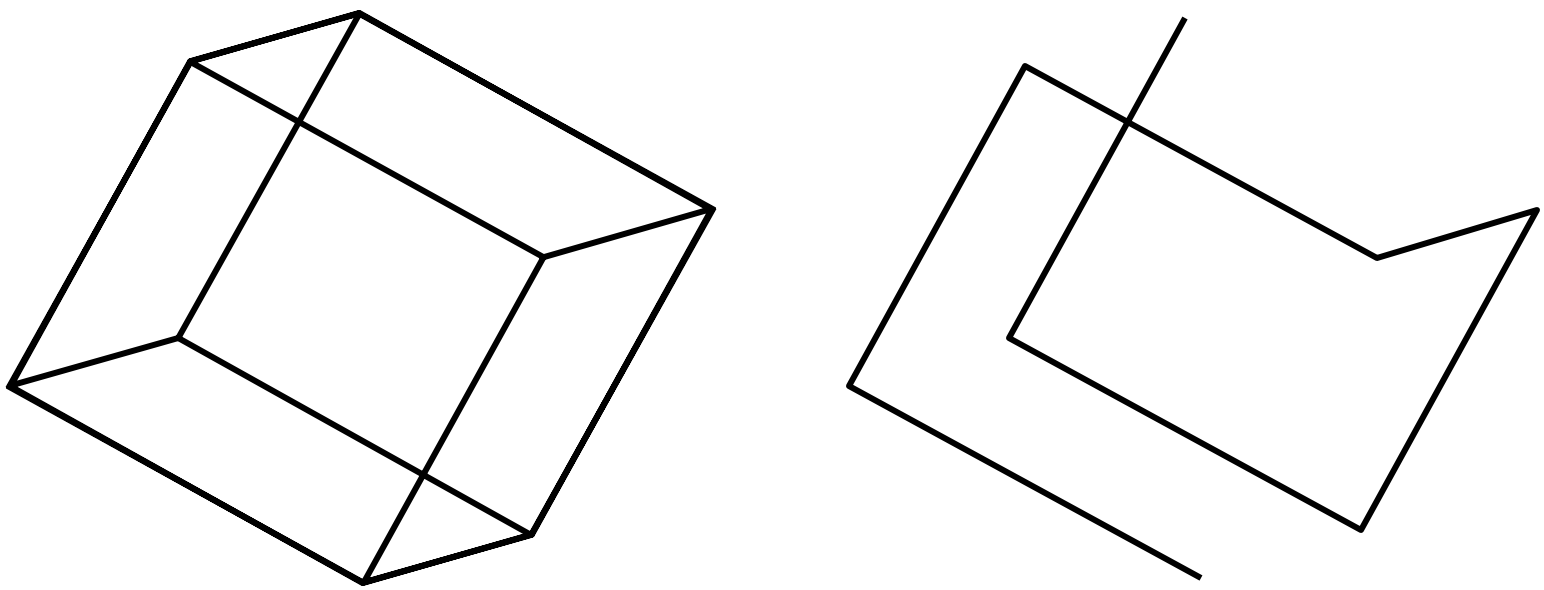

Symmetry and topology should indicate where the volume of the object is

Symmetry is a useful constraint because many (most?) objects in the real world are symmetrical

If you know that the image was almost certainly produced by a *3D symmetrical* object, you should "add" *symmetry* and *volume* to the image

Symmetry removes *N-1 df* in 3D shape recovery

Shape constraints identified in human vision:

- Maximal symmetry
- Maximal planarity
- Maximal compactness (V^2/S^3)

Demos:

http://viper.psych.purdue.edu/~pizlo/Constraint.exe

http://viper.psych.purdue.edu/~pizlo/li-demo.exe

Computational Model

- Take a single 2D retinal image
- Recover 3D shape by using constraints
- Depth cues are not used

Mirror symmetry in an orthographic image

(Vetter & Poggio, 2002)

- A 3D reflection of a 3D symmetric shape can be undone by 3D rotation

Mirror symmetry in an orthographic image

(Vetter & Poggio, 2002)

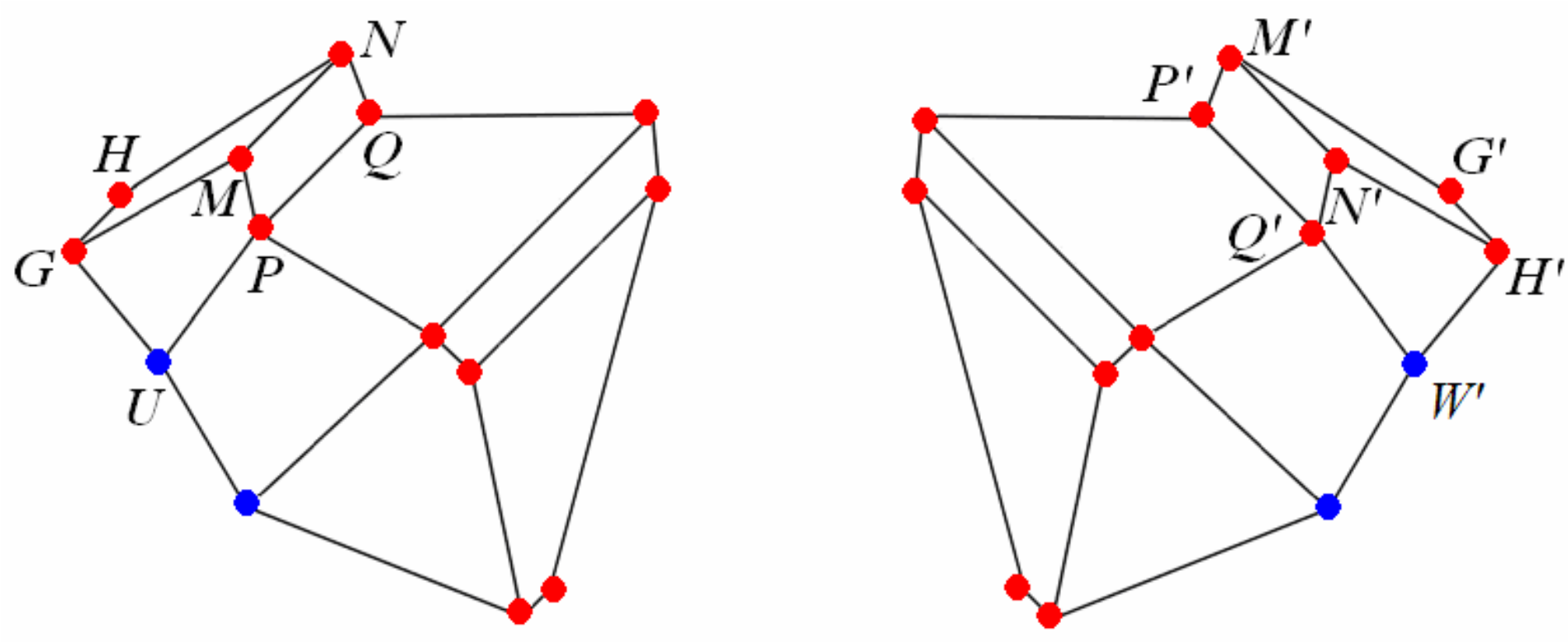

Using Symmetry Constraint

$$P_{virtual} = D \cdot P_{real},$$

$$D = \begin{bmatrix} 0 & 0 & -1 & 0 \\ 0 & 0 & 0 & 1 \\ -1 & 0 & 0 & 0 \\ 0 & 1 & 0 & 0 \end{bmatrix}$$

$$P_{real} = [X_L \; Y_L \; X_R \; Y_R]^T$$

$$P_{virtual} = [-X_R \; Y_R \; -X_L \; Y_L]^T$$

Producing one-parameter family of 3D symmetric shapes

$$\begin{bmatrix} X_i' \\ Y_i' \\ Z_i' \end{bmatrix} = \begin{bmatrix} r_{11} & r_{12} & r_{13} \\ r_{21} & r_{22} & r_{23} \\ r_{31} & r_{32} & r_{33} \end{bmatrix} \begin{bmatrix} X_i \\ Y_i \\ Z_i \end{bmatrix}.$$

$$\begin{bmatrix} X_i' \\ Y_i' \end{bmatrix} = \begin{bmatrix} r_{11} & r_{12} \\ r_{21} & r_{22} \end{bmatrix} \begin{bmatrix} X_i \\ Y_i \end{bmatrix} + \begin{bmatrix} r_{13} \\ r_{23} \end{bmatrix} Z_i.$$

$$r_{23} X_i' - r_{13} Y_i' + r_{32} X_i - r_{31} Y_i = 0.$$

Family of 3D symmetric shapes consistent with an orthographic image

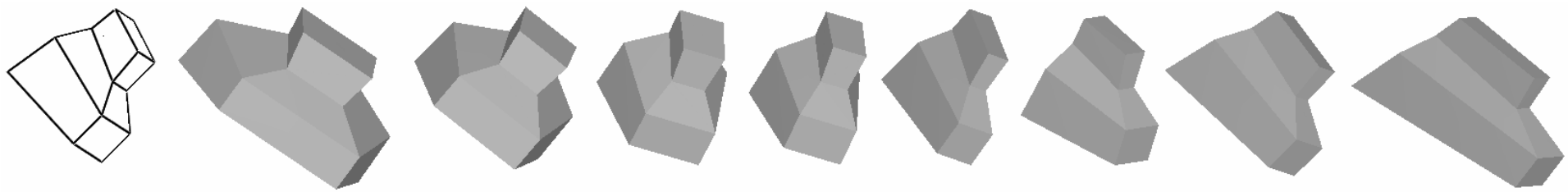

3D shape recovery

- Random opaque polyhedra
- Recovery using symmetry, planarity and compactness constraints

recovery

General Summary

- 3D shape perception is treated by the visual system as an optimization problem.
- Shape priors are necessary and sufficient for veridical shape perception
  - 3D compactness is a new shape constraint that leads to very good reconstructions based on a single randomly chosen 2D image.
- The computational model performs as well as humans do.
- 3D shape recovery can contribute to image segmentation…

The Role of 3D Shape Recovery in Image Segmentation

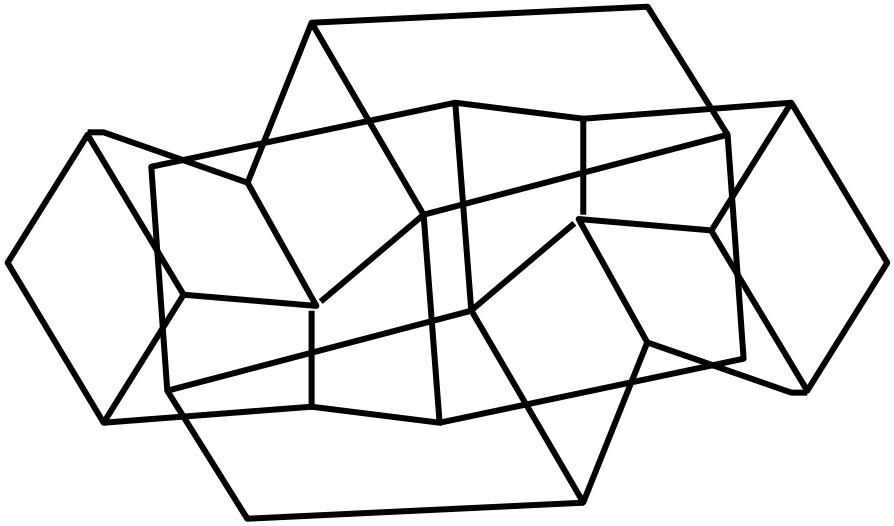

It is possible to see two different objects in this image…

The Role of 3D Shape Recovery in Image Segmentation

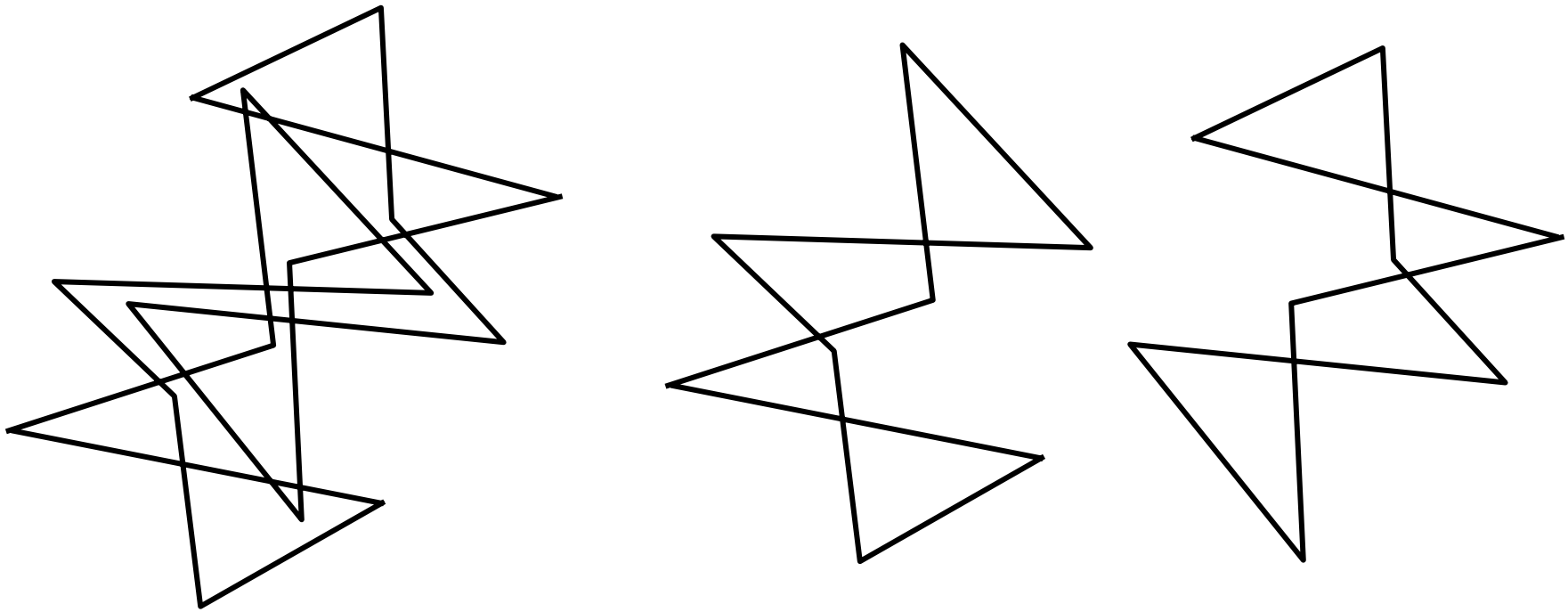

But not in this one

April 2008
6 x 9, 312 pp., 68 illus.
$38.00/£24.95
(CLOTH)

ISBN-10:
0-262-16251-2
ISBN-13:
978-0-262-16251-7

3D Shape:
Its Unique Place in Visual Perception
Zygmunt Pizlo

ADD TO CART

Future work

3. Shape familiarity (database of familiar parts)
   Perceptually motivated shape similarity metric

4. Recognition of 2D objects based on shape and texture of parts
   Adding texture to contour grouping
   Shape similarity to know contour parts + texture

5. Reconstruction and recognition of 3D objects
   Integration of 2D contour grouping based on local symmetry with the 3D reconstruction. The main link is 2D global skewed symmetry:

   2D local sym → 2D global skewed sym → 3D plane of mirror sym

   Reconstruction of 3D objects with smooth surfaces

All Solid-State Wireless Sensor Network

For

Nuclear Proliferation Detection

Sina Balkir (PI), Michael W. Hoffman (Co-PI),

Nathan Schemm (PhD Student), Walter Daniel Leon-Salas (Asst. Prof.)

Department of Electrical Engineering, 209N SEC-0511

University of Nebraska-Lincoln, Lincoln, NE 68588-0511

DOE NNSA NA-22 UITI 2007

Outline

- Project Overview and Goals
  - All Solid-State Wireless Sensor Network Development
  - Actual Implementation (Deployment Target: 10 nodes w/ Base Station)
  - Testing and Verification
- Current Research Stages
  - Development of Overall Sensor Node Architecture
  - Design, Fabrication, Test of the Computational Radiation Sensor Section
  - Design and Fabrication of Wireless Section (Ongoing)
- Future Work
  - Integration of Computational Sensor and Wireless Sections (Complete Wireless Sensor Node)
  - Design, Fabrication, and Test of Base Station
  - Implementation of Overall Wireless Sensor Network
- Milestones and Current Status

Project Overview: All Solid-State Wireless Sensor Network for Nuclear Proliferation Detection

Proposed Sensor Node

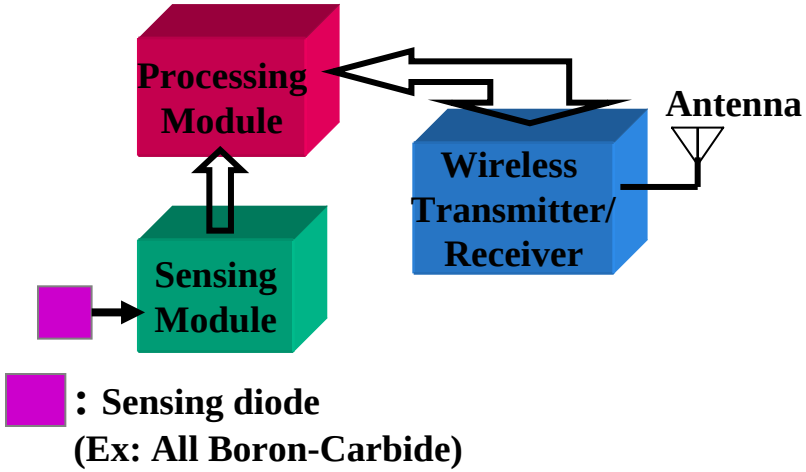

An Example 3-D Deployment of the Sensor Nodes as a Network

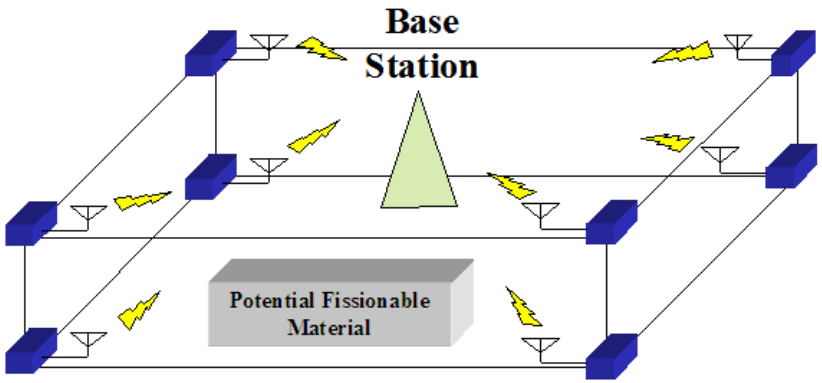

Objectives of Proposed Research:

- The design, fabrication, and test of sensor node components: Sensing Module, Processing Module, Wireless Transmitter/Receiver
- The design, fabrication, and test of a base station transmitter/receiver and the associated wireless sensor network protocol

Outcomes and Deliverables:

- A neutron detection sensor network with low-power sensor nodes for nuclear proliferation detection
- Physical dimensions of a single sensor node are similar to those of a business card for easy deployment
- 3-D sensor node configurations that allow for neutron detection with directionality
- Detection of fast neutrons (in addition to thermalized ones) by creating multiple wireless detection layers separated with moderators (such as paraffin) to slow down and capture certain fast neutrons (neutron spectroscopy application).

<u>Current Research Stage:</u> Development of Overall Sensor Node Architecture

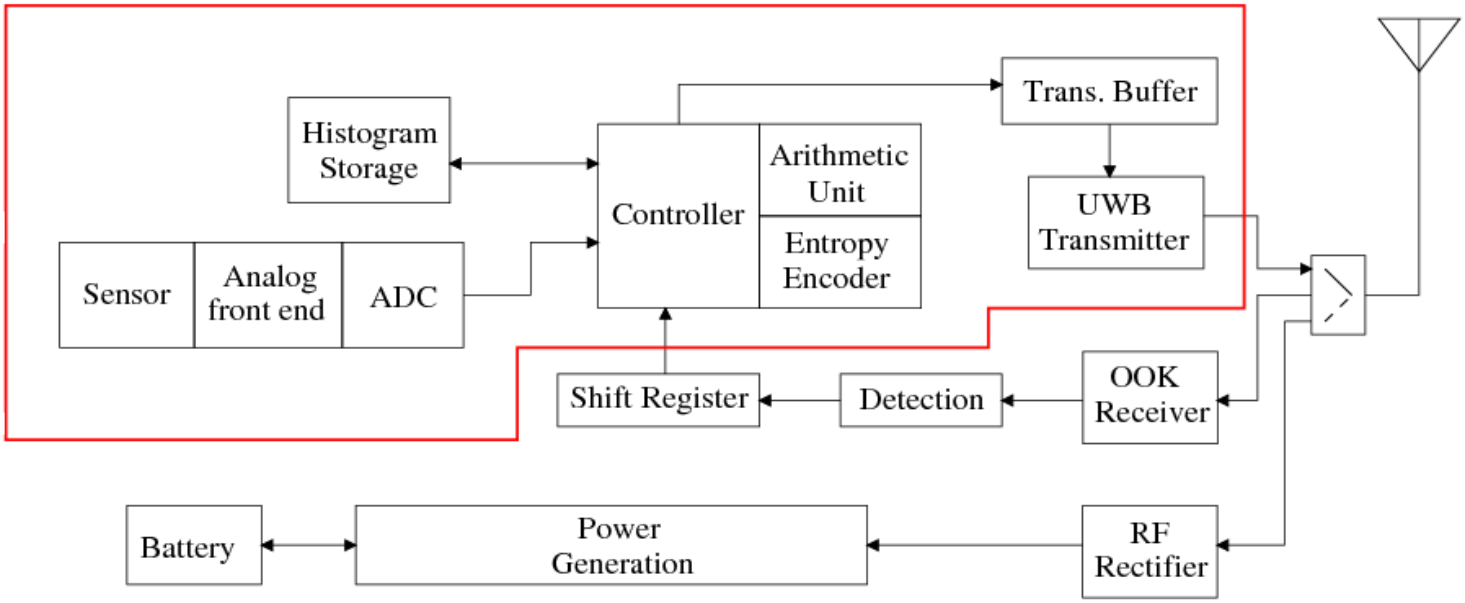

Sensor Node Architecture for Constructing the Wireless Sensor Network

- Study of feasible networking/communications protocols (OOK receiver, UWB Transmitter)
- Incorporation of a custom low-power microcontroller core and memory
- Integration of a four channel sensor analog front-end with A/D converter
- Design choices driven by low-power of operation, small area (< 5V Supply)
- Single chip solution for the wireless sensor node
- Blocks inside RED BOX comprise the computational radiation sensor section
- These blocks have been included in a test chip

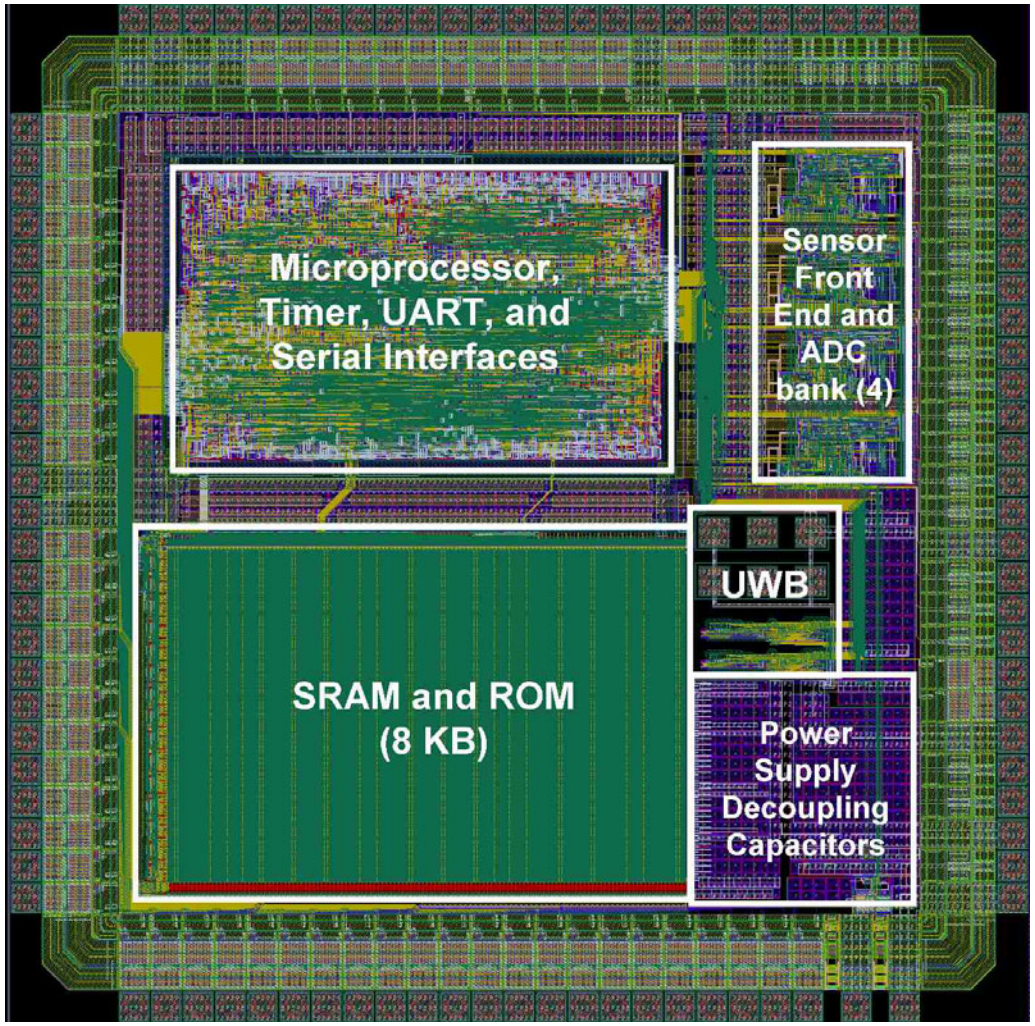

Computational Radiation Sensor Chip Layout

Main Specifications:

- 0.35 micron 4 Metal CMOS Technology
- 3.18 *mm* x 3.18 *mm* die size
- Customized and dedicated low-power microcontroller core, memory, I/O hardware, and timers.
- Analog sensor front end with quad Charge Sensitive Amplifiers (**CSA**)
- 8-bit resolution charge re-distribution A/D converter
- Packaged in QFN 100
- Tape out date: June 12, 2007
- Fabricated, packaged, and delivered: October 18, 2007

Charge Sensitive Amplifier Design

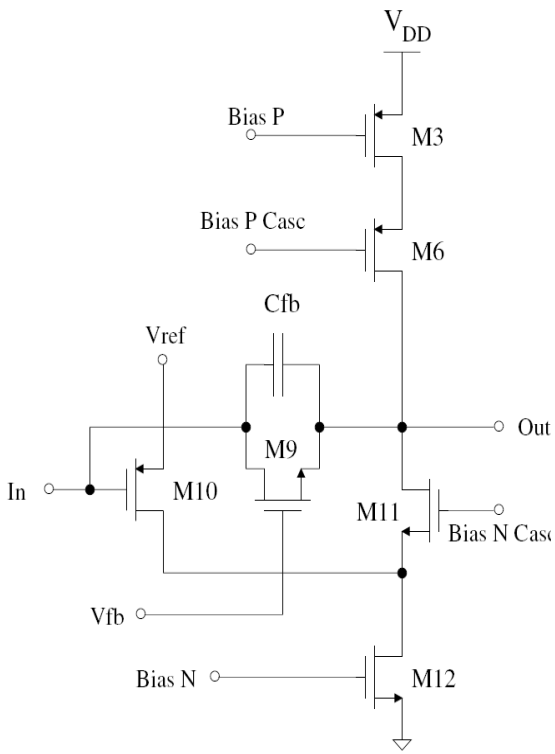

The standard CSA topology

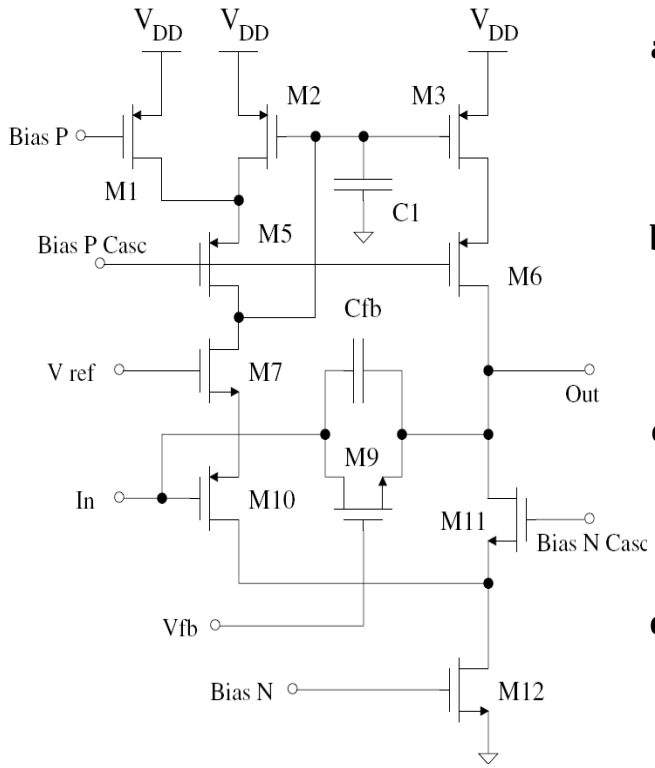

Improved version that dynamically scales the DC bias current.

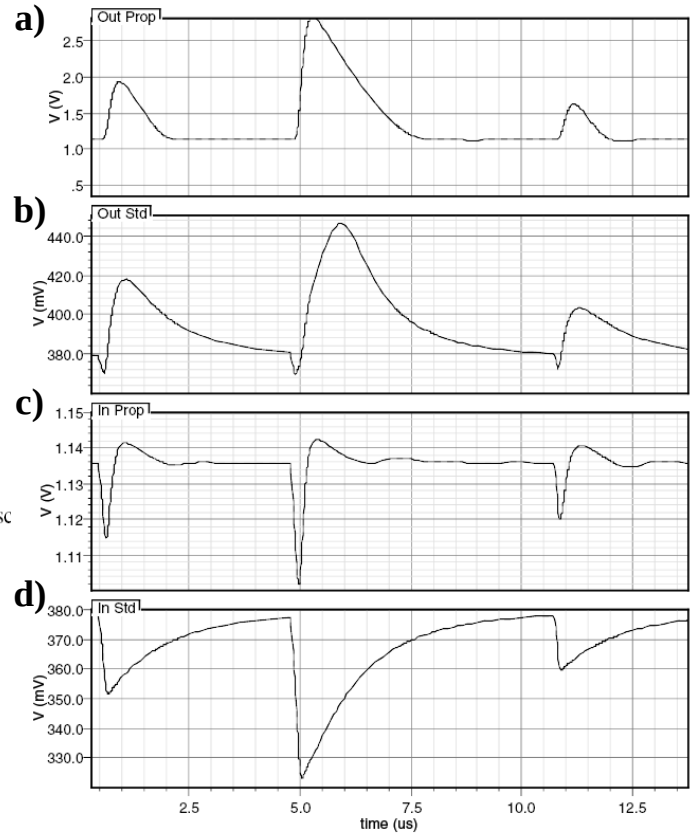

a) Output of improved CSA

b) Output of standard CSA topology

c) Input of improved CSA

d) Input of standard CSA topology

Overall Front-end Design with Event Driven (Low-power) A/D Converter

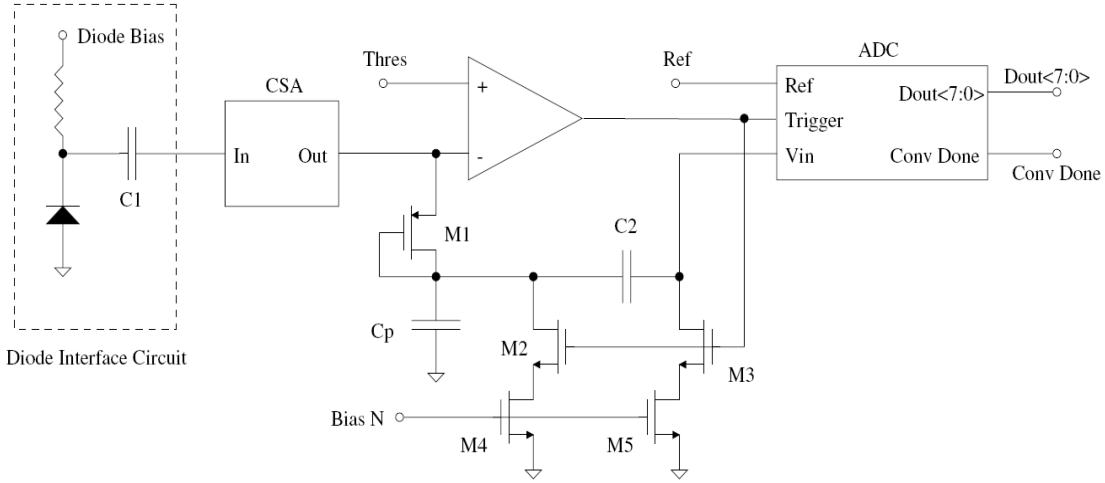

Overall Event Driven Front-end Architecture Depicting Sensor Diode Interface (Single Channel Shown)

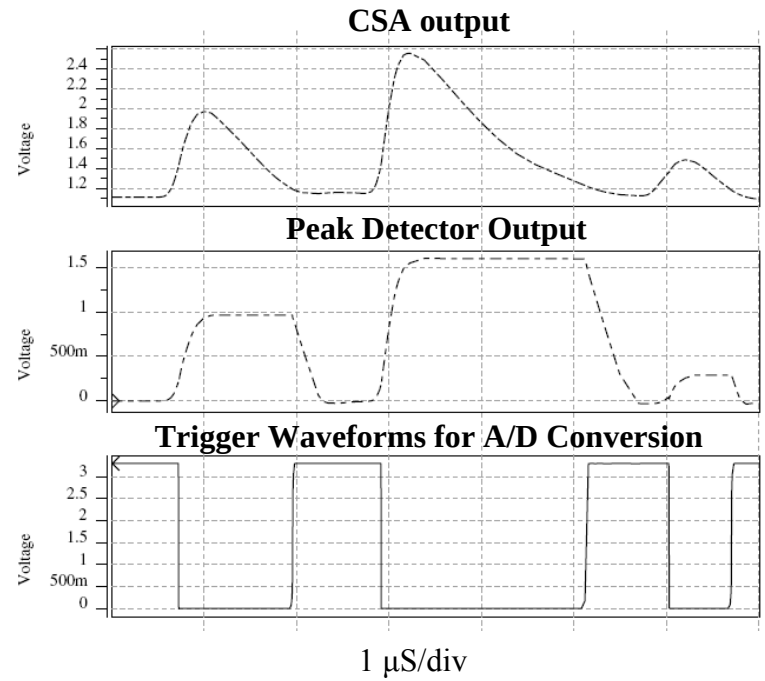

Measured Power Consumption:

- CSA enabled, no counts: 39.6 uW
- Overall Front End at 100kHz count rate: 135.3 uW

Datapath Representation of Microcontroller Core

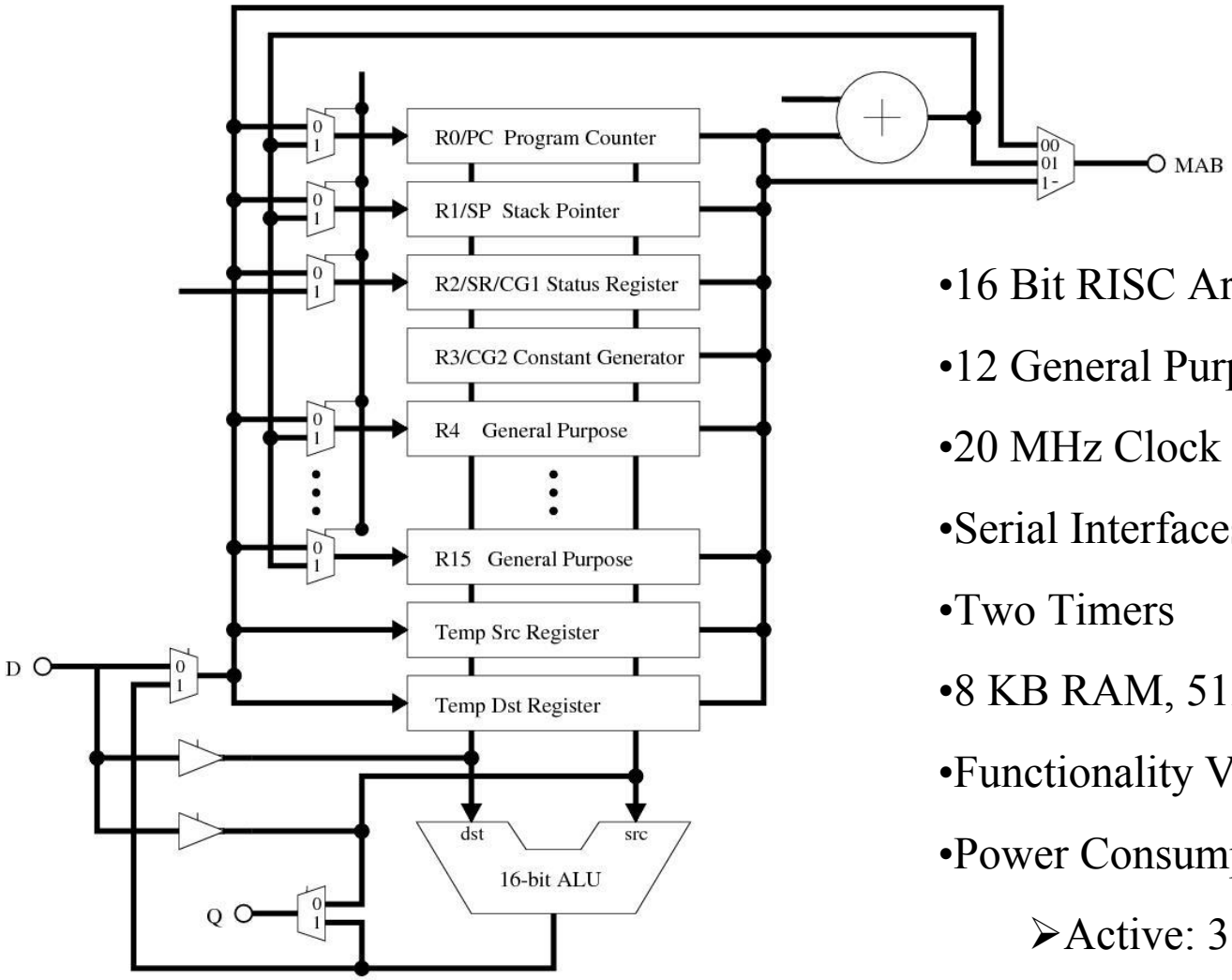

- 16 Bit RISC Architecture
- 12 General Purpose Registers
- 20 MHz Clock Speed
- Serial Interfaces (UART, SPI)
- Two Timers
- 8 KB RAM, 512 B ROM
- Functionality Verified via Test
- Power Consumption:
  - Active: 3.3 mW/MHz
  - Sleep: 422 uW

<u>Current Research Stage:</u> Fabrication of the Computational Radiation Sensor Chip

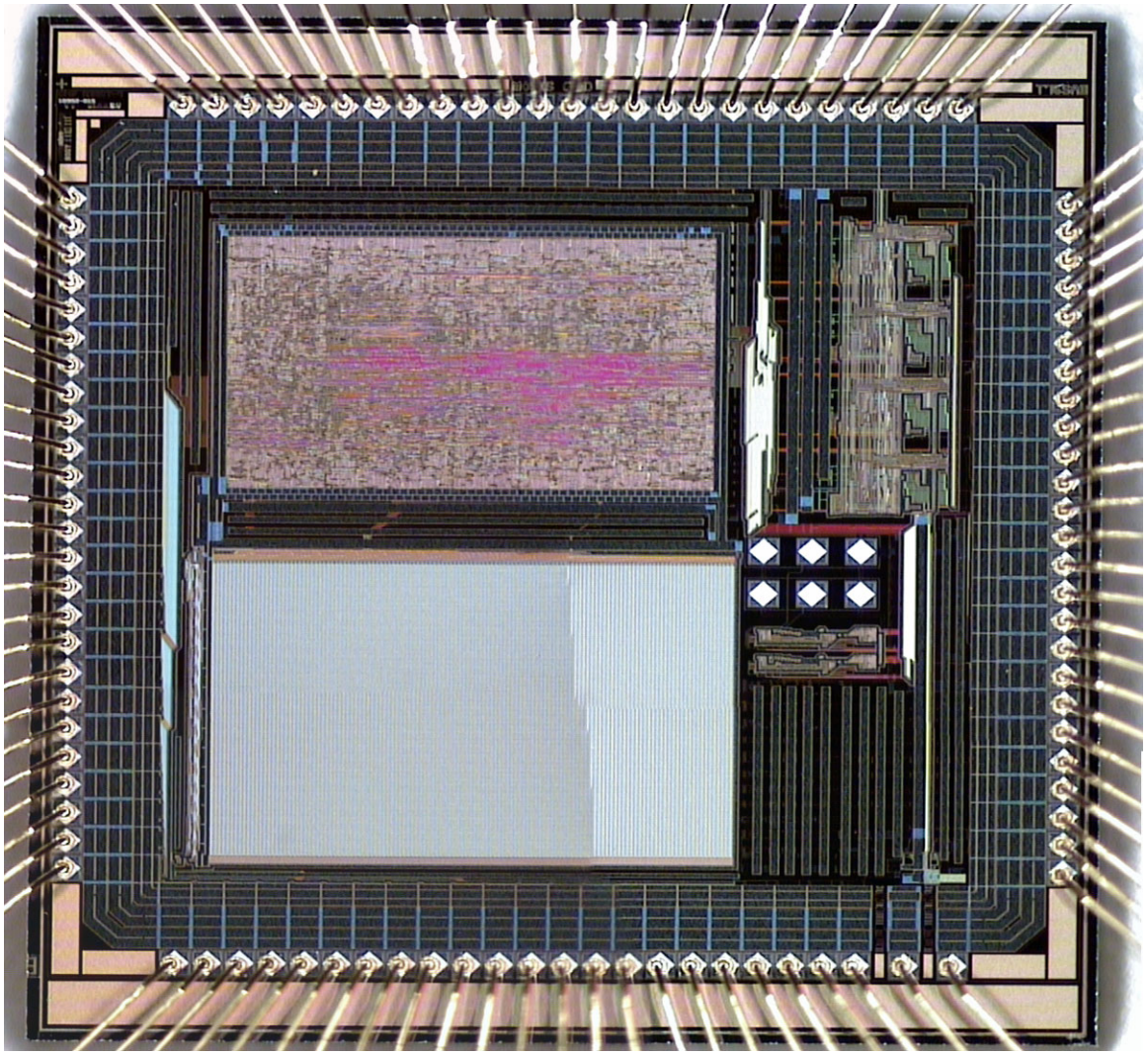

Die Photo of the Fabricated Chip *

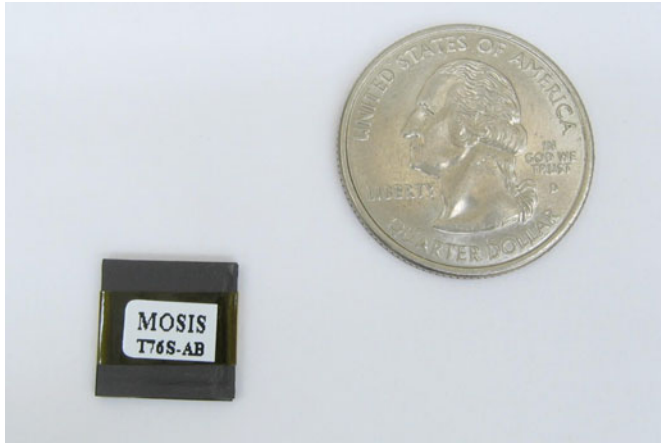

Packaged in OCP_QFN_12x12_100

*** Delivered from the Silicon Foundry on October 18, 2007**

<u>Current Research Stage:</u> Testing of the Computational Radiation Sensor Chip

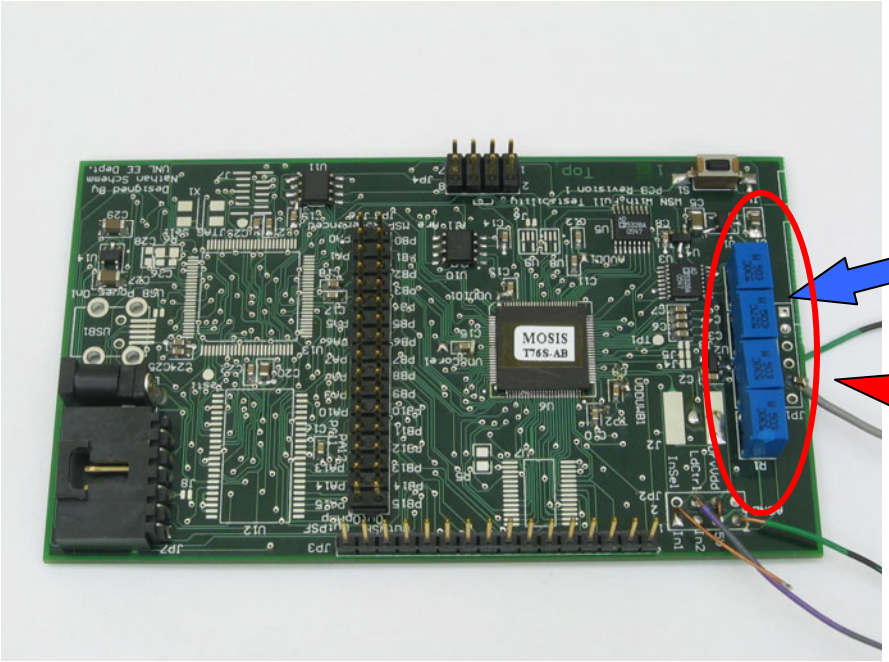

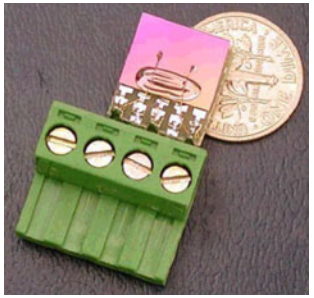

A Typical Solid-State Neutron Detection Sensor (Boron-Carbide Diode)

Four Channel Sensor Inputs

Circuit Board with Peripherals for Preliminary Laboratory Testing Displaying the Fabricated Chip

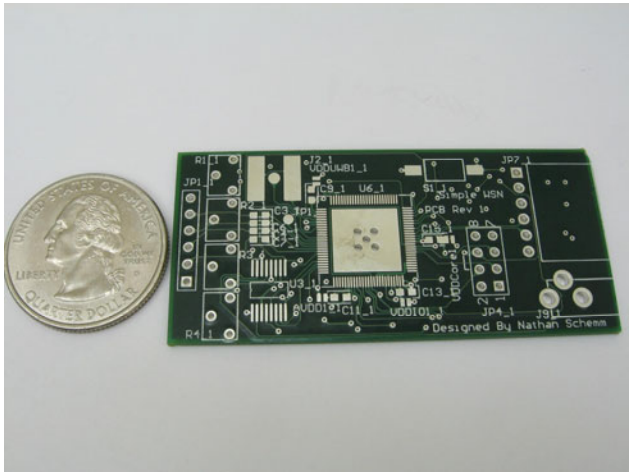

On-Site Test Board (Small Footprint)

Test Results

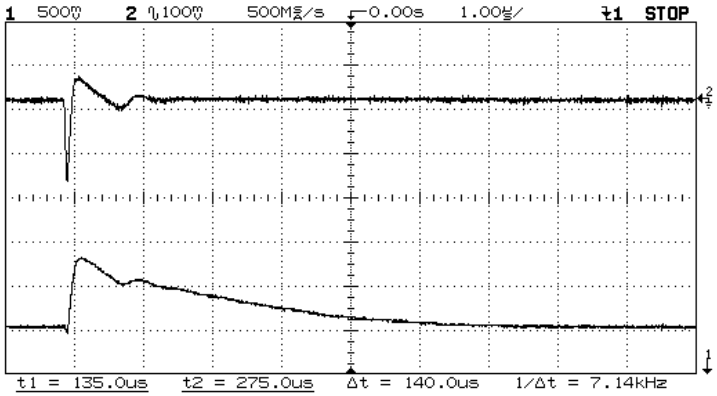

Input of Charge Sensitive Amplifier

Output of Charge Sensitive Amplifier

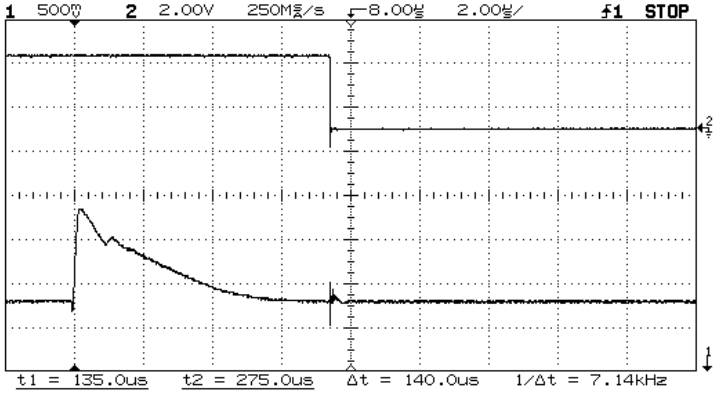

LSB of Neutron Event Counter (following the A/D Conversion Cycle)

Output of Charge Sensitive Amplifier (1V Swing)

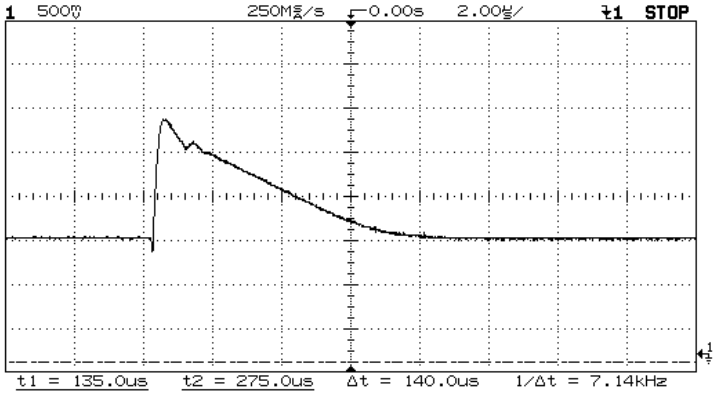

Output of Charge Sensitive Amplifier

The Boron Carbide Diode as a Neutron Detection Sensor

- Uses a specific isotope of boron, ^{10}B, to detect neutrons

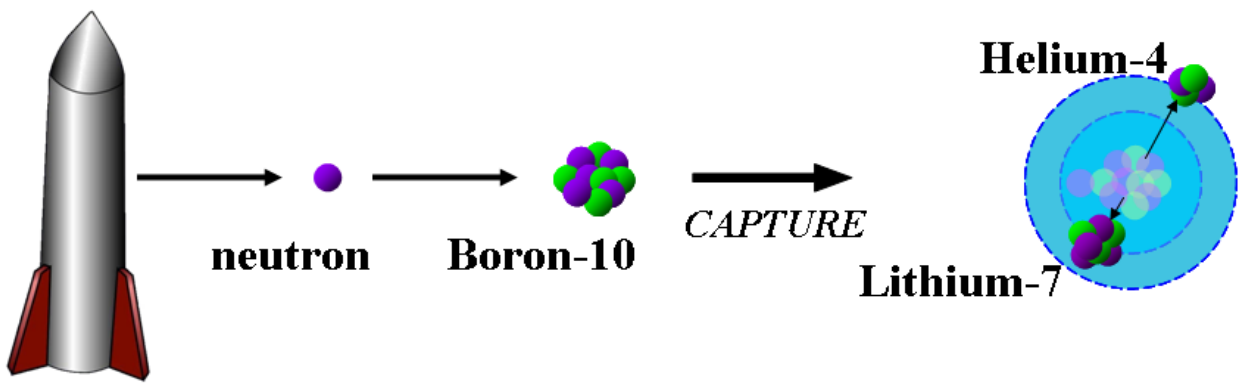

$$^{10}B + n \rightarrow {}^{7}Li(0.84MeV) + {}^{4}He(1.47MeV) + \gamma(0.48MeV)$$

or

$$^{10}B + n \rightarrow {}^{7}Li(1.02MeV) + {}^{4}He(1.78MeV)$$

The Boron Carbide Diode

J. Vac. Sci. Technol. A 10 (1992) 881

- Semiconducting boron carbide used to create a neutron sensitive diode
- p and n type layers formed from molecules identical in formula but different in arrangement
- Reverse bias applied to the diode sweeps charges out of depletion region, creating detectable current pulses through the diode

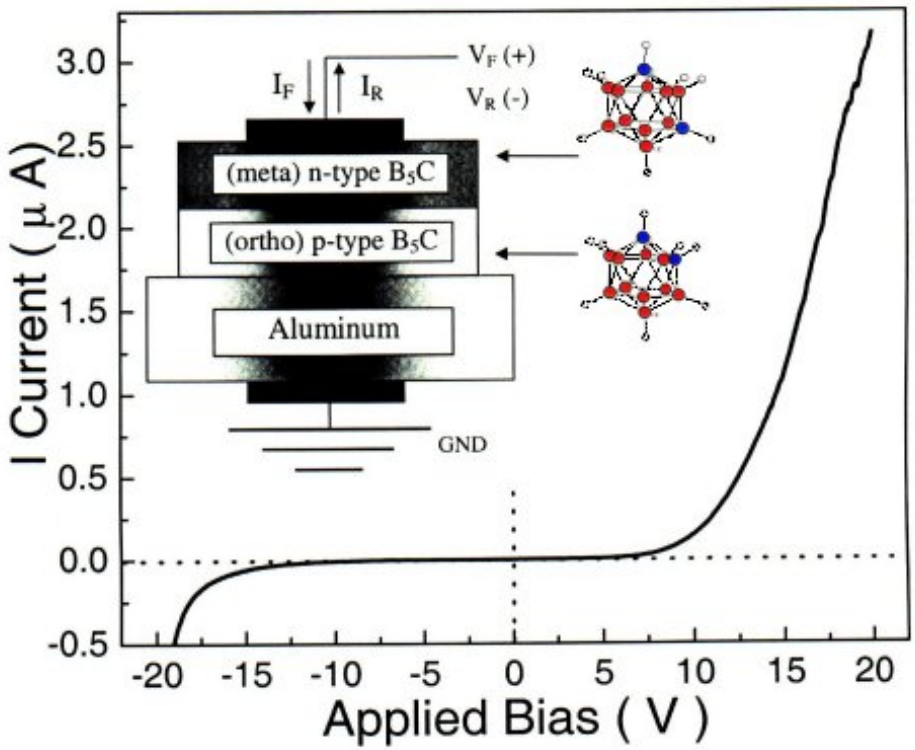

The Boron Carbide Diode

- The diodes create a detectable, real-time response to a neutron capture
- Resulting current pulses are in the range of hundreds of nanoamps for durations of 10 to 40 μsec, so the charge content is in the hundreds to thousands of fC

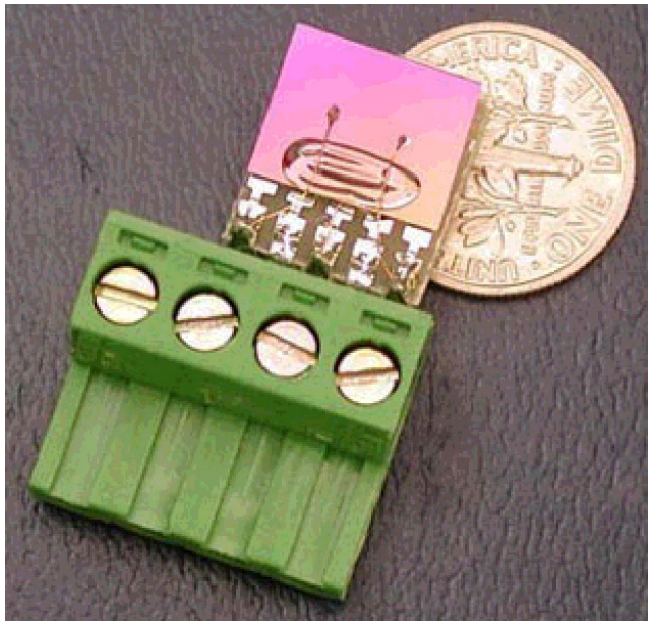

Previous Work

- Second generation hand-held neutron detector utilizing the boron carbide diode

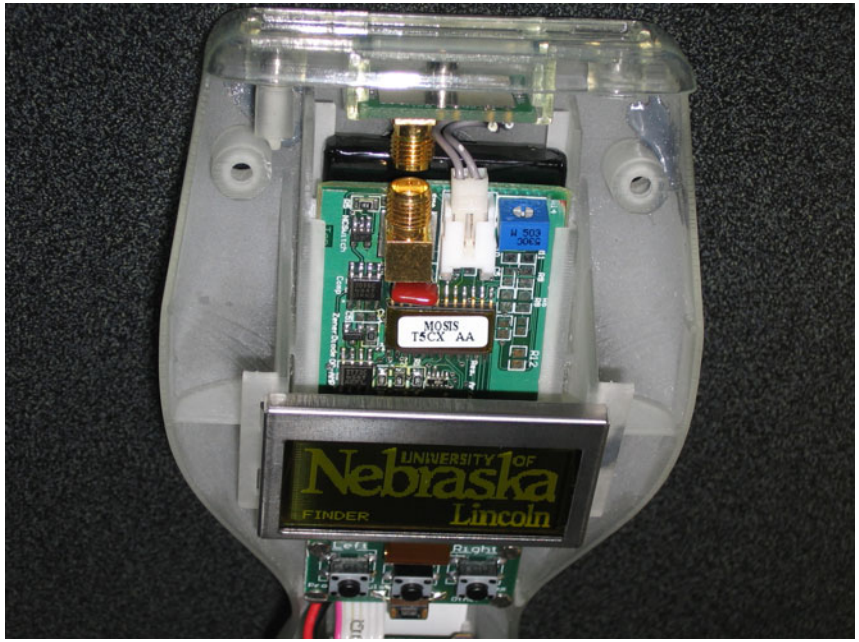

Experimental Results from Previous Work

- The blue curve is the pulse height spectra measured by the hand-held detector
- The bottom curve is the predicted spectra based on the boron carbide diode detection characteristics
- The red curve was measured when neutrons were blocked from the diode

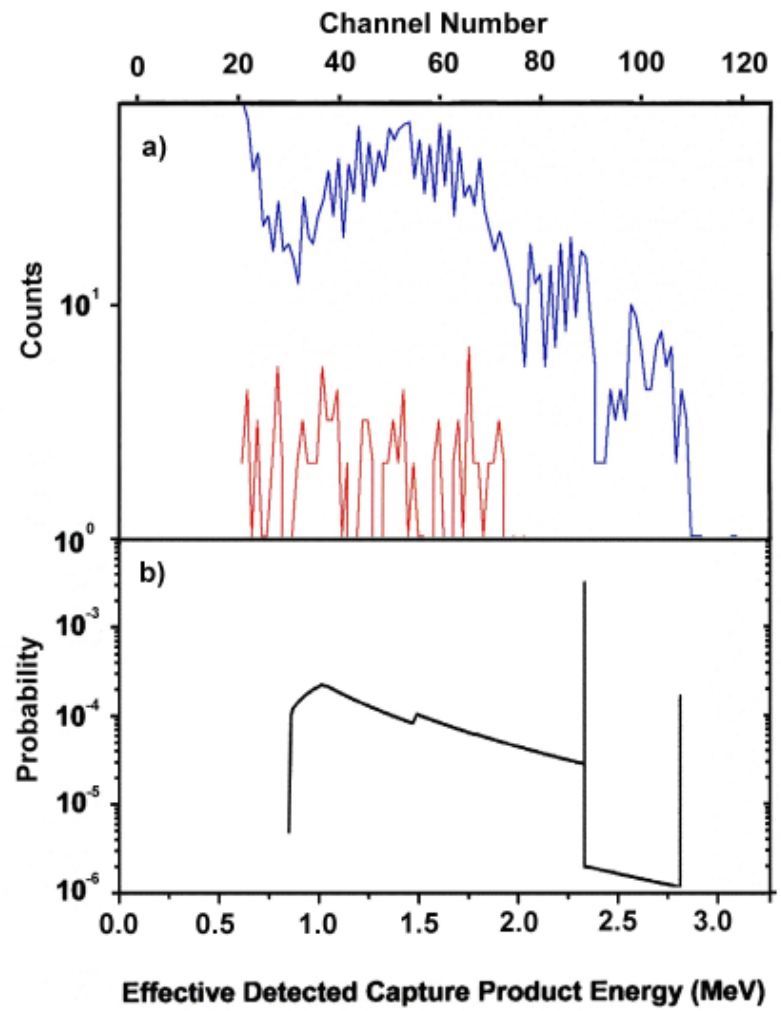

<u>Ongoing Work:</u> Integration of Wireless Sections in a Test Chip

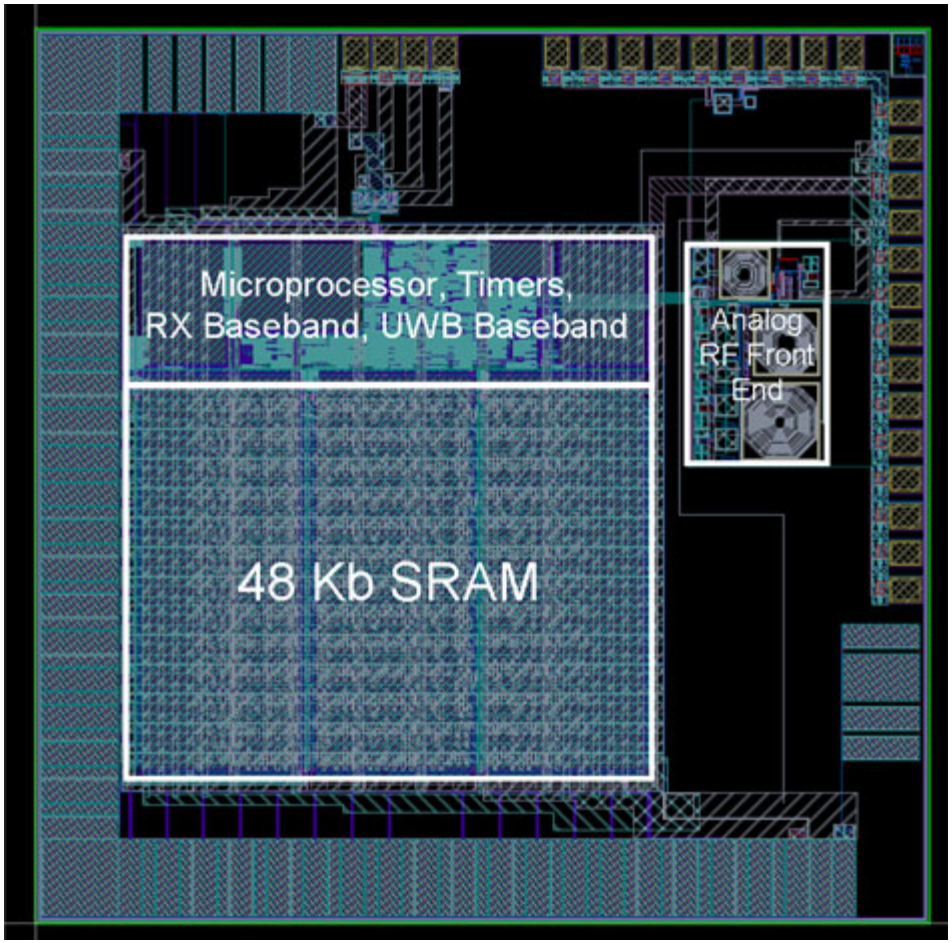

Wireless Test Chip

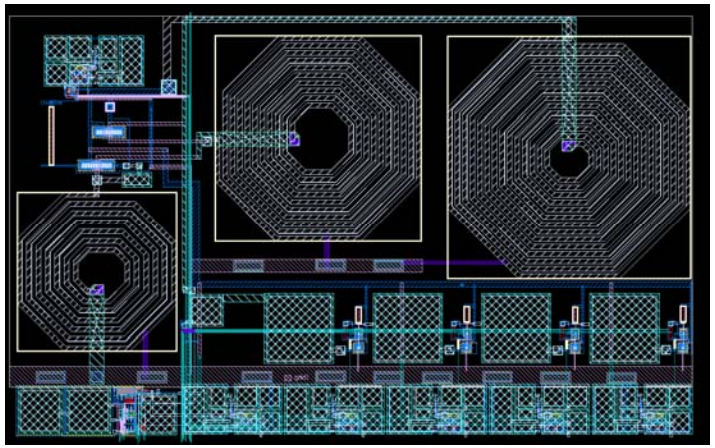

OOK Receiver Close-up

Main Specifications:

- **0.18 micron 6 Metal mixed-signal CMOS Technology**
- **3.04 *mm* x 3.04 *mm* die size**
- **Customized and dedicated low-power microcontroller core, memory, I/O hardware, and timers.**
- **Planned tape out date: December 3, 2007**

<u>Ongoing Work:</u> Design of Sensor Node Wireless Transceiver Blocks

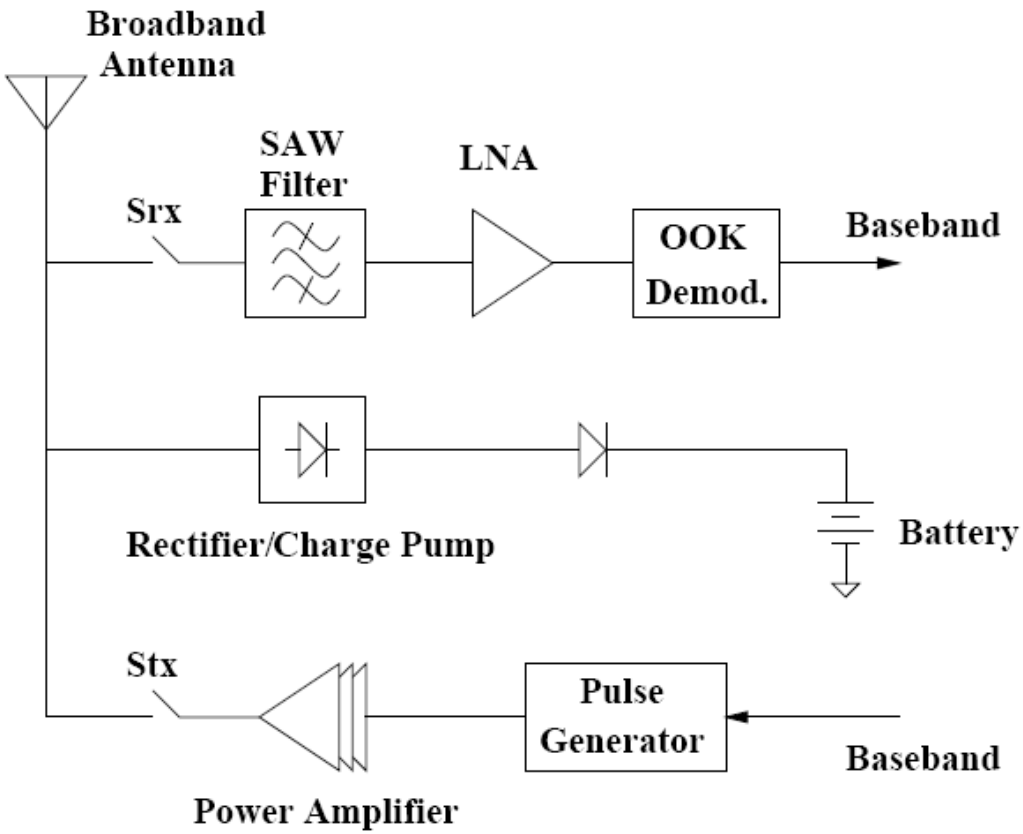

OOK - 900 MHz Center Frequency

Burst Communication Bit Rate – 100 Kbps

Symbol Synchronization Acquired During Bursts

UWB - ~50 M pulses/sec

Future Work

•**Fabrication and test of the wireless transmitter and receiver blocks.**

•**Fabrication of a second generation wireless sensor node chip**. This chip will merge both the computational sensor head and the wireless section on the same silicon substrate using a 0.18 micron RF CMOS technology.

•**Design, fabrication, and test of the base station**. As the base station is not power constrained, a mixed implementation using both off-the-shelf components and custom designed wireless blocks will be targeted. The base station's main functionality is to coordinate the sensor nodes and also provide remote battery charging capability during idle operation.

•**Implementation of the overall wireless sensor network and its associated multi-user protocol**. The whole system will be tested and verified using the test and measurement facilities available to investigators. This will complete the paradigm of the wireless neutron detection sensor network. Such a low-power and easily deployable sensor network can be utilized in various DOE operations and facilities for testing and nuclear proliferation detection

Milestones and Current Status *

- **Year 1:**
  1. Development of overall sensor node architecture. Extensive system and hardware level modeling and simulations will be conducted during the development phase of the sensor node architecture.

  2. Design, fabrication, and test of a miniaturized computational radiation sensor (0.35 *micron* CMOS) chip that interfaces with boron carbide devices to act as a low bit-rate information source. Dissemination of results in conferences and journals.

- **Year 2:**

Current Status

  1. Design, fabrication, and test of the wireless transmitter and receiver blocks using a 0.18 *micron* RF CMOS technology.

  2. Design, fabrication, and test of a second generation chip that merges both the sensor head and the wireless section on the same silicon substrate using a 0.18 *micron* RF CMOS technology. This step will finalize the realization of a single wireless sensor node. Dissemination of results in conferences and journals.

- **Year 3:**
  1. Design, fabrication, and test of the base station. A 0.18 *micron* RF CMOS technology is targeted at this stage.

  2. Implementation of the overall wireless sensor network and its associated multi-user protocol. The whole system will be tested and verified using the test and measurement facilities available to investigators.

  3. Delivery of 10 sensor nodes, the base station, and the associated system documents and user manuals. Dissemination of results in conferences and journals.

*** Total Budget: $417,191**

Test Results (Cont'd)

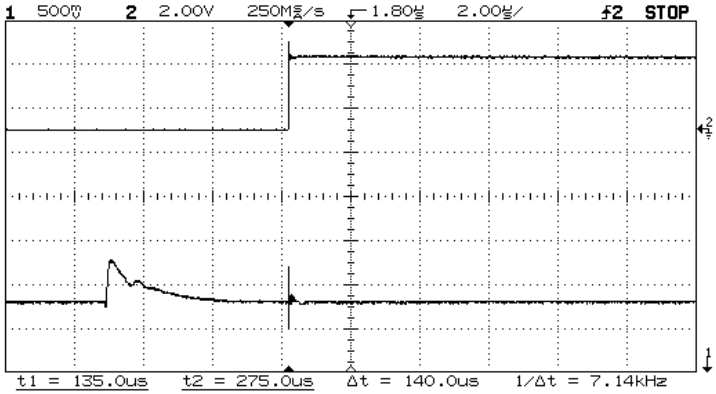

LSB of Neutron Event Counter (following the A/D Conversion Cycle)

Output of Charge Sensitive Amplifier (0.5V Swing)

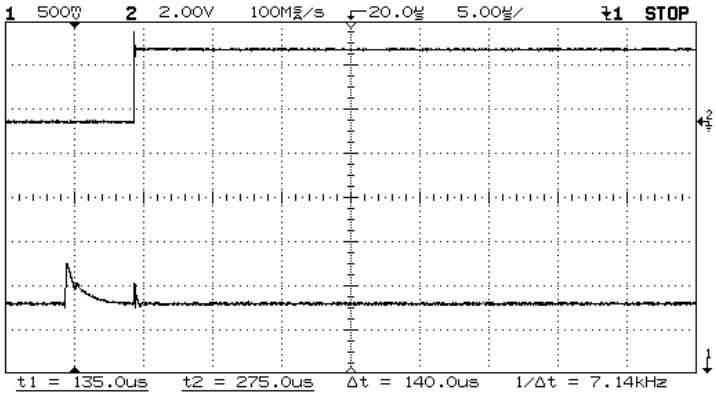

LSB of Neutron Event Counter (following the A/D Conversion Cycle)

Output of Charge Sensitive Amplifier (0.5V Swing) Showing No Re-Trigger

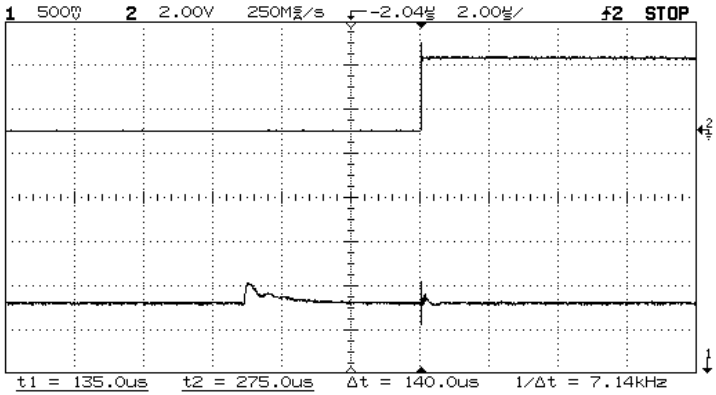

LSB of Neutron Event Counter (following the A/D Conversion Cycle)

Output of Charge Sensitive Amplifier (Min. Swing)

Test Results (Cont'd)

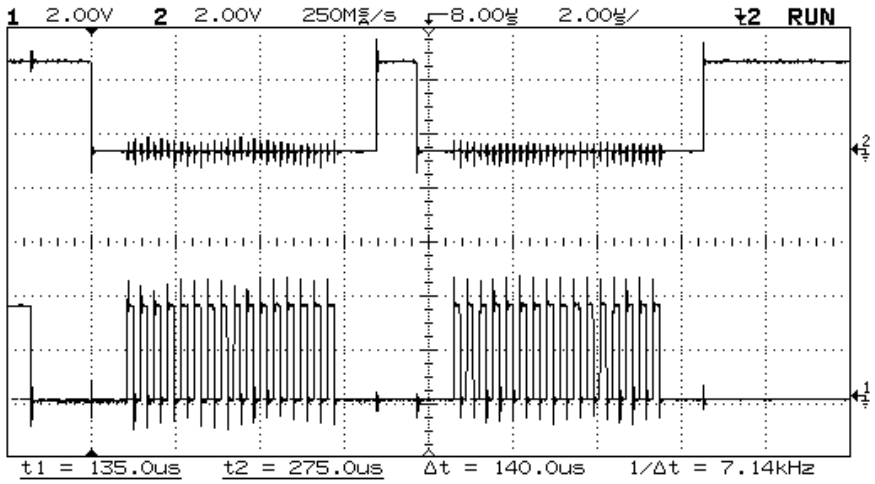

Microcontroller Operation Verification: Writing into D/A Converters on the Test Board

Architecture of On-OFF Keying (OOK) Receiver

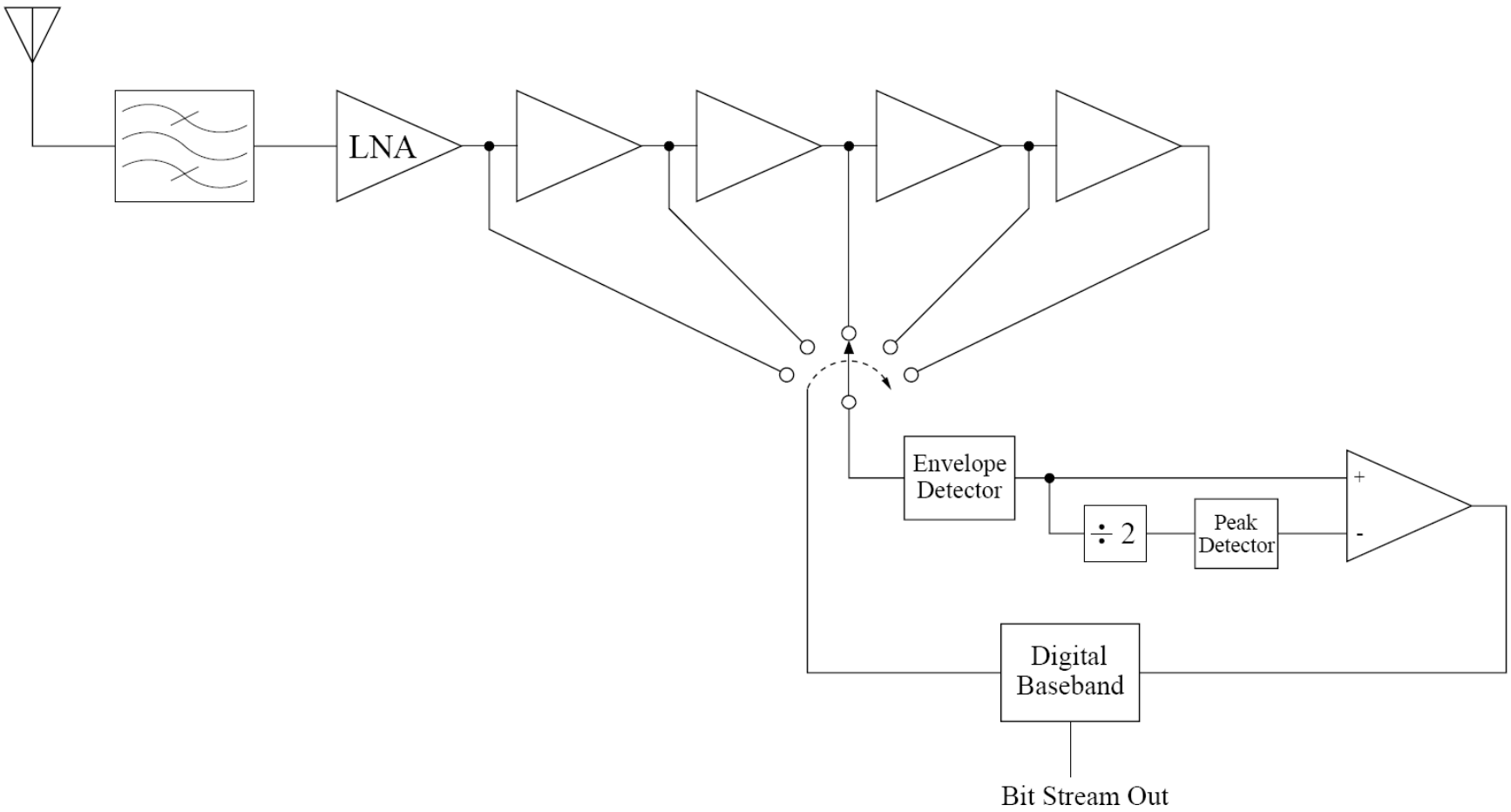

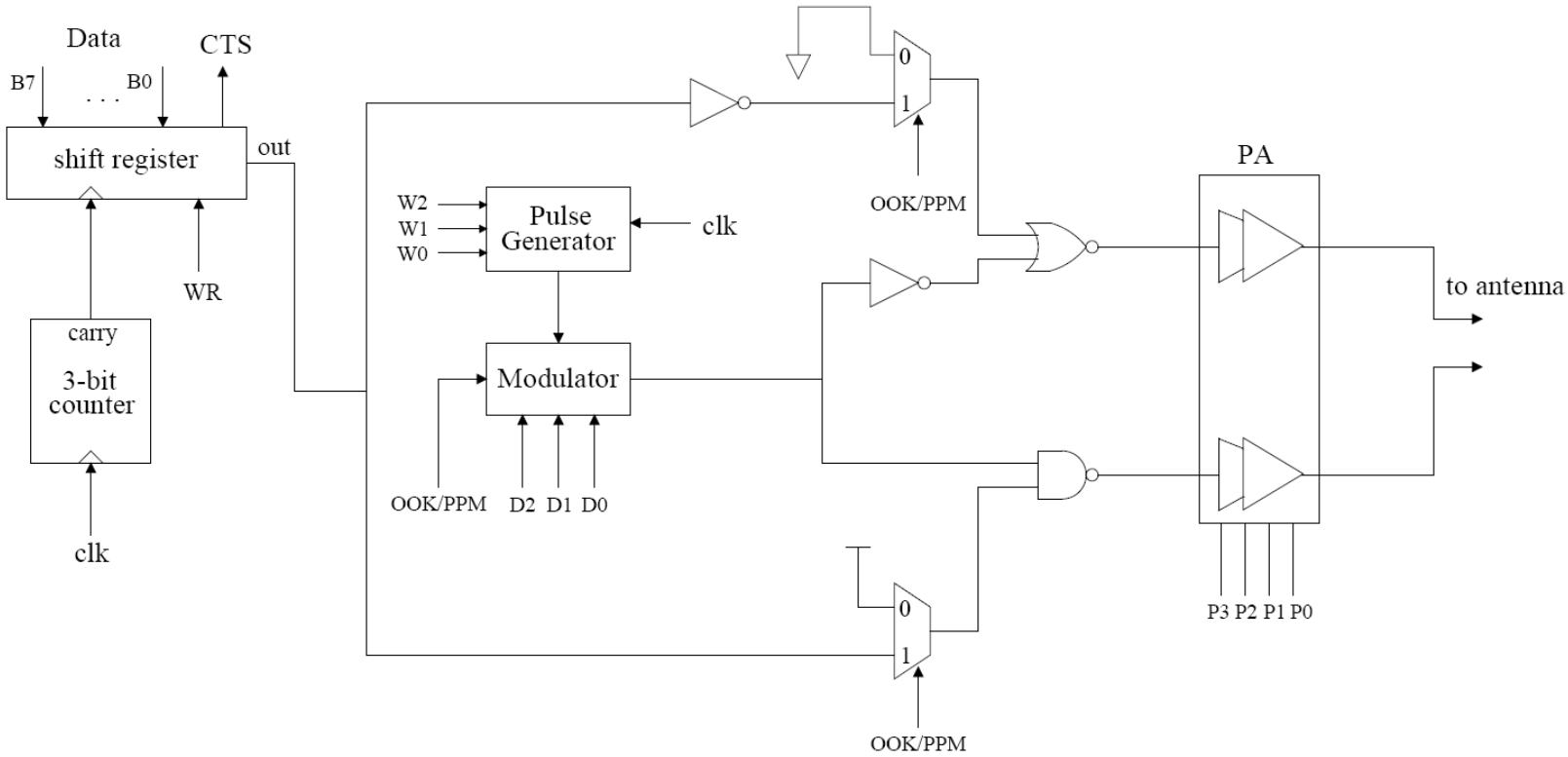

Architecture of Ultra-Wideband (UWB) Transmitter

Distributed Wireless Sensor Networks for Long-term Deployments

Yannis Paschalidis and Christos Cassandras
Contact: yannisp@bu.edu, http://ionia.bu.edu/

Center for Information and Systems Engineering (CISE),
Department of Manufacturing Engineering, and
Department of Electrical and Computer Engineering
Boston University

November 28, 2007
UITI 2007, University Information Technical Interchange Review Meeting
NNSA, DOE

Project information

Grant No.: DE-FG52-06NA27490, $ 752,117
Project Title: "Distributed Wireless Sensor Networks for Long-Term Deployments"
PIs: Ioannis Ch. Paschalidis and Christos G. Cassandras
Institution: Boston University

Project Goal: The research aims at addressing a number of fundamental issues in Distributed Wireless Sensor Networks, thus, contributing to the maturing of this technology so that it can be useful in long-term surveillance missions.

Collaborations:

1. LANL group led by Dr. Angela Mielke
2. Companies in the Sensor Network Consortium

Los Alamos NATIONAL LABORATORY

Sensor Network Consortium
Boston University

Acknowledgments: Wei Lai, Saikat Ray, X. Song, Dong Guo, Yin Chen, Wei Li, Jason Mao, Nikko Xu, Minyi Zhong

What are sensor networks ?

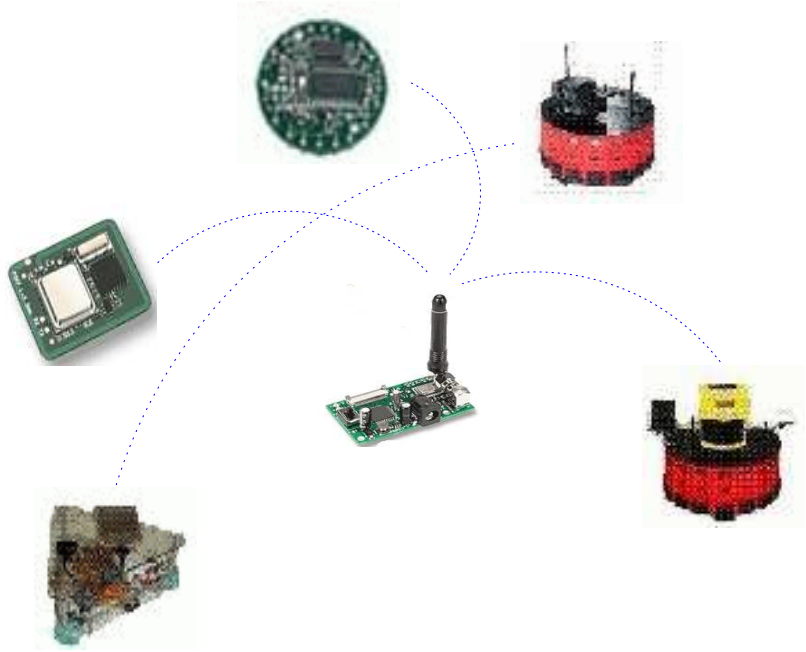

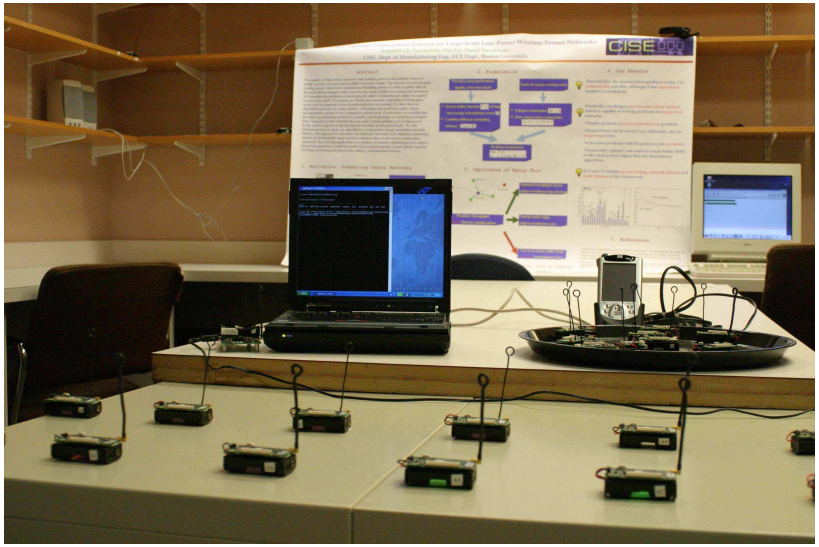

Sensor Networks (SNETs):

- consist of many (often small) devices — **the sensors** —
- communicate **wirelessly**, generally with **low power levels**;
- powered by batteries; limited processing capabilities;
- used to monitor (and **control**) a **physical** process or system.

Why are people so excited about SNETs ?




- Key characteristics: **size of sensors, wireless, battery powered**.
- Give rise to an endless list of potential applications: industrial/building automation, intelligent home networking, patient monitoring in health care, **homeland security**, **environmental monitoring**, wildlife monitoring, agriculture, **equipment and personnel tracking**.
- Brought about by **convergence** of **communications**, **computing**, and **control**.
- SNETs **interact with the physical world** vs. living in cyberspace.

Why are people so excited about SNETs ?




- Key characteristics: **size of sensors, wireless, battery powered**.
- Give rise to an endless list of potential applications: industrial/building automation, intelligent home networking, patient monitoring in health care, **homeland security**, **environmental monitoring**, wildlife monitoring, agriculture, **equipment and personnel tracking**.
- Brought about by **convergence** of **communications**, **computing**, and **control**.
- SNETs **interact with the physical world** vs. living in cyberspace. **The Internet of things !**

Research challenges

... or **What is different from communication nets we have been studying since the days of Erlang ?**

- **SNETs**: as the name suggests they **sense** (i.e., process information like **computers**) but also act as a (communication) **network**.
- **Wireless**: harder to deal with, layering is less effective.
- **Battery power**: energy conservation is important (affects protocols, network control, etc.).

Research challenges

... or **What is different from communication nets we have been studying since the days of Erlang ?**

- **SNETs**: as the name suggests they **sense** (i.e., process information like **computers**) but also act as a (communication) **network**.
- **Wireless**: harder to deal with, layering is less effective.
- **Battery power**: energy conservation is important (affects protocols, network control, etc.).
- **Efficient (i.e., optimized) operation**: not merely a desirable luxury but rather an indispensable necessity.

Outline (and Project Milestones)

- **Optimal deployment**
- **Localization**
- **Energy management**
  - **Node level: Dynamic Voltage Scaling (DVS), intelligent ON-OFF idling, and data batching**
  - **Network level: QoS-aware minimal energy routing, and energy efficient Multiple Access Control (MAC)**
- **Statistical anomaly detection**
- **Concluding remarks and future work**

Outline (and Project Milestones)

- **Optimal deployment**
- **Localization**
- **Energy management**
  - **Node level: Dynamic Voltage Scaling (DVS), intelligent ON-OFF idling, and data batching**
  - **Network level: QoS-aware minimal energy routing, and energy efficient Multiple Access Control (MAC)**
- **Statistical anomaly detection**
- **Concluding remarks and future work**

Common Theme

The role of optimization ...

Optimal Deployment

Goal: Deploy (possibly mobile) sensor nodes to maximize data source detection probability.

- Unknown data sources.
- Data sources may be mobile.

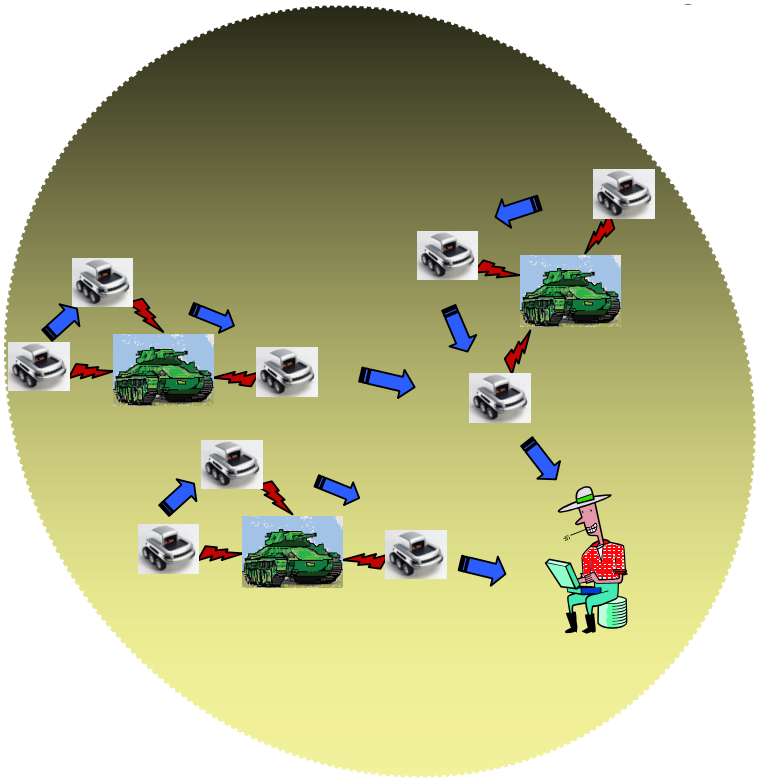

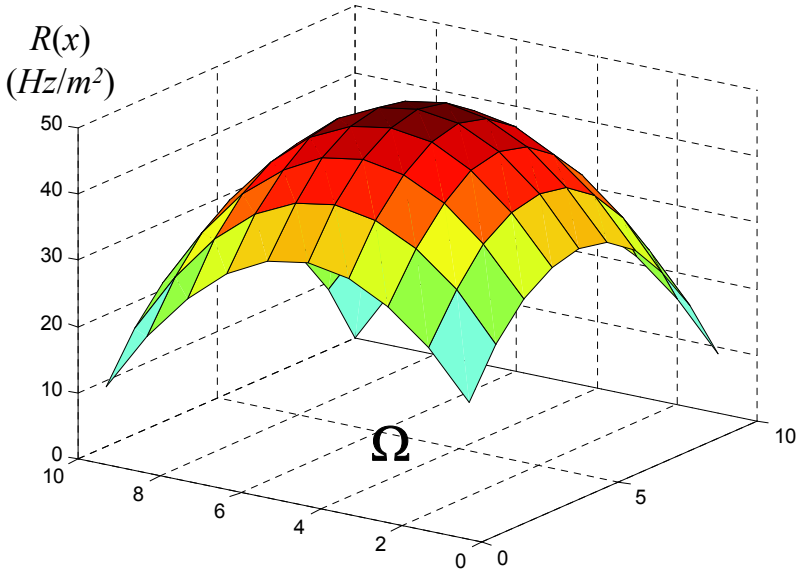

Perceived data source density over mission space

Optimal Deployment (cont.)

Formulation:

- Data source at $\mathbf{x}$ emits signal detected by sensor located at $\mathbf{s}_i$ with probability $p_i(\mathbf{x})$
- $p_i(\mathbf{x})$ is a decreasing function of distance between $\mathbf{x}$ and $\mathbf{s}_i$
- Determine locations $\mathbf{s}_i$ $(i = 1, \ldots, N)$ to maximize total detection probability
- Incorporate energy costs due to wireless communications

Optimal Deployment (cont.)

Formulation:

- Data source at $\mathbf{x}$ emits signal detected by sensor located at $\mathbf{s}_i$ with probability $p_i(\mathbf{x})$
- $p_i(\mathbf{x})$ is a decreasing function of distance between $\mathbf{x}$ and $\mathbf{s}_i$
- Determine locations $\mathbf{s}_i$ $(i = 1, \ldots, N)$ to maximize total detection probability
- Incorporate energy costs due to wireless communications

Our Solution:

- Distributed algorithm solving this maximization problem
- Limited computation within node capabilities
- Extension to allow for obstacles

Software demo:

`http://frontera.bu.edu/Applets/CoverageContr/index.html`

Optimal Deployment Demo – With Obstacles

(Deployment Demo)

Outline (and Project Milestones)

- Optimal deployment
- **Localization**
- Energy management
  - Node level: Dynamic Voltage Scaling (DVS), intelligent ON-OFF idling, and data batching
  - Network level: QoS-aware minimal energy routing, and energy efficient Multiple Access Control (MAC)
- Statistical anomaly detection
- Concluding remarks and future work

Localization

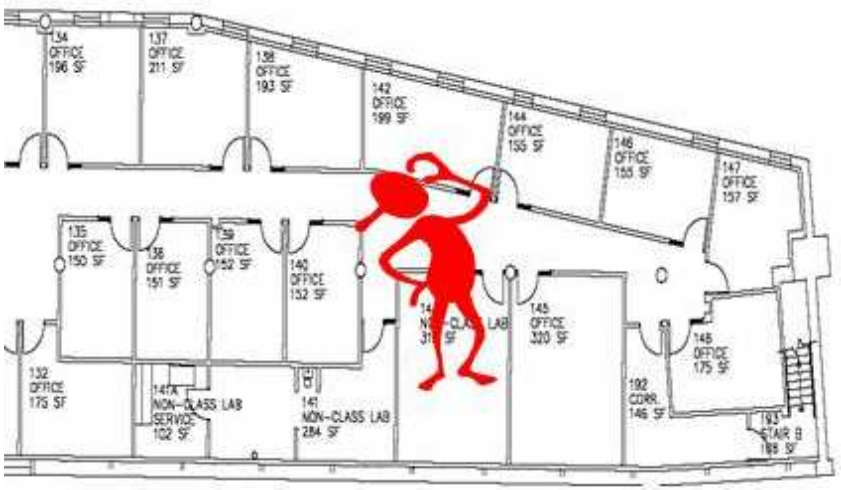

Applications:

- Location-based services: "intelligent" active maps, "smart" office applications, "smart" home applications.
- Fault/anomaly localization and maintenance in SNETs.
- "Active" RFIDs: asset and personnel tracking (e.g., in hospitals, ports, industrial sites).
- Counter-action and rescue of victims in natural or man-made disasters.

A statistical approach

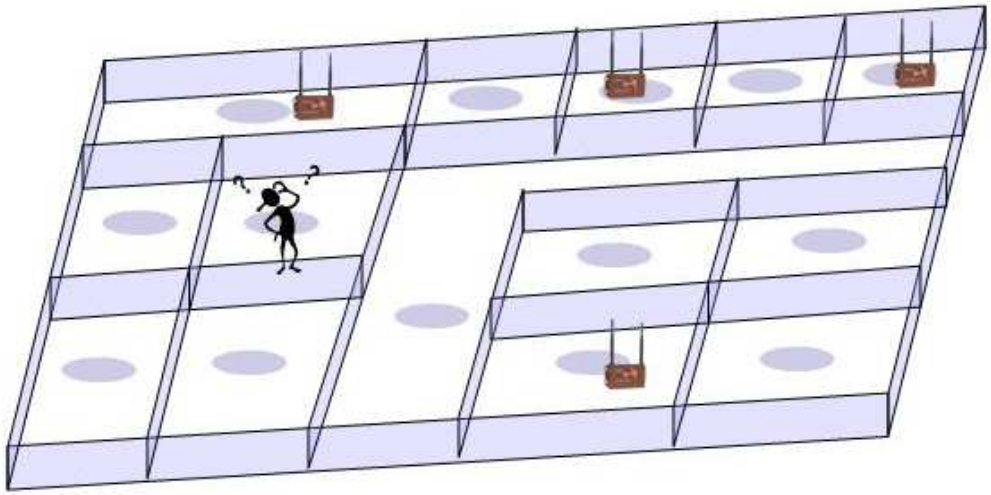

- Hierarchical SNET deployment: **sensors** and (stationary) **clusterheads**.
- When sensors transmit clusterheads receive the signal and measure **signal characteristics** (e.g., signal strength) — the **observation vector**.
- From **random** observation vector infer sensor location.
- Our approach: characterization of **probability of error**, optimal **clusterhead deployment**, **distributed** decision engine.

Boston university statistical Localization system (BLoc)

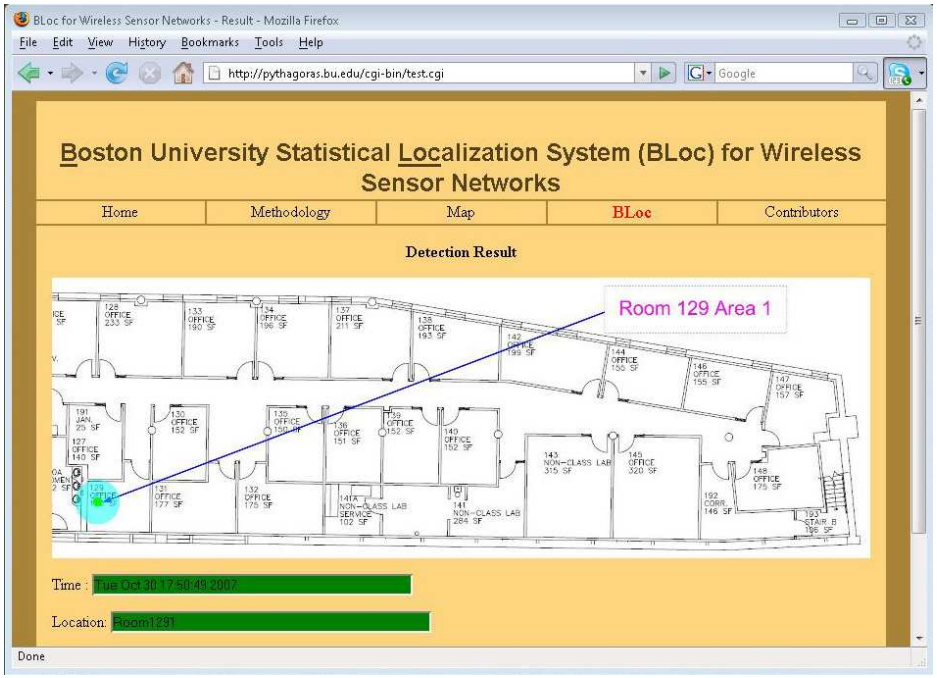

- Testbed using motes, stargates, and a Web interface covering 5.3K sq. feet.
- One clusterhead per 500 sq. feet on average.
- Mean error distance: From **8 feet to 9 inches** depending on the setup.
- A **factor of 3.6 improvement** over state-of-the-art stochastic triangulation methods.

Outline (and Project Milestones)

- Optimal deployment
- Localization
- **Energy management**
  - **Node level: Dynamic Voltage Scaling (DVS), intelligent ON-OFF idling, and data batching**
  - **Network level: QoS-aware minimal energy routing, and energy efficient Multiple Access Control (MAC)**
- Statistical anomaly detection
- Concluding remarks and future work

Dynamic Voltage Scaling (DVS)

Goal: Save battery power by dynamically varying voltage for sensing, processing, communication tasks.

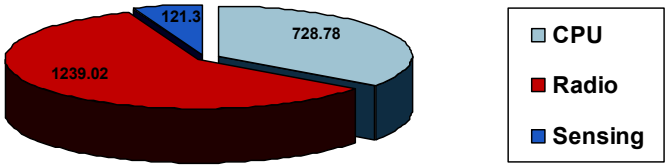

Rationale: $E = cV^2 \Rightarrow$ small reduction in V results in quadratic savings in E

Tradeoff: lower voltage $\Rightarrow$ less energy

But: lower voltage $\Rightarrow$ higher latency

Dynamic Voltage Scaling (DVS)

Goal: Save battery power by dynamically varying voltage for sensing, processing, communication tasks.

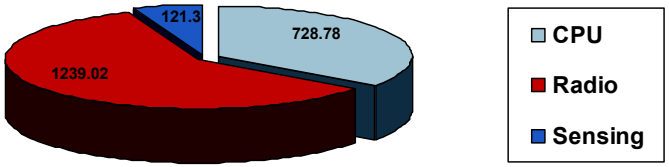

Rationale: $E = cV^2 \Rightarrow$ small reduction in V results in quadratic savings in E

Tradeoff: lower voltage $\Rightarrow$ less energy

But: lower voltage $\Rightarrow$ higher latency

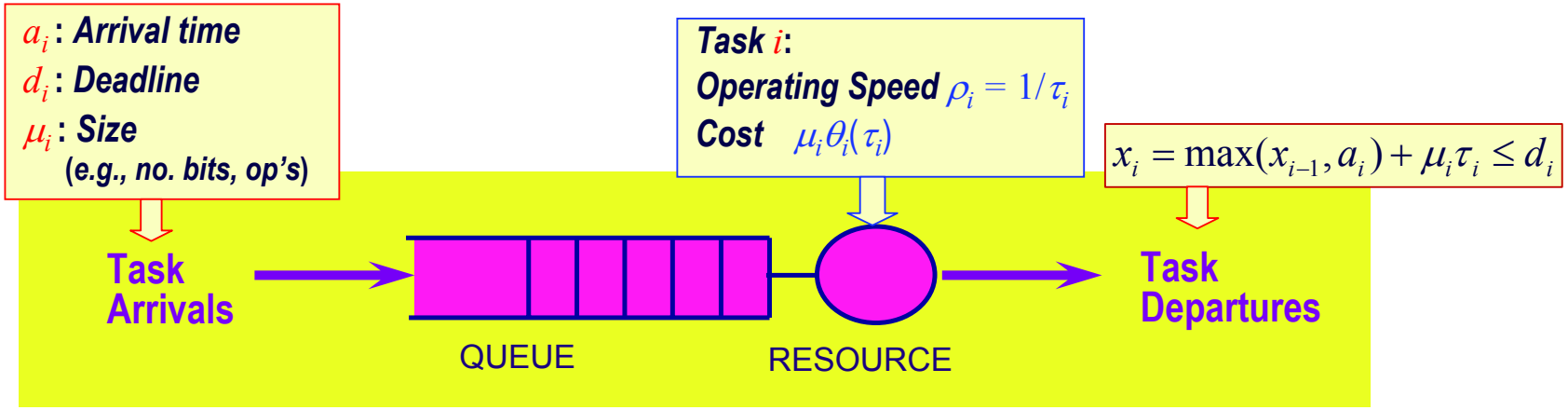

Critical Task Decomposition Algorithm (CTDA)

Formulation: Random task arrivals, random time constraint per task, non-preemptive processing

Minimize	Total Energy over all node tasks
Subject to	Timing Dynamics of tasks
	Real-time task constraints (hard time guarantees)

Our Solution:

- Exploit structural properties of the optimal solution to this problem
- Reduce problem to simple procedure for determining "critical tasks"
- Optimal solution between successive critical tasks easily obtained
- Resulting CTDA is scalable and very efficient
- At least **one order of magnitude faster than state-of-the-art**

Intelligent Node-Level ON-OFF Control

Idle Listening accounts for the largest energy waste in SNETs.

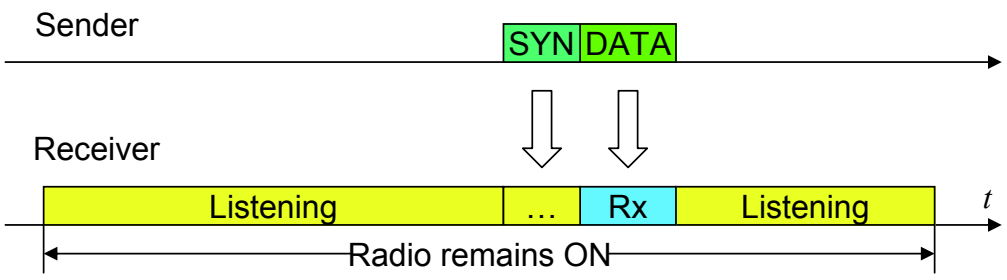

An **Intelligent** Low-Power Listening (I-LPL) approach:

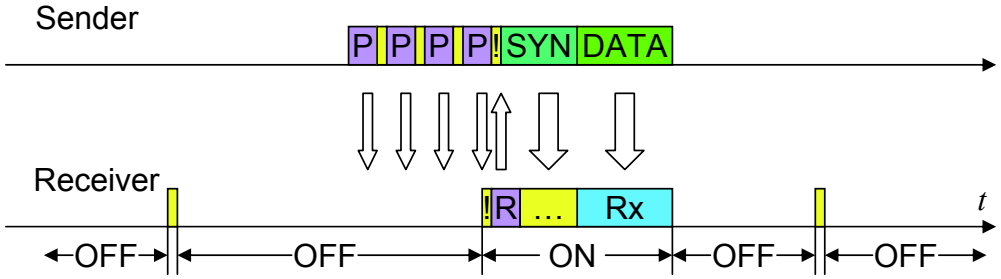

Intelligent Node-Level ON-OFF Control

Idle Listening accounts for the largest energy waste in SNETs.

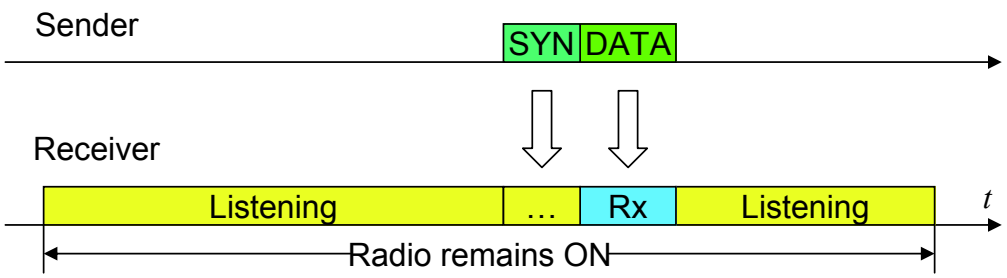

An **Intelligent** Low-Power Listening (I-LPL) approach:

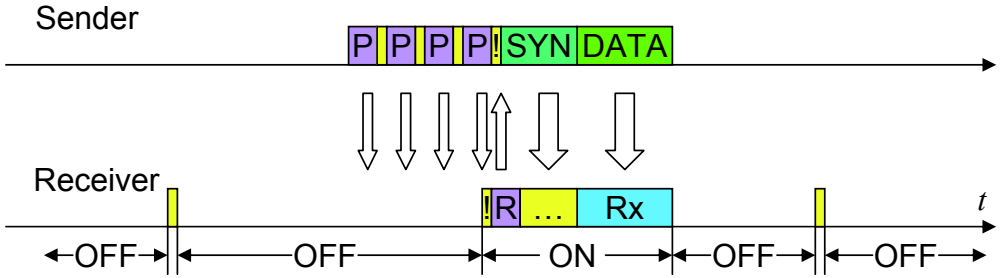

OBJECTIVE: **Minimize the total energy (Tx+Rx) spent on each message, and adapt to different network statistics.**

Intelligent Node-Level ON-OFF Control (cont.)

Key tradeoff: Poll frequently: $E_{Rx} \uparrow$, $E_{Tx} \downarrow$
vs. Poll infrequently: $E_{Rx} \downarrow$, $E_{Tx} \uparrow$
Novelty:

- Previous work (LPL): a static control of **periodic channel polling**.
- Our novel idea: sleep time should **adapt to known statistical information**.

Aperiodic channel polling:

Unlikely to have an arrival in near future	☞ **Poll Less frequently**
Likely to have an arrival in near future	☞ **Poll More frequently**

Main results:

- A quantile-based approximation/estimation of event statistics.
- An efficient algorithm to solve for optimal sleep time.
- **15%-30% improvement over the best tuned LPL without any sacrifice**.

Message Batching in SNETs

Recall Low Power Listening: Transmission triggered by external events/upstream arrivals.

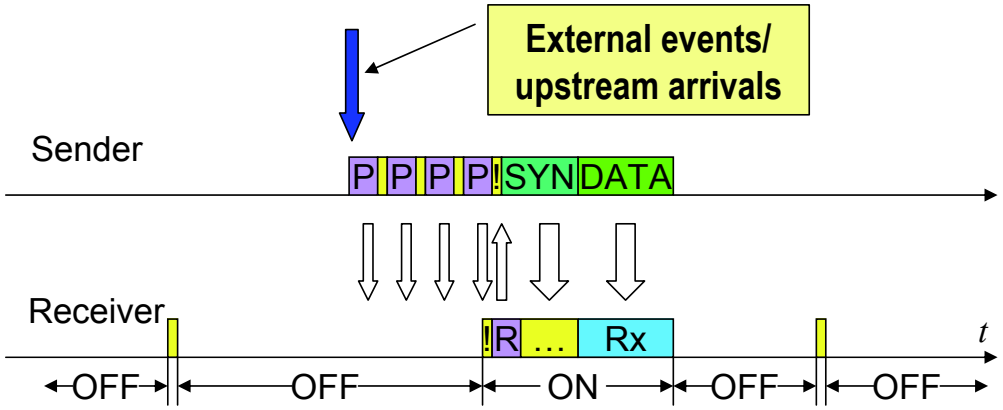

WSN traffic is generally bursty: Batching messages is desirable (**10%-40% performance improvements !**).

- Energy saved by multiple message sharing one preamble.
- Key trade-off: **delay** vs. **energy**.

APPROACH: Intentionally wait for W time before sending the preamble.
OBJECTIVE: Minimize a joint performance index of delay and energy.

Minimal energy routing with QoS guarantees

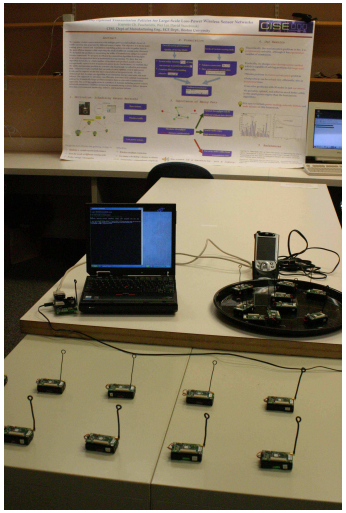

- Focus on **low data rate SNETs** serving **time-critical** applications (e.g., surveillance).
- To preserve energy have SNET nodes shut down their radios (**go to "sleep"**).
- Hence, SNETs can operate in an **event-based** sensing mode.
- This creates challenges for (timely) routing data to the gateway.
- Trade-off: Long hops (lots of **energy**) vs. short hops (large **delay**).
- **Formulation**: Minimal energy routing subject to $\mathbf{P}[\text{delay}] \leq \epsilon$.

Distributed routing discovery algorithm

(Distributed routing discovery algorithm)

MAC scheduling

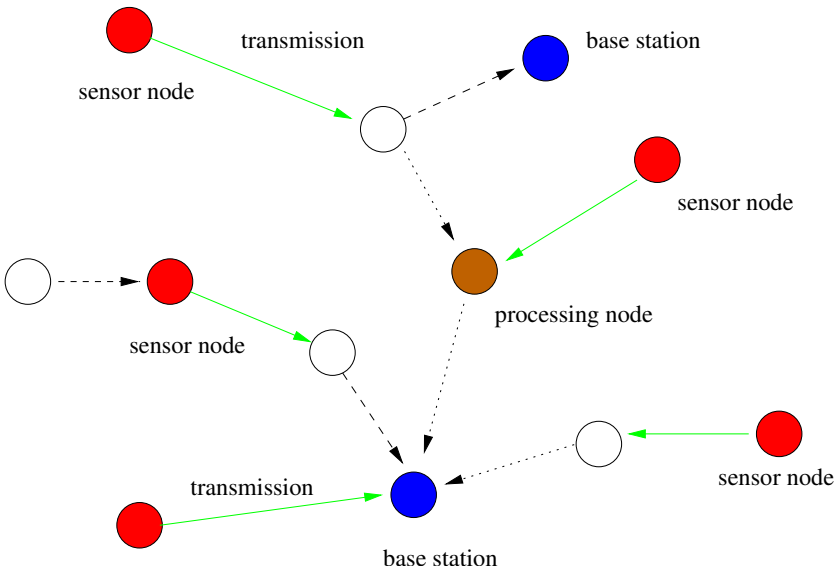

- Focus on situations where lots of data have been generated and we seek to efficiently collect them at the gateways (**data collection at congestion periods**).
- Nodes can only do one task at a time (send or receive) and concurrent transmissions cause **interference**.
- Stringent **energy constraints** (i.e., random MAC is often inefficient, benefits from multihop), hence, **transmission scheduling**.

MAC scheduling (cont.)

- Formulation:

Maximize	Utility of transmission rates
subject to	Physical layer constraints
	Node exclusion constraints
	Fairness Constraints

- Key ideas: **characterize the region of achievable rates**, $\mathscr{R}$, and optimize efficiently.
- Our approach is based on **decomposition** methods in large-scale optimization.
- Allows us to trade-off **energy** (i.e., network lifetime) **vs. performance**, **address scalability** issues, and **efficiently recover from node failures**.

Outline (and Project Milestones)

- Optimal deployment
- Localization
- Energy management
  - Node level: Dynamic Voltage Scaling (DVS), intelligent ON-OFF idling, and data batching
  - Network level: QoS-aware minimal energy routing, and energy efficient Multiple Access Control (MAC)
- **Statistical anomaly detection**
- Concluding remarks and future work

Spatio-temporal statistical anomaly detection

- Detect (significant) changes in environmental variables monitored by SNETs.
- Detect "attacks" on the SNET: **sinkholes**, **wormholes**, **selective forwarding**, **selective interference**, etc.
- **Time series** of "data" collected in various **locations**.
- **Statistical** (vs. signature-based) anomaly detection.

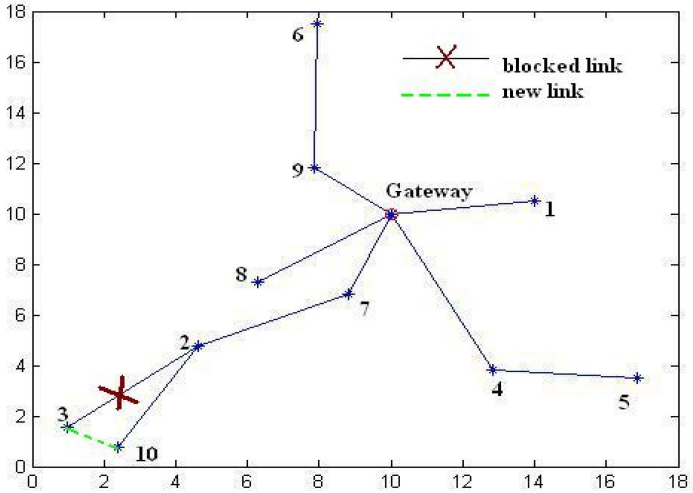

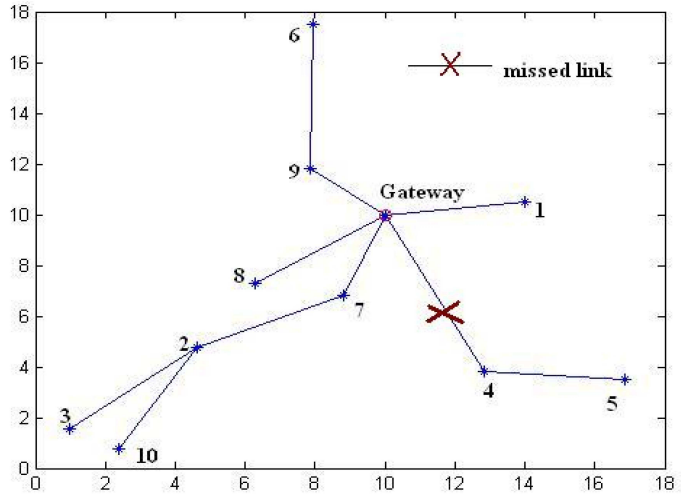

Outline (and Project Milestones)

- Optimal deployment
- Localization
- Energy management
  - Node level: Dynamic Voltage Scaling (DVS), intelligent ON-OFF idling, and data batching
  - Network level: QoS-aware minimal energy routing, and energy efficient Multiple Access Control (MAC)
- Statistical anomaly detection
- **Concluding remarks and future work**

Conclusions and future work

Wireless Sensor Networks being **extremely resource constrained** (energy, size, computational capabilities, unreliable and highly variable wireless medium) and **tied to the application** they form an exciting playground for **stochastic optimization**.

Future Work

- **Deployment:** with obstacles, dynamic setting.
- **Localization:** Location distinction, tracking.
- **Energy Management:** Batching, Protocol model in MAC scheduling.
- **Anomaly Detection:** SNET topology anomalies.

Questions, References: yannisp@bu.edu, http://ionia.bu.edu/

WSRC-STI-2007-00656

UITI2007 - University Information Technical Interchange Review Meeting

SRNL™
SAVANNAH RIVER NATIONAL LABORATORY

We Put Science To Work

Simulations and Algorithms

National Laboratory Overview

Dr. Alfred J. Garrett

November 28, 2007

SRNL™

SRNL's Core Competencies

Reactor Fuel Technology	Fuel Fabrication and Processing	Alternative Treatments, Non-Proliferation Technologies
Material Processing	Chemical Separations Technology	Legacy Material Processing, GNEP Support
High Level Waste Processing	High Level Waste Treatment Technologies	Waste Stabilization Technology / Process Development and Demonstration
Tritium Processing	Hydrogen Technology	Reservoir Surveillance Life Extension Hydrogen Storage Applications Hydrogen Production
Process Monitoring	High Sensitivity Measurements	National Security Nuclear Forensics National Law Enforcement
Environmental Restoration	Characterization and Remediation Technologies	Long Term Stewardship Monitored Natural Remediation Accelerated Closure HLW Tank Closure

SRNL

SRNL Research Emphasis Areas

National Security

- Tritium Technology
- Plutonium Technology
- Homeland Security Support
- Non-Proliferation Technology

Energy Security

- Technology for the Hydrogen Economy
- Thermochemical Production of Hydrogen
- Global Nuclear Energy Partnership
  - Fuel Technology
  - Fuel Reprocessing
  - Waste Form Development
- Renewable Energy Research
  - Biofuels for ethanol and hydrogen

Environmental and Chemical Process Technology

- Materials Stabilization and Disposition
- Cleanup and Remediation Technologies
- Characterization, Analysis and Closure Technologies

SRNL

National Security

Nonproliferation

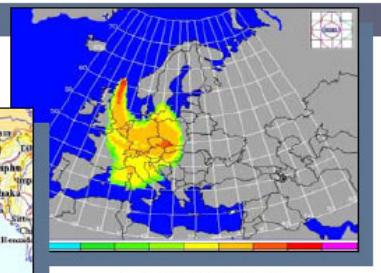

ENSEMBLE

Plume Path from Underground Nuclear Test

TRAC Vehicle- A Mobile Radiation Laboratory

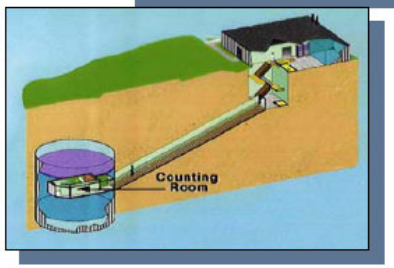

Underground Counting Facility

- **Atmospheric Transport**
  - Modeling to predict transport and fate of releases
    - ENSEMBLE participation
    - Emergency Response
- **Remote Sensing**
  - Detect proliferation nuclear testing
  - Detect reactor effluents
  - Detect and monitor nuclear proliferant undeclared operations
- **Collection/Detection**
  - Environmental signature monitoring
  - Remote sample collection systems
  - High sensitive radiation detection and measurement
  - High sensitivity material measurement technologies

High Sensitivity Measurement Technologies are vital to the Nation

SRNL

Project: Heat Flux Measurements from Imagery

- Participating Organizations: SRNL, Clemson University
- PI's and Co-investigators: A. J. Garrett (SRNL), J. R. Saylor (Clemson)
- Budget:
  - $670K in FY-06
  - $550K in FY-07
  - $500K in FY-08

SRNL

Project Overview and Goals

- Cooling lake efficiency (watts per m^2 for given weather conditions) often determines nuclear or fossil plant operating power level during summer.
- Measurement of heat losses from cooling lakes is critical to assessment of cooling lake efficiency.
  - Traditionally done with a large number of thermocouple measurements over lake
- Laboratory experiments done by John Saylor of Clemson University indicate that heat fluxes can be computed directly from thermal imagery.
- Goals of this project are to 1) determine if Saylor's results apply to actual cooling lakes and if so, 2) develop an algorithm that derives the total heat flux from the lake directly from thermal imagery with no supplementary information.

SRNL

Saylor's Laboratory Experiments

– Thermal convection experiments in a heated tank of water with and without imposed surface wind shear show a linear relationship between the standard deviation of temperature fluctuations in the thermal imagery (sigma) and the surface heat flux.

No wind stress

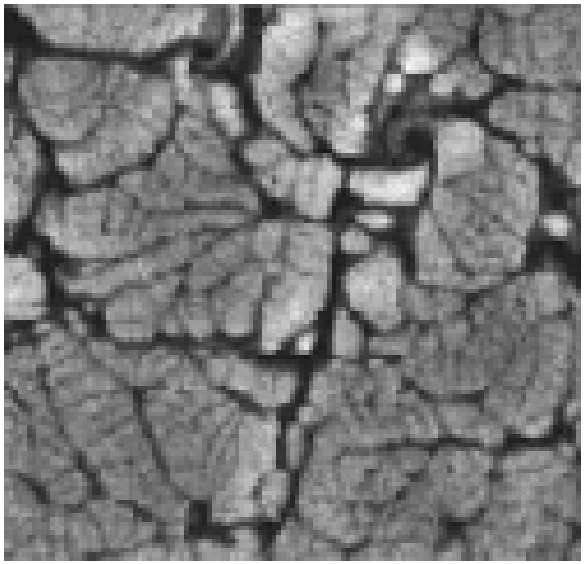

Wind Stress

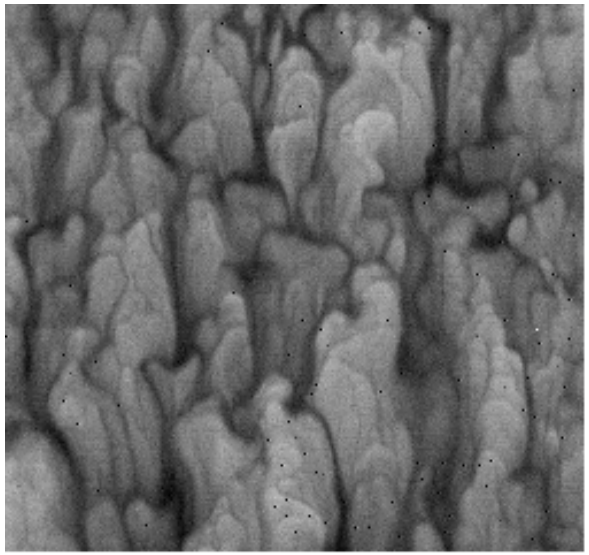

SRNL

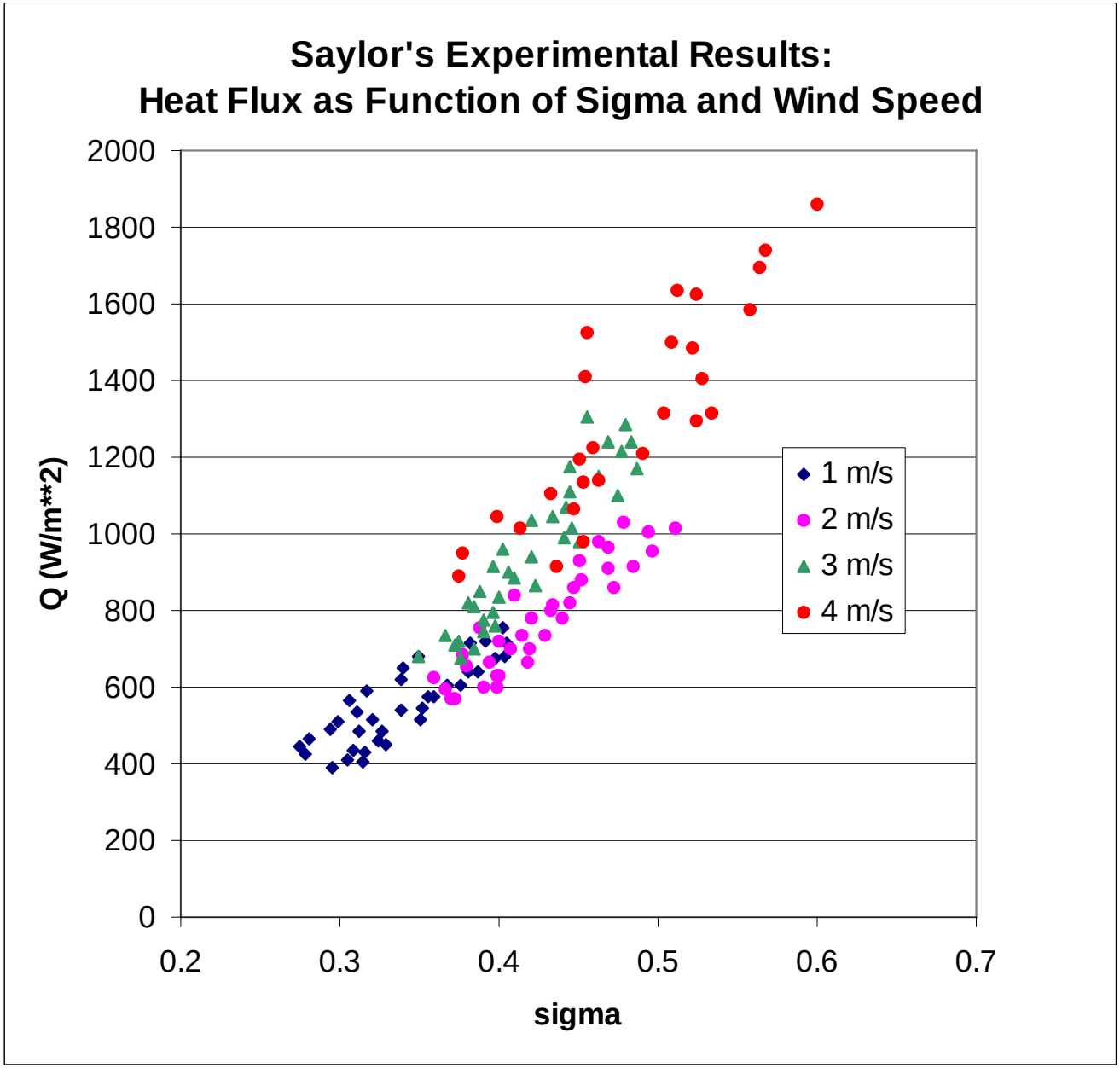
Saylor's Experimental Results:
Heat Flux as Function of Sigma and Wind Speed
Q (W/m**2)
2000
1800
1600
1400
1200
1000
800
600
400
200
0
0.2
0.3
0.4
0.5
0.6
0.7
sigma
1 m/s
2 m/s
3 m/s
4 m/s

SRNL

H. B. Robinson Power Plant Cooling Lake

Lake Robinson Collection: Run 2 Transect

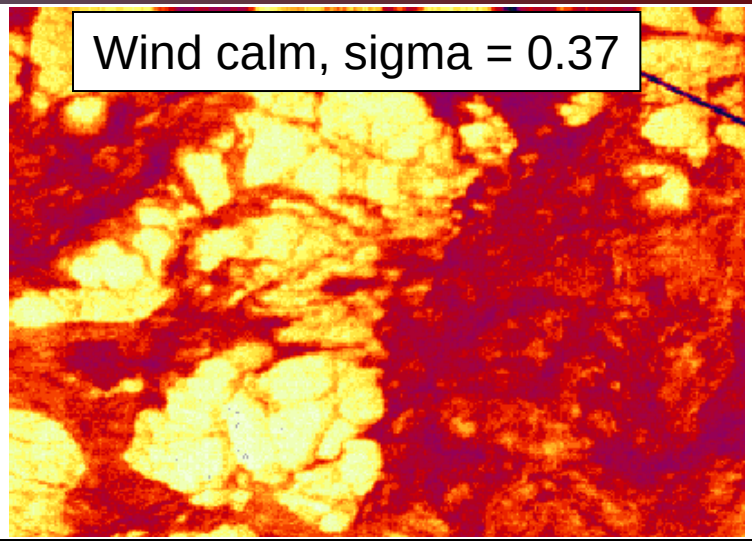

Wind speed = 3 m/s, sigma = 0.18

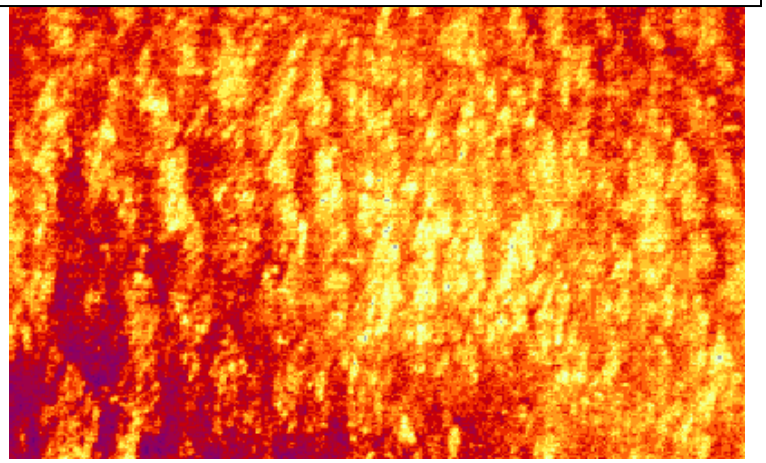

SRNL

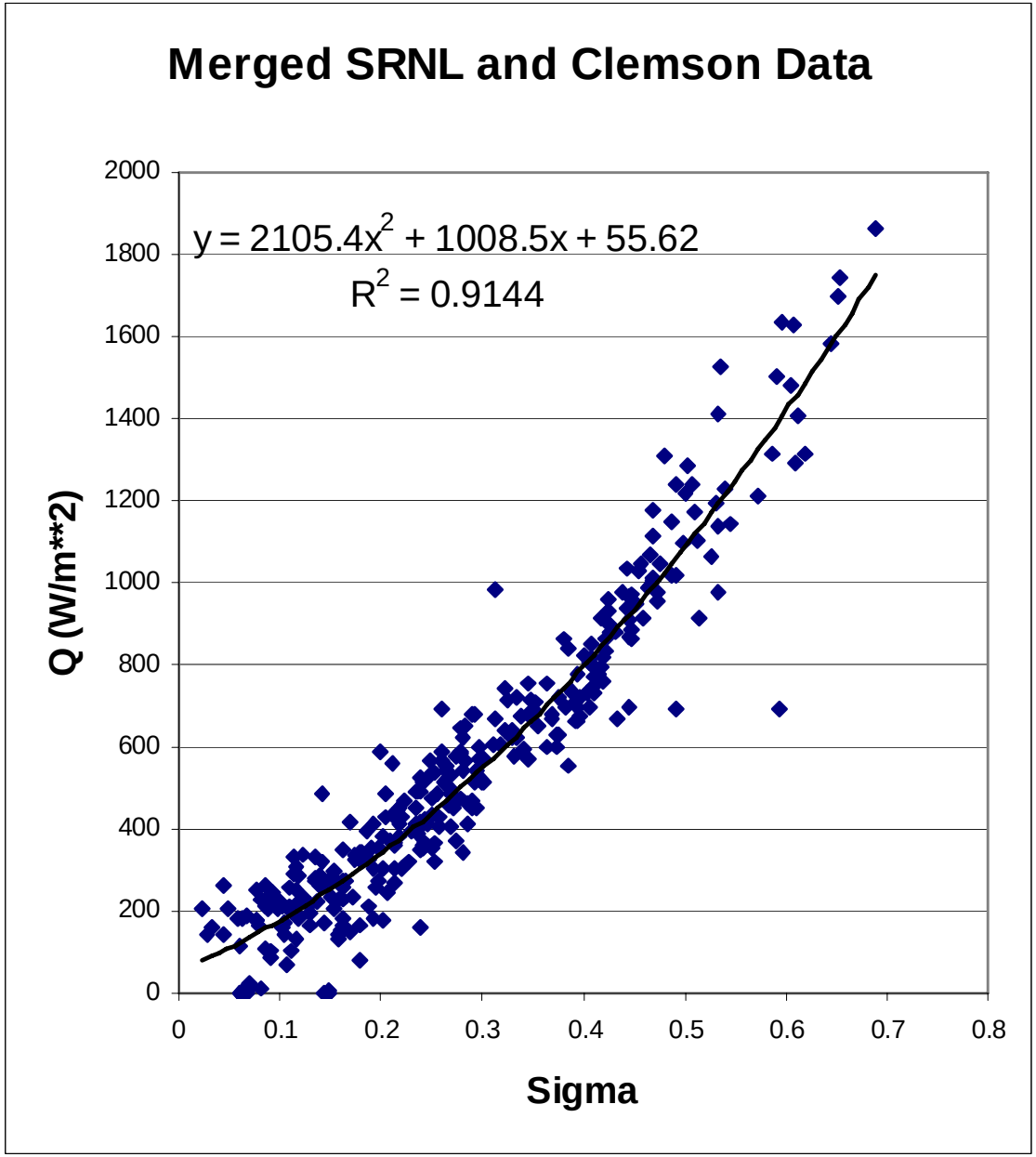
Merged SRNL and Clemson Data
y = 2105.4x2 + 1008.5x + 55.62
R2 = 0.9144
Q (W/m**2)
Sigma
0
200
400
600
800
1000
1200
1400
1600
1800
2000
0
0.1
0.2
0.3
0.4
0.5
0.6
0.7
0.8

Cooling Lake Imagery Processing

- Band pass filtering to remove camera artifacts and large scale thermal gradients that are not related to thermal convection.
- Correction to sigma – Q relationship to account for wind speed effects.
- Correction to sigma to account for truncation of spectrum of convective length scales as a function of image resolution.

SRNL

Milestones

- Verify Saylor's laboratory thermal convection experiments apply to cooling lakes by collecting imagery and ground truth
- Develop algorithm that eliminates non-convective noise from imagery and accounts for wind effects and image resolution
- Test algorithm's ability to accurately estimate total heat flux from cooling lake

SRNL

Remaining Work for Imagery Heat Flux Project

- Test validity of sigma – Q correlation with independent Comanche Peak data set.
  - Deep free convection layer
- Develop algorithm that automates band pass filtering, wind speed correction and image resolution correction to series of thermal images.

SRNL

Project: Optimal Atmospheric Characterization

- Participating Organizations: SRNL, University of North Carolina at Charlotte (UNC)
- PI's and Co-investigators: R. J. Kurzeja and B. L. O'steen (SRNL), B. Etherton (UNC)
- Budget:
  - $300K in FY-06
  - $300K in FY-07
  - $300K in FY-08

SRNL

Project Overview and Goals

- Regional scale atmospheric modeling can significantly improve weather forecasts by resolving local topographic features such as hills, valleys, land – sea contrasts and variability in surface roughness and vegetation cover, which strongly affect the atmospheric boundary layer.
- SRNL is using evolutionary programming (EP) algorithms to optimize the surface parameters used by a regional scale model (RAMS) in a way that produces the most accurate forecasts.
- Project goal is to find the most efficient and accurate version of the EP algorithm for this problem.

SRNL

Example of Improvement in Score Over Many Generations

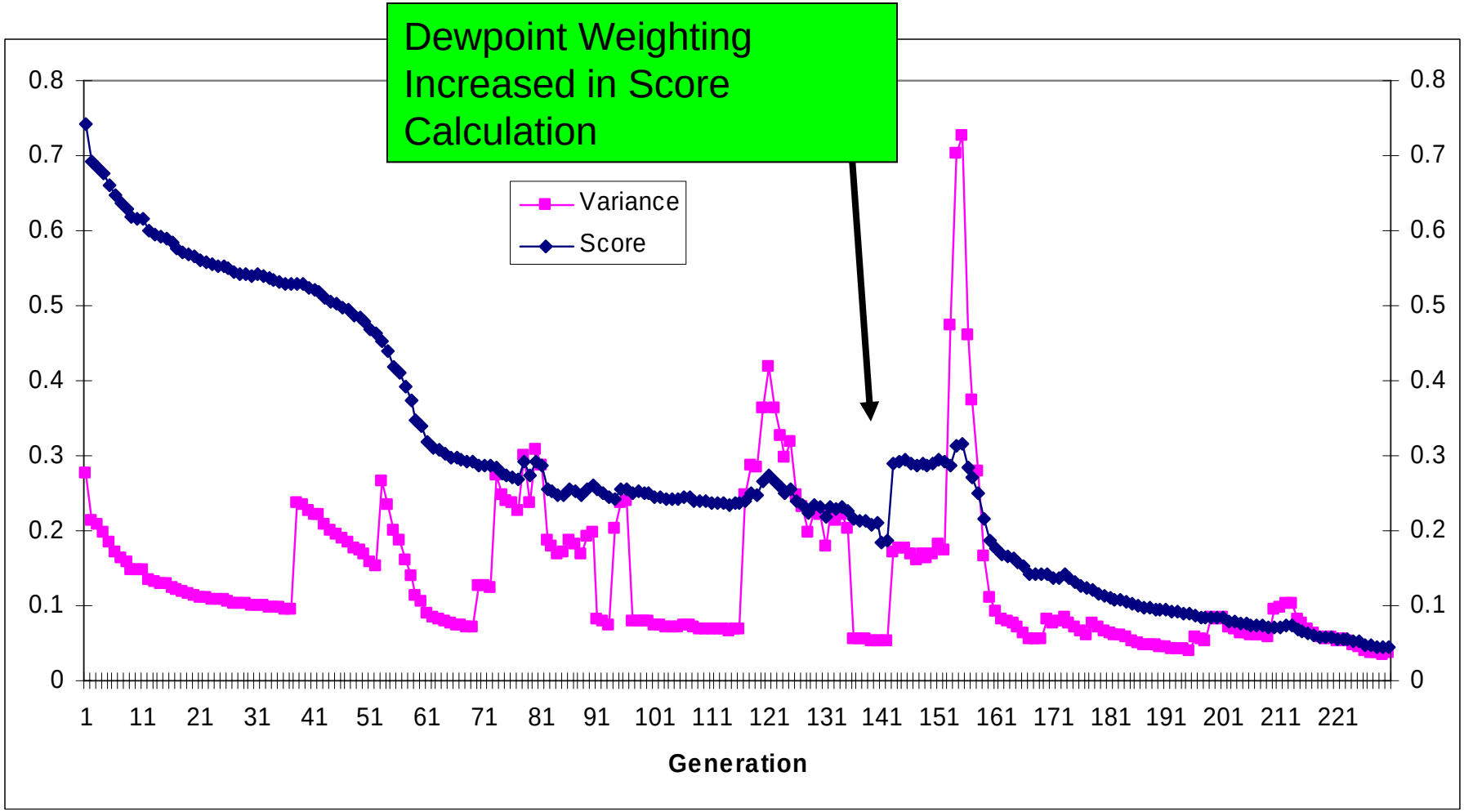

SRNL

Impact of Optimization on Speed

Single Station

Site M01

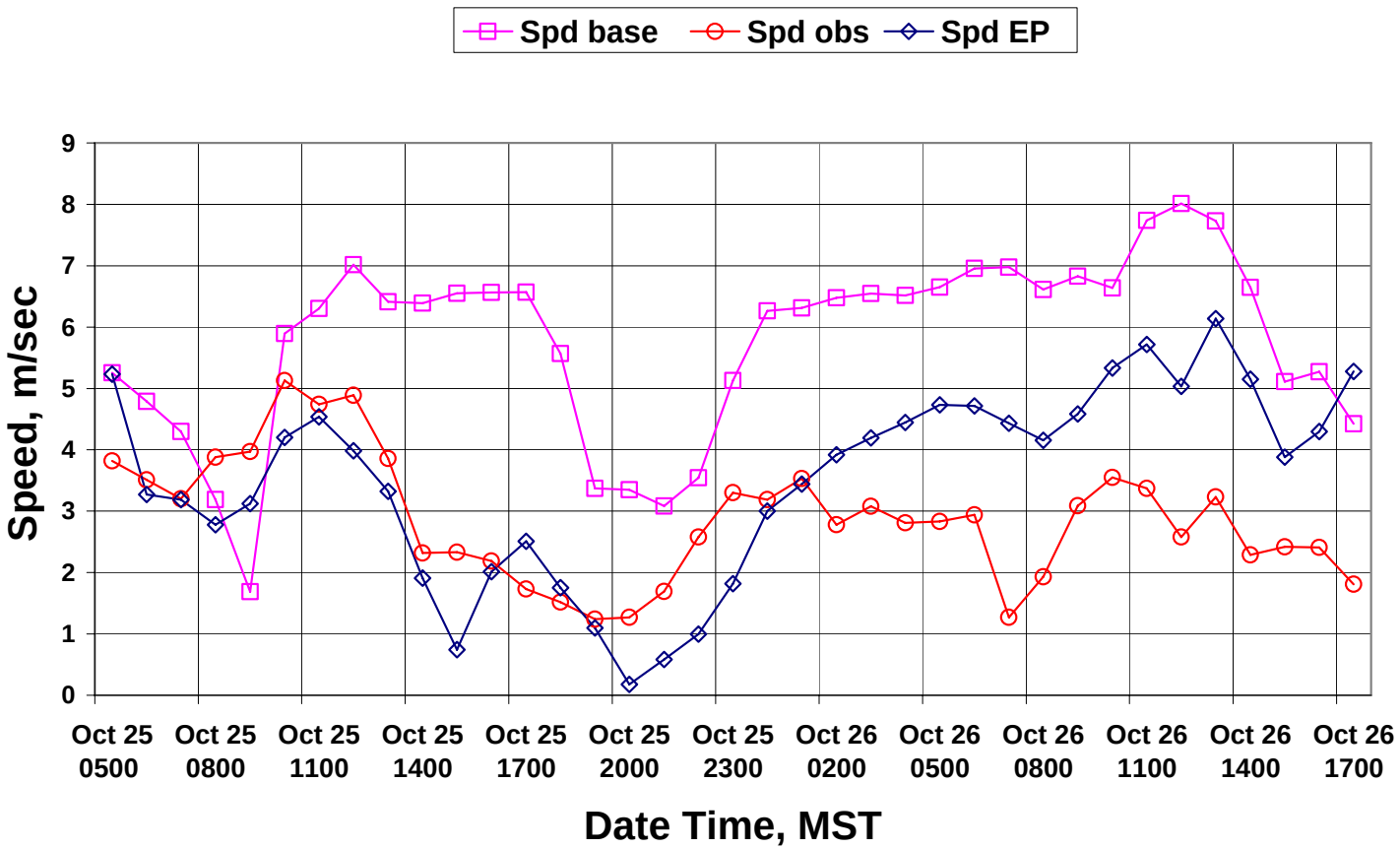

SRNL

Impact of Optimization on Temperature

12 Station Average

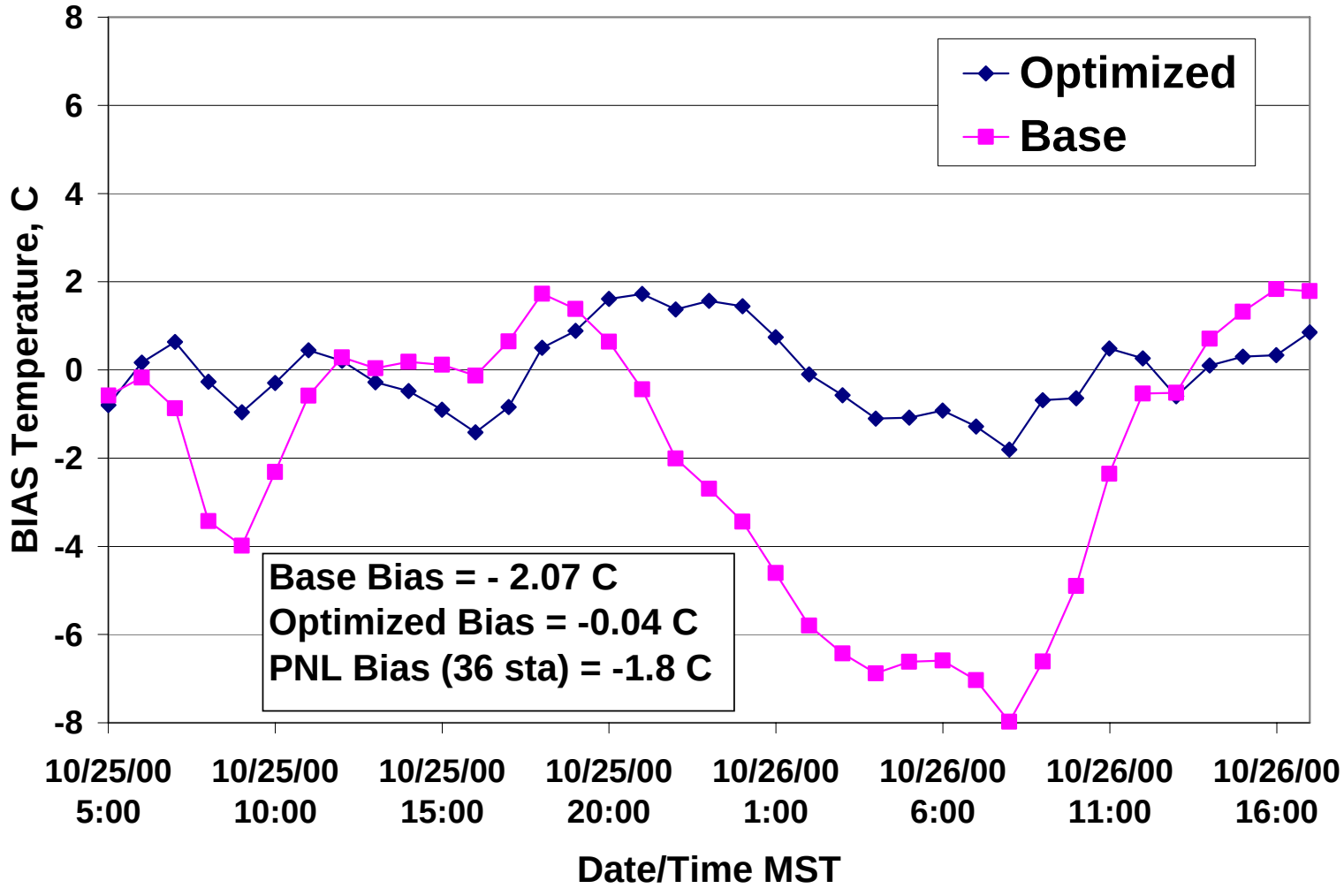

SRNL

Surface Temperature, October 26, 18z (1pm)

Target Run

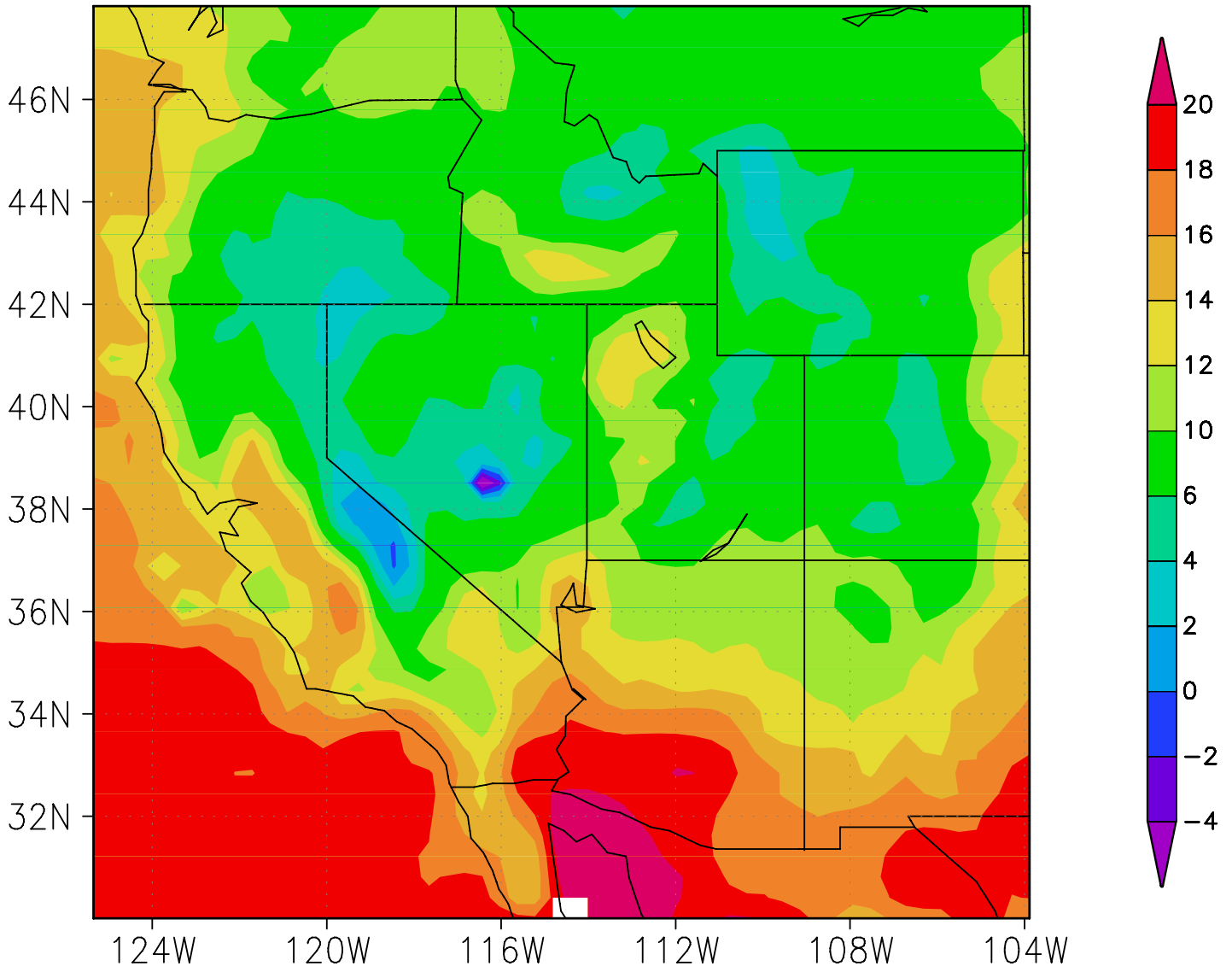

GrADS: COLA/IGES

2007−07−09−11:50

Surface Temperature, October 26, 18z (1pm)

Initial Run - Target Run

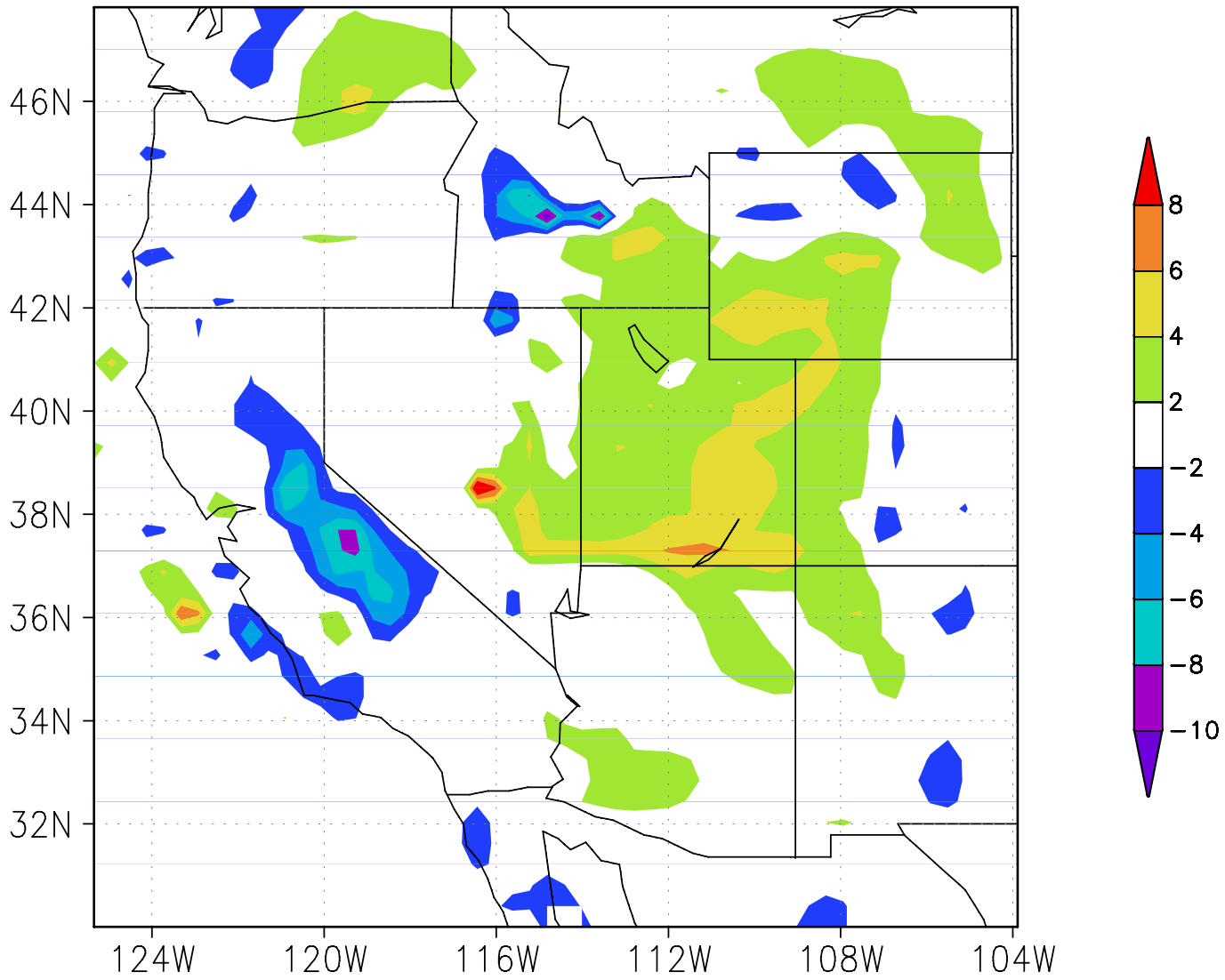

Surface Temperature, October 26, 18z (1pm)

Final Run - Target Run

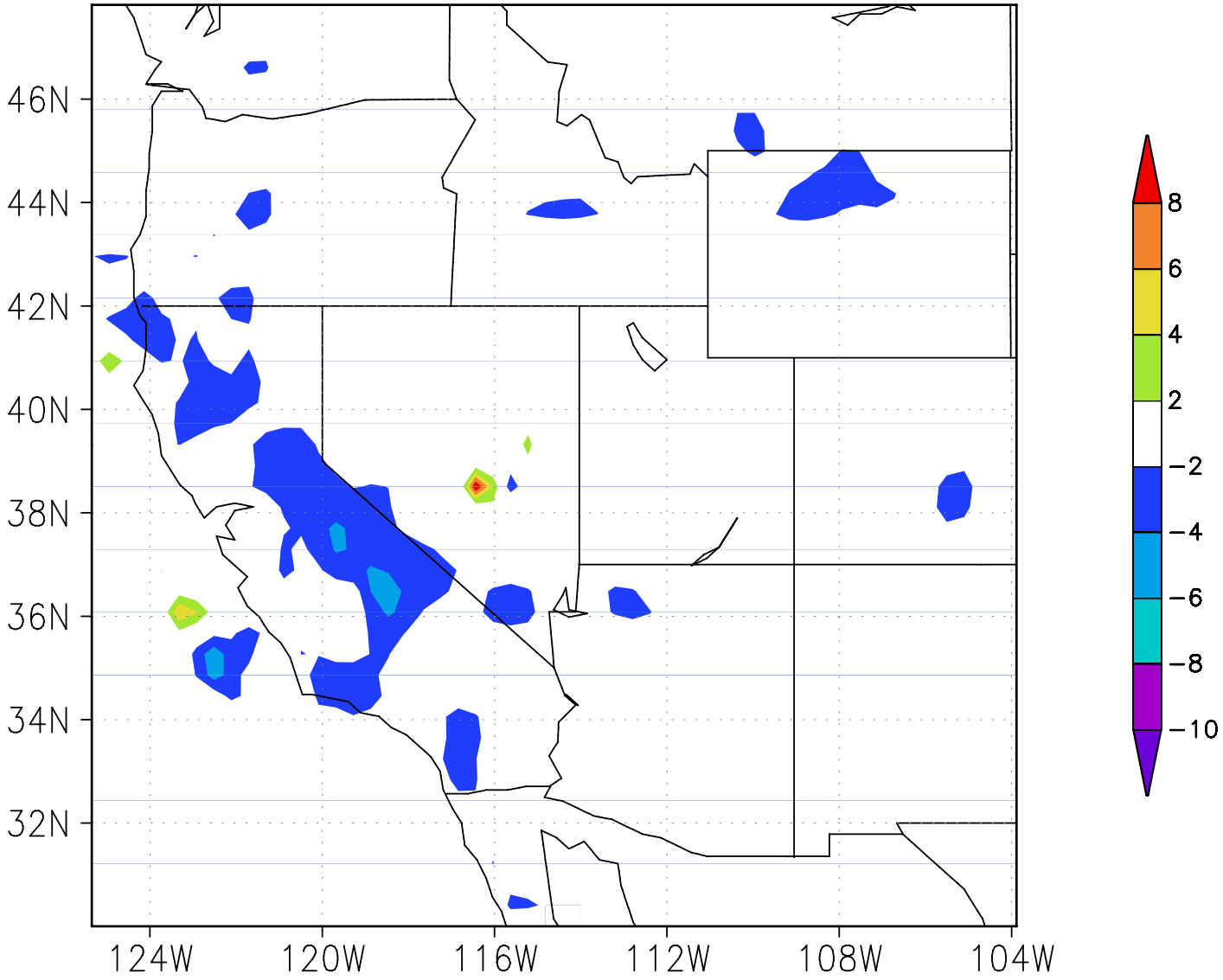

SRNL

Milestones

- Evaluate evolutionary algorithms that optimize the RAMS atmospheric model for VTMX meteorological and tracer database.
- Evaluate different evolutionary algorithms with synthetic Salt Lake valley meteorology to optimize the search efficiency and consistency.
- Apply evolutionary method to ANATEX tracer experiment and evaluate improvement in transport prediction.

SRNL

Remaining Work for Optimal Atmospheric Characterization Project

- Complete optimization tests with synthetic data sets.
- Perform validation analysis with independent (ANATEX) tracer data set.
- Determine efficacy of new data assimilation techniques
  - Incorporate remote sensing data.

SRNL

Project: Cooling Tower Assessment Tool

- Participating Organizations: SRNL, Rochester Institute of Technology (RIT)
- PI's and Co-investigators: A. J. Garrett, J. S. Bollinger (SRNL), C. Salvaggio (RIT)
- Budget:
  - $500K in FY-06
  - $450K in FY-07
  - $500K in FY-08

SRNL

Project Overview and Goals

- **MDCT's are widely used to dissipate industrial heat loads from a few megawatts up to about 100 megawatts.**
- **It is possible to derive information about cooling tower performance from accurately calibrated thermal imagery of MDCT's.**
- **Goal: develop a remote-sensing based method for deriving waste heat rejection rates (Q's) from thermal imagery of MDCT's:**
  - **Physics-based model that simulates mass and energy transfer inside the tower**
  - **3-D CFD modeling to quantify environmental effects not usually included in MDCT models (winds)**
  - **Full 3-D modeling of radiation transfer to establish quantitative relationship between throat exhaust temperature and upwelling radiance from MDCT throat**
- **Assess model performance with SRNL MDCT databases**
- **Determine impact of combined uncertainties on confidence limits of model-generated Q's.**

SRNL

Cooling Tower Photos and Flow Schematic

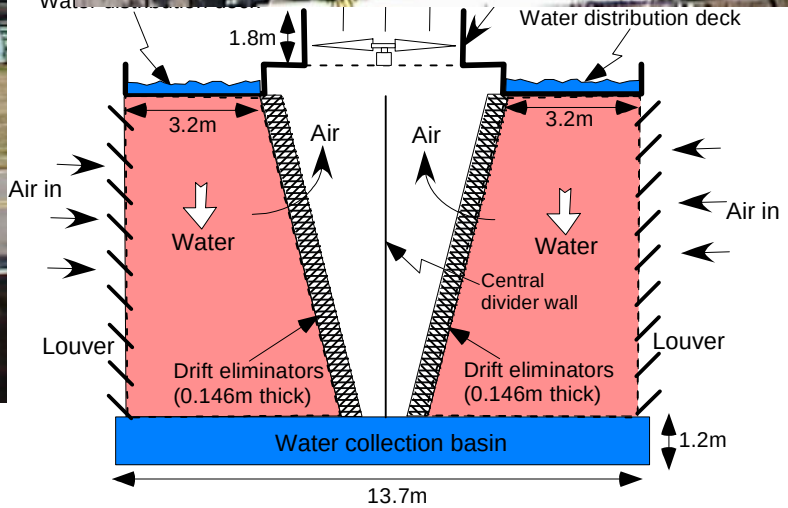

SRNL

FLUENT Simulation of Cooling Tower Thermal Exhaust and Validation Data

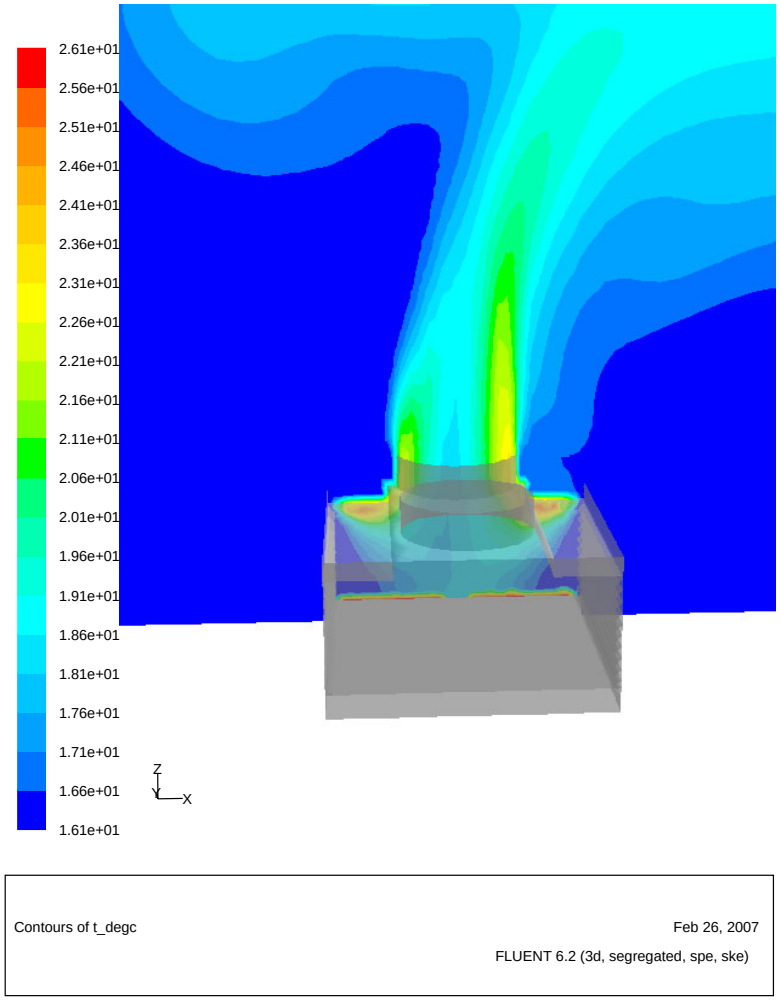

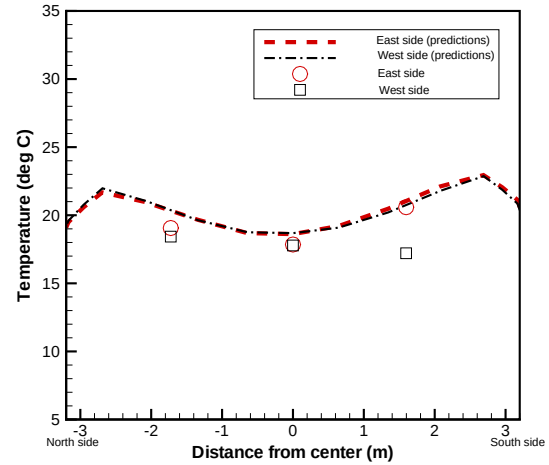

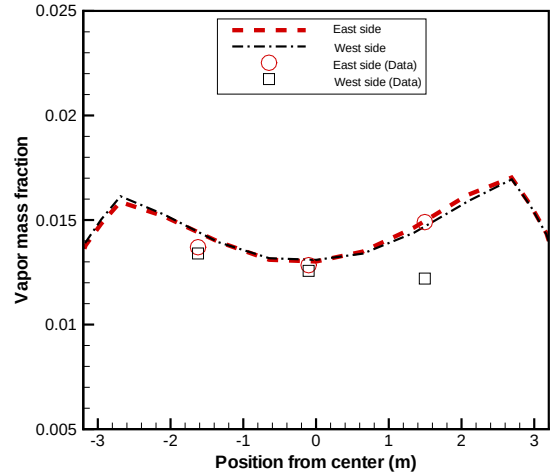

SRNL

FLUENT Simulation of Air Flow Around Tower and Falling Droplets in Tower

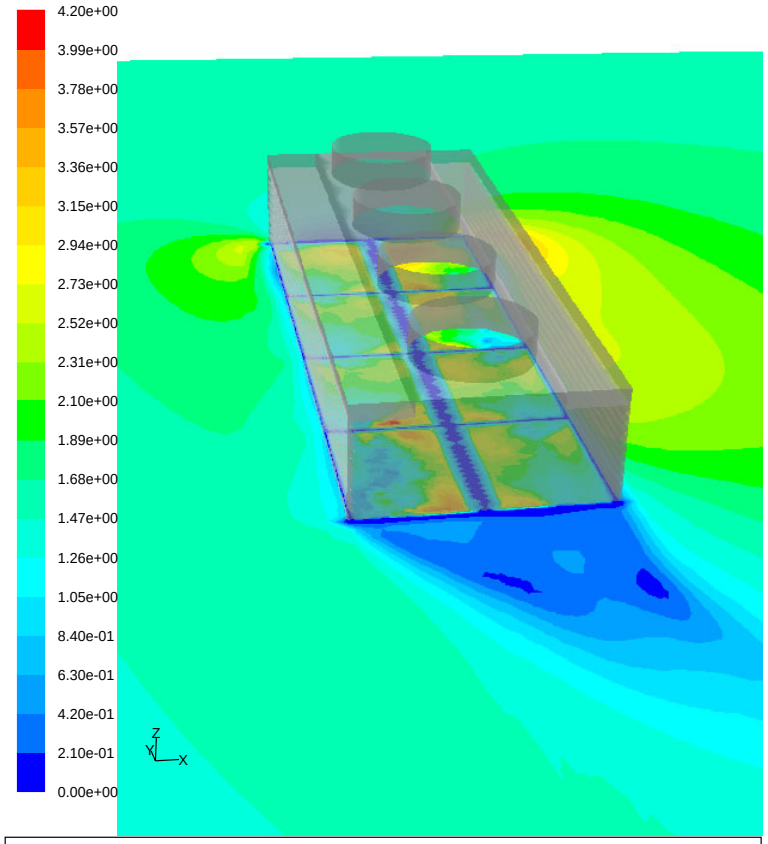

Contours of Velocity Magnitude (m/s)

Feb 26, 2007

FLUENT 6.2 (3d, segregated, spe, ske)

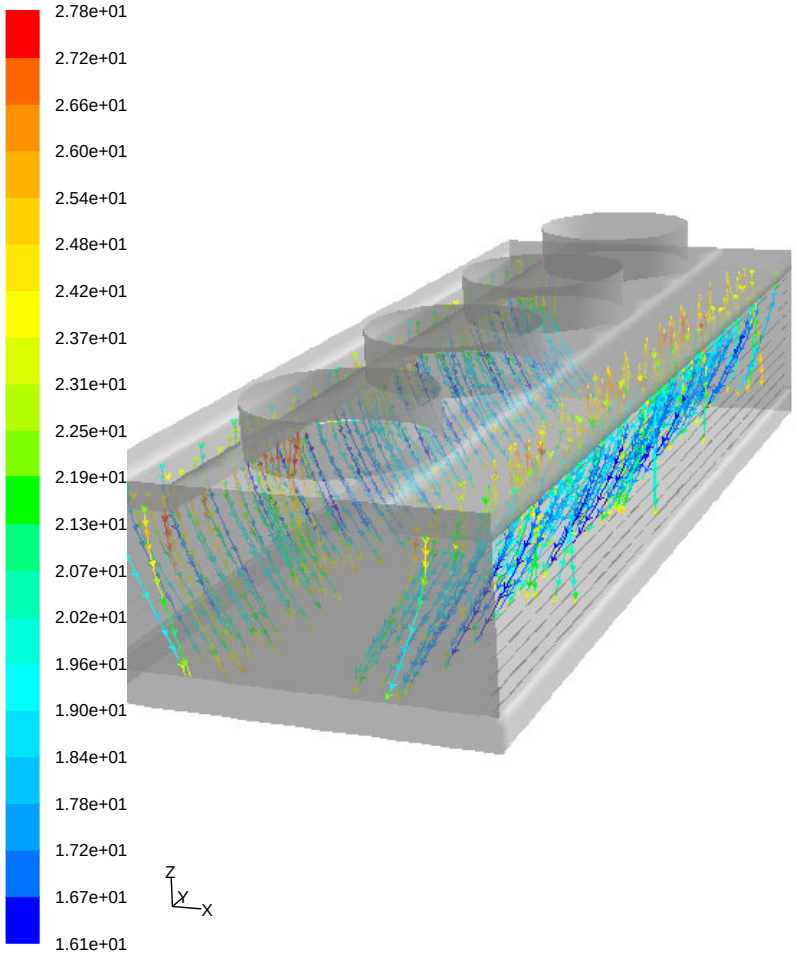

Particle Traces Colored by t_degc

Feb 27, 2007

FLUENT 6.2 (3d, segregated, spe, ske)

SRNL

Cooling Tower Thermal Images

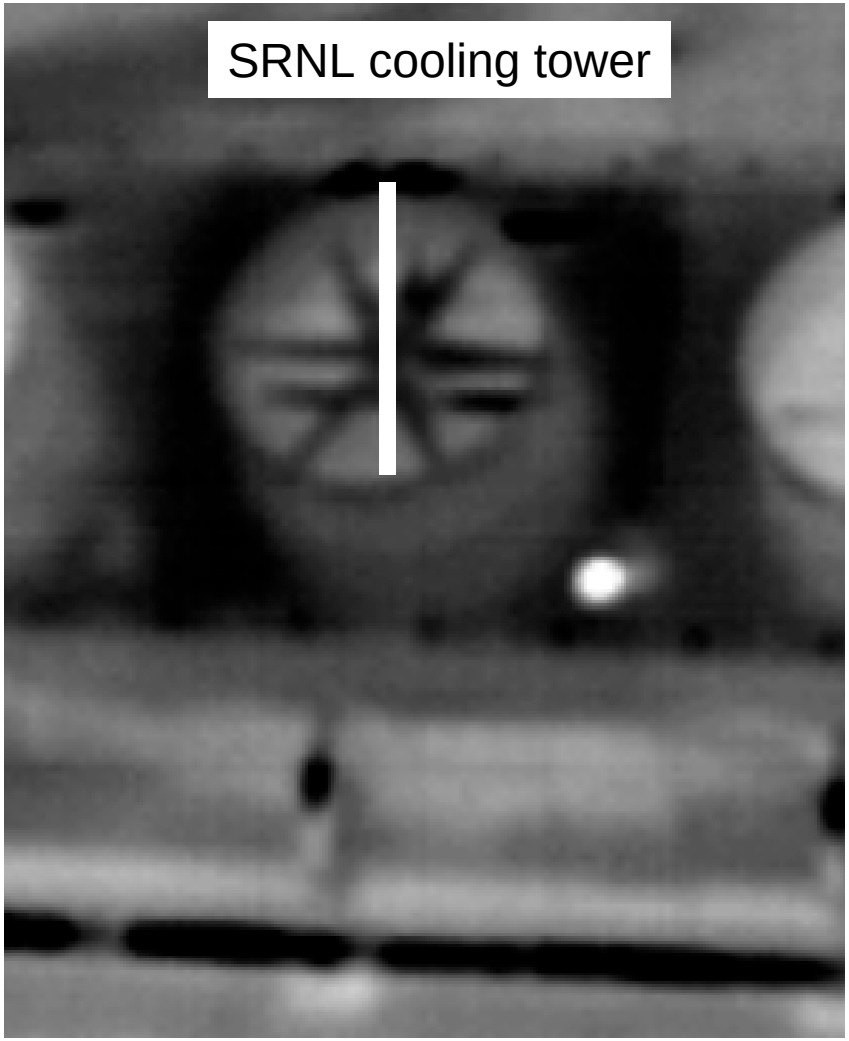

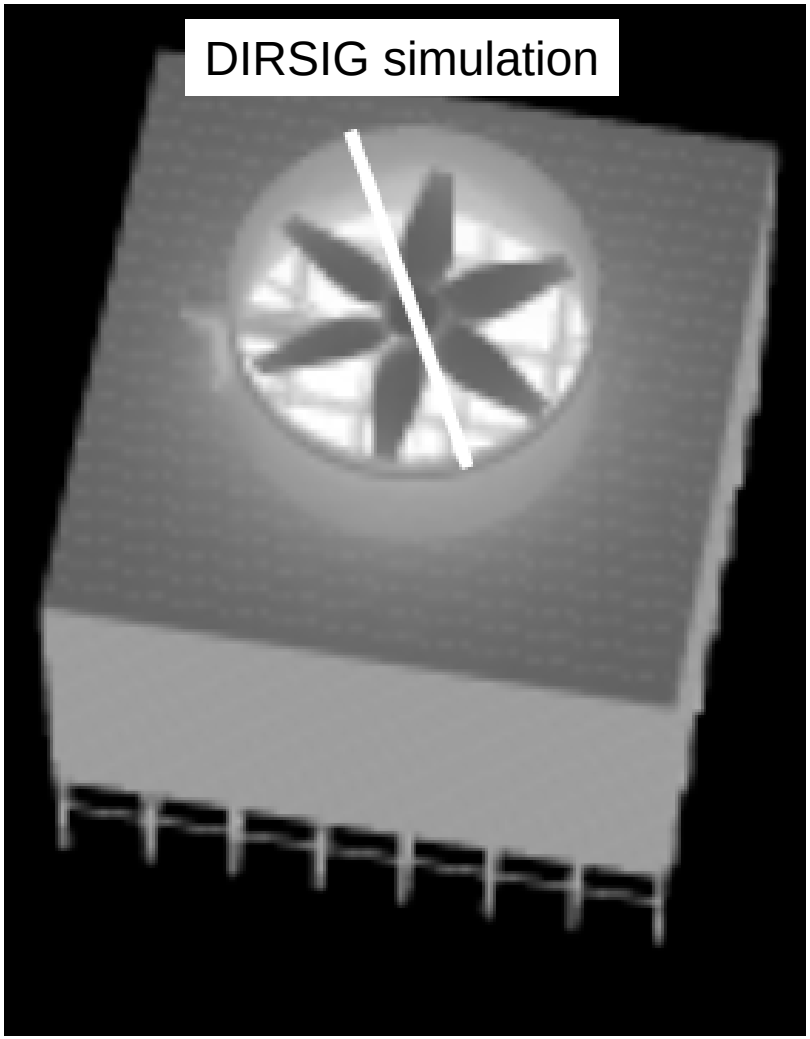

SRNL

Relative Temperature Profiles

SRNL cooling tower

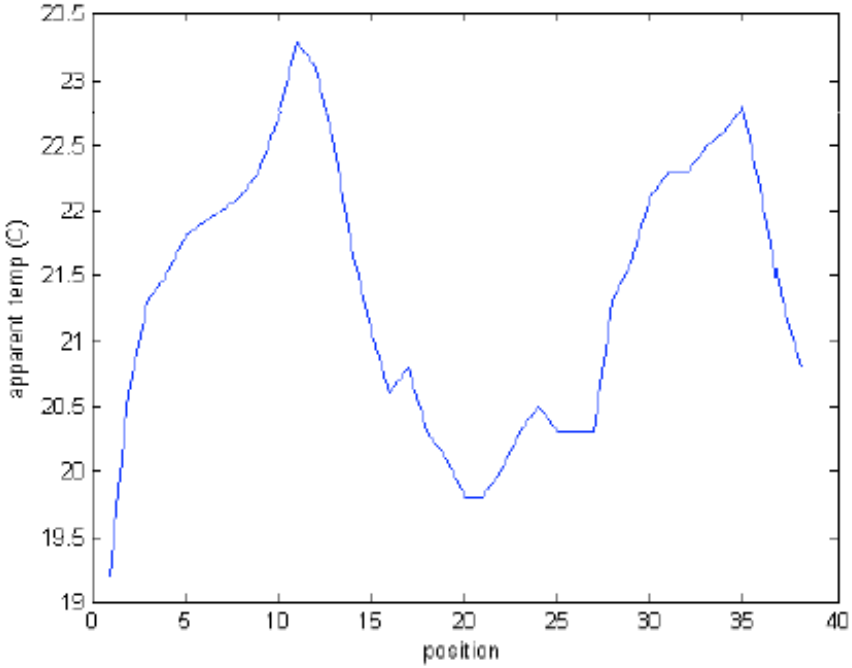

DIRSIG simulation

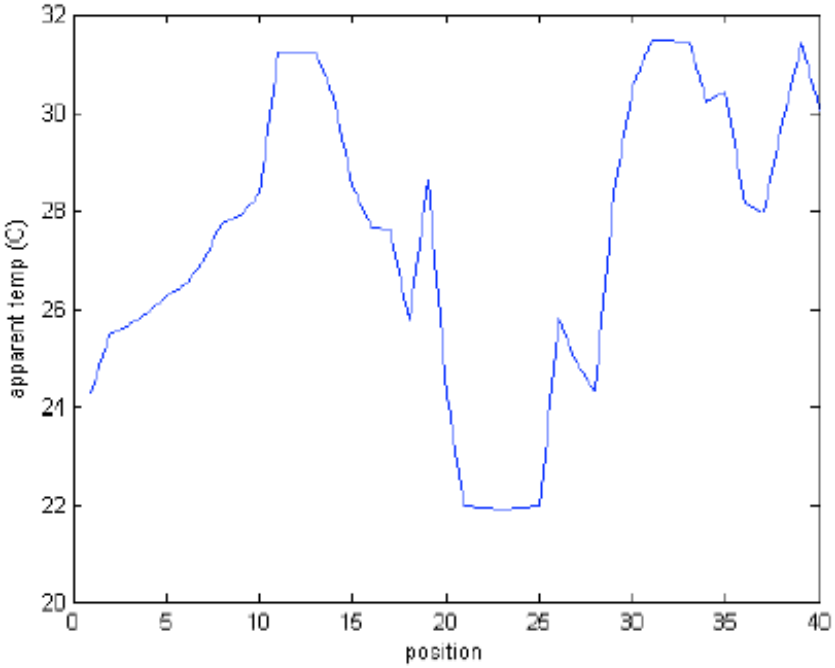

Milestones

- SRNL develops 3-D CFD models of SRS mechanical draft cooling tower (MDCT) and validates against existing and new SRS data sets.
- Rochester Institute of Technology (RIT) develops 3-D DIRSIG model of radiation transfer in MDCT throat and validates against SRS data sets.
- Develop 1-D operational physics-based MDCT model that includes 3-D hydrodynamic and radiation transfer effects via a correlation library derived from the 3-D models.

SRNL

Remaining Work for Cooling Tower Project

- Complete 3-D model validation with counter-flow cooling tower data.
- Develop multivariate correlation functions from 3-D hydrodynamic simulations that relate airflow through tower to ambient wind speed and direction for fans-off mode.
- Complete development of DIRSIG-derived relationships between cooling tower radiance measured by thermal imaging systems, cooling tower exhaust air temperature as a function of operating conditions and ambient weather conditions.
- Incorporate parameterized 3-D effects on cooling tower performance into operational 1-D model.

SRNL

DOE Award Number: DE-FG52-06NA27491

Stand off Fluorescence Detection of Uranium in Soil

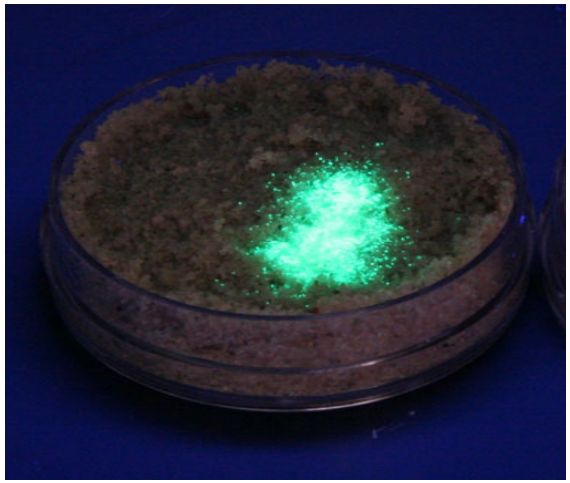

Gary Tepper, Dmitry Pestov, Chien-Cheng Chen,
John Anderson and Jean Nelson

Virginia Commonwealth University

Team Members

Gary Tepper (PI), Professor, Department of Mechanical Engineering, Virginia Commonwealth University

John Anderson (Co-PI), Research Professor, Department of Biology, Virginia Commonwealth University

Dmitry Pestov, Research Associate, Department of Mechanical Engineering, Virginia Commonwealth University

Chien-Cheng Chen, Ph.D. Student, Department of Mechanical Engineering, Virginia Commonwealth University

Jean Nelson, Ph.D. Student, Department of Biology, Virginia Commonwealth University

Project Objective

The main goal of the project is to develop fluorescence signature enhancement methods and materials for the stand off detection and identification of uranium in natural soils without sample collection or laboratory analysis

Other Studies/Hardware Development

There has been a significant investment in the development of hardware
For performing fluorescence analysis in the field.

Example:

John DiBenedetto
Kevin Kyle
Principal Investigators
Special Technologies Laboratory

Portable LIFI system developed by DOE STL

Milestone Schedule

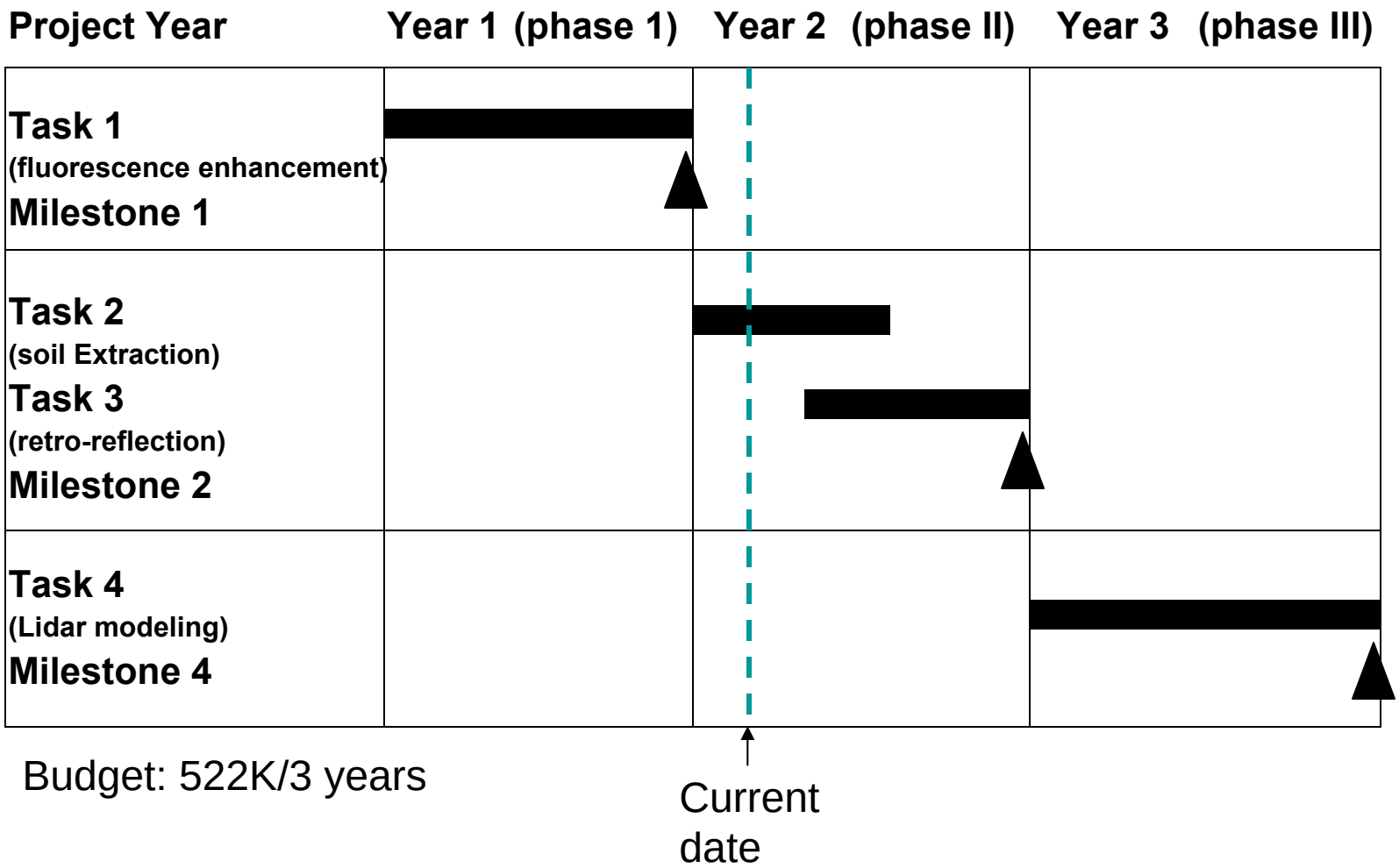

Budget: 522K/3 years

Background Information

- Uranyl ($UO2^{2+}$) is water soluble and is the most prevalent form of uranium in natural conditions and as a soil contaminant

- Uranyl has a very characteristic fluorescence spectrum and a relatively long fluorescence lifetime in comparison to most background organic compounds in soil

Absorption spectrum

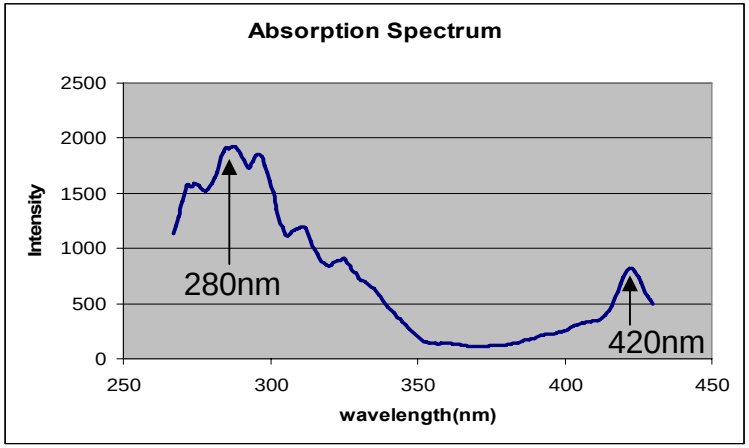

Emission spectrum

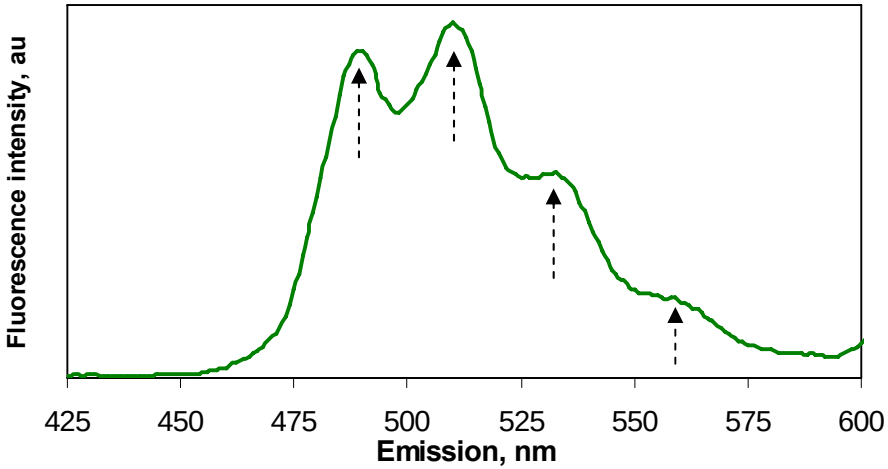

Explanation for Emission Peaks
(Diatomic Oscillator Model)

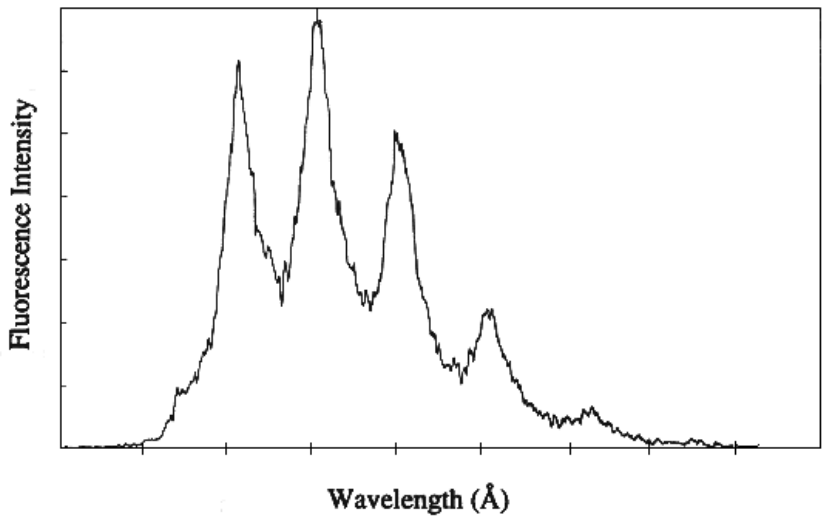

(a)

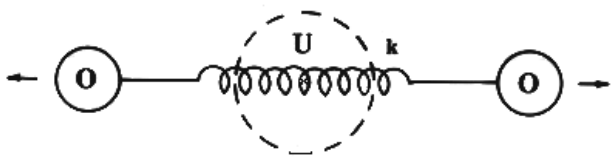

(b)

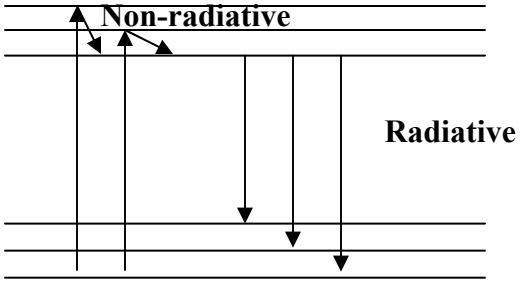

Lines in emission spectrum are due to radiative recombination to equally-spaced ground state energy levels produced by the simple harmonic motion of the 2 oxygen atoms about the massive uranium central atom.

http://cat.middlebury.edu/~PHManual/laser.html

Task 1: Fluorescence Enhancment (part 1 – in solution)

- Uranyl fluorescence in aqueous solutions is weak by itself, but can be drastically enhanced by certain chemicals.

Example: Uranyl fluorescence enhancement by KF

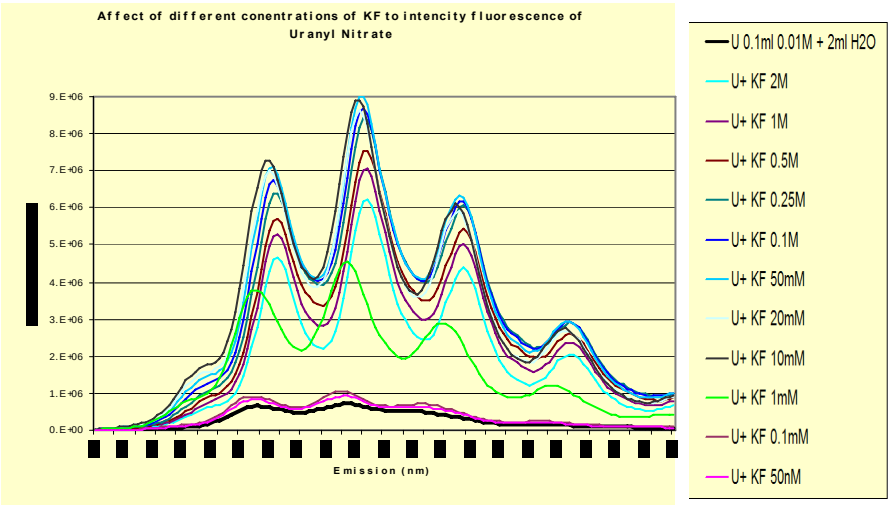

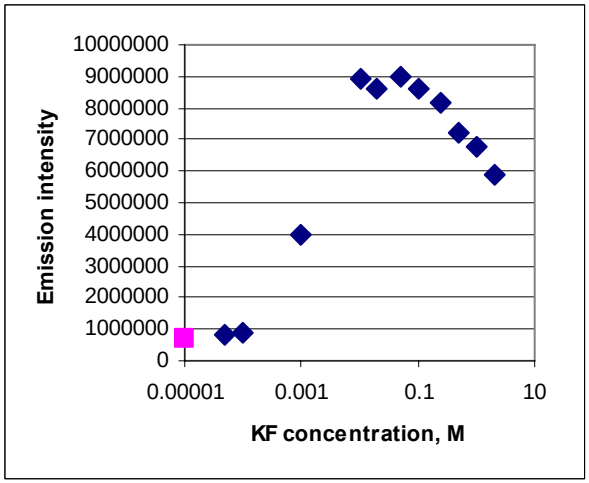

Chemical fluorescence enhancement in soils is problematic because reactions are not confined to the surface

Uranyl Detection in Soil

Requirements for stand off detection of uranyl in soil:

1. Extract and concentrate the uranyl at the surface of the soil for optical interrogation
2. Enhance the fluorescence yield
3. Enhance the fluorescence lifetime to reject background fluorescent compounds using time resolved spectroscopy

Approach:

Utilize microporous, solid-state material to simultaneously achieve all three requirements

Solid-State Fluorescence Enhancers

Materials Tested to Date

Inorganics:

- polyacrylic acidβ-tricalcium phosphate $Ca_3(PO_4)_2$
- calcium hydroxyphosphate$[Ca_5(OH)(PO_4)_3]$
- calcium fluoride CaF_2
- Silica-based materials $SiO_2 \cdot (H_2O)_x$ (following slides)

Organics

- polyacrylic acid
- poly(methacrylate-co-methacrylic acid)
- cellulose phosphate
- etidronic acid (liquid)

Result: organic compounds did not show significant uranyl fluorescence enhancement.

Silica materials exhibited the best overall performance to date

Silica materials tested

Material	Particle Size, µm	Pore Size, nm
Silica gel	40-60	4
Silica gel	40-60	6
Silica gel	40-60	15
Silica gel	5-15	6
Silica gel	60-200	6
Mesostructured silica with hexagonal framework, MCM-41 type	2-50 (estimation)	2.7
Ludox TMA colloidal silica	0.1	No porosity
Molecular sieve zeolite, type 4A	2000	0.4
Tetrabutylammonium fluoride on silica gel, ~1.5 mmol/g F^-	200-500 (estimation)	n/a

Silica gel and MCM-41structure

Silica gel and mesostructured silica MCM-41 demonstrate the most promising results – highest intensity and longest lifetime

Silica gel

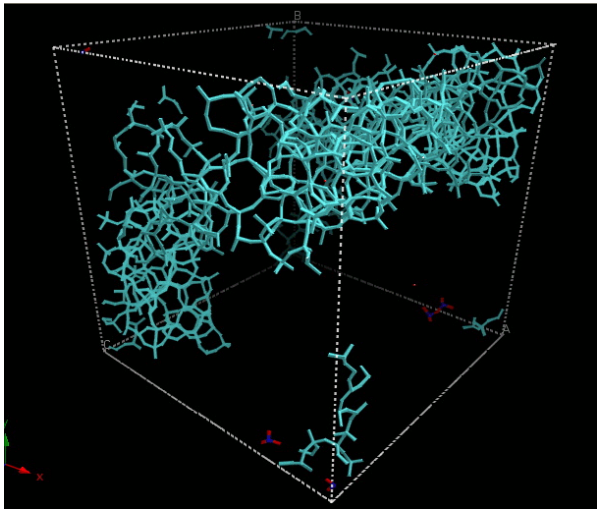

Pore size is random

Mesostructured silica

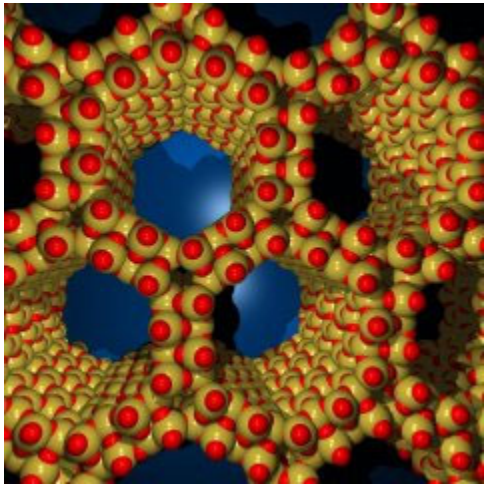

Pore size is 2.7 nm

Silica gel: Adapted from http://www.mse.engin.umich.edu/people/faculty/kieffer

MCM-41 from http://www.nusim.fraunhofer.de/simifam/contents/sim_chemistry1.html

Fluorescence Intensity Enhancement with Silica gel

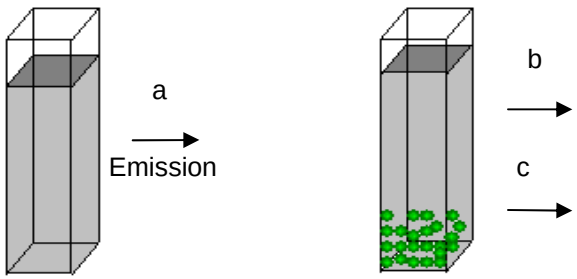

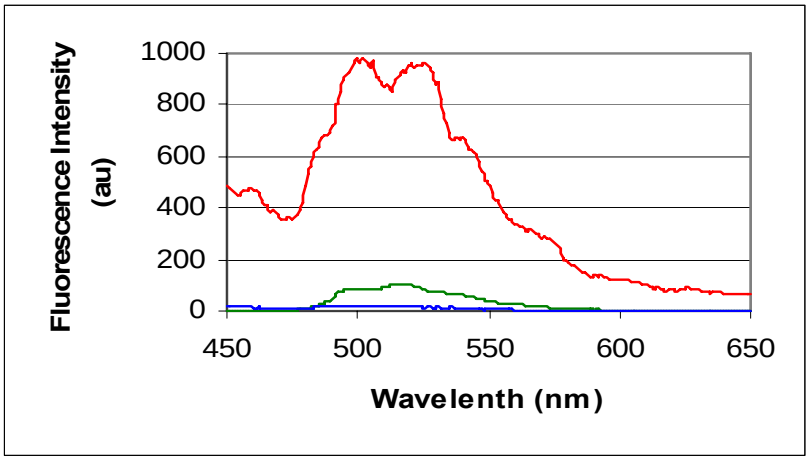

a) Fluorescence of the initial $3 \cdot 10^{-5}$M uranyl nitrate solution
b) Fluorescence of the rest amount of uranyl after 0.5g of silica gel was added to the solution
c) Fluorescence from silica gel with the absorbed uranyl

Initial uranyl nitrate concentration was $3 \cdot 10^{-5}$M.

Intensity dependence on pore and particle size during water evaporation

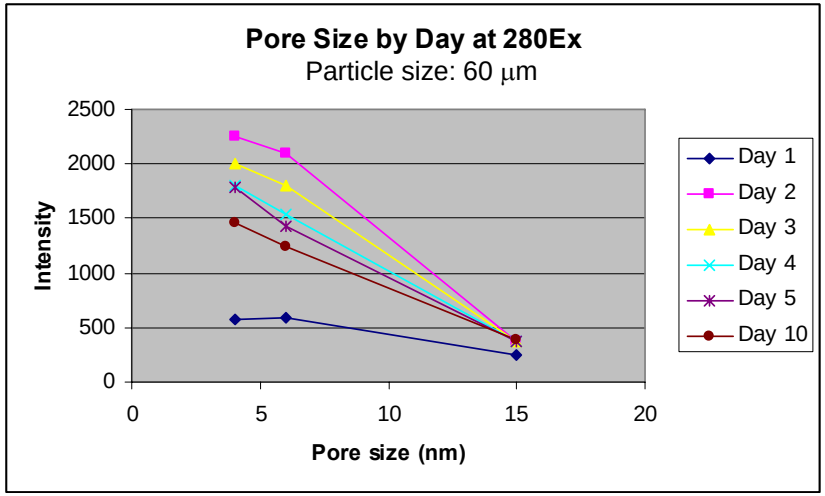

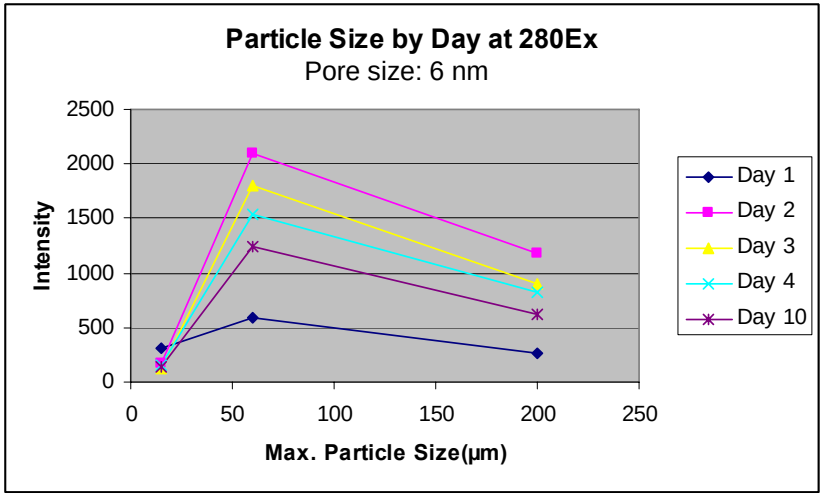

Emission intensity increases with decreasing pore size and is maximum After 24 hours of evaporation

There appears to be an optimum particle size for maximizing signal intensity

Water Evaporation Kinetics

End

Water Evaporation
From within particles
Kinetics >24 hours

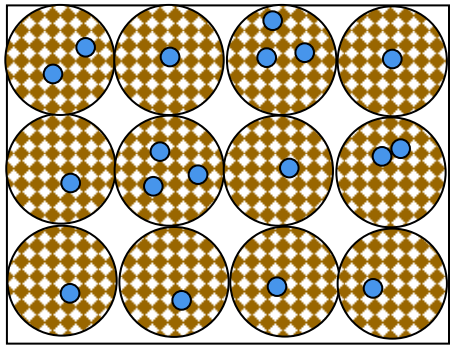

Water Evaporation
From between particles
(Kinetics ~ 24 hours)

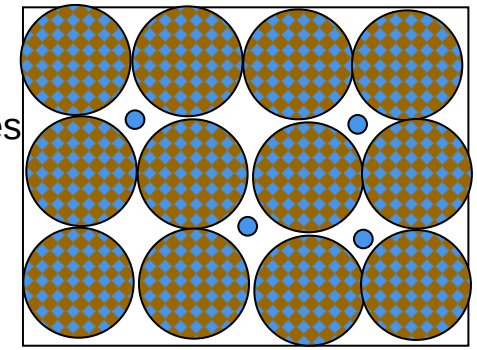

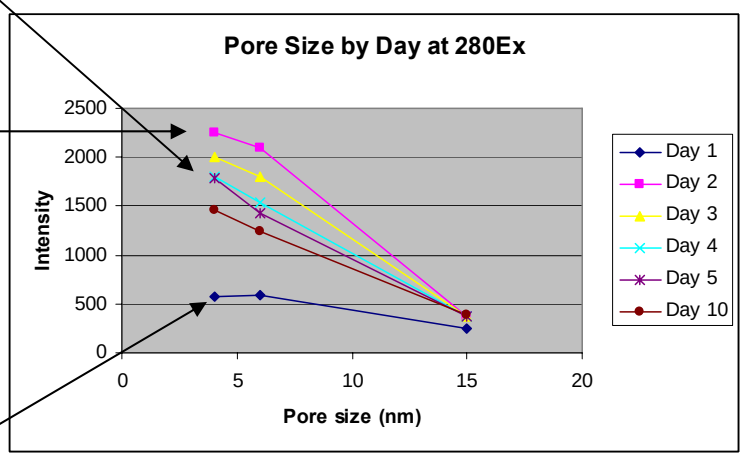

Water Saturated
Silica Gel

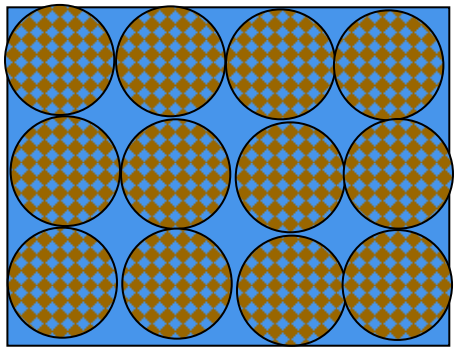

Start

Lifetime Enhancement

(498nm emission)

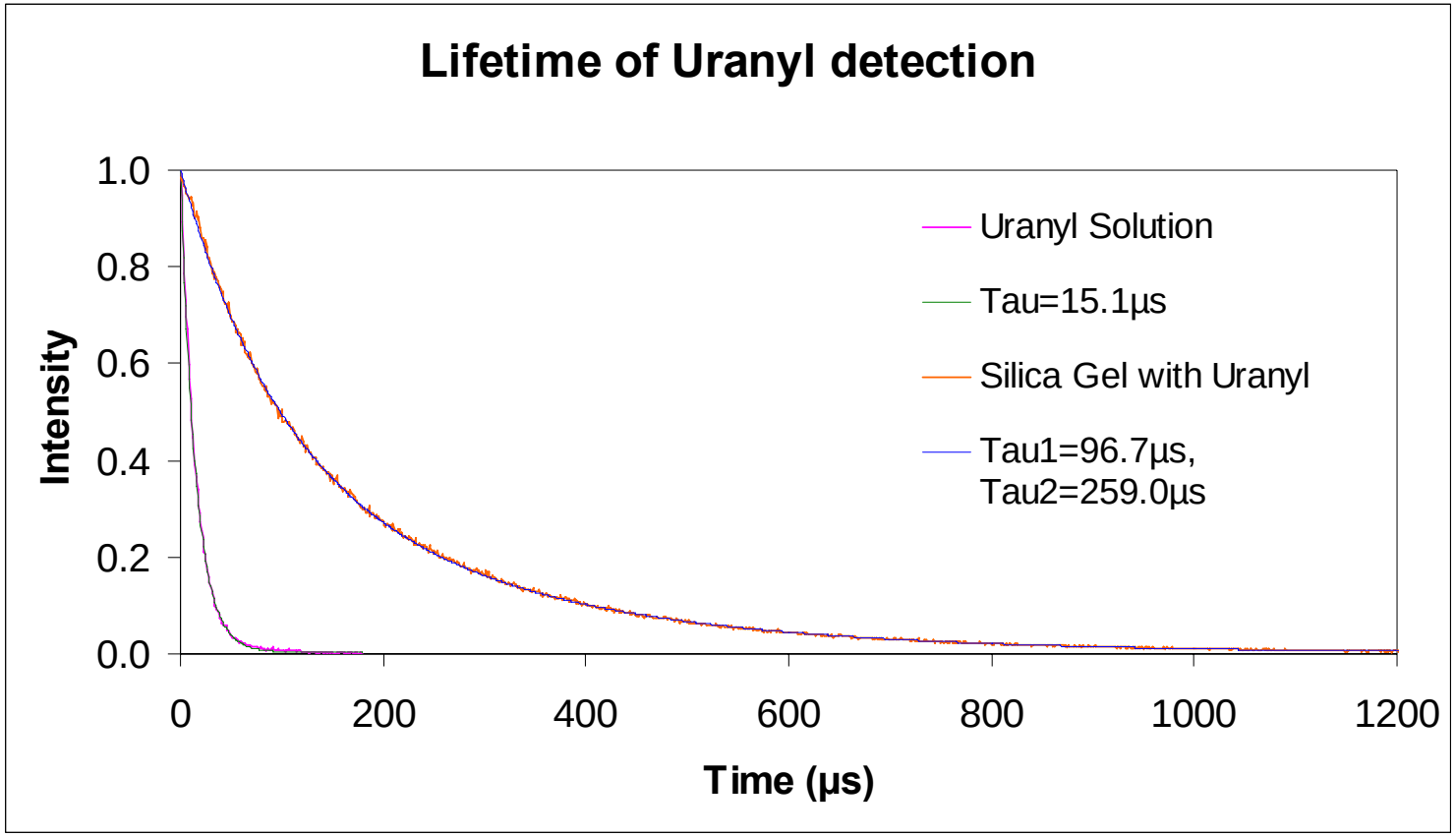

Uranyl fluorescence decay is fit using: $I(t) = A_1 e^{-t/\tau 1} + A_2 e^{-t/\tau 2}$

- 0.01M uranyl nitrate solution.
- Silica Gel (particle size=40-60µm, pore size=6nm) on the 2nd Day.

Lifetime dependence on pore size

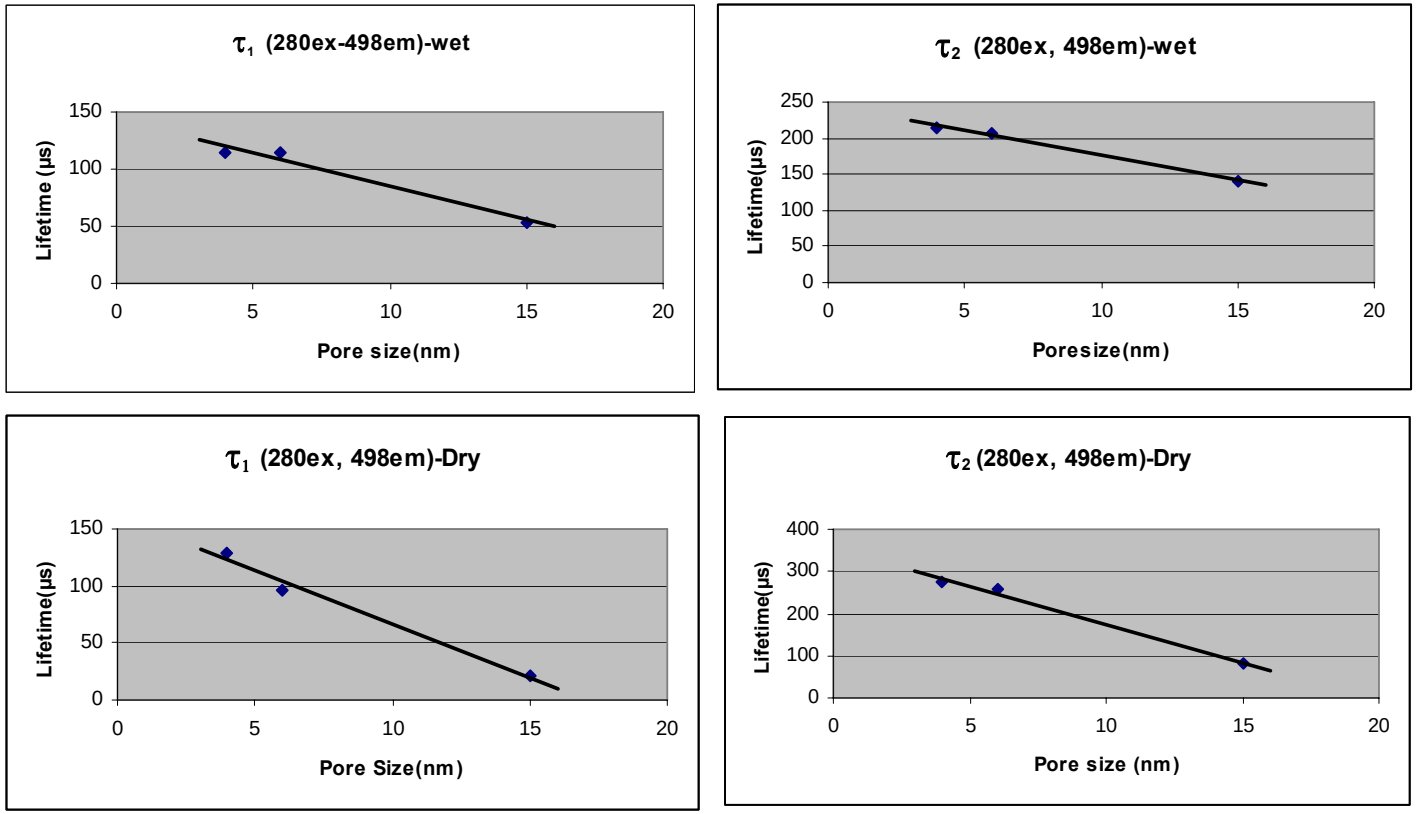

Particle diameter: 60 µm

Wet: Measurement taken from silica gel saturated with water
Dry: Measurement taken after 24 hours of drying

Lifetime increases as pore size decreases

Task 2: Soil Extraction

Silica gel deposited onto uranyl-containing sand

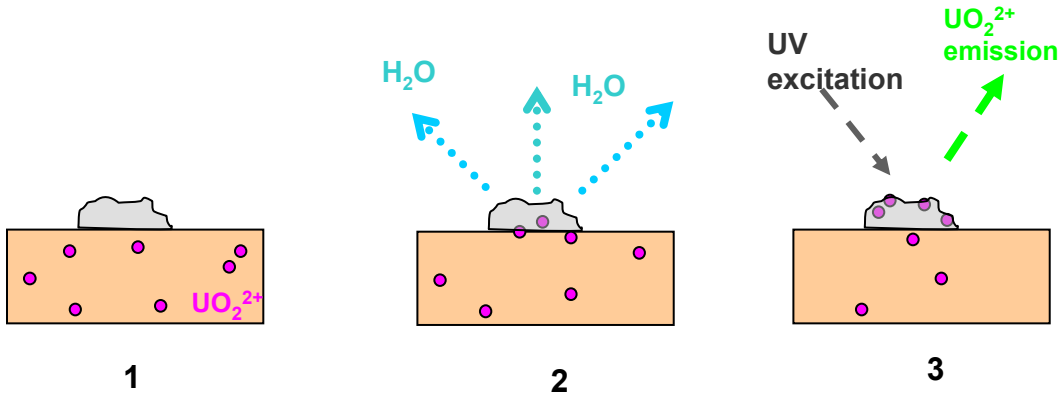

Silica gel absorbs moisture from the soil and, in the process, uranyl is transported to the surface and into the silica. The fluorescence is simultaneously enhanced by the uranyl-silica interaction.

Sand extraction and detection using silica gel

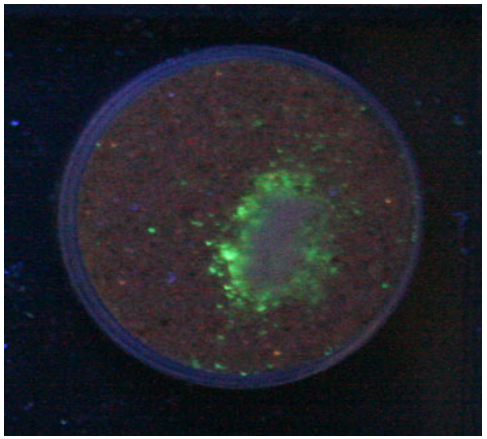

Uranyl concentration: 12ppm

UV irradiation: (peak - 254nm)

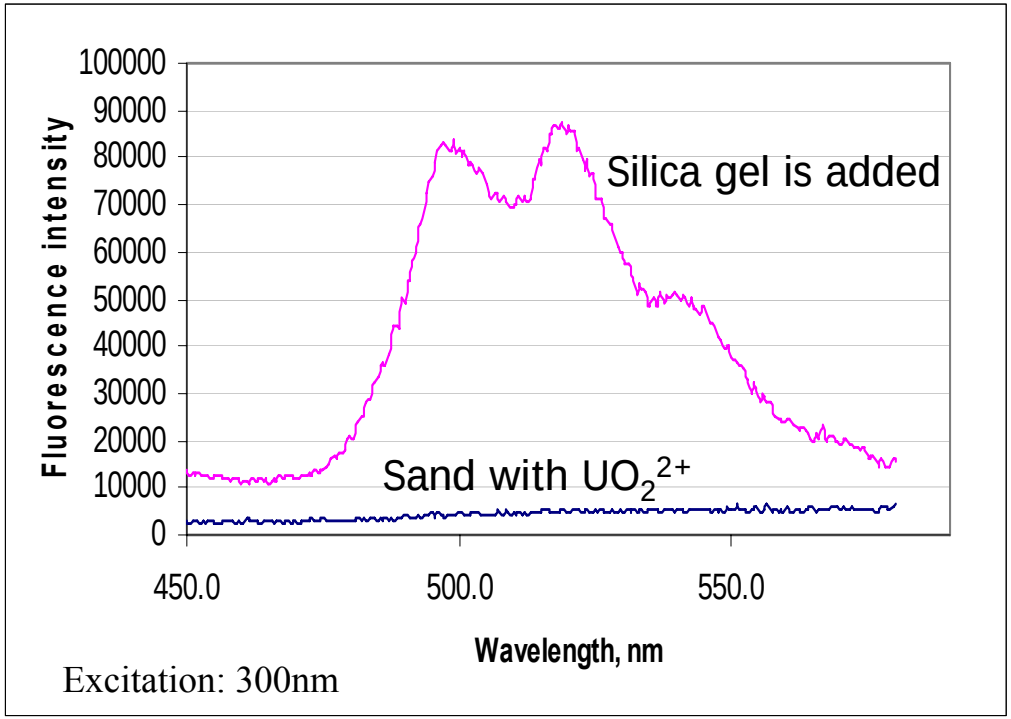

Research grade sea sand used for preliminary testing

The kinetics of the process is extremely fast ~ 1 minute

Concentration studies

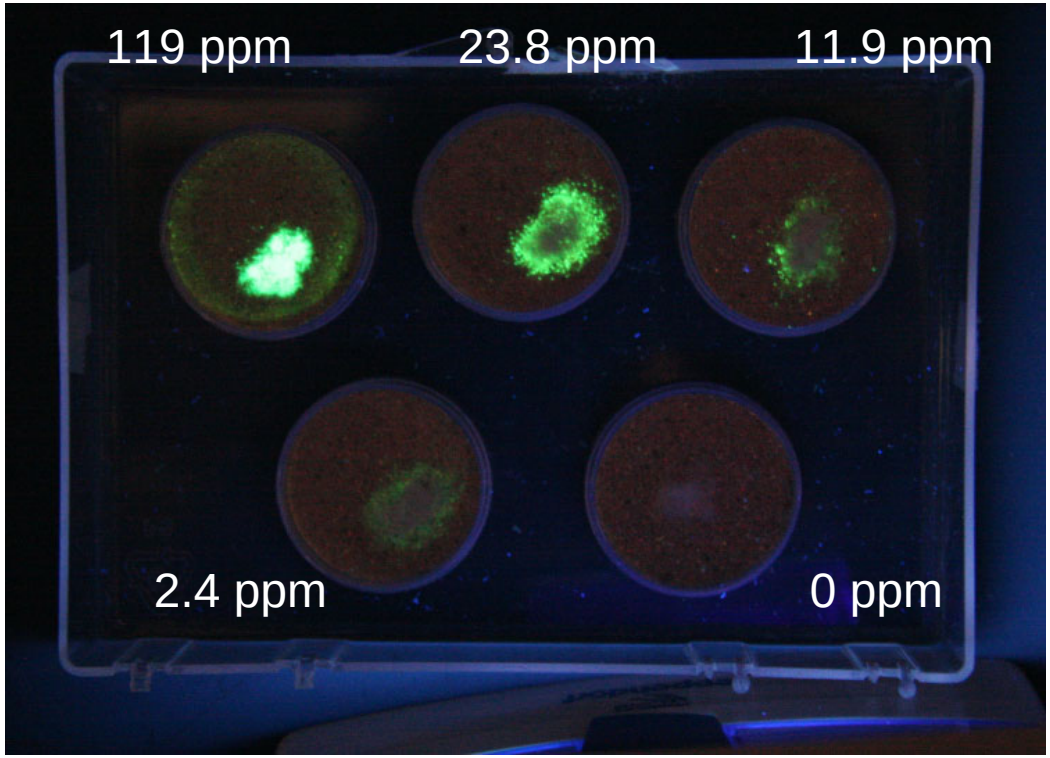

Visual (no instrumentation) detection threshold approaches ppb levels

Soil Extraction Task Status

We have demonstrated that the silica gel efficiency and rapidly absorbs water and uranyl from the near surface region.

We have also shown that uranyl can be extracted from shallow subsurface layers beneath a layer of clean sand. However, at this time, this subsurface extraction process is not optimized or quantified.

Additional testing is currently under way.

Task 3: Retroreflective Optical Beads for Signal Enhancement

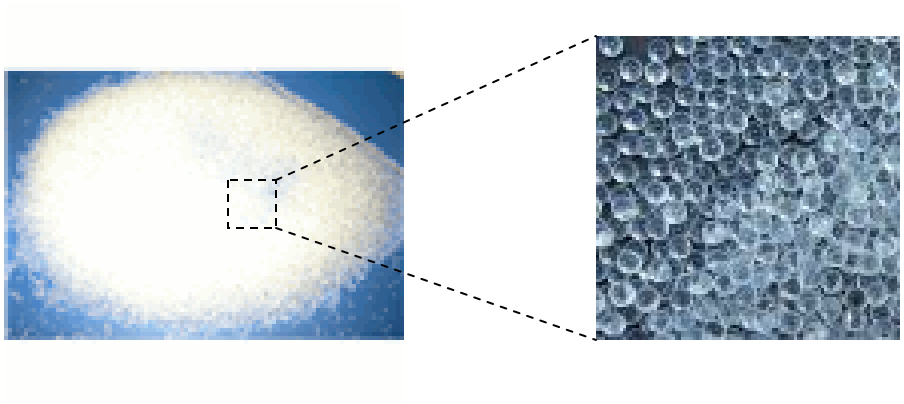

Commercially available
Optical beads

Directed Fluorescence Principle

Diffuse Reflection

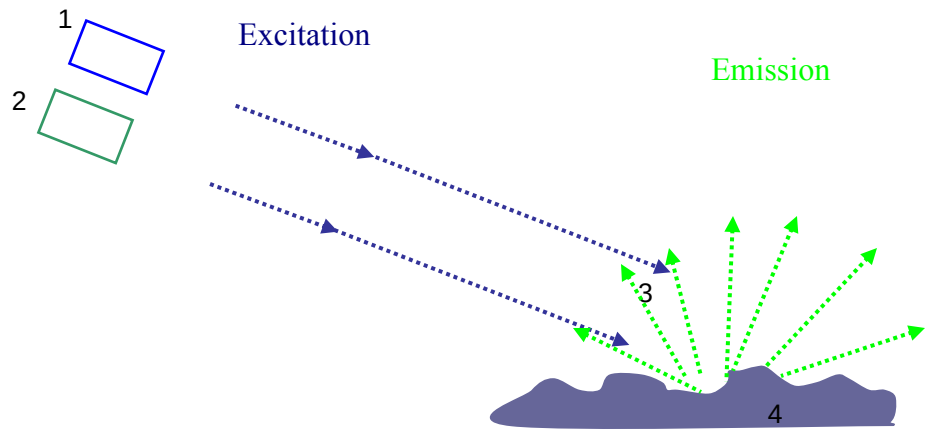

Solid silica particle with uranyl

$I \sim 1/r^2$

Directed Fluorescence System

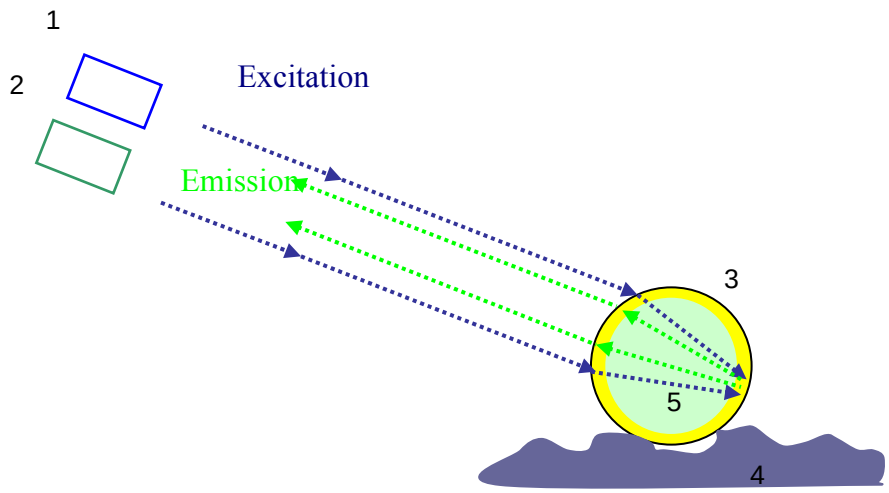

Silica gel-coated glass particle with uranyl

$I \sim 1/r^0 = \text{Constant}$

Retroreflective Glass Beads

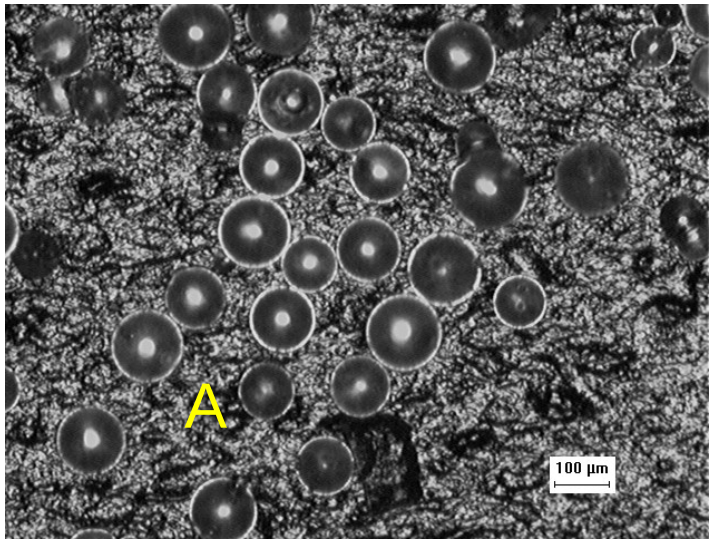

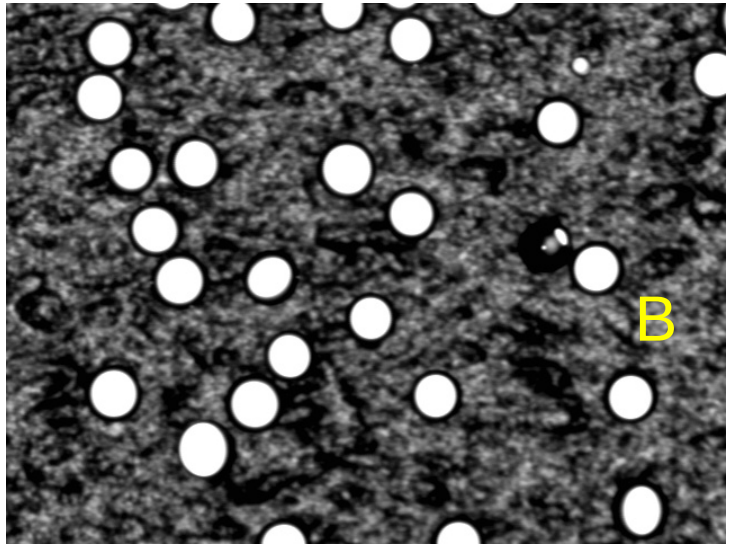

A- Regular soda lime glass beads, B – High refractive index (n = 1.95) glass beads

Combining retroreflective optical beads with soil extraction and fluorescence

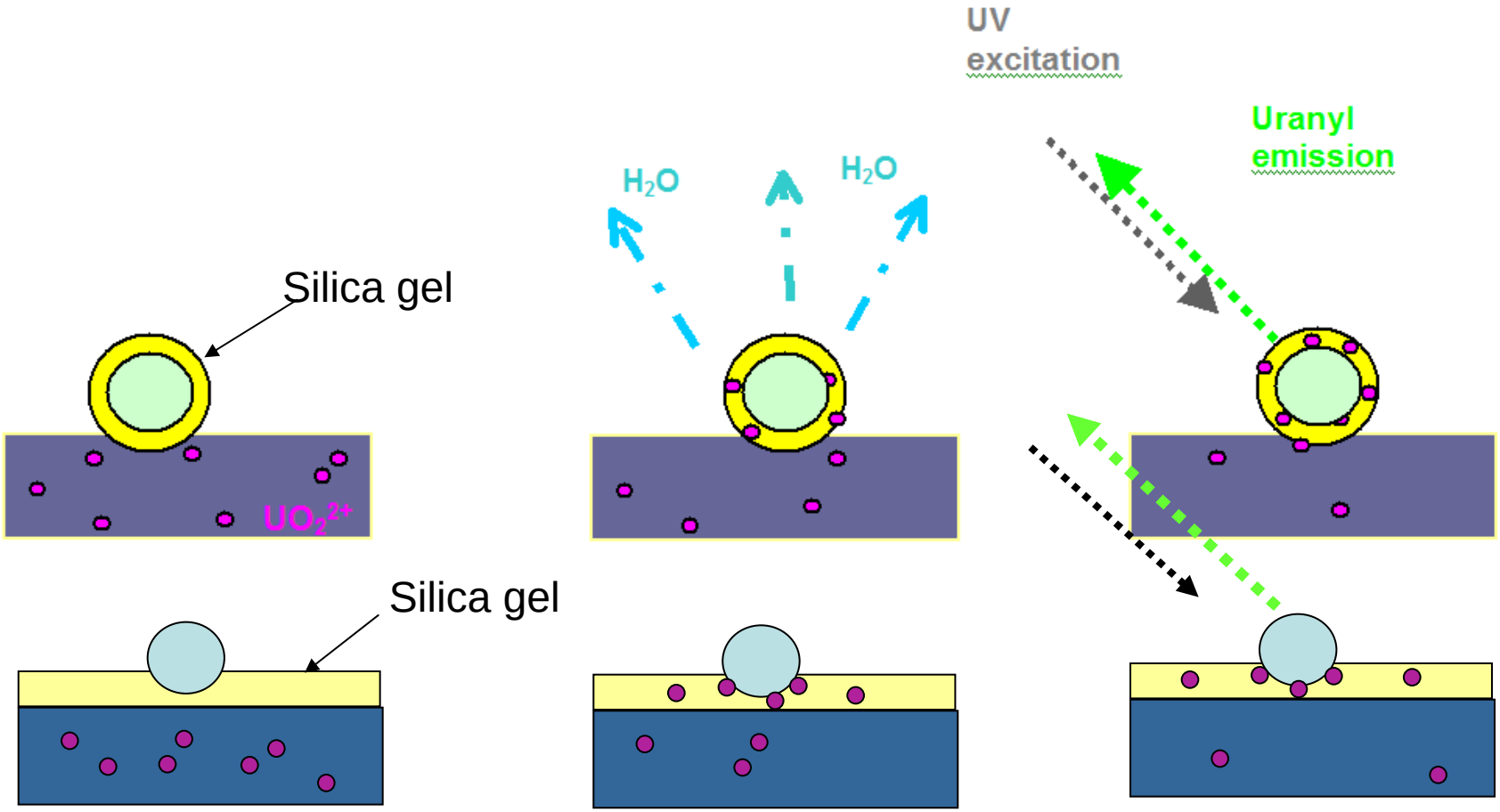

Silica gel film preparation

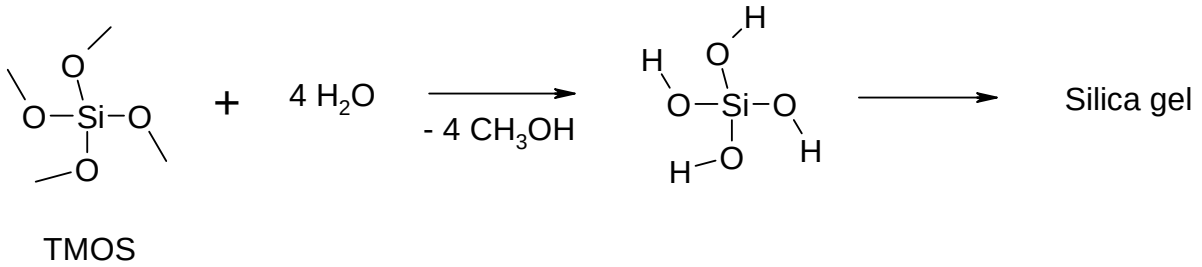

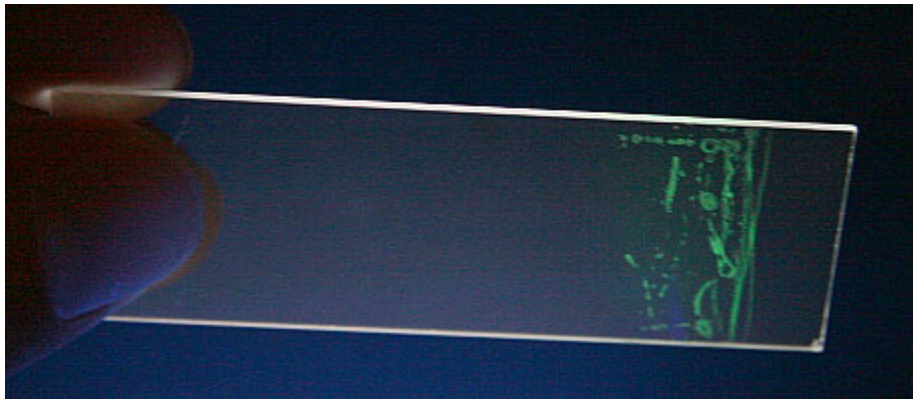

Silica gel coating onto glass slide with adsorbed. Uranyl. Irradiation UV 254 nm.

Conclusions

- Silica gel and mesostructured silica MCM-41 were identified as promising materials for uranyl soil extraction and fluorescence intensity and lifetime enhancement
- Intensity and lifetime enhancement increases with decreasing silica pore size
- The water content and silica particle size also influence the signal intensity and uranyl transport through media

Future Tasks

Task 2 (soil extraction): Status – initiated

Objective: Investigate the transport of uranyl from realistic soil environments into silica gel signal enhancers

Task 3: (Directed Fluorescence System): Status – initiated

Objective: Investigate the feasibility of using retroreflectivity for fluorescence signal enhancement

Task 4: (LIDAR model): Status – future task

Objective: Develop a LIDAR model for the system

Acknowledgements

This work was supported by a contract (#DE-FG52-06NA27491) from the US Department of Energy, National Nuclear Security Agency

Simulation, Modeling and Real-Time Algorithm Development for Fast Neutron Imaging Telescopes

James M. Ryan
University of New Hampshire

FNIT Goals

- **FNIT detector (Fast Neutron Imaging Telescope)**
  - compact size
  - Neutron/γ discrimination
  - imaging capability
  - spectroscopy <1 - 20 MeV
- **Applications**
  - SNM detection
  - Solar Orbiter / Solar Sentinels

QuickTime™ and a
TIFF (Uncompressed) decompressor
are needed to see this picture.

QuickTime™ and a
TIFF (Uncompressed) decompressor
are needed to see this picture.

Project Goals

- Characterize neutron imager/spectrometer
- Verify imaging properties
- Verify spectroscopic properties
- Verify models against data
- Implement on-line algorithms for turnkey imaging instrument. Adaptable to similar instruments.

Neutron measurement method

Two elastic n-p scatters

- measure positions, time differences, scint light
- Incident neutron energy:
  - Pulse height & scattered neutron ToF
- Neutron source image
  - neutron track lies on cone
  - draw event cones

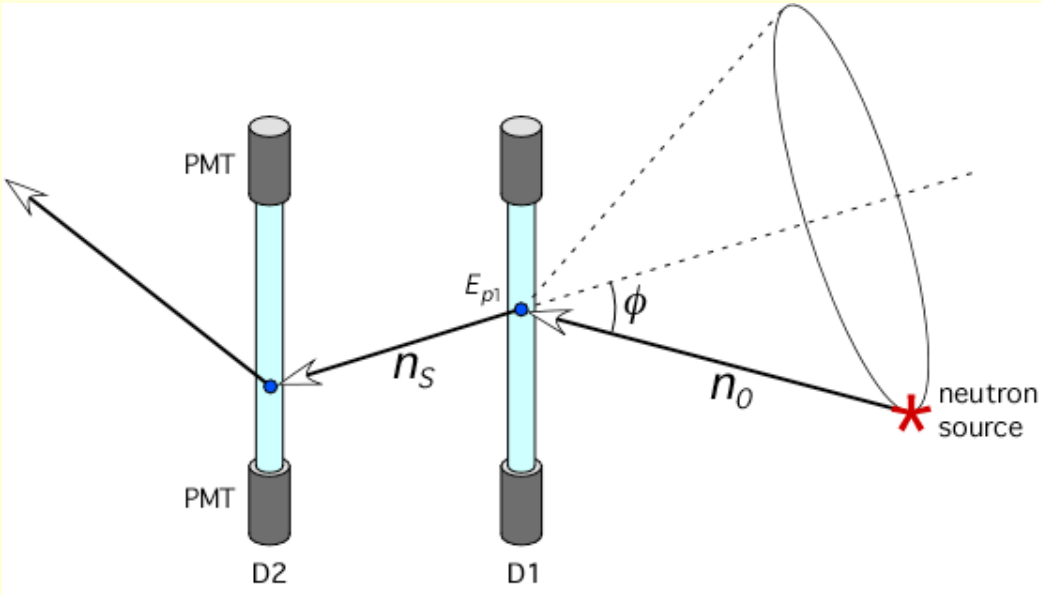

$$\sin^2\phi = \frac{E_{p1}}{E_{n_0}}$$

$$E_{n_0} = E_{p_1} + E_{n_s}$$

Imaging Technique

- **Intersecting event circles**
  - **same method used in γ-ray Compton telescopes**

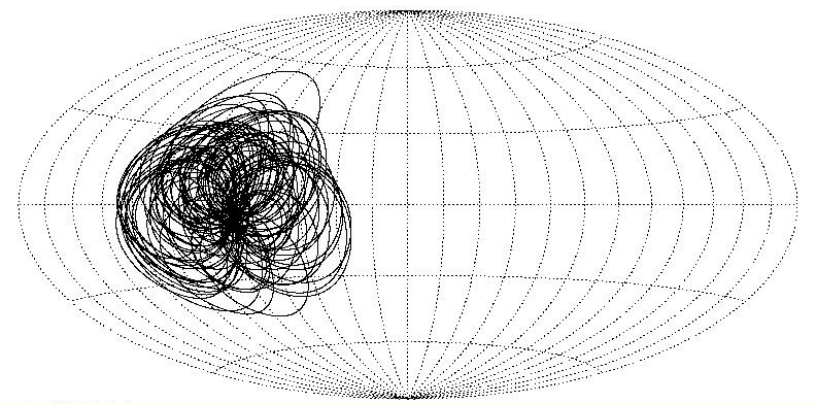

- **Demonstrated with solar neutrons**

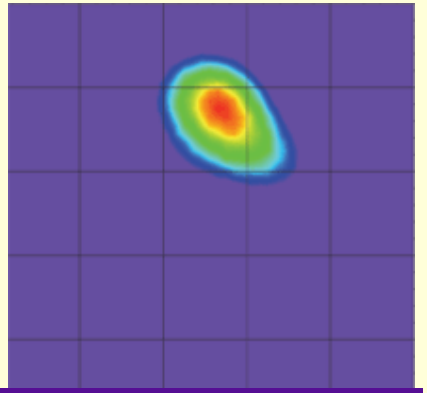

COMPTEL neutron image of the Sun
20-80 MeV, 1991 June 15.

Can do better using full information in double-scatter event—not simply adding circles.

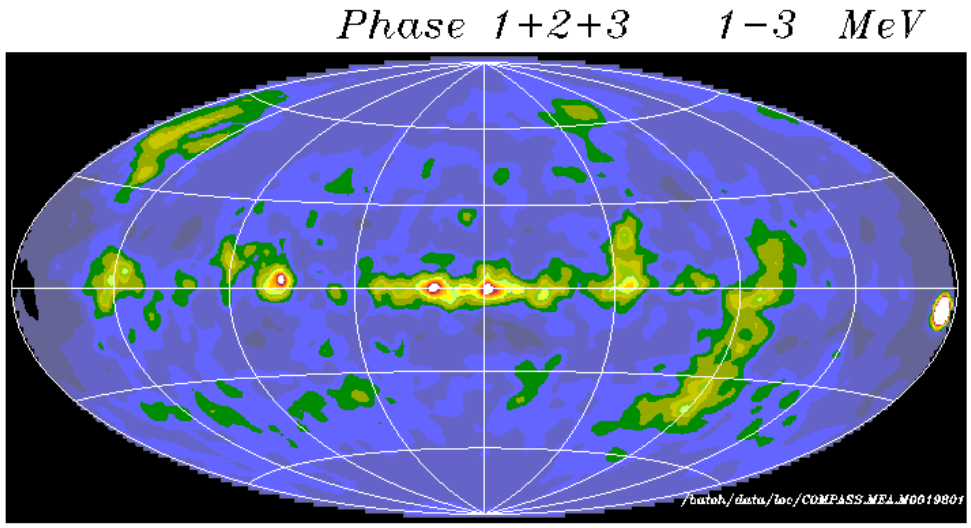

Counting circle intersections integrates over information useful for better imaging and spectroscopy.

FNIT Instrument

- Radial symmetry
  - uniform 360□ FoV
- Liquid scintillator
  - high hydrogen content
  - n/g pulse shape discrimination
- Two PMTs view each bar
  - position along *z*-axis
  - maximize light collection

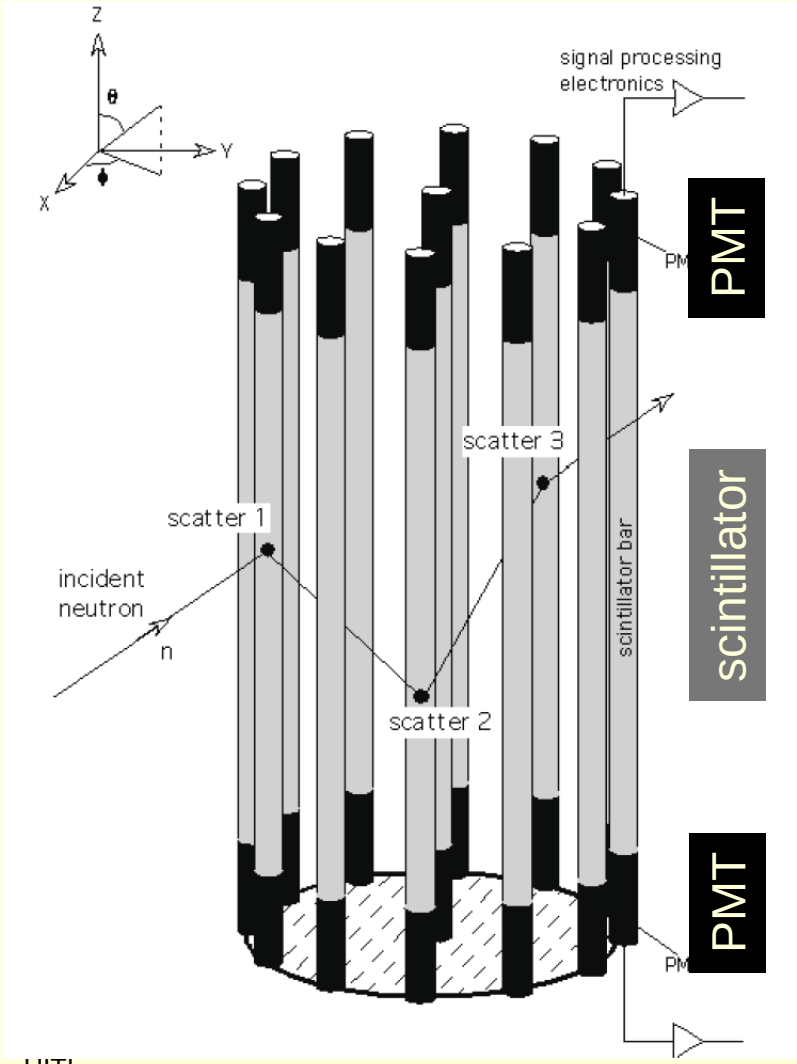

FNIT Prototype

- Three tubular liquid scintillator detectors
- NIM and VME electronics
- Test program
  - calibration with radiation sources
  - neutron beam at Crocker Lab, UC Davis, 8/2007
  - imaging of WG Pu at PNNL, 9/2007

Energy Threshold

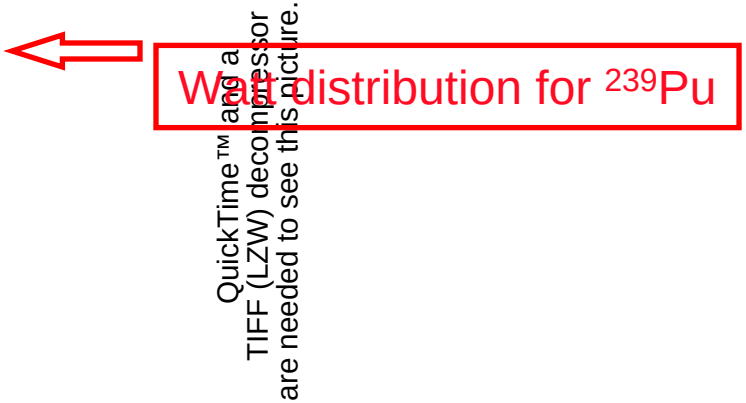

Watt distribution for ^{239}Pu

Sensitive to most of Watt spectrum

Spectral resolution

QuickTime™ and a
TIFF (LZW) decompressor
are needed to see this picture.

Event-by-event **energy resolution $\delta E/E \sim 20\%$**

Angular Resolution

$$\Theta_{actual} - \Theta_{calculated} = \Theta_{error}$$

QuickTime™ and a
TIFF (Uncompressed) decompressor
are needed to see this picture.

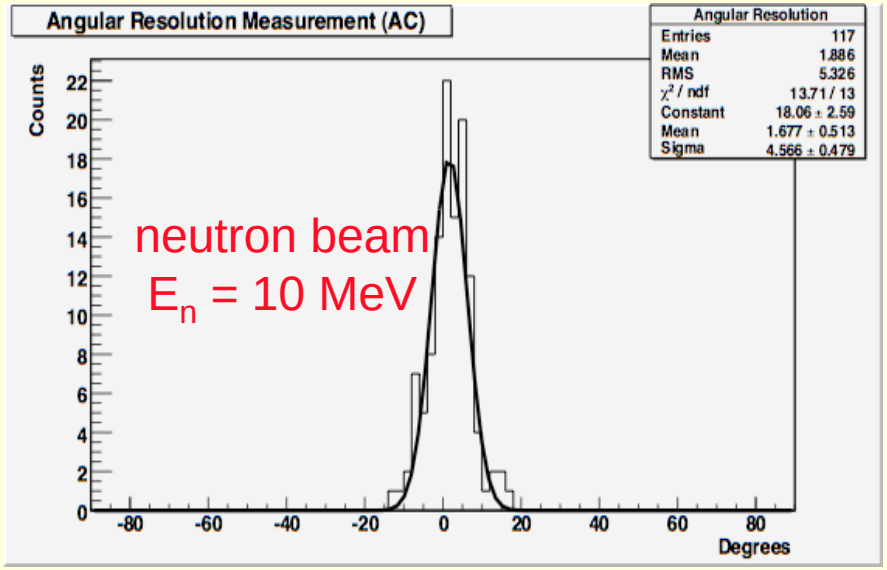

fission spectrum

QuickTime™ and a
TIFF (LZW) decompressor
are needed to see this picture.

σ = 4.5° at E_n = 10 MeV

$\langle\sigma\rangle$ = 7.4° for fission neutrons (^{239}Pu)

1st Order Imaging

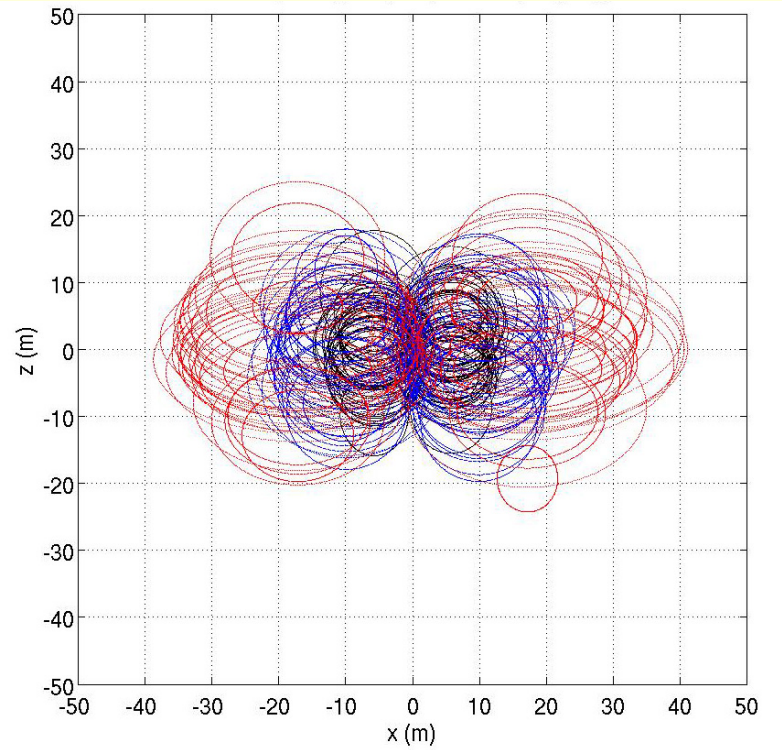

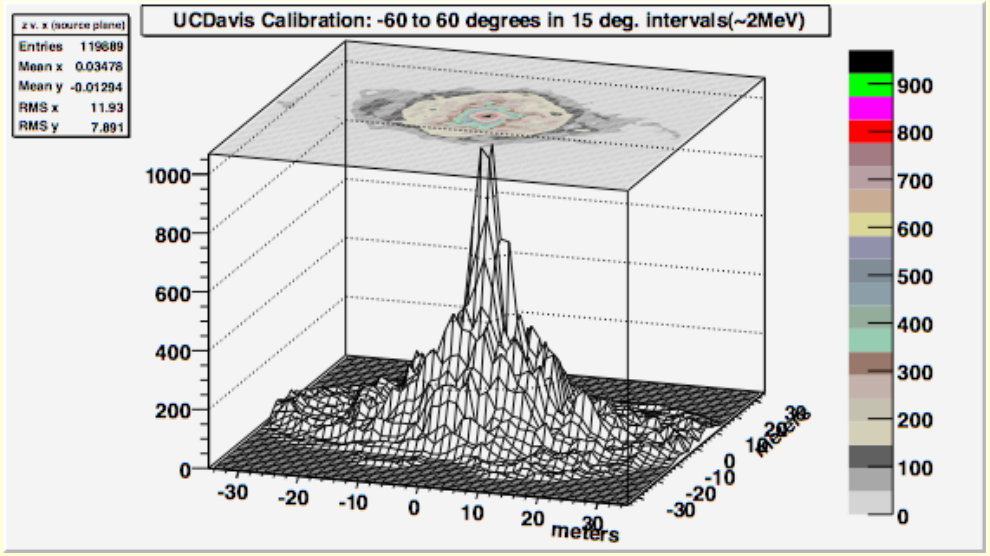

*Disclaimer

Image size $\delta\theta$ ~ 30□ in vertical dimension, but ~ 10□ in horizontal

FNIT instrument efficiency

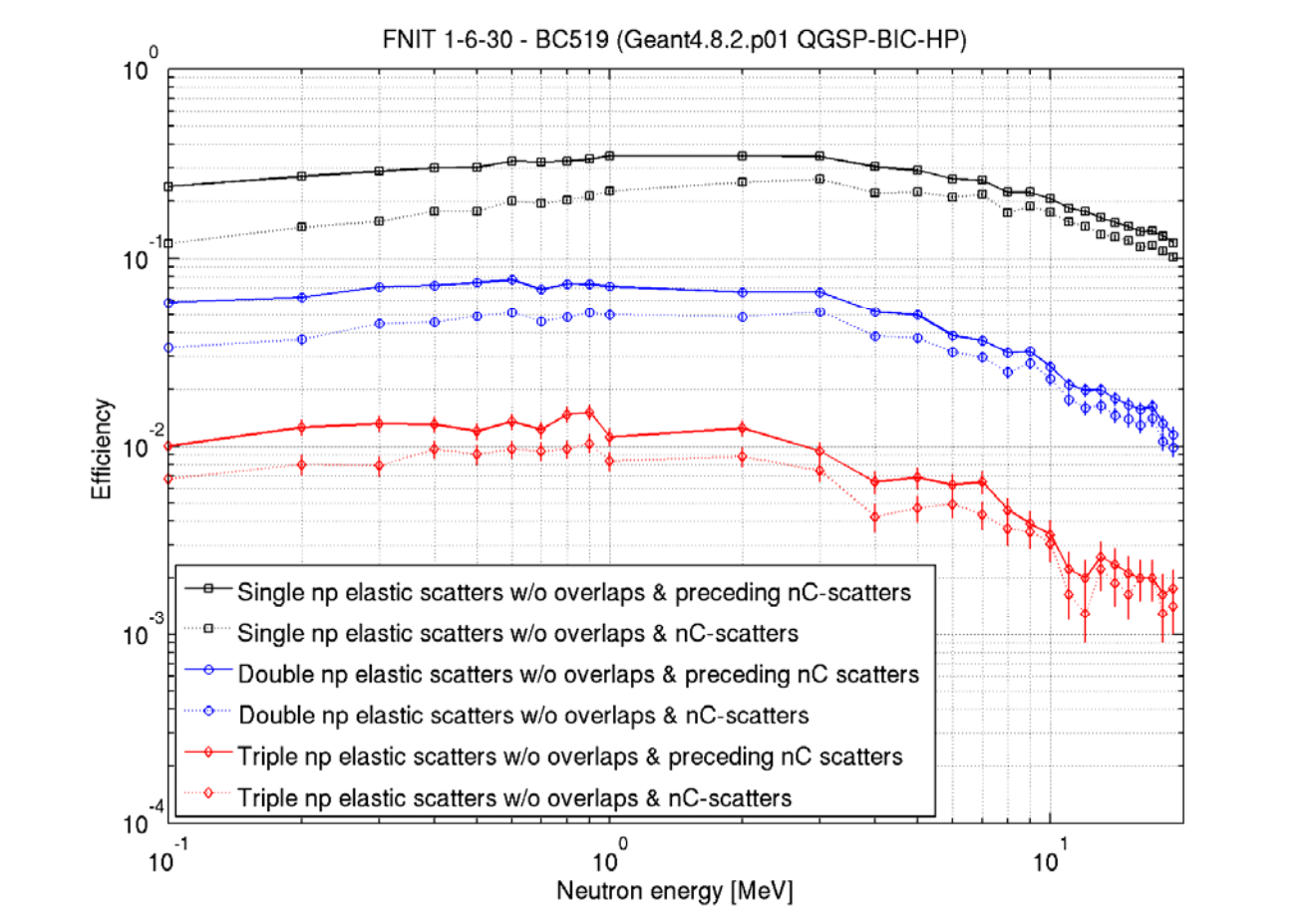

double n-p scatter efficiency ~ 5%

Energy Response (three methods)

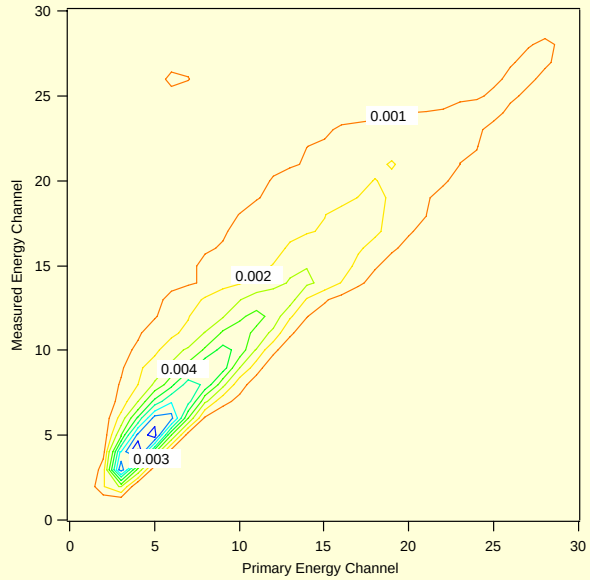

Summing pulse heights

Pulse Height & knowledge of source location

Pulse Height & ToF

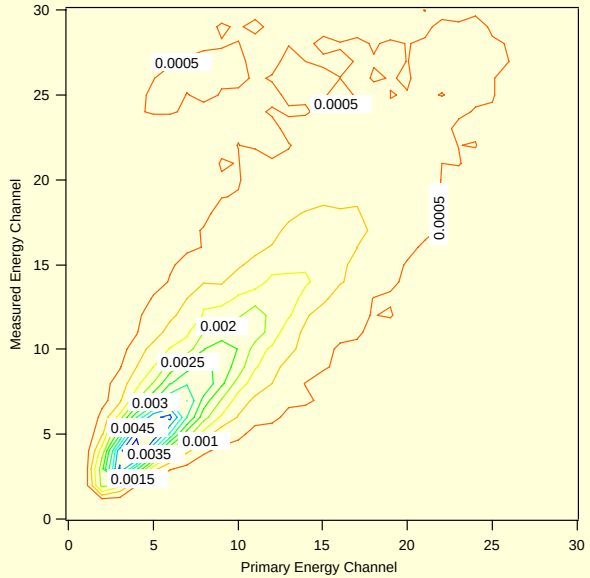

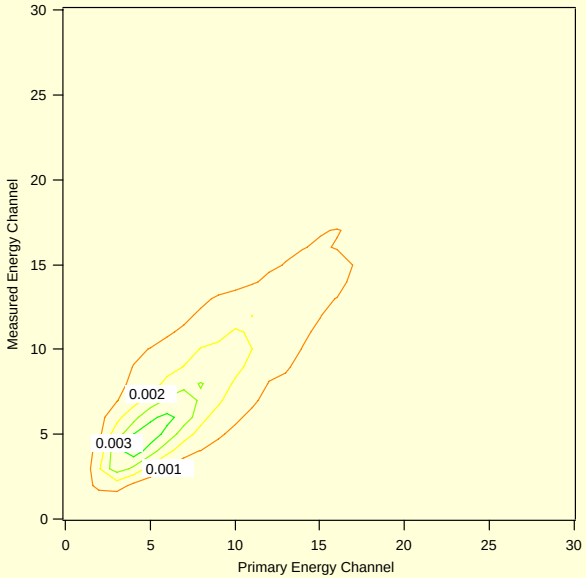

Future Work

- Continue to characterize instrument and computer model.
- Employ full instrument response into deconvolution process for imaging.
- Build "on-line" software for "real-time" imaging.

Acknowledgements

- Mitchell Woodring, Pacific Northwest National Laboratory, for help with the SNM measurements
- Carlos Castaneda, Crocker Nuclear Laboratory, UC Davis, for help with the neutron beam measurements.
- This work is supported by the DoE (NA-22) under contract numbers DE-FG52-04NA25687 and DE-FG52-06NA27493

A Framework for Dynamic Retasking and Redeployment in Sensor Networks

James Horey and Arthur B. Maccabe†

November 28 2007

University of New Mexico
Department of Computer Science

† Primary Investigator

Project Overview

- Domain specialists developing applications face enormous challenges
  - Lacking proper development and testing environments
  - Must tackle heterogeneous, distributed nature of sensor networks
- Sensor network characteristics:
  - Computation embedded in the network and
  - Computational heterogeneity
- Project Goals
  - Create a comprehensive suite of sensor network software to ensure application writers focus on the *application*, not the *system*
    - Focus on *retasking* and *redeployment*
  - Minimize overall overhead by exposing appropriate resource information to application writers

Project Overview

- Project budget
  - $750,000 over three years
  - UNM (Dept. of CS) and LANL (ISR-3, DSN project)
- Project Milestones
  - Year 1: Define basic usage models and prototype software
  - Year 2: Extend models and software for heterogeneous elements (scheduling, movement)
  - Year 3: Include dynamic elements (programming and scheduling mobile nodes)
- Students, Post-docs, and Collaborators
  - James Horey, Eric Nelson, Ann Kilzer (undergraduate at Gonzaga U.)
  - Jean-Charles Tournier, Patricia Crowley (Gonzaga U.)
  - Angela Mielke (LANL)

Scenarios

- Plume detection
  - Nodes embedded in urban landscapes
  - Must detect, classify, and respond

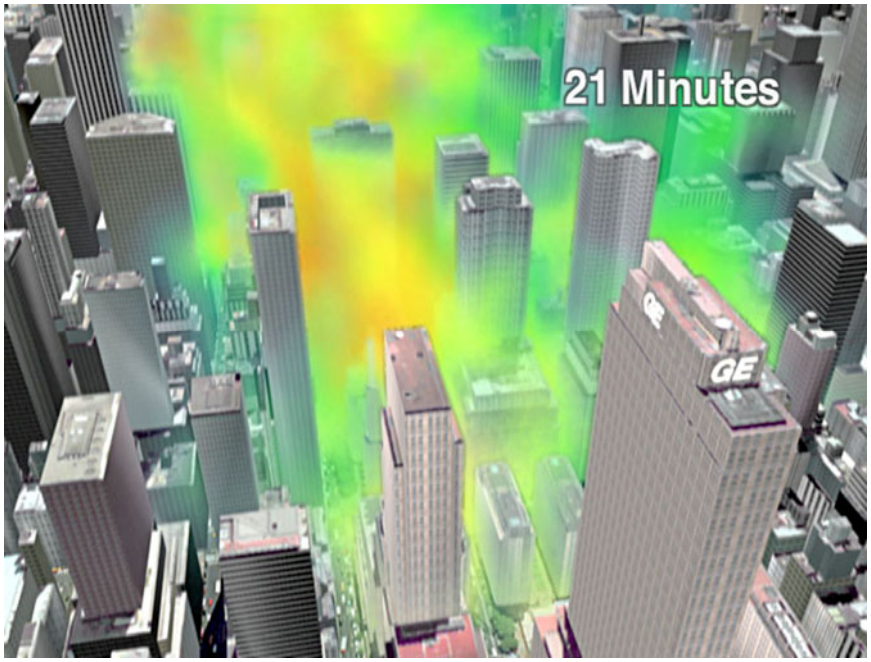

Scenarios

- Plume detection
  - Nodes embedded in urban landscapes
  - Must detect, classify, and respond
- Traffic monitoring
  - Classify traffic for better road management
  - Identify target vehicles

Scenarios

- Plume detection
  - Nodes embedded in urban landscapes
  - Must detect, classify, and respond
- Traffic monitoring
  - Classify traffic for better roa management
  - Identify target vehicles
- Homeland security
  - Report health of the building
  - Provide safety routes in emergencies

Approach

- Applications have common requirements
  - Collective and local operations
  - Must be robust to topology changes
- Different functions must run on different sensor nodes at different times
  - Mechanisms to map functions to different sensor nodes
  - Mechanisms to provide and enforce resource usage

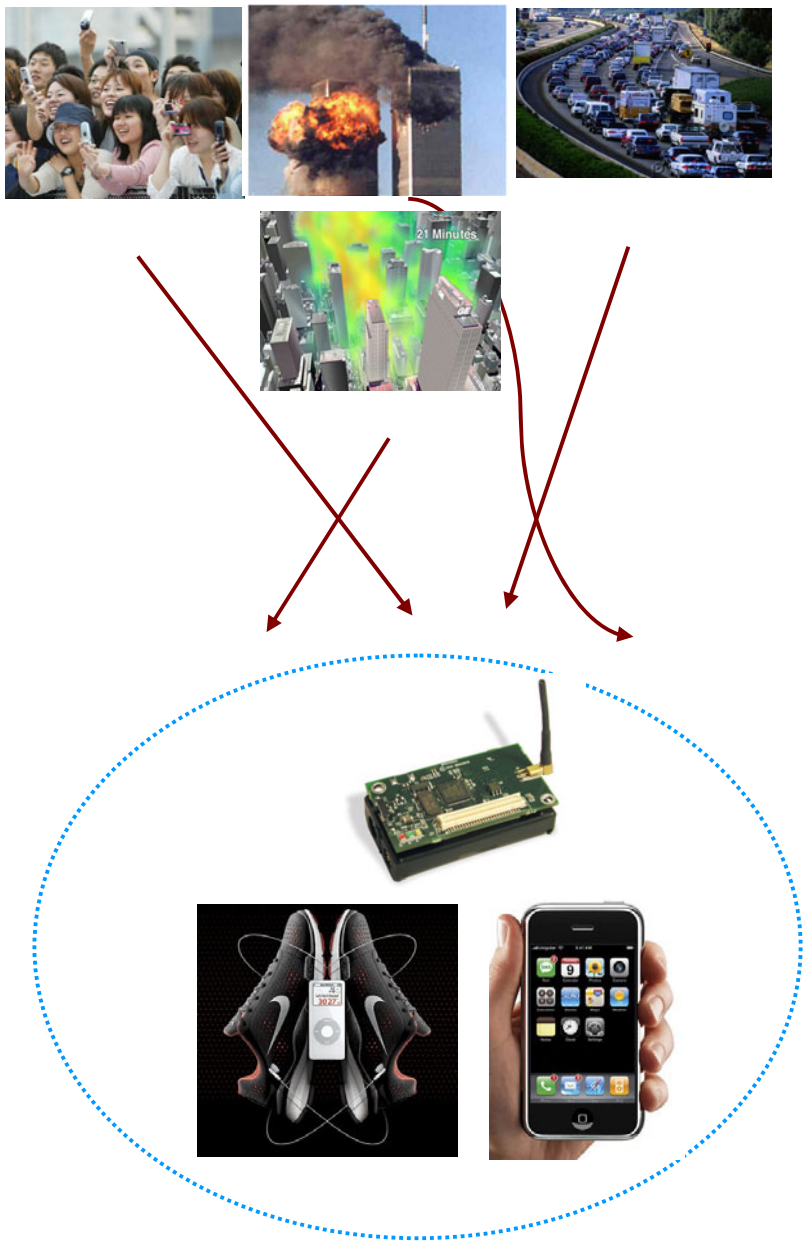

A New Software Stack

- New programming interfaces
  - *Powerful* tools that are *simple*
  - Coopt familiar interfaces: spreadsheets and filesystems
- Middleware to handle advanced communication and task mapping
  - Provide abstractions for tasking and communication
- System software to handle resource management
  - Use contracts to ensure resources for tasks and to enforce usage at runtime

Approach

- New programming interfaces
  - *Powerful* tools that are *simple*
  - Coopt familiar interfaces: spreadsheets and filesystems
- Middleware to handle advanced communication and task mapping
  - Provide abstractions for tasking and communication
- System software to handle resource management
  - Use contracts to ensure resources for tasks and to enforce usage at runtime

Tables

Programming Interfaces | Urban Applications | Privacy Algorithms

- Table-based language environment for sensor networks
- Use familiar spreadsheet metaphor to *program* the sensor network
  - Tables runs as cross-platform Java application on basestation
  - Use middleware to communicate with the sensor network
- Sensor nodes run a Tables environment
  - Data will come from sensor network
  - Functions will be executed on the network

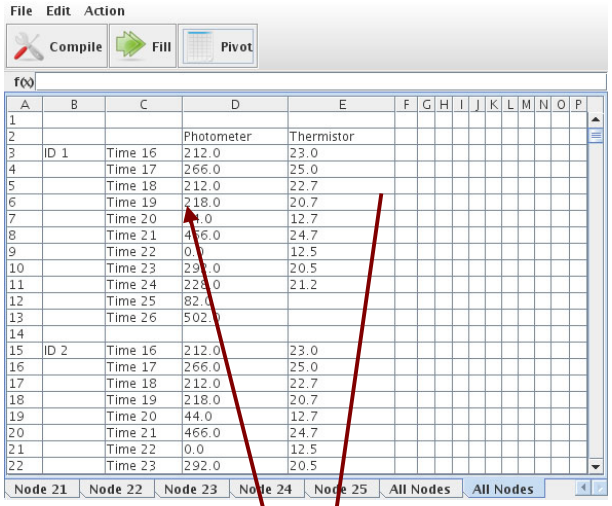

[Horey et al. in submission]

Pivot Tables

- Miniature representation of the spreadsheet
  - Users click-and-drag data items to the data and metadata panes

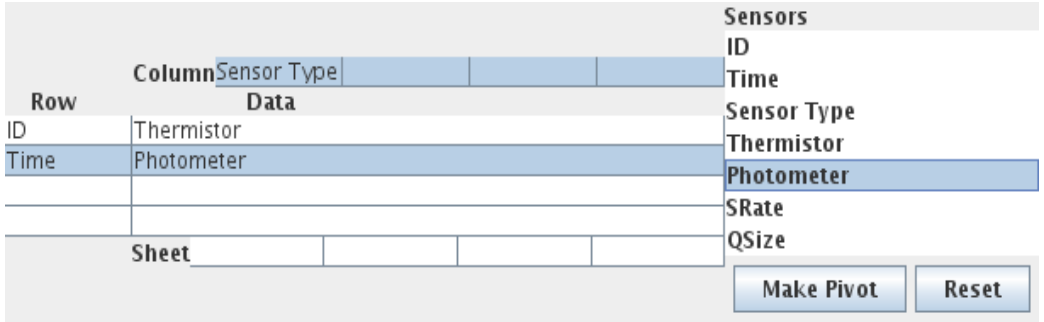

- Simple method to query the sensor network and organize the data
  - Example demonstrates construction of an environmental monitoring application

Pivot Tables

- Miniature representation of the spreadsheet
  - Users click-and-drag data items to the data and metadata panes

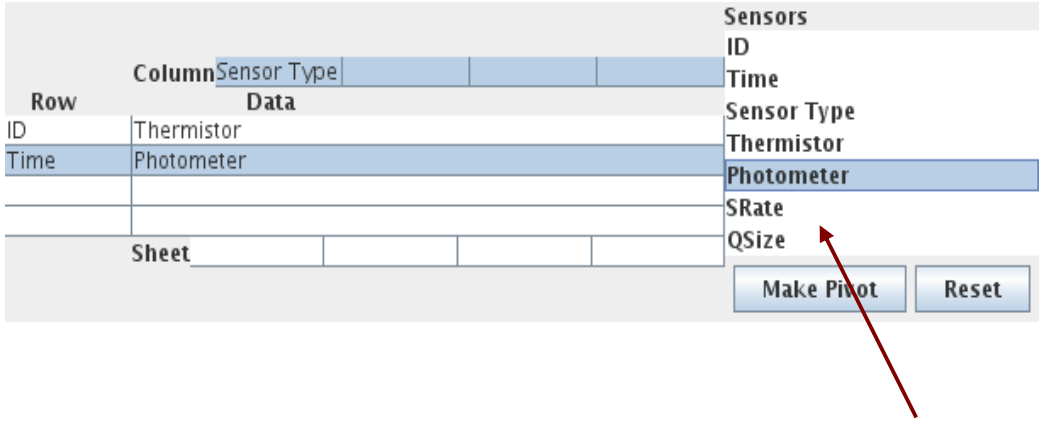

- Simple method to query the sensor network and organize the data
  - Example demonstrates construction of an environmental monitoring application
- Data list is updated automatically as new types of data are generated
  - Encourages an *iterative* workflow

Pivot Tables

- Pivot table is compiled and propagated to the sensor network
- Each sensor node continually collects environmental data and executes a pivot table processor
  - Reports back entire data queue along with metadata
- Tables uses the information from the pivot table to construct a final view

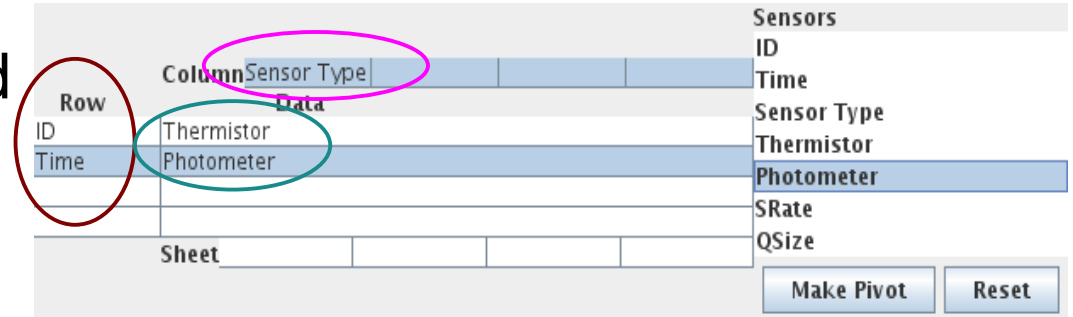

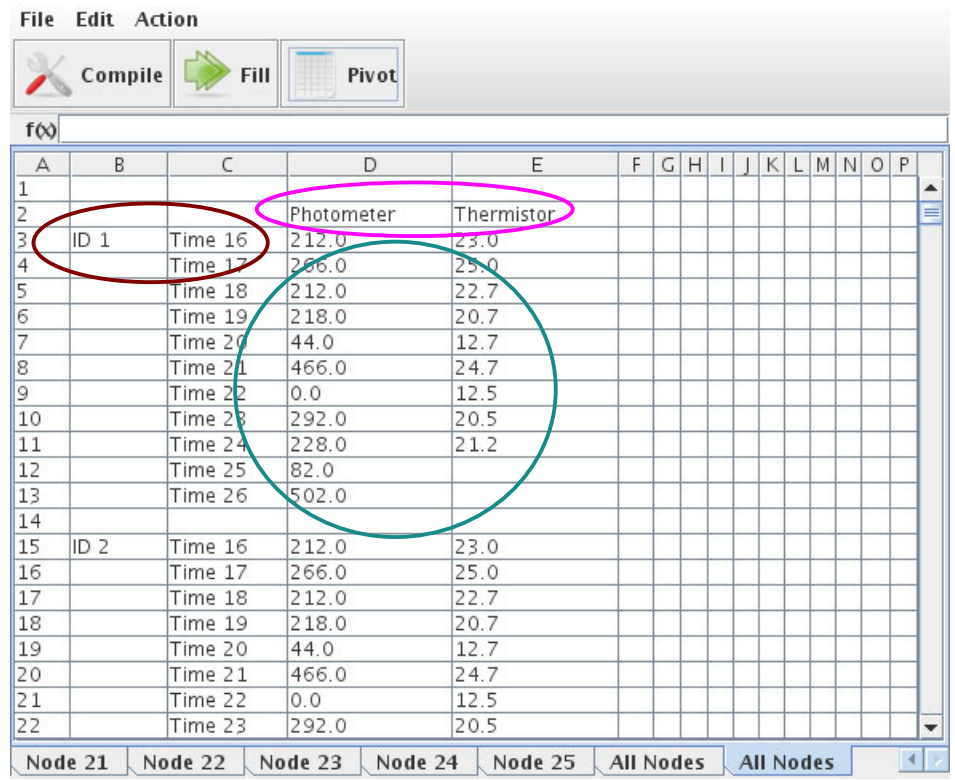

	A	B	C	D	E
1					
2				Photometer	Thermistor
3		ID 1	Time 16	212.0	23.0
4			Time 17	266.0	25.0
5			Time 18	212.0	22.7
6			Time 19	218.0	20.7
7			Time 20	44.0	12.7
8			Time 21	466.0	24.7
9			Time 22	0.0	12.5
10			Time 23	292.0	20.5
11			Time 24	228.0	21.2
12			Time 25	82.0	
13			Time 26	502.0	
14					
15		ID 2	Time 16	212.0	23.0
16			Time 17	266.0	25.0
17			Time 18	212.0	22.7
18			Time 19	218.0	20.7
19			Time 20	44.0	12.7
20			Time 21	466.0	24.7
21			Time 22	0.0	12.5
22			Time 23	292.0	20.5

Local Functions

- Users need a way to do more than simply *viewing* the data
  - Example: filtering noise
- Allow users to type in spreadsheet-like functions in empty cells
- Tables offers:
  - Arithmetic, vector (sum, average, etc), conditional, and assignment

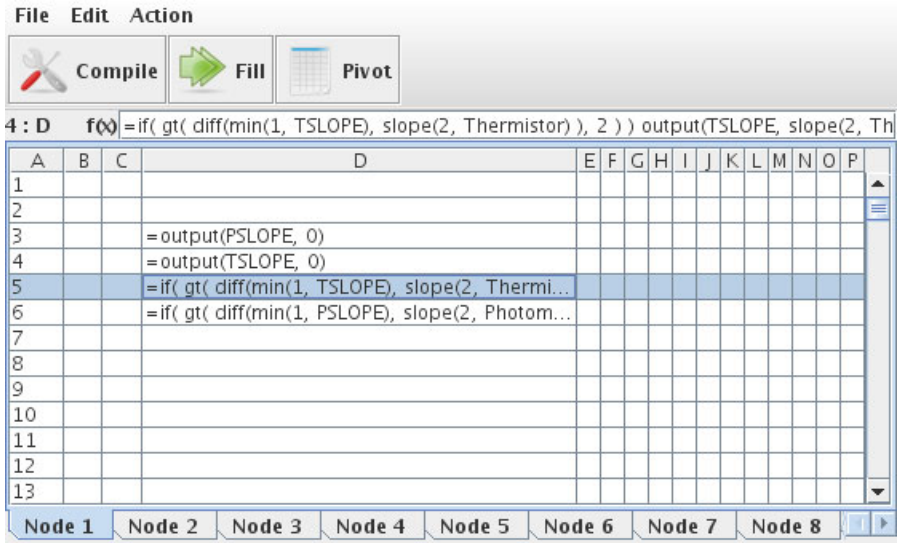

Local Functions

- Users need a way to do more than simply *viewing* the data
  - Example: filtering noise
- Allow users to type in spreadsheet-like functions in empty cells
- Tables offers:
  - Arithmetic, vector (sum, average, etc), conditional, and assignment
- Functions are propagated and executed on the sensor nodes
  - Currently using a simple interpretor

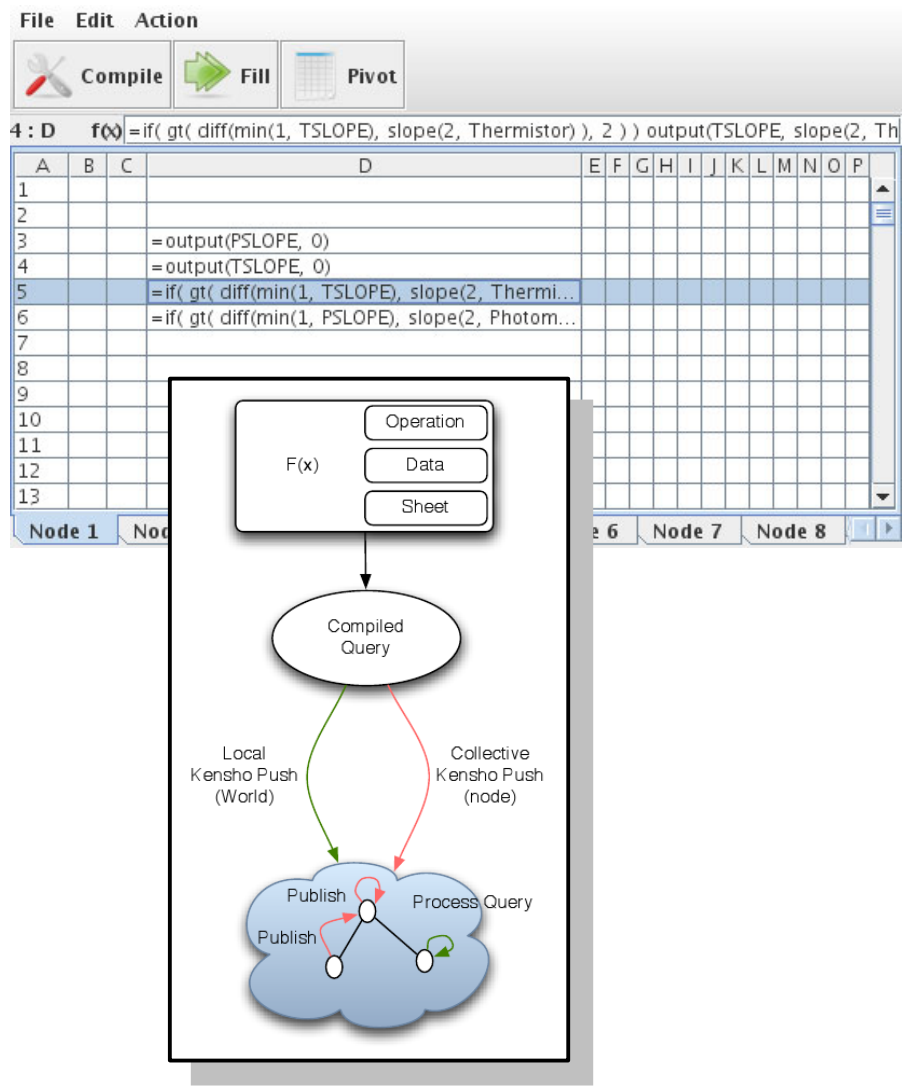

Collective Functions

- Local functions aren't enough
- Many interesting computation requires collecting data from many nodes
  - Regional averages
  - Centroid calculations
- How to do this without explicit communication?
  - Use the sheet dimension to organize the network into logical groups

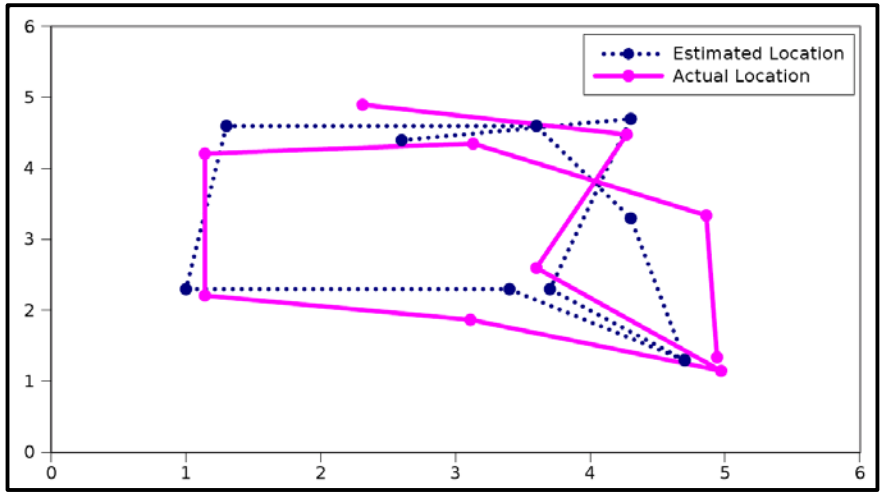

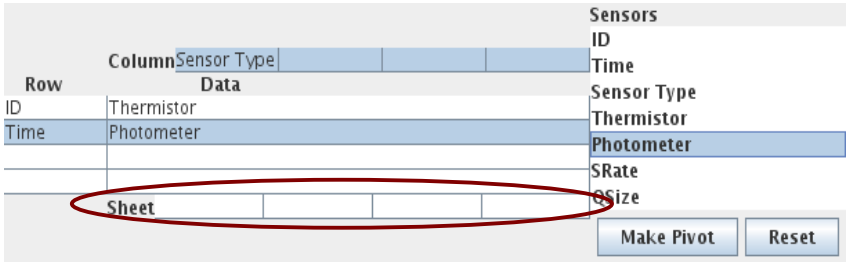

Collective Functions

- If data in a sheet is produced by multiple nodes then functions in that sheet are *collective*
  - All nodes that produce the sheet data form a *logical group* and assigns a leader
  - Each group assigns a leader
- The group leader sends a publication request
  - Nodes continually publish new data
  - Collective functions are executed with new data
- Use middleware for group formation and communication

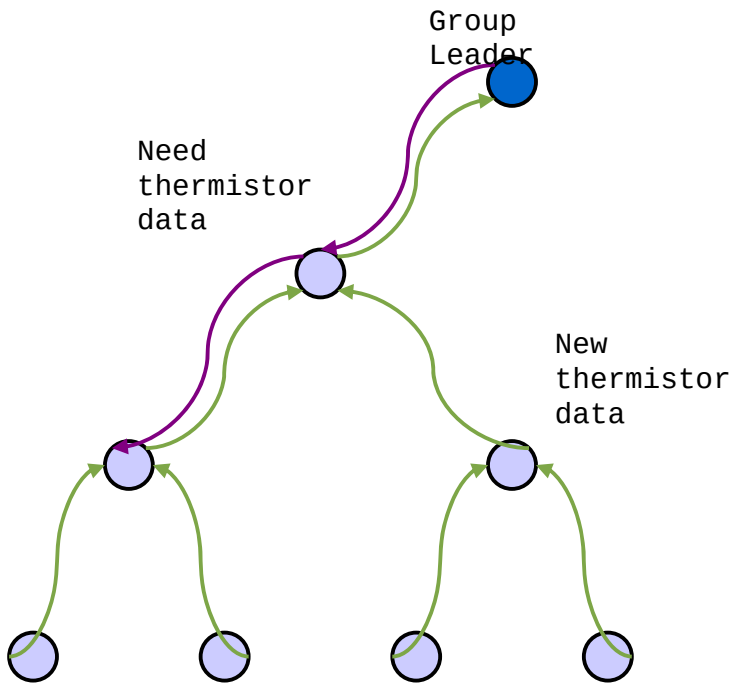

Kensho Middleware

- Provides abstractions for tasking and communication
  - Use grouping mechanisms to explicitly define roles
    - Static: Nodes in the valley perform smog monitoring
    - Dynamic: Nodes near a vehicle should perform tracking
  - Abstract *collective* and *local* tasking
  - Abstract hierarchical communication within groups

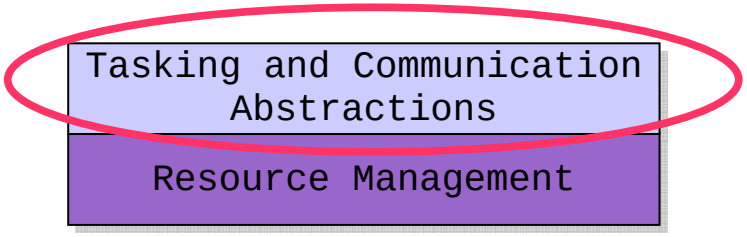

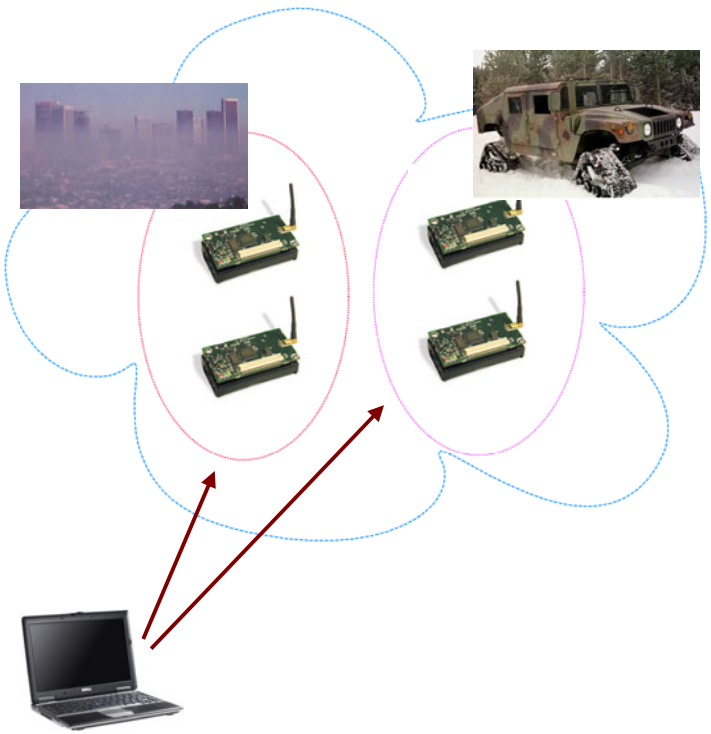

[Horey et al, WWSNA '07]

Kensho Middleware

- Provides abstractions for tasking and communication
  - Use grouping mechanisms to explicitly define roles
  - Abstract *collective* and *local* tasking
    - Map functions to run on groups, not individual nodes
    - Local: Run on every member, ie: environmental sampling
    - Collective: Run on the group, ie: data aggregation
  - Abstract hierarchical communication within groups

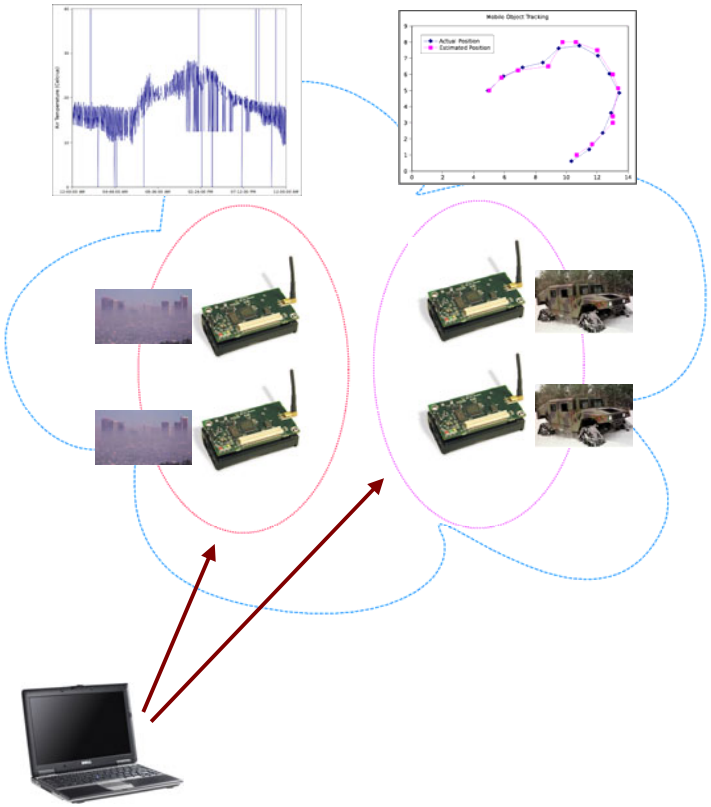

Kensho Middleware

- Provides abstractions for tasking and communication
  - Use grouping mechanisms to explicitly define roles
  - Abstract *collective* and *local* tasking
  - Abstract hierarchical communication within groups
    - Provide tuple-space data store
    - Local functions *publish* to collective functions
    - Collective functions *push* to local functions

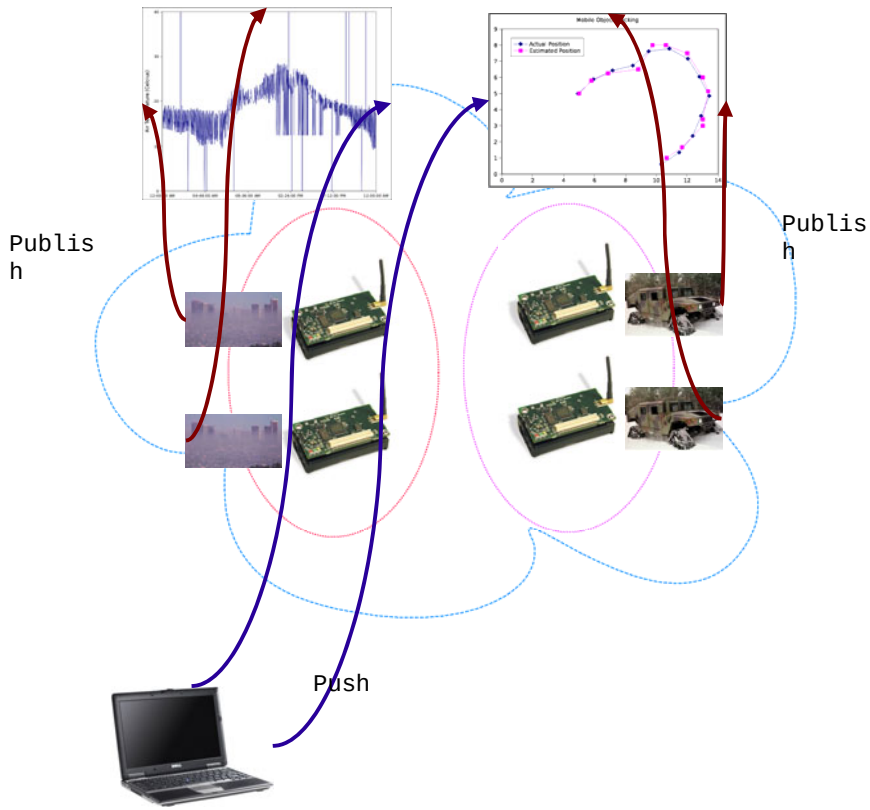

Status

- Kensho
  - Each sensor simulated by a process linked with Kensho runtime
  - Wireless communication provided by a broadcast daemon
  - Sensor values come from environmental simulator
- Tables
  - Prototype Java interface working
  - Interacts with the Kensho simulator

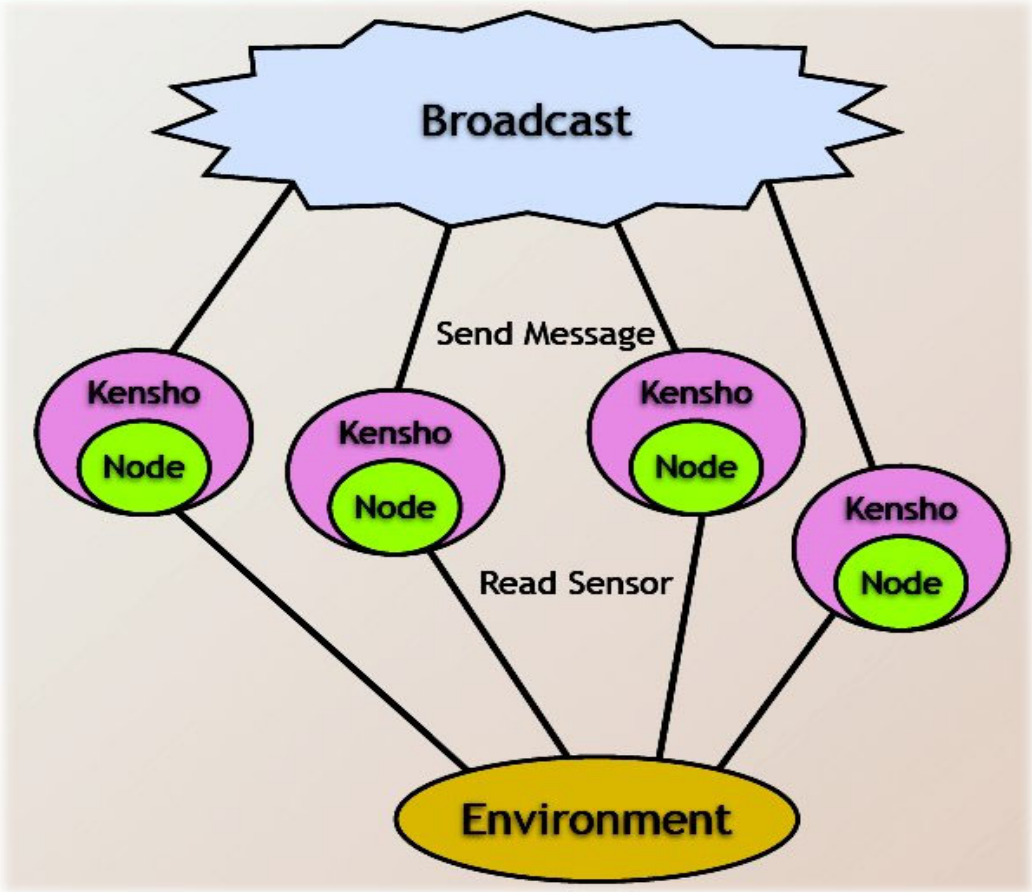

Future Work

- Systems
  - Kensho sensor node runtime in development
    - Incorporate heterogeneous hardware
    - Crossbow TelosB and Sun Spot nodes
  - Kaizen resource allocation and protection layer
    - Contract based scheduling and memory protection
- User Interfaces
  - Tables: Extend and optimize feature set
    - Incorporate function scheduling that is aware of heterogeneous hardware
  - SNFS: Using a filesystem interface to interact with and manage sensor networks
    - Allows integration with existing filesystem tools

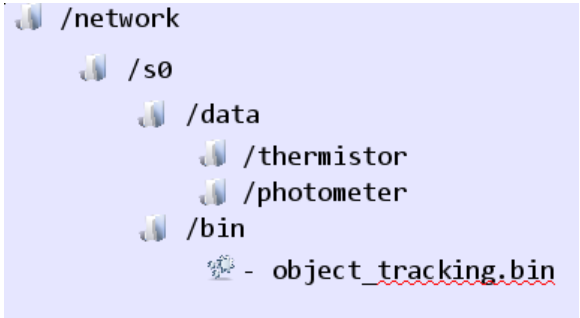

Acknowledgments

Students & Collaborators:

James Horey

Eric Nelson

Dr. Jean-Charles Tournier

Dr. Patricia Crowley (Gonzaga University)

Angela Mielke (ISR-3, LANL)

Scalable Systems Lab

UNM

Scalable Systems Lab

Bayesian Estimation of Muon Scattering Images for Detecting Heavy Radioactive materials: *Algorithms Development and Performance Evaluation*

Jinyi Qi
University of California, Davis

Muon tomography for Cargo Inspection

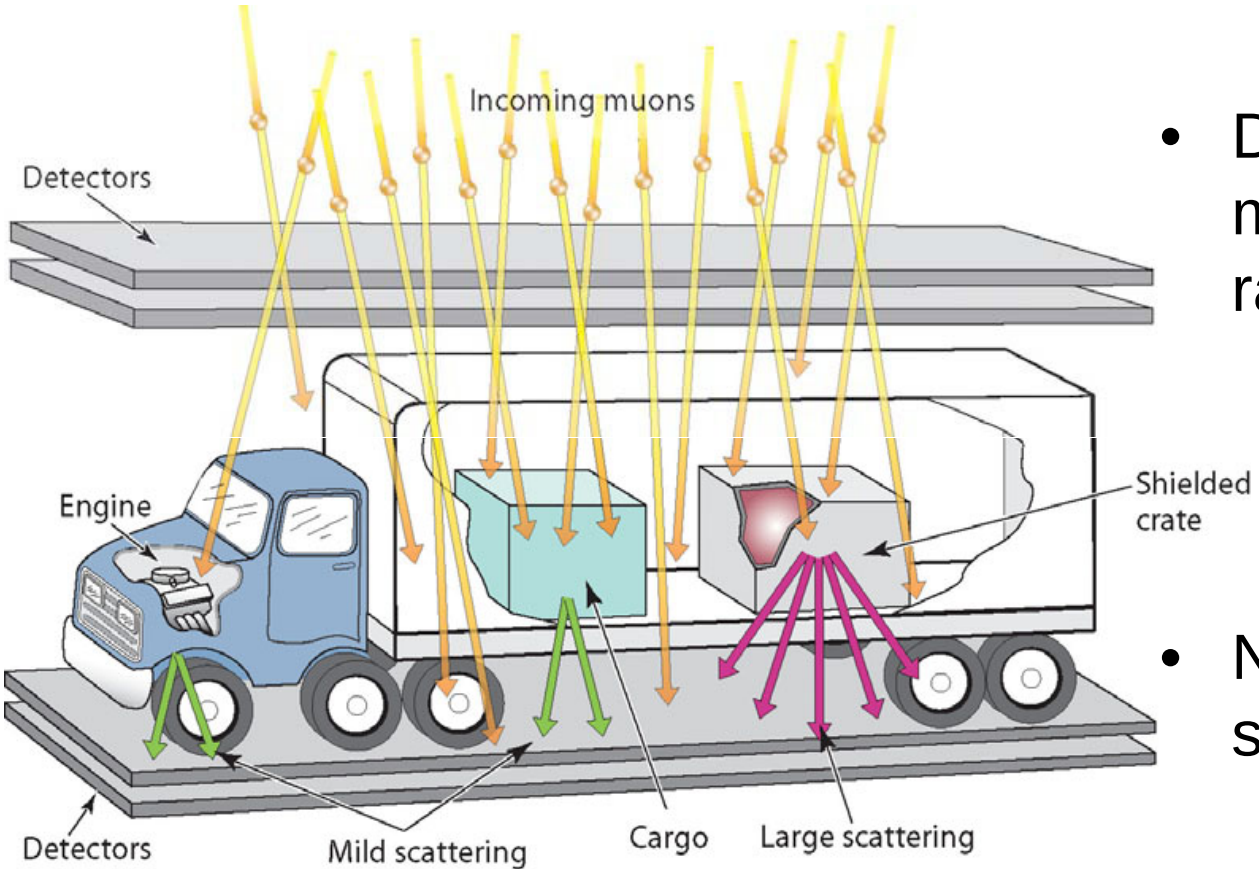

- Detect high-z nuclear material using cosmic rays
- No artificial radiation source required

Project Specific Aims

- Develop accurate models of muon interaction in objects and detectors for high-resolution, low-noise image reconstruction.
- Develop proper prior information of muon tomography images that can be used the Bayesian image estimation framework to reduce noise in muon tomography.
- Develop fast and efficient image estimation algorithms using parallel computing.
- Quantitatively evaluate the image quality of muon tomography for detecting heavy radioactive materials.

Research Team

PI: Jinyi Qi, Ph.D.,
University of California, Davis

Co-investigators

- Guobao Wang, Ph.D., University of California, Davis
- Gregory Mitchell, Ph.D., University of California, Davis

Collaborators

- Larry Schultz, Ph.D., LANL
- Christopher Morris, Ph.D., LANL
- Andrew Fraser, Ph.D., LANL

Cosmic-Ray Muon

– Primary cosmic rays interact in the upper atmosphere, producing particles including pions which decay into muons.

– Strong penetrating ability:
  - Rate: 1 muon / cm^2 / min (at sea level)
  - High energy: 3-4 GeV
  - Sufficient to penetrate meters of rock

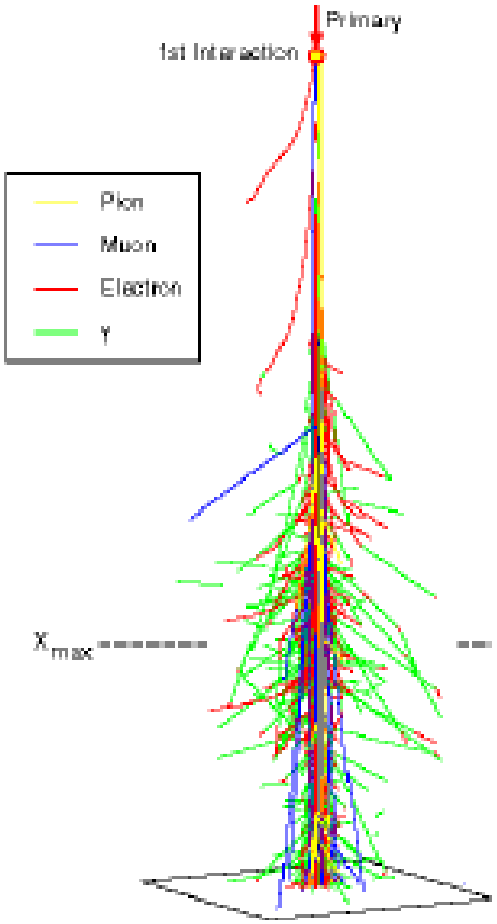

Muon Tomography

- Use attenuation of muon
  - Inspect archeological and geological objects

    (George 1955, Alvarez 1970, Minato 1988, Nagamine 1995)

- Multiple scattering
  - Coulomb scattering changes the path of muon
  - Variance of scattering depends on the material

    (Borozdin 2003; Rossi 1952, Bethe 1953)

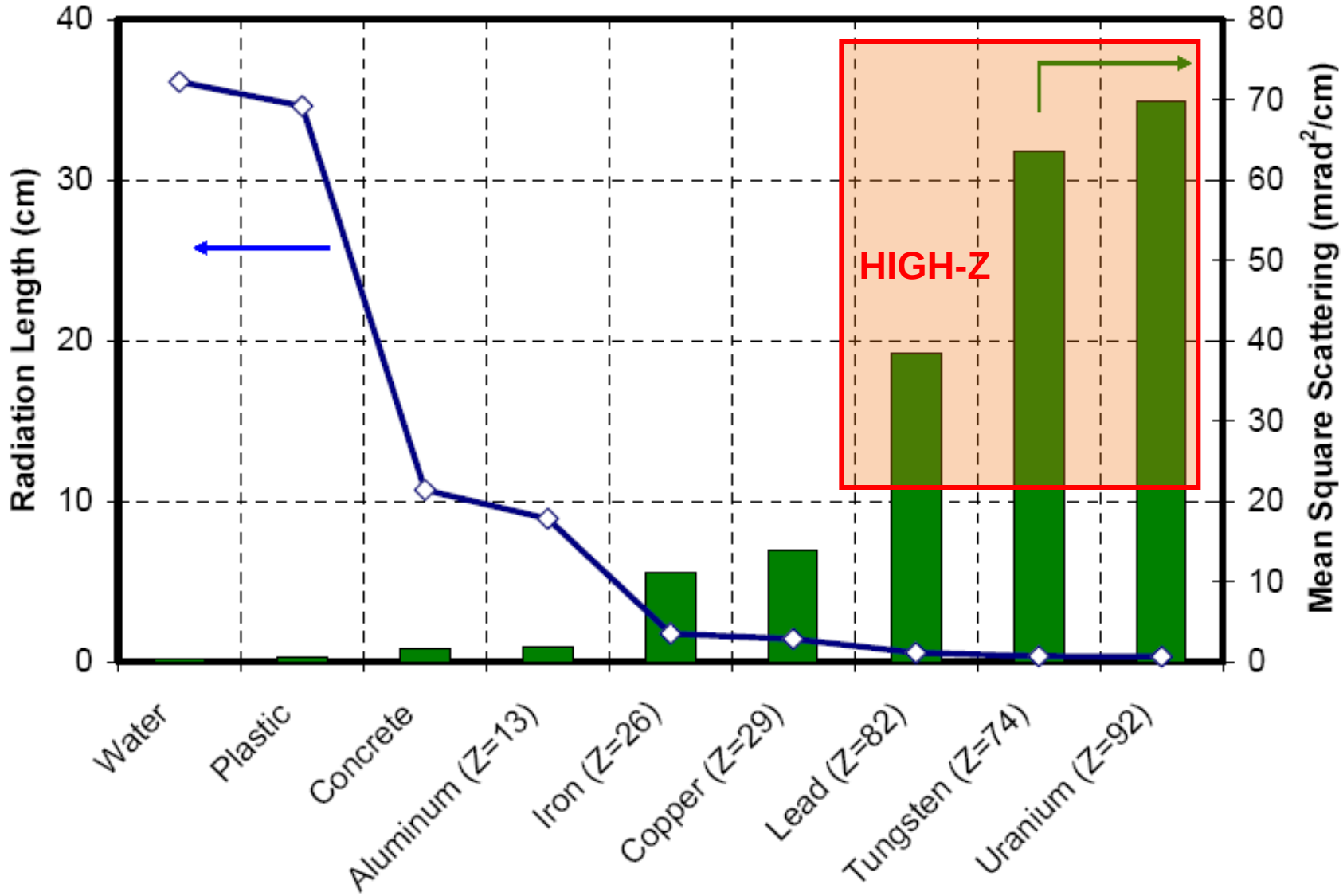
Radiation Length (cm)
Mean Square Scattering (mrad²/cm)
HIGH-Z
0
10
20
30
40
0
10
20
30
40
50
60
70
80
Water
Plastic
Concrete
Aluminum (Z=13)
Iron (Z=26)
Copper (Z=29)
Lead (Z=82)
Tungsten (Z=74)
Uranium (Z=92)

Prototype System at LANL

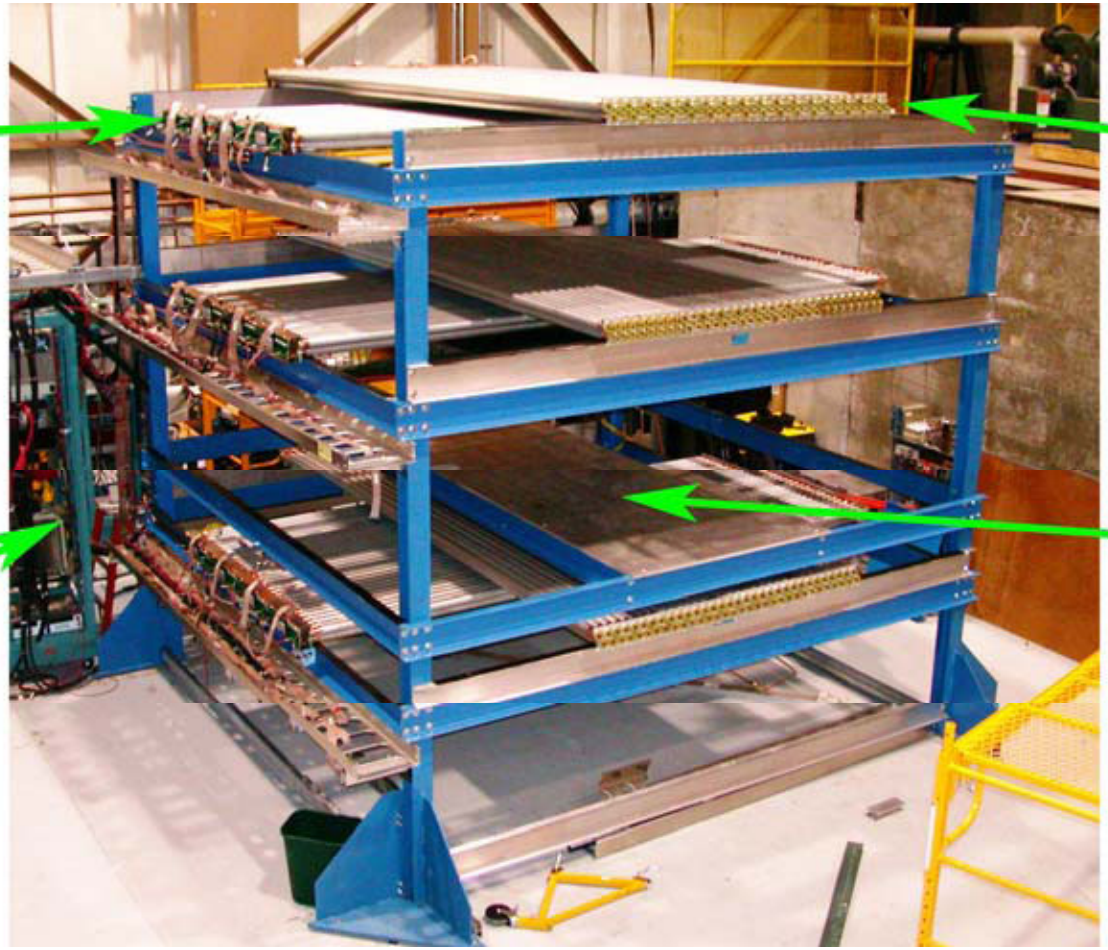

Muon Data: Gaussian Model

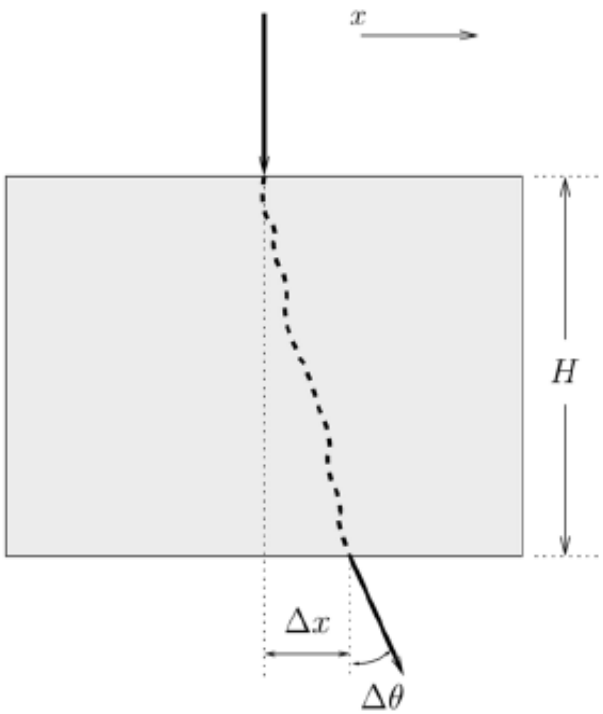

Muon measurement

$$y_i = \begin{pmatrix} \Delta x_i \\ \Delta \theta_i \end{pmatrix}$$

is usually modeled as zero-mean Gaussian random variables

$$g(y_i \mid \Sigma_i) = \frac{1}{2\pi\sqrt{|\Sigma_i|}} \exp(-\frac{1}{2} y_i' \Sigma_i^{-1} y_i)$$

The covaraince Σ_i is related to the unknown scattering density λ through

$$\Sigma_i = \sum_j H_{ij} \lambda_j$$

Maximum Likelihood: Single Gaussian

The log likelihood of the single Gaussian model is

$$L(y \mid \lambda) = -\frac{1}{2}\sum_i y_i' \Sigma_i^{-1} y_i - \log|\Sigma_i|$$

The ML estimate of λ is

$$\hat{\lambda}_{ML} = \arg\max_{\lambda > 0} L(y \mid \lambda)$$

- Expectation maximization algorithm (Schultz et al, 2007)

$$\text{E step}: \; Q_j(\lambda_j, \lambda^{(n)}) = -\sum_i (\log \lambda_j + \frac{1}{\lambda_j}\mu_{ij}) \;\; \text{where } \mu_{ij} = \mathrm{E}_z^{(n)}[z'\Sigma_i^{-1}z']$$

$$\text{M step}: \lambda_j^{(n+1)} = \arg\max Q_j(\lambda_j, \lambda^{(n)}) \Rightarrow \lambda_j^{(n+1)} = \frac{1}{2M_j}\sum_i \mu_{ij}$$

Gaussian Mixture Model

- We use a scaled Gaussian mixture model to better approximate the distribution of scattering angle
- The variance of each Gaussian function is proportional to the scattering density with a different scaling factor

$$h(y_i \mid \Sigma_i, w, s) = \sum_k w_k g(y_i \mid \Sigma_{i,k})$$

$$\Sigma_{i,k} = s_k \sum_j H_{ij} \lambda_j$$

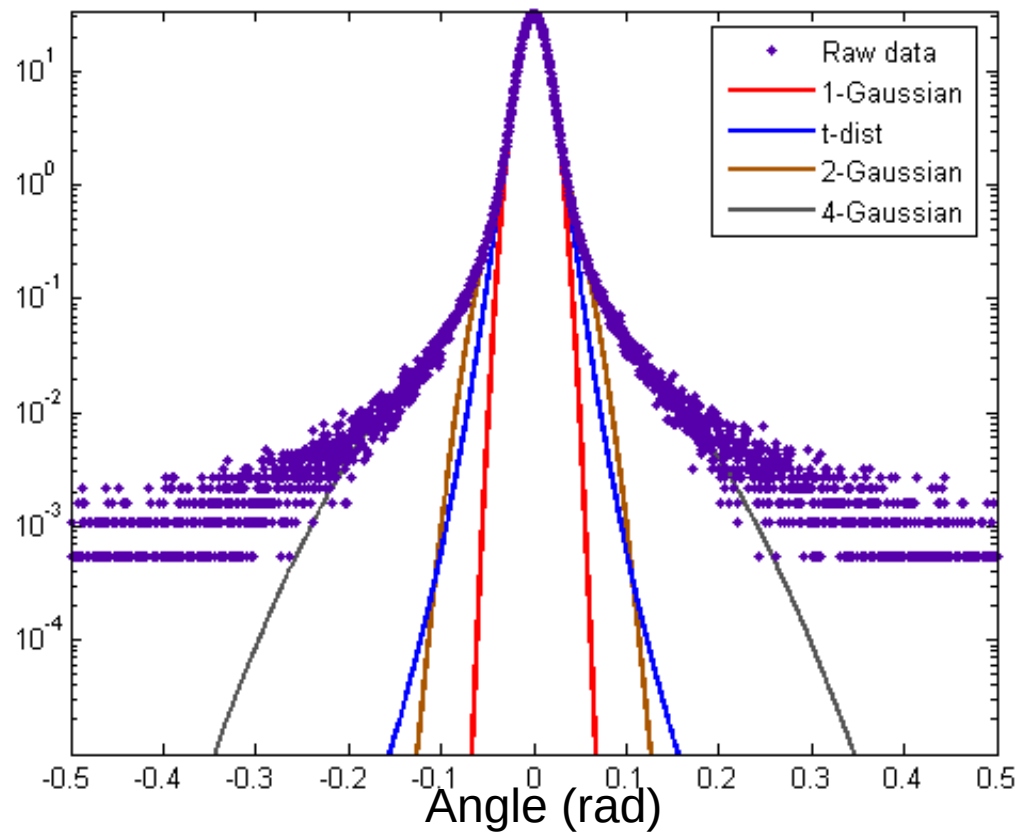

Maximum Likelihood: Gaussian Mixture

- Log likelihood function

$$L(y \mid \lambda) = \sum_i \log\left(\sum_k w_k g(y_i \mid \Sigma_{i,k}) \right)$$

- Surrogate function

$$L(y \mid \lambda) \geq \sum_i \sum_k a_{ik}^{(n)} \log\left(g(y_i \mid \Sigma_{i,k})\right)$$

$$\text{where } a_{ik}^{(n)} = \frac{w_k g(y_i \mid \Sigma_{i,k}^{(n)})}{\sum_l w_l g(y_i \mid \Sigma_{i,l}^{(n)})}$$

- The rest follows the EM algorithm

Bayesian Image Reconstruction

Bayes theorem: $p(\lambda \mid y) \propto p(y \mid \lambda)\, p(\lambda)$

MAP (maximum a posteriori) estimate is the maximizer of $p(\lambda \mid y)$

$$\hat{\lambda}_{MAP} = \arg\max_{\lambda > 0} \Phi(\lambda, y), \qquad \Phi(\lambda, y) = L(y \mid \lambda) - \ln p(\lambda)$$

Here we use Laplacian Markov random field as the image prior to model muon scattering density

$$\ln p(\lambda) = \beta_1 \sum_j \sum_{k \in N_j} w_{jk} \mid \lambda_j - \lambda_k \mid + \beta_2 \sum_j \mid \lambda_j \mid + const$$

where $\beta_{1,2}$ are the hyperparameters.

Convergent optimization algorithm has been derived.

Simulation Studies

- Geant4 Monte Carlo simulation package
- A realistic model of a passenger van containing normal and “threat” materials
- Simulate about 1 minute scan time
- 100 realizations

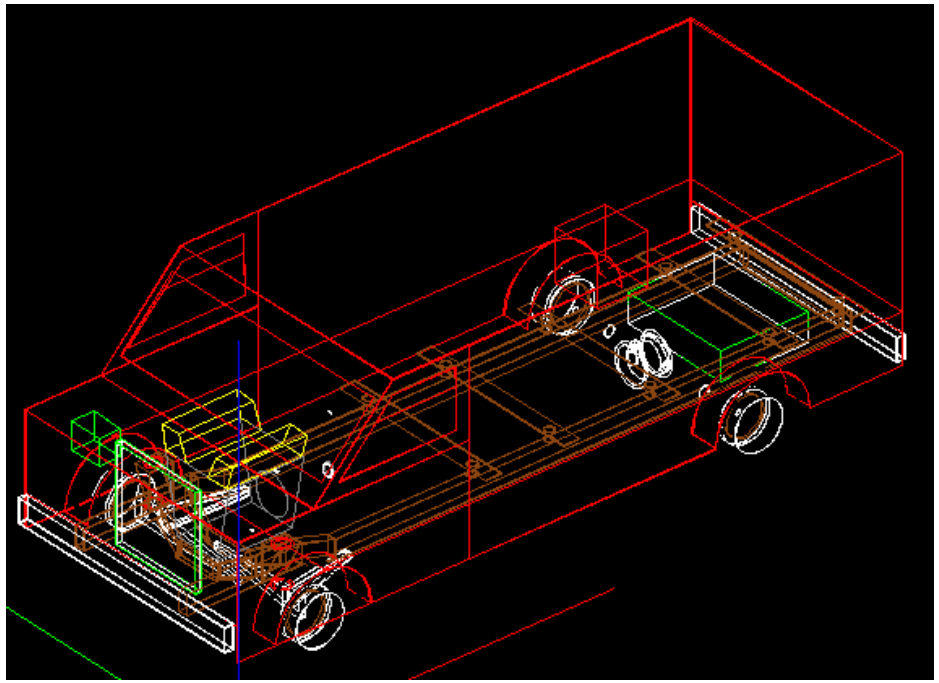

Mean Reconstructed Images

Single Gaussian

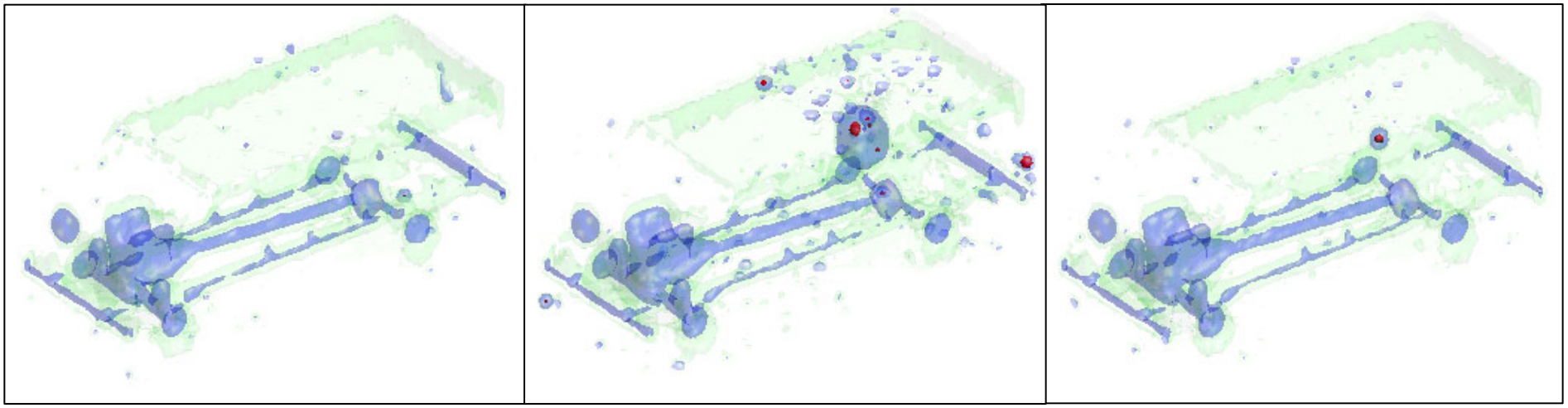

Gaussian Mixture

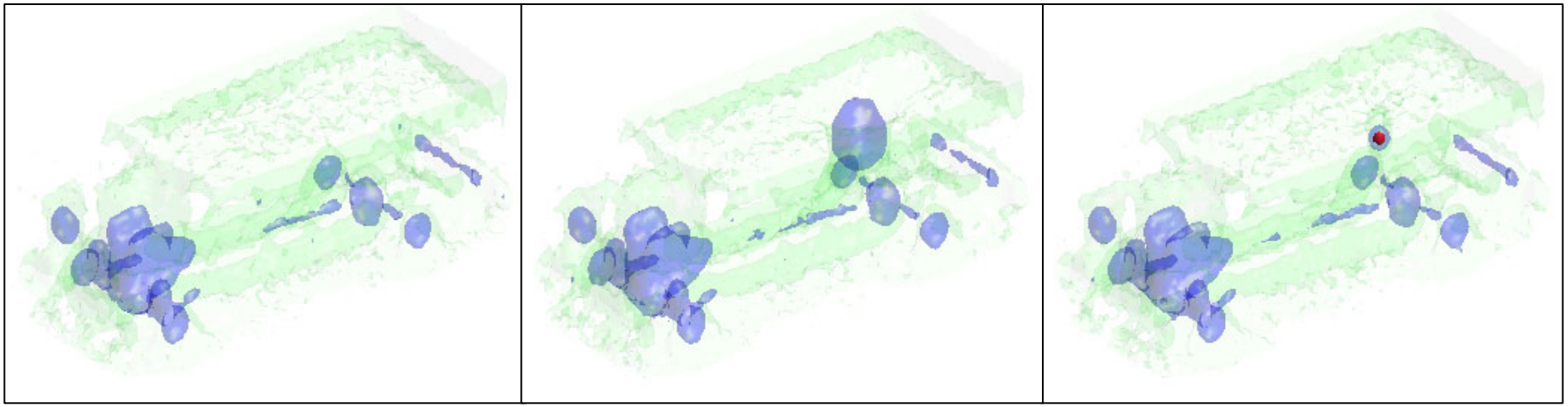

Empty | 40 cm Iron | 10 cm Tungsten

Mean Images: Bayesian Reconstruction

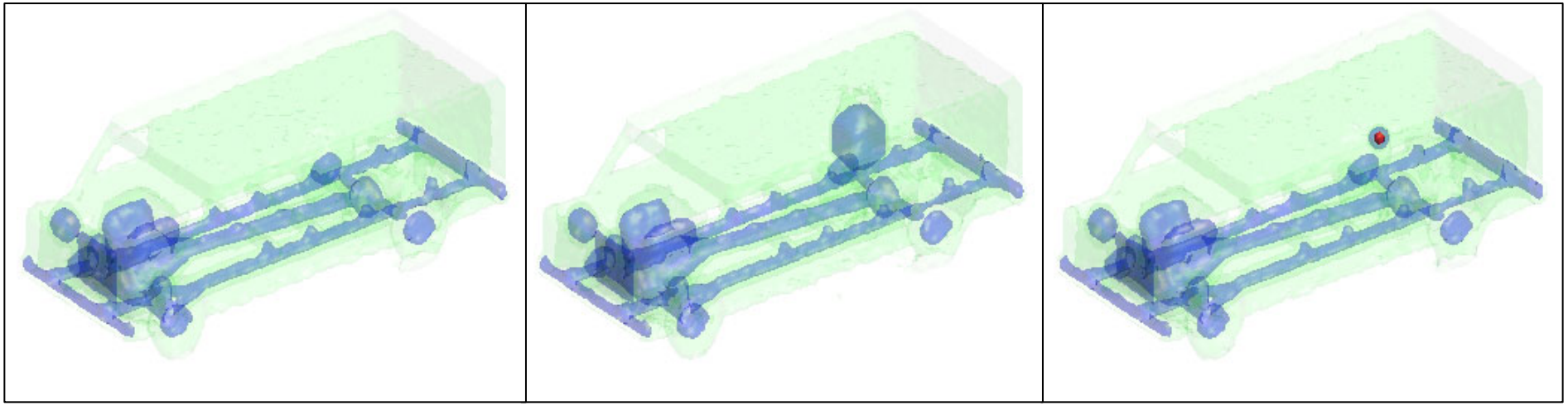

Empty | 40 cm Iron | 10 cm Tungsten

Quantitative Evaluation using LROC Curve

- Decision:
  - Maximum scattering variance > t : Positive (Alarm)
  - Maximum scattering variance < t : Negative (Pass)
- Localization ROC curve
  - Plot of ***correctly localized*** true-positive fraction vs. false-positive fraction

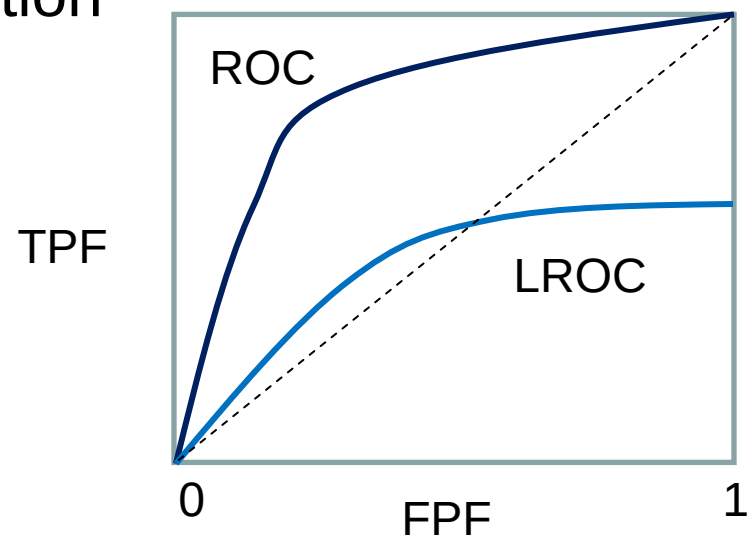

LROC Curves

- 10-cm Tungsten vs. empty van

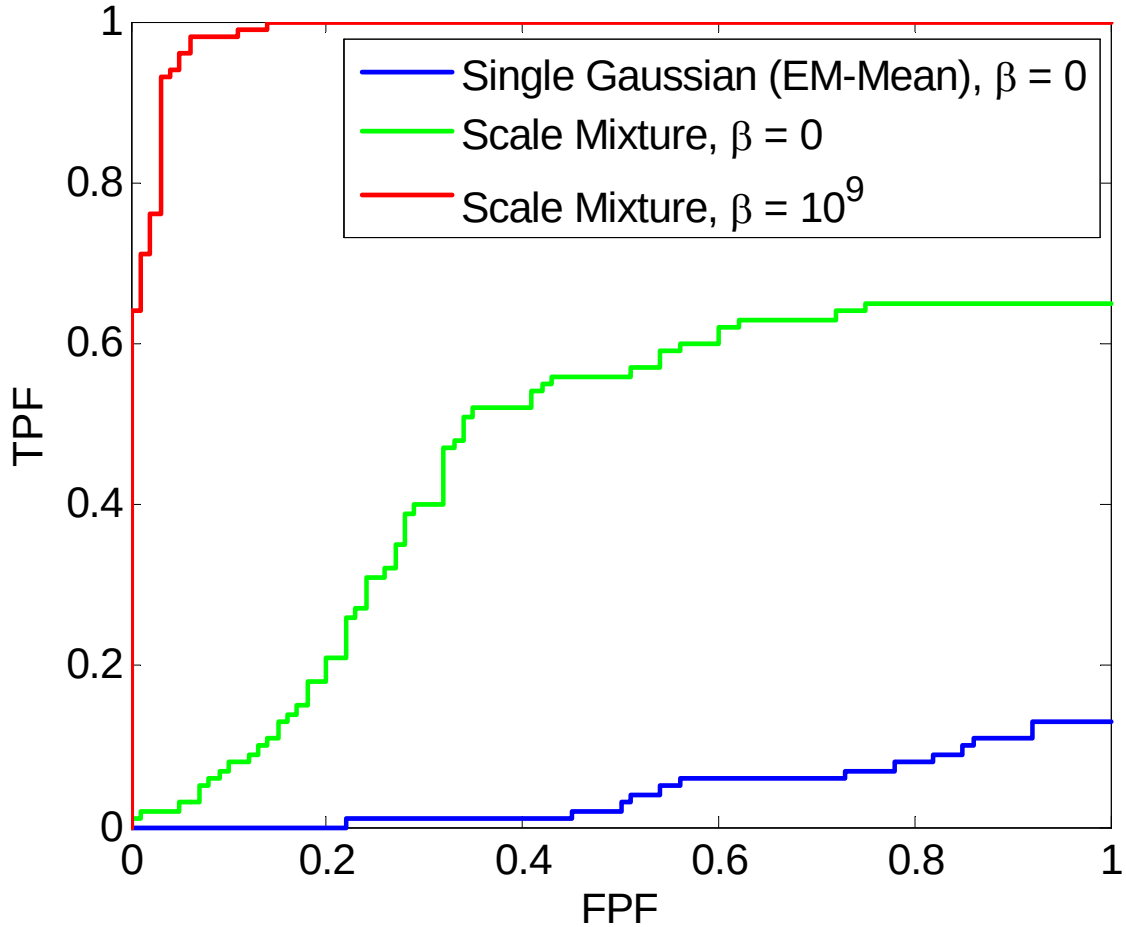

LROC Curves

- Compare with the EM-median method

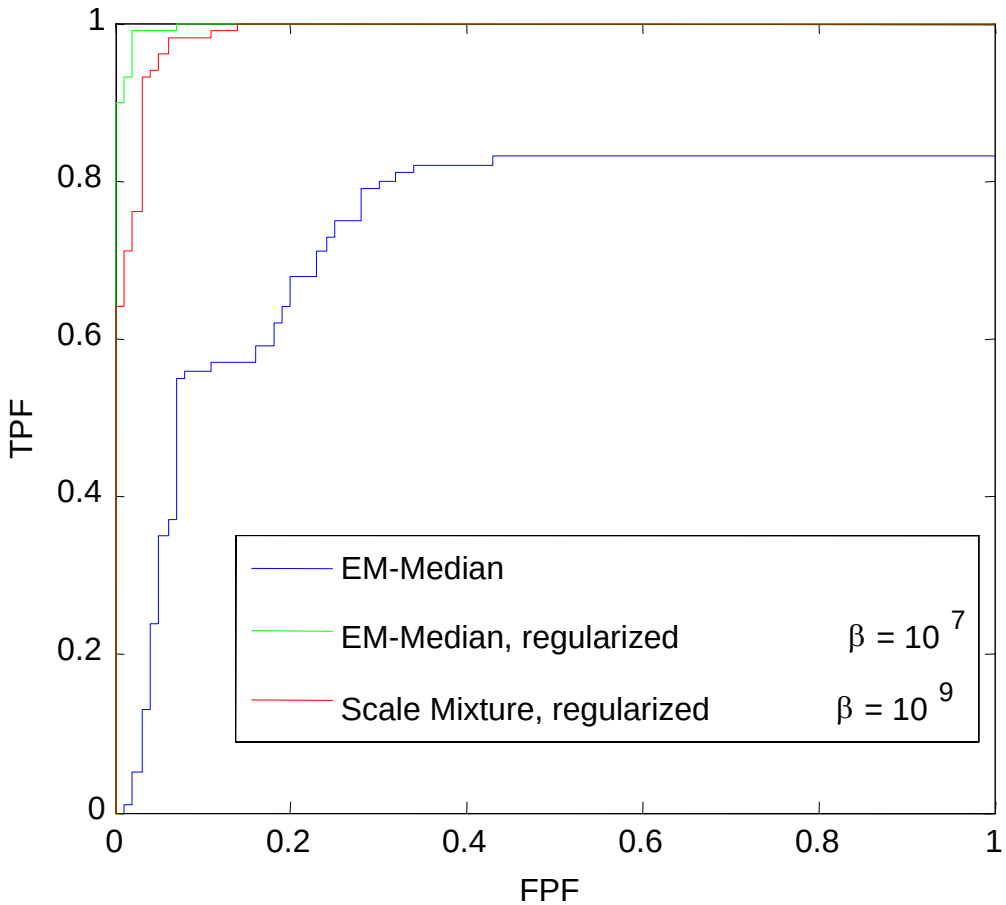

10-cm Tungsten vs. 40-cm Iron

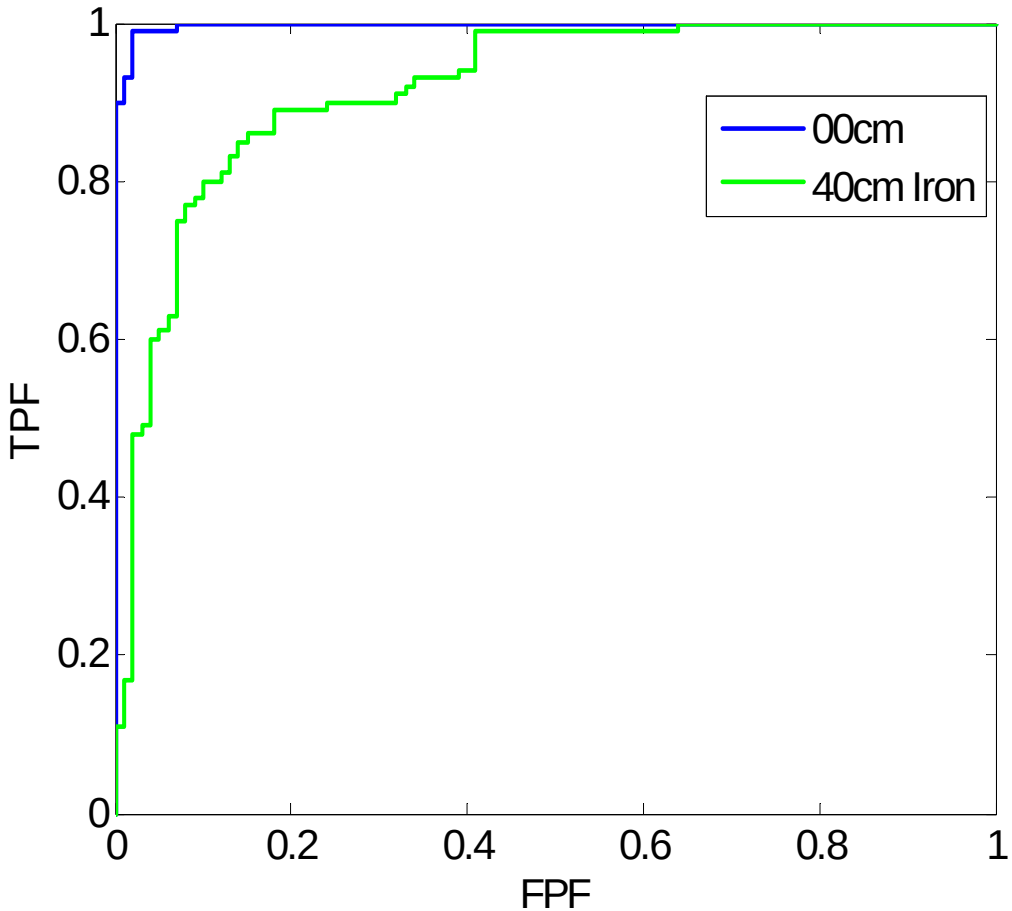

Summary

- Muon tomography is a promising tool for cargo inspections
- We have developed a Gaussian mixture model for muon scattering data and a Bayesian image reconstruction algorithm using Laplacian prior.
- Preliminary results show that the Bayesian reconstruction algorithm significantly improve the performance of muon tomography for detecting heavy nuclear materials.

Milestones

Year 1 Milestones:

- ✓ Generate models of muon scattering using Monte Carlo simulation
- ✓ Compare Monte Carlo simulated model with simplified Gaussian model
- o Cross validation between the Monte Carlo generated model with experimental measurements
- ✓ Implement new model in maximum likelihood algorithm
- – Conduct detector calibration measurements of the prototype system at LANL and incorporate into the physical model

Year 2 Milestones:

- ✓ Develop methodology for quantitative evaluation of image quality of detection performance
- ✓ Generate "normal" and "threat" data sets using Monte Carlo simulation
- o Acquire "normal" and "threat" data sets using the prototype system at LANL
- ✓ Develop and evaluate Bayesian image prior based on Markov random field
- o Develop and evaluate Bayesian image prior based on multiphase level set
- ✓ Implement Bayesian image estimation algorithm
- – Evaluate Bayesian image prior using Monte Carlo generated data and experiment data

Future work

- Extend the Bayesian image estimation algorithm to include other image priors
- Accelerate the Bayesian image estimation algorithm using parallel computing: multithread and MPI
- Acquire experimental data using the prototype system at LANL
  - Cross validation between the Monte Carlo generated model with experimental measurements
  - Incorporate the detector model in the image reconstruction algorithm
- Quantitative evaluation of the Bayesian image estimation algorithm for detecting heavy nuclear materials using simulated and experimental data
- Finalize the Bayesian image estimation software